THE JOURNAL
OF
CHEMICAL PHYSICS

VOLUME 18, NUMBER 12 DECEMBER, 1950

The Infra-Red and Raman Spectra of Cyclopentane, Cyclopentane-d_1, and Cyclopentane-d_{10}

FOIL A. MILLER
Department of Research in Chemical Physics, Mellon Institute, Pittsburgh, Pennsylvania
AND
RICHARD G. INSKEEP*,†
Department of Chemistry, University of Illinois, Urbana, Illinois
(Received June 23, 1950)

The infra-red and Raman spectra of cyclopentane, cyclopentane-d_1, and cyclopentane-d_{10} have been determined for the purpose of establishing the symmetry of cyclopentane. D_{5h} selection rules are found to hold very well. This does not constitute a rigorous criterion for structure in this case, however, because drastic alteration of the symmetry by substituting groups such as D, OH, CH_3, or Cl for a hydrogen atom does not appreciably increase the complexity of the spectra. The data have provided two strong arguments against a D_{5h} structure. (1) An assignment could not be made which simultaneously satisfied the product rule and the expected band contours. (2) The entropy of the vapor demands a low frequency (near 140 cm^{-1} for the assignment in this paper) if the symmetry is D_{5h}. This is completely incompatible with the heat capacity of the solid.

It is concluded that cyclopentane definitely does not have D_{5h} symmetry. The actual geometry of the molecule is still not known. It is shown that a rigid structure of symmetry C_s, C_2, or C_1 is consistent with the available data. A decision between this and Kilpatrick, Pitzer, and Spitzer's model with a puckered ring and a pseudorotation in place of one of the genuine normal vibrations cannot be made at this time.

Analogous spectroscopic results for perfluorocyclopentane are mentioned briefly for comparison. This molecule is definitely non-planar.

The method of preparation of the deuterium compounds is given. A Pd-on-charcoal catalyst is described which promises to be useful in other hydrogen-deuterium exchange reactions.

INTRODUCTION

THIS study was undertaken in the hope of determining whether or not the carbon ring in cyclopentane is planar. Kilpatrick, Pitzer, and Spitzer[1] have pointed out that there are forces favoring both planar and non-planar structures. A regular pentagon has interior angles which are very close to the tetrahedral value (108° *vs.* 109° 28′), so the planar structure is stabilized by the forces tending to maintain tetrahedral bond angles. Conversely this structure is destabilized by repulsions between the hydrogen atoms of neighboring methylene groups. These repulsions are at a maximum for the planar structure. They produce torsional forces around the carbon-carbon bonds which tend to pucker the ring. The problem is to determine which of the two effects predominates.

There have been many earlier physical measurements pertaining to the structure of cyclopentane. The Raman spectrum[2–8] and the infra-red spectrum[9–13] have been

* From a dissertation submitted to the Graduate School of the University of Illinois in partial fulfillment of the requirements for the degree of Doctor of Philosophy.

† Present address: School of Chemistry, University of Minnesota, Minneapolis, Minnesota.

[1] Kilpatrick, Pitzer, and Spitzer, J. Am. Chem. Soc. **69**, 2483 (1947).

[2] J. Weiler, Zeits. f. Physik **72**, 206 (1931).

[3] Canals, Godchot, and Cauquil, Comptes Rendus **194**, 1574 (1932).

[4] K. W. F. Kohlrausch and R. Seka, Ber. **69**, 729 (1936).

[5] A. W. Reitz, Zeits. f. physik. Chemie **B-33**, 179 (1936); **B-38**, 381 (1938).

[6] E. J. Rosenbaum and H. F. Jacobson, J. Am. Chem. Soc. **63**, 2841 (1941).

[7] Bazhulin, Sterin, Bulanova, Solovova, Turova-Pollak, and Kazanskii, Izvest. Akad. Nauk. S. S. S. R. Otdel Khim. Nauk. **1946**, No. 1, p. 7. Chem. Abs. **42**, 6238 i.

[8] Fenske, Braun, Wiegand, Quiggle, McCormack, and Rank, Anal. Chem. **19**, 700 (1947).

[9] Barca-Galateanu, Bull. soc. roumaine phys. **38**, No. 69, 109 (1938).

[10] P. Lambert and J. LeCompte, Ann. de physique **10** (11th series), 539 (1940).

[11] American Petroleum Institute Research Project 44 at the National Bureau of Standards. Catalog of Infra-Red Spectrograms. Serial No. 446, cyclopentane, contributed by the Shell Development Corporation.

[12] See reference 11, Serial Nos. 343 and 596, contributed by the Radiometry Laboratory of the National Bureau of Standards. Or see Plyler, Stair, and Humphreys, J. Research Nat. Bur.

reported several times. Their simplicity suggests a high degree of symmetry. Electron diffraction studies give good agreement with an assumed planar ring.[14–16] Aston, Fink, and Schumann[17] measured the heat capacity of cyclopentane from 11.1°K to room temperature, and from this determined the entropy. This was compared with the entropy calculated from spectroscopic data. They found much better agreement for a puckered ring than for a planar ring, but many of their frequency assignments are dubious.

Kilpatrick, Pitzer, and Spitzer[1] have calculated the resultant potential energy due to the two opposing forces mentioned earlier, *viz.*, the repulsions between hydrogen atoms on adjacent methylene groups, and the forces acting to preserve tetrahedral bond angles. The former was evaluated by using the potential barrier for the internal rotation in ethane, and the latter by employing a force constant carried over from other molecules. It was concluded that a puckered ring is more stable than a planar one. The calculations indicated: (a) that the maximum displacement of an equilibrium nuclear position out of the (hypothetical) D_{5h} plane is about 0.2A, and (b) that this maximum displacement is not localized at a given carbon atom, but rotates around the ring. These results make a non-planar ring appear reasonable, but hardly constitute convincing evidence for it because of the approximations involved. These authors also make a vibrational assignment and use it to calculate the entropy and heat capacity of the vapor at several temperatures. The agreement with calorimetric values is impressive, but is slightly misleading because two adjustable parameters were available for fitting the data (their q_0 and an anharmonicity coefficient).

The case for a non-planar ring rests almost entirely on the entropy argument. The most vulnerable point in this argument is the assignment of the vibrational frequencies. It therefore seemed worth while to study the vibrational spectrum in greater detail with the hope of obtaining a more reliable assignment, especially of the lower fundamentals. Still more important is the fact that one may reasonably hope to obtain completely independent evidence about the structure, since the selection rules for the planar and the non-planar forms are very different.

In this paper cyclopentane, cyclopentane-d_1, and cyclopentand-d_{10} will be referred to as d_0, d_1, and d_{10}, respectively, for the sake of brevity.

Stand. **38**, 211 (1947); E. K. Plyler, J. Opt. Soc. Am. **37**, 746 (1947).

[13] See reference 11, Serial No. 221, contributed by the Anglo-Iranian Oil Company, Ltd.; Serial No. 254, contributed by the Universal Oil Products Company. These spectra are definitely inferior to those of references 11 and 12.

[14] R. Wierl, Ann. d. Physik **8**, 521 (1931); **13**, 453 (1932).

[15] L. Pauling and L. O. Brockway, J. Am. Chem. Soc. **59**, 1223 (1937).

[16] O. Hassel and H. Viervoll, Tids. Kjemi, Bergvesen, Met. **6**, No. 3, 31 (1946).

[17] Aston, Fink, and Schumann, J. Am. Chem. Soc. **65**, 341 (1943).

EXPERIMENTAL

A. Origin of the Compounds

The d_0 used for obtaining the infra-red and Raman spectra, and also employed as the starting material in the preparation of d_{10}, was the Phillips Petroleum Company's research grade product. Its purity was 99.95±0.02 mole percent. The most probable impurity was 2,2-dimethylbutane, but no trace of this could be found in the infra-red spectrum.

Cyclopentane-d_1 was prepared by the Grignard reaction:

$$C_5H_9Cl \xrightarrow{Mg} C_5H_9MgCl \xrightarrow{DCl} C_5H_9D + MgCl_2(s).$$

Cyclopentyl chloride was dissolved in thoroughly dried *n*-butyl ether and was treated with magnesium to form the Grignard reagent. The theoretical amount of deuterium chloride, prepared by adding heavy water dropwise to benzoyl chloride according to the method of Brown and Groot[18] was bubbled slowly into the ether solution under a dry nitrogen atmosphere. The resulting d_1 was removed from the mixture by distillation and was redistilled. The fraction boiling at 47.0 to 47.7°C (uncorr.) was taken.

Cyclopentane-d_{10} was prepared by exchange between d_0 and deuterium in the apparatus shown in Fig. 1. The d_0 was refluxed in the small reservoir so that its vapor mixed with the incoming deuterium gas. The mixture passed over the heated catalyst and then through a condenser which was cooled with acetone at dry ice temperature. The condensate returned to the reservoir through a 1-mm capillary. The exit hydrogen-deuterium mixture was passed through a cold trap to insure that no product would accidentally be lost through failure of the acetone circulating system.

It is known from earlier work that exchange between cyclohexane and deuterium occurs over a platinum-black-on-platinum-foil catalyst.[19,20] This catalyst was therefore employed in the initial experiments with d_0. It worked very well at first, but its activity rapidly declined until it was useless at the end of 12 to 18 hr. An attempt to reactivate it was only slightly successful. It was realized later that the poisoning may have been due to the deposition of a film of SiO from the silicone stopcock grease used on the joints of the apparatus.[21]

Another catalyst consisting of a thin coating of palladium on activated charcoal was then tried and was found to be quite satisfactory. Measurable exchange occurred at 150°C over this catalyst, but the temperature was maintained at 190 to 210°C throughout the reaction in order to obtain a much higher rate. The

[18] H. C. Brown and C. Groot, J. Am. Chem. Soc. **64**, 2223 (1942).

[19] Horrex, Greenhalgh, and Polanyi, Trans. Faraday Soc. **35**, 511 (1939).

[20] A. Farkas and L. Farkas, Trans. Faraday Soc. **35**, 917 (1939).

[21] R. H. Savage, J. Chem. Phys. **16**, 237 (1948).

catalyst has been used for a total of 90 hr. with no lessing of activity.[22]

Eight milliliters of d_0 were exchanged with deuterium of 99.7 percent purity.[23] The rate of d_0 evaporation was kept at approximately 0.02 mole/min., and the deuterium flow at approximately 0.001 mole/min. The progress of the reaction was measured by following the disappearance of the C—H stretching band at 2950 cm^{-1}. The exchange was continued for a total of 66 hr. A yield of 5.5 ml of approximately 96 percent pure d_{10} was obtained. The chief impurity was d_9.

In order to insure that only C—H bonds were being ruptured in the exchange process, a test was carried out with d_0 and ordinary hydrogen at 250°C for an 8-hr. period. It was thought that the elevated temperature would greatly increase both the C—H rupture and any C—C rupture that might be taking place. The infra-red spectrum of the hydrocarbon was checked before and after the test and the amount of any impurity formed was below the limits of spectroscopic detection.

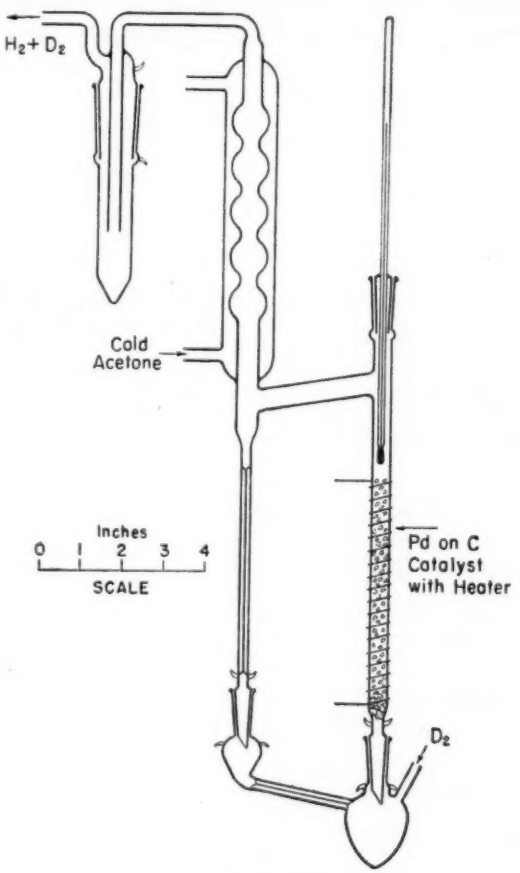

FIG. 1. Exchange apparatus.

B. Spectroscopic Measurements

The infra-red spectra presented in this paper were obtained with a modified Model 12-A Perkin-Elmer instrument equipped with a wave-length drive, a General Motors amplifier, and a Brown recorder. Prisms of KBr, NaCl, and CaF_2 were used for each sample. In addition gaseous d_0 was examined in the region from 2800 to 3000 cm^{-1} with a LiF prism.[24] Liquid d_0 was surveyed from 250 to 400 cm^{-1} with a thallium bromoiodide prism, using a 1.5-mm cell.[25] No bands were found in this range.

Band positions are estimated to have the following accuracies: 400 to 1000 cm^{-1}, ± 1 cm^{-1}; 1000 to 2000, ± 2; 2000 to 3100, ± 3. Each sample was examined in the liquid state (0.08 mm thick), and as a vapor (10- and 100-cm cells).

The spectrograph used to obtain the Raman spectra was built at Mellon Institute by Dr. A. L. Marston. It is of the type designed by Lord,[26] and described in greater detail by Stamm.[27] The collimator is a 7° off-axis parabola of 16 cm diameter and 100 cm focal length. The plane echelette grating has 15,000 lines/in. with a total ruled area 4 in. high and 6 in. wide. The blaze is in one of the first-order blue-green regions. Ghost lines are rather bad with this grating, and make it very difficult to observe Raman displacements of less than 300 cm^{-1} unless they are intense. The camera lens, obtained from the Perkin-Elmer Corporation, is $f/5.4$ with an effective focal length of 27 in. The reciprocal dispersion at the plate is 25.4A/mm.

The illuminator was closely similar to that described by Crawford and Horwitz,[28] except that each arc was backed by an elliptical reflector. Twelve General Electric Type *H*-11 mercury arcs were employed. The power supply was stabilized by two Sola constant voltage transformers, each one supplying six lamps.

Wave-length measurements were made by the method described by Stamm.[27] The Raman displacements were corrected to vacuum and are accurate to ± 2 cm^{-1} for sharp lines and about ± 5 cm^{-1} for diffuse lines. Depolarization ratios were obtained by the method of

[22] The catalyst may be prepared as follows. Make up a two or three percent aqueous solution of sodium chloropalladite (Na_2PdCl_4), and adjust its *p*H to 5 ± 1. Immerse Columbia SW activated carbon, 4/14 mesh, in this solution. Upon conclusion of the evolution of gas, decant the liquid and dry the catalyst. It is now ready for use.

Most charcoals are not suitable for this purpose, although other brands than the one mentioned can be employed. It is important that the charcoal possess a large percentage of fractures with a high metallic luster. The finished catalyst will appear to be brightly metallic.

[23] The deuterium was obtained from the Stuart Oxygen Company on allocation by the U. S. AEC. The mass spectrometer analysis was obtained through the courtesy of Mr. A. G. Sharkey and Dr. R. A. Friedel, U. S. Bureau of Mines Bruceton, Pennsylvania.

[24] The authors are indebted to Dr. N. D. Coggeshall of the Gulf Research and Development Laboratory, Harmarville, Pennsylvania, for placing facilities for the LiF work at our disposal.

[25] These measurements were made by the Radiometry Section of the National Bureau of Standards through the courtesy of Dr. C. J. Humphreys and Dr. E. K. Plyler.

[26] Harrison, Lord, and Loofbourow, *Practical Spectroscopy* (Prentice-Hall, Inc., New York, 1948), p. 515.

[27] R. F. Stamm, Ind. Eng. Chem., Anal. Ed. **17**, 318 (1945).

[28] B. L. Crawford, Jr. and W. Horwitz, J. Chem. Phys. **15**, 268 (1947).

Crawford and Horwitz.[28] The high background on most of the plates made it difficult to get accurate numerical results, but there is seldom any doubt concerning whether a line is polarized or depolarized.

Sample size was 25 ml for d_0, and 4 ml for d_1 and d_{10}. Exposure times were 1 to 6 hr. for the qualitative plates, and 24 hr. for each of the polarization exposures. All the spectra were obtained on Eastman 103*a-J* spectroscopic plates. Mercury 4358A was isolated as the exciting line by using a Wratten 2*A* filter and 1 cm of 0.005 percent aqueous solution of Dupont Rhodamine 5 *GDN* Extra. One spectrum of each compound was also taken using both Hg 4047 and Hg 4358 excitation in order to test the effectiveness of the Wratten 2*A* filter. None of the Raman lines due to 4047 appeared on plates when the Wratten 2*A* filter was employed.

RESULTS

The infra-red spectra of the three samples in the vapor phase are shown in Figs. 2a and 2b, and in the liquid phase in Figs. 3a and 3b. Table I lists the frequencies. Intensities are estimated on a scale of 0 to 10, with the pressure and cell length taken into account. The frequencies for d_0 are in reasonably good agreement with those reported by the Shell Development Corporation for the vapor,[11] and by the National Bureau of Standards for the liquid.[12] Because the infra-red spectrum of d_{10} in the region near 2900 cm^{-1} still showed evidence of hydrogen in the sample, bands appearing above 2500 cm^{-1} are not listed. A sample of the liquid was removed from the exchange apparatus before completion of the exchange and its spectrum was measured on the Perkin-Elmer spectrometer with the

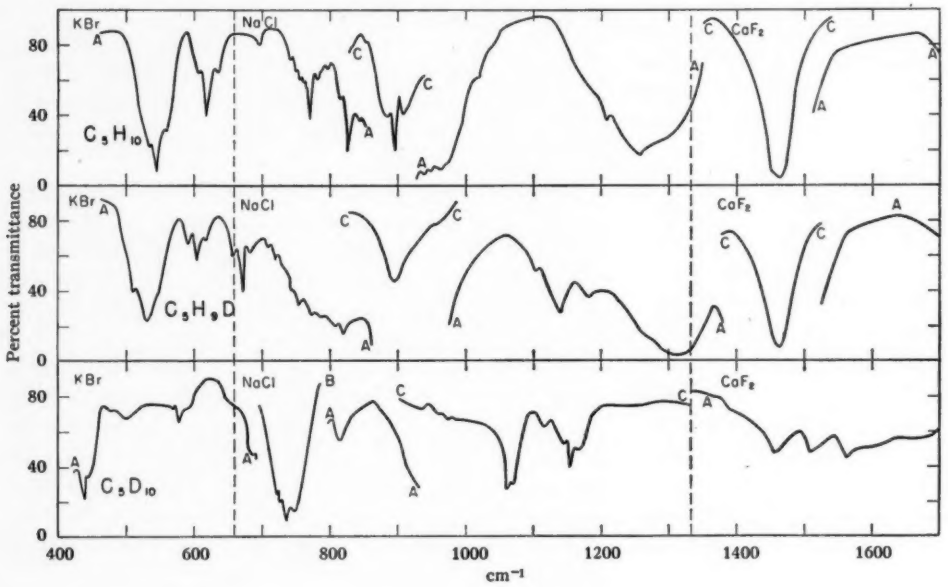

FIG. 2a. Infra-red spectra (vapor state). *A* = 100-cm cell, 220-mm pressure. *B* = 100-cm cell, 50-mm pressure. *C* = 10-cm cell, 220-mm pressure. *D* = 10-cm cell, 100-mm pressure. *E* = 10-cm cell, 25-mm pressure. *F* = 10-cm cell, 15-mm pressure. *G* = 10-cm cell, 5-mm pressure.

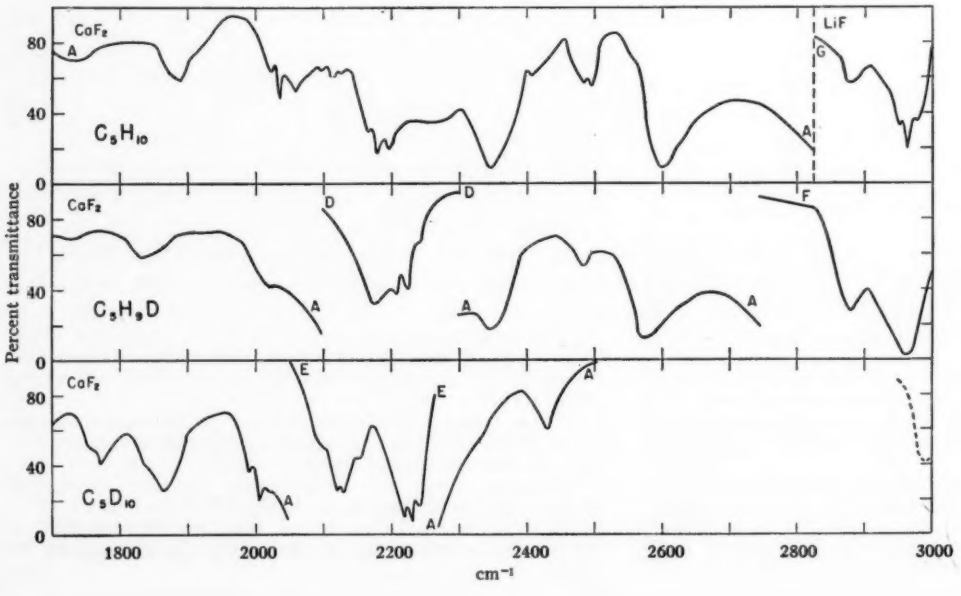

FIG. 2b. Infra-red spectra (vapor state) (continued).

KBr, NaCl, and CaF_2 prisms under the same conditions with which the final sample was measured. All bands that diminished in intensity were attributed to a molecular species containing hydrogen. All such bands were in the region above 2500 cm^{-1}.

Table II gives the best values for the Raman displacements of the three compounds. Each value is an average from several plates chosen for low background and high line intensity. The Raman lines in many cases are broad and diffuse, and the centers of the lines are difficult to determine. This is particularly true of the 1207-cm^{-1} line of d_0. The low frequency lines 283, 281, and 270 in the three compounds are of very low intensity and are obscured by grating ghosts of the exciting line Hg 4358. The frequencies, and even the existence, of these lines on our plates are open to question. There was no evidence of hydrogen in any of the Raman plates of d_{10}. Table II also compares the Raman spectrum of d_0 obtained in this work with three previous spectra of high quality. The agreement is satisfactory.

INTERPRETATION OF RESULTS

A. General Remarks

Four point groups must be considered as possibilities for cyclopentane: D_{5h}, C_2, C_s, and C_1. Table III gives the symmetry properties, number of normal vibrations, and selection rules for D_{5h} symmetry according to the conventions of Herzberg.[29] It can be seen that three

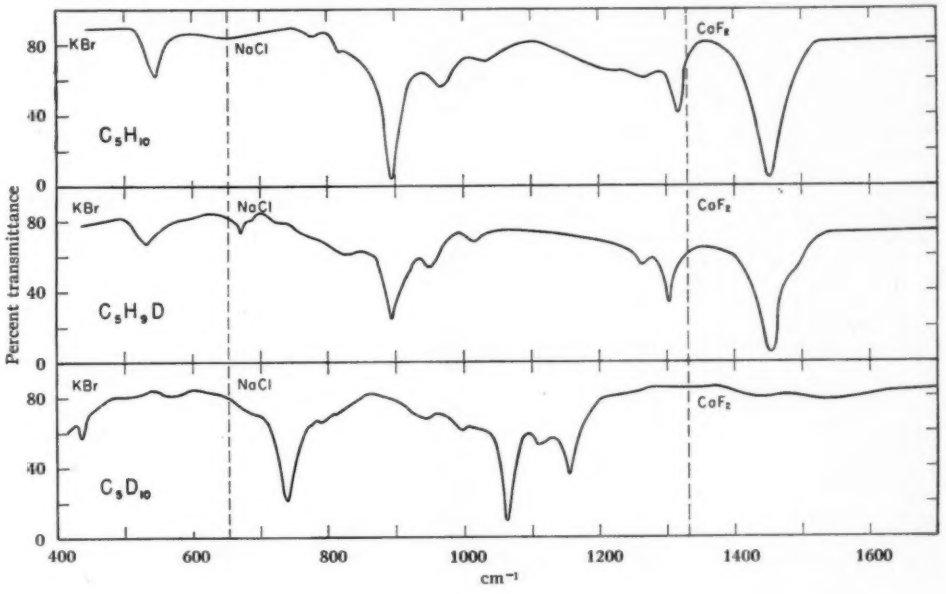

FIG. 3a. Infra-red spectra (liquid state). Cell = 0.08 mm.

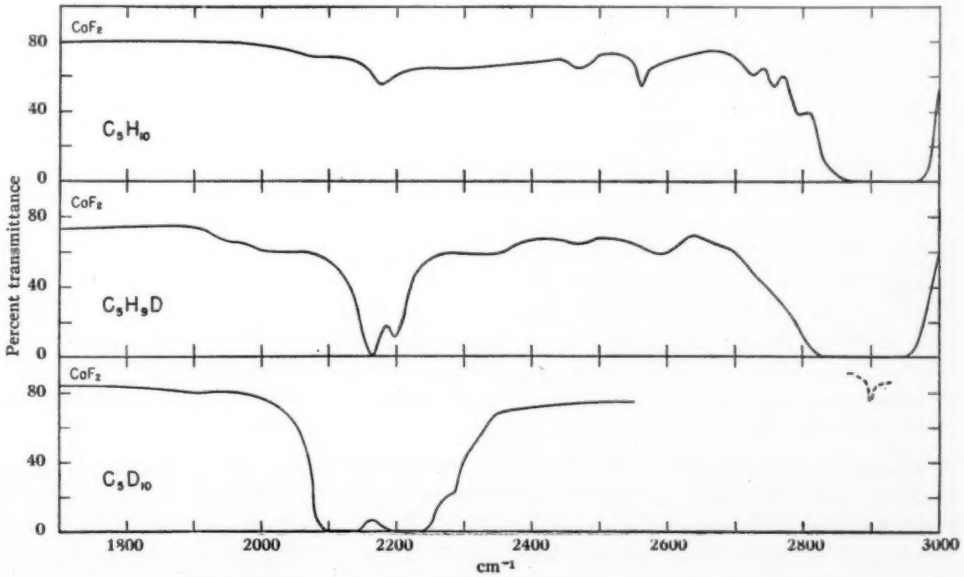

FIG. 3b. Infra-red spectra (liquid state) (continued).

[29] G. Herzberg, *Infrared and Raman Spectra of Polyatomic Molecules* (D. Van Nostrand Company, Inc., New York, 1945), pp. 117, 138, 253.

TABLE I. The infra-red spectra of the cyclopentanes.

Cyclopentane					Cyclopentane-d_1				Cyclopentane-d_{10}			
Vapor			Liquid		Vapor		Liquid		Vapor			Liquid
cm^{-1}	I	Type	cm^{-1}	I	cm^{-1}	I	cm^{-1}	I	cm^{-1}	I	Type	cm^{-1} I
535 P					511 P							
545 Q	3	?	546	3	533 Q	3	535	3	P obscured			
558 R					R obscured				438 Q	2	$\perp$(?)	438 1
602 P					590 P				446 R			
617 Q	2	∥			604 Q	1			502	0		
631 R					616 R				567 P			
697	0				659 P				578 Q	0	∥	572 0
748	0				671 Q	2	672	2	590 R			
740 P					683 R				686	0		
753 Q	0	?			708 P				722	1		
764 R					720 Q	0			728 P			
759 P					730 R				737 Q	6	$\perp$(?)	738 6
770 Q	1	$\perp$(?)	776	0	743	0			748 R			
779 R					753	0			—			791 0
					773	0			814	1		
796	0				788	0			935	0		943 1
									974	0		
812 P					808 P				—			997 1
827 Q	1	∥	817	1	820 Q	1			1061	6	?	
843 R					R obscured				1070			1064 6
882 P					895	5	895	5	1119	1		1111 1
896 Q	8	∥	896	8	949	1	951	2	1146 P			
909 R					—		1018	1	1156 Q	6	$\perp$	1155 3
					1107	0			1165 R			
937 P					1140	2						
949 Q	3	?			1180	0						
962 R					—		1264	1	1315	0		
—			964	3	1315	3	1308	4	1458	1		
1020	0											
—			1033	1	1462	6	1454	8	1510	1		
1206	0				1727	0			1562	1		
1258	3 v.b.		1264	3 v.b.	1867	1			1772	2		
—			1316	4	2021	1			1867	2		
1462	9		1456	9								
1739	0				2172	7	2166	9	1990 P			
1884	0				2210	7	2199	8	2005 Q	2	∥(?)	
2021	0				2228	7			2021 R			
2036 ?	1				2346	3			2099	5		
2060	1				2481	1	2468	0	2119	9	?	2125 10
2095 P					2597	3	2579	1	2130			
2114 Q	0	∥			2878	9	2870	10	2155	5		
2128 R					2962	10	2950	10	2203	0		
2169 P					3191	3			2219 P			
2181 Q	1	?	2175	1	3488	3	3452	2	2230 Q	10	?	2220 10
2194 R									2239 R			
									—			2283 2
2346	1								2428	2		
2405	0								~3000	5	(C−H)	~2900 2
2481	1											
2492												
—			2585	1								
2610	2											
—			2725	1								
—			2753	1								
—			2793	2								
2876	9		2890	10								
2953 P												
2965 Q	10		2960	10								
2977 R												
3196	0											
—			3202	0								
3476	1		3481	1								

Note.—v.b. = very broad.

Raman lines are polarized, six fundamentals are totally inactive, and that there are no coincidences between Raman-active and infra-red-active vibrations. On the other hand the three lower symmetries allow all thirty-nine of the fundamentals to be active in both the infra-red and Raman spectrum, and twenty or more Raman lines are polarized. Thus the results expected for a planar ring are markedly different from those for a non-planar ring. This is indicated in greater detail in Table IV for the fundamentals below 1600 cm^{-1}. It is evident that one may reasonably expect to be able to determine whether or not the molecule has D_{5h} sym-

TABLE II. The Raman spectrum of the cyclopentanes (including a comparison with earlier work).

Cyclopentane											Cyclopentane-d_1			Cyclopentane-d_{10}		
K. and S.[a]		Reitz[b]			R. and J.[d]			Present work								
cm^{-1}	I	cm^{-1}	I	ρ	cm^{-1}	I	ρ	cm^{-1}	I	ρ^f	cm^{-1}	I	ρ^f	cm^{-1}	I	ρ^f
165	0 ?	—	—	—	—	—	—	—	—	—	281?	0	—	270?	0	—
—	—	—	—	—	207	0	—	—	—	—	884	8	0.43	778	1	0.88
285	1 b.	285	1 b.	—	288	1	—	283(?)	0	—	1028	4 b.	0.92	802	9	0.49
589	00	—	—	—	—	—	—	—	—	—	1194	2 v.b.	—	937	5 b.	0.93
—	—	—	—	—	712	0	—	—	—	—	1280	2 b.	—	1021	1	—
886	9	886	9	0.08	888	10	p	886	9	0.25	1451	3 b.	0.91	1064	3 b.	—
973	½	967	0	—	—	—	—	—	—	—	1473	1	—	1124	4 b.	0.60
1028	4 b.	1028	4 b.	1.00	1032	4 b.	dp	1030	5 b.	0.86	2166	2 b.	0.69	2048	2	0.69
1102	1	1102	1	0.90	—	—	—	1104	1	—	2203	1 b.	0.75	2108	8	0.42
1216	1	1216	1	1.00[e]	—	—	—	1207[e]	3 v.b.	—	2868	9	0.46	2130	2	—
1284	2	1283	2 b.	1.04[e]	1298	1	—	1283	2 b.	—	2916	4 b.	—	2151	8	0.42
1446	5	1446	4 b.	0.92	1448	5 b.	dp	1453	4 b.	0.87	2940	9 v.b.	0.68	2214	6 v.b.	0.87
1480	1	1479	½	dp	1482	1 b.	—	1487	1	0.81	2962	9 v.b.	0.59	2304	2	0.73
2866	10	2866	10	0.26[e]	2869	10	p	2868	10	0.30						
2898	4	2898	4	—	2901	4	—	2904	4 b.	0.52						
2941	12 b.	2941	12	0.36	2943	7		2944	10 v.b.	0.46						
2964	10	2964	10		2970	6		2966	9 v.b.	0.43						

Note.—b. = broad; v.b. = very broad.
[a] See reference 4.
[b] See reference 5.
[c] Said by Reitz to be unsatisfactory.
[d] See reference 6.
[e] Exceptionally broad and diffuse. Difficult to locate center.
[f] See section on Spectroscopic Measurements.

metry. On the other hand the choice between C_2, C_s, and C_1 would be very difficult. The number of observed frequencies has been added to Table IV for comparison.

The spectra clearly suggest D_{5h} symmetry except for two features. The first is that fifteen infra-red bands are found below 1600 cm^{-1} for d_0 rather than about four. However, many of these are weak and were observed only in a meter gas cell at 220-mm pressure. Consequently one could hope to explain most of them as combination tones. The second difficulty is the spectrum of d_1. It was expected that if d_0 is D_{5h}, the substitution of one deuterium atom would lower the symmetry to C_s and would permit many more frequencies to be active. This has been found to happen with such molecules as benzene[30,31] and cyclohexane,[32] where the substitution of one deuterium atom approximately doubles the number of observed bands in the Raman spectrum of the liquid or in the infra-red spectrum of the vapor. Cyclopentane-d_1 was therefore prepared with the expectation that it might exhibit an enriched spectrum which would provide some evidence for a high symmetry in the parent molecule. At the same time degenerate frequencies and forbidden fundamentals might be located. Actually, however, the spectrum of d_1 is of about the same complexity as that of d_0 or d_{10}, and the experiment is inconclusive. It seems strange that one deuterium atom can produce a marked effect in cyclohexane, and virtually no effect in cyclopentane. This might be taken as evidence against high symmetry for the latter.

Nevertheless the spectra on the whole strongly indicate D_{5h} symmetry, so the initial effort was to make an assignment on this basis. This assignment must satisfy three criteria: (1) the calculated band envelopes, (2) the product rule, and (3) the measured entropy. The first two of these require a knowledge of the moments of inertia. For this we have used the molecular dimensions of Hassel and Vierwoll,[16] namely a planar ring, an H−C−H angle of 109° 28′, a C−H distance of 1.09A, and a C−C distance of 1.54A. The calculated moments of inertia are given in Table V.

Since a D_{5h} molecule is a symmetric top, the separation of the P and R maxima of the infra-red bands can be determined from the equations of Gerhard and Dennison.[33] The expected $P-R$ separations are included in Table V. The parallel bands will have a very intense Q branch, whereas perpendicular bands will have a less marked one. The exact appearance of the perpendicular bands cannot be predicted from the results of Gerhard and Dennison since this case is intermediate between two of theirs. The theoretical product rule ratios are

TABLE III. Symmetry properties, number of normal vibrations, and selection rules for cyclopentane (D_{5h} symmetry).

	Symmetry properties					No. of normal vibrations	Selection rules	
D_{5h}	C_5	σ_h	C_2	σ_v	T and R		Raman	IR
A_1'	1	1	1	1		3	+(p)	−
A_1''	1	−1	1	−1		1	−	−
A_2'	1	1	−1	−1	R_z	1	−	−
A_2''	1	−1	−1	1	T_z	2	−	+(∥)
E_1'	2 cos72°	2	0	0	T_{xy}	4	−	+(⊥)
E_1''	2 cos72°	−2	0	0	R_{xy}	3	+	−
E_2'	2 cos144°	2	0	0		5	+	−
E_2''	2 cos144°	−2	0	0		4	−	−

[30] A. Langseth and R. C. Lord, Jr., Kgl. Danske Vid. Sels. Math. Fys. Medd. **16**, 6 (1938).
[31] Bailey, Gordon, Hale, Herzfeld, Ingold, and Poole, J. Chem. Soc. **1946**, 299; Herzfeld, Ingold, and Poole, *ibid.* 324.
[32] A. Langseth and B. Bak, J. Chem. Phys. **8**, 410 (1940).
[33] S. L. Gerhard and D. M. Dennison, Phys. Rev. **43**, 197 (1933).

TABLE IV. Number of allowed *vs.* number of observed bands of cyclopentane.

	Theory C_1	C_s	C_2	D_{5h}	Obsv'd freqs.
1. No. of Raman-active fundamentals <1600 cm^{-1}	29	29	29	8	8
2. No. of polarized Raman fundamentals <1600 cm^{-1}	29	15	15	2	1
3. No. of infra-red-active fundamentals <1600 cm^{-1}	29	29	29	4	15
4. No. of Raman-infra-red coincidences <1600 cm^{-1}	29	29	29	0	1

TABLE V. Calculated moments of inertia (in atomic weight units $\times A^2$) and calculated $P-R$ separations for cyclopentane.

	I_x	I_y	I_z	$\Delta\nu(\perp$ bands)	$\Delta\nu(\parallel$ bands)
Cyclopentane	78.5	78.5	141	19–21 cm^{-1}	28 cm^{-1}
Cyclopentane-d_{10}	105	105	179	16–18	24

given later in Table VII. The entropy criterion will also be discussed later.

B. Analysis Based on D_{5h} Symmetry

The results of this section are summarized in Tables VI, VII, and IX. Table VI gives the numbering of the vibrations. The classification of methylene vibrations into deformations, waggings, twistings, and rockings is that defined by Linnett,[34] as modified slightly by Wilson.[35]

1. Raman-Active Species

a. *The totally symmetric vibrations (species A_1').*— The Raman spectrum of d_0 exhibits intense and highly polarized lines at 886 and 2868 cm^{-1} which can be assigned immediately to ν_3 and ν_1 respectively. In d_{10} there are polarized lines at 802, 1124, 2108, and 2151 cm^{-1}. We believe that the latter two, which have nearly the same intensities, are the results of Fermi interaction between 2×1064 (Raman) or 2×1066 (infra-red) and a fundamental very near 2130 cm^{-1}. The missing methylene frequency in d_0 can now be located by applying the product rule. It is calculated to be 1483 cm^{-1}. There is an observed Raman line at 1487 which we take to be this fundamental. Fenske, *et al.*[8] are the only workers who report it to be polarized. This may be due either to the fact that it is overlapped by the more intense depolarized line at 1453 cm^{-1}, or to an inherently high depolarization ratio.

All the assignments are collected in Table VI. The calculated and observed product rule ratios are compared in Table VII.

b. *The degenerate vibrations (species E_1'' and E_2').*— Most of the remaining Raman lines are unusually broad and diffuse. Rosenbaum and Jacobson[6] have suggested that this may be due to a slightly non-planar ring. However Herzberg[36] has pointed out that degenerate Raman frequencies of symmetrical-top molecules may be expected to be broad because the individual Q branches do not quite coincide in frequency.

It is surprising to find that the four Raman lines observed in the C—H stretching region for d_0 are all polarized, because there should be two depolarized fundamentals. There is little doubt that 2868 is the A_1' fundamental. The line at 2904 can be explained as $2\times1453=2906$, and 2966 as $2\times1487=2974$. The latter seems too intense not to be also a fundamental, and we believe that there is an accidental coincidence here. This would account for the intensity, the broad appearance, and the partial polarization. The polarization of 2944 is difficult to explain, although it may be due to overlapping with 2966. Its intensity certainly suggests a fundamental.

Considering the E_2' species first, we assign the line 283 in d_0 and 270 in d_{10} to one of the ring frequencies. This seems surprisingly low for an in-plane ring vibration. We feel, however, that it is probably an allowed fundamental frequency. We have been unable to explain it as a combination tone or difference tone. It seems improbable that it is the forbidden E_2'' out-of-plane

[34] J. W. Linnett, J. Chem. Phys. **6**, 695 (1938).
[35] T. P. Wilson, J. Chem. Phys. **11**, 369 (1943).

TABLE VI. Assignment of fundamentals on the basis of D_{5h} symmetry.

Species	Sel. rules	Description	Notation	Cyclopentane	Cyclopentane-d_{10}
A_1'	R	C—H stretching	1	2868 cm^{-1}	2130 cm^{-1}*
		CH_2 deformation	2	1487	1124
		in-plane ring	3	886	802
A_1''	F	CH_2 twisting	4	—	—
A_2'	F	CH_2 wagging	5	—	—
A_2''	I	C—H stretching	6	2965	2230
		CH_2 rocking	7	(1462)	1066
E_1'	I	C—H stretching	8	2876	2125
		CH_2 deformation	9	(1462)	1156
		CH_2 wagging	10	896	737
		in-plane ring	11	545	438
E_1''	R	C—H stretching	12	2966	2214
		CH_2 twisting	13	1207	[965±7]
		CH_2 rocking	14	1104	778
E_2'	R	C—H stretching	15	2944	2130
		CH_2 deformation	16	1453	1064
		CH_2 wagging	17	1283	1021
		in-plane ring	18	1030	937
		in-plane ring	19	283	270
E_2''	F	C—H stretching	20	—	—
		CH_2 twisting	21	—	—
		CH_2 rocking	22	—	—
		out-of-plane ring	23	—	—

R—Raman active
I—Infra-red active
F—Forbidden
[ ]—Calculated or estimated. Has not been observed experimentally.
( )—Used twice.
* —Inferred from resonance pair 2108–2151.

TABLE VII. Product rule ratios for D_{5h}.

	A_1'	A_1''	A_2'	A_2''	E_1'	E_1''	E_2'	E_2''
τ_{theor}	2.00	1.41	1.26	1.87	2.64	2.44	2.83	2.83
τ_{corr}	1.96	1.39	1.25	1.83	2.56	2.37	2.74	2.74
τ_{obs}	1.97	—	—	1.82	2.59	—	2.73	—

[36] See reference 29, p. 444.

ring vibration because it has been reported in almost every Raman study, even at moderate exposures. Considering how feeble the allowed Raman lines are, it does not seem likely that a forbidden line would be so universally found. We therefore assign 283 to one of the E_2' ring modes. The other ring vibration in d_0 is taken as 1030 because this is the lowest unassigned frequency. Since a ring vibration is expected to be about 10 percent lower in the heavy molecule, 937 is chosen as its counterpart in d_{10}. There is no doubt that the methylene deformation is 1453 in d_0 and 1064 in d_{10}. This leaves Raman frequencies at 1104, 1207, and 1283 in d_0 and at 778 and 1021 in d_{10} to be assigned to the remaining three methylene vibrations of species E_1'' and E_2'. The 778 frequency presumably has a counterpart in d_0; it can be only 1104 because either of the other two values requires a shift much larger than 2%. Furthermore the 1104–778 pair cannot belong to E_2' because there is no combination of observed C—H and C—D stretching frequencies which will satisfy the product rule. We therefore place it in E_1''. There is now only a limited number of combinations for the remaining assignments. With the help of the product rule it is readily found that two satisfactory alternatives are: (1) 1283 and 1021 belong to E_2', and 1207 and a calculated 965±7 belong to E_1'', or (2) vice versa. We find no evidence for the 965 frequency beyond this product rule calculation. The first alternative seems more probable, because the second requires fundamentals for d_{10} at 937 and 965 in species E_2'. It is unlikely that two fundamental frequencies of a highly symmetrical molecule will be this close together when they are in the same species. Therefore the first assignment is given in Table VI.

This completes the assignment of the Raman-active fundamentals. A few left-over lines are explained as overtones in Table IX.

2. *Infra-Red-Active Species*

There are 6 infra-red-active fundamentals. Far more than 6 bands were observed, but on the basis of intensity and the expected positions those at 2965, 2876, 1462, 1258, 896, and 545 are probably fundamentals for d_0. In d_{10} the bands at 2230, 2125, 1156, 1066, 737, and 438 suggest themselves as fundamentals.

The 2 parallel bands of A_2'', with their wide $P-R$ separation and their strong Q branch, should be readily apparent. The bands at 896 in d_0 and at 737 in d_{10} are obvious choices. This leaves 1462, 1258, and 545 for three of the E_1' vibrations of d_0, and 1156, 1066, and 438 for d_{10}, with the C—H and C—D frequencies still to be chosen. Unfortunately these assignments lead to serious disagreement between theoretical and observed product rule ratios for both species, regardless of what combination of the observed C—H and C—D stretching frequencies is used. This seems to be a real difficulty with the assumption of D_{5h} symmetry. If any of the observed bands are parallel fundamentals, they would appear to be 896 in d_0 and 737 in d_{10}. These are among the most intense bands in their respective spectra, their $P-R$ separations are correct, and the Q branch (at least in 896) is very prominent. There is an additional reason for assigning 896 to the A_2'' methylene rocking mode; namely that the analogous frequency in cyclopropane has been assigned to 872,[34] and in cyclobutane to 902.[35] One might therefore abandon the 737 frequency and see if any other combination will satisfy the product rule. It is found that 2965 and 896 in d_0, and 2130 and 686 in d_{10}, give a good fit. This raises two more problems, however. Why does the intense 896 band of d_0 become the weak 686 of d_{10}? How should one now explain the intense 737 band of d_{10}?

At this point we note that the 2 strong bands in d_{10} at 1065 and 1156 have completely different contours, suggesting that they belong to different species. Since there are only 2 infra-red-active species, one band must be in A_2'' and the other in E_1'. Furthermore their intensity is strong indication that they are fundamentals. If then one of these is the A_2'' methylene rocking of d_{10}, it must be somewhere near 1460 cm^{-1} in d_0. The assignment of 2965 and 1462 to the A_2'' modes of d_0, and 2230 and 1066 to d_{10}, gives excellent agreement with the product rule. Similarly in E_1' the assignment of 2876, 1462, 896, and 545 as fundamentals in d_0, and 2125, 1156, 737, and 438 as fundamentals in d_{10} gives good agreement. Thus 1462 of d_0 is assumed to be accidentally degenerate, and to split to give 1065 and 1156 on going to d_{10}.

We have now used the strongest infra-red bands of both molecules to give an assignment that fits the product rule, but at the following cost.

1. The assignment of 1462 to a CH_2 rocking frequency and of 896 to a wagging mode is in disagreement with the assignments for cyclopropane and cyclobutane. This may not be a serious objection, for these latter two analyses have never been put to the test of satisfying the product rule. Had we not had the spectrum of cyclopentane-d_{10} available so that the product rule could be applied, we certainly would also have assigned the A_2'' rocking to 896. Furthermore in ethylene oxide, which is isoelectronic with cyclopropane, the analogous rocking mode is assigned to 1379 cm^{-1} (although somewhat dubiously).[37,37a]

2. Band contours are ignored. The most likely parallel band, 896 of d_0, is placed in the species having perpendicular bands. In brief, the assignment which fits the criterion of band contours does not fit the product rule, and vice versa. Thus doubt is cast on the original assumption of D_{5h} symmetry. Conversely, there is some doubt as to how rigorous the band contour criterion is. Rasmussen, in a study of the infra-red spectrum of

[37] See reference 29, pp. 341, 351.

[37a] *Note added in proof:* Professor R. C. Lord has recently completed a study of light and heavy cyclopropane. He has kindly informed us that the A_2'' methylene wagging frequency occurs at 854 and 614 cm^{-1} respectively in these two molecules. It is unexpectedly weak in both cases.

TABLE VIII. Estimation of the E_2'' out-of-plane ring frequency.

	260°K	298.16°K
$S_{trans}+S_{rotn}$ ($\sigma=1$)	62.73 e.u.	63.82 e.u.
S_{vibn} (minus out-of-plane ring vibn.)	4.11	5.42
$-R\ln\sigma$, with $\sigma=10$.	−4.57	−4.57
S_{calc} (minus ν_{23})	62.27	64.67
$S_{measured}$	67.60	70.06
Difference	5.33	5.39
Approximate value for out-of-plane ring vibn.	130 cm^{-1}	150 cm^{-1}

cyclohexane,[38] found that the contour of one of the five bands he observed below 1500 cm^{-1} was completely different from that predicted.

We feel that the product rule is the more rigorous of the two criteria, so we shall adopt the second assignment of the infra-red bands and proceed with the analysis to see what further evidence can be obtained for or against D_{5h} symmetry.

3. *Totally Inactive Species*

There are 6 totally inactive vibrations for D_{5h} symmetry. It is possible that some of these may appear in the infra-red spectrum of the liquid. Actually there are bands at 1316, 1033, and 964 in the infra-red spectrum of liquid d_0, and at 997 and 791 in d_{10} that have no clear counterparts in the vapor spectra. The 1033 band may be due to the 1030 Raman-active vibration in d_0. The remaining four bands are probably forbidden fundamentals, but we are unable to make specific assignments. It may be noted that the 964 frequency has also been reported in three earlier Raman studies.[4,5,7]

This completes the assignment as far as we are able to deduce it from the spectra. The results are collected in Table VI. Table VII compares the theoretical and the observed product rule ratios. This table also contains a "corrected" value of τ, in which an empirical anharmonicity correction of one percent for each hydrogen bending and stretching mode in the species has been subtracted from the theoretical product rule ratio.

4. *Estimation of the E_2'' Out-of-Plane Ring Vibration (ν_{23})*

A direct comparison of the entropy calculated statistically with that obtained from calorimetric measurements cannot be made because the vibrational assignment is incomplete. In particular the E_2'' out-of-plane ring vibration, which is probably the lowest of all the fundamentals, is missing. However one can use the measured entropy to estimate this low frequency. One can then examine the spectrum to see if there is any evidence for such a frequency in the form of an allowed combination or difference tone.

The entropy of d_0 has been measured by Aston, Fink, and Schumann[17] and by Douslin and Huffman.[39] Kilpatrick, Pitzer, and Spitzer[1] have discussed these results critically and have introduced a small correction. We shall use their values.

The calculations are summarized in Table VIII. The assignments of Table VI have been used, plus the following estimated frequencies (and degeneracies) for the inactive fundamentals: 1316(2), 964(2), 2950(2), 1000(1), 1200(1). Although these frequencies are only guesses, they make such a small contribution to the entropy at the two temperatures employed that very little error is introduced. The formulas used to calculate the entropy of translation and rotation may be found in Herzberg.[40] The vibrational entropy was compiled from the tables in Taylor and Glasstone.[41]

It is seen that the out-of-plane ring frequency would have to be about 140±20 cm^{-1} to make our assignment consistent with the measured entropy. Presumably in d_{10} it would be somewhere in the range 125±20 cm^{-1}. The only prior experimental evidence supporting these values is the very faint Raman line found in d_0 by Kohlrausch and Seka[4] at 165 cm^{-1}. This line has not been reported by any other investigators, and can be assigned to ν_{23} only in violation of the selection rules.

5. *Assignment of the Left-Over Frequencies*

Table IX gives suggested assignments for the left-over frequencies. It was not possible to explain all of the observed bands, but this is to be expected because: (a) the totally inactive fundamentals are not known, (b) only binary combinations were tried, and (c) some of the weak lines in the d_{10} spectrum may actually be due to d_9.

Frequency ν_{23} can combine only with the E_1'', E_2', or E_2'' fundamentals to give infra-red-active combinations. By assuming that ν_{23} is in the range 100–200 cm^{-1}, one can compare these fundamentals with the left-over bands to see if any consistent indication is given for the value of ν_{23}. Two bands suggest that it is near 155 cm^{-1} in d_0, and 2 more suggest either 155 or 125 cm^{-1} in d_{10}. There are alternative explanations for 2 of these 4 left-over bands. The evidence is thus so slight that these values have not been entered in Tables VI and IX.

6. *Summary of the Spectroscopic Case for D_{5h} Symmetry*

The evidence favoring D_{5h} symmetry is the following. (a) The observed spectrum of d_0 is exceedingly simple, and agrees well with what is expected from the selection rules. There are very few strong bands in either infra-red or Raman spectrum, and very few coincidences between the two. The few coincidences which do occur can be reasonably explained as accidental degeneracies.

[38] R. S. Rasmussen, J. Chem. Phys. **11**, 249 (1943).

[39] D. R. Douslin and H. M. Huffman, J. Am. Chem. Soc. **68**, 173 (1946).

[40] See reference 29, p. 522.

[41] Taylor and Glasstone, *Treatise on Physical Chemistry* (D. Van Nostrand Company, Inc., New York, 1942), Vol. I, p. 654.

The number of polarized Raman lines agrees with expectations. (b) An assignment can be made which fits the product rule quite satisfactorily. (c) Left-over frequencies can be explained rather well, considering the three handicaps enumerated above.

The evidence against D_{5h} symmetry is the following. (a) Either band contours or the product rule has to be ignored in making the assignment. (b) To fit the product rule, the assignment places a methylene rocking frequency at 1462 and a wagging frequency at 896 cm^{-1}. This does not agree with assignments in cyclopropane and cyclobutane. (c) An in-plane ring vibration is assigned to 285 cm^{-1}, which seems surprisingly low. (d) There is no good independent evidence for the out-of-plane ring vibration at 140±20 cm^{-1} which is required to fit the entropy. (e) The selection rule argument favoring D_{5h} is weakened by the fact that: (1) the spectrum of d_1 is not markedly richer in bands than is that of d_0, (2) the Raman spectrum of the isoelectronic tetrahydrofuran is remarkably similar to that of d_0,[42] and (3) the Raman spectra of C_5H_9X, where X is OH, NH_2, CH_3, SH, Cl, Br, or I, are not much more complex than that of d_0 itself.[43] Apparently the effective selection rules are not sensitive to rather severe changes in symmetry. This largely nullifies one of the main arguments for D_{5h} symmetry.

Our tentative conclusion from the spectral evidence is that cyclopentane does not have strict D_{5h} symmetry, although it is certainly close enough so that D_{5h} selection rules hold very well.

C. The Heat Capacity of Solid Cyclopentane

The assignment for the D_{5h} structure postulates a doubly degenerate vibration (ν_{23}) at 140±20 cm^{-1} in order to fit the entropy. Professor R. C. Lord has suggested to us that the heat capacity of the solid might provide definite evidence concerning the reality of this value. This has proved to be the case. The results show that there is no such frequency.

The general method was that developed by Lord,[44] and used by Lord, Ahlberg, and Andrews,[45] and by Brucksch and Ziegler.[46] The basic equation is:

$$C_{v(I)}=C_p-(C_p-C_v)-C_{v(L)}, \qquad (1)$$

where $C_{v(I)}$ = "internal" heat capacity, caused by vibrations within the molecules; and $C_{v(L)}$ = "lattice" heat capacity, caused by translations and rotations of the molecules as units.

TABLE IX. Assignment of left-over frequencies (D_{5h} selection rules).

Cyclopentane				Cyclopentane-d_{10}			
cm^{-1}	I	Assignment	Active species	cm^{-1}	I	Assignment	Active species
		Raman				Raman	
2904	4	$2\nu_{16}=2906$	A_1'	2048	2	$2\nu_{17}=2042$	A_1'
				2304	2	$2\nu_9=2312$	A_1', E_2'
		Infra-red				Infra-red	
617	2(∥)	$\nu_{10}-\nu_{19}=613$	E_1'	502	0	$\nu_{18}-\nu_{11}=499$	E_1'
697	0	—		578	0(∥)	$\nu_{13}-\nu_{11}=583$	A_2''
748	0	$\nu_{18}-\nu_{19}=747$	E_1'	686	0	$\nu_3-\nu_{11}=686$	E_1'
753	0	$\nu_{18}-\nu_{19}=747$	E_1'			$\nu_{17}-\nu_{19}=691$	E_1'
770	1(⊥)	$\nu_5-\nu_{11}=771$	E_1'	722	1	—	
796	0	—		814	1	—	
827	1(∥)	$\nu_{11}+\nu_{19}=828$	A_2''	935	0	—	
949	3	$\nu_2-\nu_{11}=942$	E_1'	974	0	—	
1020	0	—		1119	2	—	
1206	0	—		1315	0	—	
1258	3	$\nu_{19}+964=1247$	?	1458	1	$\nu_{11}+\nu_{18}=1459$	A_2''
1739	0	$\nu_{16}+\nu_{19}=1736$	E_1'	1510	1	$\nu_{10}+\nu_{14}=1515$	A_2''
1884	0	—		1562	1	$\nu_2+\nu_{11}=1562$	E_1'
2021	0	—		1772	2	—	
2036	1	$\nu_2+\nu_{11}=2032$	E_1'	1867	2	$\nu_3+\nu_7=1868$	A_2''
2060	1	$2\nu_{18}=2060$	E_1'	2005	2	$\nu_6+\nu_{18}=2001$	E_1'
2114	0	—		2099	5	$\nu_9+\nu_{18}=2093$	E_1'
2181	1	$\nu_{10}+\nu_{17}=2179$	E_1'	2155	5	—	
2346	1	$\nu_3+\nu_7=2348$	A_2''	2203	0	$\nu_5+\nu_9=2206$	E_1'
		$\nu_3+\nu_9=2348$	E_1'	2428	2	—	
2405	0	$2\nu_{17}=2414$	E_1'				
2486	1	$\nu_9+\nu_{18}=2492$	E_1'				
		$\nu_{16}+\nu_{18}=2483$	E_1'				
2610	2	—					
3196	0	—					
3476	1	—					

$C_{v(I)}$ was first calculated from Eq. (1). For this purpose the observed values of C_p were employed.[17,39] The quantity (C_p-C_v) was determined from the Nernst-Lindemann equation: $C_p-C_v=0.0214C_p^2T/T_{m.p.}$. $C_{v(L)}$ was evaluated from a Debye function with six degrees of freedom in place of the usual three. The characteristic θ was calculated at 15°K from the low temperature form of the Debye equation, $C_v=928(T/\theta)^3$, and was found to be 152°. An alternative value of 155° was obtained by fitting the heat capacity curve between 0°–50°K. The former value was employed because it is free from any suspicion of being empirically adjusted. $C_{v(L)}$ was obtained at various temperatures from the usual tables.

$C_{v(I)}$ was then independently calculated from the vibrational assignments, using Einstein functions. The following frequencies (and their degeneracies) are the only ones which make any appreciable contribution at the temperatures employed: 283(2), 545(2), 886(1), 896(2), ν_{23}(2). No value was included for ν_{23}. The difference between this statistical value of $C_{v(I)}$ and the value calculated from Eq. (1) is the contribution due to ν_{23}.

The results are summarized in Table X. It is seen that a frequency in the range 140–160 cm^{-1} would contribute far too much to the heat capacity to give agreement between the two $C_{v(I)}$'s.

Similar calculations were carried out for chlorine and cyanogen to get some estimate of how accurately $C_{v(I)}$'s calculated by the two methods would agree.[47] Although the agreement in some cases was not as close as might be desired, the errors were such that there is still no doubt that a frequency of 140–160 cm^{-1} in

[42] K. W. F. Kohlrausch and A. W. Reitz, Zeits. f. physik. Chemie **B45**, 249 (1939).

[43] K. W. F. Kohlrausch, "Ramanspektren" *Hand- und Jahrbuch der Chemischen Physik*, Vol. 9, VI (1943). (Reprinted by Edwards Brothers, Inc., Ann. Arbor, Michigan), p. 331.

[44] R. C. Lord, J. Chem. Phys. **9**, 693 (1941).

[45] Lord, Ahlberg, and Andrews, J. Chem. Phys. **5**, 649 (1937). This paper does for benzene precisely what we shall do for cyclopentane—namely, eliminate the possibility of a low doubly degenerate frequency near 160 cm^{-1}.

[46] W. F. Brucksch, Jr. and W. T. Ziegler, J. Chem. Phys. **10**, 740 (1942).

[47] Data and pertinent references may be found in reference 46.

TABLE X. Vibrational heat capacity of solid cyclopentane.

T(°K)	C_p	(C_p-C_v)	$C_{v(L)}$	$C_{v(I)}$ Eq. (1)	$C_{v(I)}$ Statis.*	Diff.	Contrib'n. if ν_{23} were 140 cm^{-1}	Contrib'n. if ν_{23} were 160 cm^{-1}
50°	8.55	0.44	7.82	0.29	0.08	0.21	1.20	0.86
100	14.40	2.46	10.64	1.30	1.26	0.04	2.86	2.60
140	21.60	7.76	11.24	2.60	2.57	0.03	3.36	3.20

* Contribution of ν_{23} not included.

cyclopentane is completely incompatible with the heat capacity.

Thus the assumption of D_{5h} symmetry leads to an insurmountable dilemma. On the one hand the entropy of the vapor at room temperature demands the existence of a very low fundamental. No revision of the D_{5h} assignments can alter this fact. On the other hand the existence of such a fundamental is definitely incompatible with the heat capacity of the crystal. The only possible conclusion is that cyclopentane cannot have D_{5h} symmetry.

D. Consideration of Lower Symmetries

The other possible symmetries for cyclopentane—C_s, C_2, C_1—allow all 39 fundamentals to appear in both the infra-red and Raman spectra. The observed spectra cannot in any case be made to fit this. Kilpatrick, Pitzer, and Spitzer[1] have pointed out that if the warping of the ring away from D_{5h} symmetry is small, the hydrogen vibrations will be virtually unaffected. Their degeneracies will not be split, and they will follow the selection rules for D_{5h} fairly closely. For the ring vibrations, however, the effective symmetry is probably so low that the degeneracies are removed, and there are no forbidden fundamentals.

Table XI gives a suggested assignment for cyclopentane and cyclopentane-d_{10} based on these assumptions. The hydrogen assignments are the same as for D_{5h} except that the methylene rocking formerly put at 1492 has been changed to 896, and the methylene wagging formerly at 896 has been made 1258. Also hydrogen frequencies which are totally forbidden for D_{5h} have been assigned to weak observed bands. The ring vibrations are quite different from the D_{5h} assignments. One component of the out-of-plane mode is assigned to 285 cm^{-1}; the other component will be located with the help of the entropy. The 545 band has been split into 545 and 617. The Raman-active in-plane ring vibration ν_{19} is taken to be 769 and 827, and the 1030 band has been split into 1030 and 949.

In brief, all the observed frequencies for cyclopentane below 1500 cm^{-1} with the exceptions of 697 and 1206 are assigned to fundamental vibrations. Certain of the assignments should doubtless be interchanged, but these permutations will have no effect on the calculated entropy because all the low frequencies are taken to be singly degenerate.

The value of ν_{23b} is now estimated by comparing the measured entropy at 298°K with the entropy calculated from 38 of the 39 frequencies. The difference indicates that ν_{23b} is about 215 cm^{-1}. The only observed frequency near this value is a very faint Raman line at 207 cm^{-1} reported by Rosenbaum and Jacobson.[6] We cannot confirm this value because it is in a region where the Rowland ghosts from our grating are too intense. Nevertheless this will be taken as the value of ν_{23b}.

The assignments of Table XI provide the following calculated values for some of the thermodynamic properties.

1. Entropy of the vapor

	260°K	298°K
S_{spectros}	67.46 e.u.	70.14 e.u.
$S_{\text{calorimetric}}$	67.60	70.06
Diff.	−0.14	+0.08

The experimental error in the calorimetric value is about ±0.10 e.u. Considering that many liquid phase frequencies were used in calculating the entropy, and also that moments of inertia for a D_{5h} structure were employed, the agreement is reasonable.

2. Heat capacity of the solid

	50°K	100°K	140°K
C_p(calc.)	8.48 e.u.	14.74	21.90
C_p(obs.)	8.55	14.40	21.60
Diff.	−0.07	+0.34	+0.30

This is within the accuracy of the calculations.

3. Heat capacity of the gas

	353°K	539°K
C_p(calc.)	25.13 e.u.	39.46
C_p(obs.)	24.42	38.3
Diff.	0.71	1.2

These differences are rather large, but this is not unexpected. The assignments of the moderately high frequencies are critical, since they make large contributions to C_p at these temperatures. It is quite possible that there may be errors in some of these assignments. Furthermore anharmonicity is assuming importance. This would cause the observed C_p to be lower than the calculated value, which is found to be the case. It may be noted that the assignments of the very low frequencies are not critical, because the contribution of the low frequencies is approaching the classical value. Consequently the heat capacity of the gas at these temperatures is rather insensitive to the particular choice of ν_{23b}.

The assignments of Table XI thus fit the observed data moderately well. It is interesting to compare them with those of Kilpatrick, Pitzer, and Spitzer.[1] The agreement is not very good for the hydrogen vibrations, because these authors give only average values for groups of hydrogen frequencies. The agreement for the ring vibrations is excellent except for ν_{23}. Kilpatrick,

Pitzer, and Spitzer picture the out-of-plane ring vibration ν_{23} of D_{5h} as splitting into two parts in the puckered molecule: a vibration in which the nuclei move perpendicularly to the (hypothetical) σ_h plane, and a pseudo rotation in which the position of maximum displacement rotates slowly around the ring. This latter mode does not possess an angular momentum because any given atom moves only perpendicularly to the plane. Nevertheless it can be regarded as a kind of free rotation because the potential energy associated with this motion is zero (see their Eqs. (4) and (5)). A plane rotator energy expression is used to evaluate the contribution of this mode to the partition function.

In effect, Kilpatrick, Pitzer, and Spitzer propose that only 38 of the 39 vibrational modes are genuine vibrations, and that the remaining one is a free rotation. In this paper, all 39 have been assumed to be genuine vibrations, and a spectroscopically-observed frequency has been assigned to each. It does not seem possible to decide at this time which alternative is correct. One would have to decide in favor of the second one if the existence of ν_{23b} in the spectrum could be proved. We hope to investigate this possibility.

The conclusions of this paper may be summarized as follows.

1. Cyclopentane definitely does not have D_{5h} symmetry.
2. Its exact symmetry and geometry are not known.
3. It is not necessary to adopt Kilpatrick, Pitzer, and Spitzer's model of a puckered ring with a pseudo rotation in order to interpret the data.

COMPARISON WITH PERFLUOROCYCLOPENTANE

It may be of interest to mention the results for perfluorocyclopentane, C_5F_{10}, for comparison. One would expect this molecule to have a greater tendency to be non-planar than cyclopentane, because repulsions between fluorine atoms on neighboring carbons are probably greater than between hydrogen atoms. This is borne out experimentally. Electron diffraction results indicate that C_5F_{10} does not have D_{5h} symmetry.[48] This is confirmed by the vibrational spectrum. In contrast to the case of cyclopentane, the effective selection rules are certainly not those for D_{5h} symmetry. The Raman spectrum has approximately twice as many lines below 1400 cm^{-1} as does cyclopentane, and there are eight coincidences between the infra-red and Raman spectra in this range.[49]

[48] Bastiansen, Hassel, and Lund, Acta Chem. Scand. **3**, 297 (1949).

TABLE XI. Assignment of fundamental frequencies for a non-planar ring.

Mode of vibration	D_{5h} notation	C_5H_{10}	C_5D_{10}
C—H stretching	1	2868	2130
	6	2965	2230
	8a, 8b	2876	2125
	12a, 12b	2966	2214
	15a, 15b	2944	2130
	20a, 20b	[~2900]	[~2150]
CH_2 deformation	2	1487	1124
	9a, 9b	1462	1156
	16a, 16b	1453	1064
CH_2 wagging	5	1316	[1060]
	10a, 10b	1258	1065
	17a, 17b	1283	1021
CH_2 twisting	4	1306	943
	13a, 13b	1207	[965]
	21a, 21b	1033	791
CH_2 rocking	7	896	737
	14a, 14b	1104	778
	23a, 23b	964	[710]
Ring	3	886	802
	11a	545	438
	11b	617	502
	18a	1030	937
	18b	949	814
	19a	827	728
	19b	769	687
	23a	283	270
	23b	207	?

[ ] Estimated.

ACKNOWLEDGMENTS

One of us (R.G.I.) wishes to express his appreciation to Dr. H. P. Klug and to the Directors of Mellon Institute for placing facilities for the experimental work at his disposal.

[49] Dr. Don C. Smith of the Naval Research Laboratory very kindly furnished these spectra in advance of publication. They are now available in Naval Res. Lab. Report 3567, pp. 85, 128–129. The infra-red spectrum is also available as A.P.I. curves 992 and 993. (Reference 11.)

The Quenching of Mercury Resonance Radiation. I. The Effective Cross Sections of Paraffin Hydrocarbons*

B. DEB. DARWENT
Division of Chemistry, National Research Laboratories Ottawa, Canada
(Received June 19, 1950)

The effective cross sections of the paraffin hydrocarbons from ethane to *n*-heptane in quenching mercury resonance radiation (λ2537) have been measured by the technique of Zemansky. The effective cross section of ethane is much smaller than the value previously found by Bates. Neopentane is reasonably efficient in quenching λ2537 although it is not decomposed readily by $Hg(^3P_1)$ atoms. Increase in molecular weight and, up to a point, in branching of the carbon skeleton are accompanied by increases in the effective cross section. The quenching efficiency of the paraffins depends on the number and type of C—H bonds in the molecule and is not primarily a function of the number of carbon atoms or C—C bonds. The effective quenching diameters of the C—H bonds are: primary 0.05 to 0.10A, secondary 0.50 to 0.65A, and tertiary 1.3A; the actual values depending to some extent on the nature of the rest of the molecule. The number of collisions necessary for quenching to occur on primary, secondary, and tertiary C—H bonds is, therefore, approximately 3000, 30, and 5, respectively.

I. INTRODUCTION

THE effective cross sections (σ_Q^2) of a variety of widely differing compounds in quenching mercury resonance radiation have been measured (see for example Zemansky)[1] and Bates[2] has reported the values of σ_Q^2 for a number of paraffin hydrocarbons. However at the time that Bates' measurements were made it was not possible to obtain such pure samples of paraffin hydrocarbons as are now available, and contamination by quite small traces of olefins would have introduced serious errors. It is therefore of interest to measure again some of the values obtained by Bates, using the purest available samples, and to extend the measurements to obtain more information about the effect of molecular weight and branching of the carbon chain on the quenching cross sections.

The Measurement of Quenching Cross Sections

The quenching cross section of a volatile compound is obtained from the gas kinetic and Stern-Volmer equations by determining the effect of pressure on the intensity of fluorescent resonance radiation. Effective cross sections were originally determined by measuring the intensity of resonance radiation emitted at angles of either 45° or 90° to the incident beam of exciting radiation. Zemansky[1] has criticized those experiments, since the measured value may be considerably in error because of "imprisonment" of the radiation, and has devised a technique which fulfills the requirements of Milne's theory of diffusion of resonance radiation. In Zemansky's method the effect of pressure on the intensity of resonance radiation emitted from the back face of a thin slab of gas is measured. From a knowledge of the geometry of the cell, temperature, concentration of the absorbing species and the breadths of the incident and absorption lines he was able to calculate a relationship between Q, the extent of quenching and τZ_Q, the number of collisions per lifetime of the excited atom. Since τ the average life of $Hg(^3P_1)$ atoms is known, he was able to evaluate Z_Q as a function of the pressure of the quenching gas. Hence σ_Q^2 could be calculated by direct substitution into the usual gas kinetic equation. The apparatus and technique used in the present investigation were similar to those used by Zemansky. However, instead of measuring the relative breadths of the incident and absorption lines and carrying out the lengthy graphical integration, the relationship between Q and τZ_Q was derived in the following way. Q was measured as a function of pressure for hydrogen, one of the substances used by Zemansky, and by combining those results with Zemansky's data for the relationship between τZ_Q and pressure, the relationship between τZ_Q and Q was obtained for this apparatus. The result was checked by carrying out a similar operation with oxygen which had also been used by Zemansky.

II. EXPERIMENTAL

(a) Materials

The hydrogen and oxygen used in the preliminary experiments were taken from commercial cylinders. The hydrogen was purified by passage through a hot palladium tube followed by a trap cooled in liquid nitrogen. It was stored in a large flask and samples were taken off through the hot palladium tube and passed through a trap in liquid nitrogen. The oxygen was condensed in a trap cooled by pumped down liquid nitrogen and the stock sample taken from the liquified portion.

The hydrocarbon samples used were the purest available. Since olefins are known to be much more efficient than paraffins in quenching λ2537 it was essential for the samples used to be as free from unsaturated compounds as possible. Ethane was Phillips Petroleum Company's "Research Grade" product; it was stated to be at least 99.9 percent pure and no ethylene or other impurity could be detected by independent analyses with

* Contribution No. 2255 from the National Research Council, Ottawa, Canada.
[1] M. W. Zemansky, Phys. Rev. **36**, 919 (1930).
[2] J. R. Bates, J. Am. Chem. Soc. **52**, 3825 (1930); **54**, 569 (1932).

mass- or infra-red spectrometers.† It is probable that much less than 0.1 percent of ethylene was present as that amount would have been readily detected by the infra-red spectrum.

Propane, *n*-butane, and iso-butane were obtained from the Ohio Chemical Company. They were all at least 99 percent pure and no olefin could be detected in the samples. Neopentane was prepared by a Grignard Reaction and purified by exhaustive photo-sensitization.[3] The sample used was 99.8 percent pure, the principal impurity being 2,2-dimethyl butane, and no olefinic hydrocarbons could be detected. The other paraffins were standard samples obtained from the National Bureau of Standards, Washington; details of the purity of these samples are given below:

Paraffin	N.B.S. sample no.	Impurity (mole %)
n-pentane	201−*a*−5	0.15±0.07
iso-pentane	202−*a*−8*s*	0.09±0.06
n-hexane	205−5	0.24±0.09
2-methyl pentane	204−*a*−8*s*	0.16±0.08
3-methyl pentane	205−*a*−8*s*	0.20±0.15
2:2 dimethyl butane	206−*a*−8*s*	0.10±0.04
2:3 dimethyl butane	207 (*a*)−8*s*	0.11±0.06
n-heptane	216−5	0.10±0.05

(b) Apparatus

The apparatus, shown in Fig. 1, consisted of an exciting source C, two focusing lenses L_1 and L_2, a mercury resonance lamp R, a collimating lens L_3, an adsorption cell D, a movable photoelectric cell P, and slits S. The exciting source C was a low pressure mercury lamp with neon (3 mm) as carrier gas; it was operated at 40°C in a quartz water jacket which removed λ1849. The lamp was run off a Jefferson sign transformer at about 300 v and 100 ma. The resonance lamp R was of the usual horn-shaped quartz "light trap" type provided with polished quartz windows about 8 mm square, sealed perpendicularly to each other at a common edge. It was fitted with a wide side tube that could be maintained at any desired temperature. The lamp was thoroughly baked out and evacuated before a few drops of mercury were distilled into the side tube and the lamp sealed off. The surface of the lamp, except for the two small windows, was painted black and this, together with a suitably placed system of slits S, reduced the scattered light to a negligible fraction of the output of λ2537. The mercury supply to the lamp was maintained at 0°C, which provided a pressure of 1.85×10^{-4} mm Hg. The fluorescent radiation was taken from the second window of the resonance lamp in a direction perpendicular to the exciting beam. This radiation was collimated by lens L_3, and the size of the beam defined by the slits S_2 and S_3. The slit S_2 was provided with a shutter A and a Cellophane window B which could be used to reduce the intensity of the collimated beam by a known fraction. The absorption cell D was constructed from a ring of Pyrex glass 47 mm diameter and 8 mm deep to which two plane polished quartz windows 50 mm diameter and 3 mm thick were attached by means of a thermosetting varnish. A wide tube (20 mm i.d.) was sealed to the Pyrex ring by a short length of 6-mm tubing. A few drops of mercury were placed in the wide side tube which was kept at 20.0°C, thus providing a mercury pressure of 12.0×10^{-4} mm Hg. The absorption cell was attached to the vacuum and manometric system by a flexible glass spiral which permitted the cell to be moved in and out of the light path. The details of construction of the absorption cell and photoelectric cell are shown in Fig. 1. The photoelectric cell consisted of a quartz envelope with a platinum grid and plate sealed in by tungsten leads and quartz-to-Pyrex graded seals. The platinum surfaces were activated by passing a small discharge between the grid and plate in an atmosphere of hydrogen. After repeated activation the photo-cell was evacuated and sealed off. The internal resistance of the photoelectric cell was at least 10^{14} ohms. The output of the photoelectric cell was measured by a d.c. amplifier which was built by Dr. F. P. Lossing of these Laboratories from a design of Professor Thode of McMaster University.[4]

(c) Measurement of Q

The quenching function Q is defined as the ratio of the intensity of scattered (fluorescent) radiation in the presence of the quenching gas to its intensity in the absence of such a gas. In these experiments the intensity of scattered radiation was obtained as the difference in the readings of the photo-cell at the back face of the absorption cell (I_0) and at a distance of 75 mm away from the back face (I_∞). The function Q is given by

$$Q=[I_{0(p)}-I_{\infty(p)}]/[I_{0(v)}-I_{\infty(v)}], \qquad (1)$$

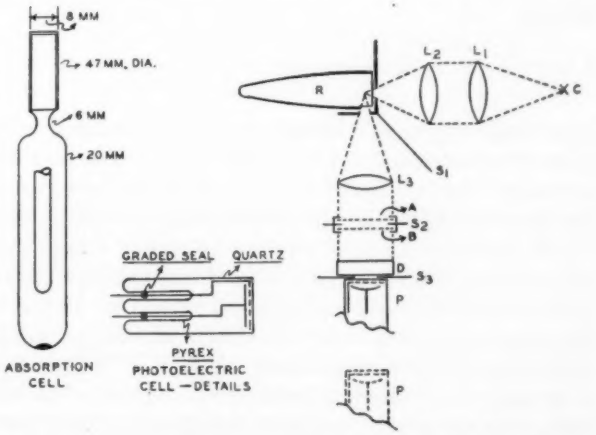

FIG. 1. Apparatus: C—exciting source, L—lens, R—Hg resonance lamp, S—slits, A—shutter, B—Cellophane window, D—absorption cell, P—photoelectric cell.

† We are grateful to Dr. F. L. Mohler, National Bureau of Standards, Washington, and to Dr. J. S. Tapp, Polymer Corporation, Sarnia, Ontario, for the mass spectra and to Dr. D. A. Ramsay of these Laboratories for the infra-red spectra.

[3] B. deB. Darwent and E. W. R. Steacie, J. Am. Chem. Soc. **70**, 2285 (1948).

[4] Graham, Harkness, and Thode, J. Sci. Inst. **24**, 119 (1947).

TABLE I. Relationship between pressure and quenching.

Hydrogen			Oxygen		
p-mm	$1/Q$	τZ_Q	p-mm	$1/Q$	τZ_Q
0.137	1.96	0.151	0.189	1.96	0.129
0.083	1.56	0.091	0.166	1.72	0.113
0.053	1.41	0.058	0.136	1.64	0.093
0.033	1.26	0.036	0.109	1.45	0.075
0.019	1.10	0.021	0.060	1.30	0.041
0.012	1.07	0.013			
0.135	1.92	0.148			
0.105	1.67	0.116			
0.057	1.49	0.063			
0.164	2.13	0.180			
0.142	1.96	0.156			
0.122	1.79	0.134			
0.041	1.32	0.045			
0.025	1.18	0.028			
0.016	1.08	0.018			
0.007	1.04	0.008			
0.155	2.17	0.171			
0.062	1.45	0.068			

where the subscripts in parenthesis (p) and (v) refer respectively to conditions in the presence of a foreign gas and in a vacuum. Since the majority of the experiments were performed at low pressures of the quenching gas, effects such as pressure broadening were negligible. Hence, the absorption coefficient of mercury in the absorption cell may be regarded as independent of the presence or absence of the foreign gas. In Eq. (1) the I_0 terms represent the sum of the intensities of the scattered, fluorescent radiation and the portion of the collimated incident radiation that was not absorbed in its passage through the cell. The I_∞ terms represent the contribution from the unabsorbed collimated radiation to the I_0 values. Since the I_∞ term is independent of the presence or absence of the quenching gas, $I_{\infty(p)}$ may be taken as equal to $I_{\infty(v)}$. This relation was checked experimentally and found to hold. It was also established that the ratio $I_{\infty(v)}/I_{0(v)}$ was constant throughout the course of the investigation. We may therefore write

$$I_{\infty(v)}/I_{0(v)}=\alpha=\text{constant},$$

whence

$$Q=\frac{1}{1-\alpha}\cdot\frac{I_{0(p)}}{I_{0(v)}}-\frac{\alpha}{1-\alpha}.$$

Also under constant conditions $I_{0(v)}$ is a constant function of the intensity of the incident beam. The incident intensity was measured by removing the absorption cell from the light path and interposing a celluloid filter which reduced the intensity to an easily measurable value. It was found that the ratio of $I_{0(v)}$ to the intensity as measured through the celluloid filter (K) increased by about 20 percent over the course of this investigation. However, measurements of $I_{0(v)}/K$ before and after each individual determination showed that the ratio was essentially constant during any one experiment. It was found that moving the photo-cell upset the equilibrium of the circuit and the quenching measurements were made by leaving the photo-cell near the back face of the absorption cell and measuring only $I_{0(p)}$ and by removing the absorption cell from the light path and measuring K the intensity through the celluloid filter. By putting

$$I_{0(v)}/K=B=\text{constant in any one experiment.}$$

We may now write

$$Q=\frac{1}{1-\alpha}\left[\frac{I_{0(p)}}{BK}-\alpha\right].$$

In these experiments α was found to be 0.53 ± 0.01.

III. RESULTS AND DISCUSSION

The data illustrating the connection between pressure and $1/Q$ for hydrogen and oxygen for this apparatus are given in Table I and Fig. 2. It is evident that the relationship may be assumed to be linear within the limits of accuracy of the experiments. The following equations were derived:

$$(1/Q_{H_2}-1)=7.15p_{H_2}, \tag{1a}$$

$$(1/Q_{O_2}-1)=4.50p_{O_2}. \tag{1b}$$

Zemansky[7] has found that

$$\tau Z_{Q(H_2)}=1.10p_{H_2}, \tag{2a}$$

$$\tau Z_{Q(O_2)}=0.683p_{O_2}, \tag{2b}$$

where p represents the pressure of the quenching gas in mm Hg. From Eqs. (1) and (2) we get:

$$\begin{aligned}\tau Z_Q&=0.154(1/Q-1)-\text{for } H_2,\\ &=0.152(1/Q-1)-\text{for } O_2.\end{aligned} \tag{3}$$

The agreement between the results obtained with hydrogen and oxygen is satisfactory, and a value of

$$\tau Z_Q=0.153(1/Q-1) \tag{4}$$

has been adopted. The relationship appears to be certain to within ±5 percent of the value given. The theoretical relation between τZ_Q and $1/Q$ as derived by Zemansky does not lead to the above linear relationship, but the deviation from linearity of Zemansky's calculated values is very small and is within the limits of accuracy of the measurements. Actually Zemansky's experimental data fit a straight line relation between τZ_Q and $(1/Q-1)$ quite closely, and it is probable that

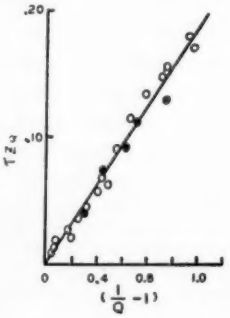

FIG. 2. Calibration of apparatus. Open circles—results obtained with hydrogen. Filled circles—results obtained with oxygen.

TABLE II. Experimental quenching data for paraffin hydrocarbons.

Neopentane			Propane			Ethane			Iso-butane		
p-mm	Q	τZ_Q	p-mm	Q	τZ_Q	p-mm	Q	τZ_Q	p-mm	Q	τZ_Q
3.72	0.44_5	0.192	1.53	0.64	0.080	4.24	0.865	0.016	1.83	0.30	0.385
2.98	0.51	0.148	1.00	0.73	0.053	2.38	0.96	0.005	1.60	0.34	0.298
2.10	0.62	0.094	0.55	0.84	0.027	1.30	1.00	0.000	1.32	0.39	0.238
1.18_5	0.73	0.055	1.85	0.57	0.107	11.0	0.70_5	0.054	1.02	0.45	0.185

n-butane			n-pentane			n-hexane			n-heptane		
p-mm	Q	τZ_Q	p-mm	Q	τZ_Q	p-mm	Q	τZ_Q	p-mm	Q	τZ_Q
1.53	0.48	0.166	0.71_5	0.37	0.262	0.92	0.24	0.485	0.44	0.28	0.394
1.15	0.55	0.126	0.52_5	0.55	0.126	0.70	0.30	0.359	0.34	0.32	0.322
0.84_5	0.61	0.098	0.32	0.73	0.057	0.56	0.34	0.300	0.20	0.46	0.180
0.45	0.75	0.053	1.40	0.24	0.485	0.19	0.57	0.116	0.11_5	0.60	0.103
			1.13	0.31	0.342				0.06	0.73	0.057
			0.81	0.41	0.221				0.24_5	0.40	0.230
			0.41_5	0.52	0.140						
			0.25_5	0.68	0.072						

2-methyl butane			2-methyl pentane			2,2-dimethyl butane		
p-mm	Q	τZ_Q	p-mm	Q	τZ_Q	p-mm	Q	τZ_Q
0.50	0.398	0.232	0.30	0.43	0.20	0.75	0.50	0.154
0.41	0.457	0.182	0.23	0.55	0.12	0.58	0.58_5	0.109
0.31	0.530	0.137	0.18_5	0.52_5	0.14	0.37	0.67	0.076
0.20	0.67	0.075	0.11	0.64	0.08_6	0.20	0.83	0.032
0.12	0.78	0.043	0.07	0.78	0.04			

2,3-dimethyl butane			3-methyl pentane		
p-mm	Q	τZ_Q	p-mm	Q	τZ_Q
0.41	0.36	0.27	0.44	0.31_5	0.33
0.31	0.52	0.14	0.33_5	0.38	0.25
0.19	0.62_5	0.09	0.19_8	0.49	0.16
0.12	0.71	0.06			
0.51	0.36	0.27			

the errors introduced by using the linear function are negligible, especially for values of τZ_Q which are not much greater than 0.2.

The relation between p, Q and τZ_Q for the paraffins are given in Table II and the τZ_Q *vs.* p relations shown in Figs. 3–5. From the slope of the straight lines the best values for $\tau Z_Q/p$ were calculated. The quenching cross section (σ_Q^2) was then calculated from the equation:

$$\sigma_Q^2 = 3.0\times 10^{-4}\mu^{-\frac{1}{2}}(\tau Z_Q/p),$$

which was derived from the gas kinetic equation for 20°C. with $\tau = 1.0\times 10^{-7}$ sec. In Table III, the values of the square root of the reduced mass of the hydrocarbon molecule and a mercury atom ($\mu^{\frac{1}{2}}$), $\tau Z_Q/p$ derived from Figs. 3–5, and σ_Q^2 are listed.

The values of σ_Q^2 of propane, n-butane, and n-heptane are in fair agreement with those obtained previously by Bates. The cross section of ethane is smaller, by a factor of 4 or 5, than Bates' value. This may be due to a trace of impurity such as ethylene or ethylbromide, both of which probably quench strongly, in Bates' sample, since he stated[2] that his sample of ethane originally contained 10 to 15 percent of ethylene which he claimed to have removed by bromination.

The results of this investigation show (Table III) that the quenching cross section increases with increasing molecular weight and, up to a point, with increased branching of the carbon skeleton. Bates[2] had previously found that σ_Q^2 increased with molecular weight for the paraffins and Norrish and Smith[5] showed that the effective diameters of the paraffin hydrocarbons in quenching Na(^{2}P) radiation increased slowly from methane to butane. Steacie and LeRoy[6] who measured the quenching of Cd($^3P_1$) radiation by hydrocarbons did not find any significant difference between the effective cross sections for methane, ethane, and propane but the butanes did appear to be rather larger.

Very little information is available from previous work about the effect of branching of the carbon skeleton on the effective quenching diameter of the paraffins. Steacie and LeRoy found a smaller cross section for iso- than for normal butane, the respective values being 0.046A^2 and 0.064A^2. The results of this investigation show that the cross section is invariably increased when branching leads to the formation of a tertiary carbon-hydrogen bond and that it is decreased when the addition of another CH_3 group to the molecule results in the elimination of a tertiary C—H bond. This is exemplified by the data given in Table III from which it may be seen that iso-butane is larger than propane and that when another CH_3 group is added to produce neopentane the effective diameter decreases; similarly, the addition of one CH_3 group to n-butane to form iso-

[5] R. G. W. Norrish and W. MacF. Smith, Proc. Roy. Soc. A176, 295 (1940).

[6] E. W. R. Steacie and D. J. LeRoy, J. Chem. Phys. 11, 164 (1943).

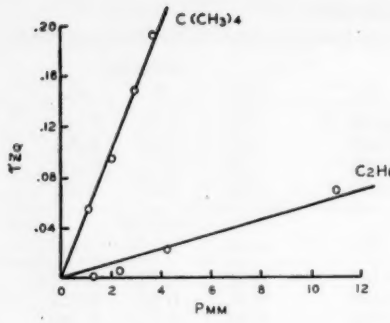

FIG. 3. Quenching results—ethane and neopentane.

pentane results in a marked increase in σ_Q, whereas we find that 2,2-dimethyl-butane is smaller than iso-pentane. The fact that iso-butane and iso-pentane are also both larger than *n*-butane and neo-pentane, which have the same number of carbon atoms, shows that the increase on forming the first branch is not caused by an increase in the physical bulk or of the number of carbon atoms or carbon-carbon bonds in the molecule. It is most likely that the increase in σ_Q on branching, which also leads to the formation of a tertiary C—H bond, is due to the fact that the tertiary C—H bond is more efficient than a secondary bond in quenching. We are thus led to the conclusion that the efficiency of the molecule as a whole in quenching mercury resonance radiation is a function of the type and number of C—H bonds.

An interesting relationship (Fig. 6) has been found between the number of carbon atoms (N) and the effective quenching diameters of the straight chained paraffins. The first part of the curve (A) shows that with methane and ethane neither of which have secondary C—H bonds, the increase of σ_Q with N is small. The second part of the curve (B) shows that the increase in σ_Q per $>CH_2$ group, from propane to heptane, is much larger. This points to a higher efficiency of quenching for secondary compared with primary C—H bonds. Also, portion B of the curve in Fig. 6 may, as a first approximation, be regarded as a straight line which can be extrapolated to cut the abscissa at approximately the point $N=2$. This suggests that, for the normal paraffins from propane to heptane, the quenching diameter is a function only of the number of secondary C—H bonds and that the terminal methyl groups contribute comparatively little to the quenching ability of the molecule. The slopes of the two straight lines in Fig. 6 indicate that each $-CH_3$ group in ethane contributes about 0.16A, or that each primary C—H bond about 0.05_5A, and that each $>CH_2$ group contributes about 1.0A, or each secondary C—H bond about 0.50A, to the quenching diameter.

The additivity found for $>CH_2$ groups in the normal paraffins cannot always be applied to the branched compounds. Thus the increase in σ_Q between 2-methyl propane and 2-methyl butane is 1.31A which is significantly larger than the value found for a methylene group in the normal paraffins. However, this discrepancy disappears when a methylene group is added to the molecule at a point that is not next to the tertiary carbon atom. Thus the difference in σ_Q between 2-methyl butane and 2-methyl pentane is 1.02A which is very close to the value found for the normal methylene group. A similar discrepancy is noted between the contributions of the $-CH_3$ groups in ethane and those in neopentane.

By the consideration of other data in Table III the effective contribution of a tertiary C—H bond appears to be about 1.3A. Thus if we assume that each $-CH_3$ group in iso-butane contributes 0.305A (being one-quarter of the value of σ_Q for neopentane) and that the tertiary C—H bond contributes the rest, we find the tertiary bond to have an effective diameter of $2.21-(3\times0.305)=1.3$A. Similarly if the 4 methyl groups in 2,3-dimethylbutane contribute as much as the 4 similar groups in neopentane, then the two tertiary bonds will be responsible for $3.86-1.22=2.63$A and each will then provide an effective contribution of 1.31A. We have adopted here the value of 0.30_5A for each methyl group which is based on neopentane rather than on ethane. The choice is arbitary but each methyl seems to contribute more in neopentane than in ethane, possibly due to some promotional effect of closely grouped methyl radicals, and the methyls in iso-butane and 2,3-dimethylbutane probably exert forces on each other which are similar to those occurring in neopentane. In any case, it is probable that the above values of 0.05, 0.5, and 1.3A assigned to the primary, secondary, and tertiary C—H bonds are approximately correct, and it is likely that in neopentane, the primary C—H bonds are promoted so that the contribution of each C—H is

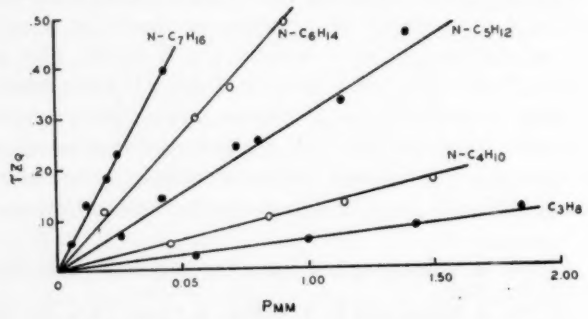

FIG. 4. Quenching results—normal paraffins.

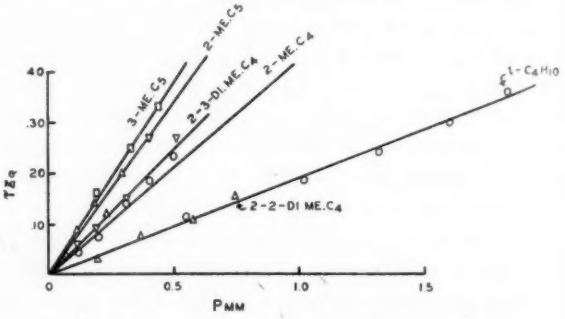

FIG. 5. Quenching results—branched paraffins.

about 0.10A or double the effective length of the C—H bonds in ethane.

If the above values for the effective bond quenching diameters are valid, we may calculate the number of collisions necessary for quenching to occur with each type of bond. The C—H bond length[7] is about 1.1A and is approximately independent of the nature of the bond. We may assume the radius of the $Hg(^3P_1)$ atom to be approximately the same as that of the normal mercury atom (1.8A). The "natural" quenching diameter will be the sum of these distances $-\sigma_N=2.9$A.

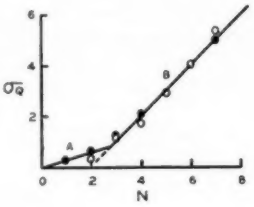

FIG. 6. Effect of size of molecule on effective diameter (normal paraffins). N = number of carbon atoms in molecule. Open circles—this investigation. Filled circles—results of Bates (reference 2).

If N is the number of collisions necessary for quenching to occur, then

$$N=\sigma_N^2/\sigma_Q^2.$$

For primary, secondary, and tertiary C—H bonds N will then have the values 3350, 34, and 5. Regarded in this way, it is evident that, contrary to general belief, the majority of the paraffin hydrocarbons are not very inefficient in quenching $Hg(^3P_1)$ radiation since only a few collisions are necessary for quenching to occur. The very much larger cross sections found for olefins may be caused by the much larger external fields associated with unsaturated compounds which will permit interaction of the olefin with $Hg(^3P_1)$ atoms to occur at distances that are quite large compared with those normally involved in collisions.

An interesting comparison may be made between the results of investigations of the mercury photo-sensitized reactions of the paraffin hydrocarbon and the above conclusions that the quenching efficiency is governed by the type and number of C—H bonds in the paraffin molecule. All information[8,9] indicates that C—H bonds are broken in the initial act of the reaction between $Hg(^3P_1)$ atoms and the paraffins. It has also been shown that the principal products of the similar reactions of propane[10] and iso-butane[11] are di-isopropyl and di-tertiarybutyl respectively. These results are in accordance with the conclusions, formed from the results of quenching measurements, that quenching occurs on the C—H bonds and that the efficiency of these bonds for quenching decreases in the order tertiary>secondary>primary. However, too much importance should not be attached to the comparison of the results of the photo-chemical with those of quenching experiments since all processes which lead to the suppression of fluorescent radiation, such as the transition of $Hg(^3P_1)$ to $Hg(^3P_0)$ are included in quenching, whereas such a transition could have no bearing on the photo-chemical reaction since the energy involved is much too small. There is also the possibility that the radicals which were identified in the final products of the photo-sensitized reactions of propane and iso-butane are not the same radicals which were produced in the initial act since isomerization of the initial radicals may conceivably have occurred before they were able to recombine. Actually, evidence has been found in the present data that high quenching efficiency does not always indicate high reactivity since it seems that the primary C—H bonds quench more efficiently in neopentane than in ethane whereas the quantum yield of the photo-sensitized reaction of ethane[9] is very much larger than for neopentane.[12] It is hoped that experiments now in progress in this laboratory will provide some information about the nature of the initial act in quenching.

TABLE III.

Paraffin	$\mu^{\frac{2}{3}}\times10^{-11}$	$\frac{\tau Z_Q}{p}$	$\sigma_Q^2\times10^{16}$ (cm²)	$\sigma_Q\times10^8$ (cm)
Ethane	1.52	0.0055	0.11	0.33
Propane	1.30	0.055	1.3	1.13
n-butane	1.16	0.116	3.0	1.73
Iso-butane	1.16	0.189	4.9	2.21
n-pentane	1.04	0.300	8.6	2.94
Iso-pentane	1.04	0.432	12	3.52
Neo-pentane	1.04	0.051	1.5	1.22
n-hexane	1.00	0.535	16	4.01
2-methyl pentane	1.00	0.682	20	4.54
3-methyl pentane	1.00	0.754	23	4.77
2,2-dimethyl butane	1.00	0.189	5.7	2.39
2,3-dimethyl butane	1.00	0.495	15	3.86
n-heptane	0.95	0.920	29	5.39

ACKNOWLEDGMENTS

It is a pleasure for the author to acknowledge his indebtedness to Dr. E. W. R. Steacie for many discussions and constant advice and to Dr. F. P. Lossing for building the d.c. amplifier and for much help with the instrument.

[7] L. Pauling, *The Nature of the Chemical Bond* (Cornell University Press, Ithaca, 1948), p. 168.

[8] E. W. R. Steacie, *Atomic and Free Radical Reactions* (Reinhold Publishing Corporation, New York, 1946).

[9] B. deB. Darwent and E. W. R. Steacie, J. Chem. Phys. **16**, 381 (1948).

[10] E. W. R. Steacie and D. J. Dewar, J. Chem. Phys. **8**, 571 (1940).

[11] B. deB. Darwent and C. A. Winkler, J. Phys. Chem. **49**, 150 (1945).

[12] B. deB. Darwent and E. W. R. Steacie, Can. J. Research **B27**, 181 (1949).

Rotation-Vibration Spectra of Diatomic and Simple Polyatomic Molecules with Long Absorbing Paths

IV. The Spectrum of Methyl Fluoroform (CH_3CF_3) from 19μ to 0.7μ

R. D. COWAN,* G. HERZBERG, AND S. P. SINHA†
*University of Chicago, Chicago, Illinois** and National Research Council, Ottawa, Canada*
(Received July 11, 1950)

The absorption spectrum of methyl fluoroform has been investigated with path lengths up to 30 meters in the region 19 to 0.7μ. Three of the fundamentals have been assigned differently from Thompson and Temple. Since the molecule is nearly a spherical top, the ⊥ bands show the same typical *PQR* structure as do the || bands except when the Coriolis interaction constant ζ is large. This seems to be the case for the degenerate C−F stretching vibration $\nu_9(\varepsilon)$ and for most binary combinations involving it. The CH_3 rocking vibration $\nu_{10}(\varepsilon)$ is split into two close components (separation 6 cm^{-1}) a splitting that is here ascribed to the presence of three potential minima separated by low potential maxima. A large number of infra-red bands can be readily interpreted as binary combinations. The relative intensities of fundamentals and of overtone and combination bands are briefly discussed.

A. INTRODUCTION

THE spectrum of fluoroform was investigated in paper I of this series.[1] From the fine structure of the photographic infra-red bands the moment of inertia of the molecule was determined. The resulting value of the C−F distance in CHF_3 was found to be appreciably smaller than in CH_3F. The more recent study of the microwave spectrum by Gilliam, Edwards, and Gordy[2] has confirmed the low value for r(C−F). It appeared of interest to ascertain whether a similar anomaly exists in other molecules containing the CF_3 group. It was with this consideration in mind that an investigation of the spectrum of methyl fluoroform (1:1:1 trifluoroethane) was undertaken. Up to now it has not been possible to resolve the fine structure of the bands of CH_3CF_3 and thus to determine the C−F distance but the results obtained concerning the vibrational structure of the spectrum appear of sufficient interest to warrant publication at this time.

After the results here to be described were obtained, a paper on the infra-red spectrum of methyl fluoroform by Thompson and Temple[3] appeared. Our results confirm in the main those of Thompson and Temple but go beyond theirs in the observation and discussion of overtone and combination bands. In addition, Thompson and Temple's assignment of fundamentals has been somewhat revised. Quite recently a spectrum of CH_3CF_3 in the region 2μ–15μ appeared in the API Catalog of Infra-Red Spectral Data (Serial No. 979, supplied by the Naval Research Laboratory).

B. EXPERIMENTAL

In the region 19μ to 2.5μ the infra-red spectrum of methyl fluoroform was recorded on the Perkin-Elmer infra-red spectrometer in the Spectroscopic Laboratory of the Physics Department at the University of Chicago using prisms of KBr, NaCl, and LiF. The absorbing path was 10 cm at various pressures. In the region 2.5μ to 0.7μ the PbS infra-red spectrometer of Dr. Kuiper[4] at Yerkes Observatory was used with an absorbing path of 30 meters, obtained in the way described in paper I of this series. This spectrometer has glass prisms. In addition the spectrum in the region 1.2μ to 0.7μ was photographed with the 21-foot grating spectrograph of Yerkes Observatory using the same long absorption tube.

In the region 19μ to 2.5μ (Perkin-Elmer spectrometer) individual fine structure lines of the bands of CO_2, CO, CH_4 and H_2O were used for calibration. In the region 2.5 to 0.7μ (Kuiper spectrometer) emission lines of He and Hg and absorption lines of H_2O as well as the zero gaps of several CO_2 bands were used as wave number standards. For the grating spectrograph iron lines of second, third, and fourth order were used.

With the prism instruments the wave number accuracy of sharp peaks in the region of maximum dispersion is estimated to be ±1 cm^{-1}. In the remaining spectral regions the accuracy may be less by a factor 2 or 3. In the region 2.2μ to 2.5μ on account of lack of standards the accuracy is probably only ±5 cm^{-1}. The accuracy in the photographic infra-red would be considerably greater than ±1 cm^{-1} if it were not for the fact that all bands in this region are quite broad and diffuse.

The methyl fluoroform was obtained through the kindness of Dr. A. F. Benning from the Jackson Laboratory of E. I. du Pont de Nemours and Company. The sample was specified as "substantially pure"

* Now Department of Physics, Friends University, Wichita, Kansas.
† Now T.D.E. Laboratory, Kanpur, India.
** This work was assisted in part by the ONR under Task Order IX of Contract N6ori—20 with the University of Chicago.
[1] H. J. Bernstein and G. Herzberg, J. Chem. Phys. **16**, 30 (1948).
[2] Gilliam, Edwards, and Gordy, Phys. Rev. **75**, 1014 (1949).
[3] H. W. Thompson and R. B. Temple, J. Chem. Soc. p. 1428 (1948), in future referred to as TT.
[4] Kuiper, Wilson, and Cashman, Astrophys. J. **106**, 243 (1947).

(b.p. $-47.5°C$) possibly with traces of CH_3CF_2Cl. It was used without further purification.

C. OBSERVED SPECTRUM

The infra-red absorption spectrum of methyl fluoroform from 500 to 6200 cm^{-1} is plotted in Fig. 1 as determined from the recordings obtained with the Perkin-Elmer and Kuiper spectrometers. Figure 2 shows a recording of the region 6000 to 11700 cm^{-1} obtained with the Kuiper spectrometer. Table I gives the wave numbers, intensities, band types and assignments of the bands below 6200 cm^{-1}. The bands above 6200 cm^{-1} are given without assignments in Table II.

In the regions 500–1550 cm^{-1} and 2850–3200 cm^{-1} which were also studied by Thompson and Temple the agreement with their absorption curve is very good except that the bands at 684 and 1135 cm^{-1} which are "weak" and "strong" respectively in their recordings, are absent in our spectra, even in those taken at a higher pressure × path than used by them. Similarly TT's "strong" band at 900 cm^{-1} is very much weaker on our records. These three bands must therefore be ascribed to impurities.

The spectral range 2850–3200 cm^{-1} is much better resolved on our records since we were able to use an LiF prism. For this reason it is believed that our value for the wave number of the band at 3034 cm^{-1} is the correct one even though it deviates by 8 cm^{-1} from the value given by TT.

Many of the infra-red absorption bands of methyl fluoroform particularly below 6000 cm^{-1} have a typical *PQR* structure, that is, a sharp central peak (*Q* branch) and two broader and less intense peaks at either side (*P* and *R* branches). These are separated from the central branch by about ± 11 cm^{-1}. There are however some bands consisting of a simple broad maximum, e.g. the strong band at 1234 cm^{-1} in Fig. 1, and others having two equally strong peaks with shoulders on the shortward and longward sides, e.g. the band at 972 cm^{-1}. At wave numbers above 6000 cm^{-1}, presumably due to overlapping of various combination bands, more and more irregular structures appear and in the photographic region very few bands show the simple *PQR* structure. Most of the photographic infra-red bands are very broad and many of these show several somewhat irregularly spaced diffuse peaks on the long- and shortward sides. Even for the bands with *PQR* structure of the photographic region it proved to be impossible to resolve the fine structure.

The intensities given in Tables I and II are based on peak heights assuming the intensity of the strongest band at 1234 cm^{-1} to be 100,000 and assuming Beer-Lambert's law to hold [that is, the intensity is taken to be proportional to $(1/pl)\log(I_0/I)$ where p and l are pressure and path length and where I_0 and I are incident and transmitted intensity respectively]. Since the dependence of peak height on slit width used and the effect of pressure broadening on peak heights has been neglected, the (relative) intensities given are necessarily quite rough. Nevertheless they are con-

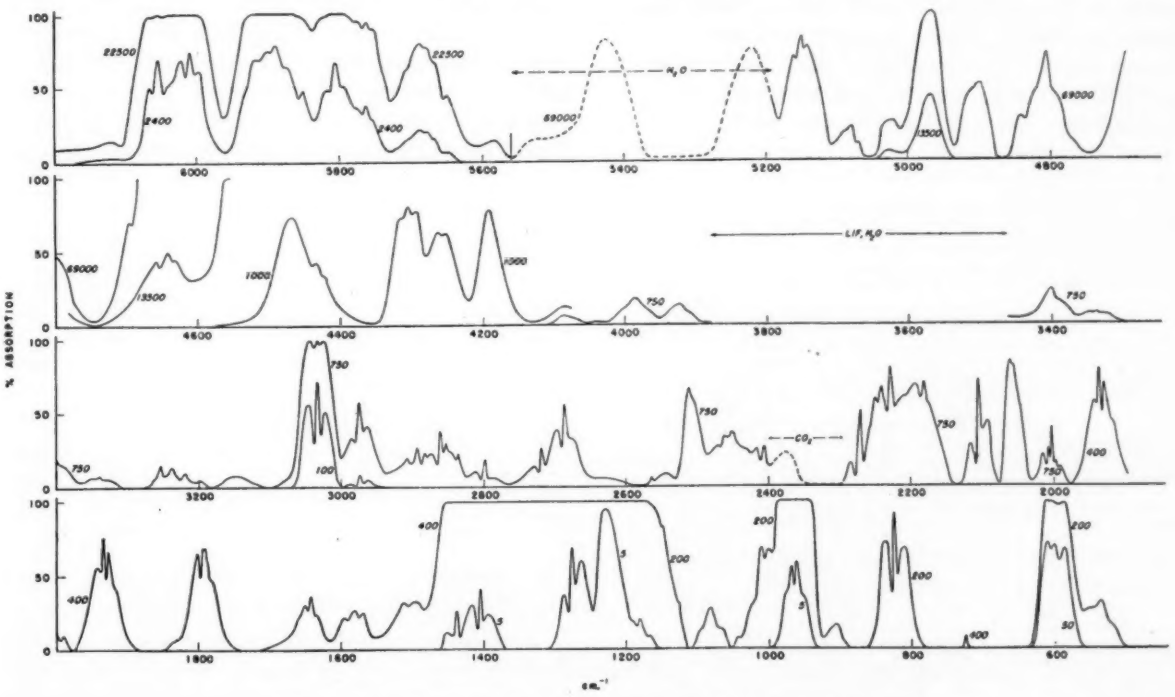

FIG. 1. Infra-red absorption spectrum of CH_3CF_3 from 500 to 6200 cm^{-1}.

The italic numbers on the curves give the product pressure×path in cm×cm. The regions marked by ⟷ are overlapped by CO_2, LiF, and H_2O bands. The broken-line curves in these regions give only an approximate representation of the absorption spectrum.

sidered to be better than the usual estimates ("strong," "medium," "weak," etc.). It may be noted that the range of intensities covered is very large, extending over seven powers of 10.

D. ASSIGNMENT OF FUNDAMENTALS

The methyl fluoroform molecule belongs to point group $\mathbf{C}_{3v}$ irrespective of whether the CH_3 and CF_3 groups are in the eclipsed or the staggered configuration. The point group $\mathbf{C}_{3v}$ has the three species A_1 (totally symmetric), A_2 (antisymmetric with respect to the planes of symmetry), and E (degenerate). It is easily seen[5] that methyl fluoroform has five normal vibrations of species A_1, one of species A_2, and six of species E. The first column of Table III describes these twelve vibrations, the second column gives the numbering chosen here, which is in conformity with general practice.[5]

All vibrations except $\nu_6(a_2)$ are infra-red active. For the a_1 vibration the dipole moment oscillates along the axis of symmetry, for the e vibrations perpendicular to it. Therefore, and since the molecule is a symmetric top the a_1 vibrations give rise to $\parallel$ bands, the e vibrations to $\perp$ bands.

On the basis of the molecular dimensions obtained from electron diffraction data by Shand and Spurr,[6] Russell, Golding, and Yost[6] calculated the moments of inertia[6a] to be $I_A=159\times10^{-40}$ $I_B=I_C=167\times10^{-40}$ g cm^2. The molecule is therefore very nearly a spherical top and consequently very little difference may be expected in the appearance of $\parallel$ and $\perp$ bands under medium dispersion. This is in agreement with the observation that a large number of the observed bands have PQR structure. Whether a given band with such a structure is a $\parallel$ or a $\perp$ band cannot be decided from the band envelope alone.

The separation of successive sub-bands of a $\perp$ band is $2[A(1-\zeta_i)-B]$ where A and B are the rotational constants corresponding to I_A and I_B and where $\zeta_i(h/2\pi)$ is the vibrational angular momentum in the degenerate upper state of the band ($|\zeta_i|\leq1$). The separation of the sub-bands of a $\perp$ band of methyl fluoroform will be very small and the band will have the same appearance as a $\parallel$ band only if ζ_i is small. If ζ_i is not small the Q branches of the sub-bands will no longer coincide and a broad rather than a sharp central maximum will arise. Similarly the P and R branches of the sub-bands will form much broader features not separated by minima from the central branch which will be the most prominent feature. An example of such a band is the strongest infra-red band of methyl fluoroform, at 1234 cm^{-1}, (see Fig. 1). This band can therefore be classified as a $\perp$ band. The same applies to other bands of this shape.

Another band type observed for CH_3CF_3 is one with two rather than three peaks. The strong band at 970 cm^{-1} (Fig. 1) is a striking example. It is suggested here that the doubling is due to a splitting of the degeneracy associated with the three potential minima of the torsional motion. As is well known[5] a splitting into two levels arises which increases with decreasing potential barrier or increasing amplitude of the torsional mode. It is to be expected that whole-molecule-vibrations such as the rocking modes can also produce such a splitting. The most natural assignment of the band at 970 cm^{-1} is indeed that of CH_3 rocking $[\nu_{10}(e)]$. It is assumed here that in the state in which this vibration is singly excited the doubling is 6 cm^{-1} while for the lowest vibrational level it is negligible. As has been shown by Koehler and Dennison,[7] with increasing K (rotation about the symmetry axis) one of the component levels splits further into two components and all

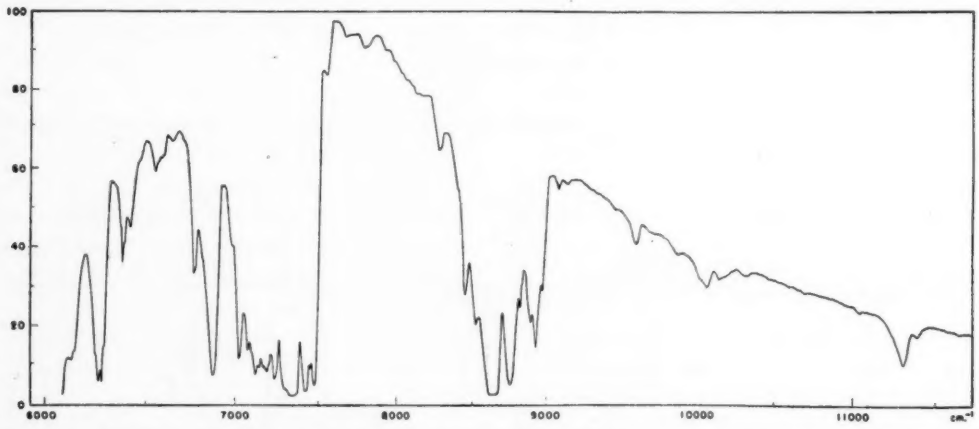

FIG. 2. Recording of the CH_3CF_3 absorption spectrum from 6000 to 11700 cm^{-1} as obtained with Dr. Kuiper's spectrometer at 70 cm pressure and 3000 cm path. In this recording unlike Fig. 1 absorption bands appear as minima of the curve.

[5] See, for example, G. Herzberg, *Molecular Spectra and Molecular Structure II. Infrared and Raman Spectra of Polyatomic molecules* (D. Van Nostrand Company, Inc., New York, 1945).
[6] W. Shand and R. A. Spurr, quoted by Russell, Jr., Golding, and Yost, J. Am. Chem. Soc. **66**, 16 (1944).
[6a] From the microwave spectrum, W. F. Edgell and A. Roberts [J. Chem. Phys. **16**, 1002 (1948)] obtained $I_B=161.8_0\times10^{-40}$ g cm^2.
[7] J. S. Koehler and D. M. Dennison, Phys. Rev. **57**, 1006 (1940).

TABLE I. Infra-red absorption bands of CH_3CF_3 from 500 to 6200 cm^{-1}.

ν_{vac}(obs.) cm^{-1}	Band type[a]	Intensity[b]	Assignment[c]	ν_{vac}(calc.)[d] cm^{-1}
526	vb *P*	240	$\nu_5(a_1)$	
541	b *Q*			
558	vb *R*			
593	vb *P*	2740	$\nu_{11}(e)$	
606	b *Q*			
616	vb *R*			
732	b	32	$2\nu_{12}(A_1, E)$	736
817	vb *P*	1490	$\nu_4(a_1)$	
830	s *Q*			
842	vb *R*			
911[e]	b	115	$\nu_5+\nu_{12}(E)$	909
967	ph doublet	21400	$\nu_{10}(e)$	
973	ph			
1015	bh	750		
1088	bh	200	$2\nu_5(A_1)$, impurity?[f]	1082
1172	b *P*?	5800	$\nu_4+\nu_{12}(E)$	1198
1187	s *Q*?			
[g]	*R*?			
1234	vb ⊥	100000	$\nu_9(e)$	
1268	b *P*	30400	$\nu_3(a_1)$	
1281	s *Q*			
1292	b *R*			
1397	b *P*	12700	$\nu_2(a_1)$	
1409	s *Q*			
1421	b *R*			
1442[h]	s *Q*	7460	$\nu_8(e)$	
1458	b *R*			
1520[i]	vb	75	$\nu_6+\nu_{10}(E)$?	1513
1586[i]	vb	66	$\nu_9+\nu_{12}(A_1, E)$, $\nu_6+\nu_8(E)$	1602, ?
1647[i]	s	115	$2\nu_6(A_1)$	1660
1797[i]	b	380	$\nu_4+\nu_{10}(E)$	1797
1806	s			1803
1883	s	14	$\nu_3+\nu_{11}(E)$	1887
1931	sh	440	$2\nu_{10}(A_1, E)$	1940
1937	s			
1945	b			
1993	b *P*	125	$\nu_2+\nu_{11}(E)$	2015
2005	s *Q*			
2008	s *Q*	55	$\nu_2+\nu_{11}+\nu_6-\nu_8$?	
2016	b *R*			
2057	ph	285	$\nu_4+\nu_9+\nu_6-\nu_8$	
2061	bh	295	$\nu_4+\nu_9(E)$	2064
2093	b *P*	255	$\nu_3+\nu_4(A_1)$	2111
2107	sh *Q*			
2116	b *R*			
2184	ph	225	$\nu_9+\nu_{10}(A_1, E)$	2204
2193	vbh			
2216	vb *P*	270	$\nu_2+\nu_4(A_1)$	2239
2231	s *Q*			
2243	bh *R*[k]			
2252	sh	140	$\nu_3+\nu_{10}(E)$	2254
2261	b *P*[l]	135	$\nu_4+\nu_8(E)$	2272
2272	s *Q*			
2285	b *R*			
(2376)[m]	?	(47)	$\nu_2+\nu_{10}(E)$	2379
2407	s	28	$\nu_8+\nu_{10}(A_1, E)$	2412
2417	ph			
2453	bh	63	$2\nu_9(A_1, E)$?	2468
2463	up			
2469	bh			
2512	bh	175	$\nu_3+\nu_9(E)$	2515
2545	b *P*	12	$2\nu_3(A_1)$	2562
2560	s *Q*			
2676	b *P*	145	$\nu_2+\nu_3(A_1)$	2690
2687	s *Q*			
2698	b *R*			
	P			
2720	s *Q*	51	$\nu_3+\nu_8(E)$	2723
2729	b *R*			
2786	b *P*	35	$2\nu_2(A_1)$	2818
2799	s *Q*			
2812	b *R*			
2836	s	40	$\nu_2+\nu_8(E)$	2851
2852	sh *Q*	52	$2\nu_8+\nu_6-\nu_8$?	
2861	s *Q*	80	$2\nu_8(A_1)$	2884
2875	b *R*			
2883	s *P*?	50	$2\nu_8(E)$	
2894	s *Q*			
2909	p *R*?			

TABLE I—*Continued.*

ν_{vac}(obs.) cm^{-1}	Band type[a]	Intensity[b]	Assignment[c]	ν_{vac}(calc.)[d] cm^{-1}
2965	b *P*	145	$\nu_1(a_1)$	
2975	s *Q*			
2986	b *R*			
3024	b *P*	2300	$\nu_7(e)$	
3034	s *Q*			
3046	b *R*			
3150	vb	(13)		
3220	s	16		
3239	s	23	$\nu_8+\nu_7$?	
3256	s	26		
3340	sh	97	$\nu_1+\nu_{12}(E)$	3343
3394	h *P*	44	$\nu_7+\nu_{12}(A_1, E)$	3402
3403	sh *Q*			
3926	vb	18	$\nu_1+\nu_{10}(E)$	3944
3983	b	31	$\nu_7+\nu_{10}(A_1, E)$	4004
4090[n]	b	9.7	?	
4192[n]	b	145	$\nu_1+\nu_9(E)$	4209
4252[n]	b	102	$\nu_1+\nu_3(A_1)$	4255
4264[n]	b	108	$\nu_7+\nu_9(A_1, E)$	4268
4295[n]	b *P*	210	$\nu_8+\nu_7(E)$	4315
4306[n]	s *Q*			
4317[n]	b *R*			
4435[n]	bh	71	$\nu_2+\nu_7(E)$	4443
4470[n]	b	145	$\nu_7+\nu_8(A_1, E)$	4476
4650	vvb	5.1	$\nu_1+\nu_8+\nu_{12}(E)$	4623
			$\nu_7+\nu_9+\nu_{12}(A_1, E, E, E)$	4636
4807	sh	2.1	$\nu_6+\nu_7+\nu_9(A_1, E)$	4809
4901	vb	1.2	$\nu_3+\nu_7+\nu_{11}(A_1, E)$	4921
4971	vb	4.8	$\nu_2+\nu_6+\nu_7(E)$	4983
5022	b	0.52	$\nu_1+\nu_4+\nu_9(E)$	5039
5081	sh	0.47	$\nu_7+\nu_8+\nu_{11}(A_1, E, E, E)$	5082
			$\nu_4+\nu_7+\nu_9(A_1, E)$	5098
5140	s *P*?	3.1	$\nu_3+\nu_4+\nu_7(E)$	5145
5151	s *Q*			
5161	s *R*?			
5220[i]	?	(2.5)	$\nu_7+\nu_9+\nu_{10}(A_1, E, E)$	5238
5429[i]	?	(1.9)	$\nu_7+\nu_8+\nu_{10}(A_1, E, E, E)$	5446
			$\nu_1+2\nu_9(A_1, E)$	5442
5583	sh	0.67	$2\nu_3+\nu_7(E)$	5596
5689	vbh	10.8	$\nu_3+\nu_3+\nu_7(E)$	5724
5755	b *P*	36	$\nu_1+2\nu_3(A_1)$	5793
5763	s *Q*		$\nu_1+\nu_2+\nu_8(E)$	5826
5775	b *R*			
5797	b *P*	56	$\nu_1+2\nu_8(A_1, E)$	5859
5807	s *Q*		$2\nu_3+\nu_7(E)$	5852
5818	b *R*			
5852	s	(32)	$\nu_2+\nu_7+\nu_8(A_1, E)$	5885
			$\nu_7+2\nu_8(A_1, E, E)$	5918
5877	b *P*	75	$2\nu_1(A_1)$	5950
5890	s *Q*			
5903	b *R*			
5920	b	(50)	$\nu_1+\nu_7(E)$	6009
5998	s *P*?	70	$2\nu_7(A_1, E)$	6068
6011	s *Q*			
6023	s *R*			
6042	h *P*?	59		
6056	s *Q*			
6067	b *R*			

[a] Abbreviations: s=sharp, b=broad, vb=very broad, h=hump (i.e., no distinct maximum), ph=peak with side humps, sh=sharp peak with side humps, bh=broad peak with side humps, u=unsymmetrical. *P*, *Q*, *R* refer to peaks that are likely to be due to *P*, *Q*, *R* branches respectively.

[b] These are relative intensities based on the value 100,000 for the strongest band at 1234 cm^{-1}. Intensities in brackets are uncertain because of overlapping.

[c] Only the infra-red active species are given.

[d] Based on the harmonic oscillator approximation.

[e] TT give a strong band with peaks at 889, 900, and 910 which can hardly be identical with the weak band at 911 reported here.

[f] This band is not given by TT but does appear in the API record. It may be due to an impurity. TT find instead a strong band at 1135 cm^{-1} which is absent here.

[g] Overlapped by the strong band at 1234 cm^{-1}.

[h] The *P* branch of this band coincides with the *R* branch of the band at 1409 cm^{-1} as confirmed by the high intensity of the 1421 cm^{-1} peak.

[i] Overlapped by H_2O lines, therefore not very accurately measured.

[j] This *P* branch seems to be overlapped by other features.

[k] This peak is higher and less broad than expected for the *R* branch of the band 2231. It is very probably overlapped by the second component of $\nu_3+\nu_{10}$.

[l] This was measured as a shoulder on a background of large slope.

[m] Overlapped by CO_2 band.

[n] These wave numbers are less accurate because of lack of good standards in this region.

three component levels, with further increase in *K*, change periodically their relative order. The intensity distribution in the wings of the band at 970 cm^{-1} is characteristically different from that in other bands. More detailed calculations will be required to ascertain whether the observed band envelope can actually be accounted for by the torsional splitting.

The other vibrations associated with the CH_3 group are easily assigned if their frequencies in other molecules containing the CH_3 group are remembered. The frequencies 2975 and 1409 cm^{-1} are due to the symmetric CH stretching and CH_3 deformation vibrations respectively while 3034 and 1442 are due to the corresponding degenerate vibrations (Thompson and Temple).[3] considered 1408 and 1442 as forming $\nu_8(e)$ with the

TABLE II. Infra-red absorption bands of CH_3CF_3 from 6200 to 14000 cm^{-1}.

ν_{vac}(obs.) cm^{-1}	Band type[a]	Intensity[b]
6260	sh } doublet	1.7
6275	sh }	1.8
6379	sh Q	0.34
6421	b	0.21
6552	bh	0.066
6645	vb	0.019
6762	b	0.44
6875	bh	1.5
7028	sh Q	1.1
7073	s[c]	0.72
7115–7250	vb[c]	1.0
7348	bh	5.2
7417	s } doublet	2.5
7427	b }	2.4
7452	s	0.40
7482	s Q?	2.2
7545	b	0.10
8272	vb	0.13
8421	b (P.I.)	(0.2)[d]
8431	b (P.I.)	(0.4)[d]
8443	b (P.I.)	0.63
8483	b (P.I.)	(0.2)[d]
8494	b (P.I.)	(0.3)[d]
8506	b (P.I.)	(0.5)[d]
8522	b (P.I.)	0.85
8536	b (P.I.)	(0.3)[d]
8556	b (P.I.)	(0.3)[d]
8574	b (P.I.)	(0.8)[d]
8593	b (P.I.)	(0.8)[d]
8604	b (P.I.)	(0.8)[d]
8613	b (P.I.)	(0.8)[d]
8624	b (P.I.)	(0.8)[d]
8640	b (P.I.)	(0.8)[d]
8650	vb (P.I.)	7.0
8758	vb (P.I.)	1.9
8814.8	sh Q (P.I.)	0.71
8887	sh	0.79
8924	sh Q (P.I.)	1.0_7
8969	h	0.52
9069.9	sh Q (P.I.)	0.052
9134	vb	0.033
9598	vb	0.099
9881	vvb	0.063
10070	vb (P.I.)	0.17
10147	vb (P.I.)	0.10_6
10180	vb (P.I.)	0.077
10325	vb	0.036
11309	vb (P.I.)	0.52
11394	vb (P.I.)	0.12
13833	vb (P.I.)[e]	(0.08)

[a] See footnote a of Table I. In addition (P.I.) refers to bands obtained with the 21-ft. grating in the photographic infra-red.
[b] See footnote b of Table I.
[c] Overlapped by H_2O, therefore not accurately measured.
[d] These are faint diffuse peaks which are superimposed on the longward wings of the main broad bands at 8443, 8522 and 8650 cm^{-1}. They have been resolved on the photographic infra-red plates only.
[e] Observed in the photographic infra-red only since it was beyond the range of Kuiper's infra-red spectrometer.

degeneracy removed and adopted $\nu_2(a_1)=1278$ cm^{-1}. However the doubling appears much too large and 1408 and 1442 are close to the symmetric and degenerate CH_3 deformation vibrations of CH_3CN and CH_3CCH.

The frequency 1281 cm^{-1} is here assigned to the symmetric C–F stretching vibration $\nu_3(a_1)$ in spite of the fact that the corresponding degenerate frequency 1234 cm^{-1} (strongest infra-red band, definitely a $\perp$ band, see above) is lower. This assignment appears necessary since the frequency 1135 used by Thompson and Temple is due to an impurity. In support of this assignment of the C–F stretching vibrations are the facts (1) that the only two frequencies of CF_3CCl_3 that can be assigned to C–F stretching modes[8] are 1250 and 1214 cm^{-1}, (2) that the means of the two $\parallel$ and the two $\perp$ C–F stretching vibrations of C_2F_6 are 1270 and 1243 cm^{-1} respectively.[9]

By comparison with other molecules containing C–C bonds the C–C stretching vibration is readily assigned to the observed band at 830 cm^{-1}; comparison with C_2F_6 yields the assignment of the CF_3 deformation vibrations $\nu_5(a_1)=541$, $\nu_{11}(e)=606$ cm^{-1}. The CF_3 rocking vibration $\nu_{12}(e)$ must very probably be identified with the Raman band 368 cm^{-1} which is beyond the region investigated in the infra-red. Thus far there is no way of assigning the torsion oscillation $\nu_6(a_2)$ unambiguously.

The frequencies thus assigned to the normal vibrations of fluoroform are summarized in the last column of Table III. The second last column gives for comparison the assignments of Thompson and Temple. The third column of Table III gives the Raman frequencies observed for liquid CH_3CF_3 by Hatcher and Yost.[10] In addition to the fundamentals given the Raman shifts 2792, 2825, and 2885 cm^{-1} were observed which presumably correspond to the infra-red bands of the gas at 2799, 2836, and 2894 cm^{-1}. Since at one time it was considered possible that the assignment of $\nu_1(a_1)$ and $\nu_7(e)$ had to be exchanged, Dr. A. E. Douglas, then at the Department of Physics of Pennsylvania State College, determined the polarization of the two Raman lines 2974 and 3040 finding the first strongly polarized, the second depolarized. This confirms the present assignment of these two frequencies. It is surprising that of the two CH_3 deformation vibrations $\nu_2(a_1)$ does not appear in the Raman spectrum while $\nu_8(e)$ does.

The relative intensities of the fundamentals in the infra-red are noteworthy: the two strongest infra-red bands are those at 1234 and 1280 cm^{-1} which are due to C–F stretching vibrations. The weakest (allowed) fundamental in the infra-red is the symmetrical C–H stretching vibration at 2975 cm^{-1} with less than 1/500 of the intensity of the 1234 cm^{-1} band.

E. OVERTONE AND COMBINATION BANDS

In addition to the fundamentals discussed in the preceding section there are a large number of overtone and combination bands (Tables I and II). As indicated in Table I most of the bands below 6200 cm^{-1} can be assigned as binary combinations of the fundamentals of Table III. Indeed, the ease with which this assignment is possible is a further strong indication of the correctness of the fundamentals. Many of the overtone

[8] G. Glockler and C. Sage, J. Chem. Phys. **9**, 387 (1941).
[9] J. R. Nielsen, C. M. Richards, and H. L. McMurry, J. Chem. Phys. **16**, 67 (1948).
[10] J. B. Hatcher and D. M. Yost, J. Chem. Phys. **5**, 992 (1937).

and combination bands whenever they can be properly resolved show the typical *PQR* structure. However it is significant that the binary combinations $\nu_4+\nu_{10}$ at 1802, $\nu_9+\nu_{10}$ at 2189 and $\nu_8+\nu_{10}$ at 2412 cm^{-1} which involve the rocking vibration $\nu_{10}(e)$ have a doublet structure similar to that of ν_{10} (see Fig. 1). Other combinations of this type are either overlapped or in regions of insufficient resolving power so that the presence of the splitting cannot be ascertained. In the case of the overtone $2\nu_{10}$ a larger splitting is expected which is further complicated by the fact that there would be a splitting into an A_1 and an E component even without the torsional splitting. The observed band at 1937 cm^{-1} does indeed show a more complicated appearance than the fundamental (see Fig. 1).

Similarly, it is noteworthy that, in all cases in which it can be ascertained, the binary combinations involving $\nu_9(e)$ do not show the *PQR* structure characteristic of most other bands but show a broad maximum in agreement with the behavior of the fundamental. This is in agreement with expectation since the ζ-value of combinations $\nu_i(a_1)+\nu_k(e)$ is the same as for $\nu_k(e)$ while for combinations $\nu_i(e)+\nu_k(e)$ it is $\zeta_i+\zeta_k$ for the E component of the resultant state.

In several cases, for example $2\nu_8$ and $2\nu_7$, the expected splitting into two bands (species A_1 and E of the upper state) is observed. The magnitude of this splitting (33 and 45 cm^{-1} for $2\nu_8$ and $2\nu_7$ respectively) is of the same order as that observed previously for CH_3I.[11]

In the last column of Table I, for all overtone and combination bands the calculated wave numbers are given, based on the assumed assignment and neglecting anharmonicity. The deviations from the observed values are of the right order of magnitude expected for the effect of anharmonicity.

Several bands in Table I are assigned as combination bands involving the inactive frequency $\nu_6(a_2)$. In case of bands of the type $\nu_i+\nu_6-\nu_6$ the peaks are very close to peaks of the main bands ν_i. While the assignment seems reasonably certain in these cases it does not allow a determination of $\nu_6(a_2)$. The assignment of difference or summation bands of the type $\nu_i\pm\nu_6$ is very doubtful in all cases. A reliable assignment and therefore an unambiguous determination of $\nu_6(a_2)$ would be possible if the effect of temperature on the difference bands $\nu_i-\nu_6$ could be established.

The bands above 6200 cm^{-1} are of necessity ternary or higher combinations. Since there are twelve fundamentals the number of ternary and higher combinations is so large that unique assignments are hardly possible particularly since it is not possible to distinguish $\parallel$ and $\perp$ bands. It is however clear that the bands in the region 7000–7500 cm^{-1} are due to ternary combinations involving two C−H stretching frequencies and a CH bending or deformation frequency while the bands in the region 8500–9000 are due to ternary combinations of the C−H stretching vibrations. The few peaks at 11350 cm^{-1} may similarly be classed as $4\nu_{CH}$ and the weak band at 13833 cm^{-1} as $5\nu_{CH}$.

[11] G. Herzberg and L. Herzberg, Can. J. Research **B27**, 332 (1949).

TABLE III. Fundamentals of CH_3CF_3.

Description	Designation	Wave number: Raman effect of the liquid	Wave number: TT	Wave number: Present work
Symmetric C−H stretching	$\nu_1(a_1)$	2974	2974	2975
Symmetric CH_3 deformation	$\nu_2(a_1)$		1278	1409
Symmetric C−F stretching	$\nu_3(a_1)$	1279	1135	1281
Symmetric C−C stretching	$\nu_4(a_1)$	829	828	830
Symmetric CF_3 deformation	$\nu_5(a_1)$	541	540	541
Torsion	$\nu_6(a_2)$			
Degenerate C−H stretching	$\nu_7(e)$	3040	3042	3034
Degenerate CH_3 deformation	$\nu_8(e)$	1450	1450 1412	1442
Degenerate C−F stretching	$\nu_9(e)$		1230	1234
Degenerate CH_3 rocking	$\nu_{10}(e)$	968	968	970
Degenerate CF_3 deformation	$\nu_{11}(e)$	603	606	606
Degenerate CF_3 rocking	$\nu_{12}(e)$	368	(368)	(368)

It is well known that the intensities of overtone and combination bands depend on the magnitude of the mechanical and the electrical anharmonicity associated with the motions involved. Since very little is known about the electrical anharmonicity no definite predictions of intensities can be made. However it is significant that the first overtones of the C−F stretching vibrations ν_3 and ν_9 are quite weak, less than 1/1000 of the fundamentals (which are the strongest bands in the spectrum), while the first overtones of the C−H stretching vibrations are much stronger relative to the fundamentals (which are quite weak, see Section D). This behavior is in agreement with the relative magnitudes of the mechanical anharmonicities.

F. CONCLUSION

As mentioned previously in spite of the use of low pressure (to avoid pressure broadening) and of high dispersion (2.5A/mm) the rotational fine structure of the photographic infra-red bands was not resolved. The reason for this must be sought in the fact that the difference between the moments of inertia of the upper and lower states is considerable so that the Q branches of the sub-bands are not line-like and, in the case of $\parallel$ bands, different sub-bands do not coincide. This is unlike the case of CHF_3 where the upper states of the overtones of the CH vibration have the same I_A as the ground state. By investigating less high overtones or fundamentals of species A_1 in the region made excessible for high resolution work by the use of photoconductive cells a determination of the moment of inertia I_B of CH_3CF_3 should be possible. For a better understanding of hindered rotation a high resolution study of bands involving the fundamental $\nu_{10}(e)$ and of difference bands involving $\nu_6(a_2)$ would be very promising.

Thompson and Temple[3] have calculated the thermo-

dynamic functions of CH_3CF_3 on the basis of the approximate moments of inertia mentioned above and of their choice of fundamentals. With the modified assignment of fundamentals given in the present work slight changes of the values of the thermodynamic functions will arise. However it does not seem worth while to carry out a recalculation at the present time before the high resolution studies suggested in the preceding paragraph have been carried out.

We are greatly indebted to Dr. A. F. Benning of the Jackson Laboratory of E. I. du Pont de Nemours and Company for putting at our disposal a generous quantity of methyl fluoroform. Our thanks are also due to Dr. G. P. Kuiper of Yerkes Observatory for letting us use his infra-red spectrometer. One of us (S. P. Sinha) wishes to express his thanks to Patna University, India, for the award of a Scholarship which enabled him to carry out this work.

THE JOURNAL OF CHEMICAL PHYSICS VOLUME 18, NUMBER 12 DECEMBER, 1950

Rotation-Vibration Spectra of Diatomic and Simple Polyatomic Molecules with Long Absorbing Paths

V. The Spectrum of Isocyanic Acid

C. REID*
National Research Council, Ottawa, Canada
(Received July 24, 1950)

The spectrum of isocyanic acid has been examined in the photographic infra-red using a 21-ft. grating spectrograph and path lengths up to 500 m. The rotational structure of several bands has been analyzed and the energy levels and moments of inertia determined. With their help the coarse rotational structure of two of the fundamentals has also been analyzed. The molecular parameters fitting best our data and published electron diffraction results for the C−N and C−O bond distances are: $r(H-N)=1.00_0A$, $\measuredangle H-N-C=125.5°$.

A. INTRODUCTION

IT has been shown in another paper[1] where a summary of previous work and a vibrational analysis is given, that the gas prepared by thermal depolymerization of cyanuric acid and loosely called cyanic acid is, in fact, isocyanic acid H−N=C=O. The basis for this assignment is (a) the marked similarity between three of the fundamentals to those of CO_2 with which H−N=C=O is isosteric and isoelectronic and (b) a comparison of the hydrogen stretching frequency with that of HNCS.

These arguments suggest also that the N=C=O group is linear as might be expected, and, since the general appearance of the spectrum is not that of a linear molecule, that the H atom is not collinear with the rest of the molecule.

Before the present investigation no analysis of the photographic infra-red spectrum of HNCO had been made. Some observations in the photographic infra-red[1] suggested that the rotational structure was rather complicated. However, if the NCO group is linear one would expect a simpler spectrum similar to that of hydrazoic acid, which has been interpreted without great difficulty.[2,3] This expectation is in fact fulfilled.

B. EXPERIMENTAL

Isocyanic acid was prepared from cyanuric acid as described in reference 1. The photographic infra-red

TABLE I. HNCO fundamentals.*

Assignment	Observed frequency cm^{-1}
$\nu_1(a')$	3531
$\nu_2(a')$	2274
$\nu_3(a')$	1527
$\nu_4(a')$	798
$\nu_5(a')$	572
$\nu_6(a'')$	670

* See reference 1.

TABLE II.

Assignment	Band center cm^{-1}	Type*	Rotational analyses*
ν_4	798	h	c
ν_1	3531	h	c
$2\nu_1+\nu_2$	9162	h	c,f
$3\nu_1$	10145.1	h	c,f
$2\nu_1+\nu_2+\nu_3$	10525	$\|\|$	c,f
$3\nu_1+\nu_4$	10988	h	f
$4\nu_1$	13217	h	f

* h=hybrid band; $\|\|$=predominantly parallel band; c=coarse rotational structure analyzed; f=fine rotational structure analyzed.

* Now at the University of British Columbia, Vancouver, B. C., Canada.

[1] G. Herzberg and C. Reid. Presented at the Faraday Society Symposium on Spectroscopy and Molecular Spectra, September, 1950.

[2] Herzberg, Patat, and Verleger, Zeits. f. Electrochemie 41, 522 (1935).

[3] E. H. Eyster, J. Chem. Phys. 8, 1935 (1940).

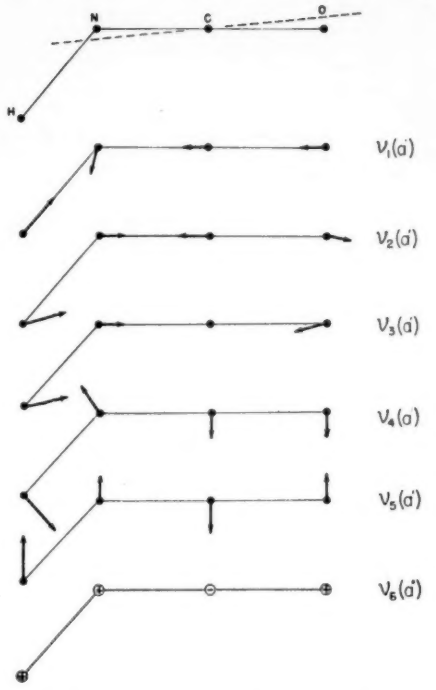

FIG. 1. Normal vibrations of HNCO. The upper diagram shows the inclination of the figure axis to the principal axis of inertia.

spectrum was obtained using the multiple reflection technique of White[4] as modified by Bernstein and Herzberg,[5] in a 5 m tube, 10 cm in diameter. With this arrangement optical path lengths up to 500 m, and pressures up to 14.5 cm of gas were used. A wedge window was found necessary to avoid interference effects produced by internal reflection in the $\frac{1}{4}$-in. plate glass window first used to close the tube. The upper pressure limit was set by the fact that at pressures above 14.5 cm of gas slow polymerization on the mirror surfaces occurred, with consequent loss of reflectivity. Photographic infra-red spectra were recorded on Eastman-Kodak *N*, *M*, and *Z* plates, using a 21-ft. grating spectrograph. Second-, third-, and fourth-order iron lines were used for comparison spectra.

The spectrum in the region 400–8000 cm^{-1} was obtained using a Perkin-Elmer model 12*C* instrument with KBr, NaCl, and LiF optics.

C. ROTATIONAL ANALYSIS

The labeling of the fundamentals is shown in Fig. 1, and their assignments are given in Table I. The bands for which a rotational analysis has been carried out are listed with their assignments in Table II.

If we presuppose that isocyanic acid has a structure in which the NCO radical is linear and the H atom displaced off the axis, the molecule is very nearly a prolate symmetric top with the large moments of inertia I_B and I_C much larger than I_A, the small moment of inertia.

In such a molecule most of the vibrations involve a change in electric moment both parallel and perpen-

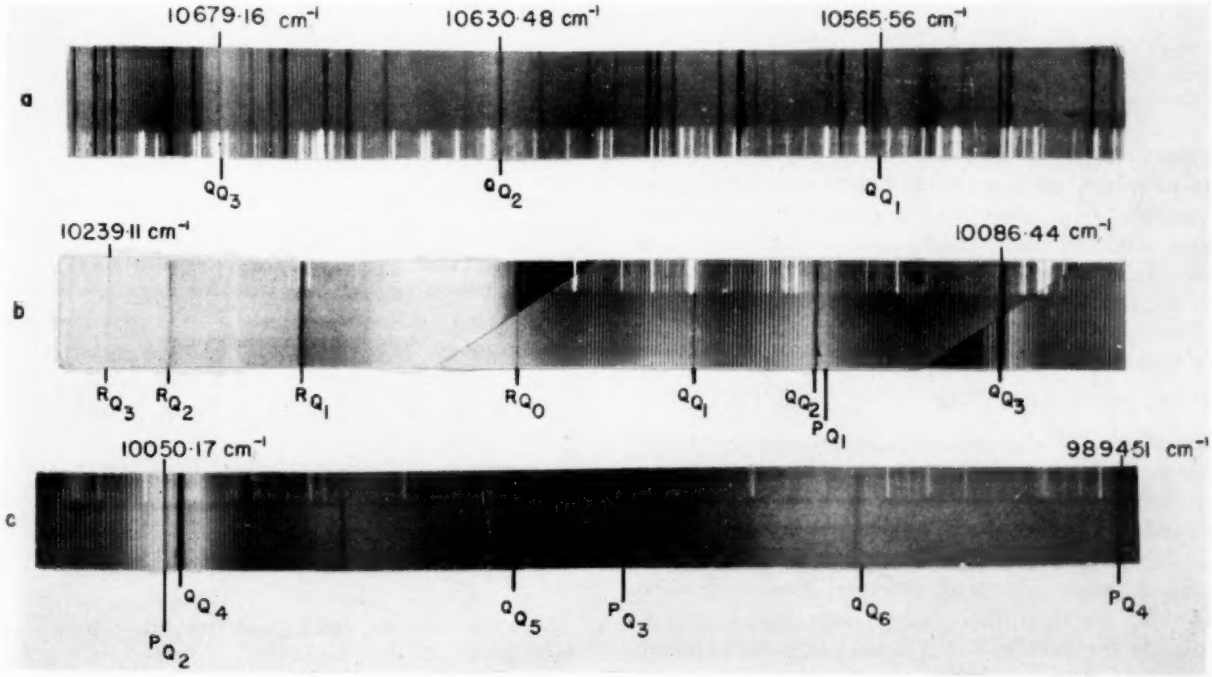

FIG. 2. (a) Part of the band $2\nu_1+\nu_2+\nu_3$ at 10525 cm^{-1}. The irregularly spaced lines are part of the 10613.12 cm^{-1} water band. (b) and (c) The band $3\nu_1$ at 10145.1 cm^{-1}.

[4] J. U. White, J. Opt. Soc. Am. **32**, 285 (1942).
[5] H. J. Bernstein and G. Herzberg, J. Chem. Phys. **16**, 30 (1948).

TABLE III(a). $2\nu_1+\nu_2+\nu_3$. Observed wave numbers.

${}^{Q}O_K$	$K=1$ 10565.56		$K=2$ 10630.48		$K=3$ 10679.16		$K=4$ 10785.63	
J	${}^{Q}R_1(J)$	${}^{Q}P_1(J)$	${}^{Q}R_2(J)$	${}^{Q}P_2(J)$	${}^{Q}R_3(J)$	${}^{Q}P_3(J)$	${}^{Q}R_4(J)$	${}^{Q}P_4(J)$
1			10632.58		10680.58			10784.77
2			33.46	10628.58*	81.28	10677.87		84.01
3	10568.51		34.16	27.61	—	76.95	10788.61	83.36
4	69.35	10562.64	34.88*	26.79	—	76.21	89.79	82.60
5	70.01	61.84	35.58*	26.06	—	75.38	90.06	81.87
6	70.81	61.15	—	25.25	84.23	74.71	90.70	81.14
7	71.49	60.48	37.09	24.59	84.98	73.91	91.45	80.42
8	—	59.74	37.76	—	85	—	92.18	79.68
9	72.95	59.02	38.51	23.15	86.43	72.49	92.90	78.81
10	—	58.28	39.20	22.44	—	71.73	93.61	78.24
11	—	57.47*	39.96	21.65	—	70.96	94.34	77.51
12	75.02	56.70	40.74	20.97	—	70.22	95.02	76.68
13	75.70	56.01	41.43	20.22	89.17	69.46	95.76	75.97
14	76.45	55.23	42.11	19.47	89.89	68.80	96.47	75.22
15	77.16	54.43	42.82	18.77	90.54	67.94	97.14	74.46
16	77.90	53.68	43.50	18.02	91.27	67.19	97.80	73.71
17	78.68	52.98	44.27	17.25	91.94	66.47	98.49	72.87
18	79.31	52.23	44.98	16.48	92.65	65.69	99.11	72.03
19	80.09	51.52	45.69	15.70*	93.40	64.93	99.82	71.27
20	80.75	50.77	46.42	14.92	94.09	64.16	10800.52	70.52
21	81.41	50.00	47.07	14.23	94.82	63.40	1.20	69.76
22	82.15	49.22	47.81	13.37	95.54	62.64	1.88	68.98
23	82.90	48.50	48.54	12.78	96.23	61.83	2.52	68.18
24	83.57	47.72	49.24	11.84	—	61.08	3.20	67.41
25	84.33		49.96*	11.10*	—	60.36	3.85	66.59
26	84.97		—	10.38*	98.36	59.60	4.51	65.87
27	85.56		—	9.61	—	58.81	5.22	65.09
28	86.24		51.86	8.79	—	58.03	5.98	64.31
29			52.55	8.00	—	57.30	6.69	63.49
30			53.28	7.25	10701.31			62.73
31			54.01	6.50	2.02			
32			54.77		2.74			
33			55.51		3.45			
34					—			
35					4.95			
36					5.66			
37					6.39			
38					7.08			

* Lines starred or absent are obscured or interfered with by H_2O lines.

dicular to the figure axis. Accordingly the expected rotation-vibration bands are of the hybrid type having both a parallel and a perpendicular component. Of the six bands observed both parallel and perpendicular components are present in four, one shows only parallel, and one only perpendicular structure.

The approximate formula for the sub-band origins in a parallel band is:[6]

$$\nu_0^{\text{sub}}=\nu_0+[(A_v'-A_v'')-(B_v'-B_v'')]K^2,$$

where $A=h/(8\pi^2cI_A)$ and $B=h/(8\pi^2cI_B)$. Single primes refer to the upper, double primes to the lower state.

In HNCO the A_v' and A_v'' values are very different because of the marked dependence of the HNC angle on vibrational quantum number, whereas the B_v' and B_v'' values are not very different from each other. $(A_v'-A_v'')-(B_v'-B_v'')$ is therefore large, and accordingly the parallel bands consist of a series of sub-bands with their origins quite well separated. In many cases however the P and R structures of these sub-bands overlap those of their neighbors.

[6] G. Herzberg, *Infrared and Raman Spectra of Polyatomic Molecules*. (D. Van Nostrand Company, New York, 1945), p. 419.

Notation

The conventional notation for rotational lines in a symmetric top has been used. P, Q or R denotes the ΔJ value -1, 0 or $+1$; P, Q or R used as a left superscript indicates the ΔJ value with the same convention. The K value for the lower state is indicated by a subscript number. The lower state J value is placed in brackets after the sub-band and branch symbol. Thus ${}^{Q}R_4(6)$ is the line with $J=6$ in the R branch of the sub-band with $K=4$ in a parallel ($\Delta K=0$) band.

In the case of the unresolved Q branches consisting of almost superposed lines of all J values the bracket is omitted so that ${}^{P}Q_3$ is the unresolved Q branch of a perpendicular band ($\Delta K=-1$) with $K=3$ in the lower state.

B-Values

The band $2\nu_1+\nu_2+\nu_3$ consists of four almost completely separated sub-bands with $K=1$, 2, 3 and 4. The $K=0$ sub-band is too weak for measurement and therefore an approximate band center only is given.

In spite of some overlapping in this region by the

TABLE III(b). $3\nu_1$. Observed wave numbers.

	$K=0$		$K=1$		$K=2$		$K=3$		$K=4$		$K=5$	$K=6$
$^{Q}Q_K$	10145.64		10138.38		10117.50		10086.44		10047.64		9993.36	9936.46
$^{P}Q_K$			10115.43*		10050.17		9975.15		9894.51			
$^{R}Q_K$	10168.44		10205.85		10228.45		10239.11					
J	$^{Q}P_0(J)$	$^{Q}R_1(J)$	$^{Q}P_1(J)$	$^{P}P_1(J)$	$^{Q}P_2(J)$	$^{Q}P_3(J)$	$^{P}R_3(J)$	$^{P}P_3(J)$	$^{Q}R_4(J)$	$^{Q}P_4(J)$	$^{Q}P_5(J)$	
4		10142.03										
5	10141.32	42.74										
6	40.55	43.42	10133.92			10081.73			10052.88	10043.27		
7	39.75	44.15	33.19			80.93		9970.21	53.47	42.51		
8	39.04	44.86	32.46					69.45	54.07	41.76		
9		45.55	31.74		10110.99			68.65	—	40.99		
10		46.24	30.99			79.01		67.88	—	40.27		
11		46.93	30.23		9.51	78.28		67.11	—	39.49		
12		47.64	29.40		8.74	77.55		66.31	57.17	38.74	9984.59	
13		48.32	28.58		7.87	76.77		65.53	57.71	38.00	83.84	
14		48.99	27.80	10105.23	7.12	76.09			58.28	37.24	83.12	
15		49.66	27.04	4.45	6.42	75.32	9986.40		—	36.48	82.42	
16		50.33	26.27		5.74	74.52	87.06		—	35.70	81.77	
17		50.84	25.51		4.89	73.73	87.76	62.68	60.63	34.94	80.95	
18		51.53	24.74		—	72.95	88.41		61.16	34.17	80.19	
19		52.20	23.93		3.27	72.18	89.19		61.70	33.37	79.42	
20		52.68	23.08		2.52	71.35	89.81			32.61	—	
21		53.33	22.26		1.80	70.55				31.81	—	
22		53.99	21.44		0.83		9991.06			31.04	—	
23		54.65	20.66		10099.99	69.69	91.73			30.27	—	
24		55.32	19.85		99.28	68.92	92.24			29.45	74.54	
25		55.98	19.06		98.53	68.11	92.86			28.59	73.54	
26		56.64	18.10		97.62	67.30				27.73	72.63	
27		57.28	—		96.82	66.50				26.90	71.79	
28		57.91	16.46		96.02	65.72				26.11	70.98	
29		58.53	15.62		95.22	64.91				25.29	70.20	
30		59.16	14.79		94.42	63.25				24.57	69.45	
31		—	13.93		93.66	62.48				23.78	68.65	
32		—	13.26		92.83					22.73	67.88	
33		61.35			91.99					21.94	66.31	
34	18.45	61.99			91.19	59.84				21.07	65.52	
35		62.59			90.39	59.06				20.42	—	
36	16.86	63.24			89.39					19.57	—	
37	16.04	63.88			88.58					18.87	—	
38	15.24	64.51*			87.76	56.41				18.12	—	
39	14.54	65.23*			—	55.63				17.37	—	
40	13.62	65.94*			—	54.85					61.94	
41		66.59*			85.27	—					61.11	
42		67.23*			84.36	—					60.27	
43					83.45	52.11					59.42	
44					82.48	51.33				12.95	58.54	
45											57.74	
46												

* Lines starred or absent are obscured or interfered with by H_2O lines.

10613.12 cm^{-1} water band the separated sub-bands were the most accurate source of B values since sub-band overlap was much worse in all the other bands observed. The B values obtained from this band were accordingly used for the calculation of molecular constants. Line positions are given in Table IIIa and a photograph of part of this band is shown in Fig. 2a. Combination differences $\Delta_2F''(J)$, from which have been subtracted values calculated using an approximate $4B$ value of 1.40, are plotted in Fig. 3.

The fine structure of the bands $3\nu_1+\nu_4$, $3\nu_1$, and $2\nu_1+\nu_2$ was also analyzed. Line positions are given in Table IIIb, IIIc, and IIId, and in Table IV are shown the ground state second differences calculated from them. The results confirm very well the values already obtained from the band $2\nu_1+\nu_2+\nu_3$.

It is noteworthy that within the accuracy of these measurements the B values are independent of K although in principle a slight dependence on K is to be expected. The smallness of this effect is to be explained by the fact that the contribution of the H atom (the only one appreciably displaced as K changes) to the B value is very small.

In the determination of B values for the upper states, combination differences were not determined. Instead the combination sum relation $R(J-1)+P(J)=2\nu_0+2(B'-B'')J^2$ was used. A plot of $R(J-1)+P(J)$ against J^2 gives a straight line of slope $2(B'-B'')$. Once the lower state B value is known that of the upper state may thus be accurately determined.

A Values

As might be expected, the small moment of inertia, depending as it does largely on the HNC angle, is very sensitive to vibrational and rotational excitation.

Ground-state first differences $\Delta_1F(K)$ were obtained

TABLE III(c). $2\nu_1+\nu_2$. Observed wave numbers.

	$K=0$		$K=1$		$K=2$		$K=3$
^QQ_K			9157.93		9143.82		9125.49
^PQ_K			9132.44		9069.36		9001.60
^RQ_K	9187.83		9232.01		9267.63		—
J	$^QR_0(J)$	$^QP_0(J)$	$^QR_1(J)$	$^QP_1(J)$	$^QR_2(J)$	$^QP_2(J)$	$^QP_3(J)$
5	9167.07		9162.36				
6	67.76		62.97				
7	68.41		63.59				
8	69.04		64.31				
9	69.76		65.03	9151.08			
10	70.43		65.70	50.34		9136.44	
11	71.06		66.40			35.11	
12	71.73					34.87	
13	72.40	9152.72			9153.58	34.00	
14	73.03	51.83		46.89	54.30	33.18	9110.54
15	73.52			46.09	54.99		9.73
16	74.10			45.25	55.56	31.51	8.88
17	74.73	49.55		44.43	56.13	30.72	7.29
18	75.32	48.64		—	56.74	29.90	6.44
19	75.95	47.71		42.81	57.36	28.99	5.55
20	76.57			42.14	—	28.24	4.69
21	77.09			41.23	58.52	27.24	3.74
22	77.65			40.39	59.10	26.41	2.90
23	78.23			39.56	59.75	—	1.99
24	78.78			38.69	60.24	24.69	1.10
25	79.27			37.82	60.78	23.74	0.24
26	79.83			37.15	61.24	22.85	9099.46
27	80.38				61.90	21.97	
28	80.93					21.12	
29						20.21	
30						19.19	
31						18.23	
32						17.37	
33						16.46	
34						15.45	
35						14.47	
36			81.48			13.41	
37			82.45			12.39	
38			83.01				
39			83.52				
40			83.97				
41			84.47				

TABLE III(d). $3\nu_1+\nu_4$. Observed wave numbers.

	^QQ_K	$K=1$ 10965.81	
	J	$^QR_1(J)$	$^QP_1(J)$
	5	10968.23	10960.16
	6	68.94	59.49
	7	69.65	58.74
	8	70.37	58.00
	9	71.07	57.22
	10	71.73	56.42
	11	72.44	55.69
	12	73.16	54.92
	13	73.84	54.15
	14	74.54	53.38
	15	75.24	52.54
	16	75.86	51.84
	17	76.55	51.08
	18	77.24	50.28
	19	77.87	49.51
	20	78.47	48.73
	21	79.20	47.98
	22	79.91	47.17
	23	80.55	46.37
	24		45.63
	25		44.80

TABLE III(e). Resolved fundamentals. Observed wave numbers.

K	^PQ_K	$^{\nu_4}Q_K$	^RQ_K	^PQ_K	$^{\nu_1}Q_K$	^RQ_K
0	—	c.798	830.2		3531	—
1	768.9	—	929.5			3609
2	711.5	840.6	1030.6	3440		c.3660
3	698.5	887.2	1129.0	3381		c.3695
4		936.8	1219.0	3322		c.3723
5		982.0		3260		
6		1025.0				
7		1066(?)				

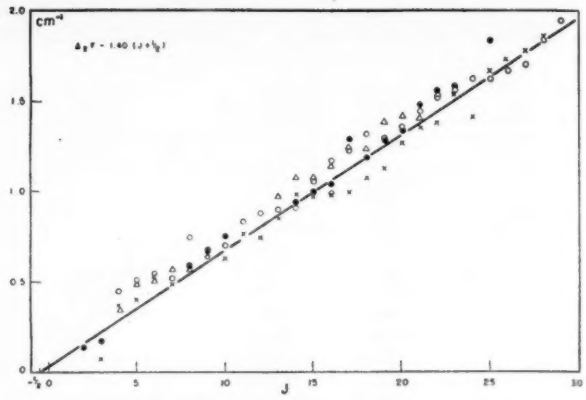

FIG. 3. Second difference curve for the band $2\nu_1+\nu_2+\nu_3$ at 10525 cm^{-1} with $1.40(J+\frac{1}{2})$ subtracted to allow a large scale plot. △ parallel sub-band with $K=1$. × parallel sub-band with $K=3$. ● parallel sub-band with $K=2$. ○ parallel sub-band with $K=4$.

from the hybrid bands at 10145.1 cm^{-1} and 9162 cm^{-1} by the two relationships

$$F''(J,K+1)-F''(J,K)={}^RQ_K-{}^QQ_{K+1}$$
$$F''(J,K+1)-F''(J,K)={}^QQ_K-{}^PQ_{K+1}$$

which were both used, to give a check on the assignments. The energy level diagram for the 10145 cm^{-1} band is shown in Fig. 4. A few lines in the incompletely analyzed band at 13217.2 cm^{-1} were fitted satisfactorily to these ground-state values, and so was the coarse

TABLE IV. Comparison of ground-state combination differences $\Delta_2F(J)$ for different bands.

J	Calculated values based on $2\nu_1+\nu_2+\nu_3$ $B=0.36645$	10145 cm^{-1} $K=1$	9162 cm^{-1} $K=2$	10988 cm^{-1} $K=1$
1	2.20			
2	3.67			
3	5.13			
4	6.60			
5	8.06	8.11		
6	9.53	9.54		9.50
7	10.99	10.95		10.93
8	12.46	12.40		12.44
9	13.93	13.87		13.96
10	15.39	15.32		15.38
11	16.86	16.83		16.81
12	18.32	18.35		18.29
13	19.79	19.85		19.78
14	21.25	21.28		21.30
15	22.72	22.72	22.79	22.65
16	24.19	24.15	24.27	24.15
17	25.65	25.59	25.66	25.68
18	27.12	26.92	27.14	27.04
19	28.58	28.45	28.50	28.51
20	30.05	29.93	30.12	29.89
21	31.52	31.26*		31.30
22	32.98	32.67		32.83
23	34.45	34.14	34.41	34.39
24	35.91	35.59	36.01	35.75
25	37.38	37.23	37.39	
26	38.84		38.80	
27	40.31	40.17	40.12	
28	41.78	41.66	41.70	
29	43.24	43.12		
30	44.71	44.60		

* Lines in P branch with $J=22$ or more are unreliable because of overlap by lines of $K=2$ sub-band.

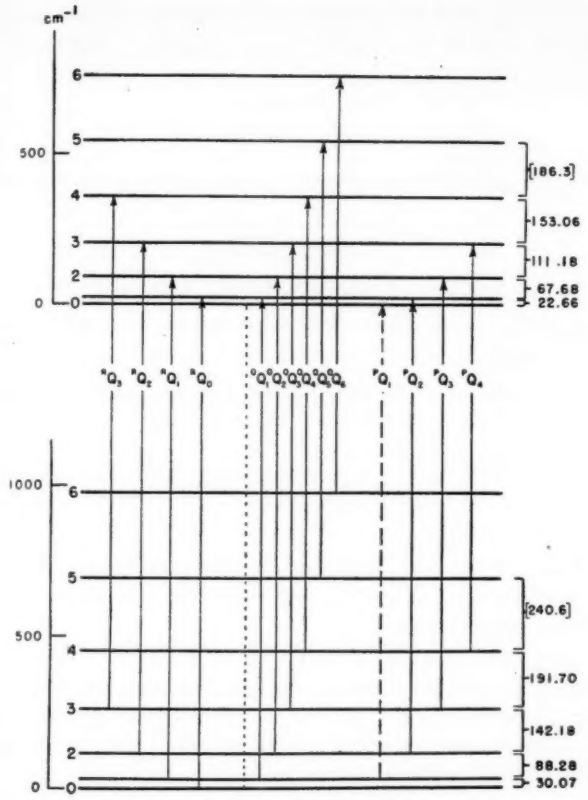

FIG. 4. Energy level diagram for the band $3\nu_1$ at 10145.1 cm^{-1}. The value of K is shown on the left and the spacing in wave numbers between levels of different K but the same J value is indicated on the right.

rotational structure of the two fundamentals ν_1 and ν_4 (Table V).

The Slawsky-Dennison formula for the energy levels of a non-rigid symmetric top is

$$F(J,K)=BJ(J+1)+(A-B)K^2-D_JJ^2(J+1)^2 -D_{JK}J(J+1)K^2-D_KK^4.$$

In view of the observed independence of the large moment of inertia on K in the present case it is permissible to neglect the cross term involving D_{JK} and use the simpler form

$$F(J,K)=BJ(J+1)-(A-B)K^2-D_JJ^2(J+1)^2-D_KK^4$$

from which one obtains

$$\frac{F(J,K+1)-F(J,K)}{K+\frac{1}{2}}=[2(A-B)-D_K]-D_K(2K+1)^2.$$

A plot of $[F(J,K+1)-F(J,K)]/K+\frac{1}{2}$ against $(2K+1)^2$ should therefore give a straight line from the slope of which, with B already known, A, and D_K could be calculated.

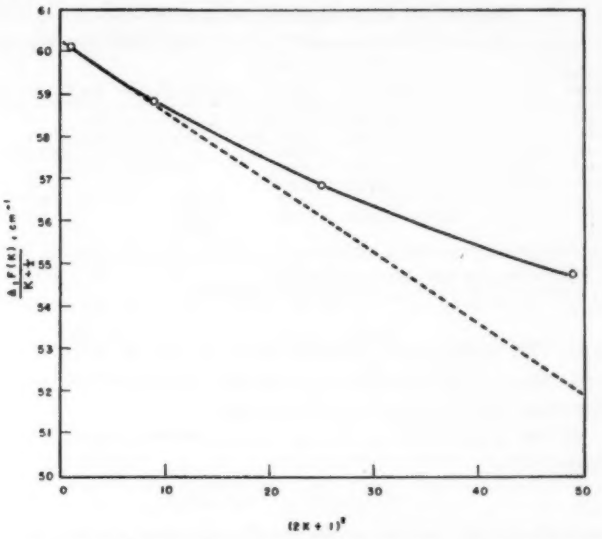

FIG. 5. Solid line. Plot of $[\Delta_1F''(K)/K+\frac{1}{2}]$ against $(2K+1)^2$. Dotted line. Straight line obtained by subtraction of $\frac{3}{8}H_K+5H_K(K+\frac{1}{2})^2+6H_K(K+\frac{1}{2})^4$ from $[\Delta_1F''(K)/K+\frac{1}{2}]$.

A straight line plot was in fact obtained for most of the upper states which were examined, but was not satisfactory in the ground state. Here the dependence of moment of inertia on K value appears to be much greater than in the excited states.

For the ground state it was found necessary to introduce a sixth-power term into the energy level expression. Again the assumption was made that no cross terms in J and K with coefficients of the kind H_{JK} are present.

The separation between successive levels of equal J is then given by

$$\frac{F(J,K+1)-F(J,K)}{K+\frac{1}{2}}=[2(A-B)-D_K+\tfrac{3}{8}H_K] -(4D_K-5H_K)(K+\tfrac{1}{2})^2+6H_K(K+\tfrac{1}{2})^4.$$

A plot of $[F(J,K+1)-F(J,K)]/K+\frac{1}{2}$ against $(K+\frac{1}{2})^2$ gives a quadratic curve with intercept $2(A-B)+(3H_K/8)-D_K$. Figure 5 shows the plot of $[F(J,K+1)-F(J,K)]/K+\frac{1}{2}$ against $(2K+1)^2$ for the ground state, together with the straight line relationship obtained by the introduction of the terms containing H_K.

A, B, D, and H values obtained from the various bands are collected together in Table VI for compari-

TABLE V. Combination differences $\Delta_1F(K)$.

	Ground state					Upper state					
K	ν_4	ν_1	$2\nu_1+\nu_2$	$3\nu_1$	$4\nu_1$	ν_4	ν_1	$2\nu_1+\nu_2$	$3\nu_1$	$4\nu_1$	$2\nu_1+\nu_2+\nu_3$
0	c.29.8	—	30.02	30.07		31.2	c.28	24.49	22.66	19.9	70.63
1	88.9	[88.3]*	88.38	88.28	88.43	128.8	83	74.28	67.48	59.6	153.20
2	142.7	141.7	142.17	142.18	141.70	188.8	136	123.84	111.18	99.2	190.86
3	192.2	196.3	191.70	[192]*		241.5	181		153.06	138.5	298.67
4	237	239	[242.14]*			285.8			[186.34]*		

* Values in brackets obtained by extrapolation.

TABLE VI. Rotational constants of HNCO.

Constant	Band ν_4	ν_1	$2\nu_1+\nu_2$	$3\nu_1$	$2\nu_1+\nu_2+\nu_3$	$3\nu_1+\nu_4$	$4\nu_1$
B''	—	—	0.3667	0.3656*	0.36645	0.3658	—
B'	—	—	0.3631	0.3644*	0.3657	0.3648	—
A''	30.1	—	30.55	30.60	—		30.65
D''	0.159	—	0.163	0.167	—		—
H''	0.0027	—	0.0028	0.00275	—		—
A'		28.40	25.23†	22.93	76.15†		20.27†
D'		0.09	0.010†	0.028	5.65†		0.012†
H'					0.23†		

* Error may be large because of overlap.
† Error may be large because few lines available.

son. The finally used ground-state A and B values are not means of all observed values but are taken from the more accurately measurable bands.

If we assume that $B_{v_1v_2}...$ fits a relationship of the form,

$$B_{v_1v_2\ldots v_i}=B_{000\ldots}-\sum_i\alpha_i v_i,$$

we obtain the following values for the α's: $\alpha_1=0.00067$ cm^{-1}; $\alpha_2=0.00199$; $\alpha_3=0.00258$; $\alpha_4=-0.00030$; α_5 not obtained; α_6 not obtained.

The A values as might be expected from their very strong dependence on vibrational level cannot be fitted to so simple a formula. The values given in Table VI for the bands $v_1\nu_1$ can be fitted approximately to the formula

$$A_{v_1}=A_0-v_1\alpha_1+v_1^2\gamma_{11},$$

where $\alpha_1=2.339$, $\gamma_{11}=0.05433$.

Using this relationship to predict A_1 gives a value 28.05 instead of the observed 28.40; but the latter value is very sensitive to small errors in the measurement of the positions of the Q branches of the parallel component from which it was obtained and its accuracy cannot be expected to be better than ±0.5 cm^{-1}, the random error probable on the Perkin-Elmer results.

The results given above show that as the angular momentum around the NCO axis is increased (increasing K) the HNC angle which is obtuse decreases just as the obtuse angle between two hinged rods would decrease on rotation of the system about an axis along the length of one of them.

The effect of vibrational excitation on the shape of the molecule is less easy to interpret. Excitation of the N—H stretching vibration decreases the A value, while excitation of the N—H bending vibration increases it very considerably. In the case of the vibration $2\nu_1+\nu_2+\nu_3$ the effect is very complicated. Excitation with no angular momentum about the NCO axis apparently leads to a considerable increase in the bond angle over its value in the ground state. With increasing K the angle then rapidly decreases towards this ground state value. This explains the abnormally large values of A', D', and H' found for this band.

D. MOLECULAR STRUCTURE

For the calculation of the moments of inertia, we use the following ground state rotational constants

$$A_0=30.57 \quad \bar{B}_0=0.36645 \quad (\bar{B}=\tfrac{1}{2}(B+C)).$$

Assuming that the molecule is a planar, nearly symmetric top, we find easily (see for example reference 6, p. 437)

$$B_0=0.36865$$
$$C_0=0.36435$$

and the principal moments of inertia of the molecule are

$$I_A=0.9153_7\times10^{-40}$$
$$I_B=75.90_7\times10^{-40}$$
$$I_C=76.82_4\times10^{-40},$$

where the relations $I_A=[27.983\times10^{-40}]/A_0$, etc., have been used.

The secular equation for the principal moments of inertia of a planar molecule takes the form

$$\begin{vmatrix} I_{xx}-I & -I_{xy} & 0 \\ -I_{xy} & I_{yy}-I & 0 \\ 0 & 0 & I_{zz}-I \end{vmatrix}=0,$$

where the I_{xx}, etc., are the moments of inertia about Cartesian axes and I_{xy}, etc., are the corresponding products of inertia.

Assuming the C=N and C=O distances to be each 1.19A, the values given by Eyster, Gillette, and Brockway,[7] we have calculated the values of the remaining two parameters which give the I_{xx}, etc., values fitting this equation. These values are

$$r(\text{N—H})=1.00_0\text{A}$$
$$\measuredangle\text{HNC}=125.5°.$$

The angle is much larger than that found in singly bonded nitrogen compounds, and suggests that the bonds are formed from sp^2 hybrid orbitals. Nitrogen in its ground state ($1s^22s^2p_xp_yp_z$) has only p orbitals for bond formation, and because of their strong directional properties, a double bond involving two such p orbitals is very unlikely.

Promotion of a $2s$ electron to a p level makes double bond formation easier, but because the promotional energy is not offset by increased bond forming power, compounds involving such double bonds will always be extremely unstable with respect to singly bonded nitrogen compounds. This expectation is borne out by the fact that almost all double-bonded nitrogen compounds are either violently explosive or readily polymerize to compounds containing only single bonds.

ACKNOWLEDGMENTS

The author would like to express his thanks to Dr. G. Herzberg who suggested this problem and provided much-needed advice and encouragement and to Dr. A. E. Douglas, without whose continued help everything would have been much harder. Thanks are also offered to the Physics Department of the University of Saskatchewan for the loan of the grating used for this work.

[7] Eyster, Gillette, and Brockway, J. Am. Chem. Soc. **62**, 3236 (1940).

THE JOURNAL OF CHEMICAL PHYSICS VOLUME 18, NUMBER 12 DECEMBER, 1950

Rotation-Vibration Spectra of Diatomic and Simple Polyatomic Molecules with Long Absorbing Paths

VI. The Spectrum of Nitrous Oxide (N_2O) below 1.2μ

G. HERZBERG AND L. HERZBERG
National Research Council, Ottawa, Canada

(Received August 16, 1950)

The photographic infra-red spectrum of N_2O has been investigated with absorbing paths up to 4500 m atmos. Thirty-four absorption bands have been found of which twenty-three have been measured and analyzed in detail. Improved vibrational constants ω_i^0 and x_{ik} have been determined which give a fair representation of all the bands. The remaining deviations which are outside the present limits of error are due to the effect of Fermi resonance between ν_1 and $2\nu_2$.

Precise values of the rotational constants $B_{v_1v_2v_3}$ have been determined for almost all vibrational levels involved in the observed bands. For the lowest vibrational level the six most accurately measured bands yield $B_{000}=0.4191_{25}$ cm^{-1}. In this case also the rotational constant D_{000} representing the influence of centrifugal stretching has been determined: $D_{000}=0.19_3\times10^{-6}$ cm^{-1}. The value of B_{000} is larger by 0.000091 than that derived from microwave data. From the $B_{v_1v_2v_3}$ values the following values for the rotational constants α_i have been obtained,

$$\alpha_1=0.0017_0 \quad \alpha_2=-0.0002_2 \quad \alpha_3=0.0033_9.$$

These values allow the determination of the rotational constant in the equilibrium position $B_e=0.4214_5$ cm^{-1} from which the moment of inertia in the equilibrium position is found to be $I_e=66.39_7\times10^{-40}$ g cm^2. The deviations of the individual $B_{v_1v_2v_3}$ values from those obtained from the formula $B_{v_1v_2v_3}=B_e-\alpha_1(v_1+\frac{1}{2})-\alpha_2(v_2+1)-\alpha_3(v_3+\frac{1}{2})$ are appreciably larger than would correspond to the errors of measurements and must be ascribed to the effect of the Fermi resonance.

A. INTRODUCTION

THE rotational fine structure of the infra-red spectrum of nitrous oxide (N_2O) was first investigated by Plyler and Barker.[1] Their observation of bands with simple P and R branches established the linear structure of the N_2O molecule, and the absence of an intensity alternation showed that the molecule is not symmetrical like CO_2, but has the structure N—N—O (point group $C_{\infty v}$).

Plyler and Barker derived a value[2] of $66.9_1\times10^{-40}$ g cm^2 for the moment of inertia of the N_2O molecule in the lowest vibrational level. More recently a much more precise value of $66.779_8\times10^{-40}$ g cm^2 has been obtained by Coles and his collaborators[3] from the microwave absorption spectrum of nitrous oxide.

For an exact calculation of internuclear distances it is necessary to know the rotational constant B_e in the equilibrium position not only for the most abundant isotopic species but also for at least one other isotopic molecule (e.g. $N^{15}N^{14}O^{16}$). The microwave spectrum gives in general only B_{000}, the rotational constant for the lowest level, which is somewhat smaller than B_e, and it gives B_{000} only if the influence of centrifugal stretching (i.e. the rotational constant D) is neglected. The effect of D is always very small but must be considered when one wants to make use of the full accuracy of the microwave data.

It was the primary purpose of the present work to determine a sufficient number of $B_{[v]}$ values so that B_e could be obtained at least for the most abundant isotopic molecule ($N^{14}N^{14}O^{16}$), and in addition it was planned to obtain an approximate value for the centrifugal stretching constant D. To this end the photographic infra-red spectrum of N_2O was investigated. Unforeseen difficulties arose on account of Fermi perturbations which cause our final B_e value to be somewhat less precise than was originally hoped for.

A second aim of this investigation was simply a better and more complete knowledge of the vibrational and rotational structure of the N_2O molecule. For very few molecules are sufficient data available that detailed formulas can be derived both for the vibrational levels and the rotational constants. N_2O appeared to be a promising example for which such formulas could be obtained and for which thus the effect of anharmonicity on the energy levels could be studied. In addition a knowledge of the higher rotational and vibrational constants is of importance for the calculation of the thermodynamic properties of N_2O.

One of the main results of this study is the conclusion that Fermi resonance plays a much more important role than is generally realized, even in cases in which the resonance is far from exact.

B. EXPERIMENTAL

The photographic infra-red absorption spectrum of N_2O was studied with the long absorbing path described in the first paper of this series.[4] The 22 m tube was filled with commercial N_2O at pressures up to 1 atmos. Absorbing paths up to 4500 m atmos. were used, corresponding to 200 traversals. For the stronger bands shorter path lengths and wherever possible reduced pressures were used in order to obtain sharper lines.

[1] E. K. Plyler and E. F. Barker, Phys. Rev. **38**, 1827 (1931); E. F. Barker, Phys. Rev. **41**, 369 (1932).

[2] The slight difference of this value from Plyler and Barker's original value (66.0×10^{-40}) is due to changes in the fundamental constants and to a more elaborate method of evaluation (see G. Herzberg, *Infrared and Raman Spectra of Polyatomic Molecules* (D. Van Nostrand Company, Inc., New York, 1945), p. 396.

[3] Coles, Elyash, and Gorman, Phys. Rev. **72**, 973 (1947); D. K. Coles and R. H. Hughes, Phys. Rev. **76**, 178 (1949).

[4] H. J. Bernstein and G. Herzberg, J. Chem. Phys. **16**, 30 (1948).

TABLE I. Band origins (ν_0), band heads (ν_h), and assignments of N_2O-bands observed in the photographic infra-red.

ν_0(vac) (cm^{-1})	ν_h(vac) (cm^{-1})	Intensity (arbitrary units)	Assignment	$o-c$† (2)	$o-c$† (3)
7998.5$_9$	8016.4$_0$	15	$2\nu_1+2\nu_2+2\nu_3$	−15.99	+3.31
8083.97	8098.5$_6$	15	$3\nu_1+2\nu_3$	−14.13	−5.03
8276.4	8298.3$_6$	2	$3\nu_1+4\nu_2+\nu_3$	−27.3	−11.27
8376.39	8393.2$_9$	10	$4\nu_1+2\nu_2+\nu_3$	−23.59	−1.49
8452.6$_9$	8470.3$_5$	3	$5\nu_1+\nu_3$	−0.06	+3.14
8657.30	8669.84	8	$\nu_2+4\nu_3-\nu_2$	−21.90	+2.10
8714.15	8726.60	30	$4\nu_3$	−14.85	+0.15
—	8752(?)	0.1	$4\nu_2+3\nu_3$	(−2)	(+2)
8877.07	8892.41	8	$\nu_1+2\nu_2+3\nu_3$	−19.26	+3.54
—	8956(?)	2	$2\nu_1+\nu_2+3\nu_3-\nu_2$	(−11)	(+17)
8976.49	8988.84	20	$2\nu_1+3\nu_3$	−18.11	−2.41
9108.39	—	1	$2\nu_1+4\nu_2+2\nu_3$	−24.13	−5.63
9219.12	9233.9$_0$	5	$3\nu_1+2\nu_2+2\nu_3$	−24.66	+3.24
9295.04	9308.4$_6$	5	$4\nu_1+2\nu_3$	−16.26	−4.15
9517.9$_2$	9534.7$_7$	0.5	$4\nu_1+4\nu_2+\nu_3$	−43.90	−15.90
9606.3$_5$	9620.8$_4$	1.5	$5\nu_1+2\nu_2+\nu_3$	−35.98	−7.08
—	9783.9	0.2	$2\nu_2+4\nu_3$	(−12.5)	+13.5
—	9850.1$_3$	0.5	$\nu_1+\nu_2+4\nu_3-\nu_2$	(−14.22)	(+19.58)
9888.53	9899.44	3	$\nu_1+4\nu_3$	−20.87	+1.13
10079.66	10092.80	2	$2\nu_1+2\nu_2+3\nu_3$	−26.22	+7.18
10163.6$_8$	10174.93	4	$3\nu_1+3\nu_3$	−24.47	−3.77
—	10441.7	0.5	$4\nu_1+2\nu_2+2\nu_3$	(−24.8)	(+11.7)
10815.35	10826.19	4	$5\nu_3$	−27.15	+0.85
10820.1$_6$	10833.05	1.5	$4\nu_2+4\nu_3$	−25.36	−2.36
—	11283.2	0.1	$3\nu_1+2\nu_2+3\nu_3$	(−25.7)	(+19.2)
—	11356.9	0.1	$4\nu_1+3\nu_3$	(−18.3)	(+7.4)
11544.5$_6$	11557.4	0.1	$4\nu_1+4\nu_2+2\nu_3$	−58.86	−11.96
11629.6$_3$	11640.9	0.1	$5\nu_1+2\nu_2+2\nu_3$	−53.05	−7.95
—	11855.8	0.1	$2\nu_2+5\nu_3$	(−29.2)	(+6.3)
—	11910.4	0.2	$\nu_1+\nu_2+5\nu_3-\nu_2$	(−28.9)	(+22.2)
11964.3$_2$	11973.2	2	$\nu_1+5\nu_3$	−32.43	+4.57
—	12820.81	0.15	$6\nu_1+2\nu_2+2\nu_3$	(−71.57)	(−17.87)
			$\nu_2+6\nu_3-\nu_2$	(−32.99)	(+25.21)
12891.1$_0$	12899.25	1	$6\nu_3$	−37.40	+7.30
—	14016.7	0.2	$\nu_1+6\nu_3$	(−39.9)	(+15.8)

† $o-c$ values in brackets refer to band heads rather than band origins and are therefore from 8 to 18 cm^{-1} higher than if band origins had been used.

The spectra above 8500A were taken in the first order, those below 8500A in the second order of the Yerkes 21-ft grating spectrograph (dispersion 2.5 and 1.25A/mm respectively). Second-, third- and fourth-order Fe lines were used as standards. A number of N_2O bands are overlapped by H_2O bands. It was usually easy to recognize the H_2O lines particularly when use was made of the tables of the solar spectrum by Babcock and Moore.[5] The relative positions of unblended lines within a given band are believed to be accurate to ± 0.03 cm^{-1}, except for faint lines; the absolute accuracy is somewhat less (probably ± 0.08 cm^{-1}) because of the possibility of a very slight shift between absorption spectrum and comparison spectrum.

C. OBSERVED SPECTRUM

A large number of absorption bands were found in the photographic infra-red. The band origins and heads of these bands are listed in Table I together with estimated intensities. In a few cases of very weak bands only the heads were measured.

Figure 1 shows as an example a spectrogram of the 8714 cm^{-1} band ($4\nu_3$). This band and all other observed bands in the photographic infra-red have P and R branches only, that is they are of the $\|$ type. A Q branch is expected to be absent in the case of $\Sigma-\Sigma$-transitions and to be very weak and usually not observed in the case of $\Pi-\Pi$-transitions. Thus far bands with strong

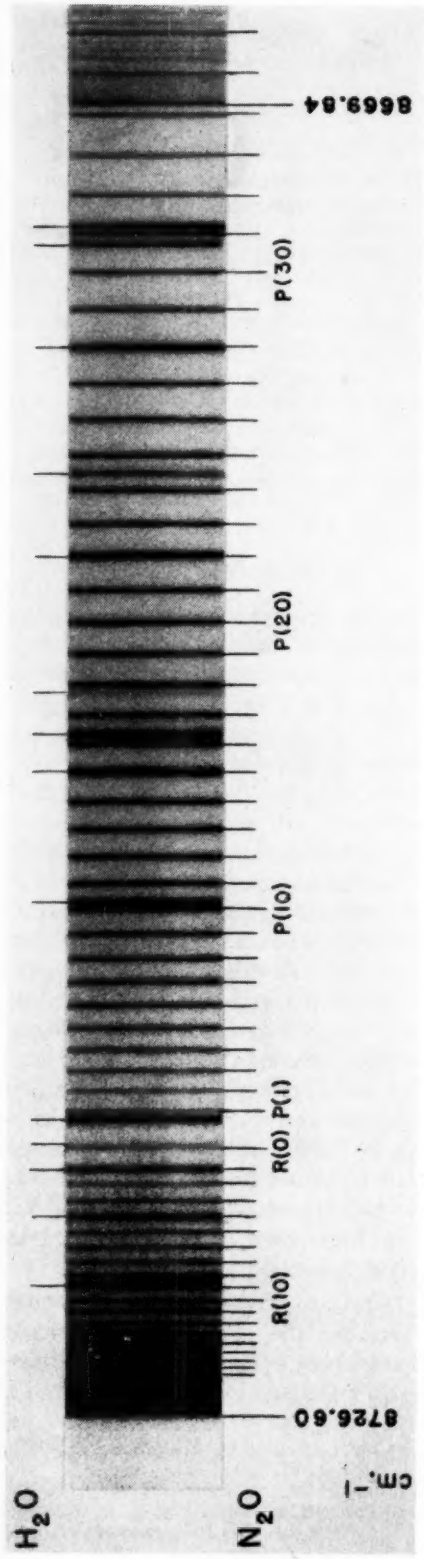

FIG. 1. $4\nu_3$ band of N_2O at 11500A. The positions of the N_2O lines and heads are indicated below the spectrogram, the overlapping H_2O lines above it. The head at the right is due to the "hot" band $\nu_2+4\nu_3-\nu_2$.

[5] H. D. Babcock and C. E. Moore, *The Solar Spectrum, λ6600 to λ13495* (Washington, D. C., 1947).

TABLE II. Wave numbers of the lines in the N_2O bands (ν_{vac}, cm^{-1}).

J	$2\nu_1+2\nu_2+2\nu_3$ $\nu_0=7998.5_9$ cm^{-1} R(J)	P(J)	$3\nu_1+2\nu_3$ $\nu_0=8083.97$ R(J)	P(J)
2			8086.3_2	8082.3_2
3			87.1_5	81.3_8
4			87.8_4	80.4_9
5	8003.2_8		88.4_9	79.5_2
6	04.0_3		89.2_2	78.6_2
7	04.6_2		89.8_4	77.5_8
8	05.2_9		90.4_7	76.6_0
9	05.9_5		91.0_4	75.6_0
10	06.5_5	7989.3_1	91.6_0	74.5_0
11	07.2_0	88.3_6	92.1_6	73.4_5
12	07.7_8	87.3_0	92.7_2	72.3_2
13		86.2_4	93.2_3	71.2_7
14		85.1_4	93.7_0	70.0_9
15		84.0_7	94.1_9	68.9_4
16		83.0_2	94.6_2	67.7_6
17		81.8_0		66.4_9
18		80.6_6		65.3_0
19		79.4_9		64.0_2
20		78.3_8		62.7_5
21		77.0_2		61.4_3
22		75.8_4		60.0_8
23		74.5_7		58.7_5
24		73.3_6		57.3_6
25		72.0_9		55.9_3
26		70.7_8		54.5_1
27				53.0_6
28				51.6_3
29				50.0_8
30				48.6_2
31				47.0_1
32				45.5_0
33				43.9_0
34				42.3_0
35				40.6_9
36				39.0_4
37				37.3_5
38				35.6_4

TABLE II—*Continued.*

J	$3\nu_1+4\nu_2+\nu_3$ $\nu_0=8276.4$ R(J)	P(J)	$4\nu_1+2\nu_2+\nu_3$ $\nu_0=8376.39$ R(J)	P(J)
3			8379.3_3	8373.8_4
4			80.2_6	72.9_1
5			80.9_9	71.9_9
6			81.6_9	71.0_8
7			82.3_5	70.1_1
8			83.0_3	69.1_8
9			83.6_2	68.1_2
10			84.2_9	67.0_9
11		8266.3_2	84.8_8	66.0_7
12	8285.9_8	65.3_1	85.4_4	64.9_8
13	86.5_1	64.2_4	85.9_9	63.9_2
14	87.1_5	63.2_5	86.5_3	62.8_0
15	87.7_2	62.1_5	87.0_7	61.7_3
16	88.3_4	61.2_4	87.5_3	60.5_4
17	88.9_3	60.2_3	88.0_2	59.3_8
18	89.4_2	59.0_1	88.4_5	58.2_1
19	89.9_5	57.9_4	88.9_0	57.0_2
20	90.5_1	56.7_5	89.3_2	55.8_0
21	90.9_5	55.5_6	89.6_9	54.5_6
22	91.5_0	54.3_7	90.0_4	53.2_9
23		53.3_7	90.4_4	52.0_4
24				50.7_1
25				49.4_2
26				48.0_3
27				46.6_4
28				45.2_6
29				43.8_8

Q branches ($\Pi-\Sigma$-transitions) have been observed for N_2O only in the ordinary infra-red.

Table II gives the wave numbers of the individual band lines of the majority of the bands. A few very weak bands which could not be analyzed properly have been omitted.

D. VIBRATIONAL ANALYSIS

The fundamentals of N_2O are $\nu_1=1285.0$, $\nu_2=588.8$ and $\nu_3=2223.5$ where ν_1 and ν_3 are the two $\parallel$ vibrations and ν_2 is the $\perp$ vibration.[6] The new photographic infra-red bands can be readily interpreted as overtone and combinations bands of these fundamentals. The assignments are given in column 4 of Table I. In Fig. 2 the observed transitions including those observed in the ordinary infra-red and Raman spectrum are represented in an energy level diagram.

Most of the observed bands correspond to transitions from the ground state to upper levels with even v_2, except a few weak bands accompanying bands of very high intensity. These weak bands obviously are "hot" bands (difference bands) arising from the lowest excited vibrational level ν_2 and leading to an upper state in which the vibration ν_2 is excited by one more quantum than in the upper state of the corresponding strong band. The observed shift between the "hot" and "cold" bands is due to the anharmonicity of the vibrations.

TABLE II—*Continued.*

J	$5\nu_1+\nu_3$ $\nu_0=8452.6_9$ R(J)	P(J)	$\nu_2+4\nu_3-\nu_2$ $\nu_0=8657.30$ R(J)	P(J)
0			8658.07*	
1			59.09*	
2			59.69	
3			60.41	8654.80*
4			61.05*	53.76
5	8457.2_0		61.78*	52.83
6	57.9_7		62.42	52.09*
7	58.7_3	8446.3_5	62.98*	50.87
8	59.2_8	45.4_7	63.67	49.85
9	59.9_6	44.4_2	64.24	48.76
10	60.5_6	43.4_6	64.78*	47.70
11	61.1_3*	42.3_6	65.17*	46.54*
12	61.7_4	41.3_4	65.75	45.45
13	62.2_3	40.2_3	66.23	44.27
14	62.8_4	39.1_7	66.63*	43.09
15	63.3_6	38.0_2	67.03	41.86
16	63.8_3	36.9_1	67.43	40.63
17	64.3_0	35.7_5	67.74*	39.35
18	64.9_6	34.5_4	68.11	38.03
19		33.3_0	68.40*	36.74*
20		32.1_0		35.34
21		30.8_1		33.96
22		29.6_6		32.55
23		28.3_4		31.12
24		27.0_6		29.63
25		25.8_1		28.24*
26		24.4_4		26.60
27		23.1_5		25.07
28				23.47
29				21.88
30				20.27
31				18.59

[6] See G. Herzberg, *Infrared and Raman Spectra of Polyatomic Molecules* (D. Van Nostrand Company, Inc., New York, 1945).

TABLE II—*Continued.*

	$4\nu_3$ $\nu_0=8714.15$		$\nu_1+2\nu_2+3\nu_3$ $\nu_0=8877.07$	
J	$R(J)$	$P(J)$	$R(J)$	$P(J)$
0	8714.96*			
1	15.84*	8713.31		
2	16.49	12.46	8879.12*	8875.25
3	17.23	11.56	80.16	74.51*
4	17.92*	10.64	80.90	73.55
5	18.60	09.69	81.63	72.64
6	19.25	08.70	82.30	71.69
7	19.87	07.71	82.89*	70.71
8	20.44	06.68	83.59	69.87*
9	20.89*	05.61	84.23	68.70
10	21.55	*	84.81	67.67
11	22.05	03.42	85.57*	66.61
12	22.54	02.27	85.92	65.53
13	22.98	8701.11	86.45	64.42
14	23.42	8699.90	86.96	63.29
15	23.81	98.62*	87.44	62.15
16	24.18	97.44	87.85*	61.11*
17	24.52	96.15	88.35	59.80
18	24.84	94.84	88.76	58.58
19	25.11	93.51	89.15	57.45*
20	25.31	92.15	89.51	56.09
21		90.76	89.87	54.86*
22		89.28*	90.22	53.50
23		87.87	90.53	52.17
24		86.42	90.77	50.82
25		84.93	91.04	49.44
26		83.40	91.28	48.08*
27		81.84		46.68
28		80.28*		45.22
29		78.65		43.82
30		77.01		42.29
31		75.35		40.74
32		73.66		39.24
33		71.93		
34		70.19		
35		68.40*		
36		66.63*		
37		64.78*		
38		62.98*		
39		61.05*		
40		59.09*		
41		57.17		
42		55.18		
43		53.21		
44		51.19		
45		49.13		
46		47.04		

* Lines marked by an asterisk are unresolved blends with an H_2O line or with another N_2O line.

TABLE II—*Continued.*

	$2\nu_1+3\nu_3$ $\nu_0=8976.49$		$2\nu_1+4\nu_2+2\nu_3$ $\nu_0=9108.39$	
J	$R(J)$	$P(J)$	$R(J)$	$P(J)$
0	8977.36			
1	78.10	8975.65		
2	78.83*	74.79		
3	79.56	73.90	9111.5_4	
4	80.26	72.98	12.3_3	9104.9_7
5	80.94	72.03	13.1_0	04.0_4
6	81.58	71.05	13.7_3	03.0_7
7	82.18*	70.06	14.4_7	02.1_0
8	82.79*	69.01	15.1_1	01.1_6
9	83.36	67.90	15.8_0	9100.2_5
10	83.88	66.90	16.4_2	9099.2_1
11	84.38	65.75	17.0_8	98.2_2
12	84.86*	64.59*	17.6_7	97.1_8
13	85.31	63.44	18.2_6	96.1_4
14	85.75	62.24	18.8_6	95.0_4
15	86.14	61.03	19.4_5	94.0_1
16	86.50	59.76	19.9_5	92.9_8
17	86.84	58.51	20.4_4	91.7_3
18	87.17	57.18	20.9_4	90.5_4
19	87.44	55.81*		89.4_8
20	87.70	54.47		88.2_9
21	87.93	53.07		87.1_8
22	88.15	51.66		85.8_9
23		50.29*		84.6_9
24		48.75		83.4_2
25		47.23		82.1_9
26		45.71		
27		44.15		
28		42.57		
29		40.97		
30		39.32		
31		37.69		
32		35.99*		
33		34.11		
34		32.50		
35		30.65		
36		28.89		
37		27.06		

It should be noted that the assignments of Table I are in conformity with the observed band structures (see above), that is, for all bands the upper state has the same species as the lower which is Σ^+ for $v_1=0$, $v_2=0$, $v_3=0$ and Π for $v_1=0$, $v_2=1$, $v_3=0$. To be sure, for configurations with $v_2>1$ several states of different species arise corresponding to $l_2=v_2$, v_2-2, v_2-4, $\cdots$ but only the ones with $l_2=0$ or 1 can combine with the lowest vibrational level.

If anharmonicity is taken into account and if no resonance occurs the vibrational levels of a linear triatomic molecule can be represented by

$$G_0(v_1, v_2, v_3)=\omega_1{}^0v_1+\omega_2{}^0v_2+\omega_3{}^0v_3+x_{11}v_1{}^2+x_{22}v_2{}^2+x_{33}v_3{}^2+x_{12}v_1v_2+x_{13}v_1v_3+x_{23}v_2v_3+g_{22}l_2{}^2+\cdots, \quad (1)$$

where l_2 is the quantum number of the vibrational angular momentum about the symmetry axis ($l_2=v_2$, v_2-2, $\cdots$ 1 or 0). For the vibrational constants ω_i, x_{ik} and g_{22} one obtains[6] from the previously known ordinary infra-red bands

$$\omega_1{}^0=1288.2_5\ \omega_2{}^0=588.0_5\ \omega_3{}^0=2237.2_5$$
$$x_{11}=-3.2_5\ \ x_{22}=-2.2_8\ \ x_{33}=-13.75 \quad (2)$$
$$x_{12}=+4.7_5\ \ x_{23}=-12.45\ x_{13}=-26.1_5\ g_{22}=+3.0_3.$$

If the positions of the new photographic infra-red bands are predicted from these constants a fair agreement is obtained as shown in the fifth column of Table I which gives the obs.−calc. values. However, the deviations are much larger than the accuracy of the observed band origins, which is ± 0.2 cm^{-1} at worst. A somewhat better agreement, as shown by the obs.−calc. values of the last column of Table I is obtained if the following slightly modified constants are used

$$\omega_1{}^0=1289.2_5\ \omega_2{}^0=588.0_5\ \omega_3{}^0=2240.9$$
$$x_{11}=-3.2_5\ \ x_{22}=-0.5_3\ \ x_{33}=-15.6 \quad (3)$$
$$x_{12}=+1.9_5\ \ x_{23}=-14.7\ \ x_{13}=-28.1_5\ g_{22}=+3.0_3.$$

However, even with these constants the deviations are much larger than corresponds to the accuracy of the measurements and in addition the representation of the ordinary infra-red bands is much poorer than with the

TABLE II—*Continued.*

J	$3\nu_1+2\nu_2+2\nu_3$ $\nu_0=9219.12$ R(J)	P(J)	$4\nu_1+2\nu_3$ $\nu_0=9295.04$ R(J)	P(J)
1			9296.5_9	
2			97.3_9	
3	9222.2_3	9216.5_8	98.1_8	9292.4_6
4	22.9_6	15.6_6	98.8_6	91.5_3
5	23.6_6	14.7_1	9299.5_6	90.6_0
6	24.3_4	13.7_0	9300.2_0	89.6_1
7	25.0_0	12.7_5	00.8_4	88.6_6
8	25.6_4	11.7_2	01.4_4	87.6_2
9	26.2_0	10.7_7	02.0_3	86.6_1
10	26.8_0	09.7_2	02.5_8	85.4_8
11	27.3_5	08.6_5	03.0_9	84.4_2
12	27.9_0	07.5_5	03.6_1	83.3_1
13	28.4_3	06.4_5	04.1_0	82.1_8
14	28.9_4	05.2_6	04.5_5	80.9_8
15	29.4_0	04.1_2	04.9_9	79.8_2
16	29.8_3	02.9_3	05.4_6	78.5_5
17	30.2_3	01.7_1	05.8_6	77.3_2
18	30.6_4	9200.5_2	06.1_9	76.0_2
19	31.0_0	9199.2_8	06.5_3	74.7_6
20	31.4_0	97.9_7		73.4_4
21	31.6_8	96.6_7		72.1_0
22		95.3_6		70.7_3
23		94.0_5		69.3_2
24		92.6_3		67.9_4
25		91.2_6		66.4_5
26		89.8_4		64.9_9
27		88.3_9		63.4_6
28		86.9_8		62.0_0
29		85.4_5		60.4_1
30		83.9_4		58.8_4
31		82.3_8		57.2_5
32		80.8_3		55.6_4
33		79.2_9		
34		77.5_6		

TABLE II—*Continued.*

J	$4\nu_1+4\nu_2+\nu_3$ $\nu_0=9517.9_2$ R(J)	P(J)	$5\nu_1+2\nu_2+\nu_3$ $\nu_0=9606.3_8$ R(J)	P(J)
0			9607.4_8	
1			08.0_8	
2			08.9_8	
3			09.5_7	
4			10.1_6	9602.9_2
5			10.8_3	9601.9_0
6		9512.3_2	11.5_6	9600.9_8
7		11.6_7	12.2_5	9599.8_8
8	9524.5_0	10.7_0	12.7_9	98.9_1
9	25.2_1	09.7_4	13.4_5	97.8_8
10	25.8_4	08.7_4	13.9_7	96.9_0
11	26.3_8	07.6_2	14.4_8	95.8_4
12	27.0_4	06.6_8	15.3_1	94.7_2
13	27.5_4	05.5_3		93.6_8
14	28.1_5	04.3_3		92.4_5
15	28.6_2	03.3_4		91.3_2
16	29.4_4	02.2_3		90.1_4
17	29.9_1	9501.1_6		88.8_8
18	30.3_9	9499.9_1		87.6_6
19	30.8_8	98.7_1		86.3_9
20		97.6_4		85.1_4
21		96.4_3		83.8_5
22		95.0_5		82.4_5
23		93.8_2		81.0_2
24		92.6_7		79.6_8
25		91.2_8		78.3_0
26		89.9_2		76.9_6
27		88.5_6		75.6_2
28		87.2_5		73.9_5
29		85.8_6		72.5_3
30		84.8_7		71.1_4
31		83.1_1		69.9_7
32		81.8_3		68.7_3
33		80.4_1		

first set. It would appear that no simple set of constants ω_i, x_{ik}, g_{22} exists that will allow a satisfactory representation of all bands. The reason for this difficulty, as has already been suggested by one of us,[6] must be sought in the occurrence of a considerable number of vibrational perturbations caused by Fermi resonance between vibrational levels of the same species and of nearly equal energy.

Indeed there is in N_2O a near equality between $\nu_1(=1285\ \text{cm}^{-1})$ and $2\nu_2(=1167\ \text{cm}^{-1})$ just as for CO_2 where $\nu_1=1388$ and $2\nu_2=1286$. For CO_2 twice the fundamental ν_2 is halfway between the two observed frequencies for ν_1 and $2\nu_2$ while for N_2O it is close to the lower value. This indicates that the resonance is much less close for N_2O than for CO_2. Nevertheless it is readily seen that the shift produced in N_2O is still of the order of the shifts produced by the anharmonic terms or even larger.

For example, in CO_2 the zero approximation levels of ν_1 and $2\nu_2$ have been found to be $\delta=16.7\ \text{cm}^{-1}$ apart[7] while the matrix element of the interaction of the two levels, due to the cubic term α_{122} of the potential function, is $W_{ni}=50.4\ \text{cm}^{-1}$. This gives rise to a shift of

TABLE II—*Continued.*

J	$\nu_1+4\nu_3$ $\nu_0=9888.53$ R(J)	P(J)	$2\nu_1+2\nu_2+3\nu_3$ $\nu_0=10079.66$ R(J)	P(J)
2	9890.92			10077.93
3	91.62	9885.92		77.05
4	92.25	84.97	10083.44	76.13
5	92.93	84.01	84.13	75.20
6	93.59	83.05	84.79	74.20
7	94.15	82.02	85.41	73.24
8	94.72	80.93	86.03	72.23
9	95.19	79.89	86.63	71.17
10	95.71	78.72	87.16	70.11
11	96.18	77.62	87.68	69.00
12	96.63	76.38	88.19	67.86
13	97.04	75.19	88.68	66.74
14	97.34	73.97	89.13	65.59
15	97.60	72.68	89.54	64.37
16	97.78*	71.38	89.93	63.14
17		70.06	90.26	61.89
18		68.66	90.61	60.62
19		67.27	90.97	59.31
20		65.83	91.27	57.94
21		64.36		56.60
22		62.88		55.22
23		61.35		53.82
24		59.77		52.39
25		58.21		50.92
26		56.56		49.41
27		54.95		47.92
28		53.23		46.36
29		51.52		44.84
30		49.77		43.23
31		48.01		41.60
32	9898.54	46.31		39.95
33	98.37	44.42		38.27
34	98.20	42.51		
35	97.98	40.57		
36	97.78*	38.70		
37		36.76		
38		34.70		
39		32.70		
40		30.60		

[7] D. M. Dennison, Rev. Mod. Phys. **12**, 175 (1940).

TABLE II—*Continued.*

	$3\nu_1+3\nu_3$ $\nu_0=10163.68$		$5\nu_3$ $\nu_0=10815.38$	
J	$R(J)$	$P(J)$	$R(J)$	$P(J)$
0	10164.41			
1	65.29	10162.92		
2	66.00	61.95	10817.53*	
3	66.74	61.08	18.32	
4	67.42	60.13	18.97	10811.62*
5	68.14	59.18	19.65	10.80
6	68.69	58.19	20.29	09.78
7	69.27	57.20	20.90	08.77
8	69.84	56.12	21.47	07.74
9	70.38	55.03	22.01	06.63
10	70.88	53.93	22.53	05.56
11	71.33	52.79	23.01	04.44
12	71.78	51.60	23.46	03.31*
13	72.19	50.42	23.87	02.08*
14	72.58	49.16	24.25	10800.82
15	72.93	47.91	24.61	10799.55
16	73.24	46.60	24.92	98.23
17	73.52	45.27	25.19	96.88
18		43.92		95.57*
19		42.53		94.13
20		41.11		92.69
21		39.68		91.23
22		38.19		89.73
23		36.69		88.19
24		35.14		86.64
25		33.56		85.01
26		31.96		83.39
27		30.36		81.70
28		28.68		79.97
29		26.98		78.21
30		25.30		76.43
31		23.52		74.39*
32		21.74		72.71*
33		19.93		70.82*
34		18.09		68.86
35		16.21		
36		14.37		
37		12.41		
38		10.46		

TABLE II—*Continued.*

	$4\nu_2+4\nu_3$ $\nu_0=10820.16$		$4\nu_1+4\nu_2+2\nu_3$ $\nu_0=11544.5_6$	
J	$R(J)$	$P(J)$	$R(J)$	$P(J)$
3		10817.53*		
4		16.64		11540.9_8
5		15.69		40.0_6
6		14.71		39.2_0
7		13.66		38.1_8
8	10826.41	12.67		37.1_1
9	26.97	11.62*	11551.4_5	36.0_0
10	27.49	10.48	52.0_3	34.9_8
11	28.01	09.38	52.5_4	33.9_3
12	28.46	08.22	53.0_7	32.7_6
13	28.93	07.05	53.5_4	31.6_0
14	29.34	05.86	53.9_8	30.3_7
15	29.75	04.64	54.3_7	29.2_4
16	30.12	03.31*	54.7_8	27.9_3
17	30.47	02.08*	55.1_3	26.7_3
18	30.81		55.4_6	25.4_1
19	31.12		55.7_8	24.0_8
20	31.41		56.0_6	22.7_2
21	31.73		56.3_4	21.3_4
22				19.9_7
23				18.6_1
24				17.0_8
25				15.6_0
26				14.1_7
27				12.6_1

TABLE II—*Continued.*

	$5\nu_1+2\nu_2+2\nu_3$ $\nu_0=11629.63$		$\nu_1+5\nu_3$ $\nu_0=11964.3_2$	
J	$R(J)$	$P(J)$	$R(J)$	$P(J)$
0			11964.97*	
1	11631.44		65.76*	11963.31*
2	32.09		66.49*	62.47*
3	32.76		67.19*	61.59*
4	33.49		67.85*	60.62*
5	34.10	11625.09	68.43*	59.66*
6	34.71	24.13	69.06*	58.65
7	35.34	23.16	69.60*	57.59
8	35.91	22.09	70.10*	56.49
9	36.46	21.01	70.57*	55.37
10	36.94	19.89	71.00*	54.19
11	37.43	18.76	71.38*	52.98
12	37.89	17.59	71.73*	51.73
13	38.28	16.39	72.04*	50.44
14	38.68	15.20	72.31*	49.11
15	39.03	14.01	72.53*	47.73
16	39.36	12.69	72.73*	46.33
17	39.66	11.38	72.89*	44.89
18	40.20	09.98		43.40
19		08.64		41.88
20		07.27		40.31
21		05.80		38.71
22		04.30		37.07
23		02.80		35.39
24		01.22	11972.89*	33.68
25			72.73*	31.93
26			72.53*	30.14
27			72.31*	28.30
28			72.04*	26.43
29			71.73*	24.52
30			71.38*	22.57
31			71.00*	20.60
32			70.57*	18.58
33			70.10*	16.51
34			69.60*	14.41
35			69.06*	12.27
36			68.48*	
37			67.85*	07.89
38			67.19*	05.59*
39			66.49*	03.43
40			65.76*	11901.03
41			64.97*	11898.67
42			64.16	96.24
43			63.31*	93.86*
44			62.47*	91.30
45			61.59*	88.83
46			60.62*	86.25
47			59.66*	83.45
48				81.21
49				77.46

either level (up for ν_1, down for $2\nu_2$) of 42.7 cm^{-1}. If the separation of the zero approximation levels were $\delta=100$ cm^{-1} the shift for the same magnitude of the cubic term in the potential function, would still be 21.0 cm^{-1}. This example shows clearly that for an accurate representation of the vibrational levels of N_2O the effect of resonance must be taken into account and that the formula (1) alone cannot be expected to represent the levels accurately.

The resonance between ν_1 and $2\nu_2$ implies of course similar resonances when in addition to ν_1 or $2\nu_2$ the vibration ν_3 is excited. We have a progression of resonance doublets (10^0v_3; 02^0v_3). Furthermore when ν_1 is doubly excited we obtain a progression of resonance triplets: (20^0v_3; 12^0v_3; 04^0v_3) and similarly higher resonance multiplets. While the resonance doublets can be

TABLE II—*Continued.*

	$6\nu_3$ $\nu_0=12891.1_0$	
J	$R(J)$	$P(J)$
0		
1	12892.65*	
2	93.21*	12889.35
3	93.90*	88.46
4	94.49*	87.52
5	95.11*	86.50
6	95.67*	85.48
7	96.18*	84.34
8	96.67*	83.23
9	97.11*	82.06
10	97.51*	80.85
11	97.94*	79.61
12	98.19*	78.32
13	98.47*	77.00
14		75.59
15		74.21
16		72.74
17		71.26
18		69.72
19		68.13
20		66.52
21		64.84
22		63.13
23		61.41
24		59.61
25	12898.47*	57.77
26	98.19*	55.91
27	97.94*	53.99
28	97.51*	52.06
29	97.11*	50.07
30	96.67*	48.01
31	96.18*	45.98
32	95.67*	43.83
33	95.11*	41.68
34	94.49*	39.49
35	93.90*	37.23
36	93.21*	34.92
37	92.65*	

expressed explicitly in terms of δ and W_{ni} this is no longer the case for the higher resonance multiplets for which cubic, quartic, $\cdots$ equations have to be solved.

Unless additional perturbations of higher order occur the sums of the wave numbers of a given resonance multiplet must follow the same formula as they would without Fermi resonance. The anharmonic coefficients x_{ik} can be determined if a sufficient number of such resonance multiplets have been observed. For example the following bands or groups of bands would be sufficient to determine the ω_i, x_{ik} and g_{22} of N_2O and similar molecules: ν_3, $2\nu_3$, $(\nu_1, 2\nu_2)$, $(\nu_1+\nu_3, 2\nu_2+\nu_3)$, $(2\nu_1, \nu_1+2\nu_2, 4\nu_2)$, $(3\nu_1, 2\nu_1+2\nu_2, \nu_1+4\nu_2, 6\nu_2)$, ν_2, $\nu_2+\nu_3$, $(\nu_1+\nu_2, 3\nu_2)$, and $(2\nu_1+\nu_2, \nu_1+3\nu_2, 5\nu_2)$. Once these have been obtained the splittings within a given resonance multiplet give the interaction constants W_{ni}.

Unfortunately not all the bands necessary for such a determination have been observed for N_2O. Only a few of the vibrational constants can be determined without neglecting the effect of resonance. From the series $v_3\nu_3$, observed to $v_3=6$, one might have hoped to obtain fairly accurate values for ω_3^0 and x_{33}. The residuals for the previously given ω_3^0 and x_{33} values are shown graphically in Fig. 3. It is clear from this figure that no values of ω_3^0 and x_{33} will give a satisfactory representation of the series. This is partly due to the fact that the infra-red values for ν_3 and $2\nu_3$ are subject to an appreciable error (as explicitly stated by Plyler and Barker)[1] and partly due to the effect of cubic and higher terms in v_3 which become noticeable when v_3 goes up to 6.

Two members of the series $\nu_2+v_3\nu_3$ have been observed in the ordinary infra-red. These give $x_{23}=-14.0$. The same constant can also be obtained from the difference between the photographic bands $4\nu_3$ and $\nu_2+4\nu_3-\nu_2$: one obtains $x_{23}=-14.1_9$ in very satisfactory agreement with the former (less accurate) value. The sum of the two bands $(\nu_1, 2\nu_2)$ is $\omega_1^0+x_{11}+2\omega_2^0+4x_{22}$ while the sum of $(\nu_1+\nu_3, 2\nu_2+\nu_3)$ is $\omega_1^0+x_{11}+2\omega_2^0+4x_{22}+2\omega_3^0+x_{13}+2x_{23}+2x_{33}$. Subtracting and substituting $\omega_3^0+x_{33}=2225.0$, $x_{23}=-14.2$ one obtains $x_{13}=-26.8$.

The unambiguous determination of the other vibrational constants must await the observation and analysis of a number of additional infra-red bands.

E. ROTATIONAL ANALYSIS

As mentioned previously all photographic infra-red bands of N_2O are $\|$ bands, that is, they consist of a single P and R branch. These branches, as given in Table II, can in most cases be picked out by inspection (compare the spectrogram Fig. 1). In a few cases on account of overlapping or of perturbations the branches were not so obvious and it was necessary to apply the method of Wood and Loomis[8] in order to find the branches. The numbering of the lines, when it was not obvious from the position of the zero gap, was established by the use of the combination differences

$$\Delta_2F''(J)=R(J-1)-P(J+1), \qquad (4)$$

which for the correct numbering must agree in different bands with the same lower state.

Some difficulty was experienced in the analysis of the bands $5\nu_3$ and $4\nu_2+4\nu_3$ whose heads lie only 8 cm^{-1} apart. In addition to the strong mutual overlapping of these two bands, one of them, $5\nu_3$, shows a strong rotational perturbation. An independent check on the correctness of the assignment was obtained by forming differences of the type

$$R_1(J-1)-R_2(J-1)=P_1(J+1)-P_2(J+1)=F_1'(J)-F_2'(J) \qquad (5)$$

with another unperturbed band. Here the subscripts 1 and 2 refer to the two bands, which have the lower state in common.

The only difference band whose fine structure could be analyzed is the band $\nu_2+4\nu_3-\nu_2$. Since the (weak) Q branch of this band could not be identified unambiguously the absolute J-numbering was found by comparing the $\Delta_2F''(J)$ values with those of the fundamental ν_2 measured by Plyler and Barker.[1]

[8] See G. Herzberg, *Spectra of Diatomic Molecules* (D. Van Nostrand Company, Inc., New York, 1950), p. 191.

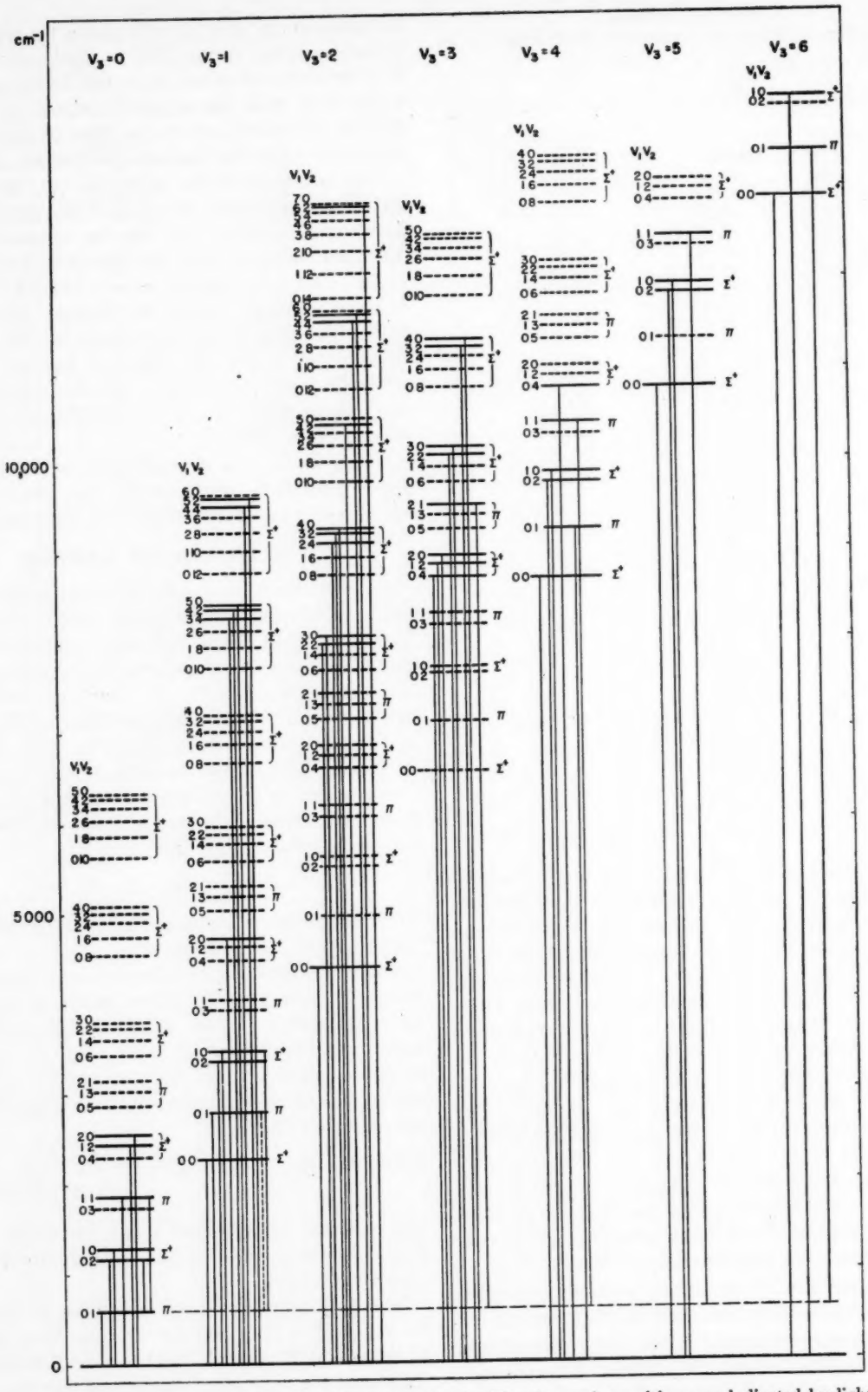

FIG. 2. Vibrational energy levels of the N_2O molecule. The observed transitions are indicated by light vertical lines (full lines for infra-red transitions, broken lines for Raman transitions). The broken-line levels are predicted but not yet observed. Only Σ^+- and Π-levels are shown. Two Δ-levels have been found: $2\nu_2^2$ and $2\nu_2^2+\nu_3$; they lie very close to the corresponding Σ^+-levels and are not shown separately in order not to make the diagram too complicated. All Σ^+-levels with $v_2=2,4,\cdots$ are accompanied by Δ-levels, all Π-levels with $v_2=3,5,\cdots$ are accompanied by Φ-levels etc. (not shown, see reference 6).

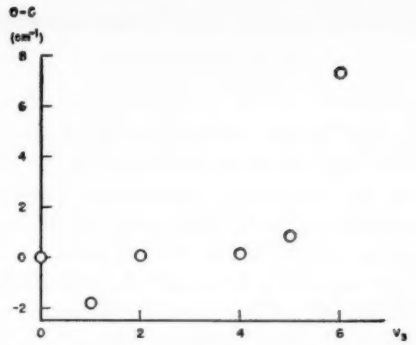

FIG. 3: Deviations of the bands $\nu_3\nu_3$ from the formula (3).

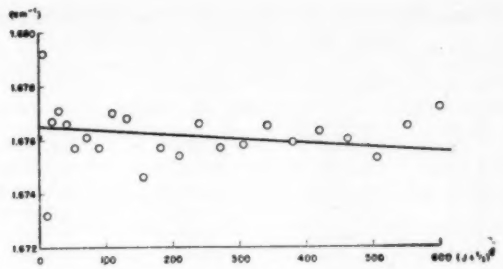

FIG. 4. Combination differences $\Delta_2F''(J)/(J+\frac{1}{2})$ for the ground state of N_2O.

The values plotted as circles are mean values obtained from the six most accurately measured bands. The value indicated by a cross is the microwave value.

In order to determine the rotational constants B_{000} and D_{000} for the vibrationless ground state of the molecule the usual graphical method[8] was applied. In Fig. 4 the mean values of $\Delta_2F''(J)/(J+\frac{1}{2})$ obtained from the six most accurately measured bands ($4\nu_3$, $\nu_1+2\nu_2+3\nu_3$, $2\nu_1+3\nu_3$, $4\nu_1+2\nu_3$, $2\nu_1+2\nu_2+3\nu_3$ and $3\nu_1+3\nu_3$) are plotted against $(J+\frac{1}{2})^2$. Since

$$\Delta_2F''(J)/(J+\tfrac{1}{2})=(4B_{000}-6D_{000})-8D_{000}(J+\tfrac{1}{2})^2 \quad (6)$$

the slope of the straight line representing best the experimental data of Fig. 4 gives $8D_{000}$ and the intercept on the ordinate axis gives $4B_{000}-6D_{000}$. One obtains

$$B_{000}=0.4191_{25}\ \text{cm}^{-1}, \quad D_{000}=0.19_3\times10^{-6}\ \text{cm}^{-1}.$$

Coles and his collaborators[3] have observed in the microwave region the transition $J=1\leftarrow J=0$ of the rotation spectrum at 25123.25 mc/sec. or, using $c=2.99776\times10^{10}$ cm/sec. at 0.8380674 cm^{-1}. Expressed in terms of the rotational constants the wave number of the $1\leftarrow0$ transition is $2B_{000}-4D_{000}$. Twice the observed value of this transition should therefore fit into the $\Delta_2F''(J)/(J+\frac{1}{2})$ curve at $(J+\frac{1}{2})^2=\frac{1}{4}$; it is marked by a cross in Fig. 4. Considering the high accuracy of the microwave results one is tempted to draw the straight line so that it goes exactly through this point. However, if that were done the resulting line giving the best representation of the other points would have very nearly zero slope and would imply $D_{000}<0.04\times10^{-6}$ cm^{-1}. On the other hand, considering that centrifugal stretching will increase both the N−N and N−O distance and thus lead to essentially the same result as a displacement according to the normal vibration ν_1, an approximate D_{000} value is obtained[6] from $4B_{000}^3/\nu_1^2$. This gives 0.18×10^{-6} cm^{-1} a value that agrees very well with the observed value. We prefer therefore to keep the evaluation of our data independent of the microwave data.

The microwave data at present available do not yield a value for D_{000}. Using our D_{000} value the microwave value for $2B_{000}-4D_{000}$ gives

$$B_{000}=0.419034_{09}\ \text{cm}^{-1}.$$

While the deviation from our B_{000} value is only -0.000091 it is perhaps slightly larger than one would expect from the accuracy of the data, particularly if the excellent agreement between microwave and photographic infra-red data (within 0.000025 cm^{-1}) obtained in the case of CO is considered.[9]

The rotational constants of most of the other vibrational levels were determined from the combination sums $R(J-1)+P(J)$ rather than from the combination differences $\Delta_2F'(J)$. One has[6]

$$R(J-1)+P(J)=2\nu_0 +2[(B'-B'')-(D'-D'')]J^2-2(D'-D'')J^4. \quad (7)$$

Since in the present case D' is very nearly equal to D'' and both are very small correction terms a plot of $R(J-1)+P(J)$ against J^2 gives a straight line whose slope is equal to $2(B'-B'')$ and whose intercept on the ordinate axis is $2\nu_0$.

Since the R branch is often not well resolved near the band head and since the lines of the outgoing and returning parts of the R branches overlap each other it is sometimes better to avoid using the lines of the R branch. $R(J-1)$ in (7) may be replaced by $P(J+1)+\Delta_2F''(J)$. Using $\Delta_2F''(J)$ values determined from the accurate B_{000} and D_{000} values given above again $2(B'-B'')$ and $2\nu_0$ can be determined. The agreement of the two methods, wherever the R lines are available, is very satisfactory.

In a few cases deviations from a straight line in plotting the observed combination sums were found: both in the $5\nu_3$ and the $\nu_1+5\nu_3$ bands there is a deviation from the straight line for small J values indicating perturbations. In addition in $5\nu_3$ and $3\nu_1+3\nu_3$ there are systematic deviations for higher J values which require anomalous D' values and in the case of $5\nu_3$ even a higher term (H') in the expression for the rotational energy. While all the other D' values are indistinguishable from D_{000} one finds in these two cases using the approximation method described by Babcock and L. Herzberg[10]

$$D_{303}=0.16_0\times10^{-6}, \quad D_{005}=0.39_3\times10^{-6},$$
$$H_{005}=-0.3\times10^{-9}\ \text{cm}^{-1}.$$

[9] G. Herzberg and K. N. Rao, J. Chem. Phys. **17**, 1099 (1949); Gilliam, Johnson, and Gordy, Phys. Rev. **78**, 140 (1950).

[10] H. D. Babcock and L. Herzberg, Astrophys. J. **108**, 1 (1948).

TABLE III. Rotational constants of the N_2O-molecule in the different vibrational levels.

v_1	v_2	v_3	$B_{obs}(cm^{-1})$	$B_{calc}(cm^{-1})$	$o-c$
0	0	0	0.4191_{25}	—	—
0	1	0	0.419_{2}	0.4193	−0.0001*
2	2	2	0.4098_{4}	0.40939	+0.00045
3	0	2	0.4073_{6}	0.40725	+0.00011
3	4	1	0.4115_{2}	0.41151	+0.00001
4	2	1	0.4090_{4}	0.40937	−0.00033
5	0	1	0.4092	0.4072	+0.0020*
0	1	4	0.405_{9}	0.4058	+0.0001*
0	0	4	0.4053_{3}	0.40559	−0.00026
1	2	3	0.4080_{3}	0.40771	+0.00032
2	0	3	0.4053_{0}	0.40557	−0.00027
2	4	2	0.4103_{4}	0.40983	+0.00051
3	2	2	0.4076_{0}	0.40769	−0.00009
4	0	2	0.4064_{2}	0.40555	+0.00087
4	4	1	0.4097_{1}	0.40981	−0.00010
5	2	1	0.4074_{0}	0.40767	−0.00027
1	0	4	0.4034_{9}	0.40388	−0.00039
2	2	3	0.4061_{5}	0.40600	+0.00015
3	0	3	0.4038_{6}	0.40386	0.00000
0	0	5	0.4036_{7}	0.40220	+0.00147*
0	4	4	0.4050_{0}	0.40646	−0.00146*
4	4	2	0.4058_{6}	0.40643	−0.00057
5	2	2	0.4043	0.4043	0.0000*
1	0	5	0.4000_{3}	0.40050	−0.00047*
0	0	6	0.3985_{2}	0.39882	−0.00030*

* $o-c$ values for B values not used in the least squares solution.

In Table III all the observed $B_{v_1v_2v_3}$ values are listed. The varying number of significant figures given indicates the accuracy ascribed to these data. The D values are not given separately since they are the same for all levels ($=0.19_3\times10^{-6}$) with the exception of the two values discussed above. The B values for the two levels v_2 and v_2+4v_3 have been obtained from the difference band $v_2+4v_3-v_2$.

As long as there are no perturbations the B values should follow the formula

$$B_{v_1v_2v_3}=B_e-\alpha_1(v_1+\tfrac{1}{2})-\alpha_2(v_2+1)-\alpha_3(v_3+\tfrac{1}{2}). \quad (8)$$

In obtaining the α_i values from the observed B values account must be taken of the fact that most of the $B_{v_1v_2v_3}$ values were obtained from the $B'-B''$ values, that is, assuming the previously given B_{000} value. An application of the least squares method can therefore not affect the B_{000} value. Using only the B values determined with maximum precision but omitting B_{005} and B_{044} which are obviously perturbed one finds the following α_i values

$$\alpha_1=+0.0017_0,\quad \alpha_2=-0.0002_2,\quad \alpha_3=+0.0033_9\ cm^{-1}.$$

The second last column of Table III gives the $B_{v_1v_2v_3}$ values calculated with these α_i values and $B_{000}=0.4191_{25}$, the last column gives the $o-c$ values. The $o-c$ values for $B_{v_1v_2v_3}$ values not used in the least squares solution are marked by asterisks. The deviations of the observed from the calculated values are appreciably larger than the estimated accuracy of the B determinations.

The reason for these discrepancies is clearly again the occurrence of Fermi resonances. In the case of two resonating levels n and i the B values are given by[6]

$$B_n=a^2B_n^0+b^2B_i^0$$
$$B_i=b^2B_n^0+a^2B_i^0 \quad (9)$$

where B_n^0 and B_i^0 are the unperturbed B values and a and b are the fractional contributions of the unperturbed to the perturbed vibrational eigenfunctions. Similar formulas apply to resonance triplets and higher multiplets. As in the case of the vibrational formula the sums of the resonating levels should follow the formula (8). Unfortunately not all bands necessary to determine the constants in this way have been measured. More work in the ordinary infra-red is required.

The series of levels 000, 004, 005, and 006 is free from the effect of Fermi resonance between v_1 and $2v_2$. In spite of that the B values of these levels do not form a smooth series (compare Table III). The reason for this is a higher order perturbation between the levels 005 and 044 which lie very close together. Indeed the $o-c$ values for these two levels are opposite and equal and in a direction to be expected from Eqs. (9). Somewhat unexpectedly there does not appear to be an appreciable vibrational perturbation between these two levels (see Table I). Probably this perturbation, affecting mainly the B values, is due to Coriolis interaction.[6] Such an interaction may also be the cause of other large deviations in Table III.

Using the α_i values given above one finds

$$B_e=0.4214_5\ cm^{-1}.$$

In view of the uncertainty of the α_i as demonstrated by the comparatively large $o-c$ in Table III it must be emphasized that B_e is less accurate than B_{000}. However, it should be accurate to $\pm0.0003\ cm^{-1}$.

F. CONCLUSION

The difficulties encountered here in the determination of the vibrational and rotational constants of the N_2O molecule are probably not peculiar to N_2O but are a fairly general property of many polyatomic molecules. They have been encountered for C_2H_2[11, 6] and H_2O.[12] The only case where comparably extensive data are available and where this difficulty does not appear seems to be the HCN molecule.[13] Here the three fundamental frequencies are so widely different that Fermi resonances have no appreciable effect on the spectrum except perhaps in a much higher order of approximation. It would be most desirable if the elementary theory could be extended to include the effects of Fermi resonance without the makeshift of introducing it as a perturbation at the end.

From the value of B_e derived above one obtains for the moment of inertia in the equilibrium position (using

[11] G. Herzberg and J. W. T. Spinks, Zeits. f. Physik **91**, 386 (1934); G. W. Funke, Zeits. f. Physik **99**, 341 (1936); T. Y. Wu and A. T. Kiang, J. Chem. Phys. **7**, 178 (1939); N. M. Nordin and R. N. H. Haslam, Can. J. Research **26A**, 279 (1948).

[12] B. T. Darling and D. M. Dennison, Phys. Rev. **57**, 128 (1940).

[13] G. Herzberg and J. W. T. Spinks, Proc. Roy. Soc. **147**, 434 (1934); E. Lindholm, Zeits. f. Physik **108**, 454 (1938).

the conversion factor of reference 8

$$I_c = 66.39_7 \times 10^{-40} \text{ g cm}^2.$$

This may be compared with the I_0 values 66.765 and $66.7797_7 \times 10^{-40}$ obtained from the present measurements and from microwave data respectively (see above).

As mentioned in the introduction a reliable determination of the internuclear distances in N_2O is possible only if I_e is obtained for an isotopic molecule e.g. $N^{15}N^{14}O^{16}$ as well as for the ordinary molecule $N^{14}N^{14}O^{16}$. Up to now only I_0 values are available for several isotopic species. The use of the I_0 values rather than the I_e values leads to somewhat contradictory values for the internuclear distances.[3]

One might be tempted to make use of the theoretical formulas for the α_i of a linear XYZ molecule (see Nielsen[14]) in determining α_i for $N^{15}N^{14}O^{16}$ from the α_i of $N^{14}N^{14}O^{16}$ here obtained, and in this way arrive at B_e and I_e values for the isotopic molecule. However, for this purpose a knowledge of both the quadratic and the cubic terms in the potential energy function of N_2O would be necessary. The ordinary force constants (quadratic terms) have recently been determined by Richardson and Wilson[15] with the aid of the observed fundamentals of $N^{15}N^{14}O^{16}$; but no overtone and combination bands of $N^{15}N^{14}O^{16}$ have yet been observed and therefore the cubic potential constants necessary for a calculation of the α_i cannot be determined.

The experimental part of this investigation was carried out in the Spectroscopic Laboratory of Yerkes Observatory. Thanks are due to the administration of Yerkes Observatory for the support of this investigation.

[14] A. H. Nielsen, J. Chem. Phys. **11**, 160 (1943).

[15] W. S. Richardson and E. B. Wilson, Jr., J. Chem. Phys. **18**, 694 (1950).

THE JOURNAL OF CHEMICAL PHYSICS VOLUME 18, NUMBER 12 DECEMBER, 1950

Molecular Orbital Calculations of the Lower Excited Electronic Levels of Benzene, Configuration Interaction Included

ROBERT G. PARR
Department of Chemistry, Carnegie Institute of Technology, Pittsburgh, Pennsylvania

AND

DAVID P. CRAIG AND IAN G. ROSS
Sir William Ramsay and Ralph Forster Laboratories, University College, London, England

(Received September 6, 1950)

The lower excited π-electron levels of benzene are calculated by the non-empirical method of antisymmetrized products of molecular orbitals (in LCAO approximation) including configuration interaction. All configurations arising from excitation of one or two electrons from the most stable configuration are considered, and all many-center integrals are retained. The results are in better agreement with experiment and valence-bond calculations than those obtained previously by Craig in a calculation neglecting many-center integrals. Configuration interaction is found to change the order of the $^1B_{1u}$ and $^1E_{2g}$ states but leave unchanged the order of the $^3B_{1u}$ and $^3B_{2u}$ states, in agreement with the assignments $^1A_{1g}-{}^3B_{1u}$ and $^1A_{1g}-{}^1E_{2g}$ for the experimental bands at 3.8 and 6.2 ev.

THE original calculation by Goeppert-Mayer and Sklar[1] of the lower excited levels of benzene by the method of antisymmetrized products of molecular orbitals has gone through several revisions[2–5] and one extension,[4] each step changing the numerical results considerably. In the present paper we report the results of repeating the calculation once more, including three-center and four-center integrals in the manner of London[2] and configuration interaction in the manner of Craig,[4] using revised values of two-center integrals as prescribed by Parr and Crawford.[6]

Our results are given in Table I. Details of the calculations will not be given, as these may be found in the papers of Goeppert-Mayer and Sklar[1] and Craig.[4] The computations, which are heavy, were carried through independently *ab initio* by RGP on the one hand, and DPC and IGR on the other.

The integrals over atomic orbitals upon which the results are based are set out in Table II. Two-center integrals were taken from the paper of Parr and Crawford.[6] Three- and four-center integrals however

[1] M. Goeppert-Mayer and A. L. Sklar, J. Chem. Phys. **6**, 645 (1938).

[2] A. London, J. Chem. Phys. **13**, 396 (1945).

[3] B. L. Crawford, Jr. and R. G. Parr, J. Chem. Phys. **17**, 726 (1949).

[4] D. P. Craig, J. Chem. Phys. **17**, 1358 (1949); Proc. Roy. Soc. **200**, 474 (1950).

[5] C. C. J. Roothaan and R. G. Parr, J. Chem. Phys. **17**, 1001 (1949).

[6] R. G. Parr and B. L. Crawford, Jr., J. Chem. Phys. **16**, 1049 (1948).

TABLE I. Electronic levels of benzene (ev).

Level	M.O.[c,d]	M.O. +configuration interaction (two-center integrals only)[e]	M.O. +configuration interaction (all integrals)	Valence bond[f]	Observed[g]
Singlets					
$A_{1g}(9)$[a]	0.0	0.0	0.0	0.0	0.0
$A_{2g}(3)$	11.1	—	12.5	—	—
$B_{1u}(6)$	7.3	4.5	9.0	—	—
$B_{2u}(5)$	5.9	2.0	4.4	4.7	4.9
$E_{1u}(11)$	9.8	6.2	9.9	7.9	7.0
$E_{2g}(11)$	10.9	—	7.7	6.6	6.2
Triplets					
$A_{1g}(4)$	13.6	—	14.9	—	—
$A_{2g}(7)$	11.1	—	11.8	—	—
$B_{1u}(5)$	3.1	—	4.1	—	3.8
$B_{2u}(4)$	5.8	—	8.2	—	—
$E_{1u}(12)$	4.4	—	4.7	—	—
$E_{2g}(9)$	8.3	—	6.4	—	—
Quintuplets[b]					
$A_{1g}(4)$	6.1	—	5.9	—	—
$E_{1u}(6)$	7.7	—	7.1	—	—

[a] The numbers of configuration wave functions used in the computations are given in parentheses.
[b] These results are based on *all* configurations. M.O. +configuration interaction (all integrals) results for $A_{2g}(2)$, $B_{1u}(3)$, $B_{2u}(2)$, $E_{2g}(6)$ quintuplet levels: 15.9, 19.8, 20.2, 9.6. The septuplet state $^7B_{1u}(1)$ falls at 11.2 ev.
[c] Method of antisymmetrized products of molecular orbitals (in LCAO approximation).
[d] This energy level scheme before configuration interaction is taken into account is a slight modification of that reported by Roothaan and Parr (reference 5). See also forthcoming publication of C. C. J. Roothaan.
[e] Reference 10.
[f] Reference 11.
[g] Assignment of reference 1 except for 6.2-ev band, for which see reference 11 and the text of the present paper.

were estimated by the method of Sklar.[7] This method applied to two-center integrals gives results generally higher than the correct ones. For example, 11|13 of Table I is 0.390 ev by Sklar's method instead of 0.376 ev, and 13|13 is 0.026 instead of 0.017 ev. An alternative approximation for these integrals is that of Mulliken,[8] which gives 0.439 and 0.017 ev, respectively, for 11|13 and 13|13. In these, and other similar cases, the success of the approximations perhaps varies too much to justify a choice between them; Sklar's method was therefore adopted to secure continuity with previous work.[5] It is certainly necessary to include these integrals because they have a considerable effect on the final results (compare columns 3 and 4 of Table I).

Integrals over molecular orbitals are expressible in terms of atomic integrals as indicated in the Appendix. Their values are set out in Table III. It is very striking that the Coulomb-exchange integrals cluster in four distinct groups. A similar (though then less striking) regularity was noted by London[2] and was shown by him to be a consequence of the approximation method for three- and four-center integrals. Exploitation of this would seem well worth while.[9]

Because the number of matrix elements increases so rapidly with increasing numbers of configurations it is important to keep the latter to a minimum. We included all the configurations obtained by excitation of one or two electrons from the lowest configuration, together with a few others which are associated with unusually large matrix components with the lowest states and are therefore important in spite of a high degree of excitation. A complete calculation (i.e., one including all configurations) of the singlet states using two-center integrals only[10] has shown that the configurations here neglected will have only a very small effect on the separations between the states. Our results should therefore represent a close approach to the best obtainable from the π-electron approximation.

In Table I our results are compared with experiment, with similar calculations excluding three- and four-

[7] A. L. Sklar, J. Chem. Phys. **7**, 984 (1939).
[8] R. S. Mulliken, J. de Chim. Phys. **46**, 497 (1949).
[9] One might, for example, assume constant values throughout each set and proceed semi-empirically, or one might seek atomic orbitals which render the approximate constancies exact.

TABLE II. Integrals over atomic orbitals.[a]

Integral[b]	Value (ev)[c]	Integral[e]	Value (ev)
11|11	16.930	1:22	0.856
11|22	9.027	1:33	0.013
11|33	5.668	1:44	0.003
11|44	4.968	1:12	1.887
11|12	3.313	1:13	0.109
11|13	0.376	1:14	0.037
11|14	0.160	1:23	0.039
11|23	1.870	1:24	0.006
11|24	0.280	1:25	0.015
11|25	0.160	1:26	0.318
11|26	0.524	1:34	0.002
11|34	1.421	1:35	0.002
11|35	0.251		
12|12	0.923[d]	S_{12}	0.25995
13|13	0.017[d]	S_{13}	0.03887
14|14	0.003[d]	S_{14}	0.01772
12|13	0.136		
12|14	0.046		
12|15	0.091		
12|16	0.677		
12|34	0.436		
12|35	0.073		
12|36	0.046		
12|45	0.383		
13|14	0.009		
13|15	0.015		
13|24	0.020		
13|25	0.009		
13|46	0.014		
14|25	0.005		

[a] The atomic orbitals employed are $2p\pi$-Slater orbitals with effective charge 3.18.
[b] $pq|rs$ is the Coulomb-exchange integral $\int\chi_p^*(1)\chi_r^*(2)(e^2/r_{12})\chi_q(1)\times\chi_s(2)d\tau(1)d\tau(2)$, where χ_p is the $2p\pi$-orbital on the pth carbon atom, and the carbon atoms are numbered consecutively around the ring.
[c] Conversion factor: 1 atomic unit = 13.602 ev.
[d] These values are derived from M. Kotani *et al.*, Proc. Phys.-Math. Soc. Japan **20**, Extra No. 1 (1938), as amended, *ibid.* **22**, Extra No. (1940). They were checked by the method of P. J. Wheatley and J. W. Linnett, Trans. Faraday Soc. **45**, 897 (1949), after changing the sign of the coefficient of H (6, 0), misprinted in that paper.
[e] $p:rs$ is the penetration integral $-\int U_p(1)\chi_r^*(1)\chi_s(1)d\tau(1)$, where $U_p(1)$ is the potential on electron 1 caused by a neutral pth carbon atom; S_{pq} is the overlap integral $\int\chi_p^*(1)\chi_q(1)d\tau(1)$.

[10] C. W. L. Bevan and D. P. Craig (to be published).

center integrals,[10] and with a previous valence-bond calculation by one of us.[11] The agreement with experiment is much improved by including three- and four-center integrals and is, for a non-empirical calculation, good. Some support is thereby lent to a proposed assignment[11] of the 6.2-ev band as an $^1A_{1g}-{}^1E_{2g}$ rather than an $^1A_{1g}-{}^1B_{1u}$ transition, and the possibility of inversion of the $^3B_{1u}$ and $^3B_{2u}$ states through configuration interaction is ruled out.[12]

RGP is indebted to J. G. Waltz and E. P. King for computational help and to the Research Corporation for a grant-in-aid. DPC is supported by a Turner and Newall Research Fellowship in the University of London and IGR by an Australian National University Scholarship. These awards are gratefully acknowledged.

APPENDIX. INTEGRALS OVER MOLECULAR ORBITALS

The molecular orbitals used in this work may be written in the form

$$\phi_j=(6N_j)^{-\frac{1}{2}}\sum_{p=1}^{6}\exp(2\pi ipj/6)\chi_p,\quad j=0,\pm1,\pm2,3, \tag{1}$$

where χ_p is the $2p\pi$-Slater atomic orbital on the pth carbon atom and N_j is a normalizing factor. The integrals over these orbitals which enter the calculations are the orbital energies

$$\epsilon_j=\int\phi_j^*(1)[\mathbf{U}_c(1)+\mathbf{T}(1)]\phi_j(1)d\tau(1) \tag{2}$$

and the Coulomb-exchange integrals

$$\zeta_{kl}{}^{ij}=\int\int\phi_i(1)\phi_j(1)(e^2/r_{12})\phi_k(2)\phi_l(2)d\tau(1)d\tau(2), \tag{3}$$

where $\mathbf{U}_c(1)$ is the mutual potential energy (operator) of electron 1 and the π-electronless $C_6H_6^{-6}$ core, $\mathbf{T}(1)$ is the kinetic energy operator for electron 1, e^2/r_{12} is the mutual potential energy (operator) of electrons 1 and 2, and integrations are over all space for the indicated electrons. The integrals

$$\gamma_{ij}=\zeta_{j-j}{}^{i-i},\quad \delta_{ij}=\zeta_{j-i}{}^{i-j}; \tag{4}$$

and

$$\xi=\zeta_{22}{}^{11},\quad \eta=\zeta_{12}{}^{12}; \tag{5}$$

are special cases of Eq. (3).

The basic integrals over atomic orbitals are

$$S_{pq}=\int\chi_p^*(1)\chi_q(1)d\tau(1), \tag{6}$$

$$(p:rs)=-\int\mathbf{U}_p(1)\chi_r^*(1)\chi_s(1)d\tau(1), \tag{7}$$

and

$$(pq|rs)=\int\int\chi_p^*(1)\chi_r^*(2)(e^2/r_{12})\chi_q(1)\chi_s(2)d\tau(1)d\tau(2), \tag{8}$$

where $\mathbf{U}_p(1)$ is the mutual potential energy (operator) of electron 1 and a neutral (assumed spherically symmetric) pth carbon atom.

Formulas for the integrals over molecular orbital in terms of integrals over atomic orbitals are as follows. First,

$$N_j=1+2S_{12}\cos(2\pi j/6)+2S_{13}\cos(4\pi j/6)+S_{14}\cos(\pi j). \tag{9}$$

Second,

$$N_j(\epsilon_j-W_{2p})=H_{11}+2H_{12}\cos(2\pi j/6)+2H_{13}\cos(4\pi j/6)+H_{14}\cos(\pi j), \tag{10}$$

where

$$H_{pq}=-\sum_{\substack{r=1\\ r\neq q}}^{6}[(r:pq)+(pq|rr)] \tag{11}$$

and W_{2p} is the energy of a $2p\pi$-electron of a carbon atom in its valence state. Finally,

$$6(N_iN_jN_kN_l)^{\frac{1}{2}}\zeta_{kl}{}^{ij}=\text{linear combination of the 30 different integrals } (pq|rs)\equiv(1,1+u|1+v,1+w)=\sum C_{uvw}(1,1+u|1+v,1+w), \tag{12}$$

where

$$\begin{aligned}C_{uvw}=(s_i/8s_m)\{&2\cos[(2\pi/6)(iu+kv+lw)]\\&+2\cos[(2\pi/6)(iu+lv+kw)]+2\cos[(2\pi/6)(ju+kv+lw)]\\&+2\cos[(2\pi/6)(ju+lv+kw)]+2\cos[(2\pi/6)(ku+iv+jw)]\\&+2\cos[(2\pi/6)(ku+jv+iw)]+2\cos[(2\pi/6)(lu+iv+jw)]\\&+2\cos[(2\pi/6)(lu+jv+iw)]\},\end{aligned} \tag{13}$$

in which the "molecular symmetry number" s_m is 1 for integrals with no axis of symmetry (e.g., 12|35), 2 for integrals with an axis of symmetry in the plane of the molecule (e.g., 11|14) and 4 for integrals with an axis of symmetry perpendicular to the plane of the molecule (e.g., 11|44), and the "integral symmetry number" s_i is the number of distinct members in the set $pq|rs=pq|sr=qp|rs=qp|sr=rs|pq=rs|qp=sr|pq=sr|pq$ (e.g., $s_i=8$, 4, 2 for 12|35, 11|14, 11|44).

TABLE III. Integrals over molecular orbitals.[a]

Integral[b]	Value (ev)	Integral[b]	Value (ev)
γ_{00}	8.627	$\epsilon_2-\epsilon_1$	5.358
γ_{01}	8.522	$\epsilon_3-\epsilon_0$	8.290
γ_{02}	8.495	$\epsilon_3-\epsilon_1$	8.112
γ_{03}	8.554	$\epsilon_3-\epsilon_0$	11.044
γ_{11}	8.474		
γ_{12}	8.517	$\zeta_{1-2}{}^{10}$	2.601
γ_{13}	8.623	$\zeta_{23}{}^{10}$	2.633
γ_{22}	8.648	$\zeta_{13}{}^{20}$	1.299
γ_{23}	8.787	$\zeta_{22}{}^{20}$	1.302
γ_{33}	8.872	$\zeta_{11}{}^{-20}$	1.375
		$\zeta_{21}{}^{30}$	0.993
δ_{01}	2.584	$\zeta_{13}{}^{11}$	1.344
δ_{02}	1.304	$\zeta_{23}{}^{3-1}$	2.772
δ_{03}	0.934	$\zeta_{22}{}^{-13}$	1.362
δ_{1-1}	1.453		
δ_{12}	2.674	N_0	1.61536
δ_{1-2}	1.074	N_1	1.20336
δ_{13}	1.338	N_2	0.71890
δ_{2-2}	1.367	N_3	0.54012
δ_{23}	2.867		
ξ	1.328		
η	1.007		

[a] The molecular orbitals employed are $\phi_j=(6N_j)^{-\frac{1}{2}}\sum_{p=1}^{6}\exp(2\pi ipj/6)\chi_p$, where the N_j are normalizing factors.

[b] For definitions of the Coulomb-exchange integrals γ_{ij}, δ_{ij}, ξ, η, $\zeta_{kl}{}^{ij}$, and of the orbital energies ϵ_j, and for formulas for them in terms of integrals over atomic orbitals, see Appendix.

[11] D. P. Craig, Proc. Roy. Soc. **200**, 401 (1950).

[12] Compare D. P. Craig, J. Chem. Phys. **18**, 236 (1950).

V-Centers in Alkali Halides

RUTH CASLER, PETER PRINGSHEIM, AND PHILIP YUSTER
Argonne National Laboratory, Chicago, Illinois

(Received July 12, 1950)

V-centers are defined as stabilized positive holes. The peak wave-lengths of three *V*-bands of KCl, KBr, and NaCl are listed. Most of the paper deals with KCl, but the results are typical for KBr and NaCl as well. Experimental data are given concerning the conditions under which the various *V*-bands are obtained and their unequal stability with regard to bleaching by light and temperature. Crystals irradiated at various temperatures and observed at room temperature show superpositions of the V_2- and V_3-bands with relative intensities depending greatly on the temperature at which the crystals were irradiated and on the nature of the primary radiation. The V_1-band can be observed only at temperatures below −100°C. These data are compared with those published by other investigators, and some remarks are made concerning the possible mechanisms which are responsible for the various phenomena.

WHEN *F*-centers are produced photo-chemically in alkali halide crystals by the capture of electrons in negative ion vacancies, positive holes (neutral halogen atoms) are left behind in the uppermost "filled" energy band of the crystal lattice. According to Seitz[1] these positive holes which have a relatively high mobility combine with positive ion vacancies and thus form *V*-centers with a characteristic absorption band in the u.v., the so-called *V*-band. In other words, a *V*-center is a positive ion vacancy surrounded by six halogens which share only five instead of six surplus electrons. When the notion of *V*-centers was introduced by Seitz, it rested on very scanty experimental data. Mollwo had obtained new bands in the absorption spectra of KBr and KI by heating these compounds in atmospheres of Br_2 and I_2 vapors respectively. The bands were diffuse, each with two incompletely resolved peaks, at 2300 and 2620A for KBr, and at 2790 and 3500A for KI. In both spectra the peaks at longer wave-lengths had by far the higher intensity.[2] Molnar,[3] whose measurements reached only to about 2400A in the u.v., observed a rise of the absorption curves of photo-chemically colored KCl and KBr in the spectral region below 2800A. Together with the *F*-band, this u.v. absorption band could be partially bleached by irradiating the crystal with *F*-light (light absorbed in the *F*-band). In additively colored crystals the new u.v. absorption was not observed.

TABLE I. Wave-lengths of *F*- and *V*-bands in *A*. (Values in parenthesis after Alexander and Schneider).

	F*	V_1†	V_2*	V_3*
NaCl	4650	3450	2226	2100 (2170)
KCl	5600	3600	2320	2155 (2205)
KBr	6200	4160	2650 (2580)	2320 (2320)

* At room temperature.
† At temperature of liquid N_2.

By extending the measurements down to 2050A almost complete *V*-bands were obtained in KBr, KCl, and NaCl.[4] It has been mentioned in a preceding paper[5] that under various conditions of excitation three bands, which are located at the short wave-length side of the *F*-band and can be interpreted as *V*-bands, were observed in the absorption spectrum of KCl. Analogous results have also been obtained with KBr and NaCl. Table I lists the peak wave-lengths of these bands. The bands characteristic of NaCl are less well-defined and thus more doubtful than those in the spectra of KCl and KBr. The V_1-bands are obtained in all these crystals only at the temperature of liquid N_2 and disappear when the crystals are warmed up to temperatures above −100°C. All *V*-bands are appreciably broader than the corresponding *F*-bands so that at equal peak intensities they would cover areas two to three times larger than those under the *F*-bands. In several instances it seems probable that an apparently simple broad band is caused by the superposition of more than one band.

Figures 1 and 2 show how V_1 of KCl vanishes together with a part of *F* when the crystal is warmed up to dry ice temperature or when it is exposed to light of 3650A absorbed in V_1. In both processes about the same fraction (30 percent) of the originally present *F*-centers is lost. Bleaching of *F* and V_1 can also be achieved, though with smaller efficiency, by exposing the crystal at −195°C to *F*-light (green and yellow Hg-lines). Figures 1 and 2 also exhibit the V_2 band of KCl at 2320A. In Fig. 2 it is practically unaffected when the crystal is bleached at −195°C by V_1-light, while in Fig. 1 even a slight increase in the intensity of V_2 and a shift of its peak towards shorter wave-lengths is noticeable after warming up for a short time to dry ice temperature. The unmistakable drop in the long wave-length tail of the band seems to indicate that still another unstable band might be submerged under V_2, but this result, although obtained repeatedly, may still be doubtful.

[1] F. Seitz, Rev. Mod. Phys. **18**, 384 (1946).
[2] G. Mollwo, Ann. d. Physik **29**, 394 (1937).
[3] J. P. Molnar, unpublished thesis, M.I.T., 1941; curve for KCl reproduced in paper quoted under reference 1.
[4] R. Casler and P. Pringsheim, ANL-4359, Quarterly Report for January, February and March, 1949; J. Alexander, and E. E. Schneider, Nature **164**, 653 (1949).
[5] Casler, Pringsheim, and Yuster, J. Chem. Phys. **18**, 887 (1950).

Figure 3 represents the complete absorption spectrum of KCl after much longer exposure to x-rays at −195°C (so that the peak of the *F*-band is too high for precise measurement) and subsequent warming up to room temperature. Immediately after the x-ray irradiation at liquid N_2 temperature the *F*-center concentration was a good deal higher. About 66 percent of the *F* centers[5] together with all the V_1-centers and an appreciable fraction of the V_2-centers are lost in the warming-up process.

A few remarks concerning the various bands on the long wave-length end of the spectrum may be inserted here. These remarks apply also to KBr and NaCl. After the primary exposure to x-rays only a relatively weak *M*-band is obtained in this spectral region. By exposure to *F*-light the *F*-band is reduced, the *M*-band is enhanced, and the *R*- and *N*-bands[6] appear. The *R*-bands are not produced directly by x-rays and, if a crystal in which *R*-bands had been formed by irradiation with *F*-light is re-exposed to x-rays, the *R*-bands are again destroyed; simultaneously the enhanced *M*-band is reduced to its previous low value which seems to correspond to an equilibrium between production and destruction by the action of x-rays. Furthermore, the *R*-bands are unstable at room temperature; after a day in the dark they decrease appreciably, while the intensity of *M* increases (*b'* in Fig. 3). After prolonged bleaching with *F*-light all bands merge into a continuous background with relatively small intensity fluctuations and finally they vanish almost completely.

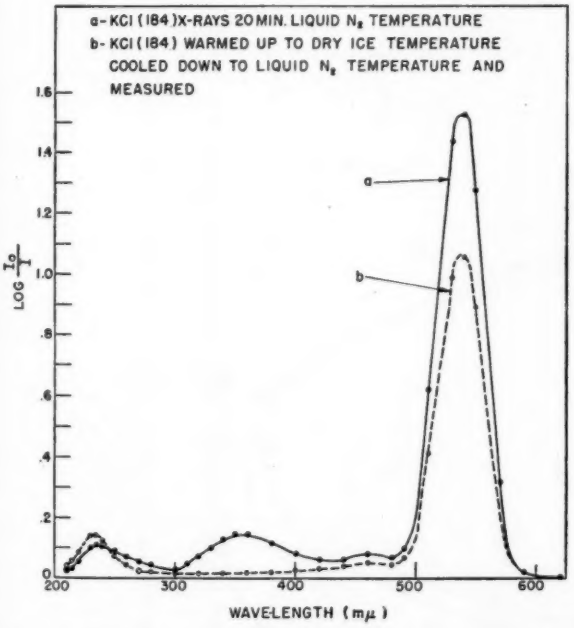
a- KCl (184) X-RAYS 20 MIN. LIQUID N₂ TEMPERATURE
b- KCl (184) WARMED UP TO DRY ICE TEMPERATURE
COOLED DOWN TO LIQUID N₂ TEMPERATURE AND
MEASURED
LOG I₀/I
WAVELENGTH (mμ)

FIG. 1. KCl exposed to x-rays at liquid N_2 temperature and partially bleached by warming up to dry ice temperature; measured at liquid N_2 temperature.

[6] P. Pringsheim, ANL-4380, Summary Report for April through September, 1949; E. Burstein and J. J. Oberly, Phys. Rev. **76**, 1254 (1949).

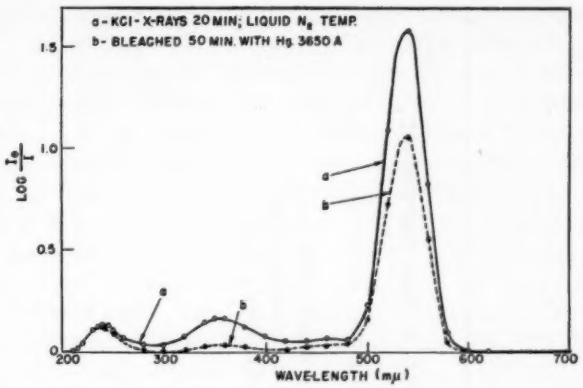

FIG. 2. KCl exposed to x-rays at liquid N_2 temperature and partially bleached by V_1-light (Hg 3650A); measured at liquid N_2 temperature.

When KCl (and similarly KBr and NaCl) containing *F*-centers is bleached by irradiation with *F*-light, the short wave-length tail of the *F*-band itself is always enhanced. The difference between the absorption curves in this part of the spectrum before and after bleaching corresponds to the formation of a new absorption band which has its peak at 4800A.

The band V_1 is completely absent in Fig. 3, but V_2 is very strongly and somewhat unsymmetrically developed, possibly with another weaker band hidden under its long wave-length tail. By exposing the crystal to *F*-light (all radiation of $\lambda < 5200$A carefully screened off) in several steps, the V_2-band is bleached in parallel with the *F*-band. However, the long wave-length part of the band disappears more rapidly than the peak and in the later steps a shift from 2320 to 2180A occurs in the peak wave-length of the band. This shift is even visible in curve *c* and is much more pronounced in curve *d*. On the last curve (*e*) only a weak band with peak at 2180A remains visible.

When a sample of KCl has been exposed to x-rays at −75°C and subsequently warmed to room temperature (Fig. 4), the *V*-band, which in this case is obviously a superposition of at least two bands, has its peak at 2200A. After bleaching the crystal with *F*-light, the component of longer wave-length disappears more and more until finally only a short wave-length component with peak at 2160A remains, but with relatively much higher intensity than in Fig. 3. Whereas the peak of the complex *V*-band drops in Fig. 3 after three hours bleaching by about 80 percent (curve *d*), it drops in Fig. 4 after three hours bleaching by only 40 percent.

In KCl exposed to x-rays at room temperature the V_3-band predominantes in the spectral region accessible to the Beckman spectrophotometer (Fig. 5). Much longer exposures to *F*-light are needed in order to obtain a drop in the *F*-band intensity of the same order of magnitude: the curves *d* in Figs. 4 and 5 correspond to bleaching times of three and forty-four hours respectively. The *F*-centers seem to be much more stable in the second instance and the V_3-band has lost

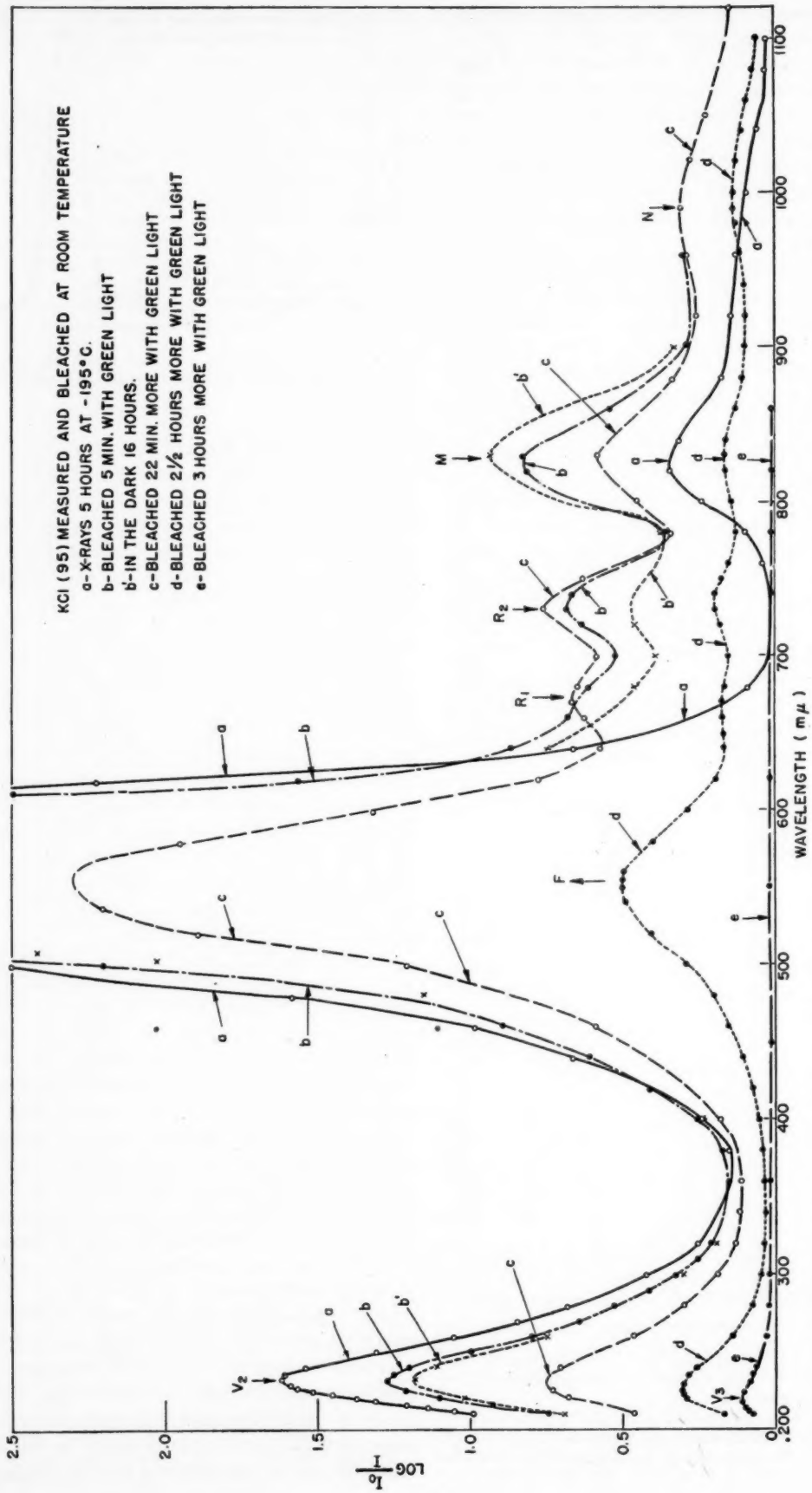
KCl (95) MEASURED AND BLEACHED AT ROOM TEMPERATURE
a - X-RAYS 5 HOURS AT - 195° C.
b - BLEACHED 5 MIN. WITH GREEN LIGHT
b' - IN THE DARK 16 HOURS.
c - BLEACHED 22 MIN. MORE WITH GREEN LIGHT
d - BLEACHED 2½ HOURS MORE WITH GREEN LIGHT
e - BLEACHED 3 HOURS MORE WITH GREEN LIGHT
WAVELENGTH (mμ)
LOG Io/I
V2
V3
R1
R2
M
N1
F

FIG. 3. KCl exposed to x-rays at liquid N_2 temperature and bleached at room temperature with *F*-light (green and yellow Hg-lines); measured at room temperature.

very little of its peak intensity even at the end of the longest bleaching period. However, the long wave-length branch of the *V*-band drops relatively much more than the peak. It is plausible to suppose that even here a weak V_2-component is superimposed on the V_3-band and this may be the cause of the decrease in the ultra-violet absorption due to bleaching by *F*-light which Molnar mentions in his thesis.

Figures 6–8 show superpositions of V_2 and V_3 at different relative intensities obtained under various conditions. The curves of Fig. 6 prove that the relative intensities of the two bands depend not only on the temperature at which they were produced, but also on the nature of the "photo-chemically active" primary radiation.* By "hard x-rays" from a 50-kv tube filtered through 1.6 mm of aluminum an almost pure V_3-band with peak at 2150A is produced (curve *c*). After irradiation with "soft x-rays" from the same tube with beryllium window, but without the aluminum filter, the *V*-band is much broader and its peak is shifted to 2200A (curve *b*). After bombardment at room temperature with 1-Mev electrons from a Van de Graaff machine the band is still appreciably wider and its peak lies at 2300A (curve *a*), but if the crystal is exposed to electron bombardment from the same source at 60°C, the *V*-band has its peak at 2160A and is again practically a

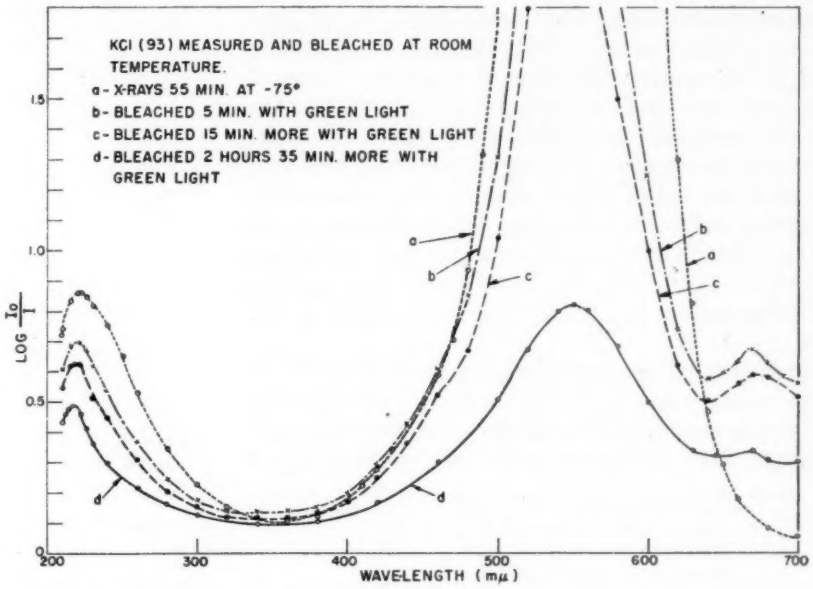
KCl (93) MEASURED AND BLEACHED AT ROOM TEMPERATURE.
a - X-RAYS 55 MIN. AT -75°
b - BLEACHED 5 MIN. WITH GREEN LIGHT
c - BLEACHED 15 MIN. MORE WITH GREEN LIGHT
d - BLEACHED 2 HOURS 35 MIN. MORE WITH GREEN LIGHT
LOG I0/I
WAVELENGTH (mμ)

FIG. 4. KCl exposed to x-rays at dry ice temperature and bleached at room temperature with *F*-light (green and yellow Hg-lines); measured at room temperature.

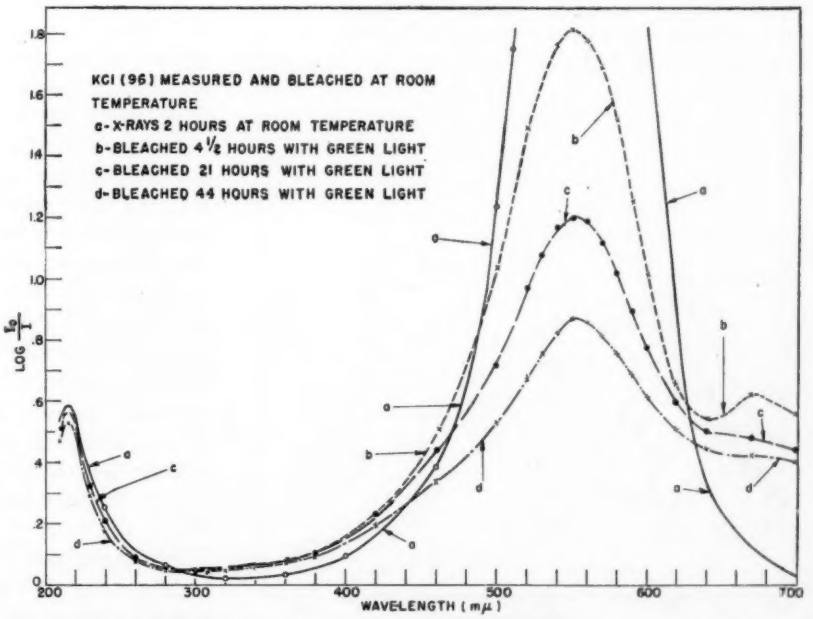
KCl (96) MEASURED AND BLEACHED AT ROOM TEMPERATURE
a - X-RAYS 2 HOURS AT ROOM TEMPERATURE
b - BLEACHED 4 1/2 HOURS WITH GREEN LIGHT
c - BLEACHED 21 HOURS WITH GREEN LIGHT
d - BLEACHED 44 HOURS WITH GREEN LIGHT
LOG I0/I
WAVELENGTH (mμ)

FIG. 5. KCl exposed to x-rays at room temperature and bleached at room temperature with *F*-light (green and yellow Hg-lines).

* By altering the nature of the primary radiation the rate of *F*-center formation and the exposure time are also changed. Experiments are now under way investigating which of these factors determines the preferential formation of one type of *V*-centers and the stability of the corresponding *F*-centers.

pure V_3-band (curve *d*). Moreover, the bands represented by curves *a* and *b* are in part unstable. After three days at room temperature in the dark they are converted into the curves *a'* and *b'*, in the main due to the weakening of their long wave-length branches, which originate from the presence of V_2-centers. Simultaneously the *F*-bands of these crystals lose some of their intensity, while the *F*- and *V*-bands of the crystals, represented by curves *c* and *d* remain practically unaltered.

If a KCl crystal, in which a complex V_3+V_2 band has been produced by irradiation with soft x-rays, is heated to 150°C, the band does not only lose intensity, but its peak is shifted to shorter wave-lengths and its half-width decreases; both effects result from the fact that the less stable V_2-centers are destroyed more rapidly than the V_3-centers. However, if a crystal irradiated with hard x-rays and containing only V_3-centers undergoes the same heat treatment, the *V*-band peak drops at a much slower rate—only by six percent in one hour against 16 percent in twenty minutes—and without any noticeable shift in wave-length. This constancy of the spectral distribution holds even through prolonged heating at 200°C (Fig. 8). The *F*-band, too, vanishes much less rapidly under heat treatment in the second case.

Figure 9 is reproduced as an example of the behavior of one of the other alkali halides. It represents the absorption spectrum of KBr exposed to electron bombardment at −70°C and corresponds very nearly to Fig. 4

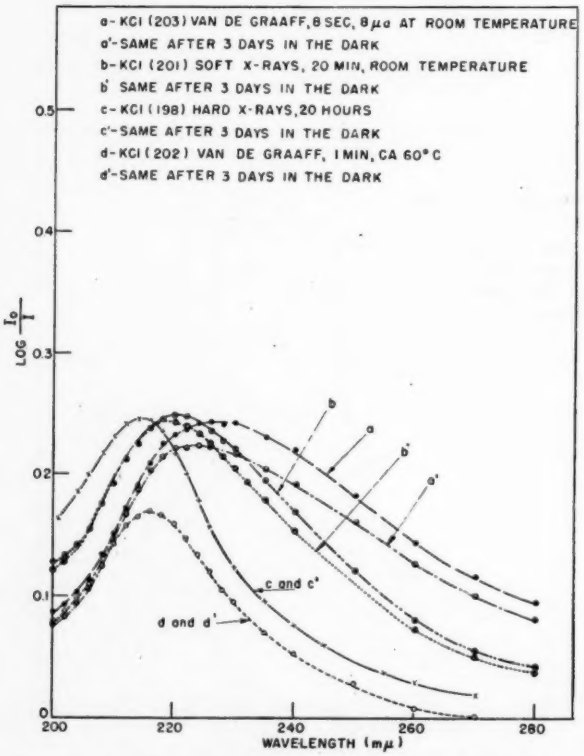

FIG. 6. *V*-bands of KCl exposed to Van de Graaff electrons, soft x-rays and hard x-rays.

for KCl. Curves corresponding to those of Figs. 1, 2, 3 and 5 were also obtained with KBr and a little less completely with NaCl.

DISCUSSION

If two or more lines or bands of an absorption spectrum are coupled so that they appear and disappear together, they can either originate from the same initial state and represent transitions to various final states or they can correspond to different initial states which are produced and destroyed by the same process. In the first case, represented by every absorption series of a vapor at moderate temperature, the relative intensities

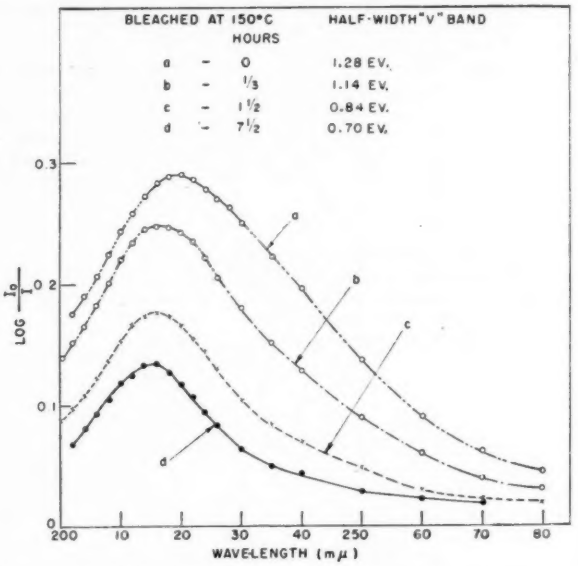

FIG. 7. *V*-bands of KCl exposed to soft x-rays at room temperature and bleached by heating to 150°C.

of the various lines or bands forming the series will be practically independent of external conditions, especially when the transitions correspond to fairly high oscillator strengths; only the intensity of a forbidden line is sometimes greatly enhanced by a strong external field. In the second case, which corresponds to Seitz's interpretation of the relation between *F*- and *V*-centers, the relative numbers of *F*- and *V*-centers can vary if there are still other electron surplus centers (such as *R*, *M*, *N*-centers) and more than one type of electron deficiency center. Without ascribing to the different *V*-centers specific configurations, each of them may be supposed to be a positive hole attached to some sort of irregularity in the crystal lattice, such as a simple positive ion vacancy, a positive ion vacancy associated with a divalent positive ion, an internal mosaic plane, etc.

Alexander and Schneider[4] report that KCl discolored by exposure to x-rays shows a single *V*-band which follows closely the theoretical absorption curve of a classical oscillator. Their values for the peak wave-lengths of *V*-bands, which do not agree too well with

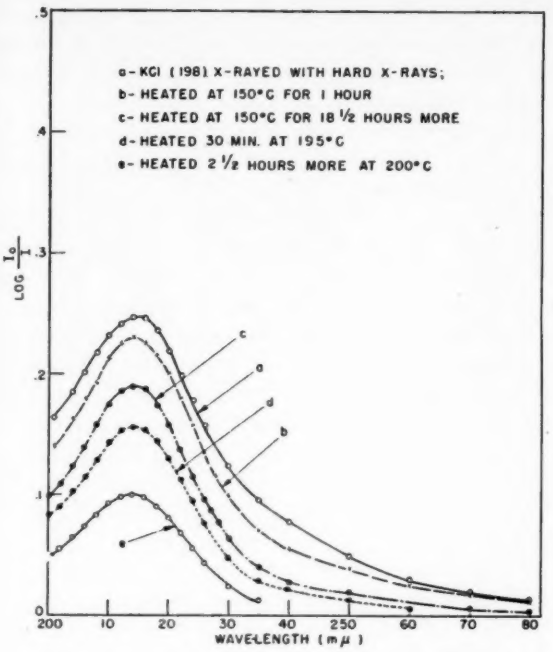
a- KCl (198) X-RAYED WITH HARD X-RAYS;
b- HEATED AT 150°C FOR 1 HOUR
c- HEATED AT 150°C FOR 18 ½ HOURS MORE
d- HEATED 30 MIN. AT 195°C
e- HEATED 2 ½ HOURS MORE AT 200°C
LOG I₀/I
WAVELENGTH (mμ)

FIG. 8. V-bands of KCl exposed to hard x-rays at room temperature and bleached by heating to 150 and 200°C.

ours, are inserted in parentheses in Table I. Figure 10 reproduces their curve representing the V-band of KCl and the curves b and c of Fig. 6 redrawn with ev instead of wave-length as ordinate. The curves are very similar, a coinciding almost completely with c. Figure 6 shows that b is converted into b' by aging and, according to Fig. 7, its peak is shifted by annealing from 2220 to 2150A; therefore it is not due to a single oscillator but corresponds to the superposition of at least two bands belonging to centers of different stabilities.

Figure 11 shows the V-band with double peaks observed by Mollwo (a), by Alexander and Schneider (b), and a curve which we obtained by bleaching a KBr crystal seventeen hours with F-light (c). Before bleaching, the crystal which had been exposed to electron bombardment at −15°C exhibited a broad absorption band with a blunt peak at 2550A. The similarities and discrepancies between the curves of Fig. 11 are obvious. Following the interpretation which Franck and Scheibe[7] proposed for similar spectra observed in aqueous solutions of alkali halides, Alexander and Schneider interpret the twin peaks as due to a typical doublet transition in one center, namely to the transition of an electron from a neighboring Br^- ion into the positive hole of the V-center, leaving the neutral Br atom either in the $P_{1/2}$ or in the $P_{3/2}$ state. In Table II the energy differences between these two states are compared with those between the V_2 and V_3 peaks. Unfortunately no well-defined V-bands could be obtained with samples of synthetic KI for which the energy gap between the P-states is twice as large as for KBr. The numerical agreement between the KBr values in lines 1 and 2 of Table II may be regarded as acceptable. However, the agreement is much poorer with respect to the V_2-V_3 value of line 3. A comparison between line 1 and line 3 for KCl certainly is not in favor of the doublet interpretation.

According to the curves in Figs. 3, 5, and 9 it is possible to prepare KBr and KCl crystals so that they exhibit a V-band with a single sharp peak either corresponding to V_2 or V_3. As stated above, it is highly improbable that such extreme differences can occur in the relative intensities of the components of a doublet due to the transitions from a common initial state. On the other hand, there is no reason to assume that under the action of F-light radiation or heat bleaching V_2-centers are partially converted into V_3-centers, for the apparent shift of the band peak is never accompanied by an increase in intensity of the short-wave-length branch of the band, so that the V_3-band emerging at the end of the treatment can well have been hidden

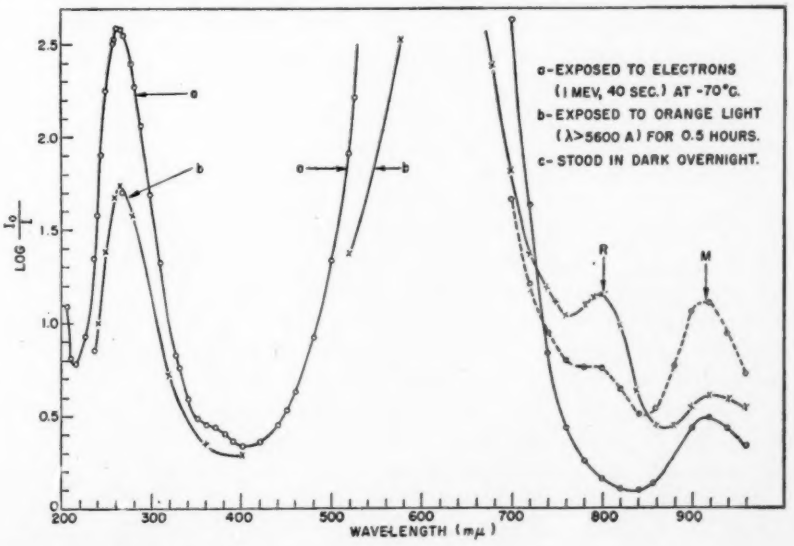

FIG. 9. KBr exposed to Van de Graaff electrons at dry ice temperature and bleached at room temperature with F-light (orange light).

[7] J. Franck and G. Scheibe, Zeits. f. physik. Chemie **A139**, 22 (1928).

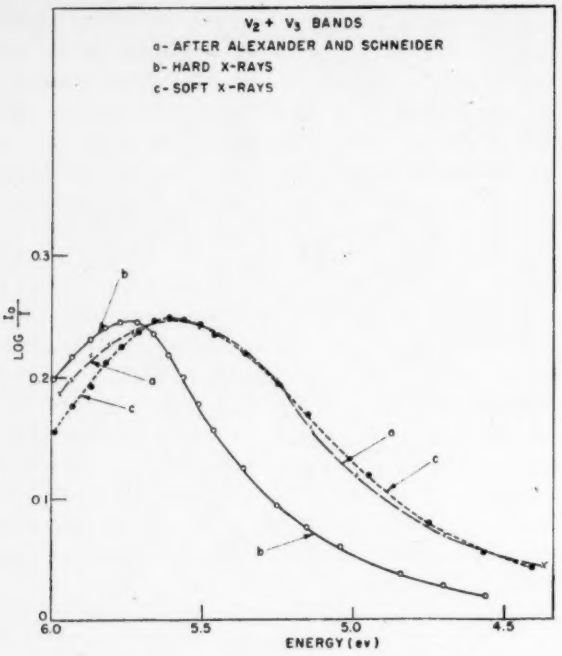

FIG. 10. V-bands of KCl on an ev scale obtained under various conditions.

previously under the original complex band. The only deviation from this normal behavior is observed in Fig. 1, where by warming a KCl sample from $-195°C$ to room temperature either a part of the V_1-centers or some others are converted into V_2-centers.

The relative numbers of the various V-centers can differ depending on the temperature at which they are produced for two reasons: because of their lower stability certain centers (e.g., V_1), even if produced at higher temperatures, vanish again spontaneously; because an activation energy must be provided for their production, other more stable centers (e.g., V_3) can be produced only at higher temperatures. It is not yet possible, however, to interpret the influence of the nature of the primary radiation (soft or hard x-rays, Van de Graaff electrons) on the relative concentrations of V_2- and V_3-centers. Alexander and Schneider found that, at higher F-center concentrations obtained by long irradiation times, V_3-centers prevail (curve b in Fig. 11), while after shorter exposure to x-rays, producing a low F-center concentration, the component at 2580A is relatively stronger than the peak at 2320A. In our experiments most of the F-centers produced by soft x-rays lie in a very thin layer near the surface, while by hard x-rays F-centers are produced uniformly throughout the crystal; therefore at equal optical densities the concentration of F-centers is much larger when they are produced by soft x-rays than when produced by hard x-rays. Nonetheless there are more V_2-centers produced in the first than in the second case.

Light absorption by a V-center is caused either by an electronic transition in the interior of the center or by the transition of an electron from a neighboring ion into the V-center. It is difficult to imagine a mechanism by which a process of the first type can be associated with the simultaneous disappearance of an F-center. Since F-centers actually disappear when KCl at $-195°C$ is exposed to V_1-light (Fig. 2), the second process must be made responsible in this particular case. A similar hypothesis has been introduced by Alexander and Schneider, except for their additional assumption concerning the two final states of the halogen atom. If, following the destruction of the V-center, an F-center also disappears and no new absorption band appears, the F-center electron must recombine with a neutral halogen atom. This need not be the identical atom which has delivered its excess electron to the V-center, but once the positive hole has been separated from the V-center it may migrate through several lattice cells before it reaches an F-center. The mobility of a positive hole should increase rather than decrease with decreasing temperatures. The energies necessary for both steps, the separation of the positive hole from the V_1-center and the transfer of the electron from the F-center to the positive hole, must be relatively small, since they occur with high probability at temperatures as low as $-100°C$. As in the case of bleaching with V_1-light, this temperature bleaching is almost certainly not initiated by the transfer of an electron from the F-center to the conduction band, but by the liberation of a positive hole from a V_1-center.

V_2-centers are bleached with a high yield by irradiating a crystal containing F- and V_2-centers at room temperature with F-light (Figs. 3, 4, and 9). In this

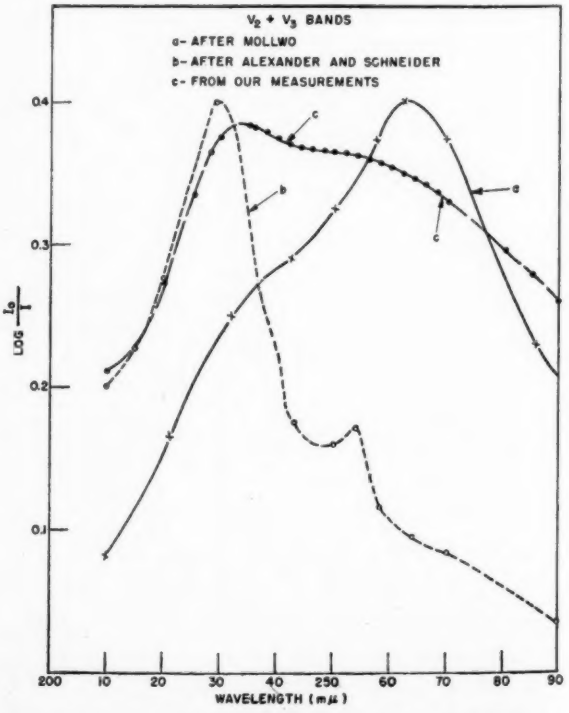

FIG. 11. Superposition of V_2- and V_3-bands in KBr obtained by various authors.

instance electrons pass through the conduction band from the F- to the V-centers and have a high probability of recombining with the latter. Apart from the fact that nothing is known about the exact oscillator strength of the V-centers, a 1:1 ratio for the bleaching rate of F- and V-centers cannot be expected, because an unknown part of the disappearing F-centers is replaced by R, M, N-centers, all of which are electron surplus centers. A part of the V_2-centers formed at low temperatures (at -195°C and even at -75°C) vanish together with a part of the F-centers when the crystals are warmed up to room temperature and also, to a smaller degree, during the first hours after they have reached room temperature (Fig. 6a and b). Later they are very nearly stable (Fig. 4). Because of this last fact their partial disappearance at relatively low temperatures can neither be due to the temperature separation of positive holes from the V_2-centers, as in the case of the V_1-centers, nor to the recombination with electrons raised from the F-centers to the conduction band, since the number of such electrons would not appreciably decrease after a few hours at room temperature. It may be, however, that without affecting the characteristic absorption bands of F- and V_2-centers, some V_2-centers lie close enough to F-centers that electrons can be transferred directly from the latter to the former by a tunnelling effect, a phenomenon which would be favored by raising the temperature. When all V_2-centers in the neighborhood of F-centers are exhausted, the remaining V_2-centers would be relatively stable.

V_3-bands are not at all, or only slightly, bleached by irradiation at room temperature with F-light. Since the probability of raising electrons from F-centers to the conduction band does not depend on the nature of the V-centers present in the crystal, it must be assumed that, in order to recombine with the positive holes stabilized in V_3-centers, electrons in the conduction band must overcome a potential barrier and that this requires an energy not available at room temperature. No new experimental data are available concerning the possibility of bleaching V- and F-centers by exposing a crystal to light absorbed in the V_2- and V_3-bands, except a qualitative observation showing that the F-band of KCl is bleached with much higher efficiency by the total radiation from a quartz-Hg-arc than by the radiation from the same source with the u.v. screened off. According to Alexander and Schneider the V-band of KCl, probably a superposition of V_2 and V_3, is bleached by V-light with a quantum efficiency ~ 1, without affecting the F-band, while a simultaneous irradiation with F- and V-light produces a rapid disappearance of both bands.

TABLE II. Energy differences between the P-levels of the halides and the V-bands of potassium halides in electron volts.

	Cl	Br	I
$P_{1/2}-P_{3/2}$	0.11	0.44	0.9
V_2-V_3 (A and S)	—	0.55	—
V_2-V_3 (Authors)	0.40	0.66	—

Most of the observations discussed above can be represented by the following picture. Absorption of F-light raises electrons to an excited level within the F-centers and from there they pass into the conduction band with a probability which at room temperature is practically 100 percent, and is still finite at -195°C. Electrons in the conduction band can combine with V_1 (and V_2) centers even at -195°C; at room temperature they are captured with high probability by V_2-centers, but not by V_3-centers. If the electrons are captured by V-centers, V- and F-centers disappear; otherwise F-centers are reformed or other electron surplus centers are produced. V-light absorption separates a positive hole from a V-center. In the case of V_1-centers the positive hole is free to drift away and thus can recombine with an F-center, destroying it. V-centers and F-centers can also be destroyed by increase of temperature. Under these conditions the separation of the positive hole from the V-center may be due rather to a positive ion jumping into the positive ion vacancy which is a part of the V-center, than to an electron jumping from a neighboring halogen ion into the positive hole.

In the case of the simultaneous disappearance at low temperatures of V_1- and F-centers the temperature bleaching seems to be due to the recombination of F-centers with positive holes which have been separated completely from the V-center, as mentioned previously. In the case of temperature bleaching at higher temperatures of crystals containing only V_2- and V_3-centers, the same may at least be partially true, while a part of the bleaching may be due to the recombination of V-centers with F-center electrons raised thermally into the conduction band, or to a direct recombination of the F-center electron with the V-center by tunnelling.

I. The Vaporization of Strontium Oxide

GEORGE E. MOORE, H. W. ALLISON, AND J. D. STRUTHERS
Bell Telephone Laboratories, Inc., Murray Hill, New Jersey

(Received July 24, 1950)

The vapor pressure of SrO was measured by studying the product evaporated from platinum filaments coated with SrO. Most of the experiments employed radiactive isotopes.* The possibility of systematic error caused by chemical reduction of the oxide or by its thermal dissociation is discussed. A value of λ_0, the heat of evaporation at 0°K computed from the results, is used to evaluate precision and to derive a vapor-pressure equation.

INTRODUCTION

SEVERAL authors discuss the nature of the products leaving hot alkaline earth oxide layers supported on metallic cores, but their conclusions are in conflict. For example, using mass spectrometer techniques, Barton, Harnwell, and Kunsman[1] concluded that Sr metal ions formed the principal product of platinum filaments, coated with a mixture of iron oxide and SrO. Similarly, Blewett and Jones[2] concluded that Sr metal ions were produced in SrO if the support metal were tungsten, or tungsten coated with platinum. Becker[3] observed thermionic activation of clean tungsten receiver filaments mounted adjacent to platinum alloy filaments coated with a mixture of BaO and SrO. He attributed the activation of the tungsten to Ba atoms (rather than ions) formed in the oxide coat by treatments which he described. However, Davisson and Pidgeon[4] and Hull[5] concluded that the material activating the receivers in their experiments was evaporated BaO, rather than Ba or Sr metal. Furthermore, the published vapor pressures for the alkaline earth oxides (CaO, SrO or BaO) are all[6,7,8] based on

(a) measurements of the total product leaving a layer of the oxide supported on heated platinum, and

(b) the assumption that this product left the oxide layer entirely in the form of oxide molecules, rather than metallic atoms of the oxide molecules. Experimental evidence to justify this assumption has never been published.

The nature of the products leaving heated filaments coated with SrO is discussed in this and the following paper. In the first (designated I) the support metal was Pt and the product essentially pure SrO. In the second (designated II) the support metal was tungsten and the product nearly pure Sr metal. Because many of the techniques are similar and comparison of the results is desirable, the two papers are presented together. The phenomena were considered thermodynamically, and it was shown that observable reduction of SrO by platinum would not be expected; this was confirmed experimentally. However, when the support is tungsten, such reduction would be expected and occurs at nearly the predicted rate.

The vapor pressure of SrO is of interest in the physics and chemistry of oxide cathodes, in the study of ionic crystals and their vapors,[9,10] and in thin film adsorption phenomena.[11] The present results are in general agreement with those of Claassen and Veenemans[6] but extend to lower temperatures.

EXPERIMENTAL

Method

In the determination of vapor pressure a number of tubes were made, each containing a platinum filament coated with SrO. The filament was operated at a controlled temperature for a known length of time during which a total mass μ of SrO molecules vaporized and deposited on the bulb. This total, μ, was reduced to mass, m, leaving each cm² of filament surface per second; m was then converted to a pressure p by the kinetic theory[12] equation:

$$m=(M/2\pi RT)^{\frac{1}{2}}p, \qquad (1)$$

where M is the molecular weight of SrO=103.63, R is the gas constant=8.314×10^7 ergs per degree, p is the vapor pressure in dynes per square centimeter, and T is the temperature in °K. Each tube thus gave an experimental value of p for a given T, and a group defined the vapor pressure curve.

Tube Design

Figure 1 shows the tube design which evolved for the measurement of evaporated products in both I and II. A long glass (702*EJ*) outer bulb B contained a glass thimble T about half as long as B and making a sliding fit in B. The filaments were of platinum coated with $SrCO_3$. The tube was pumped in the position shown, T

* The isotopes were obtained from Oak Ridge National Laboratory on allocation by the AEC.

[1] Barton, Harnwell, and Kunsman, Phys. Rev. **27**, 739 (1926).
[2] J. P. Blewett and E. J. Jones, Phys. Rev. **50**, 464 (1936).
[3] J. A. Becker, Phys. Rev. **34**, 1323 (1929).
[4] C. J. Davisson and H. A. Pidgeon, Phys. Rev. **15**, 553 (1920).
[5] A. W. Hull, Phys. Rev. **56**, 86 (1939).
[6] A. Claassen and C. F. Veenemans, Zeits. f. Physik **80**, 342 (1933).
[7] G. Herrmann, Zeits. f. physik. Chemie **35B**, 298 (1937).
[8] Blewett, Liebhafsky, and Hennelly, J. Chem. Phys. **7**, 478 (1939).
[9] O. K. Rice, *Electronic Structure and Chemical Binding* (McGraw-Hill Book Company, Inc., New York, 1940).
[10] DeBoer and Verwey, Rec. trav. chim. **55**, 443 (1936).
[11] G. E. Moore and H. W. Allison, Phys. Rev. **77**, 246 (1950).
[12] I. Langmuir, Phys. Rev. **2**, 329 (1913).

covering the filament structure while the $SrCO_3$ was dissociated to SrO. T thus intercepted any SrO or other molecules leaving the filament during this period. After exhaust and conditioning of the filament for quantitative experiment, the tube was inverted and the base AA of T assumed the position $A'A'$ indicated by dotted lines. The filament was then operated for a known length of time at a controlled temperature. Substantially all of the material leaving the filament was thus deposited on the outer bulb. T was then lowered and the bulb opened around the section AA. The interior surfaces of bulb and thimble were then washed out with 50 cc of 0.01N HCl and samples suitable for analytic determination (gravimetric, polarographic, or radioactive) made of each of two or three washings from each surface. Tests made on tubes containing radioactive coatings showed that the first wash always removed at least 99 percent of the SrO deposited on the bulb. Only the deposit on the outer bulb was used in the results stated; the deposit on the inner bulb gave control information. Getters were not used in any of the tubes in either I or II although this should be practicable in conjunction with the radioactive method of analysis used in most tubes.

The gravimetric and polarographic tests were made on tubes constructed before the thimble T was adopted. The amount of the total bulb deposit was made sufficiently large that the deposit during exhaust was only a small fraction of the total.

Preparation of Filaments

The platinum and the $SrCO_3$ were very pure. Their analysis, together with some of the pretreating, coating, and exhaust methods were described earlier.[11] The same methods were used in the present work except that

1. Pt black was added in some coatings in order to increase the spectral emissivity. The emissivity correction to be applied to observations with the optical pyrometer is appreciable; both the magnitude and probable percentage error in this correction increase with the whiteness of the coat. Higher precision was therefore expected from the filaments in which Pt black was mixed with the $SrCO_3$ but was not evident, probably because the "blackness" of these filaments tended to diminish with aging. The results with such filaments showed no trend that would distinguish them from those prepared without Pt black.

2. In most tubes, a small fraction of the $SrCO_3$ applied to the filament was radioactive. In commercial practice, the alkaline earth carbonates are generally mixed as a suspension in amyl acetate and cellulose nitrate. This homogeneous mixture is applied to the cathode support metal by a spray method, much as in commercial painting, and considerable material is lost into space. The hazard in thus handling radioactive isotopes does not exist in methods developed by B. A. Diggory. In one method he applies a drop of the $SrCO_3$-amyl acetate-cellulose nitrate mixture to an eyelet formed by bending a 1-mm nickel wire into a loop about 3 mm in diameter and then draws the filament back and forth through the center of the loop, allowing the amyl acetate in the coat to dry after each passage, until about 5 mg/cm² of $SrCO_3$ has been deposited.

Two sources of radioactive Sr were utilized. (a) Fission Sr in the form of $SrCl_2$ was mixed with non-radioactive $SrCl_2$ and the mixture then converted to $SrCO_3$ by precipitation with ammonium carbonate. The carbonate was applied to the platinum by the "eyelet" method. Fission Sr is carrier-free and consists of a mixture of Sr^{89} and Sr^{90}. Tests gave no indication of radioactive impurities other than Y^{90}, the daughter product of Sr^{90}. If any other impurity were present in appreciable quantity, its half-life was much less than the 53-day value for Sr^{89}.

(b) Purified non-radioactive Sr compounds can also be made radioactive by neutron bombardment. For many months after this treatment, the radioactivity of such samples is caused almost entirely by Sr^{89}. Although fission Sr has a specific activity many orders of magnitude greater than that of the pile-bombarded product, present coating methods limit the practical gain in sensitivity in experiments such as these to a factor of about 1000.

(3) Although the filaments produced by the eyelet technique are generally satisfactory, the method is troublesome and does not yet always give as adherent a coating as the conventional spray method. Diggory therefore suggested coating the filaments by the commercial spray method with non-radioactive carbonates and then irradiating the coated filaments at Oak Ridge. The filament support metal itself also becomes radioactive; consequently, volatile impurities in the support metal or volatile compounds formed by chemical reaction with the coat should be detectable on the bulb walls. This property was found useful in both I and II.

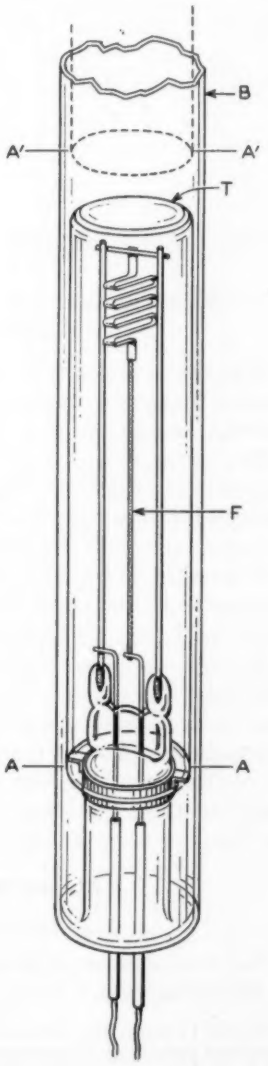

FIG. 1. Tube for measuring evaporated SrO.

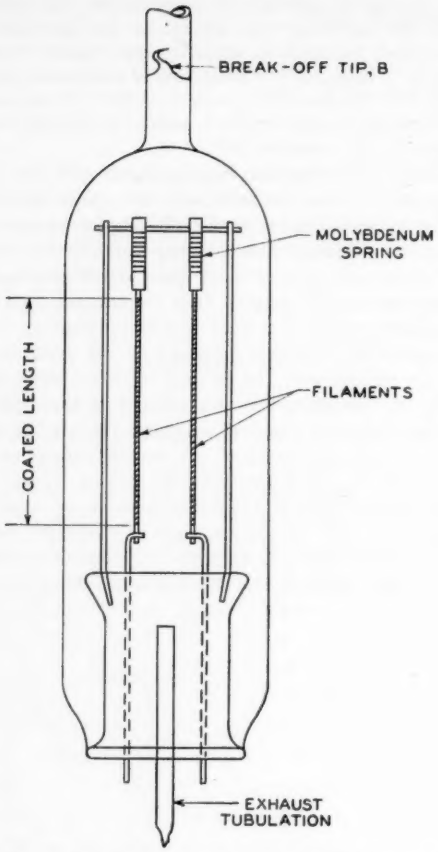

FIG. 2. Tube for determining Sr metal formed by reduction.

Measurement and Control of Filament Temperature

Apparent temperature was measured with a disappearing filament optical pyrometer. The correction for spectral emissivity was determined in a cylindrical reflectometer as described by Prescott[13] and used subsequently by others.[14,15] The correction for transmission through the glass bulb was determined in the usual way, assuming the bulb deposit to be reasonably uniform. SrO deposits, obtained in I, do not sensibly affect the pyrometer readings; but the Sr metal deposits, investigated in II, require appreciable correction.

For the platinum filaments of I, the reaction was primarily the simple physical process of evaporation and the maintenance of a constant heating current gave a reasonably constant temperature. (This was not true for the tungsten filaments of II.) In the later tubes, the radiation from the filaments was used for monitoring the temperature photoelectrically during aging.

Measurement of μ

(*a*) *Radioactive Tests*

The total number of Sr atoms (free, in SrO molecules, or otherwise) which have left the filament can be determined most conveniently by using radioactive isotopes. The "count" in a washing from the bulb is compared with the count from a known aliquot of the mixture used to coat the filament. This method implicitly assumes that the isotopes are thoroughly mixed and the isotopic ratio unaffected, within experimental precision, by the physical and chemical processes involved in the departure of the SrO molecules from the filament. The agreement observed in both I and II between gravimetric, polarographic, and other analytical methods, all using non-radioactive SrO, and the results of tests using radioactive isotopes indicates that the isotope method is accurate within the precision of these experiments. However, published evidence[16,17] indicates that exact agreement is not always found in analytical procedures depending on constant isotopic ratio.

The aliquot method should be capable of better than 3 percent precision in measuring total Sr on the bulb in amounts of 1 microgram or less; but the method does not distinguish between small amounts of SrO mechanically transferred and the amount leaving the filament by the evaporation process investigated. Accidental contamination by mechanical transfer, or otherwise, may amount to 0.1 microgram, so that the total deposit should be 1 microgram or more for precision.

The use of the thimbles until the $SrCO_3$ is dissociated eliminates the possibility that the product on the outer bulb contains an appreciable fraction of carbonate molecules; it is shown below that the fraction in the form of Sr atoms was less than 1 percent.

(*b*) *Polarographic and Gravimetric Determinations*

Polarographic.—The washing from the bulb was evaporated to dryness to remove the acid. The residue was dissolved in water and transferred to a 10-ml volumetric flask; 20 mg of tetra-methyl-ammonium iodide was added to provide the supporting electrolyte, and the solution diluted to the 10-ml volume. Polarograms were then run in the usual manner. In the earlier work, a small amount of lithium chloride was also used to provide the supporting electrolyte, but later work showed that satisfactory polarograms could be obtained with the tetra-methyl-ammonium iodide alone. Blank runs were made using the same reagents and techniques employed for the samples, and the necessary corrections were applied before calculating the amount of oxide present.

Gravimetric.—In the gravimetric analyses a few drops of sulfuric acid were added to 5 ml of the solution prepared for the polarograph, and evaporated to fuming. Any organic matter was destroyed by adding a few drops of nitric acid. The residue was then taken up in 5 ml of a 1:1 alcohol-water solution and allowed to digest overnight. The sulfates were then filtered on a microgooch crucible, ignited, and weighed. Here, also,

[13] C. H. Prescott, Jr., *Temperature, Its Measurement and Control* (Reinhold Publishing Corporation, New York, 1941), p. 1199.
[14] G. E. Moore and H. W. Allison, J. App. Phys. **5**, 431 (1941).
[15] Hannay, MacNair, and White, J. App. Phys. **20**, 669 (1949).
[16] See, for example, p. 835 in Thiers, Graydon, and Beamish, Anal. Chem. **20**, 831 (1948).
[17] P. E. Yankwich, Anal. Chem. **21**, 318 (1949).

blanks were run and the appropriate corrections applied.

Tests for Sr Metal Formed by Heating

The most direct method for measuring the Sr metal produced in either I or II involved a tube as shown in Fig. 2. After exhaust and aging at a known temperature for a suitable time interval, the tube was sealed to a gas analysis system. The break-off tip permitted introduction of water vapor without impairing the vacuum. Sr metal anywhere in the tube produced H_2 by the reaction

$$Sr+H_2O \rightarrow H_2+SrO,$$

giving one molecule of H_2 for each atom of Sr metal produced. The H_2 was identified analytically and measured manometrically.

While the other methods of analysis measure the total Sr on the bulb and do not distinguish whether it arrived in the form of Sr atoms, SrO molecules, or otherwise, the hydrogen evolution method detects only the Sr metal. The present practical sensitivity is equivalent to about 0.5 μg of Sr, presumably because of extraneous material capable of removing H_2 from H_2O. The method was developed about 1935 by L. A. Wooten.[18,19,20] Berdennikowa[21] has described much the same method, which has also been used by Jenkins and Newton.[22,23]

RESULTS

The results are given in Tables I–III and plotted in Fig. 3. LogM', the grams of SrO evaporated per cm² per *hour*, is plotted against $10^4/T$ as abscissa. These coordinates are chosen because the result is sensibly a straight line; the line plotted represents a least-squares treatment of the data of Tables I, II, and III and follows the equation

$$\log M' = -(2.366\times 10^4/T)+10.468.$$

Table I reproduces the data of Claassen and Veenemans in the temperature range 1495° to 1635°K. They employed a platinum surface of area 30 cm² and determined gravimetrically deposits of 500 to 1200 micrograms formed in periods from 0.22 to 8.00 hours. These data are shown as solid dots in the high temperature region of Fig. 3; in constructing this figure each point from Claassen and Veenemans was given the same weight as each point obtained in the present work.

Table II gives tests obtained in the present work using gravimetric and polarographic analysis. This evaporation was at lower temperatures—from 1303 to 1441°K. Because of this and a surface area of only 3.1 cm², the filaments were aged far longer, running from 707 to 3617 hours, but the total deposit analyzed in each tube was of the same order of magnitude as in the work of Claassen and Veenemans. These results are shown by open circles.

Radioactive tests were used with the tubes listed in Table III and shown by triangles. In general, the amounts of SrO deposited were about an order of magnitude smaller than with the tubes in the preceding tables. The radioactive $SrCO_3$ coating was applied by Diggory's eyelet technique to the platinum in the form of wire, the geometry most favorable for this method. In seven of the tubes as indicated, platinum black was added to the coat. This produced a filament with a spectral emissivity of the order of 0.60, in contrast to approximately 0.45 without the platinum black.

Unexpected difficulties encountered in two other groups of tubes illustrate the care necessary in using radioactive isotopes in such tests. In the first group, the radioactive coating was brush-painted on the filaments, which were in the form of ribbons. Coatings so applied gave a spectral emissivity, E_λ, of approximately 0.08 and the adherence was not adequate. This low value of E_λ requires a correction of the order of 200° to the pyrometer measurements. A series of reflectometer observations on each filament indicated that the precision with which such a low spectral emissivity could be determined was equivalent to a probable temperature error of approximately 40°. Because of this major uncertainty in the temperature and the poor adherence of the coat, the data for these tubes were not used, although the results were in substantial agree-

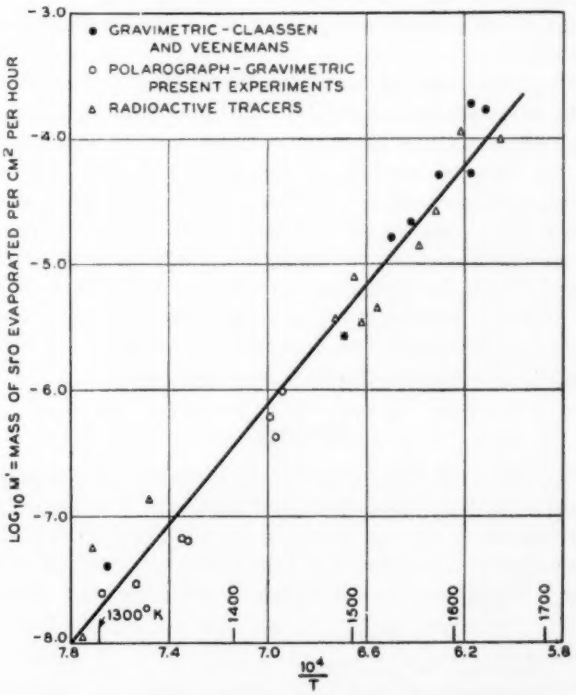

FIG. 3. Evaporated SrO as a function of temperature.

[18] L. A. Wooten, ASTM Bull. **108**, 39 (1941).
[19] L. A. Wooten, Phys. Rev. **69**, 648 (1946), oral presentation only.
[20] G. E. Moore, J. Chem. Phys. **9**, 427 (1941).
[21] T. P. Berdennikowa, Physik. Zeits. Sowjetunion **2**, 77, (1932).
[22] R. O. Jenkins and R. H. C. Newton, Nature **163**, 572 (1949).
[23] R. O. Jenkins and R. H. C. Newton, J. Sci. Inst. **26**, 172 (1949).

TABLES I–III. Experimental measurements—vaporization of SrO.

Tube no.	T°K	Hours time	Micrograms μ	logM'	λ_0
		TABLE I. Claassen and Veenemans—gravimetric.			
1	1495	8.0	500	−5.569	127,679
2	1539	1.5	540	−4.795	125,751
3	1557	1.0	500	−4.660	126,076
4	1584	1.0	1200	−4.284	125,945
5	1617	0.17	710	−3.725	123,873
6	1617	0.50	620	−4.270	127,888
7	1635	0.22	850	−3.772	125,542
		TABLE II. Present work—polarographic and gravimetric.			
420	1303	3617	270	−7.618	124,182
421	1308	3617	450	−7.396	123,405
486	1327	3617	330	−7.531	125,873
423	1361	2234	460	−7.177	126,707
422	1367	2234	440	−7.197	127,386
418	1430	707	1330	−6.217	126,621
485	1435	707	950	−6.363	128,193
419	1441	707	2120	−6.014	126,165
		TABLE III. Present work—radioactive tests.			
162[a]	1290	209	0.7	−7.950	124,962
170	1297	1611	27.5	−7.246	121,650
169	1336	1497	60	−6.876	122,694
172	1488	136	148.5	−5.439	126,101
176[a]	1505	41.5	98.8	−5.100	124,661
171	1510	136	139.5	−5.466	128,185
143[a]	1525	8.25	11.1	−5.348	128,532
158[a]	1566	1.0	4.17	−4.854	128,288
177[a]	1580	21.0	166	−4.580	127,399
175[a]	1608	2	67.4	−3.950	124,852
174[a]	1650	6	179.8	−4.001	128,363

[a] Pt black added to coat.

ment with those plotted. This experience led to the development of the eyelet method, which produced filaments in which the emissivity correction was of the order of 50° determined with a probable error of less than 10°.

In another set of tubes the filaments were sprayed with non-radioactive $SrCO_3$ and then treated in the pile. However, the platinum support metal came from a new lot and contained impurities not detected in either spectrochemical or mass spectrograph examinations. These impurities became radioactive and evaporated, together with the SrO. The evaporated product could readily be separated into three components, two of which had decay rates differing markedly from the known values for Sr. Because of the complexity of such analytical methods, the data were not used.

Precision

As indicated, the precision with which temperature can be measured and controlled is primarily responsible for the scatter of the points in Fig. 3; observations for each group are therefore compared in terms of the r.m.s. deviation, σ_T, in temperature from the least-squares curve. The fact that the spread is greater for the radioactive method, which is much more sensitive, indicates that the precision was not limited by the sensitivity of any analytical method used, but rather by the control of temperature, which is more difficult in the specially applied radioactive coats.

Group	σ_T
Gravimetric—Claassen and Veenemans	21.7°
Polarograph and gravimetric—Present tests	14.7
Radioactive isotopes	23.0

Experimental precision is best discussed by computing, for each measurement of the vapor pressure, a value of λ_0, the latent heat of evaporation at 0°K. This requires the evaluation of (1) the standard free† energy G_s of solid SrO with respect to the solid at 0°K, a function of temperature only, and (2) the free energy of SrO vapor G_g with respect to the gas at 0°K, a function of *both* temperature and pressure.

For an observed vapor pressure p_1 at a temperature T_1, the two phases are in equilibrium and

$$G_g(T_1 p_1) = G_s(T_1). \tag{2}$$

Also at any temperature,

$$G_g(T, p) = G_g(0°) + \Delta G_g(T, p), \tag{3}$$

where $G_g(0°)$ is independent of p. Also

$$G_s(T) = G_s(0°) + \Delta G_s(T). \tag{4}$$

By virtue of Eq. (2), at an observed pressure p_1 and temperature T_1, the right sides of Eqs. (3) and (4) can be equated; also at 0°K, $G \equiv H$ for any phase so that,

$$\lambda_0 \equiv H_g(0) - H_s(0) \equiv G_g(0) - G_s(0) = \Delta G_s(T_1) - \Delta G_g(T_1, p_1),$$

where H is the heat content. ΔG_s can be calculated[24] from the measured[25,26] specific heat while[27]

$$\Delta G_g = G_K + G_R + G_V + G_c, \tag{5}$$

where the subscripts K, R, and V designate translational, rotational, and vibrational terms in the free energy, respectively, and G_c is a small correction term. G_K contains the only pressure dependent term. All terms in Eq. (5) were evaluated from the band spectrum.[28,29]

The procedure is illustrated in Fig. 4 for a measured vapor pressure of 1.6×10^{-23} atmos. at $T = 1500$°K. At 1500°K, Curve PD representing G_g intersects Curve

† The International Unions (both) of Physics and of Chemistry recommended in 1947 and 1948 that the Gibbs free energy be designated by G.

[24] E. Fermi, *Thermodynamics* (Prentice-Hall, Inc., New York, 1937).

[25] C. T. Anderson, J. Am. Chem. Soc. **57**, 429 (1935). Temperatures below 300°K.

[26] J. J. Lander, Submitted to J. Am. Chem. Soc. Temperatures above 300°K.

[27] The method for computing the free energy of a diatomic gas from its molecular constants is given in J. E. Mayer and M. G. Mayer, *Statistical Mechanics* (John Wiley & Sons, Inc., New York, 1940). See especially Appendix A IX.

[28] K. Mahla, Zeits. f. Physik **81**, 625 (1933), observed the band spectrum of SrO.

[29] G. Herzberg, *Molecular Spectra and Molecular Structure* (Prentice-Hall Inc., New York, 1937), recomputed the necessary molecular constants from Mahla's data.

C representing G_s. The difference between curves C and D is the free energy of the gas at this pressure with respect to the solid, and at 0°K is the heat of sublimation of SrO. For each observed pressure, a value of ΔG_g was computed. Its high temperature ordinate is fixed only by the observed temperature and curve C, and at 1500°K will correspond to point A. Its low temperature ordinate is then determined by the observed pressure using Eq. (5). For perfect experimental accuracy, all curves corresponding to D should intersect the 0°K axis at the same point P. The scatter in the points of intersection can be reduced to a scatter in λ_0, by subtracting, from the value of ΔG_g computed from Eq. (5) for each observation, the corresponding value of ΔG_s.

A value of λ_0 so obtained is given as the final column of Tables I–III. Table IV gives the mean value of λ_0 for each group and the r.m.s. deviation from the mean in that group. There was no trend in the values of λ_0 with temperature. The value of σ for each group is 1 to 2 percent of the mean, but (fortuitously) the mean for any group does not differ by 0.1 percent from that for any other group. These facts indicate that the temperature scale used by Claassen and Veenemans is equivalent to that used in the present work. The value of λ_0 is therefore taken as 126.0 kilocalories with a probable error believed less than 1 percent. The heat of evaporation given by Claassen and Veenemans was 141 kcal. computed from the slope of their data plotted against reciprocal temperature. Their value would not represent λ_0, although it has been so used.[10] Blewett[30] assumed that the difference in specific heats of gaseous and solid SrO was $3R$ at all temperatures and obtained $\lambda_0 = 117$ kcal.

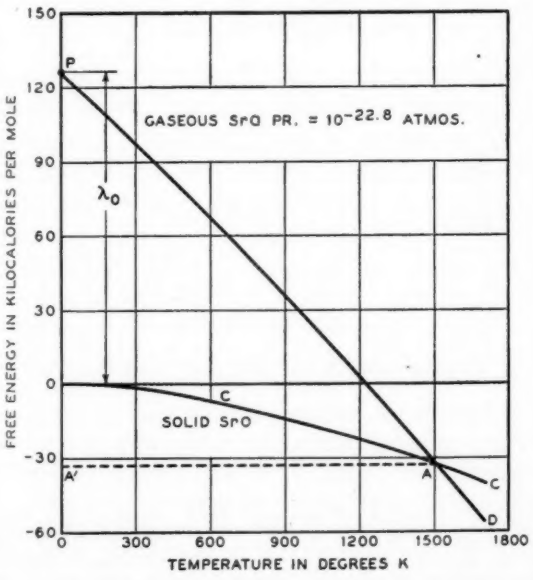

FIG. 4. Procedure for calculating λ_0 of SrO from measured vapor pressure and thermodynamic properties of solid and gaseous SrO.

[30] J. P. Blewett, J. App. Phys. **10**, 668 (1939).

TABLE IV. Mean values of λ_0.

Group no.	λ_0	r.m.s. deviation σ
1	126,043	1278
2	126,067	1486
3	125,972	2296

Evaluation of Systematic Error

Experiments of this kind measure the total Sr leaving the filament and one usually considers that it all left in the form of SrO molecules. If any left in the form of Sr atoms, these would be counted as SrO molecules and the vapor pressures stated would be too high. Such errors could occur if (a) the SrO were reduced by any mechanism which caused the oxygen atom to remain on the filament while the Sr atom moved to the bulb or (b) if the SrO dissociated thermally, both the Sr atom and oxygen molecule going to the bulb. These will be discussed in turn.

(a) *Possible Reduction of SrO*

This might occur as a result of carbon or other impurities in the platinum or the coat or by other conceivable, but not very probable, mechanisms. In the absence of accurate free energy data for these, the possibility of reduction was investigated experimentally.

Four tubes were made as in Fig. 2. Each contained two filaments of the type used for vapor pressure measurements and the $SrCO_3$ was dissociated to SrO in exhaust. The filaments were heated for prolonged periods at high temperature and then sealed to a gas analysis system. Water vapor was admitted through the breakoff tip, B, and the Sr (or any impurities capable of dissociating H_2O) analyzed by measuring the hydrogen evolved. The results are shown in Table V. The evaporated oxide listed in the fifth and sixth columns was not measured directly but was computed from the vapor pressure data of Fig. 3 because accurate measurement of evaporated oxide is not practical after admission of water vapor. In the seventh column, the apparent observed amounts of Sr metal all lie between 1 and 6 μg. These are believed upper limits to the Sr produced; the hydrogen observed might well be the result of material other than Sr, because in any of the work with the hydrogen evolution method, "blanks" of the order of 1 μg were frequently obtained in tests where no alkaline earth metal was present. However, comparison of columns 6 and 8 shows that less than 1 percent of the material leaving these filaments is Sr metal, so that less than 1 percent error is made in neglecting all conceivable mechanisms of reduction. This measurement should *not* under any circumstances be considered as giving the rate of reaction between Pt and SrO to produce Sr but may be considered as an upper limit to the rate of such a reaction.

TABLE V. Reduction of SrO.

Tube	Aged hours	Temp.	Filament area	Oxide evaporated (calculated) Total	Oxide evaporated (calculated) μg/cm²/hr	Apparent Sr (observed) Total	Apparent Sr (observed) μg/cm²/hr
A	232	1420°K	3.1 cm²	436	0.60	1.34	1.86×10^{-3}
B	3617	1308	3.1	142	0.013	1.12	1.0×10^{-4}
C	5	1618	2.6	1189	91.3	5.98	0.46
D	2.5	1610	2.6	494	75.9	3.41	0.53

(*b*) *Thermal Dissociation of SrO*

Processes which probably occur at least to a slight extent involve the thermal dissociation of SrO, as

$$SrO(s)\rightarrow Sr(g)+\tfrac{1}{2}O_2(g) \quad (6)$$

$$SrO(s)\rightarrow Sr(g)+O(g). \quad (7)$$

The Sr atoms, O_2 molecules, and O atoms would leave the filament and deposit on the bulb. Because they would reunite, free Sr atoms leaving the filament by this process would not be detected in the hydrogen evolution tests. One might not wish to designate a loss of SrO from the filament by such processes as evaporation, although the end result could not readily be distinguished experimentally from true molecular evaporation; the distinction might be observable with appropriate mass spectrometer technique.

Thermodynamic calculations performed as in II indicate that both (6) and (7) could occur at appreciable rates. The calculations employed the data of Johnston and Walker[31] for the equilibria of atomic and molecular oxygen.[32] The results suggest that up to 40 percent of the SrO determined in the analytical tests may have arrived at the bulb by a combination of processes (6) and (7) rather than by true evaporation of SrO molecules.[33] However, data from the band spectrum indicate much less than 40 percent dissociation. The fraction dissociated was computed for a sample of SrO gas, at the pressure and temperature in equilibrium with the solid phase, by using the dissociation energy $D_0=5.2$ ev, which Herzberg[29] derived from Mahla's[28] work on the band spectrum. This computation indicates that only about 0.2 percent of the SrO in the gas phase could be dissociated. To bring these two estimates of dissociation into agreement would require a decrease of D_0 by about 0.7 ev or a corresponding change in some other quantity, such as an increase in the heat of formation of solid SrO. If reactions (6) and (7) were proceeding at the rate computed from the thermochemical data, the value of λ_0 stated above should be increased to 126.6 kcal. However, it should be emphasized that such computations give the *maximum* rate at which the dissociation reactions (6) and (7) could proceed. The experimental rate might well be less, particularly if the residual oxygen pressure is 10^{-8} mm or more. In this case, or if the band spectrum data are more accurate, the value of λ_0 remains at 126.0 kcal.

Relation to Previously Published Work

Evidence from the present work is of interest in thermionic[3,4,5,11] systems activated by the particles emitted from external sources. When the external source is a pure Pt filament coated with SrO, the available thermochemical data indicate that at least 60 percent of these particles are SrO molecules; it is possible that as much as 40 percent represent SrO molecules dissociated according to Eqs. (6) and (7). If Sr atoms unaccompanied by an equivalent amount of oxygen form more than 1 percent of the particles, some reducing mechanism, such as chemical impurities, must be available. Because the ionization potential of Sr is 5.67 volts and the electron affinity[34] of the oxygen atom is only 2.33 ev, very few of the particles would be represented by SrO dissociated into Sr^+ and O^- ions. For this reason one would expect that Sr^+ ions observed in the mass spectrograph[1,2] could have been formed by the method of measurement. However, if reactions (6) and (7) occur experimentally or if a reducing mechanism is available, Sr atoms would be present and their ionization might be unavoidable in mass spectrograph technique. Dissociation of SrO molecules by electron impact and subsequent ionization of the Sr might also be encountered.

Vapor Pressure

Assuming that processes (6) and (7) are not occurring and thus taking $\lambda_0=126.0$, the vapor pressure equation for SrO molecules at any temperature can be computed from the heat capacities of solid and gaseous SrO. The pressure in atmospheres so computed in the range, 700–1600°K, is

$$\log_{10}P=1.44+1.908\log T-25{,}950/T. \quad (8)$$

CONCLUSIONS

This work is believed to show the following:

(1) The vapor pressure of SrO was measured as a function of temperature by measuring the total Sr evaporated from pure Pt filament supports coated with layers of SrO about 0.003-cm thick.

(2) The reduction of SrO with subsequent evaporation of the Sr, if it occurs at all, introduces less than 1 percent error; this result confirms the assumption of some of the previous experimenters.

[31] H. L. Johnston and M. K. Walker, J. Am. Chem. Soc. **55**, 187 (1933).

[32] Also used were J. J. Lander's specific heat data for the heat capacity of SrO and F. D. Rossini's critical value for the heat of formation of SrO. Both of these are discussed more fully in II.

[33] The method of calculation is approximately that used by A. H. White for Eq. (6), J. App. Phys. **20**, 856 (1949). The present calculations indicate that Eqs. (6) and (7) might contribute about equally to the thermal dissociation of SrO as a mechanism of producing SrO on the bulb. The numerical results for Eq. (6) in the present calculations do not differ significantly from White's values, despite the fact that Lander's specific heat data, used in our work, were not available at the time of White's computation.

[34] M. Metlay and G. E. Kimball, J. Chem. Phys. **16**, 774 (1948).

(3) Dissociation of SrO by temperature alone, the Sr atoms and O_2 molecules (or O atoms) leaving the filament and subsequently recombining on the surface on which they are deposited may represent as much as 0.4 of the total SrO leaving the filament. This conclusion is based on thermochemical data; if the band spectrum value of 5.2 ev for D_0 be accepted, the fraction is not over 0.002.

(4) The latent heat of evaporation λ_0, at 0°K is 126.0 kcal with a probable error of about 0.8 kcal. If processes (6) and (7) occur at the maximum rate thermodynamically possible, the value of λ_0 should be increased to 126.6 kcal. This increase does not seem probable because it contradicts available data from the band spectrum.

(5) The radioactive tracer method is convenient, sensitive, and accurate but must be employed with caution.

Advice from Conyers Herring during this work is gratefully acknowledged.

THE JOURNAL OF CHEMICAL PHYSICS VOLUME 18, NUMBER 12 DECEMBER, 1950

II. The Reduction of SrO by Tungsten in Vacuum

GEORGE E. MOORE, H. W. ALLISON, AND JAMES MORRISON
Bell Telephone Laboratories, Inc., Murray Hill, New Jersey
(Received July 24, 1950)

It is shown that in the temperature range 1150–1550°K, SrO is reduced by tungsten in vacuum. Both the rate of the reaction and its equilibrium constant can be calculated, giving values in substantial agreement with the experiments, which were performed under conditions such that both could be measured. The use of radioactive isotopes simplified the experimental work.

INTRODUCTION

THE performance of oxide cathodes is generally believed to depend on small quantities of excess Ba or Sr metal in the oxide lattice. Of the various methods postulated for producing this Ba or Sr, chemical reduction of the oxide by the support metal is qualitatively the best established experimentally. However, almost no quantitative work has been published on either the equilibrium or kinetics of such processes, probably because the serious difficulties, inherent in making any quantitative measurements on chemical reactions between solid phases,[1] might be accentuated in these reactions.

It has been shown[2] that the reaction between MgO and tungsten can be studied experimentally by a technique that is simple in principle and which yields simultaneously both the equilibrium constant and the rate of the reaction. The observed values were, within experimental precision, just those computed from thermodynamics and kinetic theory. White[3] has computed the free energies of several such reactions.

The present work indicates that the reaction between SrO and W can be studied quantitatively in the temperature range 1150–1550°K and the behavior is only slightly more complex than that of the MgO–W reaction.[2]

PRINCIPLE OF THE EXPERIMENTAL METHOD

Because the principle of the experimental method was not adequately discussed in the previous report[2] and because the writers hope to investigate other reactions by the same method, the principle is presented here in some detail.

Consider an evacuated glass bulb as in Fig. 2 in the preceding paper, "The vaporization of SrO" (hereinafter referred to as I), containing a W filament coated with SrO which is heated to a temperature determined pyrometrically. A reaction capable of producing Sr metal will result either in simple oxidation of the tungsten as in

$$\mathrm{SrO}(s)+\tfrac{1}{2}W(s)\rightleftarrows\tfrac{1}{2}\mathrm{WO}_2(s)+\mathrm{Sr}(g) \qquad (1)$$

or in the formation of a complex salt as in

$$\tfrac{3}{2}\mathrm{SrO}(s)+\tfrac{1}{2}\mathrm{W}(s)\rightleftarrows\tfrac{1}{2}\mathrm{SrWO}_3(s)+\mathrm{Sr}(g). \qquad (2)$$

Among the components of (1) and (2) the Sr alone will be present only in the gaseous phase in the experimental temperature range 1150–1550°K and its pressure is therefore[4] the equilibrium constant. The published vapor pressures of SrO and W are so low that they will clearly be present in the solid phase and evidence to be presented shows the same to be true of WO_2 and $SrWO_3$.

The kinetic criterion,[5] is usually employed to detect equilibrium. For this example, the temperature of the

[1] C. N. Hinshelwood, *Kinetics of Chemical Change* (Oxford University Press, London, 1940), see especially page 252.
[2] G. E. Moore, J. Chem. Phys. **9**, 427 (1941).
[3] A. H. White, J. App. Phys. **20**, 856 (1949).
[4] See for example E. Fermi, *Thermodynamics* (Prentice-Hall Inc., New York, 1937).
[5] H. Hunt, *Physical Chemistry* (Thomas Y. Crowell Company, New York, 1947), states that chemical equilibrium may be considered from the three viewpoints: "Thermodynamically, a reaction is at equilibrium when the free energy change is zero. Statistically it is at equilibrium when the mathematical probability has reached a maximum value for the system. Kinetically it is at equilibrium when the forward and reverse absolute rates are equal."

TABLE I. Experimental measurements—reaction between W and SrO.

Tube no.	T°K	Age—hr.	Total Sr micrograms	LogM'	ΔT°
Group 1a. Hydrogen evolution—SrO coat only					
928	1364	40.0	405	−5.441	62
1222	1452	2.4	1029	−3.815	22
927	1495	1.7	1108	−3.633	2
930	1520	0.67	995	−3.276	22
				r.m.s. deviation	35
Group 1b. Hydrogen evolution—SrO+W powder in coat					
1588	1228	151.0	0.26	−6.209	6
1585	1475	2.0	1907	−3.469	42
1586	1475	2.0	350	−4.203	46
1221	1515	1.0	437	−3.807	39
				r.m.s. deviation	37

TABLE II. Experimental measurements—reaction between W and SrO.

Group 2a. Radioactive $SrCO_3$ coat applied—no W powder					
125	1200	140.5	21	−6.662	3
124	1242	70.0	57	−5.931	16
129	1299	24.0	74	−5.354	11
126	1300	43.0	98	−5.487	2
127	1300	24.0	36	−5.668	19
128	1300	42.0	49	−5.775	29
				r.m.s. deviation	16
Group 2b. Radioactive $SrCO_3$ coat applied with W powder					
132	1217	74.0	48	−6.033	32
131	1350	22.5	108	−5.132	18
135	1357	22.5	159	−4.996	12
133	1395	2.0	45	−4.496	2
134	1395	2.0	27	−4.713	21
137	1430	1.0	98	−3.851	41
136	1434	1.3	80	−4.057	12
				r.m.s. deviation	23

filament would be controlled by heating the bulb in an oven. The thermodynamic system would comprise everything inside the bulb and the steady-state pressure of Sr would be determined at a series of temperatures. The forward reaction produces Sr atoms, labelled group (a), which stream outward from the filament. In the reverse reaction, incoming Sr atoms labelled group (b) again form SrO. The flux of atoms in these two groups would be equal at equilibrium. Measurement of the low equilibrium pressures would be difficult and the maintenance of a chemically inert bulb at high temperatures is not feasible.

However, if the reflection of Sr atoms is negligible at phase boundaries and if the equilibrium pressures were so low that the mean free path of Sr atoms was larger than the bulb radius, atoms of groups (a) and (b) could not interact. The two groups would be independent and one might expect Sr atoms to be produced at a rate depending only on temperature, regardless of whether *any* Sr atoms strike the filament. Experimental technique would be convenient, because only the filament need be heated, the thermodynamic system consisting only of the filament itself instead of the entire interior of the bulb. The number of (b) atoms could be reduced essentially to zero by operating the bulb at ambient temperature, at which substantially no Sr could evaporate from the glass surface. Because the filament diameter is small compared with the bulb diameter, any Sr atoms reflected from the bulb would strike the cool glass many times before returning to the filament. Therefore, almost no atoms of group (b) would be produced by reflection at the bulb unless the reflection coefficient is extremely high; negligible reflection is indicated by the sharp shadows of the filament supports observed in the experimental films of Sr metal deposited on the glass.

When atoms of group (b) can be neglected, the Sr leaving the filament per unit time can be measured and expressed as a pressure, by operating the filament at a controlled temperature for a known length of time and converting the mass of Sr observed on the bulb into pressure by Eq. I (1). The outward flux of Sr atoms at the filament surface corresponds to the pressure in the system. The cool glass surface completely removes gaseous Sr, so that the reaction will proceed as rapidly either: (1) as atoms of group (a) can leave the filament at the equilibrium pressure, or (2) as allowed by constraints of the system, such as diffusion of reactants and reaction products through solid phases. (1) is the maximum possible rate and requires that there be no reflection at phase boundaries.

It is clear that the measurement of m gives the *rate* of the reaction. The equilibrium pressure of Sr can be predicted from published thermodynamic data, as indicated below; because this computed pressure is equal to the observed value, it is believed that the measurements also give *the equilibrium pressure* of the reaction. This belief is supported by the fact that the observed values of m seem independent of large changes

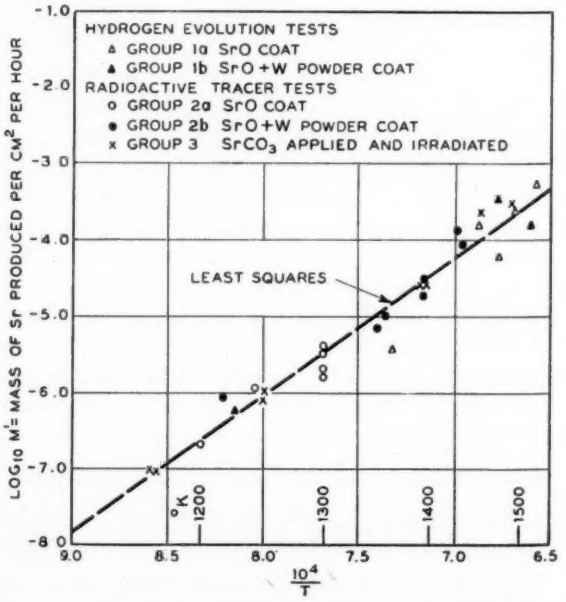

FIG. 1. Experimental measurements of the rate of production of Sr atoms by chemical reaction between SrO and W.

in the interfacial area between SrO and W, keeping the apparent surface constant.

Such considerations have previously been applied to purely physical reactions such as the vaporization of metals, but have not yet been established for the gaseous product of chemical reactions between solids.

EXPERIMENTAL

(A) Measurement and Control of Temperature

This was treated as in I. To darken the surface of the SrO and thus increase the spectral emissivity, tungsten powder was added in many filaments. Particle size analysis indicated that this powder also increased the interfacial area between tungsten and SrO by a factor of three. The probable error in determining the true temperature of a darkened filament is believed to be about 5°C; for the coats without the tungsten powder, this is approximately 10°C.

Control of temperature during runs is more difficult than its determination at individual test points. Operation at either constant current or constant voltage will not assure constant temperature. Two effects are responsible: (1) spectral and total emissivities vary as a result of chemical reaction and (2) resistivity varies during the reaction, probably because reaction products penetrate the tungsten filament. These changes were frequently large during aging periods required to produce sufficient Sr for accurate analysis. The scatter in the results for the first tubes tested amounted to about 35°C expressed as an r.m.s. deviation from the curve best fitting the experimental data. Improved temperature control was primarily responsible for decreasing this in subsequent groups. This involved frequent pyrometer and reflectometer observation of a filament during aging, which was laborious. In order to make pyrometer measurements only at the necessary intervals, the radiation from the experimental filament was monitored photoelectrically. The emission in a photo-cell which viewed the filament was calibrated as a function of filament temperature. If while aging the experimental tube, the photo-emission changed by more than the equivalent of 10°, new pyrometer and reflectometer measurements were made. This method did not correct for increased transmission loss caused by deposit of metallic Sr on the bulb, but experience indicated when this correction became appreciable, and only slight scatter was caused by the latter action.

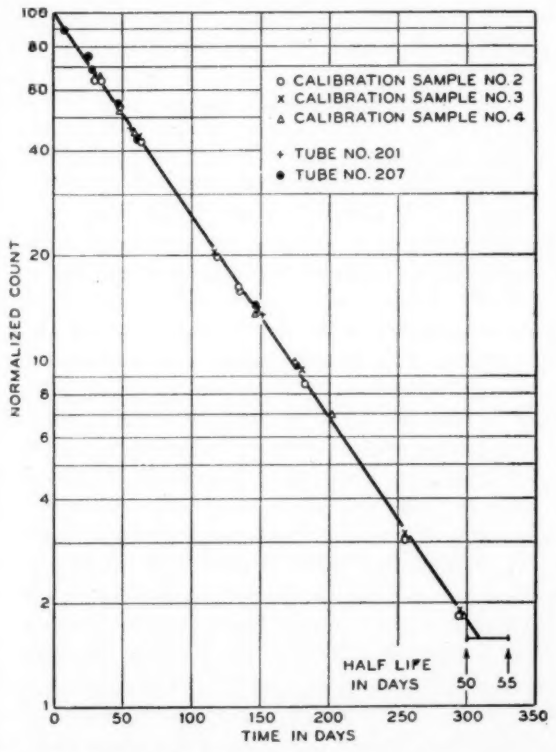

FIG. 2. Decay of radioactivity in Sr metal produced in chemical reaction. Rate of decay indicates no W in volatile reaction product.

TABLE III. Experimental measurements—reaction between W and SrO.

	$SrCO_3$ applied to filament and then irradiated				
201	—	0	0.24		
209	—	0	1.7		
211	1166	360	10.4	−7.018	3
202	1168	362	10.3	−7.023	1
207	1250	93.5	30.4	−5.965	4
210	1250	93.5	23.2	−6.082	5
212	1395	22.5	183	−4.566	5
206	1400	22.5	181	−4.571	11
204	1454	2.0	140	−3.633	43
203	1490	2.0	176	−3.532	19
				r.m.s. deviation	17

(B) Measurement of the Total Mass of Sr

Both the hydrogen evolution and the radioactive isotope methods described in I were used in this work. However, in contrast to I, the total bulb deposit, μ, measured in II was essentially the same by either method, indicating that the deposit was substantially all Sr metal.

(C) Tube Design and Exhaust

The structures of Figs. I-1 and I-2 were used and the exhaust was as described previously.

(D) Preparation of Filaments

The filament supports (or cores) were either G. E. 8111 0.010-in. wire, or ribbons rolled to 0.040 in. ×0.0005 in. from G. E. 218 "non-sag" wire. The former was analyzed spectrochemically indicating a purity greater than 99.99 percent. The coat was $SrCO_3$ of high purity and about 5 mg was applied per cm^2 of filament area. The filaments were all coated either by Diggory's "eyelet" method or coated with non-radioactive $SrCO_3$ and the coated filament then treated in the pile. Both methods are described in I. No radioactive impurities were detected in either treatment.

TABLE IV. Computed rates of reaction.

(1) Temperature °K	(2) ΔG for (3)	(3) G for SrO	(4) G for $\frac{1}{2}O_2$	(5) G for Sr	(6) ΔG for (8)	(7) $\log_{10}p_1$ for	(8) $\log_{10}M'$ (2)	(9) $\log_{10}M'$ (2)	(10) $\log_{10}M'$ method 2 for (2)
			cal./mole						
1000	−46,250	−155,540	−23,992	−14,644	71,550	−12.74	−14.07	−10.04	−9.96
1100	−44,150	−158,520	−26,899	−16,975	72,390	−10.51	−11.90	− 8.22	−8.17
1200	−42,050	−161,350	−29,846	−19,377	71,080	− 8.69	−10.07	− 6.69	−6.57
1300	−39,975	−164,430	−32,839	−21,829	70,790	− 7.09	− 8.48	− 5.40	−5.26
1400	−37,850	−167,615	−35,858	−24,377	70,530	− 5.75	− 7.15	− 4.27	−4.15
1500	−35,750	−170,900	−38,939	−27,027	70,180	− 4.56	− 5.98	− 3.30	−3.32
1600	−33,650	−174,270	−42,002	−29,627	69,995	− 3.58	− 5.01	− 2.48	−2.51

M' = grams of Sr leaving each cm² of filament surface per hour.
p_1 = outward pressure of Sr gas at filament surface in dynes per cm².
G expressed in calories per mole, elements and SrO in standard states.

RESULTS

Results are given in Tables I to III and Fig. 3. Table I gives data on tubes tested by the hydrogen evolution method; the first four filaments were coated with $SrCO_3$ only, and the second four were coated with a mixture of tungsten powder and $SrCO_3$. Table II gives data for the first set in which radioactive tracers were used. The first six were coated with $SrCO_3$ only and the second seven with $SrCO_3$ and tungsten powder. In all tubes of Table II, the $SrCO_3$ was irradiated before application to the filament. Table III gives data on ten tubes containing filaments which had been coated with $SrCO_3$ and the coated filament then irradiated. None of these 10 contained tungsten powder.

Tubes 201 and 209, Table III, served as "blanks"; that is, after assembly, the thimble was never lifted above the filament until the outer bulb was removed. Any radioactivity on the outer bulb would then result from Sr atoms which had been transferred mechanically during assembly or in other stages of preparation. The amount produced by the reaction should be much greater than the amount in such a blank if the former is to be determined with precision. The examples show that this condition was fulfilled.

The results are plotted in Fig. 1 in which the ordinates are $\log_{10}M'$, the mass in grams of Sr produced per *hour* per cm² of apparent surface. Abscissas are expressed in reciprocal temperatures. Theoretical computations and the experimental data are both sensibly straight lines in these coordinates, although exact linearity would not be expected. The dashed line shows a least square fit of the experimental data. The perpendicular distance from the point to the line was minimized although it is recognized that inaccuracy in temperature determination is probably considerably more serious than uncertainty in the mass of Sr produced. The line fits the equation

$$\log_{10}M' = -\frac{1.810\times10^4}{T} + 8.460. \qquad (5)$$

Comparison with Fig. 3 of I shows that the amount of Sr produced from a SrO coat on tungsten is considerably more than 100-fold greater than the total Sr (SrO+Sr) from a similar coat on platinum.

The deviation in *temperature* of each point from the line is listed under $\Delta T°$. The r.m.s. value of the deviation for each group is also listed. The r.m.s. deviation of all the points from the least square line is 24.9°K.

The mean *magnitude* of the deviation from the least square curve was 19°. There was no significant difference between the filaments with tungsten powder and those without. The mean deviations of the two groups from the least square line were of the order of 0.25°—an insignificant amount—but were in the opposite direction from that expected if the rate of reaction per unit apparent surface were limited by the interfacial area between W and SrO. Similarly, there was no correlation, either in magnitude or direction, between the deviation and the total amount of Sr produced by a filament.

Radioactive Decay

Decay for several samples of Sr89 in $SrCO_3$ produced by the irradiation of filaments previously coated with non-radioactive material is shown in Fig. 2. Three different calibration samples are compared with two experimentally produced deposits on glass bulbs. The calibration samples were used both to determine the absolute amounts of Sr in the experimental deposits and to judge their purity. Figure 2 illustrates only the latter use. In order to plot the data for all samples on a single curve, the activity from each was normalized by designating the initial count 100 percent and expressing all subsequent counts as a percentage. This was used as ordinate and the time in days after the first count as abscissas. If radioactive tungsten (or impurities from the W) represented some of the count initially attributed to Sr, the curves for the experimental samples would deviate from those of the calibration samples.

Specifically, after irradiation, the tungsten has 73.2 days half-life activity of 7 millicuries per gram (W185), while the Sr in the coat has a 55-day half-life activity of only 0.11 millicurie per gram. Thus the activity per microgram for tungsten is about 64 times greater than for Sr when removed from the pile. To process the tubes

requires several weeks, so because of its longer half-life, a microgram of tungsten on the bulb would give at least 2 orders of magnitude higher count than a microgram of Sr. The decay curves thus give a critical test for accumulation of W, or any compound containing W, on the bulbs. The agreement in half-life in the decay curves for calibration samples and bulb deposits therefore shows that the bulb deposit must be much less than one percent tungsten; the experiment is accordingly believed to measure only Sr (or SrO). This is supported by spectrochemical tests in which no W was found on the bulb in tests which would detect 0.5 microgram.

The curve is terminated at an ordinate of 1/64 (or 0.0156) representing 6 half-lives. The abscissas should then represent 6 times the half-life of the Sr isotope. The half-life determined in this way is between 51.5 and 52.0 days. Numerous tests on several samples consistently give half-lives of 51 to 53 days for Sr 89, while the most recent AEC Bulletins give 55 days, although earlier bulletins give 53 days. A small systematic error of unknown origin may therefore exist in the present measurements, although recent correspondence with AEC indicates that the 51- to 53-day figure may be reliable.

DISCUSSION

It was shown above that the rate at which Sr metal atoms leave a tungsten filament can be measured by two methods. However, the chemical reaction producing these Sr atoms was not identified. In this section, the rate of Sr production is discussed from a thermodynamic point of view, and a choice is made between reactions (1) and (2). It is shown that the observed rate is greater than could be justified thermodynamically if (1) occurs but is essentially that to be expected from (2). This conclusion is supported by chemical and x-ray data. In the computations, the assumed reaction [either (1) or (2)] is first resolved into simpler reactions whose sum is equivalent to that investigated, but each of which is more readily discussed than their sum.

Reaction (1)

WO_2 is the lowest recognized oxide of W; calculations indicate that the maximum rate of Sr production according to (1) would be as great as in any process forming a higher oxide; the rate would be almost identical if WO_3 were produced.

Reaction (1) is resolved into the components

$$\tfrac{1}{2}W(s)+\tfrac{1}{2}O_2(g)\rightleftarrows\tfrac{1}{2}WO_2(s) \quad (3)$$

$$SrO(s)\rightleftarrows\tfrac{1}{2}O_2(g)+Sr(l) \quad (4)$$

$$Sr(l)\rightleftarrows Sr(g). \quad (5)$$

The free energy changes in (3) and (5) are obtained from equilibrium data; in (4) the change is computed by determining a free energy G for each substance with reference to the elements at 0°K. Reactions (3), (4), and (5) will be discussed in turn.

Component Reaction (3)

ΔG for (3) can be computed from the equilibrium pressure of O_2 by the equation[4]

$$\Delta G=(RT/2)\ln P_{O_2} \quad (6)$$

using the relations for P_{O_2} given by Wohler[6] or by Chaudron[7] and Van Liempt.[8] These authors combined their own measurements of equilibria in the $W-H_2O$ system with dissociation equilibria of H_2O. The data of Wohler are preferred because they were obtained more recently, although the difference is not significant for the precision now practical in the present experiment. Values of ΔG in (3) computed from Wohler's data are listed in the second column of Table IV.

Component Reaction (4)

An absolute value for the free energy of each constituent was computed from specific heats. In I, the free

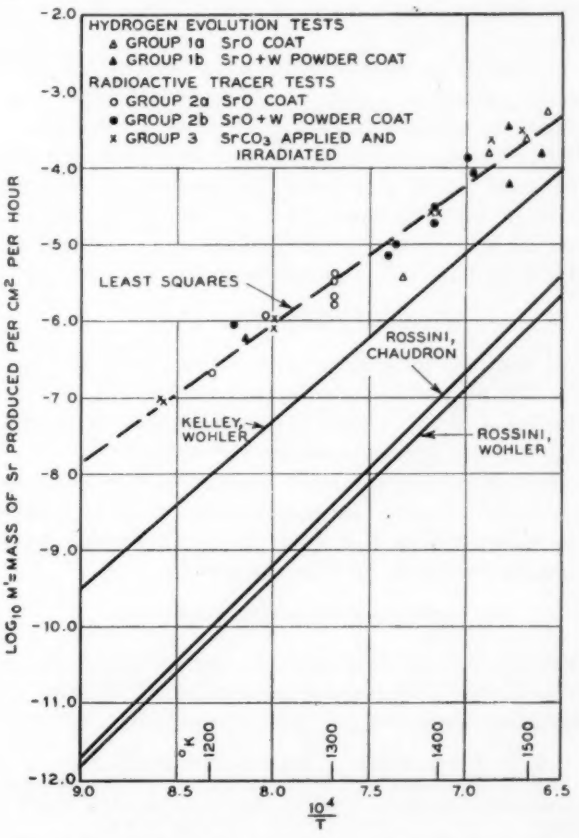

FIG. 3. Comparison of observed rate of Sr production with computed rates, assuming reaction I.

[6] Wohler, Shibata, and Kunst, Zeits. Electrochemie **38**, 808 (1932); temperature 973–1323°K.

[7] G. Chaudron, Comptes Rendus **170**, 1056 (1920); temperature 873–1373°K.

[8] J. A. M. Van Liempt, Zeits. f. Anorg. Chemie **120**, 267 (1922) and **126**, 183 (1923).

energy was referred to solid SrO at 0°K; this is satisfactory for the purely physical process of evaporation, but the basis for chemical reactions must be the elements at some reference temperature. Computation of G for SrO thus requires a value for ΔH, the heat of reaction (4). Three critically discussed values, all at 298.1°K, are available:

130,160 calories by Kelley[9] in 1935.
140,800 calories by Bichowsky and Rossini[10] in 1936.
141,100 calories by Rossini[11] in 1950.

The last is preferred although computations were carried out for each of the others. The disagreement in this quantity introduces much the most important uncertainty in the calculations. Because tabulated values of entropy are always referred to 0°K, this is used as a reference temperature. The free energy of SrO can then be computed for any temperature from specific heats[12,13] and the appropriate value for the heat of reaction. Column 3 of Table IV gives the values of G for SrO, using Rossini's value for ΔH.

For $\frac{1}{2}O_2$, values of G were computed from the specific heat data of Johnston and Walker.[14] Values are given in column 4 of Table IV.

Although no specific heats have been published for solid or liquid Sr, values can be estimated with what is probably sufficient accuracy for these experiments. A Debye temperature of 150°K was first estimated using methods[15] which give values in agreement with experiment for both Mg and Ca (as well as other metals). The specific heat curve, C_v, can then be computed. Between 100°K and 1044°K, the melting point, the equation

$$C_p = 6.25 + 0.00120T - 8120/T^2 \qquad (7)$$

was assumed in analogy with experimental values for Ca. The heat of fusion was taken as 2190 cal. and C_p of the liquid as 7.5. Values of G computed for Sr metal in this way are given in column 5 of Table IV.

By subtracting column 3 from the sum of columns 4 and 5, ΔG° is given for reaction (4) proceeding toward the right. Adding this result to that in column 2 gives column 6 which is ΔG° for the reaction

$$SrO(s) + \tfrac{1}{2}W(s) \rightarrow \tfrac{1}{2}WO_2(s) + Sr(l) \qquad (8)$$

which is the sum of (3) and (4). Because these are positive, it has sometimes been concluded[16,17] that such reactions cannot occur, for example that W cannot reduce SrO to give Sr. However, the data in column 6 show *only* that W cannot reduce SrO to give Sr *in its standard state* in the temperature range 1000–1600°K. Throughout the temperature range the standard state of Sr is liquid in equilibrium with its vapor. But the free energy decrease in the purely physical reaction (5) can be made as great as desired by isothermal vaporization of the liquid at a sufficiently low pressure. The change in free energy for the isothermal expansion of the vapor considered as a perfect gas is[4]

$$\Delta G = RT \ln(p_1/p_2), \qquad (9)$$

where p_2 is the pressure of Sr vapor in equilibrium with its solid or liquid phase. Because of this physical equilibrium, the free energy change in vaporizing any amount of the liquid at p_2 is zero. By then allowing the gas to expand from p_2 to a pressure p_1 such that by (9) the physical reaction (5) represents a loss of free energy just equal to the gain for (8), one obtains the equilibrium pressure p_1 for reaction (1). Computed values of p_1 in dynes are given in column 7 of Table IV using Dushman's[18] values for p_2. These values of p_1 were converted to mass M' of Sr in grams per cm² of filament surface per *hour* using Eq. I (1), and are shown in column 8 of Table IV. The values are plotted as full lines on Fig. 3 and compared with the observed points and the least square curve. It is seen that the measured values are several orders of magnitude *higher* than those computed for the combination of either the Wohler or the Chaudron data with the Rossini value for the heat of formation of SrO. The observed values are about one order of magnitude higher than those computed if Wohler's data are combined with Kelley's improbably low choice for ΔH in (4). Because the equilibrium pressure is the greatest that could exist over the reacting substances, the fact that the observed values are higher shows that reaction (1) cannot be occurring.

This conclusion is supported by observation. Experimentally significant quantities of W were observed on the bulbs of the tubes used in the W−MgO experiments,[2] suggesting that the reaction product containing W, presumably WO_2, possessed[19] an appreciable vapor pressure. Both spectrochemical and radioactive tests, (Fig. 2) of bulb deposits in the W−SrO reaction at the same temperature as in the MgO experiment showed no observable W. The vapor pressure of the reaction product containing W must therefore be much lower than that of WO_2.

Reaction (2)

Because the oxides of tungsten are acidic and SrO is strongly basic, chemical combination would be expected at high temperatures. Almost nothing has been published regarding such compounds. Only $SrWO_4$ has

[9] K. K. Kelley, Bureau of Mines Bulletin 384, p. 37.
[10] F. R. Bichowsky and F. D. Rossini, *The Thermochemistry of Chemical Substances* (Reinhold Publishing Corporation, New York, 1936).
[11] F. D. Rossini, private communication dated April 28, 1950.
[12] C. T. Anderson, J. Am. Chem. Soc. **57**, 429 (1935).
[13] J. J. Lander, submitted to J. Am. Chem. Soc.
[14] H. L. Johnston and M. K. Walker, J. Am. Chem. Soc. **57**, 682 (1935).
[15] N. F. Mott and H. Jones, *Properties of Metals and Alloys* (Oxford University Press, London, 1936).
[16] H. J. T. Ellingham, J. Soc. Chem. Industry (May, 1944).
[17] C. W. Dannatt and H. J. T. Ellingham, Disc. Faraday Soc., No. 4 (1948).
[18] S. Dushman, *Scientific Foundations of Vacuum Technique* (John Wiley and Sons, Inc., New York, 1949).
[19] T. Millner and J. Neugebauer, Nature **163**, 601 (1949).

been previously identified[20] and the only thermochemical datum found[10] was its heat of formation from which the heat of the exothermic reaction

$$SrO+WO_3 \rightarrow SrWO_4 \qquad (10)$$

was computed to be 56,400 calories.* No specific heat data are available. If Kopp's law be assumed[21] for $SrWO_4$, the free energy decrease in a reaction like (2) in which $SrWO_4$ was produced will be 56,400 calories greater per mole of W consumed than if WO_3 were the end product. Thus by adding $\frac{1}{3}$ of (10) to

$$SrO+\tfrac{1}{3}W \rightarrow \tfrac{1}{3}WO_3+Sr, \qquad (11)$$

one obtains

$$\tfrac{4}{3}SrO+\tfrac{1}{3}W \rightarrow \tfrac{1}{3}SrWO_4+Sr \qquad (12)$$

and by virtue of tungstate formation, reaction (12) would be driven to the right by about 18.8 kg cal. more free energy per atomic weight of Sr produced than (11), thus predicting a greater rate of Sr production. But there is no experimental evidence that $SrWO_4$ is formed. Although the tungstite, $SrWO_3$, seems more probable, no tungstites are mentioned in the literature. However, K. H. Storks at these Laboratories, observed a small amount of crystalline $SrWO_3$ in x-ray examination of some of these filaments. At about the same time Eisenstein[22] identified $BaWO_3$ (also not previously known) at the interface of nickel-tungsten alloy filaments coated with BaO. He also tentatively identified $SrWO_3$ at the interface of similar filaments coated with SrO. Because of this evidence, it is believed that the reaction occurring in the present work is (2).

In the absence of thermochemical data on $SrWO_3$, it is assumed that reaction (2) is driven toward the right by 18.8 kg cal. more free energy per atomic weight of Sr produced than (1), just as is the case with (12) relative to (11). This assumption is equivalent to taking the heat of a reaction in which WO_2 combines with SrO to be two-thirds as great as that in which WO_3 reacts with the same basic oxide. Although this is not a safe generalization, some compounds behave as postulated, and the heat and free energy of formation of WO_2 are two-thirds those of WO_3. Therefore, 18.8 kg cal. is added to the standard free energy change for reaction (1) in Table IV to give corresponding values for reaction (2). From these, the corresponding rates of reaction (2) are listed in column 9. The expected rate is plotted in Fig. 4, together with the experimental points and their least square curve, from Fig. 1. The mean square deviation of the points from the computed line (using Rossini's estimate) is 28°; from the least square fit of the experimental points, this deviation is 25°. Thus the experimental points agree nearly as well with the theoretical curve as with the best experimental fit.

Because of this agreement[23] and because the rate of reaction was not influenced by the addition of sufficient W powder to triple the interfacial area for the same surface area, it is believed that the measurements give the equilibrium pressure of Sr over reaction (2). This pressure is then given by

$$\log_{10}P_{atm}=2.286+0.5\log T-(1.810\times10^4/T).$$

Discussion of Assumptions

The magnitude of error in computing the free energy of Sr can hardly be as large as the uncertainty in the published values for the heat of formation of SrO, and will therefore not introduce any significant uncertainty into the computed rate of reaction (1) or (2). Nevertheless, the use of an estimated Debye temperature may arouse misgivings, so that the free energy of Sr vapor was estimated by another method previously used by White[3] for a different reaction. This requires the heat of vaporization of solid Sr at 298.1°K, and White assumed that this was equal to the value determined in the high temperature range by vapor pressure measurement.

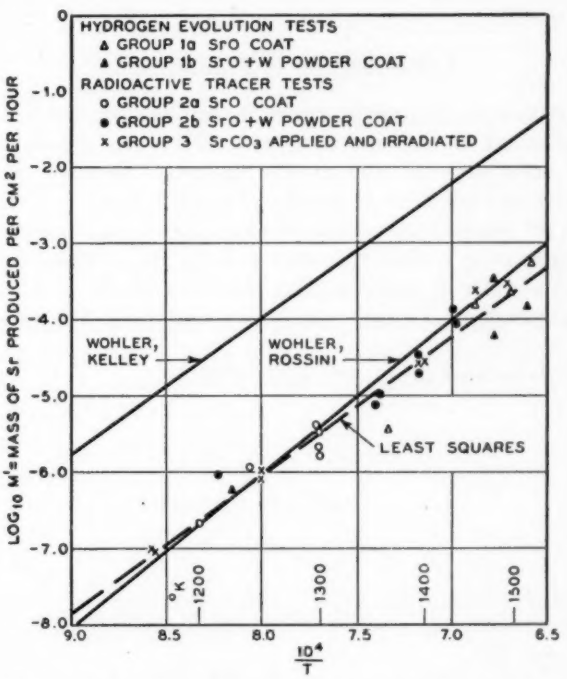

FIG. 4. Comparison of observed rate of Sr production with computed rates, assuming reaction II.

[20] J. W. Mellor, *A Comprehensive Treatise on Inorganic and Theoretical Chemistry* (Longmans, Green and Company, New York, 1931), Vol. XI.

* The heat of corresponding reaction in which MgO replaces SrO is only 3300 cal. exothermic.[10] This much smaller value probably explains why no complex compound formation was observed in the MgO experiment.

[21] H. S. Taylor, *A Treatise on Physical Chemistry* (D. Van Nostrand Company, New York, 1931).

[22] Quarterly Progress Report, December 15, 1948, Nr 074 081.

[23] W. F. Giaque, J. Am. Chem. Soc. **71**, 3192 (1949) has indicated that in some reactions between solid phases and with a gaseous reaction product, the experimental state of aggregation of the solids should be considered before identifying observed equilibria with those computed from thermodynamic data on the macroscopic properties of the solids. Such effects are not judged important here, because no effect was observed when tungsten powder was used and because SrO seems invariably to occur in very minute crystals.

This is equivalent to assuming that the specific heats of solid and vapor are equal from 298.1°K to 1000°K, which is certainly not correct but which is convenient for many calculations whose end accuracy will not be significantly influenced by the error in this assumption. Values of $\log M'$ expected from reaction (2) computing the free energy of Sr in this way are listed in column 10 of Table IV and may be compared with those in column 9.

Reflection at Phase Boundaries and Diffusion through Phases

Because this comparison of theory with experiment depends on a low reflection for Sr atoms crossing phase boundaries, the experiments are believed evidence for a reflection coefficient below 50 percent.

The fact that the rate of reaction seems unaffected by any diffusion processes occurring could not have been foretold by any method known to the writers. However, it seems to be true for a number of similar reactions on which study is not yet complete. But diffusion processes almost surely limit the rate of reaction when the cathode alloy contains a small percentage of some metal which reacts vigorously with the oxide as in the systems generally employed for commercial oxide coated cathodes.

Consideration of Equilibrium

Although one might question equilibrium constants measured in chemical reactions which are proceeding in only one direction at the maximum possible rate, there are parallels in purely physical reactions. Langmuir[24] studied the process of evaporation: i.e., tungsten atoms from a solid tungsten surface. He assumed that the number of atoms leaving the tungsten filament was independent of whether any were returning. The vapor pressures so determined were equal to those determined by the Knudsen method and technique was far easier, especially for refractory metals. Langmuir and Kingdon[25] verified the Saha equation by applying similar considerations to the ionization of Cs atoms on tungsten filaments. As a third example, the work of Mayer[26] and his students on electron affinities requires that the rate of formation and departure of negative halogen ions on a filament be determined by the number of incident halogen molecules and a true equilibrium between ions of groups (a) and (b) is not necessary.

[24] I. Langmuir, Phys. Rev. **2**, 329 (1913).

CONCLUSIONS

(1) Tungsten filaments coated with SrO produce Sr metal in the temperature range 1150–1550°K at a rate M' in grams per cm² per hour given by

$$\log_{10} M' = -\frac{1.810\times 10^4}{T} + 8.460.$$

(2) This rate is believed to correspond to the *equilibrium pressure* of Sr metal vapor in reaction (2) which is thus given by

$$\log_{10} P_{\text{atm}} = 2.286 + 0.5 \log T - \frac{1.810\times 10^4}{T}.$$

(3) The reaction occurring is

$$\tfrac{3}{2}\text{SrO}(s) + \tfrac{1}{2}\text{W}(s) \rightleftarrows \tfrac{1}{2}\text{SrWO}_3(s) + \text{Sr}(g).$$

(4) The reflection coefficient for Sr atoms in crossing phase boundaries is less than 0.5.

The writers appreciate suggestions by A. H. White and assistance in computation by Mrs. G. V. Smith, throughout this work.

[25] I. Langmuir and K. H. Kingdon, Proc. Roy. Soc. **107A**, 61 (1925).

[26] See for example P. P. Sutton, J. Chem. Phys. **3**, 20 (1935).

THE JOURNAL OF CHEMICAL PHYSICS VOLUME 18, NUMBER 12 DECEMBER, 1950

The Admittance Concept in the Kinetics of Chromatography*

J. B. ROSEN† AND WARREN E. WINSCHE‡
Columbia University and Brookhaven National Laboratory, New York
(Received July 31, 1950)

Chromatographic processes with linear kinetics can be represented by a system admittance for the case where the influent concentration varies sinusoidally. The admittance has been obtained for a variety of assumed rate controlling mechanisms and is shown to depend strongly on the type of kinetics obeyed by the system. The results indicate experimental techniques for determining the kinetics of these processes. Representative results obtained with an electronic analogue computer are presented for a case of non-linear kinetics.

THE kinetic theory of the chromatographic process, which may be defined as the process by which matter is interchanged between a fluid and a solid in relative motion, has been discussed in mathematical terms by several writers.[1–3] The problem of interest here, and in the articles referred to, is that of a liquid solution containing a single active solute moving with constant linear velocity V, through a uniformly packed column of solids, of length L.

In all cases previously discussed the problem has been solved for the bed initially at equilibrium, followed by a step increase or decrease in the value of the concentration, $c_0(t)$, of material in the liquid at the input to the bed. The desired result is the space and time distribution of concentration of material in solution, $c(z, t)$, and material adsorbed in the bed, $q(z, t)$, as the process approaches its new equilibrium state, where z is the distance from the input face of the bed and t is the time. This is shown schematically in Fig. 1. This article discusses the effect of varying the influent concentration sinusoidally, such that

$$c_0(t)=c_0[1-\alpha\cos\omega t], \quad 0\leq\alpha\leq 1. \tag{1}$$

It will be shown that this particular time variation of influent concentration leads to very useful results, which should permit the determination of the type of kinetics obeyed by a particular system in a direct manner. With this influent it is possible to describe many systems completely by a single complex quantity, the system admittance. That is to say, any two systems with the same admittance will behave identically for a sinusoidally varying influent. For systems where such an admittance can be found, the fundamental constants of the system, such as the diffusion coefficients and reaction rate constants, can readily be obtained from the system admittance. It is desirable to use a single complex admittance and its reciprocal, a complex impendance, rather than four real quantities because of the great simplification in notation thus obtained and because of the ease with which several mechanisms operating simultaneously can be taken into account by the simple assumption of several impedances acting in series.

For any physical bed with an influent given by (1), the effluent $c_e(t)=c(L, t)$ will be a periodic function of time, after a time sufficiently long for the transients to die out. Under these conditions the value of $q(z, t)$ will also be periodic at any fixed point in the bed. The period is given by $2\pi/\omega$. When $c(z, t)$ and $q(z, t)$ at any fixed point of the bed are periodic functions of time the system is said to be in a steady-state condition. In particular, for a material and bed which obey linear kinetics the steady-state effluent is given by

$$c_e(t)=c_0\{1-\alpha e^{-Y_1L/V}\cos[\omega t-(\omega+Y_2)L/V]\}. \tag{2}$$

The quantity

$$\mathbf{Y}=Y_1+iY_2=Ye^{i\phi} \tag{3}$$

is a complex admittance which is a function only of the kinetics of the system and the angular frequency ω. Y_1, Y_2, Y, and ϕ are all real quantities, the last two being given by

$$Y=|\mathbf{Y}|=[Y_1^2+Y_2^2]^{\frac{1}{2}}, \quad \phi=\tan^{-1}(Y_2/Y_1).$$

A complex impedance is also defined by

$$\mathbf{Z}=1/\mathbf{Y}=[Y_1^2+Y_2^2]^{-\frac{1}{2}}e^{-i\phi}. \tag{4}$$

Under the same conditions the steady-state distribution of adsorbed material will be given by

$$q(z, t)=c_0\{K-(\alpha Y/\omega)e^{-Y_1z/V}\times\sin[\omega t-(\omega+Y_2)z/V+\phi]\}, \tag{5}$$

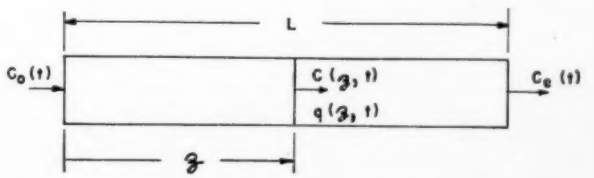

FIG. 1. Schematic of packed column.

* Part of the research covered in this paper was done at the Brookhaven National Laboratory while the first author was a Guest Research Fellow.
† AEC Predoctoral Fellow in Applied Mathematics at Columbia University.
‡ Head, Division of Chemical Engineering, Brookhaven National Laboratory.
[1] H. C. Thomas, J. Am. Chem. Soc. **66**, 1664 (1944).
[2] H. C. Thomas, Ann. N. Y. Acad. Sci. **49**, 161 (1948); ample references to the literature are given in this paper.
[3] Boyd, Myers, and Adamson, J. Am. Chem. Soc. **66**, 2849 (1947)

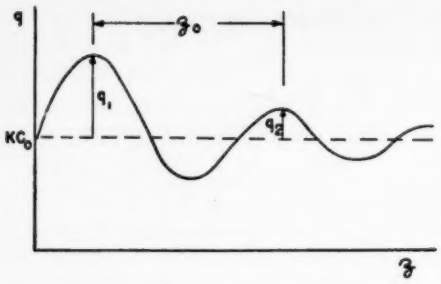

FIG. 2. Steady-state distribution of adsorbed material in bed with sinusoidal influent.

where Kc_0 is the equilibrium value of q corresponding to c_0.

Equations (2) and (5) suggest two possible experimental measurements. A time varying input of type (1) is fed into the bed, making α as close to unity as possible. This is continued until the system reaches its steady-state condition.

(a) The effluent concentration $c_e(t)$ is measured as a function of time, and observations are made of the amplitude decrease and phase shift of its time varying component relative to $c_0(t)$. Inspection of Eq. (2) shows that the relative amplitude decrease represents the effect of the term $e^{-Y_1 L/V}$ while the phase shift is produced by the term $(\omega+Y_2)L/V$.

(b) Alternately consider the process at some time, t_0. The concentration of adsorbed material $q(z, t_0)$ is measured as a function of z. Equation (5) shows that if the distance between two maxima or minima is z_0, as shown in Fig. 2, the following relation holds,

$$(\omega+Y_2)z_0/V=2\pi. \tag{6}$$

Furthermore, the ratio of any two adjacent maxima or minima, as measured from the value Kc_0, permits the value of Y_1 to be determined by means of the relation

$$Y_1 z_0/V=\log(q_1/q_2). \tag{7}$$

The second method will be of use only if it is possible to stop the process entirely in a non-equilibrium condition and analyze the solid bed material in this "frozen" state, or if the reaction is so slow that no appreciable change in solid concentration takes place in the time required to analyze the bed. The second method will therefore be applicable only in special cases. Radioactive tracer techniques will certainly prove useful in experiments based on measurements of type (a), and their use might make experiments of type (b) feasible in some cases.

It is assumed that all quantities in (2) and (5) except Y_1 and Y_2 can be obtained by other methods. Then either (a) or (b) will uniquely determine Y_1 and Y_2. If the value of ω in the influent (1) is varied over as wide a range as possible, repeating one of these measurements for each value, $\mathbf{Y}(\omega)$ is obtained as a function of ω. It will be shown that the functional relationship between $\mathbf{Y}(\omega)$ and ω depends very strongly on the type of kinetics which the system obeys. By comparison of the experimentally determined relationship with that calculated for different assumed mechanisms it should

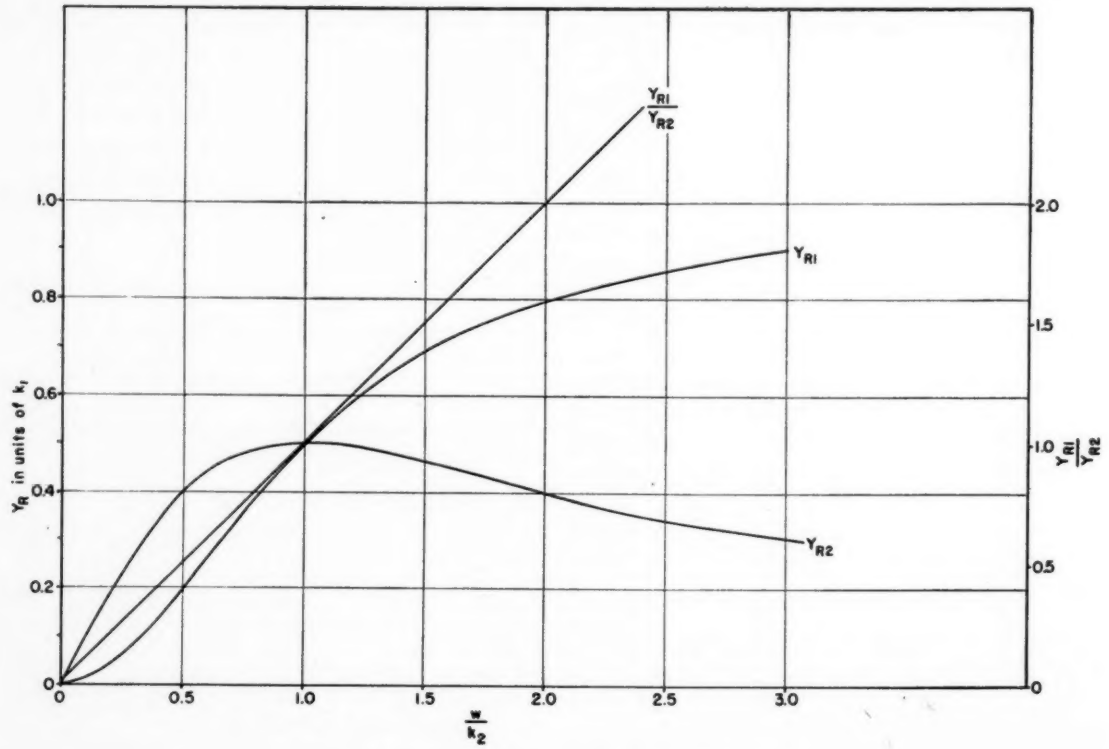

FIG. 3. Admittance for opposing first-order reactions.

be possible in many cases to determine what kinetics are actually obeyed by the system. Furthermore, if a particular mechanism is decided upon, the physical constants of the system involved in this mechanism can be uniquely determined.

In general, the concentration in the liquid and the solid will be given by Eqs. (2) and (5) for an influent of type (1) whenever the rate of adsorption of material

$$\partial q/\partial t = G(c, q) \tag{8}$$

satisfies the following two conditions:

I. The relation $G(c, q)=0$ defines a unique equilibrium value, $q_e(c)$, of q for all values of c in some given range. Furthermore, $G(c, v)$ is such that in this range

$$G(c, q)\begin{cases} >0, & q<q_e(c) \\ <0, & q>q_e(c). \end{cases}$$

Physically this condition means that the process is reversible and in addition, all transient terms die out in a sufficiently long time after a disturbance has taken place. That is, the process approaches an equilibrium condition for $c_0(t)=c_0(\text{const.})$ regardless of the initial condition of the adsorbent. This is a sufficient condition for a steady-state solution with sine influent for all cases, linear and non-linear.

II. $G(c, q)$ is linear in c and q. This ensures that all quantities vary with the fundamental angular frequency ω.

Equations (2) and (5) are derived in the appendix, assuming these conditions. Three examples of such systems will now be discussed.

A. Opposing first-order reactions.

$$G(c, q)=k_1c-k_2q. \tag{9}$$

Equation (8) holds, independently of x; then it can be written as the ordinary differential equation

$$(k_2+p)q(t)=k_1c(t), \quad p\equiv d/dt.$$

Then since p is a linear operator[4]

$$\frac{dq}{dt}=pq=\left(\frac{pk_1}{k_2+p}\right)c=\left(\frac{k_1}{1+(k_2/p)}\right)c. \tag{10}$$

To get the steady-state solution for $\mathbf{c}=c_0e^{i\omega t}$ let $p=i\omega$. Then

$$\frac{d\mathbf{q}}{dt}=\left(\frac{k_1}{1-i(k_2/\omega)}\right)\mathbf{c}=\mathbf{Y}_R\mathbf{c}. \tag{11}$$

This leads to the following value for the admittance

$$Y_{R1}=\frac{k_1}{1+(k_2/\omega)^2}, \quad Y_{R2}=\frac{k_1(k_2/\omega)}{1+(k_2/\omega)^2} \tag{12}$$

so that

$$\mathbf{Z}_R=1/k_1-i(k_2/k_1\omega). \tag{13}$$

The admittance is plotted in Fig. 3. It is seen that Y_{R2} has a maximum value at $k_2=\omega$. At this same value of ω the value of k_1 is given by $k_1=2Y_{R1}$. If this value of ω is experimentally obtainable, the above gives a simple method of obtaining k_1 and k_2. In general

$$k_2=(Y_{R2}/Y_{R1})\omega, \quad k_1=[1+(Y_{R2}/Y_{R1})^2]Y_{R1}, \tag{14}$$

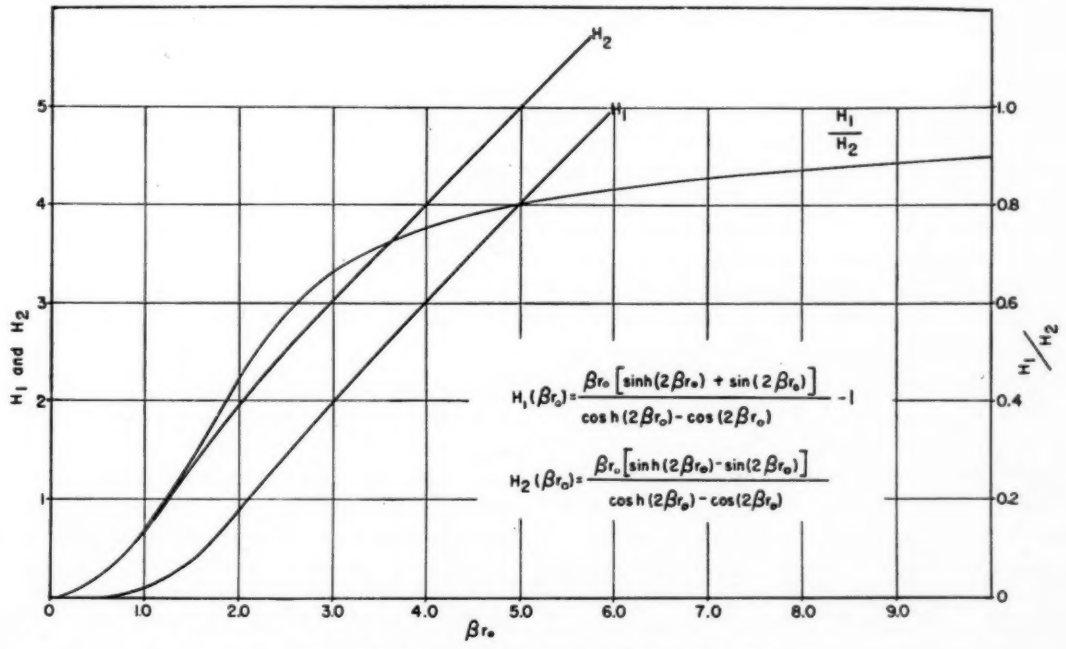

FIG. 4. Values of H-functions, $H_1(\beta r_0)$ and $H_2(\beta r_0)$.

[4] T. V. Karman and M. A. Biot, *Mathematical Methods in Engineering* (McGraw-Hill Book Company, Inc., New York, 1940), Chapter IX.

so that if this is the correct mechanism, the values of k_1 and k_2 so obtained should be independent of ω.

B. Solid diffusion into the interior of homogeneous spheres of uniform radius r_0, and diffusion constant D. The assumption is made that r_0 is small compared to the length of the column over which a significant change in solution concentration $c(x, \theta)$ occurs and that each sphere is exposed uniformly on all sides to the solution. Let $q_i(r, x, \theta)$ be the distribution of adsorbed material in the interior of the spheres. q_i must satisfy the equations

$$\partial q_i/\partial\theta = D\nabla^2 q_i, \tag{15}$$

$$q_s(x, \theta) \equiv q_i(r_0, x, \theta) = Kc(x, \theta), \tag{16}$$

where K is an effective equilibrium constant. Then by Duhamel's theorem[5] for $q_i(r, x, 0) = 0$, its value at any later time is given by

$$q_i(r, x, \theta) = K\int_0^\theta c(x, \lambda)\frac{\partial}{\partial\theta}H(r, \theta-\lambda)d\lambda, \tag{17}$$

where $H(r, \theta)$ is the solution of (15) for the boundary condition $q_i(r_0, x, \theta) = 1$. The concentration of adsorbed material is obtained from the relation

$$q(x, \theta) = \frac{3}{r_0^3}\int_0^{r_0} q_i(r, x, \theta)r^2 dr. \tag{18}$$

For this system, Eq. (8) takes the form

$$\frac{\partial q}{\partial t} = G(c, q_s) = \frac{3D}{r}\lim_{\Delta r\to 0}\left[\frac{Kc - q_i(r_0-\Delta r)}{\Delta r}\right] = \frac{3D}{r_0}\left[\frac{\partial q_i}{\partial r}\right]_{r=r_0}. \tag{19}$$

The solution of this system for a step input requires the solution of the homogeneous partial integro-differential equation in $c(x, \theta)$ obtained by substituting (17) in either (18) or (19) and then using the resulting expression for $\partial q/\partial t$ in Eq. (31). A semigraphical method of solution to this equation arising out of a similar problem in heat transfer has been presented by Lowan.[6]

For the sinusoidal influent a steady-state analytical solution can readily be obtained. The solution of (15) with the boundary condition

$$\mathbf{q}_s(t) = K\mathbf{c}(t) = Kc_0 e^{i\omega t}$$

has been obtained for the problem of heat transfer in a solid sphere.[7] The steady-state solution is

$$\mathbf{q}_i(r) = \frac{r_0}{r}\left[\frac{\sinh(1+i)\beta r}{\sinh(1+i)\beta r_0}\right]K\mathbf{c}, \quad \beta = (\omega/2D)^{\frac{1}{2}}. \tag{20}$$

Using this in either (18) or (19) gives

$$\frac{\partial \mathbf{q}}{\partial t} = \frac{3DK}{r_0^2}[H_1(\beta r_0) + iH_2(\beta r_0)]\mathbf{c} \tag{21}$$

where

$$H_1(\beta r_0) = \frac{\beta r_0[\sinh(2\beta r_0)+\sin(2\beta r_0)]}{\cosh(2\beta r_0)-\cos(2\beta r_0)} - 1$$

$$H_2(\beta r_0) = \frac{\beta r_0[\sinh(2\beta r_0)-\sin(2\beta r_0)]}{\cosh(2\beta r_0)-\cos(2\beta r_0)}$$

so that

$$\mathbf{Y}_D = Y_{D1} + iY_{D2}, \tag{22}$$

where

$$Y_{D1} = (3DK/r_0^2)H_1(\beta r_0) \tag{23}$$

$$Y_{D2} = (3DK/r_0^2)H_2(\beta r_0). \tag{24}$$

The functions H_1 and H_2 and the ratio H_1/H_2 are plotted as a function of $\beta r_0 = (\omega/2D)^{\frac{1}{2}}r_0$ in Fig. 4. Comparison of these curves with the corresponding curves in Fig. 3 indicates the essential difference between the system admittance for each of the two mechanisms considered.

It can be seen that the ratio H_1/H_2 uniquely determines βr_0. Since $Y_{D1}/Y_{D2} = H_1/H_2$ the value of βr_0 is determined once Y_{D1} and Y_{D2} are known. The accuracy of this determination is best for the middle range of values of βr_0, where the H_1/H_2 curve has its steepest slope. The accuracy decreases for larger and smaller values of βr_0. If it is possible, the range of values of ω used in any experimental work should be chosen so that βr_0 falls in the region of steepest slope. Since r_0 is assumed known, the determination of βr_0 determines D. The effective equilibrium constant K can then be determined from either (23) or (24). The values so found should be independent of ω. The limiting values given by (23) and (24) as $\beta r_0 \to 0$ are

$$Y_{D1} = \frac{K\omega^2 r_0^2}{10D}, \quad Y_{D2} = K\omega.$$

The asymptotic values as $\beta r_0 \to \infty$ are

$$Y_{D1} = Y_{D2} = \frac{3K}{r_0}\left(\frac{\omega D}{2}\right)^{\frac{1}{2}}.$$

These values are useful if it is experimentally impossible to use a value of ω which brings βr_0 into the middle range.

C. Solid diffusion as in case B but taking into account the transport of material through a thin boundary film surrounding the particles. Here the rate equation

$$\frac{\partial q}{\partial t} = G(c, q_s) = \frac{3h}{r_0}[Kc - q_s] \tag{25}$$

must be satisfied along with (15) and (18). h will depend on the diffusion constant in the solution and the film

[5] Carslaw and Jaeger, *Conduction of Heat in Solids* (Oxford University Press, London, 1947), p. 20.
[6] A. N. Lowan, Phil. Mag. **7**, 17, 914 (1934).
[7] See reference 5, p. 202.

thickness, and therefore will be a function of the velocity V. Equation (15) with the boundary condition

$$\mathbf{q}_s = q_0 e^{i\omega t}$$

leads to

$$\partial \mathbf{q}/\partial t = \mathbf{Y}_D \mathbf{q}_s / K$$

by the method used to get (21). This value of $\mathbf{q}_s$ is used in (25) and (25) is solved for $\partial \mathbf{q}/\partial t$, giving

$$\frac{\partial \mathbf{q}}{\partial t} = \frac{\mathbf{c}}{(r_0/3hK)+(1/\mathbf{Y}_D)}. \tag{26}$$

The boundary film can be considered as a resistance $R_f = r_0/3hK$ in series with the solid diffusion impedance $\mathbf{Z}_D = 1/\mathbf{Y}_D$. Then the total impedance $\mathbf{Z}_T$ is given by $\mathbf{Z}_T = R_f + \mathbf{Z}_D$, or

$$\mathbf{Y}_T = 1/\mathbf{Z}_T = 1/(R_f + \mathbf{Z}_D). \tag{27}$$

For R_f small this obviously reduces to case B. For $\beta r_0 \ll 1$, this gives

$$\mathbf{Y}_T = 1/[R_f - i/(K\omega)]$$

which is the same as case A with $k_1 = 3hK/r_0$ and $k_2 = 3h/r_0$.

In a similar manner, in principle at least, the simultaneous operation of several rate controlling mechanisms can be taken into account by using a total impedance equal to the sum of the impedances of the separate assumed mechanisms. The total effective admittance, given by the reciprocal of the total impedance, will determine the kinetics of the system. Thus, the combination of a boundary film, first-order opposing reactions on the sphere surface and internal solid diffusion leads to

$$\mathbf{Z}_T = R_f + \mathbf{Z}_R + \mathbf{Z}_D. \tag{28}$$

The preceding discussion is limited to linear systems. The analytical representation of $c_e(t)$ and $q(z, t)$ for non-linear kinetics is considerably more involved. In general, the effect of non-linearity, with an influent (1), is the generation of higher harmonic terms which appear in the steady-state values of $c_e(t)$ and $q(z, t)$. Such an analytical solution has been obtained by the first-named author for the case of opposing second-order and first-order reactions represented by the equation

$$\partial q/\partial t = k_1 c[1-(q/a)] - k_2 q \tag{29}$$

where the constant a is the total adsorption capacity of the bed. This case has been thoroughly treated by Thomas for the step function input.[2]

A large amount of labor is required to numerically evaluate analytical solutions for non-linear kinetics in those few cases for which analytical solutions are obtainable. Most non-linear cases do not lend themselves to analytical solutions. For this reason an electronic analogue computer has been constructed which is capable of solving the equations of this system for a wide range of linear or non-linear rate controlling mechanisms, including empirical kinetic equations of type (8) such that $G(c, q)=0$ leads to experimentally obtained equilibrium isotherms.

Curves of $c_e(t)$ have been obtained by use of the analogue computer for the kinetics of Eq. (29). Representative curves of the effluent obtained for a sinusoidal influent, are given in Fig. 5 as a function of the three dimensionless constants of the system

$$\omega/k_2, \quad k_1 L/V, \quad k_1 c_0/k_2 a.$$

The last constant is a measure of the non-linearity of the system, as shown by the departure of the effluent from a true sine curve as $k_1 c_0/k_2 a$ increases. It is worth

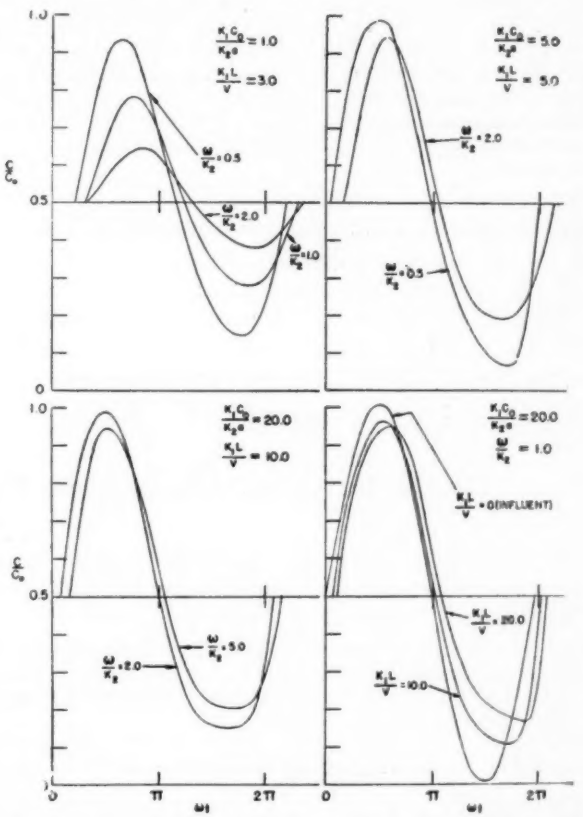

FIG. 5. Representative curves of steady-state effluent for non-linear kinetics $\partial q/\partial t = k_1 c[1-(q/a)] - k_2 q$ with influent $c_0(t) = 0.5\, c_{0O}(1+\sin\omega t)$.

mentioning that the results obtained here apply to the case of opposing second-order reactions[1] provided the constants are suitably interpreted. A study of other non-linear cases with the aid of the computer as well as a thorough investigation of the accuracy of computer solutions is now being carried out.

The authors wish to acknowledge the helpful suggestions of Professor H. C. Thomas, Sterling Chemistry Laboratory, Yale University, Professor R. H. Bretton, Department of Chemical Engineering, Yale University, and Professor F. J. Murray, Department of Mathematics, Columbia University. Special thanks are due Mr. O. A. Kuhl of the Brookhaven National Labora-

tory for help in the construction of the electronic computer. The research covered in this paper was made possible by a NRO-AEC Predoctoral Fellowship and the Brookhaven National Laboratory.

APPENDIX

The equation of conservation for the system is

$$\partial c/\partial t+V(\partial c/\partial z)=-\partial q/\partial t \tag{30}$$

where both c and q are in the same units, e.g., millimoles per gram of adsorbent. This simplifies upon the substitution

$$\theta=t-z/V, \quad x=z/V$$

to

$$\partial c/\partial x=-\partial q/\partial\theta. \tag{31}$$

This, together with the kinetic equation of the system

$$\partial q/\partial\theta=\partial q/\partial t=G(c, q) \tag{32}$$

and the boundary conditions determine a solution. Complex quantities (bold face) are used throughout, with the desired physical values being given by their real part. It is desired to obtain the steady-state solution of (31) and (32) which satisfies the boundary condition

$$\mathbf{c}_0(\theta)=c_0e^{i\omega\theta}. \tag{33}$$

Since the system is linear, a solution is assumed of the form

$$\mathbf{c}(x, \theta)=\mathbf{F}(x)e^{i\omega\theta}. \tag{34}$$

Then (31) gives

$$\partial\mathbf{q}/\partial\theta=-(d\mathbf{F}/dx)e^{i\omega\theta}. \tag{35}$$

Because of condition I, the solution of the homogeneous equation in q obtained by putting $c=0$, approaches a constant value exponentially with time. Then under steady state conditions we can obtain (32) in the form

$$\partial\mathbf{q}/\partial\theta=\mathbf{Y}(i\omega)\mathbf{c} \tag{36}$$

where the admittance $\mathbf{Y}$ is independent of q, c, x and θ. To determine $\mathbf{F}(x)$, (31) together with (34) and (36) gives

$$d\mathbf{F}/dx=-\mathbf{YF} \tag{37}$$

This has the solution satisfying (33)

$$\mathbf{F}(x)=c_0\exp(-\mathbf{Y}x). \tag{38}$$

Then

$$\mathbf{c}(x, \theta)=c_0\exp(i\omega\theta-\mathbf{Y}x)=c_0\exp[-Y_1x+i(\omega\theta-Y_2x)]. \tag{39}$$

Since the system is linear, superposition can be used to get a steady state solution for the boundary condition (1). The real part of (39), with the factor $-\alpha$, is added to the equilibrium value of c_e for the step input c_0, i.e., $c_e(\theta)=c_0$. This gives Eq. (2) directly. Integrating (36) after substitution for $\mathbf{c}(x, \theta)$ gives

$$\mathbf{q}(x, \theta)=(\mathbf{Y}/i\omega)c_0\exp(i\omega\theta-\mathbf{Y}x) \tag{40}$$

which by a similar procedure leads to (5). An alternate method of solution, leading to the same results, is by the use of the Laplace transform.

THE JOURNAL OF CHEMICAL PHYSICS VOLUME 18, NUMBER 12 DECEMBER, 1950

On the Ultrasonic Absorption in Binary Mixtures of Unassociated Liquids

DANIELE SETTE
Istituto Nazionale di Ultracustica "O. M. Corbino," Rome, Italy
(Received July 24, 1950)

Measurements of absorption coefficient were carried out in a binary mixture formed by two unassociated liquids having similar absorption coefficients. The curve absorption coefficient *versus* mole fraction has a minimum at an intermediate concentration. A theoretical interpretation of experimental results is presented.

I. INTRODUCTION

RECENTLY Pinkerton[1] and Bauer[2] gave a theoretical interpretation of ultrasonic absorption in binary mixtures of unassociated liquids with very different absorption coefficients. In this case the absorption coefficient decreases very rapidly when to the more absorbing liquid are added small quantities of the other component; the coefficient, then, gradually approaches its value for the second liquid.

Their treatments are founded on two basic ideas. The difference between classical and experimental values of absorption coefficients in unassociated liquids is, as is now reasonably well established, to be ascribed to relaxation phenomena in energy distribution among the internal degrees of freedom of the molecules. If we mix the molecules of an unassociated liquid with those of another liquid, the collisions between different molecules lead to quicker achievement of energy distributions.

Obviously, in a mixture formed by a very absorbing unassociated liquid and another one much less absorbing, the variation of the coefficient with concentration is due essentially to the decrease of energy losses in the molecules of the first liquid.

It seemed to us worth while to consider mixtures of two unassociated liquids with similar absorption coefficient. If we base our ideas on the foregoing, we must expect a decrease of the absorption coefficient, when we add small quantities of either one of two liquids to the other.

In the present paper the experimental results obtained in a mixture of this kind are given and, at the same time, a theoretical interpretation of them is presented.

[1] J. M. M. Pinkerton, Proc. Phys. Soc. **B62**, 129 (1949).
[2] E. Bauer, Proc. Phys. Soc. **A62**, 141 (1949).

II. EXPERIMENTAL RESULTS

The results of measuring the absorption coefficient in the carbon tetrachloride-benzene system are recorded in Table I.

Measurements were carried out by an optical method[3] at 8 Mc/sec. α is the amplitude absorption coefficient.

III. THEORETICAL INTERPRETATION

We can easily explain the experimental results in the carbon tetrachloride-benzene mixtures by a simple relaxation scheme, extending Bauer's treatment to mixtures formed by two unassociated liquids with similar absorption coefficients.

Let A be the more absorbing liquid and B the second. We assume with Bauer that it will only be necessary to consider binary collisions and that collisions between excited molecules may be ignored. We suppose also, for simplicity, that any molecule can find itself only at a single excited level (1) as well as in the ground state (0).

In these circumstances we are only concerned with four different kinds of collisions. If A, B, represent an unexcited molecule of liquid A and B, respectively, and A^*, B^*, an excited molecule, the collisions to be considered are: (A^*A), (B^*B), (A^*B), (B^*A).

According to Bauer's method, we introduce the transition probabilities k,g,l,h relating, respectively, to (AA), (AB), (BA), (BB) collisions.

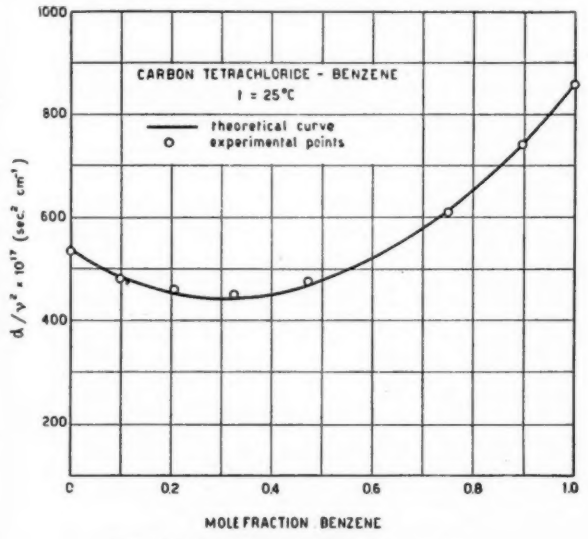

FIG. 1. Absorption coefficient in carbon tetrachloride-benzene mixture.

Let us consider 1 g mole of mixture: the fraction a of A molecules is made by the mole fractions a_1, $a_0 = a - a_1$ of excited and unexcited molecules. Similarly the fraction $(1-a)$ of B liquid is formed by the mole fractions b_1, b_0.

It is possible to set out two equations of detailed balance and, following the perturbation method used by Bauer, to arrive at the same expression he gave for the parameter α/ν^2 (α is the amplitude absorption coefficient and ν the frequency) as a function of a:

$$\frac{\alpha}{\nu^2} = 2\pi\left[\frac{\pi c}{c'^2}(\gamma'-1)\frac{1}{C_p'}\right]_a\left[\frac{aC_A}{\phi_{10}}+\frac{(1-a)C_B}{\psi_{10}}\right]. \quad (1)$$

In this equation c is the measured velocity of sound in the mixture, while c' is the velocity for frequency much higher than the mean dispersion frequency (ν_m); γ' is the ratio C_p'/C_v' between the contribution of the external degrees of freedom to the principal specific heats; C_A and C_B are the equilibrium values of the vibrational specific heats of A and B molecules. Finally, ϕ_{10} and ψ_{10} are expressed by:

$$\begin{cases}\phi_{10} = k_{10}a_0 + g_{10}b_0 \\ \psi_{10} = l_{10}a_0 + h_{10}b_0.\end{cases} \quad (2)$$

In order to make an easier comparison between theory and experiment, two approximations have to be introduced. The first is the one established by Bauer, but probably this assumption is to be considered not as justified as in the case where the two liquids have very different absorption coefficients. Assuming, nevertheless, that the quantity $[2\pi^2 c/c'^2(\gamma'^{-1})1/C'_p]$ varies linearly with concentration a, we may write it: $M_B(1-fa)$.

The second approximation refers to the efficiency of different collisions in producing inelastic transitions. It is more general than Bauer's.

Certainly an (A^*A) collision is less efficient than a (B^*B) collision from the point of view of de-excitation, because the mean dispersion frequency of A molecules ($\nu_m{}^A$) is smaller than that for B molecules ($\nu_m{}^B$). We can assume that (B^*B) collisions are $z = \nu_m{}^B/\nu_m{}^A$ times more efficient than (A^*A) collisions in producing an inelastic transition. In mathematical form this is expressed by $zk_{ij} = h_{ij}(i,j=0,1)$.

When an excited molecule (A^* or B^*) strikes against a molecule of a different kind (B or A, respectively), the collision has a higher de-excitation efficiency than when the collision occurs between two molecules of the same kind: (A^*A) or (B^*B). Generally it is, in fact, impossible in the first case that a quantum of vibra-

TABLE I. Absorption coefficient in carbon tetrachloride-benzene mixtures.

Mole fraction benzene	t (°C)	α (cm^{-1})	$(\alpha/\nu^2)\cdot 10^{17}$ (sec.^{2} cm^{-1})
0	24.9	0.3440	537.5
0.0975	24.9	0.3078	481.0
0.2061	25.05	0.2953	461.5
0.3251	24.95	0.2895	452.3
0.4739	25.05	0.3045	475.8
0.7501	24.95	0.3920	612.5
0.8975	25.1	0.4753	742.7
1	25.1	0.5491	858.0

[3] D. Sette, Nuovo Cimento 7, 55 (1950).

tional energy goes from one molecule to the other without some loss of energy. For this reason we set out: $tk_{ij}=g_{ij}$; $uh_{ij}=l_{ij}$.

To summarize, the relationships of transition probabilities which we assume to be valid are:

$$\begin{cases} zk_{ij}=h_{ij} \\ g_{ij}=tk_{ij}=th_{ij}/z \\ l_{ij}=uh_{ij} \end{cases} \quad (i,j=0,1). \tag{3}$$

Equation (1) can now be rewritten easily:

$$\left(\frac{\alpha}{\nu^2}\right)_a=\frac{2M_B}{h_{10}}(1-fa)\left[\frac{azC_A}{a+t(1-a)}+\frac{(1-a)C_B}{1+a(u-1)}\right]. \tag{4}$$

For comparison with experiment it is useful to consider the ratio α/α_B:

$$\frac{(\alpha/\nu^2)_a}{\alpha_B/\nu^2}=\frac{\alpha}{\alpha_B}=(1-fa)\left[\frac{az}{a+t(1-a)}\frac{C_A}{C_B}+\frac{1-a}{1+a(u-1)}\right]. \tag{5}$$

Equations (4) and (5) are reduced to the corresponding expressions given by Bauer, by putting $t=z$ and $u=1$.

In Eq. (5) the value of the quantity f can be found by putting $\alpha=\alpha_A$ for $a=1$. There are also the two parameters u and t which seem to be of interest in illustrating the characteristics of the molecular relaxation. Notwithstanding the roughness of our hypotheses, their introduction in our treatment, of course, has a significance if relaxation phenomena are not complicated by other factors such as, for instance, interaction between A and B molecules. It is convenient, in any case, to calculate the t and u values from the experimental results of absorption coefficients in two mixtures very rich in liquids A and B respectively. In these mixtures we can, in fact, consider that such phenomena operate as expected.

The results of our treatment in carbon tetrachloride-benzene mixture are given in Fig. 1. The curve represents Eq. (5) and the circles represent the experimental values.

The values used for C_A/C_B (0.9512), and $z=\nu_m^B/\nu_m^A(2.85)$, A being benzene and B carbon tetrachloride, are those given by Bauer. The values of u, t parameters obtained are: $t=2.40$, $u=2.06$.

As we can see from Fig. 1, there is a noticeable agreement between the theoretical variation of absorption coefficient represented by Eq. (5) and the experiment.

IV. CONCLUSIONS

The absorption coefficient in a mixture of two unassociated and not interacting liquids presents a minimum at an intermediate concentration, when the absorption coefficients of the two pure liquids are similar to one another.

A theoretical treatment is presented, as an extension to that of Bauer.

The agreement between the theoretical indications and experimental results, although achieved by rough hypotheses, seems to be a proof of the correctness of our ideas about ultrasonic absorption in unassociated liquids.

ACKNOWLEDGMENT

The author wishes to express his thanks to Professor G. Puppi for useful discussions, and to Dr. E. Bauer for having exchanged views with him.

Kinetics of the Isotopic Exchange Reaction between Carbon Monoxide and Carbon Dioxide*

T. H. NORRIS† AND S. RUBEN‡
Department of Chemistry, University of California, Berkeley, California
(Received July 24, 1950)

The rate of the exchange reaction between carbon monoxide and carbon dioxide has been studied, using C^{14} as a tracer. The reaction, whose velocity in a quartz vessel is convenient for study between 800 and 900°C appears to follow the rate law: Rate $= k(p\mathrm{CO})^{0.73}(p\mathrm{CO_2})^{0.85}$. The apparent activation energy is 77 kcal. The reaction is accelerated by added nitrogen but not argon. Packing increases the rate only slightly, giving no indication of a primarily heterogeneous reaction. However, this observation is considered questionable.

The present conclusions differ somewhat from those derived by Brandner and Urey from a similar investigation. Re-examination of these authors' data seems to resolve the apparent inconsistencies. It is concluded that their proposed reaction mechanism is invalid; however, their conclusion of heterogeneity seems more acceptable.

A probable mechanism appears to be a bimolecular exchange between the two reactants adsorbed on the catalytic surface. The acceleration by nitrogen or, as observed by Brandner and Urey, by hydrogen or water is then possibly to be ascribed to "promotion" of the catalyst by surface adsorption of these substances.

THE kinetics of the exchange reaction between carbon monoxide and carbon dioxide, using C^{13} as a tracer, have been investigated by Brandner and Urey.[1] Their data were quite poorly reproducible and did not clearly indicate any rate law or mechanism, although one particular mechanism was tentatively proposed. We, too, made a study of this same exchange reaction several years ago, using radioactive C^{14} as a tracer. However, we were dissatisfied with the reproducibility of our results, and on discovering that others were conducting a similar investigation, we discontinued our work.

In recent months, one of the present authors has had occasion, in connection with other work, to review this material. Our results, like those of Brandner and Urey, are erratic, but they do seem to indicate a not unreasonable rate law, on the basis of which it would seem that, at least in the general case, the tentative mechanism proposed by Brandner and Urey is unsatisfactory. An alternative mechanism (involving, it is true, certain assumptions) seems more plausible experimentally (and *a priori*). It appears worth while, therefore to publish our results at this time.

EXPERIMENTAL

Radioactivity Procedure

The radiocarbon, C^{14}, used in these experiments was part of the early material obtained by Ruben and Kamen[2] through irradiation of ammonium nitrate solutions with neutrons from the Berkeley 60-inch cyclotron. The reference cited gives the method of extracting the carbon from the solutions,[3] yielding radioactive calcium carbonate.

Since the available specific activity was quite low, it was necessary to employ as sensitive a counting technique as possible. All samples were counted as carbon dioxide gas introduced, in pure form, directly into a counter.[4] We used an iron-wall counter, diameter 1.8 cm, volume 25 ml, and wire diameter 0.23 mm. Carbon dioxide being a poor counting gas, the length of the plateau was only about 45 v. Argon and alcohol in the same counter gave a 200-v plateau, with about the same slope. Carbon dioxide pressures of 3 to 6 cm were used; beyond that the threshold exceeded the 2000-v limitation of our circuit. Corrections were necessary for the variation of counter sensitivity with pressure, which amounted to about 13 percent over the indicated range. Background counts were made by replacement of the sample with inactive carbon dioxide. In most cases these transfers were accomplished by use of liquid air. The fact that condensations were always rapid and complete is taken as evidence for the absence of permanent gases (e.g., air) in the samples.

The low activities used (~200 counts/min./ml CO_2, S.T.P., *versus* background ~24 counts/min.), together with the poor characteristics of carbon dioxide as a counter gas, yielded rather low accuracy in the resulting data, as is apparent from activity "balances" which compared total activities put in and recovered from a

* Taken in part from the thesis of T. H. Norris, submitted in partial fulfillment of the requirements for the Ph.D. degree, at the University of California, Berkeley, California (May, 1942).

† Present address: Chemistry Department, Oregon State College, Corvallis, Oregon.

‡ Deceased 1943.

[1] J. D. Brandner and H. C. Urey, J. Chem. Phys. **13**, 351 (1945).

[2] S. Ruben and M. D. Kamen, Phys. Rev. **59**, 349 (1941).

[3] This operation has since been extensively discussed. See, for example: Yankwich, Rollefson, and Norris, J. Chem. Phys. **14**, 131 (1946); L. D. Norris and A. H. Snell, Science **105**, 265 (1947).

[4] Carbon dioxide is now commonly recognized as a poor counter gas, and in pure form usually cannot be made to operate at all. Possibly the "slowness" of our resistance-quenched counter circuit contributed to the stability of our carbon dioxide-filled counter. W. W. Miller [Science **105**, 123 (1947)] has discussed the use of this gas in counters and reports that admixture of 2 cm of carbon disulfide vapor with the carbon dioxide (10 to 50 cm pressure, giving counting thresholds of 1800 to 4500 v) yields a satisfactory counting mixture.

TABLE I. Exchange between CO and CO_2.

Run	Time (min.)	Pressures (mm at 0°C) CO	CO_2	Sp. activities counts/min./ml, S.T.P. CO	CO_2	CO_2 (t_0)	$R^c \times 10^2$ mm/min.	av.	$k^f \times 10^4$
			Experiment at 350 to 460°C						
25	1600	27.0	32.2	<2	247			Very small	
			Experiments at 799±1°C						
27	1220	61.2	72.8	50	180	227	1.8	1.9	0.25
28	1236	59.4	71.8	55	176	218	1.9		
36*P*[a]	1214	59.1	73.9	51	155	208	2.2	2.4	0.31
37*P*	1260	63.6	75.3	51	140	186	2.5		
			Experiments at 850±1°C						
10	196	16.4	16.9	32	208		1.6		
11	356	16.4	16.9	34	220		0.88		
12	96	16.5	16.8	12	242		1.1		
13	771	16.8	16.5	58	173		0.92	1.1	1.3[g]
20	196	16.1	16.4	19	230	262	0.82		
23	375	16.5	16.6	39	186	250	1.1		
30	560	17.2	16.7		163	213	1.1[d]		
14	84	17.0	46.4	32	255		3.2		
15	887	16.5	45.4	124	217		1.7	2.5	1.2[g]
16	333	16.6	46.3	44	125		2.5		
17	189	53.8	16.8	8	211	266	2.6[d]		
18	587	53.5	16.7	30	149	264	2.2[d]	2.3	1.1[g]
19	533	53.3	16.8	15	163	264	2.0[d]		
21	153	17.2	202	119	239	266	9.2	9.2	1.3[g]
22	300	142	17.1	14	118	263	5.9[d]	5.9	1.4[g]
29	98	86.7	86.5	27	190	213	13[d]	13	1.1[g]
24[b]	469	16.6 +156 mm N_2	16.6	71	148	244	2.2	2.2	2.6
34*P*	238	23.2	24.0	40	160	210	3.2	2.8	1.9
35*P*	243	23.2	23.3	33	175	210	2.4		
			Experiments at 900±1°C						
31	127	17.4	17.0	43	169	206	4.3	4.8	5.6
32	138	17.3	15.9	51	155	206	5.2		
33	138	17.4 +92.5 mm N_2	17.2	68	131	206	8.9	8.9	9.9
39*P*	159	18.1	18.2	63	86	186	8.4[e]		
40*P*	108	17.7	17.2	38	129	176	6.5	5.1	5.5[h]
45*P*	109	17.1	17.7	24	150	158	3.3		
46*P*	117	17.5	17.3	17	161	173	2.1		
41*P*	29	62.0	59.3	17	171	176	28	28	4.3[h]
42*P*	31	17.4 +121 mm A	17.2	9	163	176	4.0	4.1	4.6[h]
43*P*	108	17.4 +117 mm A	17.2	26	131	173	4.2		

[a] Results in packed vessel indicated by *P* surface/volume ratio increased by a factor of six.
[b] Temperature 840 to 850°C.
[c] Rates corrected for reaction vessel dead space.
[d] Calculated from observed decrease in carbon dioxide specific activity.
[e] Calculated from specific activities of carbon monoxide and of initial carbon dioxide.
[f] $k = \text{Rate}/(p\text{CO})^{0.73}(p\text{CO}_2)^{0.85}$.
[g] Weighted average at 850° (excluding N_2 and packed runs): $k = 1.2 \times 10^{-4}$.
[h] Weighted average at 900° (packed): $k = 5.1 \times 10^{-4}$.

given run. Herein, perhaps, lies the most important source of error in this work.

Preparation of Reactants

Radioactive carbon dioxide, used for all the experiments, was obtained by treatment of the labeled calcium carbonate, after drying, with phosphoric acid in vacuum. The evolved gas was dried by passage through phosphorus pentoxide and condensed with liquid air in a small storage bulb. The condensate was subjected for some time to high vacuum pumping to remove any traces of permanent gas. It was then allowed to warm to room temperature (giving in this bulb about 1 atmos. pressure), again condensed and pumped to a high vacuum. The repetition of this procedure several times, both initially and periodically thereafter throughout the experimentation, insured the absence of permanent gas. Phosphorus pentoxide in the storage bulb insured the absence of moisture.

Inactive carbon dioxide, used for background counts, was taken from a commercial cylinder and purified and stored in a similar manner.

Carbon monoxide was prepared by the action in vacuum of concentrated sulfuric acid on formic acid, dried by passage through a liquid air trap, and stored over phosphorus pentoxide. The fact that this gas was oxidized by passage over hot copper oxide to a product completely and rapidly condensible in liquid air is taken as evidence for the absence of any permanent gas impurities.

Nitrogen and argon were taken from cylinders. The nitrogen was purified of oxygen by passage over hot copper turnings. Both gases were dried by passage through phosphorus pentoxide.

Run Procedure

Preliminary experiments at room temperature and at ~500°C for periods up to 1 hr. had shown no measurable exchange. Below 800° the rate was too low for convenient measurement. Like those of Brandner and Urey, therefore, these experiments were conducted in quartz. A 60-ml cylindrical quartz vessel was used in all runs. In testing for heterogeneity, the vessel was packed full of short sections of quartz tubing, whereby the surface-to-volume ratio was increased sixfold. The reaction vessel was connected to a glass high vacuum system through a graded seal, and closed by a stopcock. The 2-ml dead space between the reaction vessel and the stopcock is corrected for in the results given in Table I, assuming mixing rapid compared to the reaction rate. The alternative procedure of assuming no mixing does not make a large difference in the absolute values of the corrected figures, and makes even less in their relative values. The volume of the system was minimized by using 2-mm capillary tubing throughout and by measuring pressures with a "click" gauge. Pressures recorded in Table I have all been reduced to 0°C. The gases were handled with a Töpler pump. The furnace and temperature regulation have been described elsewhere.[5]

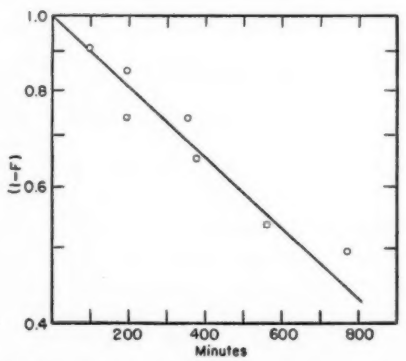

FIG. 1. Semilogarithmic plot of (one minus fraction exchange) *versus* time at 850°C. $p\text{CO} \approx p\text{CO}_2 \approx 17$ mm.

[5] M. L. Perlman and G. K. Rollefson, J. Chem. Phys. 9, 362 (1941). We are much indebted to Professor Rollefson and Dr. Perlman for the use of this apparatus.

In the majority of the experiments, the gases were premixed and introduced simultaneously into the hot quartz bulb, previously exhausted to $\sim 10^{-5}$ mm. After the desired time the gases were pumped out and circulated through a spiral immersed in liquid air, which completely removed carbon dioxide. The carbon monoxide was oxidized by several flushings over hot copper oxide. The two reactants, both now as carbon dioxide, were counted as already described.

Activities are recorded in Table I as counts/min./ml of gas measured at standard conditions. As usually filled, the counter contained a pressure of about 40 mm, which corresponds to 1.19 ml of gas at S.T.P. Hence the activities actually measured do not differ greatly from the figures in Table I.

For the sake of conservation, it was necessary to recover the more active carbon dioxide samples and restore them to the supply of labeled gas. This explains the progressive diminution of the specific activity of the stock from run to run, apparent in Table I.

Runs at a given temperature were mostly consecutive and without intervening temperature change of the reaction vessel. This may have made for greater reproducibility of results than the procedure of Brandner and Urey which involved variation of the reaction vessel temperature between runs. No special conditioning procedure was followed with our reaction vessel.

RESULTS

The experimental results are summarized in Table I, where the run numbers indicate the chronological order of the experiments. We have given the observed specific activities of the two reactant gases at the termination of the runs, as well as, in most cases, the initial specific activity of the carbon dioxide. Comparison of total activity based on the first two figures with that based on the third serves as a check on the experimental procedure. The agreement is found to be within about ten percent in every case but two (runs 19 and 39).

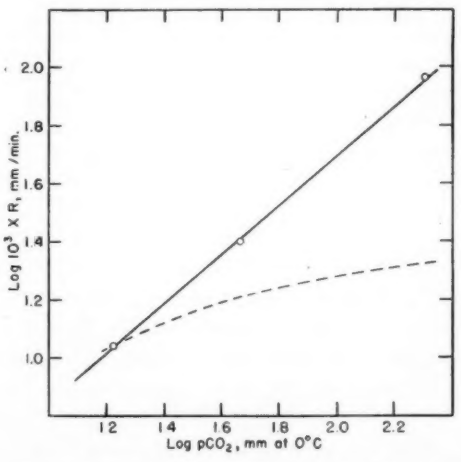

FIG. 2. Dependence of exchange rate on carbon dioxide pressure. pCO≈17 mm. Slope=0.85. Broken line calculated for Brandner and Urey, Mechanism VII.

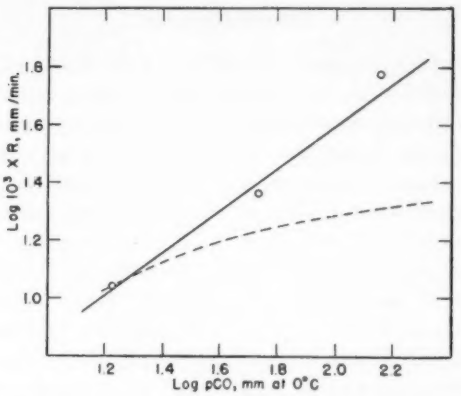

FIG. 3. Dependence of exchange rate on carbon monoxide pressure. $p\mathrm{CO_2}\approx 17$ mm. Slope=0.73. Broken line calculated for Brandner and Urey, Mechanism VII.

Carbon monoxide being initially inactive, the rate calculations have in most cases (except when there is a large excess carbon monoxide concentration) been based on the observed growth in its activity. We have calculated F, the fractional attainment of equilibrium, from expressions readily derived from the equation $F=x/x_\infty$ and the assumption $x_\infty=y_\infty$.[6,7] From F we have calculated R, the exchange rate, by means of the first-order rate law expression.[8,9]

$$R=-\frac{2.3p\mathrm{CO}\cdot p\mathrm{CO_2}}{(p\mathrm{CO}+p\mathrm{CO_2})t}\log(1-F). \qquad (1)$$

The gas pressures are those given in Table I, i.e., pressures corrected from run temperatures to 0°C. The R values recorded in Table I have, as mentioned in the experimental section, been corrected for dead space in the reaction vessel capillary. Duplicate runs, made under similar conditions, are bracketed and average R values tabulated.

An idea of the reliability and general precision of the data may be obtained from the seven runs of varying lengths made at 850° with the pressures of both reactant gases approximately 17 mm. These data have been used in Fig. 1 to show a plot of $\log(1-F)$ *versus* time. The lack of systematic deviation from the expected straight-line relationship in this plot serves as a check on the experimental procedure and the applicability of Eq. (1). Alternatively, a comparison of the Table I R values for these runs serves the same purpose.

---

[6] The symbols x and y designate respective specific activities of carbon monoxide and carbon dioxide. We assume no isotope effect with C^{14}, a procedure which seems justified in the present instance despite recent controversial reports (see reference 7) of very significant effects.

[7] See, for example: P. E. Yankwich and M. Calvin, J. Chem. Phys. **17**, 109 (1949); J. W. Weigl and M. Calvin, J. Chem. Phys. **17**, 210 (1949); J. Bigeleisen *et al.* Science **110**, 14, 149 (1949); J. Chem. Phys. **17**, 344, 425, 998 (1949); K. S. Pitzer, J. Chem. Phys. **17**, 1341 (1949).

[8] H. A. C. McKay, Nature **142**, 997 (1938).

[9] R. B. Duffield and M. Calvin, J. Am. Chem. Soc. **68**, 557 (1946).

The Rate Law

In the experiments at 850°C (unpacked vessel), the gas pressures were systematically varied so as to ascertain the effect on the rate of each reactant concentration in turn. Figure 2 gives a log-log plot of rate *versus* carbon dioxide pressure, at constant carbon monoxide pressure. The points are seen to fall almost on a straight line, the slope of which is 0.85. A similar log-log plot in Fig. 3 of rate *versus* carbon monoxide pressure, carbon dioxide remaining constant gives, with a poorer approximation to a straight line, a slope of 0.73. The poor fit of the points in Fig. 3 may be due to experimental error, estimated to be greater in the runs here involved than those above; this despite the apparently good internal consistency of runs 17 to 19 in Table I. As a tentative rate law we thus obtain

$$R=k(p\mathrm{CO})^{0.73}(p\mathrm{CO_2})^{0.85}. \qquad (2)$$

This equation has been used to calculate the values of k given in the last column of Table I. It is seen that the agreement among all the runs at 850° is fairly good, except for run 24, in which nitrogen was added. A weighted average, excluding run 24, yields $k=1.2\times10^{-4}$.

We have also plotted in Figs. 2 and 3, as broken lines, the expected rate-pressure dependence calculated on the basis of Brandner and Urey's rate law and mechanism; these call for a proportionality between R and the factor $[p\mathrm{CO}\cdot p\mathrm{CO_2}/(p\mathrm{CO}+p\mathrm{CO_2})]$. The plots are arranged to run through the lowest pressure point in each case. The disagreement with our data is striking, and seems clearly to invalidate Brandner and Urey's conclusion.

The Effect of Nitrogen and Argon. An Alternative Rate Law

Run 24, when compared to the seven first-listed 850° runs, indicates a pronounced acceleration by added nitrogen. Run 33, at 900°, shows the same effect. Argon, on the other hand (runs 42 and 43), appears to be without effect. Since a total pressure term (not to include argon) was thus suggested, we made log-log plots of rate *versus* total pressure for the corresponding nitrogen and non-nitrogen experiments at 850 and 900°. Exponents of 0.42 and 0.46, respectively, were obtained. Assuming a true value of 0.50, we then plotted the 850° data as $\log[R/(p\text{ total})^{0.50}]$ *versus* the respective logarithms of carbon monoxide and carbon dioxide pressures. The fair approximations to straight lines thus obtained yielded exponents of 0.40 and 0.49, respectively. A rate law hereby suggested appears to be

$$R=k(p\text{ total})^{0.5}(p\mathrm{CO})^{0.5}(p\mathrm{CO_2})^{0.5}. \qquad (3)$$

Although the k values calculated for Eq. (3) show about the same spread as those for Eq. (2), further graphical analysis of the data appears to give clear indication of the preferability of Eq. (2). Since, in addition, exclusion of argon from the total pressure requires rather special assumptions, we have not considered Eq. (3) further.

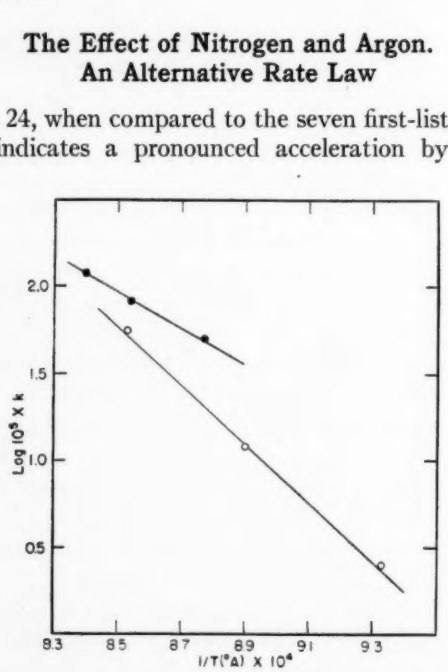

FIG. 4. Temperature dependence of rate constant. Open circles: our data; full circles: constants calculated from data of Brandner and Urey.

The Activation Energy

The average k values (unpacked, non-nitrogen) have been plotted in Fig. 4 as the logarithm of k *versus* $1/T$. The fact that the points give a reasonable approximation to a straight line implies that there is but one exchange mechanism operating over the temperature range involved. This might exclude, for instance, a reaction partly heterogeneous and partly homogeneous. The slope of this plot indicates an apparent activation energy of 77 kcal./mole, corresponding to an average temperature coefficient of the rate from 850 to 900° of 1.36 per 10°. Incidently, the same activation energy is obtained from a plot of log$R$ (in place of log$k$) *versus* $1/T$, using comparable runs at 850° (first seven) and 900° (first two).

Effect of Packing

In order to test for heterogeneity, the reaction vessel was packed with short sections of quartz tubing, thus increasing the surface-to-volume ratio sixfold. Experiments (indicated by P in Table I) were performed in the packed vessel at all three temperatures. The $k(\times10^4)$ values so obtained indicate no striking effect: +24 percent at 799°; +58 percent at 850°; and −10 percent at 900°. While there appears to be some enhancement of the rate, there is here, clearly, no evidence for a primarily heterogeneous reaction. This result, which we consider suspect, will be discussed below in connection with the work of Brandner and Urey.

DISCUSSION

The Results of Brandner and Urey

Brandner and Urey did not arrive at the same rate law as have we. In order to facilitate comparison with

our results we have calculated from their data values of rates, R,[10] and rate constants, k, based on our rate expression, Eq. (2). While the irreproducibility is such as to make for difficulty of interpretation, a detailed examination indicates no real disagreement with our rate law. We feel, in fact, that these data agree better with it than with Brandner and Urey's own rate law. This result is in marked contrast to that obtained when we tried to fit our data to this latter rate law (cf. Figs. 2 and 3).

The average Eq. (2) k values obtained for the runs with no packing are: at ~867°C, 5.0×10^{-4}; at ~898°C, 8.3×10^{-4}; and at ~917°C, 12×10^{-4}. These figures are plotted as solid circles in Fig. 4. The quantitative agreement with our results seems as good as could be expected. Incidently, this plot indicates an apparent activation energy rather lower than the estimate of 100 kcal./mole given by Brandner and Urey, and, in fact, lower than our own value of 77 kcal./mole.

Turning now to the question of heterogeneity, Brandner and Urey's conclusion of catalysis by quartz (and also silver and gold) packing seems well-founded, even though the observed effects, when calculated as average k values, are not large. This presumably is due to a smaller increase in the surface-to-volume ratio in the present instance than in our work. We thus find our observations with the packed vessel unexplained. Our data might indicate a reaction partly homogeneous and partly heterogeneous, although such an hypothesis would seem inconsistent with our straight line in Fig. 4. Alternatively one might suppose that the catalytic activity of our packing was much lower than that of the reaction vessel surface. Since only one packing was used and since this received no special standardizing treatment, it is conceivable that such might be the case: it is evident that the history of the packing was not necessarily that of the reaction vessel.

Although the data, both ours and Brandner and Urey's could be more conclusive, it seems most reasonable to believe that the reaction is primarily heterogeneous, a fact also suggested, of course, by the form of Eq. (2) as well as by the general irreproducibility of both sets of experimental data.

Brandner and Urey reported a marked acceleration by either hydrogen or water vapor. In terms of our k values, we find that their unpacked runs at ~898° indicate almost the same acceleration by 3 or 14 mm of hydrogen or alternatively 4 mm of water vapor. The average observed k enhancement factor is 5.4. This is evidently a far larger effect than we have observed with much greater added amounts of nitrogen.

[10] Brandner and Urey's rates are the slopes obtained in plots similar to our Fig. 1. Thus, since these rates do not include the pressure term in the differential form of the rate expression [cf. Eq. (1)], they do not have the same meaning as, and are not directly comparable, numerically, to our rate figures.

Conclusions

We have concluded that this exchange reaction is heterogeneous and governed by Eq. (2). The latter, has the form of a product of adsorption isotherms. This suggests that Brandner and Urey's Mechanism II, involving a rate-determining bimolecular exchange reaction between the two reactant species adsorbed on the catalytic surface, is probably the right one. This mechanism was, of course, rejected by Brandner and Urey as inconsistent with their conclusions as to rate-pressure dependence.

We have attempted to fit our data to adsorption isotherm equations derived on the assumption either (1) that the adsorbed gases mutually displace each other or (2) that they are independently adsorbed. The fit is moderately satisfactory in either case, but is not such as to permit of a choice and, further, is inferior to that shown by the empirical Eq. (2).

Since it is possible to think of the present reaction as an oxidation of carbon monoxide by carbon dioxide, it seems interesting that studies[11–14] of the (non-explosive and dry) carbon monoxide-oxygen reaction in quartz yield results showing certain similarities to the present ones. Without intending to treat these data in any detail, we may note that the reaction seems to occur at a temperature rather lower than our exchange; it is heterogeneous; and the rate appears to increase both with carbon monoxide and oxygen pressure. Here too, however, the data tend to be erratic and conflicting, both as to reaction temperature and rate law. This fact serves to emphasize the variability to be anticipated in the catalytic activity of quartz for such reactions as this oxidation and, possibly, our exchange. The comparison may indicate a possible mechanistic similarity between the two reactions. Although not wishing to strain the analogy, we might say that, with carbon dioxide as the "oxidizing agent," the high observed reaction temperature of about 850°C is not surprising.

The oxidation studies[12] indicate that, despite the heterogeneity of the reaction, at temperatures up to 400°C, the adsorption of carbon monoxide on quartz is very small. Other studies[15] indicate only weak adsorption on quartz, at 21°, of carbon dioxide, nitrogen, carbon monoxide, and argon (decreasing in that order, with the last two close together). Although correlation of these data with results at 800 to 900°C requires a considerable extrapolation, it seems safe to conclude that catalysis of our exchange must occur on but a small portion of the quartz surface; this despite the

[11] M. Bodenstein and F. Ohlmer, Zeits. f. phys. Chemie **53**, 166 (1905).

[12] A. F. Benton and T. L. Williams, J. Phys. Chem. **30**, 1487 (1926).

[13] G. Hadman, H. W. Thompson and C. N. Hinshelwood, Proc. Roy. Soc. **A137**, 87 (1932).

[14] Y. Kondo and O. Toyama, Rev. Phys. Chem. Japan **13**, 166 (1939).

[15] Hartley, Henry, and Whytlaw-Gray, Trans. Faraday Soc. **35**, 1452 (1939).

form of Eq. (2) which suggests a considerable covering of the surface.

It remains to reconcile with our conclusions the results observed with added nitrogen, hydrogen, or water vapor. Our "alternative rate law," Eq. (3), would explain the nitrogen result, but not the hydrogen or water results and not, without special assumptions, the lack of an argon effect. On the other hand, the mechanism given by Brandner and Urey for the hydrogen and water effect, besides being incompatible with the experimental observations, leaves the nitrogen effect unexplained.

One possibility is that the reaction mechanism is fundamentally different in the presence and in the absence of these accelerating additives. Such a situation has been reported[13] for the "dry" *versus* the "wet" carbon monoxide oxidation. Whether the presence of traces of any of these substances is necessary to the reaction, as Brandner and Urey thought to be the case for hydrogen or water, appears, however, to be an unanswerable question without further data.

Probably the best we can do is to assume that nitrogen, hydrogen, or water adsorbs on the catalytic surface and serves to increase its catalytic activity, functioning somewhat as a promotor. Argon, having little tendency to adsorb and being chemically inert, would then show no effect; hydrogen or water, strongly adsorbed[16] as indicated by Brandner and Urey, would show the pronounced effect they do. The smaller nitrogen effect could then be ascribed either to a feebler adsorption tendency or to a lower "reactivity" of the adsorbed nitrogen.

[16] H. N. Alyea, J. Am. Chem. Soc. **53**, 1324 (1931).

THE JOURNAL OF CHEMICAL PHYSICS VOLUME 18, NUMBER 12 DECEMBER, 1950

Intramolecular Reaction in Polycondensations. I. The Theory of Linear Systems*†‡

HOMER JACOBSON§
Department of Chemistry, Columbia University, New York

AND

WALTER H. STOCKMAYER
Department of Chemistry, Massachusetts Institute of Technology, Cambridge, Massachusetts

(Received August 3, 1950)

For three types of linear polycondensing systems, equilibrium molecular size distributions, including rings as allowable species, are derived. Average molecular weights and amounts of ring and chain fractions are calculated therefrom. The fractions of rings are shown to increase with dilution, and with molecular weight. It is shown that beyond a critical dilution it is sometimes possible to obtain 100 percent yield of rings by driving the condensation to completion. Detailed calculations are made for two important cases corresponding to condensations of the decamethylene glycol-adipic acid type: (1) for equimolar amounts of the two monomers, and (2) unequal amounts, with one monomer type completely reacted.

INTRODUCTION

PRESENT theories of the distribution of molecular species in condensation polymers[1] are severely limited by failure to account for cyclic structures formed by intramolecular reactions. A major difficulty lies in the complicated dependence of ring stability on ring size, which, in spite of considerable investigation,[2–6] has not been formulated quantitatively in general.

As a first step toward the solution of this problem, the theory of linear polycondensations at equilibrium is considered here. Useful results can be obtained when all possible ring molecules are long enough (15 skeletal atoms and up) so that short-range steric effects are not dominant. In this case, the probability of ring closure can be expressed as a well-defined function of ring size, with the aid of well-known configuration theory[7] for randomly coiled chains.

If rings are assumed to be completely absent, as in the previous theories,[1] the distribution of molecular species can be predicted from the number of unreacted end groups, or its equivalent. In the amended theory, the concentration of the polymerizing mass and the stiffness of the chains (expressed conveniently as the

* From a dissertation by Homer Jacobson submitted to the Graduate Faculty of Pure Science of Columbia University in partial fulfillment of the requirements for the degree of Doctor of Philosophy, (1948).

† Published with the assistance of the Ernest Kempton Adams Fund of Columbia University.

‡ Presented in part before the Division of Physical and Inorganic Chemistry of the American Chemical Society in Chicago, September, 1946.

§ Present address: Department of Chemistry, Brooklyn College, Brooklyn, New York.

[1] P. J. Flory, Chem. Rev. **39**, 137 (1946).

[2] H. Gilman, *Organic Chemistry*, 2nd edition (John Wiley and Sons, Inc., New York, 1943), Vol. I., p. 65.

[3] W. H. Carothers, *Collected Papers* (Interscience Publishers, Inc., New York, 1943), Vol. I, pp. 3–270.

[4] M. M. Davies, Trans. Faraday Soc. **34**, 410 (1938).

[5] M. Stoll and A. Rouve, Helv. Chim. Acta **17**, 1283 (1934); **18**, 1087 (1935); **19**, 253 (1936).

[6] G. Salomon, Trans. Faraday Soc. **32**, 153 (1936).

[7] For bibliography, see W. J. Taylor, J. Chem. Phys. **16**, 257 (1948).

effective length of a link) must also be specified. The latter might, in certain cases, be inferred from measurements of the angular dissymmetry of light-scattering,[8–11] or of intrinsic viscosity,[11–13] on related chain polymers of very high molecular weight, but for most condensation polymers it will not be readily known. However, as shown in a succeeding paper,[14] viscosity measurements on linear condensation polymers permit an estimate of the chain stiffness, thus offering a valuable supplementary method for studying the configurations of chain molecules.

Qualitatively, as would be expected, the yield of rings in a polymer system is predicted to increase on dilution. A less trivial and more interesting feature of the theory rests in the mathematical coincidence of the ring distribution equations with those expressing the thermodynamic properties of the perfect Bose-Einstein gas.[15] Thus, a critical phenomenon arises which is formally analagous to the well-known Bose-Einstein condensation; there is a critical concentration, below which the condensing system can be converted entirely into rings, but above which this is not possible.[16]

In the following sections, the theory is given for three stoichiometric types of polycondensing system. Each is named for an obvious prototype. Distribution functions and important average quantities are expressed as a function of observable parameters in each case.

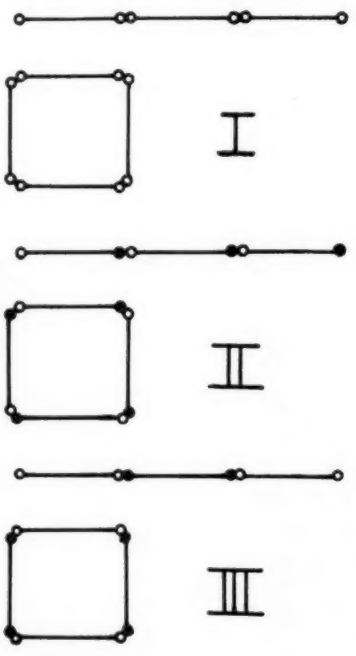

FIG. 1. Stoichiometric types of linear condensation polymers: I, "dimethylsilanediol" case; II, "ω-hydroxyundecanoic acid" case; III, "adipic acid-decamethylene glycol" case.

TYPES OF POLYCONDENSATIONS

Figure 1 symbolically shows the geometrical types of linear polycondensing system considered.

In Case I, the dimethylsilanediol case, all monomers are identical units, bearing two identical functional groups (typically OH), capable of condensing with each other. The functional groups are represented by circles, and the typical ring and chain structures are evident. Case II, the ω-hydroxyundecanoic acid case, consists of a system of identical monomers, each bearing two different functional groups (e.g. OH and COOH), each capable of reacting with the other only. The black and white terminal circles represent the two types of functional groups. Case III, the adipic acid-decamethylene glycol case, is a system composed of two different types of monomers, each of which bears two functional groups of the same kind. The arrangement is clear from Fig. 1. Most generally Case III has no restriction on the relative number of the two monomer types present in the system.

SIZE DISTRIBUTIONS AND EXPERIMENTAL OBSERVABLES

We shall first derive molecular size distributions for the condensing polymer molecules, in which rings are allowed to form. The following assumptions are made:

1. The reactivity of a functional group is independent of the size of the molecule to which it is attached. Since demonstration of its validity for polyester condensations by Flory,[17] this has been generally assumed valid. It is tantamount to postulating thermodynamic equivalence of all condensation bonds in the system.

2. The elementary steps in polycondensation are considered completely reversible. The important cases of esterification and silanol condensation[18,19] have been shown to be reversible. Attempts to derive the molecular size distribution on the basis of partial or total irreversibility of the condensation reaction introduce much cumbersome mathematics with little gain in usefulness for available polymers.

Case I. The Dimethylsilanediol Case

Let a Case I system contain N monomers combined into M molecules, of which I are rings. It will have a molecular size distribution characterized by the sets C_n and R_n, the number of n-mer chains and rings, respectively. These sets of numbers must conform to the total number of monomers, molecules, and rings, as

[8] Debye, J. Phys. and Colloid Chem. **51**, 18 (1947).
[9] Doty, Affens, and Zimm, Trans. Faraday Soc. **42B**, 66 (1946).
[10] B. H. Zimm, J. Chem. Phys. **16**, 1099 (1948).
[11] A. M. Bueche, J. Am. Chem. Soc. **71**, 1452 (1949).
[12] P. Debye and A. M. Bueche, J. Chem. Phys. **16**, 573 (1948).
[13] J. G. Kirkwood and J. Riseman, J. Chem. Phys. **16**, 565 (1948).
[14] Jacobson, Beckmann, and Stockmayer, J. Chem. Phys. **19**, 1607 (1950), hereinafter called II.
[15] See, for example, J. E. Mayer and M. G. Mayer, *Statistical Mechanics* (John Wiley and Sons, Inc., New York, 1940), Chapter 16.
[16] A trivial case, the condensation of the entire system into a single giant ring, is possible at all concentrations.
[17] P. J. Flory, J. Am. Chem. Soc. **61**, 3334 (1939).
[18] P. J. Flory, J. Am. Chem. Soc. **62**, 2255 (1940).
[19] W. Patnode and D. F. Wilcock, J. Am. Chem. Soc. **68**, 361 (1946).

TABLE I. Values of ring functions $\varphi(x, s)=\sum_{n=1}^{\infty} x^n n^{-s}$.

x	$\varphi(x, 5/2)$	$\varphi(x, 3/2)$	$\varphi(x, 1/2)$
0.1	0.102	0.104	0.108
0.2	0.208	0.216	0.234
0.3	0.318	0.338	0.385
0.4	0.434	0.473	0.570
0.5	0.555	0.625	0.806
0.6	0.684	0.798	1.122
0.7	0.822	1.003	1.580
0.75	0.895	1.122	1.903
0.8	0.972	1.258	2.338
0.85	1.053	1.418	2.970
0.9	1.139	1.614	4.022
0.95	1.232	1.884	6.377
0.97	1.274	2.038	8.702
0.99	1.317	2.272	16.22
0.995	1.329	2.366	23.30
0.997	1.334	2.422	30.88
0.999	1.339	2.501	54.58
1	1.341	2.612	∞

follows:

$$\begin{aligned}\textstyle\sum_n(C_n+R_n)&=M\\ \textstyle\sum_n n(C_n+R_n)&=N\\ \textstyle\sum_n R_n&=I.\end{aligned}\qquad(1)$$

It is clear that in complete equilibrium between ring and chain species, any subset of molecules such as the chain fraction will be in an equilibrium distribution within itself. It is consequently proper to use a molecular size distribution for the chain fraction of the same form as the distribution in the ring-free case,[1] namely:

$$C_n=Ax^n,\qquad(2)$$

where A and x are parameters to be determined from conditions (1). x is the fraction of reacted end-groups in the chain fraction, and A a normalization constant. (2) has been also rigorously derived for a ring-containing system from mass-action considerations.

In the Appendix, we have derived expressions for R_n in terms of the nature of the system:

$$R_n=BVx^n n^{-5/2}\qquad(3)$$

$$B=[3/(2\pi\nu)]^{3/2}/2b^3.\qquad(4)$$

Here V is the volume of the system, ν is the number of chain atoms per monomer unit, and b is the effective link length of the polymer chain. (3) and (4) are valid for polymer chains of many effective links. The length b can be identified with the actual bond distances in a chain (times $(1+\cos\alpha)/(1-\cos\alpha)$ where α is the bond angle), for a simplified model with completely free rotation, and no steric hindrance. These assumptions lead to prediction of more ring structures than are actually observed. Refinements of the proper value of b will be treated in the discussion of II.

The value of R_n from Eq. (3), when inserted into summations (1), presents the functions

$$\sum_{n=1}^{\infty} x^n n^{-5/2} \quad \text{and} \quad \sum_{n=1}^{\infty} x^n n^{-3/2}$$

for evaluation. After Truesdell,[20] who studied these functions and worked out practical methods for their evaluation, they are termed $\varphi(x, s)$, where s is the negative exponent of the summation index n. Table I lists values for $\varphi(x, 5/2)$ and $\varphi(x, 3/2)$ mentioned above, as well as $\varphi(x, 1/2)$, whose utility will be seen later.

Inserting (2) and (3) into (1), we obtain:

$$Ax/(1-x)+BV\varphi(x, 5/2)=M\qquad(5a)$$

$$Ax/(1-x)^2+BV\varphi(x, 3/2)=N\qquad(5b)$$

$$BV\varphi(x, 3/2)=N'\qquad(5c)$$

$$BV\varphi(x, 5/2)=I.\qquad(5d)$$

For convenience, we have defined N' by (5c). It corresponds to the total number of monomers *in the ring fraction only*.

Equations (2), (3), and (5) may be put into useful form by solving them for observable quantities. We define the following, in terms of N, N', M, and I (or R_n and C_n).

D_c = the number average degree of polymerization of the chain fraction
$=(N-N')/(M-I)$.

D_r = the number average degree of polymerization of the ring fraction
$=N'/I$.

ρ_w = the weight fraction of rings in the system
$=N'/N$.

p = the fraction of reacted functional groups in the system
$=(N-M+I)/N$.

D_{cw} = the weight average degree of polymerization of the chain fraction
$=(\sum n^2C_n)/(\sum nC_n)$.

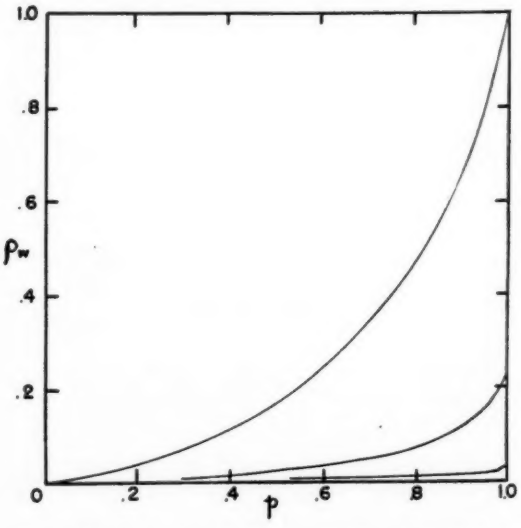

FIG. 2. Weight fraction of rings, ρ_w, as a function of the extent of reaction, p, for a Case IIIa polymer at three dilutions. Upper curve, $B'/c=0.5$; middle curve, $B'/c=0.05$; lower curve, $B'/c=0.005$.

[20] C. A. Truesdell, Ann. Math. **46**, 144 (1945).

D_{rw} = the weight average degree of polymerization of the ring fraction
$= (\sum n^2 R_n)/(\sum n R_n)$.
D_w = the weight average degree of polymerization of the system
$= \rho_w D_{rw} + (1-\rho_w) D_{cw}$.

Two more definitions are useful. They are:

$$c \equiv N/(N_0 V), \tag{6}$$

N_0 being Avogadro's number. c is clearly the concentration of monomer *units* in moles per unit volume, the so-called "ground-molar" concentration. And,

$$B' \equiv B/N_0. \tag{7}$$

From (5c), (6), and (7),

$$(B'/c)\varphi(x, 3/2) = N'/N \tag{8}$$

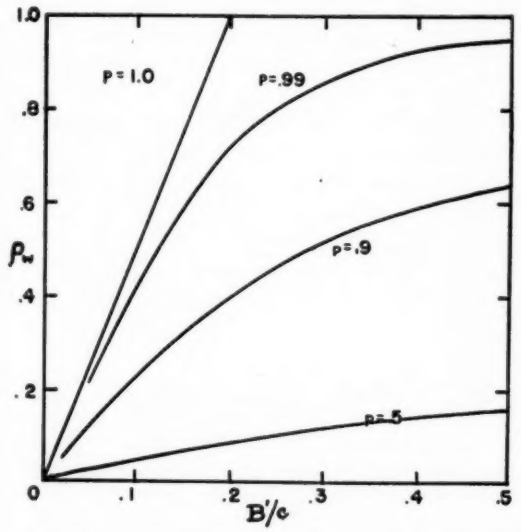

FIG. 3. Weight fraction of rings, ρ_w, as a function of dilution, B'/c, for a Case IIIa polymer at various extents of reaction, p.

a necessary relationship for solving for the quantities defined above, in terms of ordinary concentration units. Solving for them with the aid of Eqs. (2), (3), and (8), we derive:

$$\begin{aligned} D_c &= 1/(1-x) \\ D_r &= \varphi(x, 3/2)/\varphi(x, 5/2) \\ \rho_w &= (B'/c)\varphi(x, 3/2) \\ p &= x + (1-x)(B'/c)\varphi(x, 3/2) \\ D_{cw} &= (1+x)/(1-x) \\ D_{rw} &= \varphi(x, 1/2)/\varphi(x, 3/2). \end{aligned} \tag{9}$$

For any practical set of calculations, values for x must be assumed, within an appropriate range, and the remaining quantities calculated therefrom. A graphical elimination of x is then possible, as any of the other variables, say p, can be chosen as the independent one. Numerical calculations will not be made for this case.

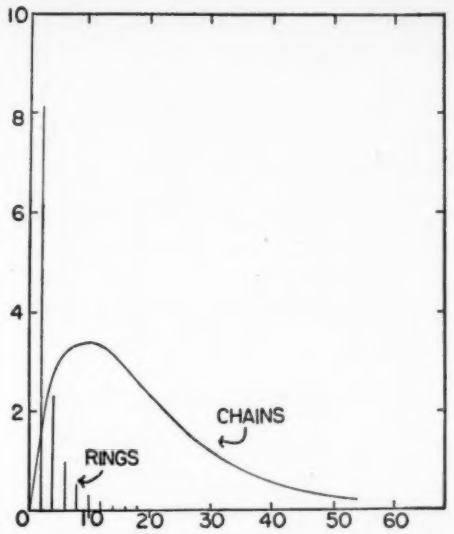

FIG. 4. Typical molecular distribution for a Case IIIa polymer. Weight percent is plotted against degree of polymerization, for $B'/c = 0.05$ and $x = 0.900$.

Case II. The ω-Hydroxyundecanoic Acid Case

For Case II, the considerations of the Appendix yield a set of equations identical with Eqs. (1) to (8), with the one difference that the constant B' (or B) has twice the numerical value given by Eq. (5b). B' is calculated from Eqs. (7) and (4) to equal 1.25 ground-moles/liter for ω-hydroxyundecanoic acid with the model of a completely freely coiling flexible chain. This value is evidently considerably too high, and leads to calculation of excessive amounts of ringed structures. Moreover, there are probably very few rings in which $n=1$ (i.e., the 12-membered lactone ring).

Case III. The Adipic Acid-Decamethylene Glycol Case

The equations for Case III analogous to (1)–(5) are reproduced below. We consider a polymer containing N and S monomers of the first and second kind, respectively, of which $N'(=S')$ is the number present in the ring fraction, and which contains M molecules of all species, of which I are rings. Characterizing the molecular size distributions by C_{ns} and R_{nn}, the numbers of n, s-mer chains and n, n-mer rings (the two indices referring to number of monomers of the first and second kinds, respectively), we have:

$$\begin{aligned} \sum_{n,s} (C_{ns} + R_{nn}) &= M \\ \sum_n R_{nn} &= I \\ \sum_{n,s} n(C_{ns} + R_{nn}) &= N \\ \sum_{n,s} s(C_{ns} + R_{nn}) &= S \\ \sum_n n R_{nn} &= N' = S'. \end{aligned} \tag{10}$$

The size distribution of the chain fraction, after Flory[1] and others, is of the form:

$$C_{ns}=Ax^n y^s/\sigma_{ns}, \tag{11}$$

where σ_{ns} is the symmetry number for n, s-mers, being one for even molecules ($n=s$), and two for odd ($n=s\pm1$), and A, x, and y are parameters to be determined from (10). As in Case I, A is a normalizing factor, while x and y are the fractions of reacted groups (in the chains) of the first and second kind, respectively. In the Appendix we derive:

$$R_{nn}=BV(xy)^n n^{-5/2} \tag{12}$$

$$B=(3/2\pi\nu)^{3/2}/2b^3. \tag{13}$$

All symbols have the same meaning as in Eqs. (3) and (4), but ν signifies the sum of the number of chain atoms of both kinds of monomer units. Putting Eqs. (11) and (12) into (10), and summing approximately, we have:

$$1/2A(x+2xy+y)/(1-xy)+BV\varphi(xy, 5/2)=M \tag{14a}$$

$$BV\varphi(xy, 5/2)=I \tag{14b}$$

$$1/2Ax(1+y)^2/(1-xy)^2 \quad +BV\varphi(xy, 3/2)=N \tag{14c}$$

$$1/2Ay(1+x)^2/(1-xy)^2 \quad +BV\varphi(xy, 3/2)=S \tag{14d}$$

$$BV\varphi(xy, 3/2)=N'=S'. \tag{14e}$$

Defining $c=(N+S)/N_0V$, as the sum of concentrations of both monomers in moles per unit volume, and B' exactly as in Eq. (7), we obtain, with Eq. (14e):

$$(B'/c)\varphi(x, 3/2)=N'/(N+S). \tag{15}$$

A calculation of the numerical value of B' for decamethylene adipate, assuming no steric hindrance, and free rotation, gives the value 0.33 ground moles/liter.

The expressions for observables obtained for Case III polymer, in the general form so far retained, become quite cumbersome. Great mathematical simplification results, however, for two important cases. Both will be treated. If (a) both monomers are present in equivalent amounts, or (b) one monomer has completely reacted, tractable expressions can be presented.

Case IIIa. The "Equivalent" Polymer

When a Case III polymer system contains equivalent quantities of the two monomers, i.e., $N=S$, we term it an "equivalent" polymer. From Eq. (10), equality of N and S demands that $x=y$. By reducing Eqs. (11), (12), and (14) thus, the observables below can be calculated. They are defined similarly to the Case I system:

$$\begin{aligned}
D_c &= (N+S-N'-S')/(M-I)=1/(1-x)\\
D_r &= (N'+S')/I=2\varphi(x^2, 3/2)/\varphi(x^2, 5/2)\\
\rho_w &= (N'+S')/(N+S)=2(B'/c)\varphi(x^2, 3/2)\\
p &= (N+S-M+I)/(N+S)\\
&= x+2(1-x)(B'/c)\varphi(x^2, 3/2)\\
D_{cw} &= [\textstyle\sum_{n,s}(n+s)^2C_{ns}]/[\sum_{n,s}(n+s)C_{ns}]\\
&= (1+x)/(1-x)\\
D_{rw} &= [\textstyle\sum_n (2n)^2R_{nn}]/[\sum_n (2n)R_{nn}]\\
&= 2\varphi(x^2, 1/2)/\varphi(x^2, 3/2)\\
D_w &= \rho_w D_{rw}+(1-\rho_w)D_{cw}.
\end{aligned} \tag{16}$$

It is possible, as in Case I, to eliminate x, the fraction of reacted groups in the chain fraction. Since it is the single parameter by which all the other observables are expressed, their mutual relations are readily obtained.

Figure 2 shows the relationship between ρ_w, the weight fraction of rings, and p, the over-all fraction of reacted end groups, for three values of B'/c. Figure 3 is a plot of ρ_w against B'/c, with p as parameter. Figure 4 is a typical molecular size distribution graph for a Case IIIa polymer.

Case IIIb. The "Hundred Percent" Case

The second type of Case III polymer treated is that for which the reaction between the two types of groups has proceeded until the type of lesser amount is totally reacted. This is entitled a "hundred percent" polymer. The only free end groups are those from the monomer type present in excess. Consequently, all chain molecules have odd numbers of monomers, including one more of the type in excess than of the other. If S is arbitrarily taken to be greater than N (i.e., the second kind of monomer is in excess) it is clear that $s=n+1$ in all chain molecules. Likewise evident is the equality of $2(S-N)$, the number of free end groups, and $2(M-I)$, the number of free end groups on chains. Substituting these relations into (14), and solving for the experimental observables, we deduce:

$$\begin{aligned}
D_c &= (1+xy)/(1-xy)\\
D_r &= 2\varphi(xy, 3/2)/\varphi(xy, 5/2)\\
\rho_w &= 2(B'/c)\varphi(xy, 3/2)\\
p &= 2xy/(1+xy)+[(1-xy)/(1+xy)]\\
&\quad \times[(2B'/c)\varphi(xy, 3/2)]\\
D_{cw} &= [1+6xy+(xy)^2]/[1-(xy)^2]\\
D_{rw} &= 2\varphi(xy, 1/2)/\varphi(xy, 3/2)\\
D_w &= \rho_w D_{rw}+(1-\rho_w)D_{cw}.
\end{aligned} \tag{17}$$

The quantity p is defined, for Case IIIb, by:

$p \equiv 2r/(1+r)$, where
$r \equiv N/S$, the ratio of monomers. From these definitions,
$p = 2N/(N+S)$, and making the substitution $N = S - M + I$, valid for a Case IIIb polymer, we have:
$p = (N+S-M+I)/(N+S)$, exactly as for Case IIIa.

All of the quantities above are parametrically given in terms of xy, which has the physical meaning of the ratio of first kind to second kind monomers, in the chain fraction alone. No numerical calculations will be made for Case IIIb.

DISCUSSION

Some study and interpretation of the calculations above is profitable. Major points of interest follow.

The amount of rings, as is well known from experimental studies, is an increasing function of the system volume. Equations (3) and (12) give R_n and R_{nn} a proportionality to V, *ceteris paribus*. For small amounts of rings, it is closely accurate to say that their amount is proportional to the volume of the system, but of course ρ_w cannot exceed unity.

The rings formed are small species, their number average degree of polymerization never rising above 4 (for Case III). Their weight average degree of polymerization is generally negligible compared to those of the chain fraction. Osmotic pressure observations would be useless in finding rings, since their sizes compare with solvent molecules. Cryoscopic measurements, on the other hand, should be successful in finding number-average molecular weights. Weight averages could be studied with light scattering, or with viscometric measurements as in II, but should give evidence only of chain structures, the rings being too small to notice except by difference.

Separation into the ring and chain fractions might be possible by any of several techniques. Small chains might be separated from rings by an end-group technique. For example, small chains in poly-ω-hydroxyundecanoic acid could be extracted by aqueous base from a chloroform solution, leaving the non-polar lactones behind. Large chains should be separable from rings by solubility behavior. Average molecular weights could then be studied on the separated fractions.

The quantity ρ_w, shown in Eq. (16) to equal $2(B'/c) \times \varphi(x^2, 3/2)$ for Case IIIa, can equal unity, for sufficiently small values of c, with $p=1$. This means a system of 100 percent rings of finite size is the stable one for a completely reacted polymer in a system of sufficient volume. Figure 3 shows this phenomenon in a striking fashion. For $p=1$, the ring fraction by weight increases linearly with B'/c, i.e. with dilution, until B'/c reaches 0.19, above which the equilibrium situation is 100 percent rings. This critical dilution, beyond which a system composed wholly of rings results, resembles the Bose-Einstein condensation phenomenon. Attention has already been called to the similarity between the φ-functions of our work, and summations appearing in Bose-Einstein statistics.

The preparative chemist interested in making cyclic structures will see that there is no great advantage in excessive dilution as far as total quantity of rings goes. The result of diluting beyond critical is chiefly to decrease the average size of the rings formed at 100 percent reaction. This must ensue from the fact that x drops off at large B'/c when $p=1$, and consequently $x^{2n}n^{-5/2} (= R_{nn}/BV)$ becomes very small for larger n's. For synthesis of very large rings, dilution as close as possible to critical is desirable.

A very heterogeneous over-all distribution of molecular sizes may ensue, especially if the chain and ring curves are peaked at different points. The chain fraction alone is reasonably homogeneous, but at high x, i.e. for large chain size, the ring fraction becomes rather heterogeneous. The typical distribution curve of Fig. 4 shows what may be expected. The chains have the typical humped distribution, but the rings are more numerous at smaller sizes.

Both the weight and number fraction of rings increase monotonically with p, x, r, or xy. Larger extent of reaction, or more even balance of monomers (Case IIIb) increases the yield of rings.

The over-all weight and number average molecular weights are not given accurately for polymers containing cyclic structures by usual measurement methods. It is the mathematical treatment developed above which will allow us to make accurate specification of such polymer systems. In II we shall apply our theory to several actual polymers, with the possibility of refinement of the theory, and better understanding of the experiments.

APPENDIX. DERIVATION OF RING SIZE DISTRIBUTION FROM CONSIDERATION OF RING-CHAIN EQUILIBRIUM

First we must derive the fraction of ring configurations leading to ring closure. Let the distribution of end-to-end distances L ("displacement lengths") for a randomly coiling chain be given by the familiar normalized Gaussian form:

$$W(L)dL = (\beta^3/\pi^{3/2}) \exp(-\beta^2 L^2) 4\pi L^2 dL \qquad \text{(i)}$$

where β is related to the mean square displacement length by the relation:

$$\langle L^2 \rangle_{Av} = 3/2\beta^2. \qquad \text{(ii)}$$

When such a chain is closed to a ring, the terminal chain atoms are constrained to positions at, or nearly at, some small distance s (corresponding to the bond length) from each other. In other words, if one of these atoms is fixed, the other must lie in a small volume v_s at a mean distance s from the fixed atom. As will be seen subsequently, further specification of v_s is unnecessary, as it plays no role in the final results. For sufficiently long

chains (such that $\beta s \ll 1$), the probability P that a chain be in a configuration corresponding to a ring is then:[21]

$$P = \int_{v_s} W(L)dL \simeq (\beta^3/\pi^{3/2})v_s. \qquad \text{(iii)}$$

We desire P for a chain of νn links, composed of n monomer units contributing ν links each. Following others[10,13] we can define an effective link length b by the relation:

$$\langle L^2 \rangle_{Av} = \nu n b^2 \qquad \text{(iv)}$$

and use the ratio of b to the actual link length as a convenient measure of chain stiffness. Substitution of Eqs. (ii) and (iv) into (iii) gives:

$$P = (3/2\pi\nu n)^{3/2}(v_s/b^3) \qquad \text{(v)}$$

as the fraction of chain configurations permitting ring closure.

We now desire to predict ring-chain equilibria in terms of P and other quantities. For this purpose, we consider the equilibrium:

(1) $$C_{n+m} \rightleftharpoons C_m + R_n$$

of the type encountered in Cases I or II, where the symbols C and R, as in the text, denote chains and rings respectively. The mass-action product in terms of numbers of molecules, is:

$$K_1 = C_m R_n / C_{m+n} = R_n / x^n, \qquad \text{(vi)}$$

the last equality following from the substitution of Eq. (2) for the chain size distribution. Since reaction (1) involves no change in the number of bonds, we may assume to a good approximation that it is attended by negligible change of energy, so that the task or predicting K_1 reduces to that of evaluating the entropy change. This is most clearly accomplished by breaking up reaction (1) into the steps:

(2) $$C_{n+m} \rightleftharpoons C_n + C_m$$

(3) $$C_n \rightleftharpoons R_n.$$

In these reactions, by-products (such as water) are omitted, since they do not appear in the over-all reaction.

For reaction (2), consider one of the skeletal atoms forming the bond that breaks. Before breaking, it is confined to a volume v_s situated near the atom to which it is bonded, but after breaking it may be anywhere in the volume V of the system as a whole. For Case I systems, we must also recall that the symmetry number of a chain molecule is 2. The entropy change is then:

$$\Delta S_2 = k \ln(V/2v_s). \qquad \text{(vii)}$$

For reaction (3), the change in configurational entropy is found at once from (b). Since the symmetry number of an n-mer ring is $2n$ for Case I, we obtain:

$$\Delta S_3 = k \ln(P/n). \qquad \text{(viii)}$$

The desired mass-action product is thus:

$$K_1 = \exp(\Delta S_1/k) = (3/2\pi\nu)^{3/2}(V/2b^3)n^{-5/2} \qquad \text{(ix)}$$

and it is seen that the "bond volume" v_s has been eliminated, as could be expected from the consideration that reaction (1) is merely a bond interchange. With the use of Eq. (vi), we may write, for Case I:

$$R_n = BVn^{-5/2}x^n, \qquad \text{(x)}$$

with

$$B = (3/2\pi\nu)^{3/2}/2b^3, \qquad \text{(xi)}$$

corresponding to (3) and (4) of the text.

For Case II systems, the only difference from Case I lies in the symmetry numbers, which are unity for chains and n for n-mer rings. Therefore K_1 (and hence B) is just twice as large as for Case I.

In Case III, a new equilibrium must be considered, since two different kinds of monomer unit are involved:

(4) $$C_{n+m,\,n+s} \rightleftharpoons C_{ms} + R_{nn}.$$

The mass-action product for this reaction is:

$$K_4 = C_{ms}R_{nn}/C_{n+m,\,n+s} = R_{nn}/x^n y^n, \qquad \text{(xii)}$$

the last equality resulting from the use of Eq. (11) for the chain distribution. In the evaluation of K_4, again only the symmetry numbers are different. These are unity for chains with even numbers of monomer units, 2 for chains with odd numbers of monomer units, and $2n$ for rings with n units of each type. The final result is:

$$B_{nn} = BVn^{-5/2}x^n y^n \qquad \text{(xiii)}$$

for the ring distribution, corresponding to Eq. (12). The constant B is given by Eq. (xi), just as for Case I, but with the important difference that ν now represents the *sum* of the number of links in the two kinds of monomer unit, since the ring contains n monomer units of each kind. For example, in the system decamethylene glycol-adipic acid, $\nu = 18$.

We have also succeeded in deriving the above equilibrium relationships by considering the kinetics of the forward and reverse reactions, but here we confine ourselves to several brief remarks. The factor $1/n$ in the entropy formula, Eq. (viii), arose there from considerations of symmetry number; in the kinetic treatment it appears as a consequence of the availability of n equivalent bonds for the reverse (ring-opening) reaction. The kinetic approach has of course one additional advantage, in that estimates of the time required to reach equilibrium may be made if the correct reaction mechanism has been assumed. For example, in experiments with adipic acid-decamethylene glycol polymers reported in II, we were able to distinguish between aqueous degradation and ester interchange leading to ring formation by observations on the rate of the process.

[21] In treating the cure of a rubber molecular network, H. M. James and E. Guth, J. Chem. Phys. 15, 669 (1947), have made use of similar arguments.

THE JOURNAL OF CHEMICAL PHYSICS VOLUME 18, NUMBER 12 DECEMBER, 1950

Intramolecular Reaction in Polycondensations. II. Ring-Chain Equilibrium in Polydecamethylene Adipate*†

HOMER JACOBSON‡ AND CHARLES O. BECKMANN
Department of Chemistry, Columbia University, New York, New York

AND

WALTER H. STOCKMAYER
Department of Chemistry, Massachusetts Institute of Technology, Cambridge, Massachusetts

(Received August 3, 1950)

Decamethylene adipate polymers prepared in the absence of solvent undergo a reversible decrease in solution viscosity when heated for long times in chlorobenzene. This phenomenon is shown to be due to ester interchange reactions which establish equilibrium between ring and chain molecules. Quantitative agreement with the equilibrium theory of the previous paper is obtained if the effective length of a chain link is taken as 4.5±0.2A, which is of the order of magnitude to be expected from hindered rotation and steric effects. Measurements of ring-chain equilibrium thus appear to offer a useful method for characterizing the stiffness of relatively short and flexible chains.

INTRODUCTION

To test the theory developed in the previous paper,[1] we have studied ring-chain equilibrium in decamethylene adipate polyesters by means of solution viscosity measurements. Such polymers, when heated in chlorobenzene solution for extended times, attain equilibrium values of the dilute-solution viscosity, which depend on dilution and on the extent of esterification in the predicted[1] fashion. Numerical treatment of the results then gives a measure of the stiffness of the polymer chains.

In a polyester system, ring molecules can form by two mechanisms. First, an intramolecular esterification between the terminal hydroxyl and carboxyl groups of a linear chain leads directly to a ring of the same polymerization degree, with elimination of a molecule of water. Second, an intramolecular transesterification (ester interchange) of a chain gives a smaller chain and a ring; for example, a tetrameric chain may transesterify into a dimeric chain and a dimeric ring. Since both esterification and transesterification are reversible reactions, ring formation by either of these mechanisms will approach an equilibrium state. High extent of reaction, as well as high dilution, should favor an equilibrium state with larger amounts of ringed structures.[1] For experimental observation of rings, it is necessary that one or the other mechanism be employed, with both extent of reaction and dilution sufficient to give a sensible quantity of rings at equilibrium.

The esterification equilibrium is determined primarily by the vapor pressure of water in the system. Consequently, to establish an equilibrium state with a high extent of reaction, when starting with monomers and solvent, it would be necessary to remove most of the water formed in the esterification reaction. To do so without removing solvent from the system is seen to be experimentally inconvenient. On the other hand, when starting with an already prepared polymer of high extent of reaction, together with sufficient solvent, the water removal problem does not occur. In this case, without removal of water, esterification can proceed to an equilibrium state with a high extent of reaction. Formation of ringed species occurs here primarily by ester interchange, very few of the chains present being small enough to give rings directly by intramolecular esterification. This is the procedure followed in all our experiments.

Chlorobenzene was chosen as the solvent because of its inertness and convenient boiling point, and because solution viscosities of polydecamethylene adipates in this solvent had already been investigated by Flory and Stickney.[2] In our work, previously prepared polymers were dissolved in chlorobenzene at the desired dilution, together with *p*-toluenesulfonic acid in small amounts. As shown by Flory,[3] the latter substance catalyzes both esterification and transesterification. The solutions were heated for various times, then cooled and diluted with more chlorobenzene to polymer concentrations of the order of one percent for the measurement of dilute-solution viscosities at 25°C. The process of heating the solutions until constant dilute-solution viscosities are reached will be called "equilibration."

EXPERIMENTAL METHODS

Materials

Adipic acid was Eastman Kodak Company O. P. grade, recrystallized three times from water, m.p.

* From a dissertation by Homer Jacobson submitted to the Graduate Faculty of Pure Science of Columbia University in partial fulfillment of the requirements for the degree of Doctor of Philosophy (1948).

† Published with the assistance of the Ernest Kempton Adams Fund of Columbia University.

‡ Present address: Department of Chemistry, Brooklyn College, Brooklyn, New York.

[1] H. Jacobson and W. H. Stockmayer, J. Chem. Phys. **18**, 1600 (1950), hereinafter referred to as I.

[2] P. J. Flory and P. B. Stickney, J. Am. Chem. Soc. **62**, 3032 (1940).

[3] P. J. Flory, J. Am. Chem. Soc. **62**, 2255, 2261 (1940).

TABLE I. Equilibration of "hundred percent" polydecamethylene adipate in chlorobenzene at 130°C.

Weight fraction of polymer	Time (hr.)	$[\eta]^c$	ρ_w	D_{cw}	$B'\left(\frac{\text{mole}}{\text{liter}}\right)$
∞ [a]	—	36.0	0	83.0[d]	—
1.000	0	34.7	0.024	81.0	(0.050)
0.202	0.6	32.1			
	1.3	31.1			
	2.5	31.0			
	∞ [a]	30.8	0.097	75.0	0.041
0.131	5	28.5			
	10	27.6			
	20	27.3			
	∞ [a]	27.0	0.172	68.7	0.048
0.091	20	26.1			
	36	24.5			
	50	24.0			
	∞ [a]	23	0.256	61.7	0.050
0.091[b]	4	26.1			
	8	25.5			
	12	25.0			
	∞ [a]	24	0.234	63.6	0.045
0.060	20	22.5			
	40	18.7			
	80	16.9			
	∞ [a]	16	0.42	48	0.058
0.031	80	16			
	160	12			
	320	9			
	∞ [a]	8	0.66	28	0.051
				Average	0.049

[a] Extrapolated.
[b] Equilibration at 170°C.
[c] Inherent viscosities at one percent concentrations in chlorobenzene, 25°C.
[d] From melt viscosity.

152.4–153.1; neutral equivalent 73.2_0, 72.9_8, theoretical 73.07.

Decamethylene glycol (Edwal) was recrystallized three times from reagent benzene. A cooling curve indicated less than 0.05 percent impurities insoluble in the crystal lattice.

P-toluenesulfonic acid catalyst (monohydrate) was used as obtained from Eastman Kodak Company.

Chlorobenzene was carefully dried by distillation at 130–131° from a single batch of c.p. chlorobenzene (Amend Drug Company). It was dispensed from an automatic buret, provided with drying tubes.

Solution Viscosity Measurements

Solution viscosities were taken in a modified Bingham viscometer, a constant pressure head type. Both efflux times and pressure heads were simultaneously measured at 25.00±0.05°. Times of about 200 sec. and kinetic energy and head corrections allowed viscosities to be measured and reproduced to within 0.1 percent.

Polymer Preparation

Preparation of polymer samples was effected in a ground-glass-joint stoppered vessel, surrounded by vapors of boiling toluene. Weighed portions of adipic acid, decamethylene glycol, and catalyst were heated at constant temperature (109°), with passage of bubbles of prepurified nitrogen through the melt to remove water and keep the melt homogeneous. Oxidation was avoided by the use of high grade nitrogen (Air Reduction Products Company), containing less than 0.002 percent of water, oxygen, or hydrogen.

Miscellaneous Techniques

Titrations were performed with 0.02 normal alcoholic potassium hydroxide. The solution was standardized at frequent intervals against freshly prepared solutions of adipic acid or potassium acid phthalate, to a phenolphthalein end point.

Polymer concentrations were obtained from direct weighing of polymer and solvent on an analytical balance. Frequently concentrations were checked, particularly after titrations, by evaporation of solvent at 110°, and getting dry weight.

Equilibration of polymer in solvent with catalyst was performed in sealed ampoules of appropriate size. To eliminate effects of moisture, evaporation, or oxidation, the sample, immediately after introducing into the ampoule, was subjected to aspirator vacuum through a drying tube, cooled in dry ice-acetone mixture, and sealed. The sample was then placed in an oven with a bimetallic thermostat control and forced-draft air circulation, and left at the desired temperature for the stated time.

Control experiments performed in sealed ampoules to test the stability of the *p*-toluenesulfonic acid catalyst in chlorobenzene solution, in the presence of decamethylene glycol, showed that a week at 130° decreased the acidity by less than five percent.

RESULTS

Two sets of measurements were made, with polymer concentration and degree of esterification as respective variables. In the first set, a single polymer sample of known initial average molecular weight was equilibrated at various dilutions in chlorobenzene. This polymer, hereinafter called P-IV, was prepared in the absence of solvent from a monomer mixture containing a five percent excess of decamethylene glycol, and the esterification was driven to virtual completion ("hundred percent" polymer). This mixture, when esterified until all carboxyl groups have reacted, should produce (in the absence of ring formation) a linear polyester with a weight-average polymerization degree of 81. After 124 hours at 109° in the presence of 2.4 percent *p*-toluenesulfonic acid catalyst, the melt viscosity of the mixture had become essentially constant at 65 poises, corresponding[4] to a weight-average polymerization degree

[4] P. J. Flory, J. Am. Chem. Soc. **62**, 1057 (1940).

of 83. This slight excess over the stoichiometric limit is probably due to some volatilization of glycol.[4]

Samples were removed from the oven at various times during the equilibration process for the measurement of dilute-solution viscosities at 25°. For the first few runs, these viscosities were measured over a range of concentrations, and it was found that the inherent viscosity, $\{\eta\}=c^{-1}\ln(\eta/\eta_0)$, (where c is the concentration expressed as weight fraction of polymer, η the viscosity of the solution, and η_0 that of the pure solvent) decreased only slightly with increasing concentration.[2] Hence, for convenience, subsequent viscosity measurements were restricted to a concentration of one percent, and the tabulated values of $\{\eta\}$ correspond to this figure.

The results for a series of equilibrations of P-IV at 130°C are given in Table I. It is seen that the values of $\{\eta\}$ decrease with time to a limit, greater decreases being observed at higher dilutions. In Fig. 1, the final values of $\{\eta\}$ are plotted against the reciprocals of the polymer concentrations at which equilibration was conducted. The curve shown in Fig. 1 and the last three columns of Table I were calculated with the aid of the theory,[1] as described later.

The reversibility of the equilibration process was demonstrated by prolonged heating of equilibrated solutions of P-IV in capped but unsealed vessels, thus permitting slow evaporation of solvent. As the solvent evaporated, the inherent viscosity of the polymer increased again.

Before attributing the observed decreases in $\{\eta\}$ to ring formation by intramolecular transesterification, it is necessary to eliminate alternative explanations, such as hydrolysis by unexcluded moisture, which would

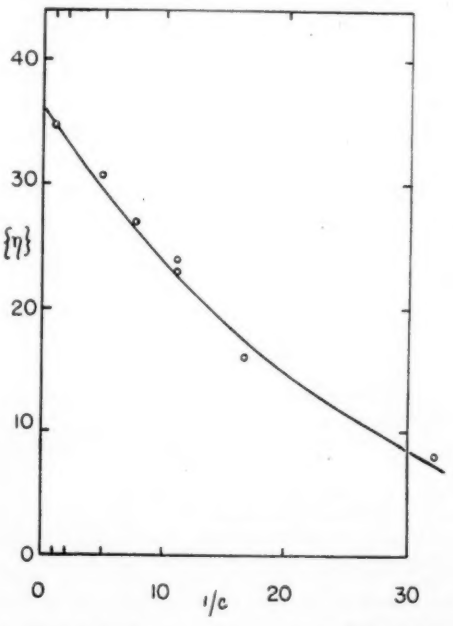

FIG. 1. Final inherent viscosities, $\{\eta\}$, of "hundred percent" decamethylene adipate polymer, equilibrated at various concentrations in chlorobenzene. The abscissas are reciprocals of the polymer concentration in weight percent.

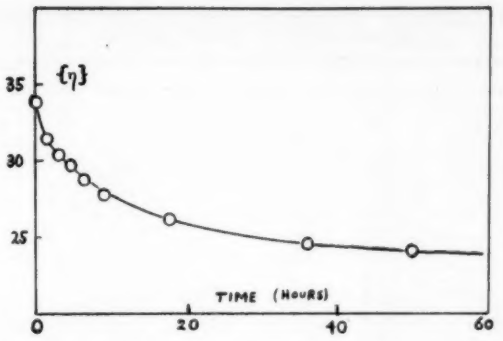

FIG. 2. Equilibration of a 9.1 percent solution of "hundred percent" decamethylene adipate polymer (P-IV) in chlorobenzene at 130°C. The ordinates are inherent viscosities at 25°C of one percent solutions in chlorobenzene.

simply produce shorter chains. The observed rate of the viscosity decrease indicates that hydrolysis cannot account for the results. The course of one equilibration (the fourth sample in Table I) is depicted in Fig. 2, where it is seen that the half-time of the process is about 7 hours. This is in good agreement with a value of about 10 hours calculated from Flory's rate constants for ester interchange,[3] while direct observation of the hydrolysis of a purposely moistened solution of P-IV gave a half-time of about 10 minutes.

The above observations rule out hydrolysis as the primary cause of the observed decreases in the viscosity of P-IV, but cannot assure its complete absence. This uncertainty was not present in the second set of measurements (Tables II and III), which were made with "equivalent" polymers (i.e., containing equimolar quantities of glycol and acid) of various initial degrees of polymerization. These equilibrations were all conducted at 10 percent concentration, and the carboxyl end groups in the samples were assayed by titration, both before and after equilibration.

The results with equivalent polymers are shown in Fig. 3. Inherent viscosity (at one percent concentration) is plotted against D_t, defined as the quantity $(1+p)/(1-p)$, where p is the fractional extent of esterification as determined by end-group titration. If the polymer contained no rings, D_t would be its weight-average polymerization degree. The upper curve (from Table II) gives the inherent viscosities of polymers prepared without solvent, while the lower curve (from Table III) is for samples subjected to equilibration at 10 percent concentration in chlorobenzene. The upper curve is in fair agreement with the results of Flory and Stickney,[2] and the points are reproduced to within one percent by the equation

$$\log_{10}\{\eta\}=0.295+0.655\log_{10}D_t. \qquad (1)$$

It is clear that the difference between the two curves of Fig. 3 cannot be ascribed to hydrolytic degradation, which would only lead to shorter chains and thus merely cause shifts *along* the upper curve. A change in inherent viscosity without accompanying changes in end-group

TABLE II. Inherent viscosities of "equivalent" polydecamethylene adipates prepared without solvent.

D_t[a]	$\{\eta\}$[b]
7.8	7.5
11.1	9.4
11.8	10.0
18.4	13.1
19.3	13.8
28.0	17.5
30.5	18.7
41.4	22.4
43.4	23.4
61.9	29.3
94.9	39.9

[a] $D_t=(1+p)/(1-p)$, where p is the fractional extent of esterification as determined by titration.
[b] Inherent viscosity, $c^{-1}\ln(\eta/\eta_0)$, at one percent concentration in chlorobenzene, 25°C.

content can occur only by ring formation through intramolecular transesterification, or perhaps by some other type of pyrolytic or oxidative degradation. The reversibility of the equilibration process argues against the latter alternatives. Moreover, the absence of oxidative degradation is indicated by the three experiments in ampoules sealed without evacuation of air (Fig. 3). These samples, presumably containing 10 to 100 times as much oxygen as the evacuated ones, show no evident deviation from the curve established by the other points.

The absence of appreciable temperature effect is also indicated in Fig. 3, the points on the lower curve being obtained at several temperatures between 90° and 170°C. The significance of this result is discussed later.

COMPARISON OF EXPERIMENT AND THEORY

Consider a polyester sample that has attained ring-chain equilibrium, consisting of a weight fraction ρ_w of rings with a weight-average polymerization degree D_{rw} and a weight fraction $(1-\rho_w)$ of chains with weight-average polymerization degree D_{cw}. Since it has been shown that $\{\eta\}$ depends only slightly on concentration (i.e., that $\ln\eta/\eta_0$ is a nearly linear function of concentration), the inherent viscosity of the sample can be closely approximated as

$$\{\eta\}=(1-\rho_w)f_c(D_{cw})+\rho_w f_r(D_{rw}), \qquad (2)$$

where $f_c(D_{cw})$ represents the inherent viscosity of the chain fraction alone and $f_r(D_{rw})$ that of the ring fraction along. These have been written as functions of weight-average polymerization degree; this procedure is valid whatever the form of the functions, since the equilibrium distributions of chains and rings are unique. In addition, Eqs. I(16) or I(17) show that D_{rw} and D_{cw} are not independent quantities, either one being fixed if the other is specified.

The second relation of importance is that between D_{cw} and the observable quantity D_t, defined as $(1+p)/(1-p)$. From Eqs. I(16) or I(17), we get

$$D_{cw}=D_t(1-\rho_w)-\rho_w, \qquad (3)$$

but the last term is completely negligible for all our samples. Since $\{\eta\}$ and D_t are measured quantities,§ there are just two independent unknown quantities, which we take at this point to be D_{cw} and ρ_w, and these can be calculated if the functions f_c and f_r are known.

The simplest method of calculation is based on two assumptions of approximate validity: (a) the rings will be small in size,[1] so that f_r can be taken as zero, and (b) the polymers prepared without solvent contain negligible quanties of rings, so that for them $D_{cw}\cong D_t$ and $f_c=KD_{cw}^{\epsilon}$, where the constants $K=1.97$ and $\epsilon=0.655$ are obtained from Eq. (1). Using these assumptions in Eqs. (2) and (3), and multiplying these together, we obtain

$$\{\eta\}D_t=KD_{cw}^{1+\epsilon}=KD_{cw}^{1.655}. \qquad (4)$$

Equation (4) gives D_{cw} directly, and ρ_w then follows from Eq. (3).

After preliminary results are obtained as just described, improved assumptions can be made. First, Kramers[5] has shown that under conditions given Staudinger's rule ($\epsilon=1$) the inherent viscosity of a ring polymer is half that of a chain of the same molecular weight. We therefore take $f_r=\frac{1}{2}KD_{rw}^{\epsilon}$, obtaining D_{rw} from the preliminary values of D_{cw} by means of Eqs. I(16) or I(17). Second, the polymers prepared without solvent contain some rings, but since ρ_w at equilibrium is nearly proportional to dilution,[1] we may assume that for them ρ_w is about one-tenth as large as for sam-

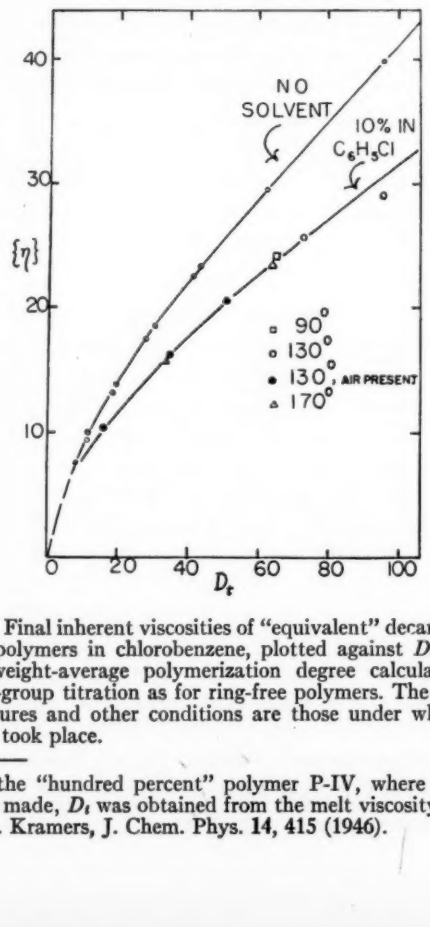

FIG. 3. Final inherent viscosities of "equivalent" decamethylene adipate polymers in chlorobenzene, plotted against D_t, the apparent weight-average polymerization degree calculated from carboxyl-group titration as for ring-free polymers. The indicated temperatures and other conditions are those under which equilibration took place.

§ For the "hundred percent" polymer P-IV, where titrations were not made, D_t was obtained from the melt viscosity.

[5] H. A. Kramers, J. Chem. Phys. 14, 415 (1946).

ples equilibrated at 10 percent concentration; this causes an increase in the numerical value of K. With the incorporation of these changes, each of which raises ρ_w by about ten percent, our final values of D_{cw} and ρ_w are obtained from Eqs. (2) and (3). These are the figures given in Tables I and III.

The theory can now be tested by observing the constancy of the quantity B', which is easily calculated from D_{cw} and ρ_w. For the "hundred percent" polymers of Table I, Eqs. I(17) give

$$D_{cw}=(1+6xy+x^2y^2)/(1-x^2y^2),$$
$$\rho_w=2B'\varphi(xy, 3/2)/c. \tag{5}$$

The parameter xy is determined from D_{cw} by the first relation, and B' then follows from the second, the polymer concentrations c being expressed in ground-moles per liter. It is seen in the last column of Table I that a reasonably constant value of B' results. The solid curve of Fig. 1 was obtained by taking the average B'-value of 0.049 mole/liter and reversing the above method of calculation, and is seen to give a good fit of the experimental points.

A similar procedure is used for the more reliable data of Table III, except that we must use the relations

$$D_{cw}=(1+x)/(1-x),$$
$$\rho_w=2B'\varphi(x^2, 3/2)/c, \tag{6}$$

which come from Eqs. I(16). For these experiments, B' is more nearly constant, and the average value of 0.037 mole/liter is about 25 percent lower than that of Table I. By using this average value and reversing the calculations, the lower solid curve of Fig. 3 is obtained, and again a good representation of the experimental results is secured.

The disagreement between the two sets of values of B' appears to be outside the experimental error, and is believed to be due to some hydrolytic degradation of the "hundred percent" polymers. As explained earlier, hydrolysis can cause no error in the results of Table III, but would elevate the apparent values of B' obtained in Table I. If we therefore assign to the results of Table III three times as much weight as to those of Table I, we obtain a figure of $B'=0.039\pm0.005$ mole/liter as a "best" value of this constant.

DISCUSSION

The effective length b of a chain link in polydecamethylene adipate may now be calculated. From Eqs. I(7) and I(13), we have

$$B'=(3/2\pi\nu)^{3/2}/2N_0b^3, \tag{7}$$

where N_0 is Avogadro's number. For polydecamethylene adipate, $\nu=18$, and with $B'=0.039\pm0.005$ we obtain $b=4.5\pm0.2$A. This figure must now be compared with the actual length of a link, and with values of b for other polymers.

The quantity b is defined in terms of the mean square extension of a long chain of n links by the relation

TABLE III. Ring-chain equilibrium in "equivalent" polydecamethylene adipates at 10 percent concentration in chlorobenzene.

Temp. (°C)	$[\eta]$	D_t	D_{cw}	ρ_w	$B'\left(\frac{\text{mole}}{\text{liter}}\right)$
130	29.0	94.9	76.7	0.192	0.040
130	25.6	72.2	60.5	0.162	0.035
90	24.1	64.5	54.6	0.154	0.034
170	23.4	63.4	53.0	0.164	0.036
130[a]	20.6	49.9	42.6	0.146	0.034
130[a]	16.2	34.4	29.4	0.146	0.038
170	15.9	34.3	29.0	0.156	0.040
130[a]	10.3	15.5	13.9	0.102	0.035
				Average	0.037

[a] Air present.

$\langle L^2\rangle_{Av}=nb^2$. If successive links were joined at a fixed valence angle α and if rotation about the bonds were otherwise completely unbiased, b would be related to the actual link-length l_0 by the expression[6]

$$b^2=l_0^2(1+\cos\alpha)/(1-\cos\alpha). \tag{8}$$

With $l_0=1.54$A for single carbon-to-carbon bonds and $\cos\alpha=\frac{1}{3}$ for tetrahedral bond angles, Eq. (8) gives $b=2.18$A. Our observed value is greater than this by a factor of 2.05 ± 0.1, which clearly indicates the presence of other effects.

Taylor[7] and Benoit[8] have treated the problem of chains in which hindrance to free rotation is localized; that is, in which the direction of a link depends only on that of the two previous links. The direction of a link may be specified by the azimuthal angle ϕ which it makes about the axis defined by the previous link. If ϕ is assigned the value zero when the chosen link is in the *trans*-position with respect to the two previous links, and if $p(\phi)d\phi$ is the normalized probability that this angle lies in $d\phi$ at ϕ, then for long chains that are not too stiff

$$b^2=l_0^2\left(\frac{1+\cos\alpha}{1-\cos\alpha}\right)\left(\frac{1+a}{1-a}\right), \tag{9}$$

with

$$a=\int_0^{2\pi}\cos\phi\, p(\phi)d\phi=\langle\cos\phi\rangle_{Av}.$$

It is seen that a is zero for completely unbiased rotation and unity for completely stiff chains with all links in the *trans*-configuration. Our value of b for polydecamethylene adipate, when used in Eq. (9), leads to $a=0.62\pm0.03$.

With the aid of Pitzer's[9] estimate of about 800 cal./mole for the difference in potential energy between the *gauche* ($\phi=\pm2\pi/3$) and *trans*-($\phi=0$) positions, Taylor has calculated $a=0.35$ for paraffin chains at 130°C,

[6] H. Eyring, Phys. Rev. **39**, 746 (1932).
[7] W. J. Taylor, J. Chem. Phys. **16**, 257 (1948).
[8] H. Benoit, J. Polymer Sci. **3**, 376 (1948).
[9] K. S. Pitzer, J. Chem. Phys. **8**, 711 (1940); see also Szasz, Sheppard, and Rank, *ibid.*, **16**, 705 (1948).

corresponding to $b=3.14$A. This is seen to be appreciably smaller than our experimental value, and in fact a potential energy difference of about 1400 cal./mole would be required to give $a=0.62$ at 130°C. It will be recalled, however, that we found no perceptible temperature-dependence of B' from 90° to 170°C. Our estimated experimental error is large enough so that a potential energy of 800 cal./mole would not be incompatible with the results, but a figure of 1400 cal./mole is definitely too large. It may be remarked that extremely accurate measurements of ring-chain equilibrium would be needed to give a reliable temperature-coefficient, since the practically accessible temperature range is not great.

If the Taylor-Pitzer assessment of local hindrance is accepted, a factor of 1.4 in the value of b remains to be explained by long-range steric effects. Equation (9) includes contributions from many chain configurations which should be excluded because they correspond to the overlapping of the covolumes of several parts of the chain. The problem of properly excluding such forbidden configurations presents very formidable mathematical difficulties, and has thus far been solved only approximately.[10–13] However, H. Kuhn[14] has estimated a factor of 1.3 in the effective link length of paraffin chains as due to this cause, and G. W. King[15] finds a factor of about 1.6 by punched-card calculations for chains of up to 30 links. These figures are in gratifying agreement with our results,|| especially when it is recalled that most of the rings formed in polydecamethylene adipate consist of 18 or 36 chain atoms, which is rather small for the application of the asymptotic formulas for very large rings.

The value 0.62 for a found here for decamethylene adipate chains of short lengths can be compared with those for other high polymers, as inferred from light-scattering measurements. Cellulose acetate[16] has an extremely stiff chain corresponding to a value of a very near unity. For chains of this stiffness, Taylor's mathematical treatment must be refined.[17]

Light-scattering measurements on polystyrene in various solvents[18–20] show an effective link length of three to five times that predicted from a free-rotation-no-hindrance model, leading to values of a between 0.72 and 0.93.

These results are for chains stiffer than the predominantly paraffinic chain of decamethylene adipate. Flexible chains do not lend themselves readily to the light-scattering method, since, even with fairly high molecular weights, the molecules are not sufficiently extended to give measurable dissymmetry of light scattering. Quantitative measurement of ring formation, however, is especially suited to flexible chains of low molecular weight for finding information about chain stiffness and length. The present data can be taken to give some picture of the stiffness of a chain composed principally of methylene groups, with an occasional ester linkage.

[10] R. Simha, J. Research Nat. Bur. Stand. **40**, 21 (1948).
[11] P. J. Flory, J. Chem. Phys. **17**, 303 (1949).
[12] J. J. Hermans, Rec. Trav. Chim. des Pays-Bas **69**, 220 (1950).
[13] E. Montroll, J. Chem. Phys. **18**, 734 (1950).
[14] H. Kuhn, J. Chem. Phys. **15**, 843 (1947).
[15] G. W. King, private communication.
|| In general, the long-range factor depends on the solvent-solute interactions, being largest in the best solvents and approaching unity in poor solvents (see references 11 and 20). The estimates of Kuhn and King are for athermal (i.e., rather good) solvents. Chlorobenzene is a good solvent for polydecamethylene adipate (see reference 2), and is probably not far from being athermal.
[16] R. S. Stein and P. M. Doty, J. Am. Chem. Soc. **68**, 159 (1946).
[17] H. Benoit and C. Sadron, J. Polymer Sci. **4**, 473 (1949).
[18] B. H. Zimm, J. Chem. Phys. **16**, 1099 (1948).
[19] A. M. Bueche, J. Am. Chem. Soc. **71**, 1452 (1949).
[20] Outer, Carr, and Zimm, J. Chem. Phys. **18**, 830 (1950).

The Microwave Spectrum and Structure of Methyl Acetylene*

RALPH TRAMBARULO AND WALTER GORDY
Department of Physics, Duke University, Durham, North Carolina

(Received August 4, 1950)

From measurements of the $J=1\rightarrow2$ rotational transitions of methyl acetylene and some of its isotopic modifications, the moments of inertia, I_B (in the units 10^{-40} gm cm^2), were found for the ground vibrational state: for CH_3CCH, 98.17_{23}; for $CH_3C^{13}CH$, 98.21_{32}; for $C^{13}H_3CCH$, 100.91_{93}; for $CH_3CC^{13}H$, 101.19_{92}; for CH_3CCD, 107.72_{34}; and for CD_3CCD, 124.58_{06}. The centrifugal distortion constants, D_{JK}, in mc/sec. are 0.16_1, 0.1_6, 0.1_6, 0.1_3, 0.1_4, and 0.0_9, respectively. The $J=2\rightarrow3$ rotational transition of CH_3CCH was also measured, and the distortion constant D_J was found to be 0.00_5 mc/sec. Four lines of CH_3CCH corresponding to the $J=1\rightarrow2$ transition and six lines for the $J=2\rightarrow3$ transition in the excited vibrational state $v_{10}=1$ and six lines for the $J=2\rightarrow3$ transition in the excited state $v_9=1$ were measured and interpreted according to Nielsen's theory of l-type doubling in symmetric tops. The calculated structure for the ground vibrational state is: C−H (acetylenic), 1.056A; C≡C, 1.207A; C−C, 1.460A; C−H (methyl), 1.097A; ∠HCH, 108°14′.

INFRA-RED spectra[1] and electron diffraction[2] studies have shown that single bonds adjacent to triple bonds in the acetylenes and cyanides are significantly shorter than the normal tetrahedral carbon bond. Recent microwave studies of linear acetylenes[3,4] and of cyanides[4,5] also show this. The vibrational bands of the infra-red and Raman spectra indicate that methyl acetylene is a symmetric top;[6] that is, the $\backslash$ $-C-C\equiv C-H$ configuration is linear. These features $/$ are confirmed by the present study, which also provides the first complete determination of the structure of this molecule.

PROCEDURE

The $J=1\rightarrow2$ and $2\rightarrow3$ rotational absorption lines were found with a video detection sweep spectroscope[7] and were measured with a frequency standard[8] monitored by means of *WWV*.

The methyl acetylene was prepared by dropping propylene bromide into a boiling 6 normal solution of KOH in *n*-butanol.[9] The evolved vapors were passed through an ice trap, and the methyl acetylene collected in a receiver cooled in a dry ice and acetone bath. The sample was further purified by fractionation in a vacuum system. The sensitivity of the spectroscope was sufficient for observation and measurement of the C^{13} isotopic species in their natural concentrations with the absorption cell cooled to dry ice temperature. For the detection of CH_3CCD, a portion of the methyl acetylene was exchanged with a solution of NaOD in D_2O at room temperature for several weeks. The CH_3CCD content was enriched to about 70 percent. The CD_3CCD was prepared by reacting D_2O with Mg_2C_3, which was formed by passing isopentane over magnesium powder heated to 700°C for several hours.[10] Impurities were removed by fractionation in a vacuum system.

RESULTS

The measured frequencies of the $J=1\rightarrow2$ and $2\rightarrow3$ transitions are given in Table I.

Rotational constants for the ground vibrational states appear in Table II. For calculation of I_B the value of Planck's constant used was $h=6.62373\times10^{-27}$ erg sec.

EXCITED VIBRATIONAL TRANSITIONS

The four lines between 34,246.30 and 34,313.21 mc/sec. and the six between 51,369.12 and 51,469.85 mc/sec. are $J=1\rightarrow2$ and $2\rightarrow3$ rotational transitions of CH_3CCH in the first excited vibrational state for which $\omega_{10}(e)$ is 336 cm^{-1}.[6] This corresponds to the $C-C\equiv C$ degenerate bending mode. The pattern of the $J=1\rightarrow2$ transition is that predicted by Nielsen[11] for l-type doubling in symmetric tops. There is a pair of closely spaced lines approximately midway between two lines separated by 66.91 mc/sec.

The spectrum of the $J=2\rightarrow3$ transition for the first excited $C-C\equiv C$ bending state consists of four rather closely spaced lines midway between two lines which

* The research reported in this document has been made possible through support and sponsorship extended by the Geophysical Research Directorate of the Air Force Cambridge Research Laboratories under Contract No. W19-122-ac-35. It is published for technical information only and does not represent recommendations or conclusions of the sponsoring agency.

[1] Herzberg, Patat, and Verleger, J. Phys. Chem. **41**, 123 (1937).
[2] Pauling, Springall, and Palmer, J. Am. Chem. Soc. **61**, 927 (1939).
[3] A. A. Westenberg and E. B. Wilson, Jr., J. Am. Chem. Soc. **72**, 199 (1950).
[4] Westenberg, Goldstein, and Wilson, J. Chem. Phys. **17**, 1319 (1949).
[5] Kessler, Ring, Trambarulo, and Gordy, Phys. Rev. **79**, 54 (1950).
[6] G. Herzberg, *Infra-Red and Raman Spectra of Polyatomic Molecules* (D. Van Nostrand Company, Inc., New York, 1945), pp. 337–9.
[7] W. Gordy and M. Kessler, Phys. Rev. **72**, 644 (1947).
[8] R. R. Unterberger and W. V. Smith, Rev. Sci. Inst. **19**, 580 (1948).
[9] Hurd, Meinert, and Spense, J. Am. Chem. Soc. **52**, 1138 (1930).
[10] H. C. Rueggeberg, J. Am. Chem. Soc. **65**, 602 (1943).
[11] H. H. Nielsen, Phys. Rev. **77**, 130 (1950).

TABLE I. Observed frequencies for the rotational transitions of methyl acetylene and some isotopic species.

Species	Transition[a]		Frequency[b] (mc/sec.)
CH_3CCH	$J=1\rightarrow2$	$K=0\rightarrow0$	34,183.37
		$K=1\rightarrow1$	34,182.71
	$J=1\rightarrow2$	Excited vib. state,	34,246.30
		$v_{10}=1$	34,277.05
			34,278.98
		(C−C≡C bending)	34,313.21
	$J=2\rightarrow3$	$K=0\rightarrow0$	51,274.75
		$K=1\rightarrow1$	51,273.76
		$K=2\rightarrow2$	51,270.86
	$J=2\rightarrow3$	Excited vib. state,	51,280.45
		$v_9=1$	51,296.33
			51,304.05
		(C≡C−H bending)	51,305.93
			51,307.47
			51,334.81
	$J=2\rightarrow3$	Excited vib. state,	51,369.12
		$v_{10}=1$	51,410.51
			51,415.35
		(C−C≡C bending)	51,418.23
			51,418.75
			51,469.85
$CH_3C^{13}CH$	$J=1\rightarrow2$	$K=0\rightarrow0$	34,169.13
		$K=1\rightarrow1$	34,168.47
$C^{13}H_3CCH$	$J=1\rightarrow2$	$K=0\rightarrow0$	33,252.88
		$K=1\rightarrow1$	33,252.22
$CH_3CC^{13}H$	$J=1\rightarrow2$	$K=0\rightarrow0$	33,160.94
		$K=1\rightarrow1$	33,160.35
CH_3CCD	$J=1\rightarrow2$	$K=0\rightarrow0$	31,152.56
		$K=1\rightarrow1$	31,152.00
CD_3CCD	$J=1\rightarrow2$	$K=0\rightarrow0$	26,937.24
		$K=1\rightarrow1$	26,936.87

[a] Transitions are for the ground vibrational states unless otherwise noted.
[b] Absolute frequencies are accurate to ±0.10 mc/sec. The frequency of the $J=1\rightarrow2$, $K=0\rightarrow0$ and $K=1\rightarrow1$ transitions for $CH_3C^{13}CH$ are measured relative to those of CH_3CCH to ±0.04 mc/sec.

are 100.74 mc/sec. apart. The solutions to the secular equation indicated by Nielsen[11] for $J=3$ are

$$\epsilon=T_v+12B_v-9(B_v-C_v)+6\zeta C_v-144D_J-108D_{JK}-81D_K,$$
$$T_v+12B_v-4(B_v-C_v)+4\zeta C_v-144D_J-48D_{JK}-16D_K,$$
$$T_v+12B_v-(B_v-C_v)-2\zeta C_v-144D_J-12D_{JK}-D_K\pm12B_e^2a/\omega_s,$$
$$T_v+12B_v-5(B_v-C_v)-2\zeta C_v-144D_J-60D_{JK}-41D_K\pm\{(4[(1-\zeta)C_v-B_v]-48D_{JK}-40D_K)^2+60B_e^4a^2/\omega_s^2\}^{\frac{1}{2}},$$
$$T_v+12B_v-2(B_v-C_v)-2\zeta C_v-144D_J-24D_{JK}-8D_K\pm\{[2(1-\zeta)C_v-2B_v-24D_{JK}-8D_K]^2+120B_e^4a^2/\omega_s^2\}^{\frac{1}{2}}.$$

In the expressions for the last two roots, the terms involving square roots may be expanded and higher order terms of the expansion neglected to give the values:

$$\epsilon=T_v+12B_v-9(B_v-C_v)-6\zeta C_v-144D_J-108D_{JK}-81D_K+\frac{15B_e^4a^2/2\omega_s^2}{(1-\zeta)C_v-B_v-12D_{JK}-10D_K},$$
$$T_v+12B_v-(B_v-C_v)+2\zeta C_v-144D_J-12D_{JK}-D_K-\frac{15B_e^4a^2/2\omega_s^2}{(1-\zeta)C_v-B_v-12D_{JK}-10D_K},$$

and

$$\epsilon=T_v+12B_v-4(B_v-C_v)-4\zeta C_v-144D_J-48D_{JK}-16D_K+\frac{30B_e^4a^2/\omega_s^2}{(1-\zeta)C_v-B_v-12D_{JK}-4D_K},$$
$$T_v+12B_v-144D_J-\frac{30B_e^4a^2/\omega_s^2}{(1-\zeta)C_v-B_v-12D_{JK}-4D_K}.$$

The positions of the spectral lines for the $J=2\rightarrow3$ transition are then

$$6B_v-108D_J-\frac{24B_e^4a^2/\omega_s^2}{(1-\zeta)C_v-B_v-12D_{JK}-4D_K}$$

corresponding to $K=0$, $l=\pm1$;

$$6B_v-108D_J-6D_{JK}\pm6B_e^2a/\omega_s \quad \text{for} \quad K=\pm1, \quad l=\pm1,$$

$$6B_v-108D_J-6D_{JK}-\frac{15B_e^4a^2/2\omega_s^2}{(1-\zeta)C_v-B_v-12D_{JK}-10D_K}$$

for $K=\pm1$, $l=\mp1$;

$$6B_v-108D_J-24D_{JK}+\frac{24B_e^4a^2/\omega_s^2}{(1-\zeta)C_v-B_v-12D_{JK}-4D_K}$$

for $K=\pm2$, $l=\pm1$; and

$$6B_v-108D_J-24D_{JK} \quad \text{for} \quad K=\pm2, \quad l=\mp1.$$

Additional centrifugal stretching terms to be added to the transition frequencies are: $12(2D_J+D_{JK})\zeta$ for $K=\pm1$, $l=\pm1$; $-12(2D_J+D_{JK})\zeta$ for $K=\pm1$, $l=\mp1$; $24(2D_J+D_{JK})\zeta$ for $K=\pm2$, $l=\pm1$; and $-24(2D_J+D_{JK})\zeta$ for $K=\pm2$, $l=\mp1$.

The identification of the $J=1\rightarrow2$ and $J=2\rightarrow3$ transitions for $v_{10}=1$ are given in Table III. From this assignment of the spectrum $B_v=8{,}569.7_{64}$ mc/sec., $D_J=0.00_3$ mc/sec., $D_{JK}=0.15_3$ mc/sec., $\zeta_{10}=1._1$, and $\alpha_{10}=-23.92$ mc/sec. If we take $\omega_{10}=336$ cm^{-1} and $B_e\approx B_0=8{,}545.84$ mc/sec., then $a=1.15$.

The group of lines between 51,280.45 mc/sec. and 51,334.81 mc/sec. are probably due to the first excited C≡C−H bending vibration for which $\omega_9(e)=643$ cm^{-1}. The grouping of the lines fits Nielsen's theory qualitatively; however, no reasonable assignment of the lines could be made.

MOLECULAR STRUCTURE

For a rigid symmetric top model with a linear $-C-C\equiv C-H$ configuration, the moment of inertia I_B may be written

$$I_B=(3/2)M_HY^2+3M_HX_H^2+M_CX_C^2 +M_{C'}X_{C'}^2+M_{C''}X_{C''}^2+M_{H'}X_{H'}^2,$$

where Y is the distance of each hydrogen in the methyl group from the figure axis, the X's are the components along the figure axis of the distance of each atom from the center of gravity, and the M's are the masses of the atoms. The subscripts denote the atoms indicated in the figure:

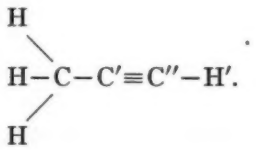

The distance of a particular atom along the figure axis from the center of gravity in the original molecule may be obtained from the moments of inertia of this species and of one in which an isotope has been substituted for the atom from the expression,

$$X=[(I_B'-I_B)(M+\Delta M)/M\Delta M]^{\frac{1}{2}},$$

where X is the distance from the center of gravity of the original molecule, I_B and I_B' are the moments of inertia of the original and of the substituted species, M is the mass of the original molecule, and ΔM is the increase in mass as a result of the isotopic substitution. Symmetrical isotope substitution for the hydrogens in the methyl group leads to the following relationship,

$$(I_B'-I_B)/\Delta M=Y^2/2+MX_H^2/(M+\Delta M).$$

(Here, ΔM is the total increase in molecular mass as a result of isotopic substitution.)

One more moment of inertia than is necessary for the complete solution of the structure is known. The set of parameters which best fit the data is given in Table IV. The atomic masses used are: H=1.00813 a.m.u., D=2.01473 a.m.u., C=12.00386 a.m.u. and C^{13} =13.00761 a.m.u. A comparison of the moments of inertia of the various isotopic species of methyl acetylene calculated from the parameters in Table IV and the observed values are listed in Table V.

An estimate of the limits of error in the molecular dimensions is given. The largest factor in the error is the assumption in the calculations that substitution of isotopes does not change the interatomic distances for the ground vibrational state.

DISCUSSION OF THE STRUCTURE

With assumed values for other parameters, Herzberg, Patat, and Verleger[1] found by infra-red measurements the C−C single bond length to be 1.462A. From electron diffraction measurements, Pauling, Springall, and Palmer[2] obtained 1.46A and 1.20A for the C−C and C≡C distances. These values are essentially confirmed by our study, which also provides a determination of the remaining dimensions of the molecule. It is interesting to compare the ≡C−H and C≡C distances in methyl acetylene with those in cyanoacetylene, chloroacetylene, and methyl cyanide. (See Table IV.)

The ≡C−H link in methyl acetylene, like that in acetylene, is 0.037A shorter than the C−H link in methane. Pauling has suggested that this shortening may be due to the use of a carbon orbital differing from that of a tetrahedral orbital. The C−C bond adjacent to the triple bond is likewise shortened, and there is an additional shortening of about 0.05A, which, as suggested by Pauling, Springall, and Palmer,[12] may be explained by resonance of the most probable structure I with the less stable structures of type II and III.

I. II. III.

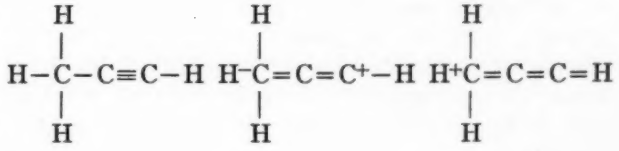

The observed length would require the single CC bond to have about 12-percent double bond character. This resonance could also account for the fact that the methyl

TABLE II. Rotational constants for the ground vibrational states of methyl acetylene and some isotopic modifications.

Species	B_0 (mc/sec.)[a]	D_{JK} (mc/sec.)	D_J (mc/sec.)	I_B ($\times10^{-40}$ g cm^2)
CH_3CCH	8,545.84±0.03	0.16_1	0.00_5	98.17_{23}
$CH_3C^{13}CH$	8,542.28±0.03	0.1_6	···	98.21_{32}
$C^{13}H_3CCH$	8,313.23±0.03	0.1_6	···	100.91_{93}
$CH_3CC^{13}H$	8,290.24±0.03	0.1_3	···	101.19_{92}
CH_3CCD	7,788.14±0.03	0.1_4	···	107.72_{34}
CD_3CCD	6,734.31±0.03	0.0_9	···	124.58_{06}

[a] Relative accuracy for the first two species is ±0.01 mc/sec.

TABLE III. Assignment of the rotational transitions $J=1\rightarrow2$ and $2\rightarrow3$ for $v_{10}=1$.

Frequency (mc/sec.)	Transition		
34,278.95	$J=1\rightarrow2$	$K=0$,	$l=\pm1$
34,277.07		$K=\pm1$,	$l=\pm1$
34,246.30 } 34,313.21 }		$K=\pm1$,	$l=\mp1$
51,418.23	$J=2\rightarrow3$	$K=0$,	$l=\pm1$
51,415.35		$K=\pm1$,	$l=\pm1$
51,369.12 } 51,469.85 }		$K=\pm1$,	$l=\mp1$
51,418.75		$K=\pm2$,	$l=\pm1$
51,410.51		$K=\pm2$,	$l=\mp1$

[12] L. Pauling, *Nature of the Chemical Bond* (Cornell University Press, Ithaca, New York, 1939), p. 152. See also Pauling, Springall, and Palmer, reference 2.

TABLE IV. Structure of methyl acetylene and related compounds.

Molecule	∠HCH	Distances in Angstroms C–H (methyl)	C–C	C≡C	C–H (acetylenic)	Ref.
CH_3CCH	108°14′±1°	1.097±0.010	1.460±0.002	1.207±0.002	1.056±0.008	
HCCCN			1.382	1.203	1.057	3
HCCCl				1.211	1.052	4
CH_3CN	109°49′	1.092	1.460			5

configuration found for the methyl acetylene differs from that of methane. Though the deviations observed are in the right direction they are within the limits of error and thus may not be real. The structural features mentioned here have also been accounted for by Mulliken, Rieke, and Brown[13] with the molecular orbital theory.

TABLE V. Comparison of the observed and calculated moments of inertia, $I_B(\times 10^{-40}$ g cm^2), of methyl acetylene isotopic species.

	Molecule CH_3CCH	$CH_3C^{13}CH$	$C^{13}H_3CCH$	$CH_3CC^{13}H$	CH_3CCD	CD_3CCD
observed	98.17_{33}	98.21_{32}	100.91_{93}	101.19_{92}	107.72_{34}	124.58_{96}
calculated	98.171	98.212	100.924	101.201	107.726	124.638

We wish to thank H. Ring, H. D. Edwards, and O. R. Gilliam for assisting with the preliminary work.

[13] Mulliken, Rieke, and Brown, J. Am. Chem. Soc. **63**, 41 (1941).

THE JOURNAL OF CHEMICAL PHYSICS VOLUME 18, NUMBER 12 DECEMBER, 1950

Absolute Intensity of Light Scattering from Pure Liquids and Solutions*

C. I. CARR, JR.† AND B. H. ZIMM
Department of Chemistry, University of California, Berkeley, California

(Received July 31, 1950)

The absolute scattering powers of several strongly scattering solutions of polystyrene were measured by three independent methods, using transmission, integrated scattering, and scattering at right angles respectively. When a number of factors involving the geometry of the measuring system and the refraction of the light at interfaces are taken into account all the methods give results in excellent agreement. The absolute scattering power of benzene and carbon tetrachloride were then determined by comparison with the polystyrene solutions and were found to be in good agreement with Einstein's theoretical equation, though at variance with most of the previously reported experiments. The scattering from solutions of dibenzyl and sucrose octaactetate were also measured and found to give results in good agreement with those calculated theoretically from the molecular weights of these substances. In the course of the measurements it was also necessary to study the reflection properties of $MgCO_3$ and MgO surfaces in more detail than has been published heretofore.

I. INTRODUCTION

LIGHT scattering investigations have become of increasing importance in recent years because of the applicability of this method to the molecular weight determination of high polymers in solution. Prior to high-polymer application, work in the field was confined primarily to the scattering from pure liquids and gases in efforts to examine the theories of scattering developed by Lord Rayleigh[1] for gases and Einstein[2] for liquids. Experimental attempts met with some success in the case of gases, but examination of liquids presented a more difficult problem and there has been no satisfactory determination of the validity of the liquid theory or even agreement between different investigators as to the extent of the scattering from a given liquid. Bhagavantam[3] has very satisfactorily summarized the work in this field.

The absolute scattering has been expressed in various ways. Rayleigh's ratio, $i_{90}r^2/I_0$, which is a constant for a given medium, has been generally used where i_{90} and I_0 are the irradiances (energy sec.$^{-1}$ cm^{-2}) of the transversely scattered light per unit volume of fluid and of the incident light, respectively, and r is the distance from the scattering volume to the point of observation. We will hereafter symbolize Rayleigh's ratio by S, indicating by a subscript u or v whether the incident light is unpolarized or vertically polarized.

In current literature the term "turbidity," having the symbol τ, is frequently used. Turbidity may be defined as the fractional decrease in the irradiance of the incident light per centimeter of medium or represented by the expression,

$$\tau = 2\pi \int_0^{\pi} (i_\vartheta r^2/I_0) \sin\vartheta d\vartheta, \qquad (1)$$

* This paper represents part of a thesis submitted by C. I. Carr, Jr. to the Graduate Division, University of California, in partial fulfillment of the requirements for the degree of Doctor of Philosophy, September, 1949.

† Present address, General Laboratories, U. S. Rubber Company, Passaic, New Jersey.

[1] Lord Rayleigh, Scientific papers **1**, 87, (1871); **4**, 397 (1899).

[2] A. Einstein, Ann. d. Physik **33**, 1275 (1910).

[3] S. Bhagavantam, *Scattering of Light and the Raman Effect* (Chemical Publishing Company, Brooklyn, New York, 1942).

where ϑ is the angle between the incident and scattered rays. The turbidity is thus a measure of the total light scattered, and for small scattering is approximately equal to the extinction coefficient.

From a consideration of fluctuation theory, Einstein[2] showed that Rayleigh's ratio for a dilute colorless binary solution of small isotropic particles with unpolarized incident light was given by the equation,

$$S_u=\frac{2\pi^2}{\lambda_0^4N_0}\left[RT\beta(\rho ndn/d\rho)^2+\frac{M_1Cn^2(dn/dc)^2}{\rho_1(-d\ \ln f_1/dc)}\right], \quad (2)$$

where λ_0 is the wave-length of the incident light in vacuum, N_0 is Avogadro's number, β is the isothermal compressibility, ρ density of solution, ρ_1 is the density of the solvent, M_1 is the molecular weight of the solvent, n is the refractive index of the solution, c is the concentration of solute in grams per milliliter of solution, f_1 is the fugacity of the solvent, and R and T have their usual significance. The first term represents scattering due to fluctuations in density and the second term is due to concentration fluctuations. For a pure liquid the second term is zero.

For a dilute solution the density scattering is essentially the same as that due to the pure solvent, so that the second part of Eq. (2) may be considered as an excess scattering caused by the solute. This excess scattering is related to the molecular weight of the solute, as may be seen if the following extended form of the van't Hoff law is used for $\ln f_1$:

$$\ln f_1=-\frac{M_1c}{M_2\rho_1}-\frac{M_1A_2c^2}{\rho_1}.$$

A_2 is an empirical constant.

Appropriate modifications must be made when the scattering particles are either anisotropic or large compared to the wave-length. If the horizontal plane is defined as that containing the incident and scattered beams, the light scattered transversely from fluids composed of isotropic particles is completely polarized with the electric vector vibrating in the vertical plane. However, if the particles are anisotropic the effects of the varying polarizability along the different axes results in a horizontally vibrating component in the scattering and the total scattering is greater than given by Eq. (2). We must introduce the depolarization ratios, ρ_u and ρ_v, for unpolarized and vertically polarized incident light respectively; these are the ratios of the intensities of the horizontally vibrating to the vertically vibrating components in the scattered light. Equation (2) may then be corrected by introducing the appropriate Cabannes factors, $(6+6\rho_u)/(6-7\rho_u)$ for unpolarized light and $(3+3\rho_v)/(3-4\rho_v)$ for polarized light.

We now write down the equations in the forms in which they are finally used. For a pure liquid illuminated with unpolarized light,

$$S_u=\frac{2\pi^2RT\beta}{\lambda_0^4N_0}\left(\rho n\frac{dn}{d\rho}\right)^2\left(\frac{6+6\rho_u}{6-7\rho_u}\right). \quad (3)$$

For a dilute solution, the excess scattering, S, obeys the formulas:

$$S_u=\frac{2\pi^2c}{\lambda_0^4N_0}\left(n\frac{dn}{dc}\right)^2\left(\frac{6+6\rho_u}{6-7\rho_u}\right)\frac{1}{2A_2c+1/M_2} \quad (4a)$$

$$S_v=\frac{4\pi^2c}{\lambda_0^4N_0}\left(n\frac{dn}{dc}\right)^2\left(\frac{3+3\rho_v}{3-4\rho_v}\right)\frac{1}{2A_2c+1/M_2} \quad (4b)$$

the former for unpolarized incident light and the latter for vertically polarized incident light. The depolarization ratios to be used in Eqs. (4a) and (4b) are to be calculated from the horizontal and vertical components of the excess scattering only. The molecular weight of the solute, M_2, may be obtained from either of the last two equations by extrapolation to infinite dilution of the ratio c/S. Either Eq. (4a) or (4b) may be written in the form,

$$Kc/S=1/M_2+2A_2C, \quad (5)$$

where K includes all the constant factors.

In some simple cases the depolarization ratios are zero and the intensity of scattering as a function of angle is proportional to $1+\cos^2\vartheta$ for unpolarized illumination. Under these circumstances Eq. (1) may be integrated to yield,

$$\tau=16\pi S_u/3=8\pi S_v/3, \quad (6)$$

as an explicit relation between S and τ.

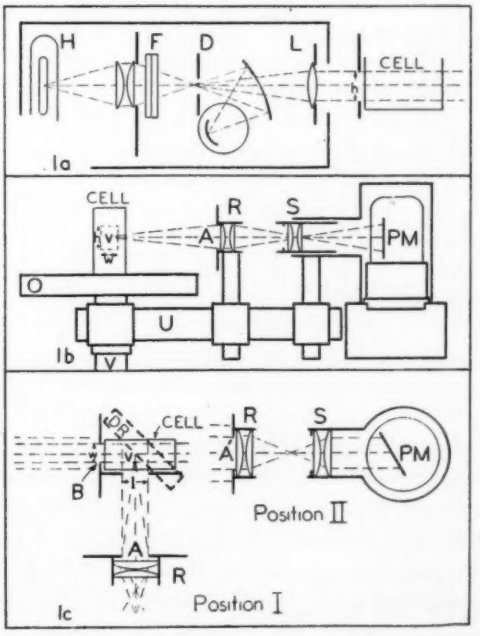

FIG. 1. Apparatus, schematic only. 1a. Side view of optical projector system. 1b. Side view of solution cell and photometer. 1c. Top view of solution cell and photometer.

Either the Rayleigh ratio, S, or the turbidity, τ, may be measured directly. In this research we first report a comparison of the independent measurements of both quantities on some solutions of high scattering power that should obey Eq. (6). Satisfactory agreement is obtained. By comparison with the strongly scattering solutions Rayleigh ratios are then obtained on some substances of scattering power too low to measure directly. Among the latter substances are two pure liquids, benzene and carbon tetrachloride, and some solutions of compounds of known molecular weight, dibenzyl and sucrose octaacetate, to test the validity of Eqs. (3) and (4).

The theory of scattering from liquids and solutions has recently been discussed by several writers.[2,4,5]

II. THEORY OF ABSOLUTE SCATTERING MEASUREMENTS

Three independent methods were used in this research to determine the scattering power of a strongly

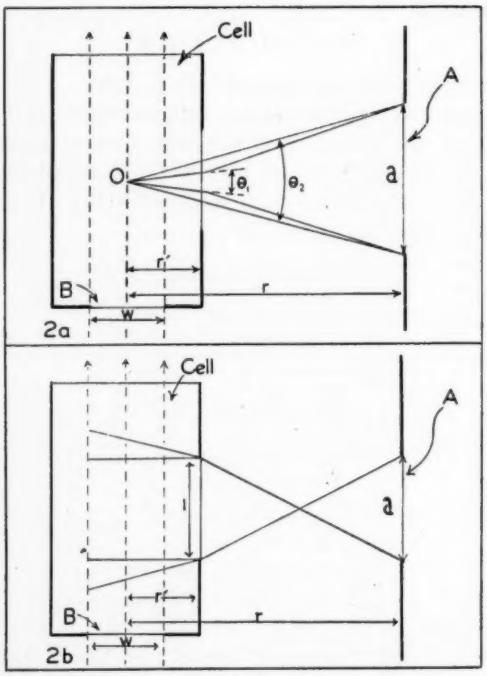

FIG. 2. Derivation of correction factors. 2a. Refractive index correction. 2b. Volume correction.

scattering solution. These were the measurement of the transmission of the solution, measurement of the total scattering by means of an integrating sphere, and measurement of the transverse scattering only. The necessary formulas for the three methods are developed here; apparatus and results are described subsequently.

[4] P. Debye, J. App. Phys. **15**, 456 (1944); J. Phys. and Coll. Chem. **51**, 18 (1947).
[5] G. Oster, Chem. Rev. **43**, 319 (1948).

1. Transmission Method

We denote photometer readings by F. The irradiance of a parallel beam of light is measured before (F_1) and after (F_2) passing through a known length, l, of solution. If it is assumed that true absorption is absent, the turbidity may be calculated from the expression,

$$\tau=(1/l)\ln(F_1/F_2). \tag{7}$$

High accuracy is required in the measurement of F_1 and F_2 because of the small value of τ; in fact, this method is not suitable for most pure liquids and dilute solutions.

2. Integrated Scattering Method

This method involves the use of a hollow sphere with a dull, white, smooth inner surface. Any light which enters this sphere through a small opening is multiply reflected from the surface. An even illumination on the surface results, the magnitude of which represents the intensity of the entering light.

If a turbid solution is placed in a small cell within the sphere, and a second opening made in the sphere opposite the first so that the incident beam may pass through the solution cell and out the opposite side of the sphere, the light scattered by the solution is the only light collected within the sphere. The magnitude of the scattering is then proportional to the illumination on the surface of the sphere. The incident beam flux is proportional to the illumination when a white plug is placed in the exit hole.

Let the total flux entering the sphere be represented by the photometer reading F_3. The excess flux scattered by the solute in a solution cell of length, l, when the exit plug is removed, is represented by F_4. The turbidity can be calculated from the expression,

$$\tau=F_4/lF_3. \tag{8}$$

F_4 is the reading after a "blank" for the cell filled with solvent alone has been subtracted. The ratio of the photometer readings thus gives the excess turbidity due to the solute directly.

3. Transverse Scattering Method

This method involves a measurement of the intensity of the light scattered at an angle of 90° to the incident beam. Equation (6) shows that turbidity is proportional to the ratio of the irradiance of the scattered light to that of the incident light. The ratio may be obtained by direct measurement or by comparing the solution to a secondary standard of known reflectance or transmittance and intensity distribution.

A measure of the irradiance of the incident light may be obtained by attenuating the parallel incident beam a fraction t_1 and revolving the photometer into the incident beam. If the aperture stop that defines the area of the beam observed is referred to as A', the total flux collected is represented by a reading F_1,

$$F_1=I_0A't_1. \tag{9}$$

A top view of a typical arrangement is shown in Fig. 1c. Aperture B is a rectangular aperture of dimensions w (width) by h (height). Aperture l is a tall rectangular aperture of width l. Apertures B and l determine the volume, V, of liquid observed by the photometer.

Position I shows the photometer at 90° to the incident beam for transverse scattering measurements, and position II shows the photometer directly in the incident beam for measurements of the irradiance of the incident light.

If the volume of scattering solution is illuminated by parallel incident light and observed at 90° and distance r by the small photometer aperture of area A, the flux collected is $i_{90}A$ and is represented by the reading, F_5,

$$F_5 = i_{90}A = \frac{3I_0hwl\tau A}{16\pi r^2}. \tag{10}$$

The ratio of F_5 and F_1 gives an expression for the turbidity in terms of measurable quantities,

$$\tau = \frac{16\pi F_5 r^2 A t_1}{3F_1hwlA'}. \tag{11}$$

Measurement of the turbidity by this method is difficult experimentally because the order of magnitude of the ratio, F_5/F_1, for the unattenuated incident light is approximately 10^{-6}. It thus is necessary to reduce the irradiance of the incident light by about this factor to obtain comparable readings of the photometer.

The use of a diffusely reflecting secondary standard reduces the ratio of the two measurements by a factor of 10^3 and eliminates all dimensional measurements except that of l. The diffuse reflectors magnesium oxide and magnesium carbonate were employed as secondary standards in this research.

The intensity of the reflected light from a perfect diffuse reflector, which follows Lambert's "cosine law," decreases as the cosine of the angle between the normal to the surface and the direction of observation. The flux striking the surface of a reflector, DR, position I Fig. 1c, placed at an angle of 45° to the incident beam is I_0hw and the flux emitted is I_0hwr_f where r_f is the total reflectance. By integrating the irradiance of the reflected light, i_α, over the surface of a hemisphere of radius r, where α is the angle between the direction of observation and the normal to the plane of the surface, the photometer reading, F_6, for α equal to 45° is found to be,

$$F_6 = (0.707I_0hwr_ft_2A)/(\pi r^2), \tag{12a}$$

and

$$\tau = (16\times 0.707r_ft_2F_5)/(3F_6l), \tag{12b}$$

where t_2 is the fractional reduction of the incident light necessary to make F_5 of comparable magnitude to F_6.

The reflectance, r_f, of the material may be obtained by comparing F_1 and F_6. In this case the following relation would be applicable,

$$r_f = (\pi F_6 r^2 A' t_1)/(F_1hwAt_2\sin\alpha). \tag{13}$$

It should be noted that the preceding expressions for turbidity are accurate only in the case where refraction corrections need not be applied; that is when the observer is in the same medium as the scatterer or when the intensity distribution around the cell holding the scattering liquid is independent of the shape of the cell. Thus they would apply to a sphere with the scatterer at the center. For square or cylindrical cells appropriate correction factors must be applied (see below).

A further assumption is that the area of the diffuse reflector illuminated, and the volume of the liquid observed, are small compared with the distance to the aperture stop, A, of the photometer.

4. Correction Factors

It is very difficult, if not impossible, to eliminate experimentally all the complicating factors inherent in an absolute turbidity measurement made at 90°. Therefore it is necessary to introduce appropriate calculated corrections. The equations previously given are derived without regard to these factors, and indeed they have frequently been overlooked.

In this photometric method there are essentially four correction factors that must be applied caused by (1) the reflectance of the diffuse reflector, (r_f), (2) the greater sensitivity of the photo-multiplier tube to horizontally polarized light, (C_p), (3) the spreading of the light rays on leaving the cell containing the medium because of refractive index differences, (C_n), and (4) the difference in actual volume observed by the photometer and that defined by the apertures, (C_v).

The reflectance correction, r_f, has been mentioned previously. The polarization correction, (C_p), arises from a greater sensitivity of the photo-multiplier tube to horizontally polarized light than to vertically polarized light. This difference in our photo-multiplier tube varied from 7 to 12 percent depending on the size of the image on the cathode surface.

The refractive index correction, C_n, depends on the shape of the glass cell containing the liquid, and on the refractive indices of the medium which contains the scattering particles and the medium which contains the photometer.[6] The correction is apparent from a consideration of Fig. 2a. The diagram represents a top view of the rectangular scattering cell and photometer aperture A of width a enlarged for the purpose of the discussion. The scattering particle is located at point 0, a distance r from the aperture stop, A, of the photometer; r' is the distance from the particle to the outer edge of the cell.

If the liquid is of refractive index, n, and the observer is in air of refractive index unity, the light rays

[6] For a general discussion of this type of effect, see, for example, A. C. Hardy and F. H. Perrin, *The Principles of Optics* (McGraw-Hill Book Company, New York, 1932), page 411.

are refracted on leaving the liquid, and the flux the photometer actually collects is contained in the angle, Θ_1. Our previous formulas have been derived assuming no refraction, so that the photometer would collect the flux contained in the angle, Θ_2. The ratio of the quantities of flux in the two angles is, $(\Theta_2/\Theta_1)^2$, and represents the correction factor, C_n, which is found to be

$$C_n=(\Theta_2/\Theta_1)^2=n^2\left[1-\frac{r'(n-1)}{rn}\right]^2. \tag{14}$$

The volume correction, C_v, is indicated by Fig. 2b which represents a top view of the solution cell and aperture A of the photometer. A slightly greater volume, the excess volume, is seen by the photometer than that represented by the volume, V, defined by lwh. Aperture A defines the solid angle of scattered light observed from the scattering elements in the volume V, but it is apparent that this same solid angle does not apply for the elements in the excess volume. The solid angle for the latter decreases linearly as the elements approach the outer edge. Hence only one-half as much light per scattering element is picked up from the excess volume as compared to the volume V. The correction, C_v, is the ratio of the amount of light picked up from V to that from the actual volume and is found to be,

$$C_v=1-\frac{r'(a+l)/(r-r')}{2[nl+r'(a+l)/(r-r')]}. \tag{15}$$

The total correction is the product of the above four factors, r_f, C_ρ, C_v, C_n, for a cell with plane faces. The quantities r and r' in C_n and C_v may be taken to be the distances from the center of the beam to the photometer aperture and to the outer edge of the cell, respectively.

The validity of the refractive index correction was verified experimentally by observing the ratios of intensities of light scattered from spherical, cylindrical, and square cells filled with liquid where the scattered light originated from a scattering body at the center of the cells. The correction factor is unity in the case of the spherical cells, and $(C_n)^{\frac{1}{2}}$ for cylindrical ones. In all cases the agreement with theory was good. The volume correction was satisfactorily verified by observing the relative scattering from a given solution with l the only variable.

It should be noted that it is not necessary to correct for reflection at the face where the beam enters, as has been done in some instances, as the same fraction is reflected back through the liquid at the exit face and the reflections are self-compensating.

III. EXPERIMENTAL

1. Apparatus

The general design of the electronic circuit has been discussed previously.[7] The technique of balancing the circuit has been modified by introducing a twin triode and galvanometer type of synchronous detector in place of the magic eye of the original circuit. The detector is sensitive to the phase and the frequency of the signal from the photomultiplier and integrates over other frequencies and noise. The high sensitivity of the detector makes it possible to use an untuned amplifier with a gain of 5000–10,000 and thus eliminates the necessity of the twin-T feedback network of the original design. This detector makes possible more rapid and certain determination of the null point than is possible with the magic eye or oscilloscope tracing, and represents a definite improvement.

The photometer and optical system shown in Fig. 1 has the distinct advantage of flexibility, an absolute essential in experimental measurements of this nature. The projector optical system as previously described[7] is shown in Fig. 1a with a side view of the photometer assembly in Fig. 1b. An RCA 931A photo-multiplier tube was used throughout this work except for transmission measurements where the less sensitive RCA 929 photo-cell was required.

The light source, H, is a 100-watt medium-pressure mercury arc, General Electric type AH-4. The filters, F, for monochromatic light are a combination of Corning filters, No. 3389 and No. 5113 for the 4358A line of the Hg spectrum and No. 3484, No. 5120, and No. 4303 for the 5461A line of the Hg spectrum. The transmittances of these filters were measured with a monochromator and multiplier photo-cell and found to be less than 0.5 percent of the maximum at $\pm$50A for λ4358A and at $\pm$100A for λ5461A. The lamp is operated by 60 cycles per second current and the light has therefore a strong 120 cycles per second component which is measured by the electronic circuit.

The size and shape of diaphragm D may be readily adjusted. The lens, L, can be moved laterally on the optical bench and can be substituted by others different in diameter and focal length for variation of the position of the image of the secondary source, D, and to vary the convergence of the beam.

The optical bench which supports the projector system and the photometer assembly is 2 meters long. The assembly may be changed as desired to obtain the optimum position for the experiment in question and for making absorption and integrating sphere measurements.

The photometer assembly, Fig. 1b, is adjustable and mounted on the rod U. The distance of the photomultiplier housing from the center of the table 0 can be varied as desired and the housing can be rotated around the axis of U and revolved around the table 0 on a bearing at V. The table is graduated showing the angle of observation.

Scattered light from a cell mounted on the center of the table is received by the objective lens R, and an image of the cell is focused on the rectangular diaphragm at S. The lens S forms an image of the diaphragm A on

[7] B. H. Zimm, J. Chem. Phys. 16, 1099 (1948).

the cathode of the photo-multiplier tube, *PM*. The diaphragm at *S* serves as a field stop for the system for elimination of stray light, and the diaphragm *A* is the aperature stop determining the solid angle of light received from the scattering solution. The lenses at *S* and *R* and the stops are readily removed for variation in design.

The use of the diaphragm and lens at *S* insures that the image on the photo-multiplier cathode remains constant in size, shape, and uniformity of illumination as the photometer is moved or as the shape and size of the scattering object is changed. This is an important consideration as the photo-cathode varies in sensitivity over its surface, and when a solution in the cell, Fig. 1c, is replaced by a reflectance standard, the sensitivity would be different if this feature were not present.

2. Filters

Reduction of the incident light a known fraction by filters is another rather difficult problem. It was found that photographic plates, wire screens, and color filters were unsatisfactory and not reproducible, although reproducibly positioned in the beam, apparently because of large scattering by the filters.

A grey solution was finally used and was very satisfactory. It was a water solution composed of nickel sulfate heptahydrate, potassium chromium alum, and cobalt sulfate hexahydrate in weight ratios of 5.3: 1.23:1.0. The final technique was to use four glass cells with optically clear and parallel faces 1 cm apart. Each cell filled with solution transmitted about 27 percent. The calibration was made at the time of measurement by observing a reading of the photometer with the cell successively in and out of the light beam when the photometer was collecting the light scattered from the $MgCO_3$. The ratio of the two readings gave the fractional reduction of the beam due to the particular cell and solution, and reflections between faces of the cells were automatically considered.

3. Cells

Another factor of some importance is the use of containers with minimum background light when measuring small scattering. Extraneous light in the pure liquid measurements was minimized by using a Rayleigh type horn or cross (Bhagavantam,[2] p. 48). The cross has the advantage of a perfectly black background against which the scattered light is observed. Optically clear, flat, Pyrex faces were fused on the horn to form a flat surface for the incident light to enter and for the scattered light to leave. A mixture of red lead and Bakelite also serves very well for sealing on glass faces and is insoluble in most organic compounds after baking. It was also found that rectangular glass cells, inner dimensions 1×5×5 cm, were quite satisfactory in most cases if due regard was given to providing a black background and masking out stray radiation from the incident light by appropriate shields. This type of cell was used generally for measurements of solutions.

TABLE I. Relative intensity values of light scattered from $MgCO_3$ as a function of α, the angle of reflection. (*V*-vertically polarized, *H*-horizontally polarized, *U*-unpolarized incident light.)

α	cosα	*U*	*V*	*H*	*V*+*H*	Harrison
25°	0.906	0.926	0.902	0.938	0.920	0.910
15°	0.966	0.990	0.978	1.00	0.989	0.974
5°	0.996	1.00	1.00	1.01	1.00	1.00
0°	1.00	1.00	1.00	1.00	1.00	1.00
5°	0.996	0.996	1.00	0.987	0.994	0.995
15°	0.966	0.965	0.970	0.941	0.957	0.952
25°	0.906	0.899	0.920	0.872	0.897	0.902
35°	0.819	0.812	0.837	0.775	0.806	0.815
45°	0.707	0.714	0.745	0.671	0.707	0.702
55°	0.573	0.561	0.594	0.530	0.562	0.572
65°	0.423	0.409	0.438	0.378	0.408	0.419
75°	0.259	0.254	0.264	0.227	0.246	0.250
85°	0.087	0.10	0.100	0.090	0.095	

4. Materials

The liquids were repeatedly distilled into the cell from an all-glass still until no dust particles could be seen by low angle scattering. Measurements were made at 25°C and 30°C after the liquids had come to the temperature of a thermostated dark room.

The benzene measured was Baker's reagent meeting A.C.S. specifications and was twice crystallized by successively freezing out about one third of the original amount. The solidifying temperature was 5.2°C. Carbon tetrachloride was purified as described by L. E. Fieser, *Experiments in Organic Chemistry*, and had a constant boiling point of 76.6°C (corr.)(lit. 76.7). This procedure includes shaking the carbon tetrachloride with a mixture of concentrated potassium hydroxide solution and alcohol, and then washing with water and finally treating with concentrated sulfuric acid. After drying over calcium chloride it is finally distilled.

The sucrose octaacetate used in the molecular weight determinations was recrystallized four times out of ethanol. The dibenzyl was purified by distilling in vacuum and twice recrystallizing from ethanol giving the previously reported melting point, 51–52°C.

The solutions were filtered through an asbestos filter pad that had been impregnated with Bakelite and baked. Centrifugation at 15,000 times gravity was used when necessary. Solvents were treated in the same manner as the solutions. Solutions were transferred to the cell either by directly filtering into the scattering cell or by successively adding, with a dust-free pipette, known amounts of a stock solution to a measured amount of solvent in the scattering cell and stirring with a dust-free glass stirrer.

Several solutions of high scattering power and negligible depolarization were made by dissolving a commercial polystyrene in butanone, dichlorethane, or toluene. The polystyrene was a sample of Dow Styron furnished us by Drs. Debye and Bueche of Cornell

TABLE II. Excess turbidities at λ5461A.

Sample	Transverse scattering	Transmission	Integrating sphere
1	13.0×10^{-3}	13.3×10^{-3}	12.2×10^{-3}
2	12.1×10^{-3}	12.0×10^{-3}	12.7×10^{-3}
3	13.9×10^{-3}	13.7×10^{-3}	14.1×10^{-3}
4	10.5×10^{-3}	10.8×10^{-3}	—
5 ($Et\,Cl_2$)	2.78×10^{-3}	2.76×10^{-3}	—

TABLE III. Excess turbidities at 4358A.

Sample	Transverse scattering	Transmission
4	28.5×10^{-3}	29.1×10^{-3}
5 ($Et\,Cl_2$)	8.61×10^{-3}	8.85×10^{-3}

University, and which has been used as a standard material in several laboratories.

5. Diffuse Reflectors

The substances which have been the subject of the most study as diffuse reflectors have been magnesium oxide and magnesium carbonate. These are particularly suitable because of their high reflectance and the ease of forming smooth, clean surfaces. MgO from the burning metal can be smoked on a metal or plaster of paris surface to a depth of 1 or 2 millimeters. Any smaller depth results in some loss of light because of the transparency of MgO. Blocks of $MgCO_3$ may be purchased and a smooth surface formed by scraping with a clean straight edge.

Since the determination of absolute turbidity depends on the reflectance of $MgCO_3$ or MgO, and their conformity to Lambert's "cosine law," it is important that these factors be investigated before applying Eq. (12b).

Reflectance of a substance is ordinarily determined by collecting all the light scattered from the surface in an integrating sphere. The reflectance obtained in this manner is called the total reflectance. In this work, the angle of incidence and the angle of observation are 45°. If Lambert's "cosine law" is not obeyed, the light scattered at 45° may not be the same as would be calculated from the total reflectance.

Benford, Schwartz, and Lloyd[8] by an absolute method have recently found the total reflectance of $MgCO_3$ and MgO to be 0.965 and 0.982 at λ4358A and 0.980 and 0.989 at λ5461A, respectively, and V. C. W. Harrison[9] has shown that the intensity distribution of reflected light from a MgO surface follows the "cosine law" with light of 45° incidence. Harrison, however, measured the intensity distribution in one plane only.

In Table I are the results of both Harrison's and our measurements of the scattering in the plane normal to the surface and containing the incident beam, with the incident beam at 45° to the surface. Measurements on the different components of polarization of the scattered light are included. It can be seen that there is some deviation from the cosine law but that the deviation is small for the total scattering except at a few angles not actually used in subsequent experiments. There is some polarization of the scattered light, however.

Measurements were also made at various angles in the vertical plane, i.e., the plane normal to the surface and normal to the plane containing the incident beam and the normal to the surface. No significant deviations from the cosine law were found here.

Therefore, it would seem that the intensity of the light scattered at 45° from $MgCO_3$ illuminated at 45° can be safely computed from the total reflectance. This conclusion was checked by a number of direct measurements of the scattering from $MgCO_3$ and MgO made with different photometer arrangements and using Eq. (13). While the precision of these measurements was not high, the results were reproducible and inspired confidence in the photometric technique.

6. Measurements of Turbidity

For the determination of turbidity by transmission, two cells, five, and ten centimeters in length, with optically clear and parallel faces were used. A small integrating sphere (prepared as described below) with an RCA 929 photo-cell was used as a photometer, since this arrangement is relatively insensitive to small displacements of the beam due to the cells. Successive readings were made on both the solution and solvent with the cell in and out of the incident beam. Corrections were made for the effect of solvent and reflections at the interfaces, and the excess turbidity determined by Eq. (7).

For the integrating sphere method, a sphere with a 13.5 cm inner diameter was used. It was made by forming a two-piece plaster of paris cast around a one liter spherical flask. The inner surface of the plaster was painted with a ZnO collodion paint and smoked with MgO by burning metallic magnesium, giving a very smooth white surface.

Three holes of approximately 1 cm diameter were cut in the sphere. Two holes were cut opposite to each other to permit the incident light to pass in and out through the center of the sphere. The third hole in the horizontal plane and at an angle of 90° to the first two was adapted for the photo-multiplier tube, which could view the opposite wall of the sphere.

A pedestal, of minimum possible surface area, was placed near the exit of the sphere to support the solution cell. A small shield was placed to protect the photo-multiplier tube from observing the directly scattered rays. For the incident beam measurement a $MgCO_3$ plug was placed in the exit hole. The incident light had to be attenuated about 70 percent while it was being measured to make the photometer readings comparable.

[8] Benford, Schwartz, and Lloyd, J. Opt. Soc. Am. **38**, 445, 964 (1948).
[9] V. C. W. Harrison, Phys. Soc. London **58**, 408 (1946).

This was done by using a 1 cm cell of the grey solution mentioned above.

Variations in the method included using a cone of $MgCO_3$ with its vertex directly in the beam for the incident light measurement. The cone was the same size as the cell and was placed on the pedestal in the same position as the cell. Convex and concave surfaces were also used. All gave results agreeing within two percent.

The solution cell was cylindrical, of clear glass, 2 cm long, with a diameter of about 1.5 cm, and with plane end windows. The photometer reading for the solvent was subtracted from the solution reading to obtain the turbidity due to the solute only by Eq. (8). Another pedestal was made later and placed in the center of the sphere (instead of off center) with results agreeing within five percent of the other measurements.

A correction of about three percent had to be applied due to the increase in the efficiency of the sphere when the $MgCO_3$ plug was placed in the exit hole for the direct beam measurement.

This method, although the least accurate of the three, certainly gave results consistent to six or seven percent and the average of a series of measurements was reproducible.

The transverse scattering measurements were made using the method previously described, Eq. (12b), and as shown in Fig. 1c, position I. The field stop of the photometer was adjusted to minimum size to eliminate stray reflections. Measurements were made of the solution and $MgCO_3$ successively and a blank due to solvent and cell was subtracted to give the excess turbidity due to solute alone. The solution was contained in a rectangular cell with optically clear parallel faces and sides, and of inner dimensions $5\times5\times1$ cm. The calculated correction factors were $r_f=0.96$, $C_n=1.81$, $C_v=0.95$, and $C_p=1.05$. Appropriate dimensions were $r=7.75$ cm, $r'=0.65$ cm, $l=1.075$ cm, $a=0.8$ cm. Table II shows the results of the three methods for a number of polystyrene butanone solutions of about one percent concentration. Sample 5 is a dichlorethane solution of polystyrene. The incident light was unpolarized and of wave-length 5461A in vacuum.

Slightly more difficulty was encountered with light of λ4358A. The butanone, which was the purest available and had a boiling point 79.0°–80.0° (lit. 79.6) absorbed about 2 percent of the light per centimeter and thus invalidated the transverse measurements when 5 cm cells were used unless a rather uncertain correction was applied. This was partially circumvented by using a small square cell made from 13-mm square tubing. A one percent solution of polystyrene in dichlorethane (sample 5) was also prepared for these measurements (Table III).

Sample 4 was measured in the small square cell made from 13-mm square tubing at both wave-lengths and also in the "horn" that was prepared to measure the scattering from pure liquids. The two measurements agreed well. Sample 4 was a 0.75 g per 100 cc butanone solution of the Dow polystyrene furnished by Debye and Bueche.

TABLE IV. Comparison of dn/dt and $(\alpha/\beta)(dn/dp)$.

	$\alpha\times10^3$	$-\beta\times10^6$ (atm^{-1})	dn/dp $\times10^6$	$-(\alpha/\beta)(dn/dp)$ $\times10^3$	dn/dt $\times10^3$(exp)
Benzene	1.202	91.2	49.0	64.8	63
Carbon disulfide	1.175	96.4	63.9	78	78
Methanol	1.217	119.7	40.4	41	39
Toluene	1.095	88.0	46.5	58	60
Chloroform	1.260	96.9	47.3	61.5	59
Water	0.207	46.45	15.1	6.7	9

IV. PURE LIQUIDS

With the absolute scattering power of several solutions of the Dow Styron sample known, it was then an easy matter to determine by comparison the scattering powers of several other liquids and solutions of more general interest. The first such determinations were done for carbon tetrachloride and benzene in order to investigate the validity of the theoretical Eq. (3). The materials were contained in a Rayleigh "horn" for the measurements and the correction factors discussed above were all applied.

Rayleigh's ratios of pure liquids have been measured directly by Martin and Lehrman[10] (ether), and Peyrot[11] (benzene). Indirect measurements have been made by Cabannes and Daure[12] who investigated benzene by comparing with ethyl chloride gas, and Bai[13] who has compared carbon disulfide with oxygen. Blaker, Badger, and Gilman[14] in a direct measurement of carbon disulfide scattering attempted to eliminate the corrections by using porcelain suspended in carbon disulfide as a standard.

Brice and Speiser[15] have used opal glass as a standard and have determined the Rayleigh's ratio of benzene. We understand, however, that this work is under reinvestigation.[16]

Many of the investigators have attempted to compare their experimental results to Einstein's equation by assuming an expression relating refractive index to density, $f(n)=\rho\times$(constant), where ρ is the density. Bhagavantam has summarized this work with the conclusions that the Maxwell relation, $f(n)=(n^2-1)$, is correct in preference to the Lorentz-Lorenz relation, $f(n)=(n^2-1)/(n^2+2)$. Ramanathan[3] has justified the use of the Maxwell relation by assuming that the properties of the medium surrounding the small volume element used in fluctuation theory are not related to the fluctuations in the element.

[10] W. Martin, S. Lehrman, J. Phys. Chem. **26**, 75 (1922).
[11] P. Peyrot, Comptes Rendus **184**, 1512 (1936); Ann. de physique **9**, 335 (1930).
[12] J. Cabannes, P. Daure, Comptes Rendus **184**, 520 (1927).
[13] S. Bai, Proc. Ind. Acad. Sci. **15**, 357 (1942).
[14] Blaker, Badger, and Gilman, J. Phys. Coll. Chem. **53**, 794 (1949).
[15] B. A. Brice, R. Speiser, J. Opt. Soc. Am. **34**, 364 (1946).
[16] Private communication from B. A. Brice.

TABLE V. Comparison of experimental $(\rho ndn/d\rho)^2$ with theoretical and empirical relations.

Liquid	n	$(\rho ndn/d\rho)^2$	Maxwell	Lorentz-Lorenz	Gladstone-Dale	Eykman
Benzene	1.5044	0.62	0.398	0.80	0.575	0.655
Carbon tetrachloride	1.4631	0.448	0.325	0.618	0.455	0.52
Carbon disulfide	1.6319	1.175	0.69	1.66	1.06	1.23
Methanol	1.3307	0.183	0.148	0.235	0.192	0.215
Toluene	1.4999	0.675	0.39	0.785	0.563	0.64
Chloroform	1.4486	0.46	0.298	0.56	0.423	0.47
Water (20°)	1.3330	0.185	0.195	0.245	0.209	0.234

TABLE VI. Calculation of Avogadro's number (6.03×10^{23}).

Liquid	$-\beta\times10^{12}$ (dyne^{-1})	T, °K	λ_0(A)	n	$[(ndn/dt)/\alpha]^2$	$S_u\times10^6$	ρ_u	Av. no.
Carbon tetrachloride	112	303	5460	1.4575	0.43	5.88	0.050	5.77×10^{23}
Carbon tetrachloride	112	303	4358	1.4709	0.457	15.8	0.050	5.62×10^{23}
Benzene	101	303	5460	1.4985	0.625	16.95	0.40	6.20×10^{23}
Benzene	101	303	4358	1.5203	0.685	49.5	0.41	5.85×10^{23}

TABLE VII. Absolute scattering powers of some materials.

Material	Wavelength	Temperature	$S_u\times10^6$	τ
0.75 percent Dow Styron in butanone*	4358A	25°C	1720	0.0288
	5461A	25°C	632	0.0106
1.00 percent Dow Styron in dichlorethane*	4358A	25°C	522	0.00873
	5461A	25°C	165	0.00277
0.5 percent Dow Styron in toluene*	4358A	25°C	208	0.00348
Benzene	4358A	25°C	48.5	—
	5461A	25°C	16.3	—
	4358A	30°C	49.5	—
	5461A	30°C	16.9	—
Carbon tetrachloride	4358A	30°C	15.8	—
	5461A	30°C	5.88	—

* "Excess" scattering of solution, i.e., scattering of solution less scattering of solvent.

It is known that neither the Lorentz-Lorenz nor the Maxwell expressions adequately represent the relation between the refractive index and the density of a liquid. The Gladstone-Dale relation, $f(n)=(n-1)$, and Eykman relation, $f(n)=(n^2-1)/(n-0.4)$, have also been used. The latter applies particularly well to benzene while the former has been shown to be applicable to many solutions.

The validity of such relations can be determined by comparison with experimental quantities. The relation between $dn/d\rho$ in Eq. (3) and dn/dt, an experimentally determined quantity, can be represented very closely by the equation,

$$\rho n(dn/d\rho)=(n/\alpha)(dn/dt),$$

where α is the coefficient of thermal expansion and dn/dt is the derivative of the refractive index with respect to temperature. The use of the dn/dt values can be supported by comparing with dn/dp data through the relation,

$$dn/dt=-(\alpha/\beta)(dn/dp),$$

where β is the isothermal compressibility and dn/dp is the derivative of the refractive index with respect to pressure. Such a comparison is shown in Table IV as an example of the reproducibility of the dn/dt and dn/dp data taken from the literature. All data were taken at a temperature of 15°C and refractive index quantities are for light of wave-length 5893A in vacuum. Table V shows a comparison of $(\rho ndn/d\rho)^2$, the factor that enters Einstein's Eq. (3), for a few liquids as determined experimentally and as calculated from the various relations. The experimental conditions are the same as for Table IV.

The isothermal compressibilities are those given by Freyer, Hubbard, and Andrews[17] determined from the velocity of sound in the various media. These agree well with the results of Tyrer[18] determined by another method.

The coefficients of expansion were obtained also from the work of Freyer, Hubbard, and Andrews[17] who give data for the density and dv/dt, where v is the specific volume. These values agree generally within 0.5 percent with those given in the *Handbook of Chemistry and Physics*. The dn/dp data were taken from the work of several investigators including F. Himstedt and I. Wertheimer,[19] I. Eisele,[20] and W. C. Rontgen and L. Zehnder.[21] The dn/dt values are those given by Timmermans[22] and co-workers.

As seen from Table V the Gladstone-Dale and Eykman expressions agree with experiment much better than the theoretical equations. The closest correspondence is obtained with the Gladstone-Dale equation for carbon tetrachloride and is within the experimental error of the dn/dt value made with a Pulfrich refractometer.

The use of Maxwell's relation would result in large errors for any of the liquids examined, and its application to the light scattering equation, in addition to the experimental errors in determining reduced intensities, is apparently one reason for the large discrepancies between previous experiments and the theory.

The depolarization of carbon tetrachloride is 0.05 $\pm$0.005 and thus the error in correcting for this factor is not greater than two percent. Benzene on the other hand has a large depolarization but has been investigated by other workers and would make a convenient standard in calibrating light scattering instruments.

The depolarization was found by measuring the scattered light successively with vertically and horizontally polarized incident light and applying a correction for the greater sensitivity of the photo-multiplier tube to horizontally polarized light.

[17] Freyer, Hubbard, and Andrews, J. Am. Chem. Soc., **51**, 759 (1929).
[18] D. Tyrer, J. Chem. Soc. **105**, 2534 (1914).
[19] F. Himstedt and I. Wertheimer, Ann. d. Physik **47**, 395 (1922).
[20] I. Eisele, Ann. d. Physik **76**, 396 (1925).
[21] W. C. Rontgen and L. Zehnder, Ann. d. Physik **44**, 24 (1891).
[22] J. Timmermans and F. J. Martin, J. Chim. Phys. **27**, 747 (1926); **25**, 411 (1928); **27**, 401 (1930).

The results of the measurements are shown in Table VI. Following tradition, we compare theory and experiment by calculating Avogadro's number from the experimental results and Einstein's equation.

The refractive indices were obtained from the International Critical Tables. Corrections to 30°C and the desired wave-lengths were made with the dn/dt values and the dispersions given in those tables.

The most questionable experimental quantity is dn/dt. For carbon tetrachloride the values used were 55×10^{-5} and 56×10^{-5} at 5461A and 4358A respectively as determined by Timmermans and Martin at 15°C. Those for benzene were 65×10^{-5} and 67×10^{-5} for the same wave-lengths. If the Gladstone-Dale relation is used to calculate the quantity $(ndn/dt/\alpha)^2$ at 30°C for carbon tetrachloride, one gets 0.445 instead of 0.43 at a wave-length of 5461A and 0.48 instead of 0.457 at 4358A or an increase of 3.5 and 5 percent respectively which is the estimated experimental error of $(dn/dt)^2$. The light scattering measurements are felt to be accurate to five percent.

As shown in Table VI, Avogadro's number obtained is 5.77×10^{23} and 5.62×10^{23} for light of wave-length 5461A and 4358A respectively. Use of the Gladstone-Dale relation for dn/dt would give 5.97×10^{23} and 5.9×10^{23}. The comparison of the values for the two wave-lengths is felt to be very satisfactory considering the number of possible sources of error in the experimental procedure.

The values for benzene are not as reliable because of the large depolarization correction factor. The depolarization of 0.40 and 0.41 for light of λ5461A and λ4358A, respectively, compares well with that found by Raman and Rao.[23] The difference in the values 6.20×10^{23} and 5.85×10^{23} for the wave-lengths 5461A and 4358A could very easily be caused by an error in the depolarization.

The values of Rayleigh's ratio found in this research are somewhat higher than those previously obtained. The values for benzene at 25° for example are 16.3×10^{-6} and 48.4×10^{-6} at 5461A and 4358A respectively. These compare with Cabannes and Daure's value[12] of 11.2×10^{-6} at 5461A and Peyrot's value[11] of 34.8×10^{-6} at 4358A. The difference is undoubtedly due to the corrections for the optics of the instruments as well as to the intrinsic difficulty of measuring scattering intensities that are only 10^{-6} of the intensity of the incident light.

For the convenience of other investigators our measurements of the turbidities and Rayleigh ratios of several easily obtained materials are given in Table VII.

V. MOLECULAR WEIGHTS

The molecular weights of dibenzyl and sucrose octaacetate were determined, the former dissolved in 1,2-dichlorethane and butanone and the latter in methanol. Light of wave-length 5461A was used for the dibenzyl solutions while two wave-lengths, 5461A and 4358A, were used for the sucrose octaacetate solutions. The molecular weights were determined from the values of Kc/S extrapolated to zero concentration using Eqs. (4) and (5), and were corrected for depolarization by the Cabannes factor corresponding to zero concentration.

[23] C. V. Raman and K. S. Rao, Phil. Mag. **45**, 625 (1923).

TABLE VIII. Molecular weight and depolarization of dibenzyl ($M=182$) in 1,2-dichlorethane and butanone with vertically polarized and unpolarized incident light at 5461A.

	1,2-dichlorethane		butanone	
	vertical	unpolarized	vertical	unpolarized
$(Kc/S)\times10^3(\lim c\to0)$	3.88	3.05	4.18	3.77
Depolarization, ρ $(\lim c\to0)$	0.15	0.26	0.105	0.14
Molecular weight	184	181	186	195
dn/dc	0.141		0.205	

TABLE IX. Molecular weight of sucrose octaacetate ($M=678$) in methanol with light of wave-length 5461A and 4358A.

	5461A	4358A
$(Kc/S)\times10^4(\lim c\to0)$	14.20	14.60
Depolarization, ρ_u	0.02	0.02
Molecular weight	677	660
dn/dc	0.114	0.114

TABLE X. Representative values of Kc/S and depolarization for four concentrations of dibenzyl in 1,2-dichlorethane with vertically polarized and unpolarized incident light at 5461A.

Conc. (g/ml)	0.0812	0.1625	0.217	0.325
$(Kc/S)\times10^3$ (unp)	3.53	3.94	4.38	4.96
Depolarization (unp)	0.290	0.328	0.350	0.390
$(Kc/S)\times10^3$ (vert)	4.62	5.10	6.06	6.83
Depolarization (vert)	0.185	0.230	0.242	0.295

Measurements of the dibenzyl solutions were made with both vertically polarized and unpolarized incident light. Vertically polarized light was used to reduce the effect of any fluorescence which was noticed to be considerable in unpurified dibenzyl solutions but seemed negligible after purification.

Tables VIII and IX show the results of these measurements. Table X contains the Kc/S values and the depolarizations for four concentrations of dibenzyl in 1,2-dichlorethane. The small scattering of the dibenzyl solutions, the long extrapolations to infinite dilution, the uncertainty of the dn/dc values determined with a Pulfrich refractometer, and the large depolarization correction do not allow better than 20 percent accuracy.

Figure 3 contains Kc/S *versus* concentration for the sucrose octaacetate solutions. As indicated in Table IX, the molecular weight was found to be 677 and 660, compared to the formula weight, 678, using light of wave-lengths 5461A and 4358A respectively. These measurements are felt to be accurate to plus or minus five percent. The dn/dc value is that given by Brice[17] for light of wave-length 4358A. It was also used for light of 5461A as little dispersion was to be expected.

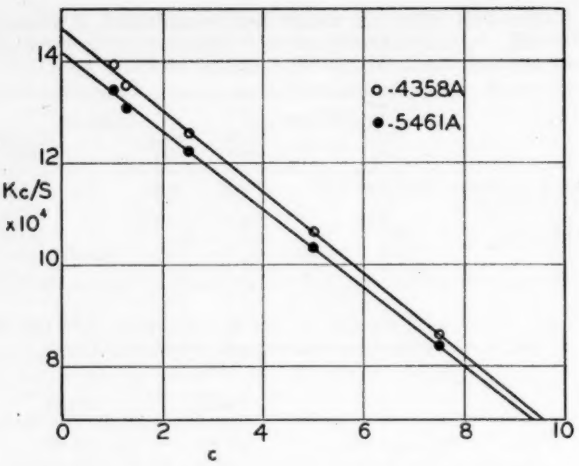

FIG. 3. Kc/S against concentration for sucrose octaacetate in methanol at two wave-lengths.

VI. DISCUSSION OF DESIGN

It is evident that a light scattering technique must be carefully examined for experimental errors which may not be immediately apparent. Therefore, it is appropriate to mention some precautions which we have found important.

The fundamental requirements of an instrument are (1) a linear measuring system, (2) a constant intensity light source or a compensating photo-cell as used in our apparatus, and (3) a flexible photometric assembly of appropriate design to minimize the sources of error. The first two have been satisfactorily obtained, but the last is more difficult and the following precautions may be mentioned:

1. Appropriate shields should be introduced to eliminate extraneous light and surfaces should be blackened to reduce background reflections. The effect of background may be estimated by observing the light scattered at 90° from a liquid of small known depolarization with horizontally and vertically polarized incident light successively.

2. It seems impossible to eliminate satisfactorily the refractive index correction, C_n, without using spherical cells or having the photometer aperture stop directly against the side of the cell; either method would introduce other complications. To determine this correction accurately it is necessary to have a well-defined aperture stop in the photometer and to know its position. It must be noted that C_n must be introduced even when measurements of one liquid relative to another are made.

3. The volume correction is negligible when comparing the relative scattering from liquids, but may be appreciable for an absolute measurement. It requires a knowledge of the dimensions of the volume of liquid and of the aperture stop. These dimensions must therefore be well defined. The correction can be minimized by adjustment of the dimensions of the photometer.

4. The sensitivity of the photo-multiplier to the polarization of light may be eliminated by introducing a depolarizer, however, the light intensity may also be considerably reduced which decreases the ability of the instrument to measure small scattering.

There are many other minor factors to consider, but the above are of primary importance in design.

The Small-Angle Scattering of X-Rays by Nitrogen*

ROBERT L. WILD†
Department of Physics, University of Missouri, Columbia, Missouri
(Received August 7, 1950)

An experimental study has been made of the scattering of x-rays by nitrogen at various pressures and temperatures in the general region of the critical point. Particular attention was given to the scattering at small angles. Copper $K\alpha$-radiation used with a single-crystal spectrometer and narrow slits provided the means of attaining low values of $\sin\theta/\lambda$ where 2θ is the scattering angle and λ the wave-length of radiation. A qualitative demonstration of the effect of pressure and temperature upon the small-angle scattering from a fixed volume of sample was made by observing at a fixed angle the amount of scattering from the sample as it was made to approach and then cross the liquid-vapor transition curve. At 29 selected conditions of pressure and temperature, more complete patterns were taken in an attempt to make a quantitative application of theoretical expressions to obtain values of the isothermal compressibility and the sizes of regions of inhomogeneity which give rise to the small-angle scattering. Values of compressibility from this work are roughly comparable to those obtained by other methods. The regions of inhomogeneity are found to be small at low temperatures, and they increase in size as the P—T conditions approach the critical region. Typical values for the radii of the regions of inhomogeneity are found to be 3.8A at 115°K and 18.7 atmospheres, and 8.1A at 128°K and 36.8 atmospheres.

I. INTRODUCTION

INFORMATION concerning atomic distributions in amorphous materials has long been obtained from the analysis of the x-ray scattering patterns. Following the method of Zernike and Prins,[1] as modified by Debye and Menke,[2] a Fourier inversion of the scattering pattern yields an atomic distribution curve which describes the average atomic environment about any given atom. Considerable work has been done on elements in the liquid state[3] for which the theory is the most exact and requires the fewest approximations. Most of the work has been done with well-defined liquids, but several attempts have been made to study the effect on the scattering patterns of varying the pressure and temperature over selected ranges. Ether[4] and isopentane[5] were studied in the general region of the critical point primarily for the change in position of the first liquid peak. It was found[6] that the results could be explained in a semi-quantitative way by the utilization of an approximate theory developed by Debye.[7] Harvey[8] studied the scattering pattern of nitrogen gas at room temperature and under pressures up to 100 atmospheres over a small angular range not exceeding 15 degrees. He also compared his work with Debye's theory and showed systematic deviations of the observed scattering curves from the scattering of independent molecules. The most complete study of this kind was made by Eisenstein and Gingrich[9] with argon at 26 different combinations of temperature and pressure. One incidental observation in this work disclosed the existence of unusually large scattering at very small angles from the fluid, particularly in the critical region. This small-angle scattering was not observed in the fluid near the triple point, but it became progressively larger as the fluid approached the critical temperature and pressure.

Small-angle scattering of x-rays has been observed by many workers in the case of solids which are in a finely divided state. A considerable collection of theory exists[10] for interpreting this small-angle scattering as being due primarily to diffraction at the boundaries of the particles, very much as in the case of the diffraction of light. In a perfectly homogeneous material of infinite extent there would be no effect of this kind. It is therefore reasonable to suppose that this small-angle scattering of x-rays from liquids arises from inhomogeneities in the density of scattering material. Since this scattering takes place at small-angles it is likely to be due to relatively large aggregates of scattering material. This problem was attacked theoretically in 1948 by Vineyard[11] who made a detailed analysis of the scattering from amorphous materials. From this analysis an expression was found that can be used to determine the extent of the inhomogeneities that are necessary to account for the observed small-angle scattering.

Since the previous work on nitrogen has been either

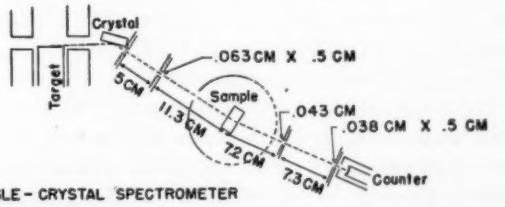

FIG. 1. Showing experimental arrangement and slit system.

* Extracted from a dissertation submitted to the University of Missouri in partial fulfillment of the requirements for the Ph.D. degree.

† Present address, Department of Physics, University of North Dakota, Grand Forks, North Dakota.

[1] F. Zernike and J. Prins, Zeits. f. Physik **41**, 184 (1927).
[2] P. Debye and H. Menke. Ergeb. Tech. Rontgenk. II (1931).
[3] N. S. Gingrich, Rev. Mod. Phys. **15**, 90 (1943).
[4] G. W. Stewart, Trans. Faraday Soc. **29**, No. 148, 982 (1933).
[5] C. A. Benz and G. W. Stewart, Phys. Rev. **46**, 703 (1934).
[6] N. S. Gingrich and B. E. Warren, Phys. Rev. **46**, 248 (1934).
[7] P. Debye, J. Math. and Phys. **4**, 133 (1925).
[8] G. G. Harvey, Phys. Rev. **46**, 441 (1939).
[9] A. Eisenstein and N. S. Gingrich, Phys. Rev. **62**, 261 (1942).
[10] A. Guinier, *Radiocrystallographie* (Dunod, Paris, France 1945), Chapter XII.
[11] G. H. Vineyard, Phys. Rev. **74**, 1076 (1948).

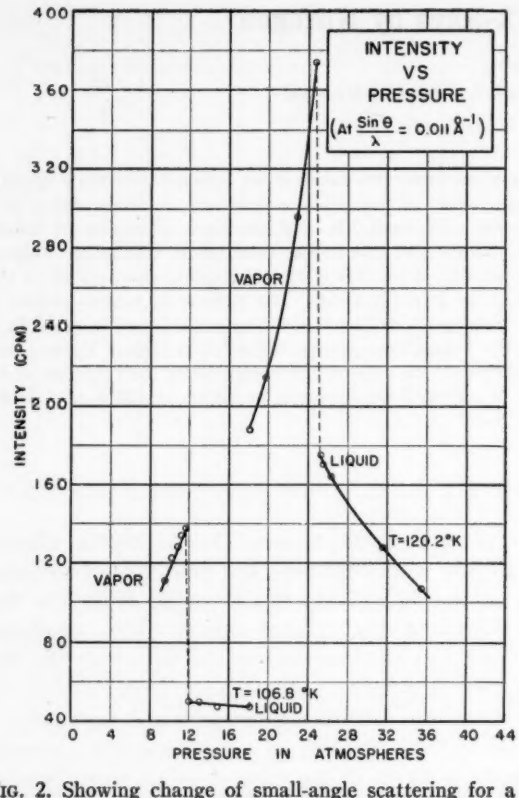

FIG. 2. Showing change of small-angle scattering for a fixed volume of sample at a fixed temperature and a fixed scattering angle as the liquid-vapor transition is crossed.

with a well-defined liquid[12, 13] or with a permanent gas[8, 14] which was far from the critical temperature, this investigation was undertaken to provide data on the small-angle scattering of x-rays from nitrogen in the general region of the critical point in order to verify the phenomena as observed incidentally in the study on argon and to yield, on analysis, some quantitative knowledge of the change in structure or molecular arrangement as a substance changes from liquid to vapor.

II. EXPERIMENTAL

Full-wave rectified voltage and current of 40 kv and 12 ma, respectively, were supplied to a Machlett type *A*-2 copper-target diffraction tube equipped with beryllium windows at the x-ray port. X-rays from the target were monochromatized by reflecting the copper $K\alpha$-wave-length from a rock salt crystal. The experimental arrangement for collimating and detecting the radiation is indicated schematically in Fig. 1.

The nitrogen cell, which was perpendicular to the main beam, consisted of a 5-mm square hole in a brass block 3.44 mm thick, with beryllium windows of thicknesses 0.66 and 0.56 mm sealed by indium gaskets to the x-ray entrance and exit ports, respectively. The upper part of the brass sample block was threaded to hold a heating coil for use in controlling the temperature, and a copper-constantan thermocouple for measuring the temperature was soldered as close to the nitrogen cell as possible. The cell assembly was suspended by 3 screws from the bottom of a metal liquid-air Dewar inside a vacuum "camera." The experimental arrangement was essentially the same as that pictured in the aforementioned article.[9]

The oil-pumped nitrogen gas of 99.6 percent purity was brought to the sample cell by a 10-ft length of small Super-Nickel tubing. Pressure was established by a dead-weight pressure gauge, in which continuous rocking of the weights prevented binding of the piston. The limit of accuracy on the measurement of the pressure was 0.1 atmosphere although the variation of pressure was believed to be considerably less than this over the time required to make a run.

The copper-constantan thermocouple, which was compared with a standard thermocouple previously calibrated by the Bureau of Standards, was used both to measure the temperature and to activate the device[15] for controlling the temperature. In the determination of the temperature, it was found necessary to evaluate a small horizontal thermal gradient in the sample cell. This was done by holding the temperature at some fixed value, increasing the pressure in increments of 0.3 atmosphere, and noting by x-ray absorption measurements just where the liquid-vapor line was crossed. With all variations taken into account, it is believed that the temperature was known to within 0.4°K.

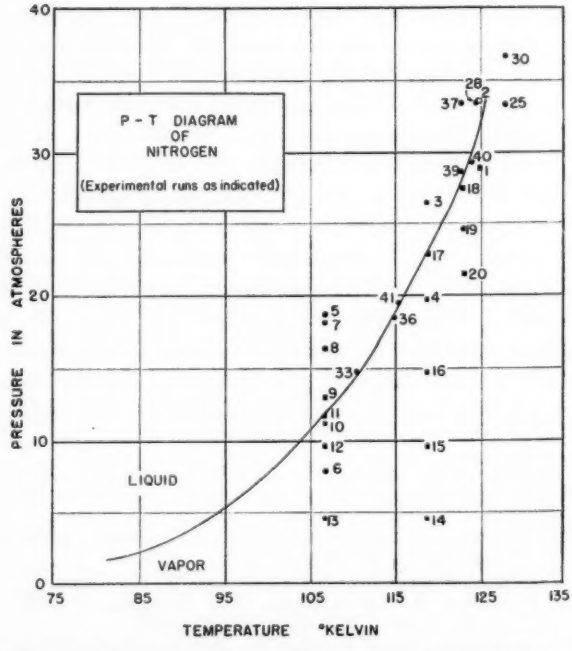

FIG. 3. Pressure-temperature diagram for nitrogen with boxed in datum points referring to small-angle scattering only and circled datum points referring to complete diffraction patterns.

[12] W. A. Keesom and J. de Smedt, Proc. Amst. Akad. Sci. **26**, 112 (1923).
[13] P. C. Sharrah, J. Chem. Phys. **11**, 435 (1943).
[14] E. O. Wollan, Phys. Rev. **37**, 862 (1931).
[15] R. M. Zabel and R. R. Hancox, Rev. Sci. Inst. **5**, 28 (1934).

The x-rays were detected by a Geiger counter, designed especially for soft x-rays, mounted on the spectrometer arm. The amplified pulses were counted and recorded by a conventional scale-of-sixteen coupled to a mechanical counter. With the narrow slit system used, the scattering pattern could be obtained to within 1° without appreciable interference by the main beam. In order to check the zero, the small-angle scattering was measured on both sides of the main beam.

III. EXPERIMENTAL RESULTS

A qualitative demonstration of the effect of pressure and temperature on the small-angle scattering as the condition of the experimental sample approaches and crosses the liquid-vapor transition curve is shown in Fig. 2, where for two typical runs the small-angle intensity for a fixed sample volume is plotted against the pressure with the temperature and the scattering angle held fixed. The increase in x-ray small-angle scattering as the liquid-vapor line is approached indicates that the physical picture of regions of fluctuating density, which increase in size, giving rise to the small-angle scattering, is essentially correct. The discontinuity in the curve comes about as a combination of (1) a change in absorption and scattering power caused by a change in density and (2) a change in isothermal compressibility which is proportional to the small-angle scattering.[16] No attempt was made to correct these curves for absorption, since as far as is known to the writer no quantitative theoretical significance can be attached to the adjusted values. This work affords an interesting parallel to recent work on light scattering in the critical region from ethylene and ethane.[17,18]

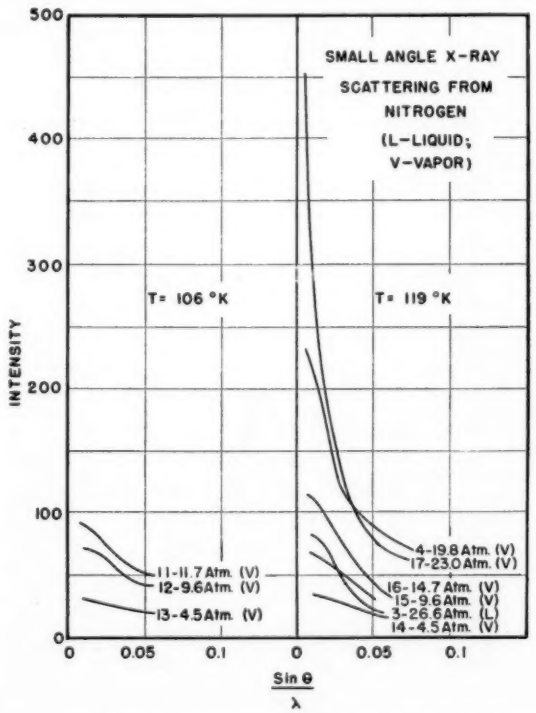

FIG. 4. Small-angle scattering for a fixed volume of sample in relative units *vs.* sin θ/λ at 106°K (P−T conditions 11, 12, 13) and 119°K (P−T conditions 3, 17, 4, 16, 15, 14).

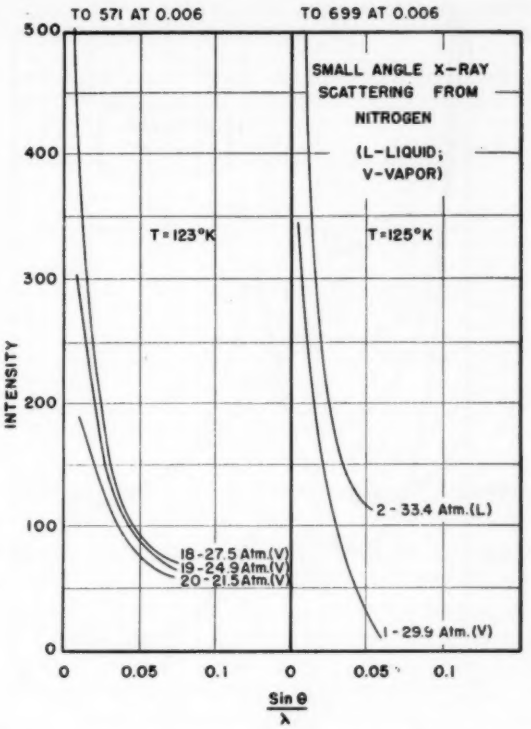

FIG. 5. Small-angle scattering for a fixed volume of sample in relative units *vs.* sin θ/λ at 123°K (P−T conditions 18, 19, 20) and 125°K (P−T conditions 2, 1).

On the nitrogen P−T diagram of Fig. 3, boxed-in datum points refer to conditions of pressure and temperature at which small-angle scattering patterns alone were obtained, while circled datum points refer to complete scattering patterns out to the limits of the experimental apparatus. The results of the small-angle scattering measurements are shown in Figs. 4 and 5, where the increase in the amount of scattering and the slope of the curves indicate the growth in size of the regions of inhomogeneity as the liquid-vapor transition is approached at a fixed temperature. These curves have not been placed on an absolute intensity basis of electron units, since the theory to be applied requires only relative intensity. For the lowest temperature studied (106°K), the plots of the liquid patterns taken (5, 7, 8, and 9) were not included, since in none of them could the small-angle scattering be detected above the background. Patterns 6 and 10 were also omitted since they were essentially the same as 12 and 11, respectively.

The diffraction patterns out to the limits of the apparatus have been corrected[3] for the natural counter background, scattering by the beryllium windows, and

[16] M. J. Yvon, J. de phys. et rad. 7, 201 (1946).

[17] H. A. Cataldi and H. G. Drickamer, J. Chem. Phys. 18, 650 (1950).

[18] A. L. Babb and H. G. Drickamer, J. Chem. Phys. 18, 655 (1950).

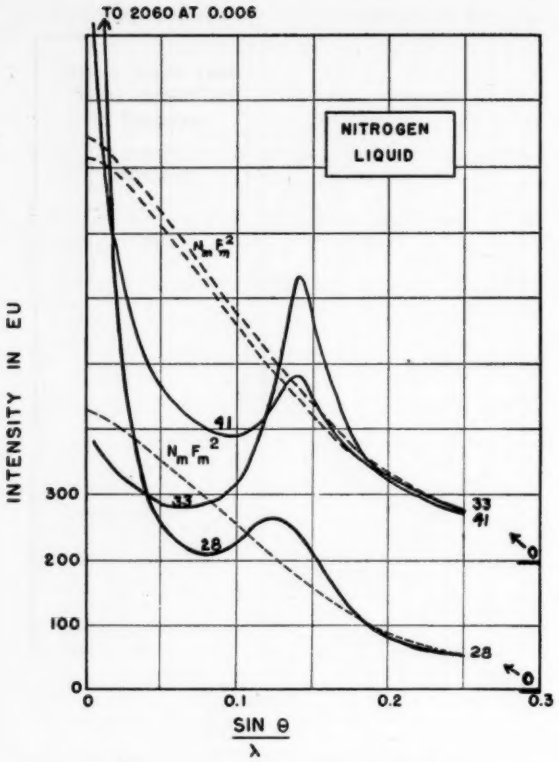

FIG. 6. Intensity patterns for nitrogen liquid in electron units *vs.* $\sin\theta/\lambda$ for P−T conditions 33, 41, and 28.

absorption and polarization, and placed on an absolute intensity basis of electron units in order to determine the isothermal compressibility from the x-ray data. A series of curves along the liquid side of the saturated vapor curve, up into the permanent gas side of the critical point, and back along the vapor side of the saturated vapor curve are given in Figs. 6, 7, and 8. In order to obtain sufficient intensity for the large-angle portion of these curves, it was found necessary to replace the narrow collimating slits of Fig. 1 by a slit 0.1 cm wide. These curves have been fitted with the molecular coherent scattering function, N_mF_m,[2] for N_m molecules, instead of the atomic coherent scattering function, Nf^2, for N atoms, since the former is required in the formula for the compressibility. The molecular coherent scattering function may be expressed as $F_m^2=2f^2(1+\sin kr/kr)$, where f^2 is the atomic coherent scattering function, k is $4\pi\sin\theta/\lambda$, and r is the equilibrium interatomic distance.

The change in position and sharpness of the first liquid diffraction peak is qualitatively the same as in the previous work on argon.[9] No attempt was made to perform Fourier inversions of these scattering patterns in order to obtain atomic distribution curves, since experience has shown that it is likely that little would be contributed to the information already obtained from previous work.

IV. ANALYSIS AND RESULTS

The analysis of the small-angle scattering patterns in order to determine the radii of the regions of inhomogeneity requires that either the theoretical expression,[11] $I_{sa}=A\Phi^2(ka)$, or its exponential approximation, $I_{sa}=A\exp[-(ka)^2/5]$ be fitted to the observed data, where $\Phi(ka)$ is the well-known spherical shape function,[19] k is $4\pi\sin\theta/\lambda$, and a is the radius of the scattering entity. The fitting of the exponential, method (a), is accomplished in the usual manner, i.e., plotting log I *vs.* k^2, the radius being determined from the slope of this curve. The other method, method (b), fits the square of the spherical shape function to the observed pattern at two selected points. It is unlikely that either method is entirely correct, since a small latitude of fitting is permitted in both schemes; and, hence, both methods and their average are listed in Table I for a selected set of curves along the liquid side of the saturated vapor curve, up into the permanent gas side of the critical point, and back along the vapor side of the saturated vapor curve. A definite and regular trend in the growth of these regions is readily apparent.

Values of isothermal compressibility may be determined from the x-ray data[16] with the aid of the following formula,[11]

$$\beta=I(0)V/N_mF_m^2RT,$$

where $I(0)$ is the extrapolated value of zero angle

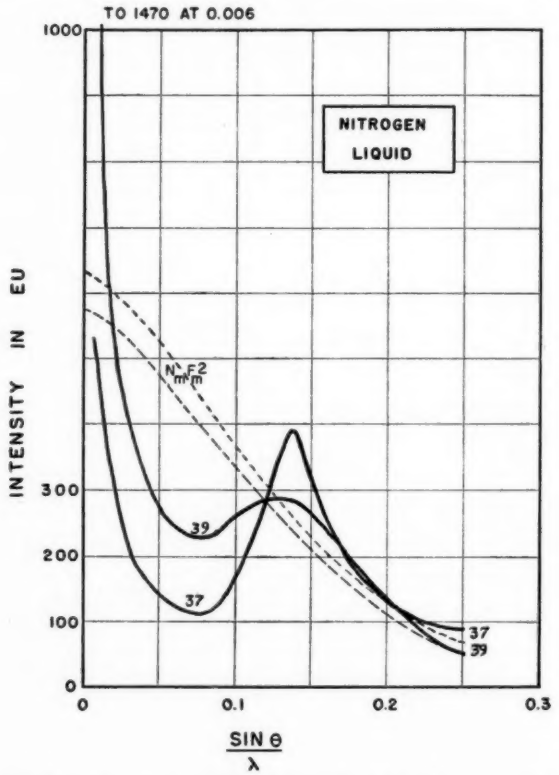

FIG. 7. Intensity patterns for nitrogen liquid in electron units *vs.* $\sin\theta/\lambda$ for P−T conditions 39 and 37.

[19] A. L. Patterson, Phys. Rev. **56**, 972 (1939).

TABLE I. Radii of regions of inhomogeneity and values of isothermal compressibility for a selected set of curves along the liquid side of the saturated vapor curve, up into the permanent gas side of the critical point, and back along the vapor side of the saturated vapor curve.

Pattern	State	Temp.	Press.	Method (a)	Method (b)	Av.	$\beta \times 10^3$
33	liquid	110.4°K	14.7 atmos.	4.6A	3.9A	4.3A	1.46 atmos.$^{-1}$
41	liquid	115.6	19.6	6.2	5.6	5.9	6.11
39	liquid	122.8	28.6	5.3–8.6	6.9	6.9	11.6
37	liquid	122.8	33.4	7.2	6.3	6.6	5.13
28	liquid	124.6	33.4				27.3
30	gas	128.0	36.8	8.8	7.4	8.1	88.3
25	gas	128.0	33.4	7.4	6.3	6.7	72.0
25[a]	gas	128.0	33.4				105.0[a]
40	vapor	123.8	29.5	6.6	6.3	6.4	69.2
17	vapor	119.0	23.0	5.9	6.2	6.0	
36	vapor	115.0	18.7	4.1	3.6	3.8	47.2
11	vapor	106.0	11.7	4.0	3.9	4.0	

[a] Calculated from Onnes and van Urk, reference 20, pp. 41–42.

scattering, $N_m F_m^2$ is the value of the molecular coherent scattering function at zero angle, V is the molar volume at temperature T°K, R is the gas constant, and β is the isothermal compressibility. The extrapolated values of $I(0)$ were obtained from the plots of $\log I$ *vs.* k^2, and the results for the series of curves in Figs. 6, 7, and 8 are also listed in Table I. Values of isothermal compressibility as determined from the slope of the isotherms previously obtained by Onnes and van Urk[20] could have been available for comparison with values obtained from patterns 25 and 30, except that pattern 30 falls near a point of inflection on their isotherms and the slope to be used is uncertain. The agreement of both values for the condition of pattern 25 may be seen in Table I.

V. DISCUSSION

The growth in size of the regions of inhomogeneity as the saturated vapor curve or the critical point is approached is consistent with the naive picture of tiny drops of liquid forming in the vapor, or small bubbles of vapor appearing in the liquid. However, the calculated size of these regions is too small to lend credence to this over-simplified representation. The maximum radius, 8.1A, is not much greater than the 5.66A intermolecular spacing of the unit cell of crystalline nitrogen. Indeed, the smaller regions, containing even less volume than a unit cell, are impossible to picture as regions having a phase distinct from the material as a whole. The regions indicated for vapor pattern 40 would contain about 10 molecules at a density corresponding to the liquid side of the saturated vapor curve at the same point, while a similar calculation for pattern 36 yields less than 3 molecules! This is strong evidence that this physical model has been oversimplified.

A more plausible arrangement has been suggested by Vineyard,[11] in which there need not be macroscopic inhomogeneity, the effective inhomogeneity being on a molecular scale. This type of arrangement may be imagined as one in which the macroscopic region model has the boundaries of the regions made diffuse and the shapes of the regions all different and highly irregular. The data on nitrogen indicating small regions and a definite growth in size as the critical point is approached lends strong support to the picture of the dynamic association of molecules rather than the distinct macroscopic regions of inhomogeneity. However, the analysis of the data by means of the theory derived from the simple assumption of identical spherical regions should still be correct to an order of magnitude.

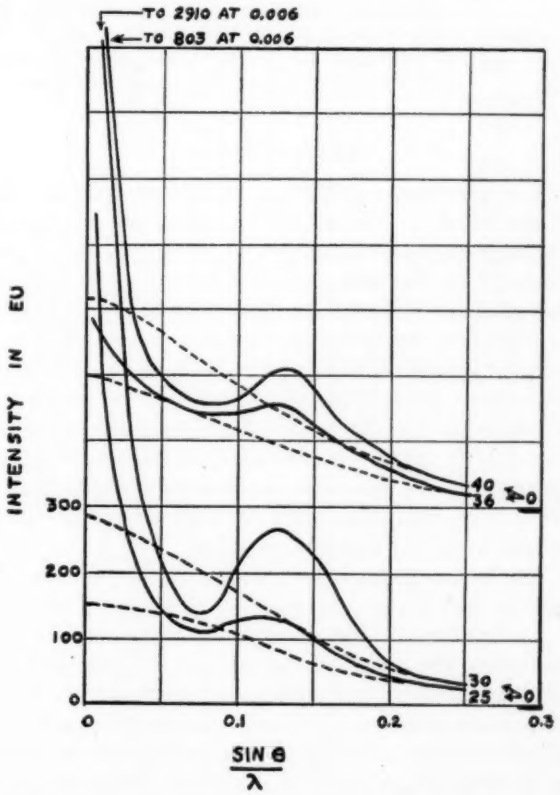

FIG. 8. Intensity patterns in electron units *vs.* $\sin\theta/\lambda$ for nitrogen gas, P–T conditions 25 and 30, and for nitrogen vapor, P–T conditions 40 and 36. Dotted curves represent respective $N_m F_m^2$ curves.

[20] Onnes and van Urk, Commun. Phys. Lab. Univ. Leiden, No. 169 d, 33 (1924).

Although not complete in itself, this type of experiment and subsequent analysis seems to offer an effective means of obtaining direct experimental evidence for the structure or molecular arrangement of a substance when it makes the difficult-to-investigate transition from vapor to liquid.

In the determination of isothermal compressibilities from the x-ray data, the most serious objection is having to obtain the value of zero-angle scattering by some means of extrapolation of the observed data. Even so, since all values of $I(0)$ listed in Table I were obtained in the same manner, the relative values of the compressibility should be significant. Without a more reliable means of determining this zero-angle scattering, however, the reliance to be placed on the absolute values is doubtful. The most that can be said is that good agreement, considering inaccuracies inherent in both means of determining the compressibility, was obtained for the points where experimental conditions overlapped.

VI. ACKNOWLEDGMENTS

The author wishes to express his appreciation to Professor N. S. Gingrich, whose suggestions led to the undertaking of this problem and under whose guidance it was completed. Special appreciation is expressed also to Professor G. H. Vineyard for many helpful discussions and for aid in the analysis of the experimental data. To the O. M. Stewart Fund Committee, the author is deeply indebted for the support which made this work possible.

THE JOURNAL OF CHEMICAL PHYSICS VOLUME 18, NUMBER 12 DECEMBER, 1950

Kinetics of the Reaction of Atomic Hydrogen with Acetylene

J. R. DINGLE* AND D. J. LE ROY
Department of Chemistry, University of Toronto, Toronto, Canada
(Received August 7, 1950)

A study has been made of the rate of recombination of atomic hydrogen in the presence and in the absence of the homogeneous catalyst, acetylene. The recombination in the absence of acetylene has a negative temperature coefficient and an order between one and two. The acetylene catalyzed recombination was found to be first order in atomic hydrogen and first order in acetylene, with a rate constant of $1.3_4\times10^{-14}$ cc molecules^{-1} sec.$^{-1}$ at 17°C. The effect of temperature on the reaction corresponded to a collision theory activation energy of 1.5 kcal./mole and a steric factor of 4×10^{-4}.

INTRODUCTION

IN a previous publication[1] Tollefson and Le Roy described a method of studying the elementary reactions of atomic hydrogen in which the atoms were produced by the dissociation of hydrogen on tungsten filaments and detected by their heat of recombination on platinum. Applying the method to the reaction of atomic hydrogen with acetylene, they found that only a very small proportion of the atomic hydrogen was consumed in the formation of hydrogenated products. The greatly increased rate of consumption of atomic hydrogen in the presence of acetylene was found to be due to the catalytic affect of that substance on the recombination of atomic hydrogen.

The improvements made in the method of Tollefson and Le Roy have now made it possible to allow for recombination in the absence of other reactants, to determine the order of reaction in both reactants and to obtain activation energies and steric factors for the elementary reactions of atomic hydrogen with a number of hydrocarbons. The present paper reports the results of a reinvestigation of the reaction between atomic hydrogen and acetylene. The kinetics of the reactions of atomic hydrogen with ethylene and ethane will be reported in a later publication.

APPARATUS

The dissociator, reaction chamber, and detector are shown in some detail in Fig. 1. Purified hydrogen entered the water-cooled dissociator chamber *7* through the inlet tube at the top. This tube and the dissociator filament were mounted on a ground joint which could be removed to replace filaments or to re-poison the inner walls of the apparatus.

Acetylene from the calibrated burette (*9*, Fig. 2) entered through the tube *16*, between the dissociator and reaction chambers. The acetylene inlet tube was provided with a capped ground joint through which a platinum wire could be inserted to clear the tube of the phosphoric acid poison, if necessary.

The reaction chamber, approximately 25 cm long and 23 mm i. d., was surrounded by a jacket; a steady flow of tap water through this gave a temperature of approximately 17°C. For experiments near 0°C ice water was circulated through the jacket; thermometers were inserted at the entrance and exit. For higher temperatures appropriate liquids were boiled in the jacket

* Present address: Atlantic Fisheries Experimental Station, Halifax, Nova Scotia.
[1] E. L. Tollefson and D. J. Le Roy, J. Chem. Phys. **16**, 1057 (1948).

at atmospheric pressure by means of the external heater *15*. A reflux condenser (not shown) was attached to the upper outlet and the temperature was measured at this point by a thermometer immersed in the vapor. The return from the condenser was fed into the lower inlet of the jacket. In every case the temperatures were steady throughout a determination to about ±0.5°C.

The lower half of the reactor assembly is shown to the right of the dissociator and reactor in Fig. 1. The fixed central tube served as a guide for a long sliding glass tube which carried the detector head. This sliding tube floated on the mercury surrounding the guide tube and the position of the detector could be adjusted by manipulation of the pressure in the attached reservoir. The position of the detector relative to the acetylene inlet tube was found by measuring the distance between fiducial points on the outer and sliding tubes.

The detector is shown on a larger scale at the right of Fig. 1. The detector head consisted of a short length of glass tubing with two tungsten wires sealed into its closed end. These carried nickel wires to which coiled platinum or tungsten filaments were silver-soldered. The filaments were 0.0025 in. in diameter in the case of platinum, 0.004 in. in the case of tungsten. After attaching the detector filament, the upper parts were dipped into fused potassium chloride to poison the catalytic effect of nickel on the recombination of atomic hydrogen. The filament was then washed with water. The detector head fitted snugly into the upper end of the sliding tube. One of the leads was soldered to a long copper wire dipping into mercury in the central guide tube; the other was taken out through a hole in the side of the head tube and soldered to a second copper wire which was attached to the outside of the sliding tube with de Khotinsky cement and made contact with the mercury in the outer tube. Detector heads could thus be easily interchanged. Both pools of mercury were connected through tungsten seals to the Wheatstone bridge circuit. Changes in the position of the sliding tube had no significant effect on the resistance of the circuit.

The circuit used to determine the energy liberated by the recombination of atomic hydrogen was similar to that described previously,[1] except that the milliammeter was placed in series with one of the lead wires to the bridge, rather than in the same arm as the detector. As before, the response of the platinum detector was independent of its temperature over a range from 50° to 350°C. In some experiments tungsten detector wires were used and found to be as satisfactory as platinum.

The temperature of the dissociator filament was calculated from its resistance at 0°C and the temperature coefficient of resistance. The values agreed to within 50° with the results obtained with a disappearing filament pyrometer. In practice the current for the dissociator was supplied by storage batteries and adjusted to give the required voltage and current readings. On the few occasions when the dissociator was overheated the response of the detector fell off drastically; this was believed to be due to the deposition on the detector of poison dislodged from the walls, since the response could be partially restored by washing the detector.

No measurable concentration of atomic hydrogen was obtained when the walls of the apparatus were bare because of the high recombination coefficient on glass. The loss was reduced to about 50 percent or less in a reaction time of 0.2 sec. by coating the inner walls of the dissociator and reaction chambers with a poison prepared from approximately equal amounts of orthophosphoric acid and phosphorus pentoxide. The mixture was first heated in a platinum dish until the volume was reduced by about 30 percent; the hot poison was then drawn into a glass tube, blown onto the walls, and spread with the glass tube while rotating the reactor. The ground surfaces were protected with dummy joints and the reactor rotated until the coating cooled. When cool the poison formed a very viscous, glassy layer which did not run appreciably even at 150°C. As shown in Fig. 1, it was cooled in the vicinity of the dissociator by passing cooling water through a number of turns of rubber tubing wound around the tube at this point. Just below its jacket the reaction tube was expanded to form a gutter to catch any drainage from the poison and so prevent the fouling

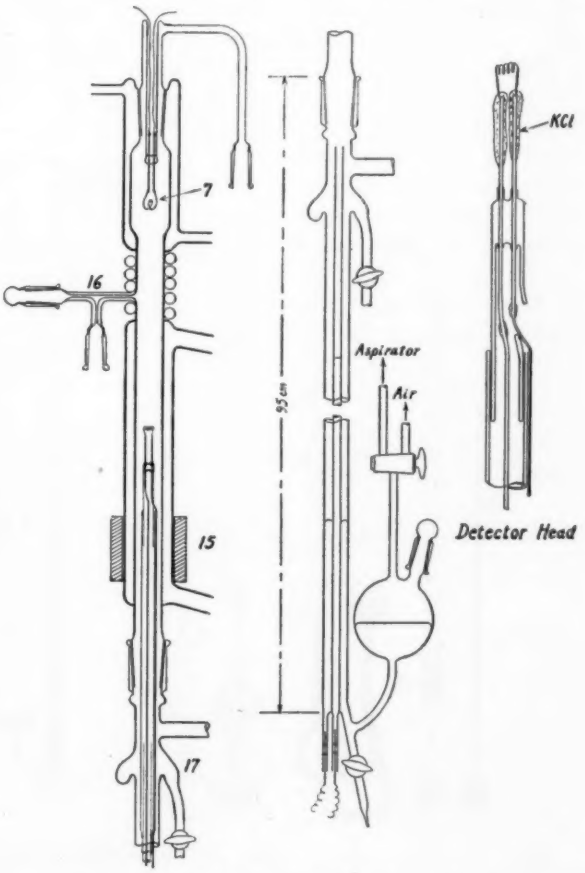

FIG. 1. Detailed view of the dissociator, reaction chamber, and detector.

of the mercury surface. Provided water vapor and oxygen were excluded from the apparatus, the efficiency of the poison would remain practically constant for a period of several months as shown by the rate of decay of H atom concentration in the absence of acetylene.

The arrangement of the apparatus (except for the analysis and acetylene purification systems) is shown in Fig. 2. Purified acetylene, stored in the 4-liter volume, was admitted to the water-jacketed burette *9* through the Fugassi valve *8*. The pressure in the burette was measured on the manometer *10*. As the acetylene entered the reaction chamber through the capillary at the top of the burette the pressure in the burette was kept constant to a fraction of a millimeter by the automatic electrolysis of an aqueous sodium sulfate solution in the cell *11*. The current through this cell was controlled by a relay operated by contacts on the vacuum arm of the manometer *10*.

Commercial electrolytic hydrogen was purified by passage over platinized asbestos in the furnace *1* and through the traps *2* containing silica gel at liquid air temperature. The hydrogen flow rate was measured on the flow meter *4*. The pressure in the reaction cell was controlled by the needle valves *5* and *6*. Condensible products could be collected in the coiled trap cooled with continuously pumped liquid air. The non-condensible gases were removed from the system through a mercury diffusion pump and a mechanical pump with a capacity of 15 cu. ft./min.

EXPERIMENTAL

A. H Atom Consumption in the Absence of Acetylene

The recombination of atomic hydrogen has been studied by a number of workers, and has recently been treated theoretically by Schuler and Laidler.[2] While the present investigation was concerned primarily with the kinetics of the reaction of atomic hydrogen with acetylene, it was necessary to have some knowledge of the recombination reaction in order to correct the observed rates in the presence of acetylene.

Amdur,[3] using a phosphoric acid-poisoned surface and a total pressure in the range 0.276 to 1.044 mm, found that his experimental results could be fitted to any one of five mechanisms. Each of these involved at least two

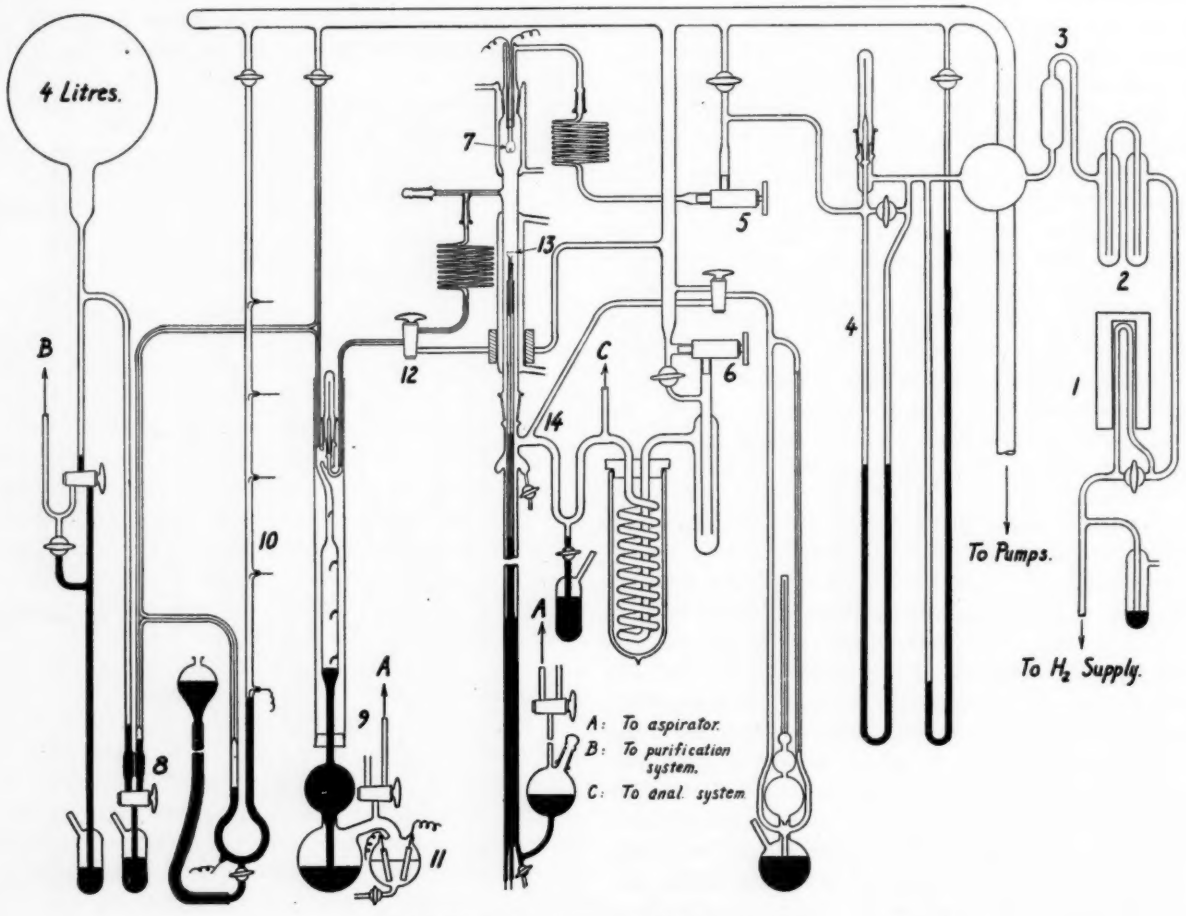

FIG. 2. General arrangement of the apparatus.

[2] K. E. Schuler and K. J. Laidler, J. Chem. Phys. **17**, 1212 (1949). References to previous work are given in this paper.
[3] I. Amdur, J. Am. Chem. Soc. **60**, 2347 (1938).

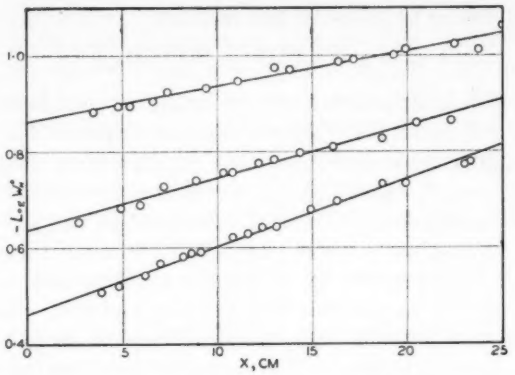

FIG. 3. First-order plots of H atom decay in the absence of foreign gas for different initial H atom concentrations.

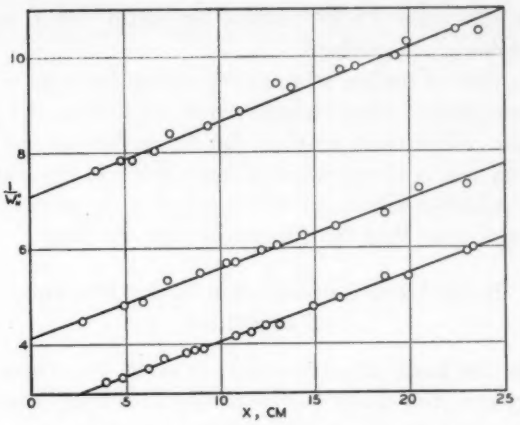

FIG. 4. Second-order plots of H atom decay in the absence of foreign gas, using the same data as in Fig. 3.

simultaneous reactions of different order. On the other hand, Smith,[4] using water vapor as the poison and a total pressure of less than 0.1 mm, concluded that neither three-body collisions nor second-order wall recombination occurred under these conditions.Schuler and Laidler's treatment[2] is based on the assumption of a first-order wall recombination.

Our measurments, as were those of Amdur, were based on isothermal calorimetry and involved no correction for radiation. Smith, however, assumed that the H atom concentration at the probe was a linear function of the temperature difference between the probe and its surroundings, although the temperature difference was, in some cases, as high as 400°C.

In the case of our experiments straight lines could be drawn through the points obtained by plotting the log of $W_H{}^0$ against the time t, where $W_H{}^0$ is the wattage due to H atom recombination on the detector in the absence of acetylene and t is the product of the reciprocal of the flow rate and the distance, x, of the detector from the acetylene inlet. Since the H atom concentration at the detector is undoubtedly proportional to $W_H{}^0$, the decay appeared to be first order. Many of these plots, however, showed some indication of concavity toward the time axis, suggesting the presence of a second-order reaction.

In Fig. 3 are shown three curves of $-\log W_H{}^0$ *vs.* x for different dissociator temperatures but otherwise for identical conditions of flow rate, hydrogen pressure, etc. Two series of measurements were made at each dissociator temperature. Although curvature is not pronounced, the slopes of the curves (proportional to the first-order rate constant) are seen to decrease with decreasing H atom concentration. The second-order plots of the same data are shown in Fig. 4. Here any curvature is within the experimental error and the slopes (proportional to the second-order rate constant) are more nearly the same at different initial H atom concentrations. Clearly the choice of the order of the recombination reaction is open to question.

The temperature coefficient of the recombination reaction was found to be negative. This is shown in Table I; the data were obtained from pairs of experiments carried out at different reactor temperatures but otherwise under similar conditions.

The tabulated first-order rate constants, k' were obtained as the average of four or more slopes of corresponding $\log W_H{}^0$ *vs.* t plots. Values of k''/f, rather than the second-order rate constant k'' were given in Table I; they may be interpreted as second-order rate constants having the dimensions watt^{-1} sec.$^{-1}$, since f is the constant of proportionality between [H] and $W_H{}^0$; they were obtained as the average of four or more slopes of corresponding plots of $1/W_H{}^0$ against t.

If the recombination reaction is actually first order, a negative temperature coefficient would be predicted by Schuler and Laidler's low temperature mechanism for a water vapor poisoned surface.[2] However, our temperature range was scarcely large enough to apply the detailed theory.

A value for the recombination coefficient γ may be calculated from the first-order rate constant through the relation[2]

$$\gamma = (2k'r)/\bar{v}.$$

For example, the value of γ corresponding to a k' of 4.80 sec.$^{-1}$ at 5°C is 4.5×10^{-5}, in reasonable agreement

TABLE I. Recombination of atomic hydrogen in the absence of foreign gas.

Temperature °C	k' sec.$^{-1}$	k''/f watt^{-1} sec.$^{-1}$	k_a'/k_b'	k_a''/k_b''	H_2 pressure mm
(a) 5.0	4.80	31.2	1.11	1.08	3.86
(b) 59.5	4.32	28.9			3.87
(a) 4.3	4.88	28.3	1.60	1.53	3.70
(b) 99.0	3.06	18.5			3.83
(a) 2.3	4.12	25.8	1.60	1.47	3.73
(b) 98.6	2.58	17.6			3.72

[4] W. V. Smith, J. Chem. Phys. 11, 110 (1943).

with the value 2×10^{-5} found by Smith[4] for a metaphosphoric acid surface.

In view of the uncertainty regarding the order of the recombination reaction under our conditions, the procedure adopted in making the correction to the observed rate in the presence of acetylene was to compare the values obtained on the basis of each mechanism. It was found that the differences were not large.

B. H Atom Consumption in the Presence of Acetylene

On the basis of a first-order decay in the absence of acetylene, the decay in the presence of acetylene was assumed to be given by the relation

$$-d[\mathrm{H}]/dt = k'[\mathrm{H}] + 2k_1[\mathrm{C_2H_2}][\mathrm{H}], \qquad (1)$$

in which k_1 is the rate constant for the reaction $\mathrm{H}+\mathrm{C_2H_2} = \mathrm{C_2H}+\mathrm{H_2}$ or $\mathrm{H}+\mathrm{C_2H_2} = \mathrm{C_2H_3}$ (see reference 1). Since no appreciable decomposition of acetylene occurred, the over-all reaction in the presence of acetylene would be first order in [H] with a rate constant k_{ov} given by the expression $k_{ov} = k' + 2k_1[\mathrm{C_2H_2}]$. Defining W_H as the wattage developed by H atom recombination on the detector in the presence of acetylene, a plot of $-\log W_H$ against t should give a straight line with slope 0.4343 k_{ov}. A few of these plots are shown as the upper curves of Fig. 5.

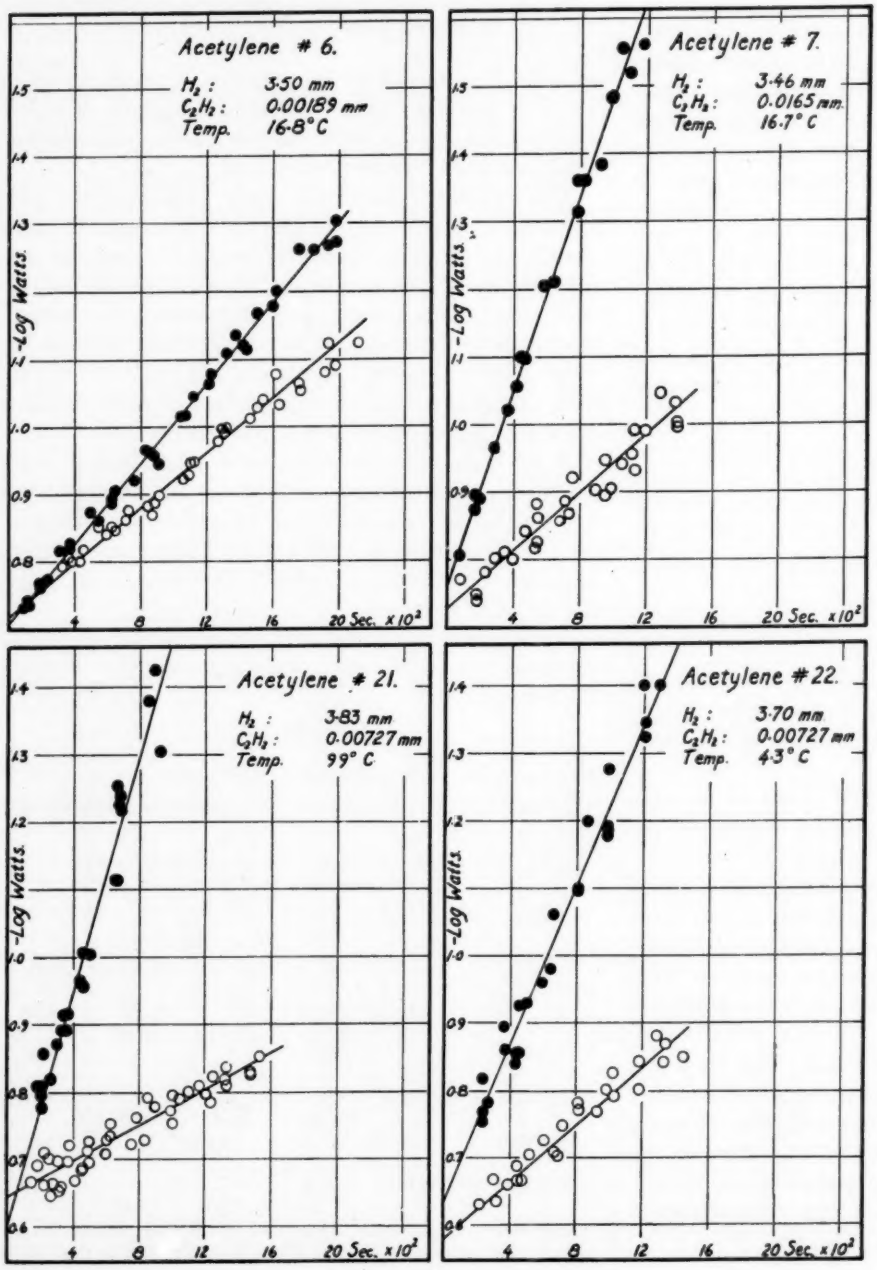

FIG. 5. Plots of $-\log W_H$ (upper curves) and $-\log W_H^0$ (lower curves) *vs.* t for four of the experiments.

The lower curves in Fig. 5 are the plots of $-\log W_H{}^0$. The points on these show considerable scattering; however, they are, in general, the result of four determinations, two before and two after adding the acetylene. The points for any single determination usually lay on fairly good straight lines, but frequently the lines for different determinations were shifted up or down relative to one another while still remaining nearly parallel. This was probably the result of slight changes in the H atom concentration entering the reaction vessel.

The linearity of the $-\log W_H$ *vs.* t plots suggests that the reaction with acetylene is first order in [H]. The

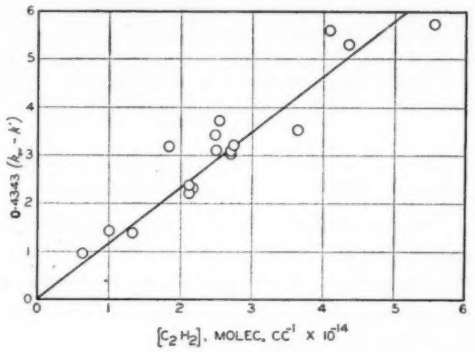

FIG. 6. $0.4343(k_{ov}-k')$ *vs.* $[C_2H_2]$ for the experiments at 17°C. The straight line corresponds to a value for k_1 of 1.34×10^{-14} cc molecules^{-1} sec.$^{-1}$.

difference in the slopes of the $-\log W_H$ and the $-\log W_H{}^0$ plots $(=0.4343(k_{ov}-k')=0.4343\times2k_1[C_2H_2])$ should then be linear in $[C_2H_2]$. That this is so can be seen from Fig. 6. The value of k_1 corresponding to the straight line is 1.34×10^{-14} cc molecules^{-1} sec.$^{-1}$ at 17°C. The value obtained by Tollefson and Le Roy[1] was 8.6×10^{-14} at 25°C.

On the basis of a second-order decay in H atom concentration in the absence of reactant, the decay in the presence of acetylene was assumed to be given by the expression

$$-d[H]/dt=k''[H]^2+2k_1[C_2H_2][H]. \quad (2)$$

Assuming, as before, that $[H]=W_H/f$, then

$$-(1/f)dW_H/dt=k''(W_H/f)^2+2k_1[C_2H_2]W_H/f,$$

or

$$\log\{2k_1[C_2H_2]+(k''/f)W_H\}/W_H = 2k_1[C_2H_2]t+\text{const.} \quad (3)$$

TABLE II. Kinetic data for the reaction $H+C_2H_2$.

Temp. °C	k_1, Eq. (1) cc molecules^{-1} sec.$^{-1}$ $\times10^{14}$	k_1, Eq. (2) cc molecules^{-1} sec.$^{-1}$ $\times10^{14}$	E_1, Eq. (1) kcal./mole	E_1, Eq. (2) kcal./mole	p_1, Eq. (1) $\times10^4$	p_1, Eq. (2) $\times10^4$
(a) 5.0	1.37	1.66	1.31	1.27	2.6	2.9
(b) 59.5	2.20	2.64				
(a) 4.3	1.72	2.19	1.65	1.35	6.0	4.4
(b) 99.0	4.28	4.74				
(a) 2.3	1.06	1.36	1.72	1.45	4.3	3.4
(b) 98.6	2.80	3.16				
		Mean	1.59	1.39	4.3	3.6

Equation (3) does not permit a direct solution for k_1, but this quantity can be obtained by successive approximations. In the first approximation the value of k_1 obtained from Eq. (1) was used; the left-hand side of (3) was then plotted against t to give a second approximation, etc.

In Table II are shown the values of k_1 derived from Eqs. (1) and (2) for three pairs of experiments. Table II also gives the corresponding values of the activation energy E_1 and the steric factor p_1. In calculating E_1 allowance was made for the term in $T^{\frac{1}{2}}$ appearing in the frequency factor. The steric factors were calculated from corresponding values of k_1 and E_1 using a value of 2.72A for the mean collision diameter.[1]

CONCLUSIONS

It is seen from Table II that the form of the rate law assumed for the decay of H atom concentration in the absence of acetylene makes little difference in the values calculated for E_1 and p_1. The low collision efficiency of the reaction with acetylene, as evidenced by a p_1 value of approximately 4×10^{-4}, is not surprising.[5] The activation energy of 1.5 kcal./mole, while small, is believed to be real, since particular reliance can be placed on the relative rates of any of the pairs; the second was always done immediately after the first, without interrupting the hydrogen flow.

The authors are indebted to the Associate Committee on Scientific Research of the University of Toronto for supporting this research.

[5] Glasstone, Laidler, and Eyring, *The Theory of Rate Processes* (McGraw-Hill Book Company, Inc., New York, 1941), p. 19.

THE JOURNAL OF CHEMICAL PHYSICS VOLUME 18, NUMBER 12 DECEMBER, 1950

The Separation of the Rotational Coordinates from the N-Particle Schroedinger Equation*

C. F. CURTISS AND J. O. HIRSCHFELDER
Department of Chemistry and Naval Research Laboratory,

AND

F. T. ADLER**
Department of Physics, University of Wisconsin, Madison, Wisconsin

(Received August 10, 1950)

By group theoretical arguments, it can be shown that a wave function, $\psi_\mu{}^L$, for a system of N particles corresponding to a total angular momentum quantum number, L, and a quantum number, μ, referring to the z component of angular momentum may be written as a sum of terms:

$$\psi_\mu{}^L = \Sigma_s D^L(R)_{\mu s}{}^* \chi_s{}^L.$$

The $D^L(R)_{\mu s}$ are the representation coefficients for the Lth irreducible representation of the three-dimensional rotation group, and are functions of the three coordinates specifying the orientation of the system of particles in space. The $\chi_\mu{}^L$ are functions of the $3N$-6 coordinates specifying the relative configuration of the N-particle system. The set of coupled differential equations for the functions, $\chi_\mu{}^L$, is obtained explicitly. The special case of the three-particle system is discussed in detail. The present treatment is more directly usable than the previous discussions since the basic equations do not involve implicit relationships between the variables.

IN classical mechanics, the three components of linear and the three components of angular momentum are constants of motion of a mechanical system moving in free space. Corresponding to each of these constants of motion a coordinate can be separated from the classical equations of motion or from the quantum-mechanical Schroedinger equation. The constancy of the linear momentum leads to the separation of the motion of a set of particles into the motion of the center of gravity of the system and the motion in the center-of-gravity coordinate frame. Similarly the constancy of the angular momentum leads the separation of the motion into the rotation of the system as a whole as described, e.g., by the three Eulerian angles, and the "internal" motion of the set of particles. In the case of two particles this separation of the rotational motion introduces a "virtual" potential, the centrifugal potential. In the case of N particles the separation leads to the introduction of similar terms but of more complicated structure.

There are a number of possible applications. For example, one of the most important problems in the spectroscopy of polyatomic molecules is the interaction of rotations and vibrations. This problem is usually considered from the standpoint of small perturbations, and each symmetry type of molecule is considered as a special case. The present treatment could be used to obtain more general results.

The separation of the rotational coordinates from the N-body Schroedinger equation is the first step in a theory of collisions between molecules. Such a theory of collisions between molecules should lead to a knowledge of the transition probabilities for the transfer of energy between the translational and the internal degrees of freedom. This knowledge is of course fundamental to an understanding of the kinetic theory of molecules and related phenomena. The application of the results presented here to the theory of collisions is being carried out and will be presented elsewhere.

The wave function for a system of N particles in free space can be written as a product of a function of the coordinates of the center of gravity and a function of the $3N$-3 coordinates specifying the position of the N particles in a center-of-gravity coordinate frame. If the potential depends only upon the internal configuration and this is invariant under a rotation, the function of the $3N$-3 coordinates can be written as a sum of products of functions of the three coordinates specifying the orientation of the system and functions of the $3N$-6 coordinates specifying the internal configuration of the system. In the present paper we obtain the set of differential equations determining these functions of the internal coordinates. The coordinates used here were chosen to clarify the derivation in the general case. For any particular N and for any particular problem it will be possible to simplify the equations considerably by transforming to a set of coordinates especially adapted to the problem in question. This procedure is illustrated for the case $N=3$.

The viewpoint and procedures used here are similar in many respects to those of Hirschfelder and Wigner.[1] However, their results were not directly usable for the problems under consideration. Their final equations were expressed in terms of a set of variables which were not independent. Then, too, they used an inconvenient standard configuration. In the present paper, the three-body problem is considered explicitly and reduced to a simple set of equations which can be solved explicitly

* This work was carried out under Contract NOrd 9938 with the Navy Bureau of Ordnance.

** Present address: Carnegie Institute of Technology, Pittsburg, Pennsylvania.

[1] J. O. Hirschfelder and E. P. Wigner, Proc. Nat. Acad. Sci. 21, 113 (1935).

for certain types of potentials. Similar procedures could be used for the solution of any particular N-body problem.

I. THE SEPARATION OF VARIABLES

The wave equation for a system of N particles may be written

$$-\frac{\hbar^2}{2}\sum_{n,k}\frac{1}{m_n}\frac{\partial^2\Psi}{\partial x_{nk}^2}+V\Psi=E'\Psi, \tag{1}$$

where x_{nk} is the kth coordinate of the nth particle, m_n is the mass of the nth particle, V is the potential energy, and E' is the total energy of the system. If the potential, V, is independent of the position of the center of gravity of the system, then Ψ may be written as the product

$$\Psi=f(X_k)\psi(y_{nk}) \tag{2}$$

of a function f of the coordinates of the center of gravity and a function ψ of a set of $3N$-3 coordinates y_{nk} specifying the configuration relative to the center of gravity. For definiteness we take the set y_{nk} to be the Cartesian coordinates of the first N-1 particle in a coordinate frame with origin at the center of gravity and axes parallel to those of the original frame. The position of the remaining Nth particle is then specified.

By straightforward manipulation it can be shown that Eq. (1) separates into an equation for f and an equation for ψ. The f equation is the usual equation for a free particle,

$$(-\hbar^2/2m)\sum_k \partial^2 f/\partial X_k^2=E_t f, \tag{3}$$

where E_t is the translational energy of the system and

$$m=\sum_i m_i \tag{4}$$

is the total mass of the system. The ψ-equation is

$$-\frac{\hbar^2}{2}\sum_{nn'k}\left(\delta_{nn'}-\frac{m_n}{m}\right)\frac{1}{m_n}\frac{\partial^2\psi}{\partial y_{nk}\partial y_{n'k}}+V\psi=E\psi. \tag{5}$$

Here $E=E'-E_t$ is the energy associated with the rotation and the internal motion of the system.

If the potential energy is invariant under a rotation of the coordinate system, the wave functions will form bases of representations of the three-dimensional rotation group. Let $\psi_s{}^L$ be a wave function specified by the total angular momentum quantum number, L, and the quantum number referring to the z component of the angular momentum, μ. Then, if R is the rotation of the coordinate system, $P_R\psi_s{}^L$ will be a linear combination of the $\psi_\mu{}^L$ belonging to the same L, i.e., a rotation will mix the set of $2L+1$ degenerate quantum states. In particular,[2]

$$P_R\psi_s{}^L=\sum_\mu D^L(R)_{\mu s}\psi_\mu{}^L \tag{6}$$

where the set $D^L(R)_{\mu s}$ is the set of representation coefficients for the Lth irreducible representation of the rotation group.

Now let us choose a "standard configuration" corresponding to each configuration of the N atoms in such a way that all configurations which differ only by a pure rotation correspond to the same standard configuration. Then if R is the rotation of the coordinate system which bring the set of atoms into a standard configuration

$$P_R\psi_s{}^L=\chi_s{}^L \tag{7}$$

depends only on the relative configuration, i.e., $\chi_s{}^L$ depends upon three less coordinates than $\psi_s{}^L$. Using the orthogonality of the representation coefficients

$$\sum_s D^L(R)_{\mu' s}{}^* D^L(R)_{\mu s}=\delta_{\mu'\mu} \tag{8}$$

and Eq. (7), the definition of $\chi_s{}^L$, one can easily obtain from Eq. (6)

$$\psi_\mu{}^L=\sum_s D^L(R)_{\mu s}{}^*\chi_s{}^L. \tag{9}$$

This expression is a factorization of the wave function into a sum of products of functions of the rotational coordinates and the internal coordinates. In many respects Eq. (9) is similar to Eq. (2). However, in Eq. (9) the degeneracy of the group representations leads to a possible mixing of the states and thus to a sum in Eq. (9) instead of the single term as in Eq. (2).

If the expression for $\psi_\mu{}^L$ as given in Eq. (9) is substituted into Eq. (4) one could in principle separate variables and obtain equations for the various functions. However, since the functions $D^L(R)_{\mu s}$ are well known[3] it is not necessary to obtain such detailed information. Instead one integrates over the rotational coordinates and obtains immediately equations for the functions $\chi_s{}^L$. However, the manipulations involved in this procedure are somewhat lengthy and are discussed in detail below.

II. THE WAVE EQUATION FOR THE N-PARTICLE SYSTEM

First one must obtain the derivatives of the $D^L(R)_{\mu s}$. If one coordinate, y_{nk}, is changed by a small amount, the rotation necessary to bring the system into a standard configuration is changed by an infinitesimal rotation, S^{nk}. The rotation R depends upon the three coordinates specifying the orientation of the system. These coordinates in turn depend upon the set of coordinates y_{nk}. Hence by definition

$$\partial R_{ij}/\partial y_{nk}=\lim_{\delta y_{nk}\to 0}[(RS^{nk})_{ij}-R_{ij}]/\delta y_{nk}. \tag{10}$$

The infinitesimal rotation matrix S^{nk} can be written in the form,

$$\begin{aligned} S_{ii}{}^{nk}&=1+0(\delta y_{nk})^2 \\ S_{ij}{}^{nk}&=\epsilon_{ij}{}^{nk}\delta y_{nk}; \quad i\neq j, \end{aligned} \tag{11}$$

where the $\epsilon_{ij}{}^{nk}$ are functions of the y_{nk} depending upon the choice of the standard configuration. Then using

[2] E. P. Wigner, *Gruppentheorie und Ihre Anwendung auf die Quantenmechanik der Atomspedtren* (J. W. Edwards, Ann Arbor, Michigan, 1944).

[3] See reference 2, p. 180.

these relations, Eq. (10) becomes

$$\partial R_{ij}/\partial y_{nk}=\sum_{l\neq j} R_{il}\epsilon_{lj}{}^{nk}. \tag{12}$$

Hirschfelder and Wigner[1] have carried out the differentiation of the explicit form of the representation coefficients, $D^L(R)_{\mu s}$. The result in terms of the $\epsilon_{lj}{}^{nk}$ defined above is

$$\begin{aligned}\partial D^L(R)_{\mu s}/\partial y_{nk}=&is\epsilon_{21}{}^{nk}D^L(R)_{\mu s}\\&-\tfrac{1}{2}\lambda_-(L,s)(\epsilon_{32}{}^{nk}-i\epsilon_{13}{}^{nk})D^L(R)_{\mu,s-1}\\&+\tfrac{1}{2}\lambda_+(L,s)(\epsilon_{32}{}^{nk}+i\epsilon_{13}{}^{nk})D^L(R)_{\mu,s+1}\end{aligned} \tag{13}$$

where

$$\lambda_+(L,s)=[L(L+1)-s(s+1)]^{\frac{1}{2}} \tag{14}$$

and

$$\lambda_-(L,s)=[L(L+1)-s(s-1)]^{\frac{1}{2}}. \tag{15}$$

Carrying out the differentiation of Eq. (9), and using Eq. (13), one obtains

$$\begin{aligned}\partial\psi_\mu{}^L/\partial y_{nk}=&\textstyle\sum_s D^L(R)_{\mu s}{}^*\\&\times\begin{bmatrix}(\partial\chi_s{}^L/\partial y_{nk})-is\epsilon_{21}{}^{nk}\chi_s{}^L\\-\tfrac{1}{2}\lambda_+(L,s)(\epsilon_{32}{}^{nk}+i\epsilon_{13}{}^{nk})\chi_{s+1}{}^L\\+\tfrac{1}{2}\lambda_-(L,s)(\epsilon_{32}{}^{nk}-i\epsilon_{13}{}^{nk})\chi_{s-1}{}^L\end{bmatrix}.\end{aligned} \tag{16}$$

In order to obtain the functional form of the $\epsilon_{ij}{}^{nk}$ it is necessary to specify the standard configuration and a particular set of $3N$-6 internal coordinates explicitly. The standard configuration is chosen so as to simplify the separation of the rotational coordinates and obtain a set of differential equations for the $\chi_s{}^L$ explicitly in terms of $3N$-6 variables. In order to solve the resulting equations it will usually be convenient to make a further transformation to a set of variables suitable for the particular problem under consideration. The standard configuration can be defined in such a manner as to apply to any general problem. It is convenient to specify the standard configuration in terms of the positions with respect to the center of gravity of two specified particles in the following manner: Particle "1" is placed on the positive z axis, and particle "2" is placed on the positive half of the x, z plane. In general, if y_{nk} is the coordinate of a particle before the rotation and z_{nk} is the coordinate after,

$$z_{nk}=\textstyle\sum_j R_{jk}y_{nj}. \tag{17}$$

The $3N$-6 internal coordinates are then:

$$\begin{array}{cccc}z_{13}, & z_{23}, & z_{33}, \cdots, & z_{N-1,3}\\0, & 0, & z_{32}, \cdots, & z_{N-2,2}\\0, & z_{21}, & z_{31}, \cdots, & z_{N-1,1}.\end{array}$$

From the definition of the standard configuration, z_{12}, z_{22}, and z_{11} are identically zero so that

$$\textstyle\sum_j R_{j1}y_{1j}=0, \tag{18}$$

$$\textstyle\sum_j R_{j2}y_{1j}=0, \tag{19}$$

$$\textstyle\sum_j R_{j2}y_{2j}=0. \tag{20}$$

These three equations essentially define the three coordinates of orientation of the system in terms of the y_{nk} coordinates. From the properties of an infinitesimal rotation matrix we have

$$\epsilon_{ij}{}^{nk}=-\epsilon_{ji}{}^{nk}. \tag{21}$$

Using this relation and Eq. (12) one obtains on differentiating Eq. (18)

$$\epsilon_{13}{}^{nk}=\delta_{1n}R_{k1}/z_{13}. \tag{22}$$

In a similar manner one obtains from Eqs. (19) and (20)

$$\epsilon_{32}{}^{nk}=-\delta_{1n}R_{k2}/z_{13} \tag{23}$$

and

$$\epsilon_{21}{}^{nk}=\left[\delta_{2n}-\frac{z_{23}}{z_{13}}\delta_{1n}\right]\frac{R_{k2}}{z_{21}}. \tag{24}$$

The derivatives of the internal coordinates z_{nk} with respect to the y_{nk} are obtained in a straightforward manner from Eq. (17). In general (where z_{11}, z_{12}, and z_{22} are defined to be zero),

$$\partial z_{n'k'}/\partial y_{nk}=\delta_{nn'}R_{kk'}+\sum_{l\neq k'} z_{n'l}\epsilon_{lk'}{}^{nk}. \tag{25}$$

Since the $\chi_s{}^L$ depend only upon the internal coordinates z_{nk},

$$\frac{\partial\chi_s{}^L}{\partial y_{nk}}=\sum_{n',k'}\frac{\partial z_{n'k'}}{\partial y_{nk}}\frac{\partial\chi_s{}^L}{\partial z_{n'k'}} \tag{26}$$

where the sum is over all the $3N$-6 internal coordinates.

Now using Eqs. (25) and (26) it is easily seen that Eq. (16) can be written in the form

$$\partial\psi_\mu{}^L/\partial y_{nk}=\sum_{s,j} D^L(R)_{\mu s}{}^*R_{kj}\Lambda_{nj}\chi_s{}^L \tag{27}$$

where the Λ_{nj} are a set of operators defined by the following equations:

$$\begin{aligned}\Lambda_{n1}=&\sum_{n'=2}^{N-1}\left(\delta_{nn'}-\frac{z_{n'3}}{z_{13}}\delta_{1n}\right)\frac{\partial}{\partial z_{n'1}}+\sum_{n'=2}^{N-1}\delta_{1n}\frac{z_{n'1}}{z_{13}}\frac{\partial}{\partial z_{n'3}}\\&-\frac{i}{2}\frac{\delta_{1n}}{z_{13}}(\lambda_+\sigma_++\lambda_-\sigma_-)\end{aligned} \tag{28}$$

$$\begin{aligned}\Lambda_{n2}=&\sum_{n'=3}^{N-1}\frac{z_{n'2}}{z_{21}}\left(\delta_{2n}-\frac{z_{23}}{z_{13}}\delta_{1n}\right)\frac{\partial}{\partial z_{n'1}}\\&+\sum_{n'=3}^{N-1}\left[\delta_{nn'}-\left(\frac{z_{n'3}}{z_{13}}-\frac{z_{n'1}}{z_{21}}\frac{z_{23}}{z_{13}}\right)\delta_{1n}-\frac{z_{n'1}}{z_{21}}\delta_{2n}\right]\frac{\partial}{\partial z_{n'2}}\\&+\left[\sum_{n'=3}^{N-1}\delta_{1n}\frac{z_{n'2}}{z_{13}}\frac{\partial}{\partial z_{n'3}}\right]-\frac{is}{z_{21}}\left(\delta_{2n}-\frac{z_{23}}{z_{13}}\delta_{1n}\right)\\&+\frac{\delta_{1n}}{2z_{13}}(\lambda_+\sigma_+-\lambda_-\sigma_-)\end{aligned} \tag{29}$$

$$\Lambda_{n3}=\sum_{n'=1}^{N-1}\delta_{n'n}\partial/\partial z_{n'3}. \tag{30}$$

Here σ_+ and σ_- are operators, which are defined by

$$\sigma_+\chi_s^L=\chi_{s+1}^L \tag{31}$$

and

$$\sigma_-\chi_s^L=\chi_{s-1}^L. \tag{32}$$

Differentiating Eq. (27) once again one obtains

$$\frac{\partial^2\psi_\mu^L}{\partial y_{n'k}\partial y_{nk}}=\sum_j\left[\frac{\partial R_{kj}}{\partial y_{n'k}}\sum_s D^L(R)_{\mu s}{}^*\Lambda_{nj}\chi_s^L+R_{kj}\frac{\partial}{\partial y_{n'k}}\sum_s D^L(R)_{\mu s}{}^*\Lambda_{nj}\chi_s^L\right]. \tag{33}$$

In the differentiating of ψ_μ^L, χ_s^L was an arbitrary function of the internal coordinates. In Eq. (33), $\Lambda_{nj}\chi_s^L$ can be treated as another function of the internal coordinates, and the differentiation of the second term can be carried out in a similar manner. Thus

$$\frac{\partial^2\psi_\mu^L}{\partial y_{n'k}\partial y_{nk}}=\sum_{s,j}\frac{\partial R_{kj}}{\partial y_{n'k}}D^L(R)_{\mu s}{}^*\Lambda_{nj}\chi_s^L+\sum_j R_{kj}\sum_{s,j'}D^L(R)_{\mu s}{}^*R_{kj'}\Lambda_{n'j'}\Lambda_{nj}\chi_s^L. \tag{34}$$

Now using Eqs. (12), (22), (23), (24), and the orthogonality condition of the R_{ij},

$$\sum_k R_{kj}R_{kj'}=\delta_{jj'}, \tag{35}$$

one obtains

$$\sum_k\frac{\partial^2\psi_\mu^L}{\partial y_{n'k}\partial y_{nk}}=\frac{1}{z_{21}}\left(\delta_{2n'}-\frac{z_{23}}{z_{13}}\delta_{1n'}\right)\sum_s D^L(R)_{\mu s}{}^*\Lambda_{n1}\chi_s^L+2\frac{\delta_{1n'}}{z_{13}}\sum_s D^L(R)_{\mu s}{}^*\Lambda_{n3}\chi_s^L+\sum_{sj}D^L(R)_{\mu s}{}^*\Lambda_{n'j}\Lambda_{nj}\chi_s^L. \tag{36}$$

These derivatives can now be substituted back into the modified Schroedinger equation, Eq. (4). The rotational coordinates can be eliminated from the resulting equations by making use of the orthogonality relations among the representation coefficients, i.e., multiplying both sides of the equation by a particular representation coefficient $D^L(R)_{\mu s}$, integrating over all rotations, and using Eq. (8). As a result one obtains the following equations:

$$\sum_{n=1}^{N-1}\sum_{n'=1}^{N-1}\frac{1}{m_n}\left(\delta_{nn'}-\frac{m_n}{m}\right)\left[\frac{1}{z_{21}}\left(\delta_{2n'}-\frac{z_{23}}{z_{13}}\delta_{1n'}\right)\Lambda_{n1}\chi_s^L+2\frac{\delta_{1n'}}{z_{13}}\Lambda_{n3}\chi_s^L+\sum_j\Lambda_{n'j}\Lambda_{nj}\chi_s^L\right]=(2/\hbar^2)(V-E)\chi_s^L. \tag{37}$$

Equations (37) apply to systems of any number of particles. In each case the internal configuration is specified by z_{13}, z_{21}, z_{23}, and z_{nk} ($k=1,2,3$; $n=3,4\cdots N$-1). This choice of coordinates was convenient in the development up to this point. However, Eq. (37) are quite cumbersome. It seems clear that for any particular N and for any particular type of problem it would be more convenient to use another set of coordinates to describe the internal configuration. The set of χ_s^L equations for three particles in terms of such a system of coordinates is discussed in the following section.

III. THE WAVE EQUATION FOR THE THREE-PARTICLE SYSTEM

For a system of three particles, in order to solve Eq. (37), it is convenient to specify the internal configuration by means of a new set of coordinates illustrated in Fig. 1, where ρ is the distance from particle 1 to the center of gravity of 2 and 3; ξ is the distance between 2 and 3; and φ is the angle between the line joining particle 1 with the center of gravity of 2 and 3 and the line joining 2 and 3. In terms of the z_{nk} we have

$$\rho=[m/(m_2+m_3)]z_{13} \tag{38}$$

$$\xi=\frac{m_2+m_3}{m_3}\left[z_{21}{}^2+\left\{z_{23}+\frac{m_1}{m_2+m_3}z_{13}\right\}^2\right]^{\frac{1}{2}} \tag{39}$$

and

$$\tan\varphi=\frac{z_{21}}{z_{23}+[m_1/(m_2+m_3)]z_{13}}. \tag{40}$$

Now taking Eq. (37), setting $N=3$, and changing variables to the ρ, ξ, φ system, one can obtain the set of equations for χ_s^L. The procedure is straightforward but somewhat cumbersome. The result is

$$\frac{1}{\mu}\left[\frac{\partial^2}{\partial\rho^2}+\frac{2}{\rho}\frac{\partial}{\partial\rho}-\frac{1}{\rho^2}\{L(L+1)-2s^2\}\right]\chi_s^L+\frac{1}{M}\left[\frac{\partial^2}{\partial\xi^2}+\frac{2}{\xi}\frac{\partial}{\partial\xi}\right]\chi_s^L+\left\{\frac{1}{\mu\rho^2}+\frac{1}{M\xi^2}\right\}\left[\frac{\partial^2}{\partial\varphi^2}+\cot\varphi\frac{\partial}{\partial\varphi}-s^2\csc^2\varphi\right]\chi_s^L+\frac{i}{\mu\rho^2}\left[\lambda_+(L,s)\left\{\frac{\partial}{\partial\varphi}+(s+1)\cot\varphi\right\}\chi_{s+1}^L+\lambda_-(L,s)\left\{\frac{\partial}{\partial\varphi}-(s-1)\cot\varphi\right\}\chi_{s-1}^L\right]=(2/\hbar^2)(V-E)\chi_s^L, \tag{41}$$

where M is the reduced mass of the "molecule" consisting of particles 2 and 3,

$$M=m_2m_3/(m_2+m_3), \tag{42}$$

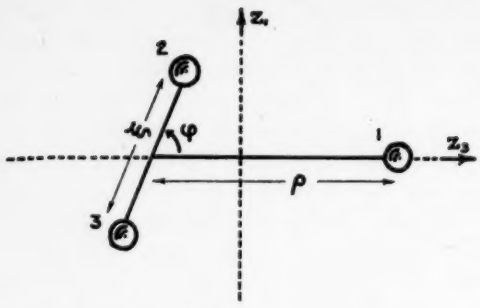

FIG. 1.

μ is another reduced mass,

$$\mu = m_1(m_2+m_3)/[m_1+(m_2+m_3)], \tag{43}$$

and $i=(-1)^{\frac{1}{2}}$.

Equations (41) are coupled differential equations for the internal functions χ_s^L for a system of three particles. The individual terms can be given some physical interpretations. The first bracket represents the relative translational motion of the "atom" and the "diatomic molecule" with the usual centrifugal potential. The second bracket represents the internal motion of the "molecule." The third is due to the relative rotation of the two systems; while the fourth is due to the coupling of the various rotations. This equation has been solved in a number of special cases of interest in collision problems and they will be discussed in a forthcoming paper. If the potential energy is a function of the separation of particles 2 and 3, only (i.e., a non-interacting atom and molecule), the solution to Eq. (41) can be determined exactly. For an arbitrary potential energy, perturbation methods, similar to those used by Zener,[4] can be used.

The authors wish to thank Dr. Eugene Wigner for many helpful discussions.

[4] C. Zener, Phys. Rev. **37**, 556 (1931).

THE JOURNAL OF CHEMICAL PHYSICS VOLUME 18, NUMBER 12 DECEMBER, 1950

Rotational Isomerism and the Vibrational Spectrum of 1,2-Dibromoethane

JOHN T. NEU AND WILLIAM D. GWINN
Department of Chemistry, University of California, Berkeley, California

(Received August 14, 1950)

An assignment of the vibrational frequencies of CH_2BrCH_2Br and CD_2BrCD_2Br has been made. The Raman spectra of these compounds have been redetermined using the new "Toronto"-type mercury arcs. It was possible, in the case of CH_2BrCH_2Br, to obtain a number of combination and overtone bands which were of assistance in the assignment. The liquid phase infra-red spectra of both compounds have been redetermined with greater resolution and spectral range than had been previously reported. The solid infra-red spectra of the same compounds were also determined in order to separate bands due to the *trans* isomer from those due to the *skew* isomer. Evidence for the C_2 symmetry of the high energy form has been given.

DIBROMOETHANE, CH_2BrCH_2Br, has been shown to exhibit rotational isomerism.[1–4] The low energy isomer has been generally accepted as being the *trans*-configuration (C_{2h} symmetry). The assignment of the high energy isomer however has not been generally agreed upon, being taken by some investigators to be the *cis*-configuration (C_{2v} symmetry), and by others to be the *skew* configuration (C_2 symmetry). A representation of these configurations is given in the first column of Table I.

Assignments of the observed Raman and infra-red bands have been made by Wu[2] and by Kohlrausch and Wittek,[5] using the *trans*- and *cis*-configurations. Mizushima and co-workers[1,4] have made a partial assignment of the observed frequencies on the basis of the *trans*- and *skew* configurations.

Calculating thermodynamic quantities, Gwinn and Pitzer[6] have used Wu's[1] assignments with the C_{2v} frequencies transformed to a C_2 (staggered) model. They note, however, that it is impossible to obtain agreement between the calculated and the experimentally determined thermodynamic properties for CH_2BrCH_2Br.

This research was undertaken to remove, in so far as possible, the uncertainties in the configuration of the rotational isomers and in the vibrational assignments for these isomers.

The following methods were used.

[1] Mizushima and Morino, Sci. Papers Inst. Phys. Chem. Research (Tokyo) **36**, 281 (1939).
[2] Ta-you Wu, *Vibrational Spectra and Structure of Polyatomic Molecules* (J. W. Edwards Brothers, Inc., Ann Arbor, Michigan, 1946), p. 306.
[3] G. Herzberg, *Infrared and Raman Spectra of Polyatomic Molecules* (D. Van Nostrand Company, Inc., New York, 1945), pp. 346, 350.
[4] Odan, Mizushima, and Morino, Sci. Papers, Inst. Phys. Chem. Research (Tokyo) **42**, 29 (1944).
[5] K. W. F. Kohlrausch and H. Wittek, Zeits. f. physik. Chemie B, **47**, 55 (1940).
[6] W. D. Gwinn and K. S. Pitzer, J. Chem. Phys. **16**, 303 (1948).

(a) Examination of de Hemptinne's[7] data on the various isomers obtained by the substitution of hydrogen by deuterium permitted the positive identification of the symmetry of the high energy form.

(b) Coincidence (or its absence) between the Raman and infra-red spectra and comparison of the solid and liquid phase spectra were used to separate the bands into groups corresponding to the two rotational isomers.

(c) Raman polarization data, selection rules, combination and overtone bands from the Raman as well as the infra-red spectra, and general characteristic frequency ranges of the various groups were used to make the actual assignments.

(d) The totally deuterated analog was prepared and

TABLE I. Configuration and Raman frequencies of 1,2-dibromoethane isomers.

CONFIGURATION					
FORM	CH_2BrCH_2Br	$CH_2BrCHDBr$	CH_2BrCD_2Br	$CHDBrCD_2Br$	CD_2BrCD_2Br
LOW ENERGY C_{2h}	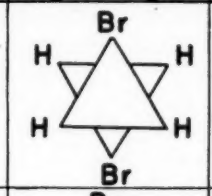	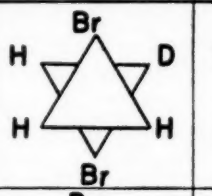	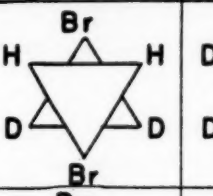	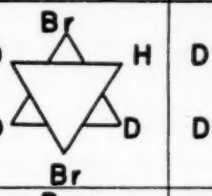	
HIGH ENERGY C_{2v}	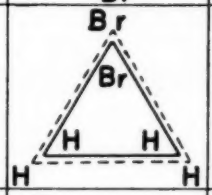	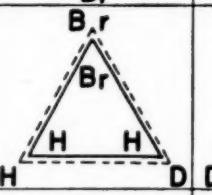	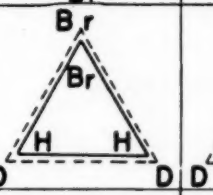	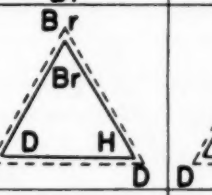	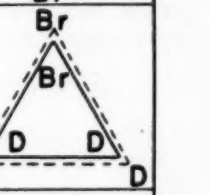
HIGH ENERGY C_2	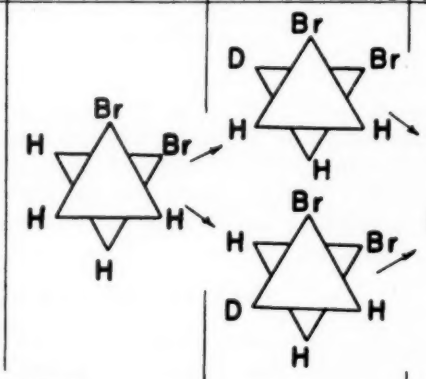		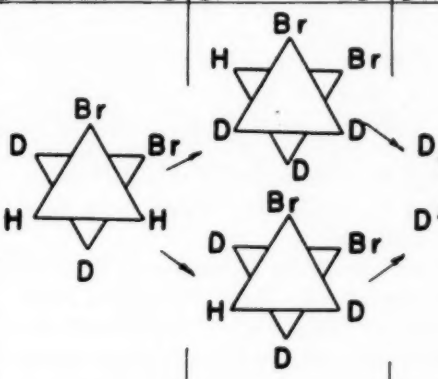		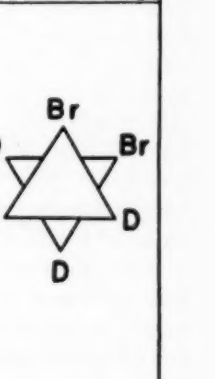
FREQUENCIES					
C_{2h}	188 (10)	188 (10)	188 (5)	187 (10)	188 (10)
C_2	356 (2)	[313 (1)] 342 (1) 352 (1)	341 (1)	321 (1) 333 (1)	316.5 (2)
C_2	552 (5)	532 (4) 546 (4)	528 (3)	518.5 (4) 523 (2)	517 5 (8)
C_2	581 (1)	565.5 (2) 580 (3)	551 (1) [571 (3)] $_{C_{2h}\nu_{17}}$	540 (2)	526.5 (3) [563.5 (0.5)] $_{C_{2h}\nu_{17}}$
C_{2h}	660 (15)	640 (15)	639 (6)	617 (10)	607 (15)

[7] M. de Hemptinne, Contrib. etude structure mol. Vol. commem Victore Henri, 151, (1947/48).

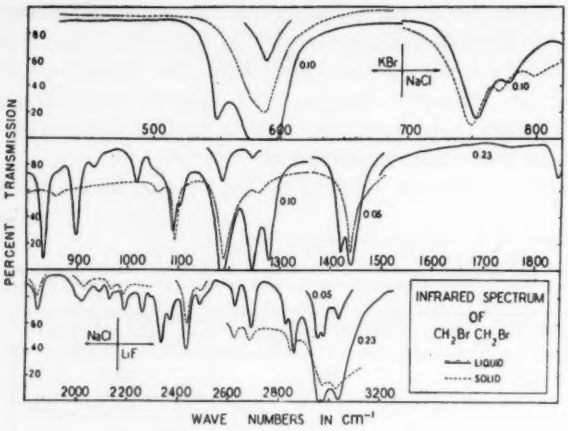

FIG. 1.

the Raman and infra-red spectra obtained. These data permitted the verification of the assignment by use of the product rule.

SELECTION OF THE CONFIGURATIONS OF THE ISOMERS

The experimentally observed spectra, used in conjunction with the selection rules and polarization of the Raman bands (see Table II) do not allow the assignments of the high energy configuration to be made with as much confidence as would be desired. Conclusive evidence in favor of the C_2 rather than C_{2V} symmetry was obtained however on examination of the Raman spectra of CH_2BrCH_2Br, $CHDBrCH_2Br$, CH_2BrCD_2Br, $CHDBrCD_2Br$ and CD_2BrCD_2Br, which have been recorded by de Hemptinne.[7]

If the high energy form were of symmetry C_{2V}, the four hydrogen atoms in this form of CH_2BrCH_2Br would be equivalent, and the molecules $CHDBrCH_2Br$, and $CHDBrCd_2Br$ would each give only one high energy rotational isomer, and would allow the same number of Raman lines as do CH_2BrCH_2Br, CH_2BrCD_2Br. If, on the other hand, the symmetry were C_2, two rotational isomers would be possible for the high energy forms of both $CHDBrCH_2Br$ and $CHDBrCD_2Br$ (see Table I) and two separate but similar Raman spectra originating from the two isomers would be expected to appear. CH_2BrCH_2Br, CH_2BrCD_2Br, and CD_2BrCD_2Br in the low energy form would exist in only one spatial isomer.

Examining the data of de Hemptinne,[7] we find that frequencies above 800 cm^{-1} are rather difficult to trace through the deutero isomers, but that the bromine stretching and bending frequencies show a regular behavior from one compound to another. Consequently frequencies corresponding to the bromine vibrations in these molecules, which may be grouped with some certainty, were taken for study and are listed in Table I. De Hemptinne's[7] data were used throughout in order that spectra obtained under similar conditions might be compared.

These data show that the high energy form has the symmetry C_2,* since, as deuterium atoms are added the bands assigned to the high energy form split and converge exactly as expected for the C_2 symmetry. Each successive substitution of a deuterium atom lowers the frequencies slightly.

The discrepancies which appear in Table I may be logically explained. Bands at 571 cm^{-1} in CH_2BrCD_2Br and at 563.5 cm^{-1} in CD_2BrCD_2Br are obviously due to a frequency (ν_{17}) of the *trans*-form. The 540 cm^{-1} band in $CHDBrCD_2Br$ is not reported as double, but it

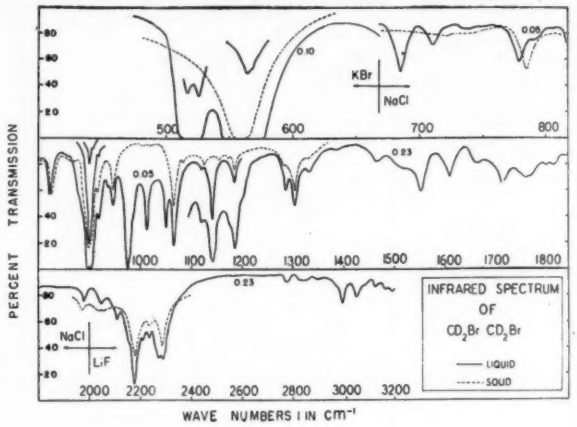

FIG. 2.

is possible that the doublet has such a small separation that it is not resolved. The band at 313 cm^{-1} in $CH_2BrCHDBr$, which was not reported in de Hemptinne's first paper,[8] is probably a combination or difference band.

CLASSIFICATION OF BANDS

The observed Raman and infra-red bands were separated into groups corresponding to the species present. The presence or absence of coincidence between the Raman and infra-red bands is one criterion for this classification. The low energy form (C_{2h}) has a center of symmetry, and therefore allows no coincidences, while for the high energy form, which has been shown to have C_2 symmetry, complete coincidence of the two spectra is allowed. In practice, however, this method is not without difficulty, since some allowed fundamentals occur very weakly or are not observed at all, and some forbidden fundamentals do appear in the liquid or solid phase.

It has been shown by Mizushima and Morino[9] that on freezing the dihaloethanes are converted to the C_{2h} form, and therefore spectra taken of the solid

* It should be pointed out that we have shown only that the high energy form is of C_2 symmetry. The data allows no decision between the eclipsed or staggered C_2 form. Since the low energy form is known to be the *trans*-configuration (staggered) we consider it very unlikely that the high energy form would be eclipsed configuration.

[8] M. de Hemptinne and C. Velghe, Physica **5**, 958 (1938).

[9] Mizushima and Morino, Proc. Ind. Acad. Sci. **8**, 315 (1938).

phase, when compared with the liquid phase spectra permit classification into groups. It must be remembered that experimental difficulties involved in obtaining Raman spectra of solids limit the completeness of the spectrum, and only the strong lines are obtained. We have used the data of Mizushima and Morino[1,9] on the Raman spectrum of solid CH_2BrCH_2Br and CD_2BrCD_2Br. We have obtained three exposures of the Raman spectrum of solid CD_2BrCD_2Br, and the appearance of the lines found by Mizushima and Morino was confirmed, and one additional very weak line (919 cm^{-1}) was found. In contrast to the Raman spectrum, the infra-red bands obtained from the solid are of intensity comparable to the corresponding bands of the liquid. We have obtained the liquid and solid infra-red spectra of both CH_2BrCH_2Br and CD_2BrCD_2Br. The liquid infra-red spectrum of 1,2-dibromoethane had been determined previously with less resolution by Cheng and Lecomte,[10] and more recently by Mizushima and co-workers.[11]

EXPERIMENTAL

The sample of CD_2BrCD_2Br was prepared by the steps shown in the following equations:

$$2D_2O+CaC_2=Ca(OD)_2+C_2D_2$$
$$PBr_3=3D_2O=3DBr+D_3PO_3$$
$$C_2D_2+2DBr+h\nu(\lambda=2537A)=CD_2BrCD_2Br.$$

About 20 cc were prepared. A small fractionating column operated at reduced pressure (14 mm) was used to fractionate the sample. The bulk of the material distilled at 78°C, the temperature at which the hydrogen compound distilled under the same pressure. A 6 cc middle fraction, thought to be of high purity, was used for spectra determinations. The Raman plates, however, showed that there was a weak fluorescence taking place, which prevented the determination of combinations and overtone lines. Besides the material causing the fluorescence, the most likely impurity in the sample would be $CHDBrCD_2Br$. Fortunately, the Raman spectrum of this compound is available[7] and it does appear that at least two of the Raman lines found are due to the trideuterated compound. Strong lines of $CHDBrCD_2Br$ which coincide with lines found in the CD_2BrCD_2Br sample are noted in Table V. The infra-red spectrum of $CHDBrCD_2Br$ is not available for comparison.

The sample of CH_2BrCH_2Br, obtained from Eastman Kodak Company was washed with concentrated H_2SO_4, then washed with water and dried over $MgSO_4$. The sample was finally distilled in a thirty plate column, the Raman sample being distilled directly into the Raman tube.

The infra-red spectra were obtained with a Perkin-Elmer spectrometer, model 12*C*, using KBr, NaCl, and LiF prisms. Dr. Earl K. Plyler[12] of the Bureau of Standards very kindly obtained the spectra of these compounds for us in the liquid phase using a thallium bromide-iodine prism and he also obtained the liquid spectrum of CD_2BrCD_2Br in the KBr region. The liquid phase spectra in the KBr, NaCl, and LiF regions

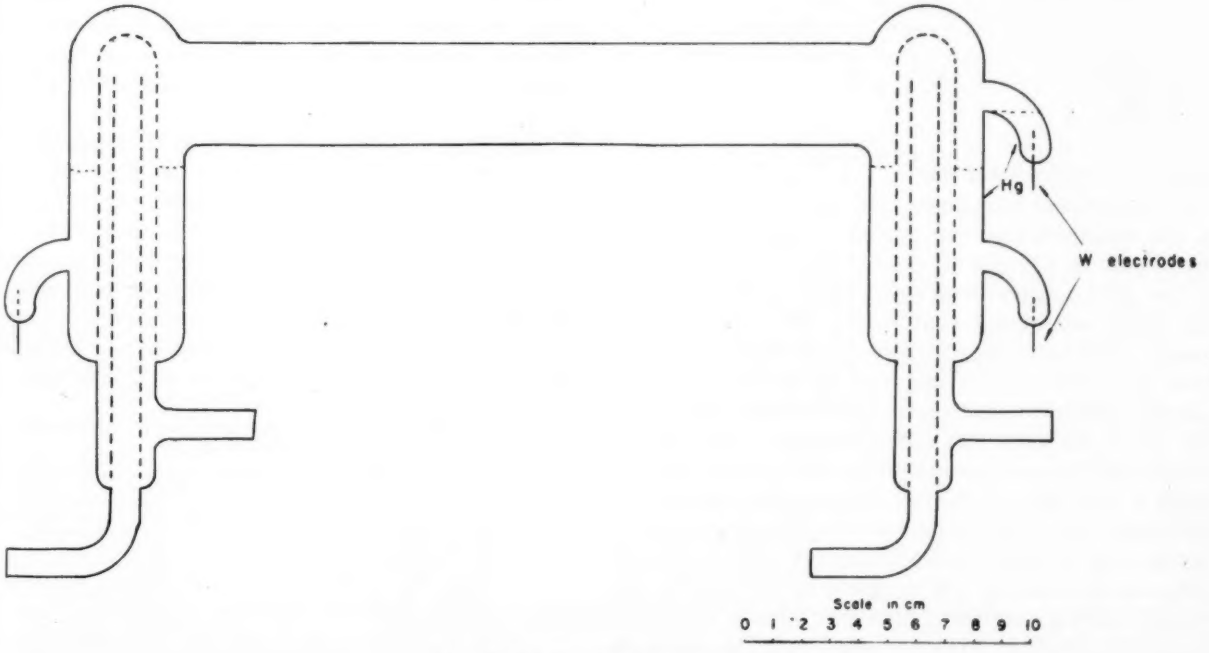

FIG. 3. Water-cooled mercury arc.

[10] Cheng and Lecomte, J. de phys. et rad. **6**, 477 (1935).
[11] Mizushima, Morino, Watanabe, Simanouti, and Yamaguchi, J. Chem. Phys. **17**, 591 (1949).
[12] Earl K. Plyler, J. Chem. Phys. **17**, 218 (1949) and private communication from Dr. Plyler.

TABLE II. Previous assignments of class A_g (*trans*-) fundamentals.[a]

	C−H stretching	CH_2 bending	CH_2 wagging	C−C stretching	C−Br stretching	CH_2Br deformation
Frequency assignment by Wu[b]	2972	1255	1052	932	659	190
CD_2Br-CD_2Br frequency	2180	992	907	[711]	607	188
$\left(\frac{\nu_D}{\nu_H}\right)^2$	0.542	0.625	0.743	0.588	0.848	0.979
$\prod_{i=1}^{6}\left(\frac{\nu_D}{\nu_H}\right)_i^2=0.124$ Calculated 0.126						
Frequency assignment by Kohlrausch[c]	2972	1438	1255	932	659	190
CD_2BrCD_2Br frequency	2180	1155	992	[791]	607	188
$\left(\frac{\nu_D}{\nu_H}\right)^2$	0.542	0.645	0.625	0.721	0.848	0.979
$\prod_{i=1}^{6}\left(\frac{\nu_D}{\nu_H}\right)_i^2=0.131$ Calculated 0.126						
Frequency assignment by Odan *et al.*[d]	2972	1438	1255	1052	659	190
CD_2BrCD_2Br frequency	2180	1155	992	907	607	188
$\left(\frac{\nu_D}{\nu_H}\right)^2$	0.542	0.645	0.625	0.743	0.848	0.979
$\prod_{i=1}^{6}\left(\frac{\nu_D}{\nu_H}\right)_i^2=0.135$ Calculated 0.126						

[a] To avoid confusion, the numerical values of frequencies found in this work were used.
[b] See reference 2.
[c] See reference 5.
[d] See reference 4.

represented by a solid line in Fig. 1 were obtained in the conventional type liquid cells. Due to uncertainties in the cell thickness, the percent transmission of the liquid may be in error by as much as ten percent.

The solid spectra were obtained in a cell similar to the liquid cell except that in the place of the rings usually used to clamp the salt plates together, hollow brass rings were used. These were flat on the side which pressed against the salt plates and had openings at the top for introduction of the refrigerant. The sample was placed between the salt plates in the usual manner using a lead spacer, the salt plates were clamped together by means of the hollow brass rings and the assembly was fastened in the light path. The light path between the housings not occupied by the sample was encased with a cardboard tube and filled with dry air to prevent fogging of the salt windows. The spectrum was traced with the sample in the liquid phase; the chart paper was then turned back to the starting point and the spectrum was retraced with the sample frozen by the introduction of dry ice and acetone into the hollow rings. The solid, of course, scattered a large percent of the light and in order to get a trace comparable to the liquid, the deflection was increased by opening the slit and advancing the gain of the amplifier to the point that the deflection was approximately equal to that of the liquid. Consequently, although the percent transmission for the solid, indicated by a dotted line in Figs. 1 and 2 has little meaning, the positions of the bands and their relative intensities are significant.

Recently, a new type of mercury arc[13] has been developed using water-cooled electrodes. This arc gives a very high intensity 4358A exciting line with an exceedingly low continuous background. In the past, it has been found that with the G.E. AH2 or AH11 arcs, very long exposures were not fruitful since the continuous background from the mercury arc was sufficient to blanket weak lines. Filters have been devised to reduce this background and isolate the exciting line but they are only partially successful. As a result of this difficulty combination and overtone bands have seldom been observed in the Raman effect. With the water-cooled mercury arc, however, it has been possible to obtain long exposures without the prohibitive continuous background formerly encountered. The arcs used (see Fig. 3) were patterned after arcs already described.[13] Water was circulated through the space provided at each electrode. A d.c. potential was applied across the lower electrodes and the arc was started by application of a spark coil to the upper electrode. The arcs were operated from the 110-volt d.c. line using a resistance in series. Each arc was operated at about 750 watts (25 amp., 30 volts). A type GH Steinheil spectrograph with f10 collimator and camera optics was used. The dispersion was about 10A/mm. Eastman 103aO and 103aJ plates were employed.

Two arcs were used in obtaining the spectra. The Raman tube and the arcs were parallel, with the Raman tube in the middle. A reflector of polished chromium plated copper was placed around the arcs and Raman tube. The 4358A mercury line was used for excitation. A Wratten 2A gelatin filter was used to eliminate 4047A excitation and a water solution of Rhodamine 5GDN extra was used to reduce light from the arcs on the long length side of 4358A. Water was

TABLE III. The carbon-carbon stretching frequency in several substituted ethanes.

Compound	Frequency
$ClCH_2CH_2Cl$[a]	1054 (3)[a]*P*[a]
$BrCH_2CH_2Br$[a]	1052 (8)[a]*D*[a]
ICH_2CH_2I[a]	1038 (3)[a]
$ClCH_2CH_2Br$[b]	1056 (3)[b]*D*[a]
$ClCH_2CH_2I$[b]	1050 (3)[b]
$BrCH_2CH_2I$[b]	1051 (6)[b]

[a] See reference 5.
[b] Mizushima, Morino, Miyahara, Tomura, Okamoto, Sci. Pap. Inst. Phys. Chem. Res. Tokyo **39**, 387 (1942).

[13] Welsh, Crawford, and Scott, J. Chem. Phys. **16**, 97 (1948).

TABLE IV. Spectrum of $CH_2Br\ CH_2Br$.

Raman					Infra-red				
Solid[a]	Int.	Liquid	Int.	[b]	Solid	Int.	Liquid	Int.	Assignment
		91	2	*D*					ν_{10}' (A)
187	7	190	9	*P*					ν_8 (A_g)
		231	2	*P*					ν_6' (A)
		325(?)	0						
		355	4	*D*			355[d]		ν_{18}' (B)
		375	0						$2\nu_6$ (A_g)
		390	0						$\nu_4-\nu_5$ (A_g)
							402[d]		$\nu_{17}-\nu_6$ (B_u)
		470	1						$\nu_8-\nu_6$ (A_g)
		551	8	*P*			550	*m*	ν_5' (A)
		581	4	*D*					ν_{17}' (B)
					589	*s*	589	*s*	ν_{17} (B_u)
656	10	659	10	*P*					ν_5 (A_g)
		753	1		750	*s*	753	*s*	ν_9 (A_u)
					770	*m*	773	*w*	$\nu_6+\nu_{17}$ (B_u)
		781	1						$\nu_2-\nu_6$ (A_g)
					797(?)	*w*			$\nu_5+\nu_{18}$? (B_u)
		836	2	*D*			836	*s*	ν_{13}' (B)
		856(?)	0		856	*vw*			$\nu_6+\nu_5$ (A_g)
		898	2	*P*			898	*m*	ν_9' (A)
933	0	932	1	*P*			930	*vw*	ν_{13} (B_g)
		943(?)	0						
		1017	1				1019	*m*	ν_4' (A)
1057	5	1052	8	*D*	1058	*vw*			ν_4 (A_g)
					1092	*m*	1087	*m*	ν_8 (A_u)
		1104	1	*D*			1104	*w*	ν_8' (A), ν_{12}' (B)
1157	1	1169	1	?					ν_{12} (B_g)
		1186	0	*D*	1191	*s*	1186	*vs*	ν_{16} (B_u)
		1243	1				1245	*s*	ν_{16}' (B)
1254	8	1255	9	*P*	1259	*vw*			ν_3 (A_g)
		1276	2	?			1278	*m*	ν_3' (A)
		1418	3	*D*			1420	*m*	ν_2' (A), ν_{15}' (B)
1436	3	1438	4	*D*?					ν_2 (A_g)
					1441	*s*	1441	*vs*	ν_{15} (B_u)
		1507	0						$2\nu_9$ (A_g)
		1709	1						$\nu_4+\nu_5$ (A_g)
					—		1844	*w*	$\nu_{18}+\nu_5$ (B_u)
		1911	1						$\nu_3+\nu_5$ (A_g)
					2026	*w*	2019	*w*	$\nu_8+\nu_{13}$ (B_u)
							2081	*vw*	$\nu_{16}'+\nu_{13}'$ (A)
		2092	1						$\nu_5+\nu_2$ (A_g)
					2123	*w*	2121	*w*	$\nu_{13}+\nu_{16}$ (A_u)
							2145(?)	*vvw*	$\nu_4+\nu_8$ (A_u)
		2172	0						$\nu_3'+\nu_9'$ (A)
					2177	*w*	2183	*w*	$\nu_2+\nu_9$ (A_u)
							2256	*w*	$\nu_2'+\nu_{12}'$ (B)
							2292	*vw*	$\nu_3'+\nu_4'$ (A)
		2304	1						$\nu_3+\nu_5$ (A_g)
					—[c]		2336	*w*	$\nu_3+\nu_8$ (A_u)
		2370	1						$2\nu_{16}$ (A_g)
		2404?	0						
					2437	*w*	2434	*m*	$\nu_3+\nu_{16}$ (B_u)
					2483	*w*	2486	*vw*	$\nu_4+\nu_{15}$ (B_u)
					2625	*w*	2625	*w*	$\nu_2+\nu_{16}$ (B_u)
					2685	*w*	2690	*m*	$\nu_{15}+\nu_3$ (B_u)
		2827	1				2826		$2\nu_2'$ (A)
2848	2	2860	3	*P*	2844	*w*	2858	*m*	$2\nu_2$ (A_g)
		2953	8	*P*			2953	*vs*	ν_1' (A), ν_7' (A)
2968	8	2972	9	*P*					ν_1 (A_g)
					2974	*s*	2974	*vs*	ν_{14} (B_u)
		3005	5						ν_{11}' (B), ν_{14}' (B)
3020	2	3018	6	*D*					ν_{11} (B_g)
					3025	*s*	3037	*s*	ν_7 (A_u)
							3244	*vw*	$\nu_{11}'+\nu_6'$? (B)
							3308	*vw*	
							3357	*vw*	

[a] Data of Mizushima and Marino (see reference 9).
[b] These polarizations data were taken from a review of the existing data made by Kohlrausch and Wittek (see reference 5).
[c] No data obtained.
[d] Data of Dr. E. K. Plyler (see reference 12).

TABLE V. Spectrum of $CD_2Br\ CD_2Br$.

Raman					Infra-red				
Solid[a]	Int.	Liquid	Int.		Solid	Int.	Liquid	Int.	Assignment
		87	2						ν_{10}' (A)
188		188	8	*P*					ν_6 (A_g)
		317	3	*D*?			319[c]	*s*	ν_{18}' (B)
							376[c]	*w*	$\nu_9-\nu_6$ (A_u)
							429[c]	*w*	$\nu_3-\nu_9$ (A_u)
		518	6	*P*			517	*s*	ν_5' (A)
		526	3	*D*?			526	*s*	ν_{17}' (B)
		564	1		560	*s*	564	*vs*	ν_{17} (B_u), ν_9 (A_u)
605		607	10	*P*					ν_5 (A_g)
		612	2						$CD_2Br-CHDBr$[d]
		657	1						$\nu_9+\nu_{10}$ (A_g)
		686	1				685	*m*	ν_{13}' (B)
		712	2				711	*w*	ν_9' (A)
		738?	0				738	*w*	$\nu_{15}'-\nu_{18}'$ (A)
					783	*m*	779	*m*	ν_8 (A_u)
		791	1				791	*vw*	ν_8' (A), ν_{12}' (B)
		824	1		826	*m*	823	*m*	$CD_2Br-CDHBr$[d]
					876	*w*			
					900	*s*	900	*vs*	ν_{16} B_u
907		907	4	*P*			905	*vw*	ν_4 (A_g)
919[aa]		919	1		919	*w*	919	*w*	ν_{12} (B_g)
							936	*vw*	$\nu_3'-\nu_{10}'$ (A)
		947	0				947	*m*	ν_4' (A)
		979[b]					975	*s*	ν_{16}' (B)
989		992	7	*P*					ν_3 (A_g)
		1015	2	*P*			1013	*m*	ν_3' (A), $CD_2Br-CDHBr$[d]
		1029[b]							
		1051	2				1050	*m*	ν_{15}' (B)
					1064	*s*	1067	*s*	ν_{15} (B_u)
					1083	*vw*	1090	*vvw*	$\nu_{16}+\nu_6$ (B_u)
					1122	*w*	1120	*vw*	$CHDBrCD_2Br$[d]
							1141	*s*	ν_2' (A)
1154		1155	4	*P*	1151	*vw*	1154	*vvw*	ν_2 (A_g)
					1171	*vw*	1170	*vvw*	$\nu_5+\nu_9$ A_u
		1186	1		1187	*m*	1186	*m*	$CHDBrCH_2Br$[d]
							1204(?)	*vw*	$\nu_{13}'+\nu_5'$ B
							1227	*vw*	$\nu_9'+\nu_5'$ (A)
					1283?	*vvw*	1287	*w*	$CHDBrCD_2Br$[d]
					1305	*w*	1305	*w*	$\nu_{14}-\nu_4$ (B_u)
							1331	*w*	$\nu_3'+\nu_{18}'$ (B)
							1465(?)	*vw*	$\nu_4'+\nu_5'$ (A)
							1553	*w*	$\nu_{17}+\nu_3$ (B_u)
							1612	*w*	$\nu_{13}+\nu_{16}$ (A_u)
							1661?	*vw*	$\nu_9'+\nu_4'$
							1710	*w*	$\nu_{17}+\nu_2$ (B_u)
					1978	*w*	1978	*w*	$\nu_{15}+\nu_4$ (B_u)
					2046	*w*	2046	*w*	$\nu_1+\nu_{18}$ (?)
		2098	0						
							2107	*w*	$2\nu_{15}'$ (A)
		2130	1	*P*					
		2150	0				2158(?)	*vw*	$\nu_2'+\nu_3'$ (A)
		2174	6	*P*	2174	*m*	2174	*s*	ν_1' (A), ν_7' (A)
2180		2187	8	*P*			2189	*vw*	ν_1 (A_g)
					2209	*w*	2209	*w*	ν_{14} (B_u)
							2234	*w*	ν_{11}' (B)
		2271	1				2272	*m*	ν_{14}' (B)
		2280	1						ν_{11} (B_u)
					2290	*w*	2290	*s*	ν_7 (A_u)
							2278(?)	*vw*	$\nu_{14}'+\nu_5'$ (B)
							2838?	*vw*	$\nu_{17}+\nu_{11}$ (A_u)
							2890?	*vw*	$\nu_5+\nu_7$ (A_u)
							2997	*w*	$\nu_{13}+\nu_7$ (B_u)
					3050?	*vw*	3050	*vw*	$\nu_8+\nu_{11}$ (B_u)
							3080	*vw*	$\nu_1+\nu_{16}$ (A_u)
							3132	*vw*	$\nu_{14}+\nu_{12}$ (A_u)
							3165	*vw*	$\nu_{11}+\nu_{16}$ (A_u)
					3190?	*vw*	3190	*vw*	$\nu_7+\nu_4$ (A_u)
					3267	*w*	3267	*m*	$\nu_1+\nu_{15}$ (B_u)
					3342?	*vw*	3342	*m*	$\nu_{15}+\nu_{11}$ (A_u)
					3440?	*vw*	3440	*w*	$\nu_7+\nu_2$ (A_u)

[a] The values were taken from the work of Mizushima and Morino (see reference 1).
[aa] Data obtained in this research (see text).
[b] This value was not observed in this research and was taken from reference 7.
[c] Data of E. K. Plyler, (see reference 12).
[d] Raman bands of $CHDBrCD_2Br$ which might be confused with CD_2BrCD_2Br bands: 610(10), 824(7), 1014(10), 1123(5), 1185(10), 1286.5(0.5). (See reference 7.)

TABLE VI. Spectrum of CH_2ClCH_2Cl.

Raman					Infra-red			
Solid[a]	I	Liquid[b]	I	Polarization[c]	Gas[d]	I	Contour[d]	Assignment
		124	(5b)	*P*				ν_{10}' (A)
		223[a]	(00)					ν_{18} (B_u)
		264	(4)	*P*	272[e]			ν_6' (A)
302	(5)	301	(10)	*P*				ν_8 (A_g)
		410	(4)	*D*	412[e]			ν_{18}' (B)
		454	(00)					
					543	*m*		$\nu_6+\nu_{18}$ (A_u)
		653	(12)	*P*				ν_5' (A)
		676	(5b)	*D*	695	*m*	triplet	ν_{17}' (B)
					728	*s*	doublet	ν_{17} (B_u)
750	(10)	753	(15)					ν_5 (A_g)
					772	*w*	singlet	ν_9 (A_u)
					832	*vw*		
		881	(3)	*D*	890	*m*	triplet	ν_{13}' (B)
		943	(5)	*P*	946	*m*	doublet	ν_9' (A)
992	(3)	991	(1)	*P*	993	*w*		ν_{13} (B_g)
		1032	(1)		1027	*w*		ν_4' (A)
1059	(3)	1054	(3)	*P*				ν_4 (A_g)
		1143	(1)	*D*	1124	*w*		ν_3' (A)
		1207	(5)	*P*				ν_3' (A)
					1235	*s*	doublet	ν_{16} (B_u)
1265	(2b)	1263	(2)	*D*				ν_{12} (B_g)
					1291	*s*	triplet	ν_{16}' (B)
1301	(5b)	1302	(5)	*P*				ν_2 (A_g)
					1319	*w*		
		1428	(5)	*D*	1425	(*s*)[a]		ν_2' (A)
1448	(2b)	1442	(3)	*D*				ν_2 (A_g)
					1460	*m*	doublet	ν_{15} (B_u)
					1531	*w*		
		2845	2b	*P*				
2874	(3)	2873	3	*P*	2881	*m*		
2964	(10)	2956	12	*P*				ν_1 (A_g)
3005	(6)	3002	6b	*D*				ν_{11} (B_g)
					3029	*s*		ν_7 (A_u), ν_{14} (B_u)

[a] Mizushima, Morino, Watahabe, Simanouti, and Yamaguchi, J. Chem. Phys. **17**, 591 (1949).
[b] See reference 5.
[c] J. T. Neu and W. D. Gwinn, J. Chem. Phys. **16**, 1004 (1948).
[d] H. J. Bernstein, J. Chem. Phys. **17**, 258 (1949).
[e] This band was observed in the liquid by Plyler, see reference 12.

circulated through a jacket around the Raman tube and filters to keep them approximately at room temperature (25°C). A large Raman tube (100 cc) was used for CH_2BrCH_2Br since an ample sample was available. This tube was mounted directly in front of the slit. Due to limited amount of sample, a small (6 cc) Raman tube was used for CD_2BrCD_2Br. It was placed about 18 inches from the spectrograph and a lens was used to focus the light on the slit. The polarization data listed in Table V were obtained when it became evident that pairing of the lines between the two compounds was going to be difficult. The data are only qualitative and were obtained by the two exposure methods first used by Edsall and Wilson.[14] The data on CH_2BrCH_2Br, CD_2BrCD_2Br, and $CH_2ClClCH_2Cl$ are listed in Tables IV, V, and VI, respectively.

ASSIGNMENT OF FREQUENCIES

The nature of the vibrational modes in dibromoethane has been described by both Wu,[1] and Kohlrausch and Wittek.[3] The rather extensive data now available make it possible to improve the original assignment of the vibrational frequencies (Table VII).

C_{2h} (*trans*-)

Class A_g (Raman active, totally symmetric)

The Raman lines in the totally symmetric class may have a degree of depolarization ranging from zero (completely polarized) up to 6/7 (depolarized), and it has been found that in most compounds they are the most intense lines.

The class A_g assignments of the previous authors are shown in Table II. It is seen that there is complete agreement on the CH stretching vibration (2972 cm^{-1}), the C—Br stretching vibration (659 cm^{-1}), and the Br—C—C—Br bending vibration (190 cm^{-1}). Since our data are consistent with these selections, the above frequencies have been adopted. A fourth frequency, 1255 cm^{-1}, has also been assigned in this class by all authors, though not as the same vibrational mode. Two additional frequencies are necessary to complete this class, and the only selections which are at all plausible are among those made by the previous authors (see Table II). A choice of these frequencies may

[14] J. T. Edsall and E. B. Wilson, Jr., J. Chem. Phys. **6**, 124 (1938).

be made by application of the product rule of the observed bands in the light and heavy compounds. On the basis of polarization data and the solid spectrum it is possible to pair with some certainty the frequencies of the deuterium compound corresponding to the frequencies of the hydrogen compound for all possible A_g bands except 932 cm^{-1}. For this band, which has no apparent analog, an observed frequency which gives product rule agreement was selected. The results are shown in Table II.

The Raman bands of the deuterium compound selected to correspond to the 932 cm^{-1} band in the assignments of Wu[1] and Kohlrausch[3] are ones which obviously belong to the C_2 form. (They do not appear in the solid, and have comparable intensity in the infra-red and Raman spectra.) Furthermore, the above selections required the C—C stretching frequency to shift more than the frequencies corresponding to hydrogen motions. Any other possibility such as pairing the 932 cm^{-1} band with the 907 cm^{-1} band introduced even greater discrepancies. Therefore, the assignments of Wu[2] and Kohlrausch[5] were not accepted.

In the third assignment, in which the pairing of frequencies is complete, the agreement between the calculated and observed product rule values is good, as has been pointed out earlier by Mizushima and Morino.[1] The discrepancy (about one percent per frequency) is of the magnitude and direction to be expected on the basis of the anharmonicity of the vibrations involved. Furthermore, the individual frequencies change in a very reasonable manner, in going from the hydrogen to the deuterium compounds. The two bromine vibrations are practically unchanged. The hydrogen stretching mode changes by a factor of approximately 2 ($\nu^2_{heavy}/\nu^2_{light}=0.542$). The other two hydrogen modes change by large factors (for CH_2 bending, $\nu^2_{heavy}/\nu^2_{light}=0.645$; and for CH_2 wagging, $\nu^2_{heavy}/\nu^2_{light}=0.625$). For the C—C stretching mode this change is an intermediate value ($\nu^2_{heavy}/\nu^2_{light}=0.743$).

It is felt that on the basis of characteristic frequencies the assignment of Mizushima and Morino[1] is the most reasonable. There are, however, two points which do not seem to be entirely consistent with this assignment: the 1052 cm^{-1} band is listed as depolarized, and 932 cm^{-1} is listed as polarized. In regard to the polarization of Raman lines, it might be said that the determination of the polarization of isolated intense Raman lines which are strongly polarized presents essentially no difficulty experimentally. Unfortunately, however, all lines of interest do not occur in this category. The complications of low intensity, the overlapping by other Raman lines or the exciting line, and weak polarization tend to make a decision as to whether a line is polarized or depolarized, difficult or impossible. Furthermore, a band determined as depolarized is not necessarily ruled out of a "polarized class," for the depolarization factor of a totally symmetric vibration may take on any value up to the limiting value expected for a depolarized band. Consequently the reported depolarization of 1052 cm^{-1} is not a direct contradiction of the assignment. (The assignment of 932 cm^{-1} is discussed under class B_g.)

An examination of the frequencies and the polarization of the corresponding bands in other substituted ethanes is of interest in this regard. When the bromine atoms are replaced by other halogens (I, Cl) a frequency at 1052 cm^{-1} seems to remain almost constant throughout several molecules, as shown in Table III. The last three compounds were measured in the solid state, and the frequencies listed are the only ones found which are in the range of the C—C vibration. It is considered likely that in all cases this frequency corresponds to the C—C stretching vibration, which is essentially a vibration involving only the $CH_2—CH_2$ skeleton.

Additional support for this assignment is found on examination of the observed combination bands. The Raman combination bands occur with very low intensity, and consequently these bands are most likely to be of class A_g, which contains the strongest fundamental bands. It will be seen in Table VI that all the Raman combinations except one may be explained as belonging to class A_g. The band at 1052 cm^{-1} is found in combination with two class A_g bands. (See the bands at 1709 cm^{-1} and at 2304 cm^{-1} in Table IV.) This lends support to the assignment of 1052 cm^{-1} as an A_g frequency.

Class B_g (Raman active, depolarized)

There are three weak Raman bands which persist in the solid spectrum and were not assigned in Class A_g. This is the number of bands required for this class. The bands are: 3018 cm^{-1} reported as depolarized, 1169 cm^{-1} of questionable polarization, and 932 cm^{-1} reported as polarized. The assignments of 3018 cm^{-1} and 1169 cm^{-1} to the C—H stretching vibration and the CH_2 twisting vibration are straightforward.

The assignment of 932 cm^{-1} to the rocking modes is reasonable, however, the reported polarization datum is not consistent with this assignment. There are no plausible combinations or differences of fundamentals which can account for this band, so it must be assumed that it is a fundamental. This band is very weak, and it is possible that the recorded polarization datum is in error. A careful examination of a strongly exposed Raman plate shows that this line is probably double, with bands appearing at 932 cm^{-1} and 943 cm^{-1}, the latter being somewhat the weaker of the two. Possibly the reported polarization is due to a polarized band superimposed on a depolarized line, the polarized line remaining in the spectrum of the solid. These two possible explanations, while reasonable, are not very satisfactory, and 932 cm^{-1} is assigned in this class, subject to some uncertainty.

There are only two bands unassigned in the deutero compound, namely 2280 cm^{-1} and 919 cm^{-1}, and they

TABLE VII. Frequency assignment.

	Trans-C_{2h}					Skew C_2					CH_2Cl-CH_2Cl			
	CH_2Br-CH_2Br		CD_2Br-CD_2Br		$\left(\frac{\nu_D}{\nu_H}\right)^2$	CH_2Br-CD_2Br		CD_2Br-CD_2Br		$\left(\frac{\nu_D}{\nu_H}\right)^2$	*trans*-C_{2h}		Skew C_2	
	Raman	*IR*	Raman	*IR*		Raman	*IR*	Raman	*IR*		Raman	*IR*	Raman	*IR*
Class A_g in C_{2h}														
Class A in C_2														
ν_1 (C−H stretching)	2972		2187		0.542	2953	2953	2174	2174	0.542	2956		2956	
ν_2 (CH_2 bending)	1438		1155		0.645	1418	1420		1141	0.647	1442		1428	
ν_3 (CH_2 wagging)	1255		992		0.625	1276	1278	1015	1013	0.630	1302		1207	
ν_4 (C−C stretching)	1052		907		0.743	1017	1019	947	947	0.867	1054		1032	
ν_5 (C−Br stretching)	659		607		0.848	551	550	518	517	0.884	753		653	
ν_6 (C−C−Br bending)	190		188		0.979	231	—	—	—	0.80	301		264	272
Product rule check for Class A_g in the *trans*-form: $\prod_1^6 \left(\frac{\nu_D}{\nu_H}\right)^2 = 0.135$ Calculated 0.126														
Class A in C_2 (cont.)														
Class A_u in C_{2h}														
ν_7 (C−H stretching)		3037		2290	0.569	2953	2953	2174	2174	0.542		3029	2956	
ν_8 (CH_2 twisting)		1087		779	0.514	1104	1104	791	791	0.513			1143	1144
ν_9 (CH_2 rocking)		753		564	0.561	898	898	712	711	0.629		772	943	946
ν_{10} (torsion)			Calculate		0.817	86		86		0.893			125	
Product rule check for Class A_u in the *trans*-form: $\prod_6^{10} \left(\frac{\nu_D}{\nu_H}\right)^2 = 0.136$ Calculated 0.128														
for Class A in the skew form: $\prod_1^{10} \left(\frac{\nu_D}{\nu_H}\right)^2 = 0.0212$ Calculated 0.0165														
Class B_g in *trans*-														
Class B in *skew*														
ν_{11} (C−H) stretching)	3018		2280		0.517	3005			2234	0.553	3002		2956	
ν_{12} (C−H_2 twisting)	1169		919		0.617	1104	1104	791	791	0.513	1256		—	
ν_{13} (CH_2 rocking)	932		712		0.584	836	836	686	686	0.673	991		881	
Product rule check for Class B_u in the *trans*-form: $\prod_{11}^{13} \left(\frac{\nu_D}{\nu_H}\right)^2 = 0.206$ Calculated 0.190														
Class B_u in *trans*-														
Class B in *skew* (cont.)														
ν_{14} (C−H stretching)		2974		2209	0.552	3005		2271	2272	0.571		3029	2956	
ν_{15} (C−H_2 bending)		1441		1061	0.548	1418	1420	1051	1050	0.549		1460	1428	1425
ν_{16} (CH_2 wagging)		1186		900	0.576	1243	1245		975	0.614		1235		1291
ν_{17} (C−Br stretching)		589		564	0.917	581	—[a]	526	526	0.820		728	676	695
ν_{18} (C−C−Br bending)	[140]	—	—	—		355	355	317	319	0.803	223		410	412
Product rule check for Class B in the *skew* form: $\prod_{11}^{18} \left(\frac{\nu_D}{\nu_H}\right)^2 = 0.024$ Calculated 0.021														

[a] The strong band at 589 cm^{-1} due to the *trans*-form probably masks this band.

may be paired with 3018 cm^{-1} and 1169 cm^{-1} respectively. If 932 cm^{-1} is taken as the third frequency, a band at about 710 cm^{-1} would be required to give product rule agreement. The observed band at 711 cm^{-1} appears also in the infra-red, and hence has been assigned to the C_2 form. Possibly a weak C_{2h} band in this region is not observed, or coincides with the C_2 band. It was found that the combination band at 1612 cm^{-1} could be explained if a 712 cm^{-1} class B_g band were assumed. ν_{15} is assigned as 712 cm^{-1} in Table VII, and is listed in parentheses, but is subject to considerable doubt.

Class B_u (infra-red active)

Better resolution of the liquid spectrum, and the determination of the solid infra-red spectrum have made obvious the necessity of rather extensive revision of the previous infra-red assignments. For example, the infra-red active C−Br stretching frequency in class B_u can now be confidently assigned to the 569 cm^{-1} band of the *trans*-form, since it remains strong in the solid spectrum. Wu[2] and Kohlrausch[5] have, however, assigned this band to the *skew* form.

The CH_2 bending, CH_2 wagging, and C−Br stretching in this class are essentially the same as the corresponding modes in class A_g, except that the end groups vibrate out of phase. They would be expected therefore to have approximately the same frequency. On this basis the assignements of 1441 cm^{-1} (CH_2 bending), 1186 cm^{-1} (CH_2 wagging), and 589 cm^{-1} (C−Br stretching) have been made. There is no suitable infra-red frequency available which could have been used in the place of 1441 cm^{-1} or 589 cm^{-1}. However the band at 1087 cm^{-1} might be substituted for 1186 cm^{-1}. The decision between these two lines was made by examination of the gas phase band contour of 1186 cm^{-1}. The gas phase band contour was determined by placing a beaker of dibromoethane under the front housing of the spectrograph, and allowing the vapor to fill the housing. The 1186 cm^{-1} band was the only one which was intense

enough to be determined in this manner. A class B_u vibration should have a doublet contour, and a class A_u a singlet contour. The fact that the line was found to be doubled placed it definitely in the B_u class.

Two suitable bands (3018 cm^{-1} and 2974 cm^{-1}) appear in the CH_2 stretching region. The 2974 cm^{-1} was somewhat arbitrarily placed in this class, and 3018 cm^{-1} was placed in class A_u.

The C—CBr bending frequency ν_{18}, was too low to be observed on a prism instrument. Since ν_{18} is important in the calculation of the partition function, it is very desirable to obtain this frequency and a direct measurement of this band by a grating infra-red instrument would be highly desirable. We do have two indications that the band may have a frequency of about 140 cm^{-1}. A weak infra-red band at 797 cm^{-1} in the solid spectrum of CH_2BrCH_2Br can be explained if a band at 138 cm^{-1} is assumed $659_{\nu_5}+138_{\nu_{18}}=797$. No other suitable combination could be found for this band. Also, a long exposure of CHDBrCHDBr shows a very weak line at about 140 cm^{-1} which is possibly due to ν_{18}, forbidden in CH_2BrCH_2Br but appearing weakly in CHDBrCHDBr because of reduced symmetry. We are endebted to Mr. Gordon Barrow who prepared CHDBrCHDBr and obtained its Raman spectra.

The pairing of the light and heavy compound frequencies is given in Table VII. The only difficulty was the selection of the C—D stretching frequency. Just as the choice between 3037 cm^{-1} and 2974 cm^{-1} as the CH stretching frequency of class B_u was arbitrary, so also was the choice between 2209 cm^{-1} and 2290 cm^{-1} arbitrary. Since the lower of the two was selected for the C—H motion, so also was the lower of the two selected for the C—D motion. The product rule calculations are only slightly affected by this choice, and therefore it introduces little error. Assuming an anharmonicity correction of one percent per frequency, it is found that the expression $\nu_{18}^2(\text{heavy})/\nu_{18}^2(\text{light})$ equals 0.86. Since this is a reasonable value, we conclude that our choice of B_u frequencies is consistent with the product rule.

Class A_u (infra-red active)

The selection of 3037 cm^{-1} as ν_7 and 1087 cm^{-1} as ν_8 has been discussed under class B_u. The band at 753 cm^{-1} is the only unassigned strong infra-red band, and may be reasonably assigned to the CH_2 rocking frequency. The torsional vibration was not observed.

In making the product rule calculations, it was assumed that the square of the ratio of the torsional frequencies was equal to the reciprocal of the ratio of the reduced moments of inertia for internal rotation.

$$\frac{\nu_{10}^2(\text{heavy})}{\nu_{10}^2(\text{light})}=\frac{Im\ (\text{light})}{Im\ (\text{heavy})}=\frac{22.14\ (\text{at. wt., A}^2)}{27.10\ (\text{at. wt., A}^2)}=0.817.$$

With this assumption, the agreement is satisfactory.

C_2 *Skew* Form

Assignments for the C_2 symmetry form are more difficult to make since the aids derived from high symmetry are absent and also, the bands are weaker due to the lower population of the high energy form which especially adversely affects the Raman polarization data. It was possible, however, to make use of the expected similarity between C_{2h} (*trans*-) and C_2 (staggered) frequencies in making these assignments.

Most of the C_2 assignments are reasonably straight forward and will not be dealt with in detail. It might be noted, however, that only one suitable frequency occurs in the CH_2 bending range, one in the CH_2 twisting range, and two in the C—H stretching region. In each case twice as many frequencies are required but were not observed, probably because the bands were very weak. This has made necessary duplicate assignment of the observed frequencies.

The application of the product rule where so many frequencies occur in a class, is of only limited value. In class B a check of

$$\prod_{i=11}^{i=18}(\nu'_{\text{heavy}}/\nu'_{\text{light}})^2=0.0241$$

against a calculated value of 0.021 is considered reasonable in view of the number of frequencies involved. In calculating the product rule for class A, the value of the ratio of the square of the frequencies for ν_{18}' was used for the missing value of ν_6'. The discrepancy of $i=10$

$$\prod_{i=1}^{i=10}(\nu'_{\text{heavy}}/\nu'_{\text{light}})^2=0.0212$$

against a calculated value of 0.0165 is not excessive, since it amounts to less than two percent per frequency.

APPENDIX

The moments of inertia were calculated using tetrahedral angles, bond distances CC=1.54A, CH=CD=1.09A, C—Br=1.92A, and atomic weights C=12.01, H=1.008, D=2.0147, Br=7.916. The numerical values are shown in the following table.

Trans-(C_{2h}) form	CH_2Br-CH_2Br	CD_2Br-CD_2Br
I_x	29.72×10^{-40}	44.78×10^{-40}
I_y	1412×10^{-40}	1418×10^{-40}
I_z	1431×10^{-40}	1442×10^{-40}
I_m (internal rotation)	36.80×10^{-40}	45.0×10^{-40}
Skew (C_2 staggered) form		
I_x	122.6×10^{-40}	151.5×10^{-40}
I_y	876.1×10^{-40}	903.4×10^{-40}
I_z	781.3×10^{-40}	794.3×10^{-40}
I_m (internal rotation)	64.7×10^{-40}	71.2×10^{-40}

The Structure of Para-di-chloro-benzene*

B. D. SAKSENA
Department of Physics, University of Allahabad, India
(Received August 7, 1950)

Two low frequency spectra of the crystal of para-di-chloro-benzene are reproduced, one showing the frequencies 27, 54, and 93 and the other 45, 57, and 84 cm^{-1}. The former represent the spectra of a single crystal very slowly cooled from melt, and the latter of a crystal rapidly cooled. The three frequencies in the spectra of the single crystal have been shown to be rotational oscillations, the smallest frequency representing an oscillation about the axis of greatest moment of inertia which is the axis perpendicular to the plane of the molecule. From the x-ray data it is noticed that the molecules in the crystals of para-di-chloro-benzene and para-di-bromo-benzene are differently orientated, but they can be brought into juxtaposition by a rotation about this axis. The different orientations of the molecules in these crystals are however incompatible with the fact that these crystals are isomorphous and form mixed crystals. It has therefore been postulated that the crystal of para-di-chloro-benzene has a tendency to become disordered by the excitation of free rotation about the axis perpendicular to the plane of the molecule which results in the vanishing of the frequency 27 as noticed in the second spectrum. The apparently discordant results of Sircar and Venkateswaran on the temperature independence of Laue spots and Raman spectra and also those of Sircar and Vuks on the spectra of mixed crystals have been explained on this basis, and the frequencies of mixed single crystals of para-di-chloro- and para-di-bromo-benzenes have been calculated in good agreement with the observational data.

THE low frequency spectrum of *p*-di-chloro-benzene has been investigated by several workers. Vuks[1] reported two different low frequency spectra namely 27.5, 46.5, 54, and 93 cm^{-1} below 32°C and 43, 55, and 82 cm^{-1} above 32°C. Sircar and Gupta[2] and also Venkateswaran[3] could not confirm the change of the spectrum with temperature, and reported frequencies at 40, 53, and 82 cm^{-1}. Rousset and Linchet,[4] however, favour the data of Vuks below 32°C, and consider the results of Sircar and co-workers as incomplete. Vuks[5] also investigated the spectra of mixed crystals of *p*-di-chlorobenzene and *p*-di-bromobenzene, and found that the frequencies 20.1 and 37.8 of 100 percent *p*-di-bromo-benzene progressively increase with increased concentration of di-chloro-benzene to 27.5 and (46.5 and 54) in 100 percent di-chloro-benzene. Sircar and Bishui[6] find no such progressive shift, and report only two frequencies at 36 and 47 cm^{-1}, the former corresponding to *p*-di-bromo-benzene and the latter to *p*-di-chloro-benzene, which change in intensity but not in frequency in the spectra of different mixed crystals.

Two low frequency spectra of this crystal are reproduced here, the molecular frequencies being the same in the two cases. (See Fig. 1.) One is that of a single crystal obtained by very slow cooling from melt, and the other of a solid rapidly cooled after melting. The author is thankful to the late Shrimati S. Bai for the latter picture. The single crystal was grown in several days according to the method described by Nedungadi.[7] For solid (I) we observe the frequencies at 27, 54, and 94 cm^{-1}, and for the other at 45, 57, and 84 cm^{-1}. The frequency 27 is present in the spectrograms (a), (e), (f) for solid (I) but not in the spectrograms (b), (c), and (d) for solid (II). The intensities of the spectra also differ considerably. For solid (I), the frequency 54 is very strong and has almost twice the intensity of the other strong frequency at 27 cm^{-1}, while in solid (II) the frequencies 45 and 57 are of comparable intensity, the frequency 45 being stronger. The molecular frequencies also, chiefly the low frequencies at 308 and 330 cm^{-1}, show different relative intensities in the spectra of the two solids.

The structures of *p*-di-chloro-, *p*-di-bromo-, and *p*-chloro-bromo-benzenes were investigated by Hendricks.[8] The crystals are isomorphous and belong to the symmetry class C_{2h}^5. The unit cell contains two molecules, and there is a center of symmetry at each molecule. The plane of the benzene ring in di-chloro- and di-bromo-benzene crystals is parallel to the two-fold '*b*' axis. According to Hendricks, in the projection of the unit cell in the '*ac*' plane, the molecules are along the '*a*' axis (the elongated axis) in *p*-di-chloro-benzene, but inclined to the '*a*' axis in *p*-di-bromo-benzene. The molecules of one compound can be brought to the position of the other by a rotation about the axis perpendicular to the plane of the molecule. In para-chloro-bromo-benzene, Hendricks finds a complete randomness of orientation in the positions of the halogens which can be accounted for by a 180° rotation of the molecule. Gross and Korshunov,[9] however, think that since the crystals are isomorphous and possess so high a degree of similarity that they form mixed crystals, the structures of their lattices and the orientations of the molecules in them must be the same.

* Read before the meeting of the American Crystallographic Association held at Pennsylvania State College.

[1] M. Vuks, C. R. (Doklady) **1**, 73 (1936).
[2] S. C. Sircar and J. Gupta, Ind. J. Phys. **10**, 473 (1936).
[3] C. S. Venkateswaran, Proc. Ind. Acad. Sci. **8**, 448 (1938).
[4] Rousset and Linchet, J. de Phys. **3**, 146 (1942).
[5] M. Vuks, Acta Phys. Chem. (U.S.S.R.) **6**, 11 (1937).
[6] S. C. Sircar and Bishui, Ind. J. Phys. **11**, 418 (1937).
[7] T. M. K. Nedungadi, Proc. Ind. Acad. Sci. **13**, 161 (1941).
[8] S. B. Hendricks, Zeits. f. Kryst. **84**, 85 (1933).
[9] Gross and Korshunov, Acta Phys. Chem. (U.S.S.R.) **20**, 353 (1945).

TABLE I.

Concentration Cl_2	Concentration Br_2	Calculated ν_1	Calculated ν_2	Observed (Vuks)[a] ν_1	Observed (Vuks)[a] ν_2
100	0	27.5	50.2	27.5	50.2
91	9	26.0	48.0	26.2	50.0
78	22	24.8	45.6	24.0	46.3
53	47	22.8	42.1	22.0	42.1
22	78	21.0	39.3	20.2	39.5
0	100	20.1	37.8	20.1	37.8

[a] See reference 5.

Following Brester[10] and Placzek,[11] the vibrational spectrum of the first order in a crystal may be analyzed by considering the number of molecules in the unit cell as the basis. Since there are two molecules in the unit cell, the three translations and the three rotations of each molecule may be combined in the same or opposite phases for the two molecules to give the twelve external modes of the crystal, six of which are translational and six rotational. Only the rotational modes will be active in the Raman effect because each molecule is a center of symmetry. Since the crystal has a point-group C_{2h}, there are only two Raman-active classes, and three of the rotational modes are symmetric and three anti-symmetric. We do not expect the frequencies of the symmetric and the anti-symmetric modes to be very different on account of coupling, and so we may expect only three Raman lines. Bhagavantam[12] also arrives at the same results with the help of the group theory. The frequency of a rotational mode will naturally depend in some way upon the moment of inertia involved in a given vibration. On this basis, the frequencies 93 and 27 will represent rotational oscillations about the axes of least and greatest moment of inertia, while 54 will be an oscillation about the axis of intermediate moment of inertia. The former (i.e. the axis of least inertia) is an axis lying in the plane of the molecule and passing through the halogens, and the latter (the axis of greatest inertia) is the axis perpendicular to the plane of the molecule. Since the positions of the halogens are unaltered in a rotation about the axis of least inertia, the frequency 93 should be present in the spectra of p-$C_6H_4Cl_2$, p-$C_6H_4Br_2$ and p-C_6H_4BrCl, which is actually observed. The assignment of the frequency 27 to a rotational mode about the axis perpendicular to the plane of the molecule is also supported by the fact that this frequency becomes the weakest in some orientations while the frequency 54 always remains the strongest. The above analysis is in substantial agreement with the work of Rousset and Linchet and of Gross and Korshunov. Vuks[13] has reversed the assignments of the frequencies 27 and 54 given above, but his argument is rather arbitrary, and not based upon experiment. Gross as well as Vuks consider that the frequencies of these modes are given by the relation $\nu=1/2\pi(c/I)^{\frac{1}{2}}$ where ν is the frequency, 'c' the restoring couple per radian, and I the moment of inertia.

It was first pointed out by Bech and Ebbinghaus[14] that when p-di-chloro-benzene is cooled below 39°C, a sudden contraction in volume takes place which is due to a modification of the lattice. Vuks, however, considered that the change occurs 32°C, and is due to a rotation of the molecules, and thereby involves no change in volume. This was contradicted by Sircar and Gupta[15] who investigated the variation of the Laue pattern with temperature, and found no change. However, since the low-frequency spectra of crystals are very susceptible to a change of structure, (compare the low frequency spectra of calcite and aragonite or of anhydrite and gypsum), the two specimens of di-chloro-benzene whose spectra are reported here should have different structures. It is likely that the change of structure is a phase-transition from the ordered to the dis-ordered state on account of the incidence of the free rotation about an axis perpendicular to the plane of the molecule. The frequency of the rotational mode about this axis would then be absent from the spectrum of the crystal. The possibility of such a transition is suggested by the vanishing of the frequency 27 which is the rotational mode about an axis perpendicular to the plane of the molecule, and also by the fact that the different orientations of the molecules in the crystals of para-di-chloro- and di-bromo-benzenes are not compatible with their tendency to form mixed crystals. A similar result is reported by Menzies and Mills[16] in NH_4Cl, where the frequency 183 of the low temperature modification is either absent from or becomes very weak in the spectrum of the room temperature modification. The spectrum of solid (II) reported here is the same as reported by Sircar and Gupta and also by Venkateswaran, and it is likely that the crystals used by them had the same structure. It is possible that once the crystal has become disordered, the change of temperature alone is unable to bring it back to the ordered state for, since the crystal is very soft and also volatile, the internal strains on crystallization and heating tend to keep it disordered. This, perhaps, may be the reason why Sircar and Venkateswaran fail to observe the temperature dependence of the Laue spots and the low frequency spectrum.

The spectrum of a mixed crystal may also be explained on the basis of the above ideas. If we grow a mixed crystal from two single crystals which have no disorder, we can regard each lattice point of the mixed crystal as a statistical average of two types of molecules. Thus if there are x percent molecules of $C_6H_4Cl_2$ and $(100-x)$ percent of $C_6H_4Br_2$, the moment of inertia of the molecule of the mixed crystal will be $[xI_{Cl}+(100-x)I_{Br}]\times 1/100$, where I_{Cl} and I_{Br} are the

[10] C. J. Brester, Zeits. f. Physik **24**, 324 (1924).
[11] G. Placzek, Handbuch der Radiol. Bd. **6**, Vol. 2, (1934).
[12] S. Bhagavantam, Proc. Ind. Acad. Sci. **13**, 161 (1941).
[13] M. Vuks, Acta. Phys. Chem. (U.S.S.R.) **20**, 851 (1945).
[14] Bech and Ebbinghaus, Ber. **29**, 3870 (1906).
[15] S. C. Sircar and J. Gupta, Ind. J. Phys. **11**, 287 (1937).
[16] Menzies and Mills, Proc. Roy. Soc. **148**, 407 (1935).

moments of inertia of the para-di-chloro and *p*-di-bromo-benzene molecules. The frequency for this concentration is given by the relation

$$\nu_3^2=\frac{xI_{Cl}\nu_{Cl}^2+(100-x)I_{Br}\nu_{Br}^2}{xI_{Cl}+(100-x)I_{Br}}.$$

The relation can be easily derived from the expression for the rotational frequency given earlier. When $x=0$, $\nu_3=\nu_{Br}$ where ν_{Br} is the frequency for $C_6H_4Br_2$, and when $x=100$, $\nu_3=\nu_{Cl}$ where ν_{Cl} is the corresponding frequency for $C_6H_4Cl_2$. If I_1 and I_2 are the moments of inertia about an axis perpendicular to the plane of the molecule, and the axis in the plane of the molecule at right angles to its length we have

$$I_1^{Br}=3155,\quad I_2^{Br}=3004,\quad I_1^{Cl}=1384,$$
$$I_2^{Cl}=1234\times10^{-40}\ \text{g}\times\text{cm}^2.$$

If ν_1 and ν_2 are the frequencies of the rotational oscillations about these axes in cm^{-1}

$$\nu_1^{Br}=20.1,\quad \nu_2^{Br}=37.8,\quad \nu_1^{Cl}=27.5,$$
$$\nu_2^{Cl}=(46.5+54)/2.$$

The frequencies for the various mixed crystals may now be calculated as shown in Table I.

The agreement between the observed and calculated values suggests that the lattice point of a mixed crystal may be treated as a statistical average of two types of molecules having the same orientation. In *p*-chloro-bromo-benzene, where Hendricks finds a complete randomness in the position of the halogens, the molecular orientation is not arbitrary (being either 0° or 180°) so that each lattice point can be treated as an average effect. With disordered crystals the molecular orientation will no longer remain fixed, and so the lattice point of a mixed crystal cannot be considered as a statistical average. In the spectrum of such a mixed crystal one can only expect the frequencies of rotational oscillations of both the crystals separately irrespective of the ratio in which these crystals are mixed, while the frequency of the rotational oscillation about the axis of free rotation will be missing from the spectrum. This is what is observed in the spectra of mixed crystals reported by Sircar and Bishui.

We can now analyze the spectrum of solid (II). It is likely that the frequencies 45, and 57 correspond to the frequencies 46.5 and 54 observed in the case of a single crystal, while the frequency 84 corresponds to the frequency 93 of the single crystal. The diminution of the latter frequency also indicates a change of the structure. It is interesting to note that in *p*-$C_6H_4I_2$, which is rhombic, Gross and Korshunov report this frequency at 115 cm^{-1}.

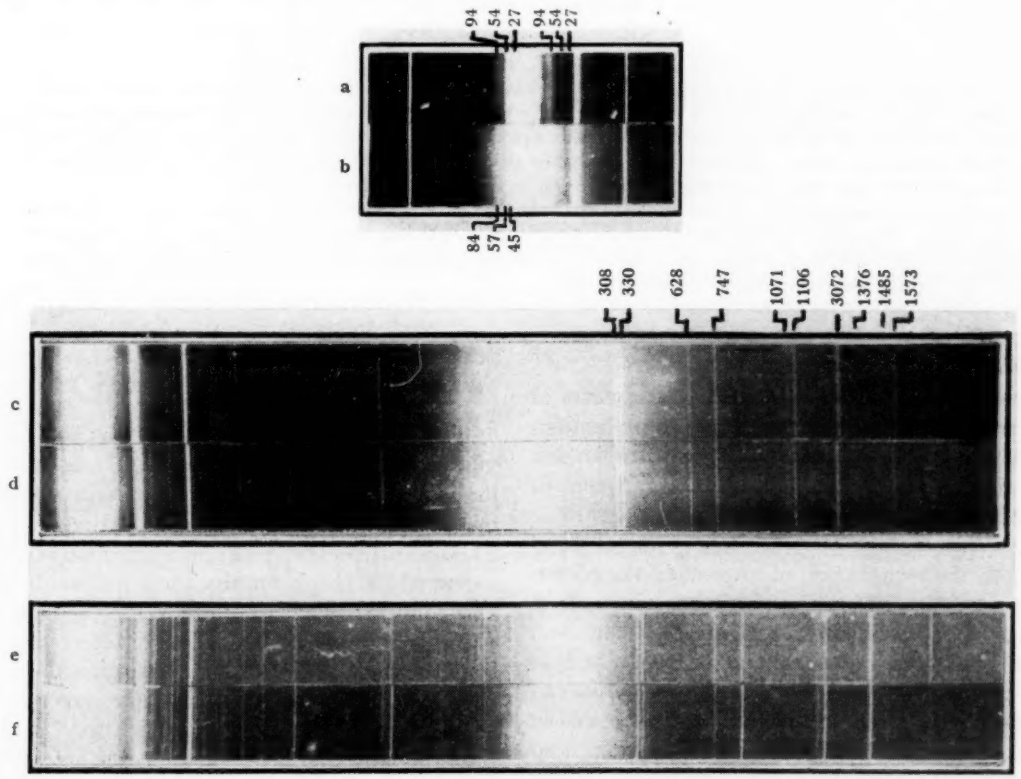

FIG. 1. Raman spectrograms of solid *p*-di-chlorobenzene. (a) Low frequency spectra of the single crystal in the 4046 and 4077 excitation. (b) Low frequency spectra of the disordered crystal (solid II) in the 4046 and 4077 excitations. (c) and (d) Two spectrograms showing the molecular frequencies of solid II the disordered crystal. (e) Raman spectra of the single crystal (solid I) with symmetry axis of the crystal and the electric vector in the direction of observation. (f) Raman spectrum of a single crystal with the symmetry axis in the direction of observation and the electric vector in a direction at right angles to the directions of illumination and observation.

The molecular frequencies are the same in the spectra of solids (I) and (II), and in the liquid. The frequencies 330, 747, 1071, 1106, and 3072 are found to be polarized in the liquid spectrum and therefore represent the planar vibrations of the molecule, while the frequencies 1573, 1376, 628, and 308 are depolarized. According to Sponer and Kirby-Smith,[17] the latter are the out-of-plane frequencies of the molecule. The different behavior of the planar and the out-of-plane vibrations in the solid is seen in the spectrograms (e) and (f), which represent the spectra taken with the symmetry axis of the crystal along the direction of observation *OY* and the electric vector either along the direction of observation *OY* (spec. e), or along the line perpendicular to the directions of illumination *OX* and of observation *OY* (spec. f). In the former case, the electric vector will lie in the plane of the molecule. The planar frequencies 747, 1071, 1106, and 3072 are seen to be somewhat weaker in (e) than in (f), while the out-of-plane vibrations 1573, 1376, and 628 show an opposite behavior. This is due to the fact that these planar vibrations are also the totally symmetric vibrations of the molecule, and therefore produce an induced moment in the direction of the electric vector. Since the electric vector is in the direction of observation, they appear weak. The out-of-plane vibrations, on the other hand, give fairly large induced moments perpendicular to the direction of observation, and therefore appear much stronger. The relatively large intensity of the planar vibrations in the spectrogram (e) is due to the fact that they are both symmetric and antisymmetric oscillations for the crystal. (Saksena).[18]

[17] H. Sponer and Kirby-Smith, J. Chem. Phys. **9**, 667 (1941).

[18] B. D. Saksena, Proc. Ind. Acad. Sci. **11**, 229 (1940).

THE JOURNAL OF CHEMICAL PHYSICS VOLUME 18, NUMBER 12 DECEMBER, 1950

The Infra-Red Spectra of $N^{15}N^{14}O^{16}$ and $N^{14}N^{15}O^{16}$. Some Thermodynamic Properties of the Isotopic N_2O Molecules*

JACOB BIGELEISEN AND LEWIS FRIEDMAN
Chemistry Department, Brookhaven National Laboratory, Upton, New York

(Received August 18, 1950)

The three fundamental frequencies of $N^{15}N^{14}O^{16}$ have been studied in the infra-red. One stretching frequency and the bending frequency in $N^{14}N^{15}O^{16}$ have similarly been investigated. The bending frequencies in $N^{15}N^{14}O^{16}$ and $N^{14}N^{15}O^{16}$ are found to be in good agreement with calculations from the product rule. Some slight changes are made in the force constants for the stretching vibrations in N_2O. The stretching frequency ω_3 in $N^{14}N^{15}O^{16}$ provides a good independent check on the force constants.

The partition function ratios for isotopic exchange reactions involving nitrogen and oxygen in N_2O are calculated. The isomerization equilibrium $N^{15}N^{14}O^{16}=N^{14}N^{15}O^{16}$ has been calculated over the temperature range 273.16°–1000°K. A correlation is drawn between the structures of the isotopic isomers, $N^{15}N^{14}O^{16}$ and $N^{14}N^{15}O^{16}$, and the isomerization equilibrium.

INTRODUCTION

In the course of an investigation of some aspects of the controlled thermal decomposition of ammonium nitrate into nitrous oxide and water, we prepared a sample of nitrous oxide enriched in N^{15} exclusively in the end position.[1] The availability of such a sample afforded the opportunity of determining its infra-red spectrum with the expectation of improving the potential function for the vibrations of nitrous oxide. In a concurrent and independent investigation, Richardson and Wilson[2] have described the preparation of a sample of nitrous oxide containing 60 percent N^{15} in the end position and the infra-red spectrum of this molecule in the fluorite and rock salt regions of the spectrum, and have evaluated the stretching force constants in the potential function

$$2V=f_1\Delta r_1^2+f_2\Delta r_2^2+2f_{12}\Delta r_1\Delta r_2. \quad (1)$$

We have measured the shift in the three fundamental vibrational frequencies of N_2O on substitution of N^{15} for N^{14} in the end position and in two of the fundamental vibrations on N^{15} substitution in the center. The measurements on the $N^{14}N^{15}O^{16}$ molecule afford an independent check on the force constants in Eq. (1) and confirm Richardson and Wilson's force constants. A slight improvement of their force constants results from the combination of our measurements on $N^{15}N^{14}O^{16}$ and theirs as evidenced by a better agreement with the product rule and the spectrum of $N^{14}N^{15}O^{16}$. The potential function (1) and the product rule have been used to calculate the vibrational frequencies of $N^{14}N^{14}O^{18}$. From the vibrational frequencies the partition function ratios of the various isotopic N_2O molecules can be calculated. The partition function ratio, f, $N^{14}N^{15}O^{16}/N^{15}N^{14}O^{16}$ is just the equilibrium constant for the

* Research carried out at the Brookhaven National Laboratory under the auspices of the AEC.

[1] L. Friedman and J. Bigeleisen, J. Chem. Phys. **18**, 1325 (1950).

[2] W. S. Richardson and E. B. Wilson, Jr., J. Chem. Phys. **18**, 694 (1950).

isomerization equilibrium,

$$N^{15}N^{14}O^{16} = N^{14}N^{15}O^{16}. \quad (2)$$

Thus, we can calculate the equilibrium between a pair of isotopic isomers. The results of the measurements and calculations are presented below.

EXPERIMENTAL

The preparation of a sample containing 7.5 percent N^{15} in the end position has been described previously.[1] A sample of N_2O containing 31.4 percent N^{15} in the center position and 0.4 percent N^{15} in the end position was prepared from 31.4 percent $N^{15}-HNO_3$ as a starting material. The nitric acid was obtained from the Eastman Kodak Company. Five millimoles of the enriched nitric acid were titrated with ordinary ammonium hydroxide to the stoichiometric end point; brom-phenol blue was used as an external indicator. The solution was evaporated to dryness and the solid ammonium nitrate was decomposed to give N_2O by the method described previously.[1] It has been shown[1,2] that the decomposition of $N^{15}H_4N^{14}O_3$ yields $N^{15}N^{14}O$ exclusively. Therefore, the decomposition of a sample of ammonium nitrate enriched in N^{15} in the nitrate ion yields N_2O enriched in N^{15} in the middle position.

The spectra were measured with a Baird Associates, Inc., Model B infra-red recording spectrophotometer. The shifts in the ν_1 and ν_3 bands, 1285.4 and 2224.1 cm^{-1}, respectively, in $N^{14}N^{14}O^{16}$, were measured with a rock salt prism; those in the ν_2 band were measured with a KBr prism. The cells were 5 cm long and equipped with KBr windows. A sample of tank N_2O was used in the reference cell. The shifts were measured from experiments in which the pressure in the reference cell was equal to the total pressure of N_2O in the sample cell. The shutter in front of the mirror in the sample beam was adjusted to give roughly 50 percent transmittance in a spectral region of no absorption. Under these conditions an excess transmittance, negative absorption, appears at the absorption frequencies of $N^{14}N^{14}O^{16}$ corresponding to the amount of absorption for one of the N^{15} substituted molecules at its corresponding frequency. This negative absorption provides an internal wave-length calibration of the instrument. The wave-length shift was determined using the dispersion of the instrument as furnished by the manufacturer. The frequency shift over a small spectral region is given by the relation

$$\Delta\nu = -\bar{\nu}^2\Delta\lambda, \quad (3)$$

where $\bar{\nu}$ is the average of the frequency determined by Plyler and Barker[3] and the corresponding N^{15} substituted frequency and is easily calculated to a higher precision than the present experimental measurements. Determinations of the wave-length shifts were made by measurements of recorded spectra as well as point-by-point manual scanning of the spectrum. The latter gave better precision and reproducibility because of the fact that the response time of the bolometer and recording system is not negligible in comparison with the time to scan an absorption peak.

The above procedure for measuring small frequency shifts was checked by measurement of the separation of close absorption lines in the ammonia spectrum. The separations measured in this way were compared with the precise grating measurements of Barker.[4] No systematic deviations were found and the accuracy of our determinations was limited by the precision to which the wave-length shift could be measured. The corresponding errors in the shifts in the N_2O spectrum on N^{15} substitution are indicated along with the experimental results.

TABLE I. Frequency shifts on N^{15} substitution in N_2O (cm^{-1}).

Designation	$N^{14}N^{14}O^{16}$[a]	$N^{14}N^{14}O^{16} - N^{15}N^{14}O^{16}$[b]	$N^{14}N^{14}O^{16} - N^{14}N^{15}O^{16}$	$N^{14}N^{14}O^{16} - N^{14}N^{14}O^{18}$
ν_1	1285.0	17.5	16.1±1.4	...
ν_2	588.8	...	4.2±0.3	12.9±0.2
ν_3	2223.5	22.5	29 ±4	46.5±2.0

[a] Measurements of Plyler and Barker (reference 3) reduced to vacuum (reference 6).
[b] W. S. Richardson and E. B. Wilson (reference 2).

RESULTS

The shifts in the bending frequency, ν_2, were easily resolved by the KBr optics and were determined from the separation of the pronounced Q branches. In accord with expectations no shift could be found in the low stretching frequency, ν_1, for the $N^{14}N^{15}O^{16}$ molecule. In the case of the $N^{15}N^{14}O^{16}$ molecule the shifts in ν_1 in both the P and R branches were clearly resolved and measured. In the measurements of the ν_3 shift in $N^{15}N^{14}O^{16}$ the R branch of the $N^{15}N^{14}O^{16}$ molecule was completely unresolved from the P branch of the $N^{14}N^{14}O^{16}$. The separation between the R branch of $N^{14}N^{14}O^{16}$ and the P branch of $N^{15}N^{14}O^{16}$ was measured. The shift in the band origin was calculated from this measured separation and the value of 28 cm^{-1} estimated for the $P-R$ separation.[3,5] The shift in ν_3 in the $N^{14}N^{15}O^{16}$ molecule was sufficiently large so that the P and R branches of both the $N^{14}N^{14}O^{16}$ and $N^{14}N^{15}O^{16}$ molecules appeared distinctly. The experimentally determined frequency shifts are given in Table I.

The shifts determined for the $N^{15}N^{14}O^{16}$ agree with the measurements made by Richardson and Wilson within the limits of the experimental errors of both measurements. As will be shown below, their shift in ν_3 is undoubtedly more accurate than ours as a result of their use of a fluorite prism to measure this shift.

The experimental zero-order stretching frequencies are tabulated in Table II. The zero-order frequencies

[3] E. K. Plyler and E. F. Barker, Phys. Rev. **38**, 1827 (1931).

[4] E. F. Barker, Phys. Rev. **55**, 657 (1939).

[5] C. P. Snow, Proc. Roy. Soc. **A128**, 294 (1930).

TABLE II. Zero-order stretching frequencies for the isotopic N_2O molecules (cm^{-1}).

Molecule	$N^{14}N^{14}O^{16}$			$N^{15}N^{14}O^{16}$				$N^{14}N^{15}O^{16}$			$N^{14}N^{14}O^{18}$
Designation	Observed	Calculated from force constants A, Table IV	Calculated from force constants C, Table IV	Observed R+W	Observed this research	Calculated from force constants A, Table IV	Calculated from force constants C, Table IV	Observed	Calculated from force constants A, Table IV	Calculated from force constants C, Table IV	Calculated from force constants C, Table IV
ω_1	1299.8	1298.8	1299.8	1281.9	1283.3	1283.0	1283.5	—	1296.2	1297.6	1256.2
ω_3	2276.5	2277.1	2276.5	2252.9	2246.2	2252.3	2252.6	2227.8	2228.8	2228.1	2270.8

TABLE III. Zero-order bending frequencies for the isotopic N_2O molecules (cm^{-1}).

Molecule	ω_2 observed	ω_2 calculated (product rule)
$N^{14}N^{14}O^{16}$	596.5	...
$N^{15}N^{14}O^{16}$	592.2	592.9
$N^{14}N^{15}O^{16}$	583.2	582.8
$N^{14}N^{14}O^{18}$	...	591.9

TABLE IV. Force constants[a] and product rule check for the stretching frequencies in N_2O.

Quantity	A Richardson and Wilson	B $N^{15}N^{14}O^{16}$ (this research)	C See below[b]	Product rule
f_1	18.98	22.22	18.71_7	
f_2	11.50	10.31	11.61_1	
f_{12}	1.43	3.56	1.312_7	
$\omega_1\omega_3/\omega_1^i\omega_3^i$	1.0246	1.0265	1.0240	1.0235

[a] Force constants in units of 10^5 dynes/cm.
[b] Calculated from $\omega_3(N^{15}N^{14}O^{16})$ from Richardson and Wilson and $\omega_1(N^{15}N^{14}O^{16})$ from the average of R and W and this research.

for $N^{14}N^{14}O^{16}$ are those calculated by Herzberg[6] from the observed fundamentals, combination and overtone bands. The zero-order frequencies for $N^{15}N^{14}O^{16}$ and $N^{14}N^{15}O^{16}$ have been calculated from the ones for $N^{14}N^{14}O^{16}$, the observed shifts in Table I, and the approximate relations introduced by Dennison,[7]

$$\omega_j = \nu_j(1+\alpha_j), \tag{4}$$

$$\omega_j^i \simeq \nu_j^i[1+\alpha_j(\nu_j^i/\nu_j)]. \tag{5}$$

The zero-order bending frequencies are given in Table III.

The first check that can be made on the isotopic zero-order frequencies is by means of the Teller-Redlich product rule.[8] For the linear XYZ molecule the rule states

$$\omega_1\omega_3/\omega_1^i\omega_3^i = (m^iM/mM^i)^{\frac{1}{2}}, \tag{6}$$

$$\omega_2/\omega_2^i = (m^iMI/mM^iI^i)^{\frac{1}{2}}, \tag{7}$$

where the superscript i refers to the isotopically substituted molecule, m is the mass of the isotopically substituted atom, M is the mass of the molecule, and I is the moment of inertia of the molecule. The bending vibrations ω_2^i have been calculated from Eq. (7) with the value of ω_2 calculated from Plyler and Barker's data.[6] The moments of inertia of $N^{14}N^{14}O^{16}$, $N^{15}N^{14}O^{16}$, and $N^{14}N^{15}O^{16}$ have been determined by microwave spectroscopy.[9,10] The experimentally determined microwave frequencies were used directly, since $I\alpha 1/\nu$. The moment of inertia of $N^{14}N^{14}O^{18}$ was calculated using 1.126A and 1.191A for the N−N and N−O bond distances,[9] respectively. The values of ω_2 calculated from the product rule are compared with experiment in Table III. The agreement between the observed and calculated frequencies is satisfactory. The deviations can be ascribed to experimental error and the reduction of the observed frequencies to zero-order frequencies by Dennison's approximation.

The product rule check for the stretching frequencies is given in Table IV. It is clear from the product rule check that Richardson and Wilson's value for ω_3 for $N^{15}N^{14}O^{16}$ is to be preferred to ours. The best agreement with the product rule is obtained by using their value for ω_3 and our value for ω_1 for $N^{15}N^{14}O^{16}$, together with Plyler and Barker's measurements on $N^{14}N^{14}O^{16}$. This combination gives for the ratio of the product of the stretching frequencies 1.0235, in perfect agreement with the product rule. There is no other reason to prefer our measurements for ω_1 over those of Richardson and Wilson. Therefore, we have chosen as the best set of values for the zero-order frequencies for $N^{15}N^{14}O^{16}$ their value for ω_3 and the average of their value and ours for ω_1.

The force constants in the potential function (1) can be calculated from the zero-order frequencies by the use of the following relations:

$$\lambda_1+\lambda_3 = (\mu_x+\mu_y)f_1+(\mu_y+\mu_z)f_2-2\mu_y f_{12}, \tag{8}$$

$$\lambda_1\lambda_3 = (\mu_x\mu_y+\mu_x\mu_z+\mu_y\mu_z)(f_1f_2-f_{12}^2), \tag{9}$$

where $\lambda=4\pi^2\omega^2$ and $\mu_k=1/m_k$. Equations (8) and (9) have been solved for the force constants from the zero-order frequencies of $N^{14}N^{14}O^{16}$ and $N^{15}N^{14}O^{16}$. Three sets of force constants are listed in Table IV corresponding to three sets of frequencies for $N^{15}N^{14}O^{16}$. The force constants in column A are those calculated by Richardson and Wilson; those in column B are calculated from our measurements on $N^{15}N^{14}O^{16}$; those in column C are calculated from Richardson and Wilson's value for ω_3 and the average of their value and ours for ω_1. Our value of ω_3 leads to an unsatisfactory set of force constants. The resulting value of f_1, corresponding to N−N

[6] G. Herzberg, *Infra-Red and Raman Spectra of Polyatomic Molecules* (D. Van Nostrand Company, Inc., New York, 1945), p. 278.
[7] D. M. Dennison, Rev. Mod. Phys. **12**, 175 (1940).
[8] See reference 6, pp. 112, 231 ff.
[9] Coles, Elyash, and Gorman, Phys. Rev. **72**, 973 (1947).
[10] D. K. Coles, and R. H. Hughes, Phys. Rev. **76**, 178 (1949).

stretching, is higher than the force constant in the nitrogen molecule, which seems unreasonable. The interaction constant, f_{12}, is also rather large. There is little difference between the force constants in column C and those in column A. As has been pointed out by Richardson and Wilson, the interaction constant is most sensitive even to the slight changes which we have introduced in Richardson and Wilson's values for the frequency shifts.

The stretching frequencies in the molecules $N^{14}N^{14}O^{16}$, $N^{15}N^{14}O^{16}$, $N^{14}N^{15}O^{16}$, and $N^{14}N^{14}O^{18}$ have been calculated from the force constants in Table IV. They are compared with experiment in Table II. The only independent check on the force constants is afforded by the measured value of ω_3 for $N^{14}N^{15}O^{16}$. The agreement of both force constant sets A and C is well within the limits of the experimental error. Set C gives a slightly better agreement than does set A. Either set of force constants can be used to calculate the stretching frequencies of any one of the isotopic N_2O molecules to a few tenths of a wave number.

THERMODYNAMIC PROPERTIES

The vibrational frequencies for $N^{14}N^{14}O^{16}$, $N^{15}N^{14}O^{16}$, $N^{14}N^{15}O^{16}$, and $N^{14}N^{14}O^{18}$ in Tables II and III can be used to calculate nitrogen and oxygen exchange equilibria involving N_2O. The equilibria are most readily calculated with the aid of the tables published for calculating partition function ratios.[11] The partition function ratios, f values,[11] for nitrogen and oxygen substitution in N_2O are given in Table V. The stretching frequencies used in the calculations were those calculated from force constants C in Table IV, the bending frequencies were those calculated in Table III. The conversion factor, hc/k, was taken as 1.43847.[12]

The partition function ratio, f, $N^{14}N^{15}O^{16}/N^{15}N^{14}O^{16}$, is the equilibrium constant for the isomerization reaction (2). This can readily be seen from the definition of f.[13] The values for this equilibrium constant are about as large as most of the ones which arise from the exchange of nitrogen atoms between different chemical species.[14] This may appear surprising and counter to the expectation that isotopic isomerization equilibrium constants

TABLE V. Partition function ratios and exchange equilibria involving N_2O.

$T°K$	$f\ \frac{N^{15}N^{14}O^{16}}{N^{14}N^{14}O^{16}}$	$f\ \frac{N^{14}N^{15}O^{16}}{N^{14}N^{14}O^{16}}$	$f=K\ \frac{N^{14}N^{15}O^{16}}{N^{15}N^{14}O^{16}}$	$f\ \frac{N^{14}N^{14}O^{18}}{N^{14}N^{14}O^{16}}$	$K\ \frac{N^{14}N^{14}O^{18}}{N^{14}N^{14}N^{16}}\ \frac{H_2O^{16}}{H_2O^{18}}$
273.16	1.0911	1.1420	1.0467	1.1127	1.0359
298.16	1.0811	1.1262	1.0417	1.0916	1.0233
300	1.0805	1.1252	1.0414	1.0908	
400	1.0539	1.0838	1.0284	1.0586	1.0116
500	1.0386	1.0603	1.0209	1.0408	1.0056
600	1.0290	1.0454	1.0159	1.0299	1.0023
700	1.0225	1.0354	1.0126	1.0227	
800	1.0179	1.0283	1.0102	1.0179	
900	1.0146	1.0232	1.0085	1.0144	
1000	1.0122	1.0192	1.0069	1.0118	

should be smaller than equilibrium constants for exchange between different kinds of molecules. The large equilibrium constant in the present case can be understood from the nature of the normal modes of vibration and the product rule. The shift in the stretching frequencies on N^{15} substitution is distributed between the modes corresponding to ω_1 and ω_3. In the mode ω_1 the central nitrogen atom is virtually at rest; and, therefore, N^{15} substitution in the central position puts almost all of the shift in the high frequency ω_3. This makes a large contribution to f by virtue of the larger values of both the factor $G(u)$ and also Δu. The bending mode, which is doubly degenerate, also has a larger shift on N^{15} substitution in the center rather than on the end because of the fact that the center atom is very close to the center of gravity of the molecule.

The oxygen exchange equilibrium constant between gaseous N_2O and H_2O is also included in Table V. The partition function ratios for the water molecules are taken from Urey's tabulation.[14] This equilibrium has been calculated previously by Rosenthal,[15] who obtained the value 1.056 at 0°C. The discrepancy between Rosenthal's calculations and those in Table V arises from the fact that her stretching frequencies for $N^{14}N^{14}O^{18}$ were calculated from a potential function based entirely on the spectrum of $N^{14}N^{14}O^{16}$.

ACKNOWLEDGMENTS

We wish to thank Mr. W. S. Richardson and Professor E. B. Wilson, Jr. for sending us a copy of their manuscript on the infra-red spectrum of $N^{15}N^{14}O$ prior to publication.

[11] J. Bigeleisen and M. G. Mayer, J. Chem. Phys. **15**, 261 (1947). See Eq. (11a) and Table I.

[12] "Selected values of chemical thermodynamic properties" (Nat. Bur. Stand., June 30, 1948).

[13] See Eq. (7), reference 11.

[14] H. C. Urey, J. Chem. Soc. **1947**, 562.

[15] J. E. Rosenthal, J. Chem. Phys. **5**, 465 (1937).

Factors Influencing Bond Dissociation Energies

M. SZWARC
Chemistry Department, University of Manchester, Manchester, England
(Received August 20, 1950)

The calculations leading to estimates of resonance energies of various molecules and radicals are analyzed and the ambiguities involved are stressed. It is suggested that an alternative approach to problems of molecular energetics may be provided by analyzing the variations in bond dissociation energies. Consideration of bond dissociation energies leads to estimates of "experimental resonance energies" of radicals, and to an evaluation of a "strengthening effect" influencing the undissociated molecule. The new approach is one of several possible variants which might be used to arrive at a better understanding of energetic relationships in molecules.

DURING the last twenty years the problems connected with the energy of a molecule have formed the subject of extensive and intensive research. The main method of attack has been based on the concept of average bond energy.* By adding the average bond energies corresponding to all the bonds in a given molecule, a value is obtained which can be compared with the experimentally determined heat of atomization of this molecule. The difference between the sum of bond energies thus calculated and the observed heat of atomization has been interpreted as the resonance energy of the molecule.[1] Similarly, the resonance energy of a radical may be derived by comparing the sum of the respective average bond energies with the experimentally estimated heat of atomization of this radical.

It follows that all such calculations of resonance energies defined in this way require a knowledge of the numerical values of average bond energies. However, the concept of average bond energy is not capable of precise definition, and therefore the numerical values of this quantity cannot be derived in an unambiguous manner.[2] Furthermore, the average bond energy is in principle an unmeasurable quantity and therefore it cannot be determined by a direct experiment. Attempts were made to overcome these difficulties by postulating relationships between the average bond energy and some property of a bond which can be measured directly. From such considerations various empirical scales of average bond energies were proposed.[3]

Among these empirical scales, that based on the stretching force constant is particularly ambiguous and unsatisfactory. While a relationship might be expected between the average bond energy and the deformability of a bond,† there is no justification for relating the former entity to the stretching force constant. Moreover, in the present state of our knowledge the numerical values of the stretching force constants are ambiguous, since they depend on the nature of the molecular force field *assumed* in the computations. Hence, it seems that the average bond energies obtained from a scale based on stretching force constants[4] should be discarded completely.

The length of a bond provides a much more satisfactory basis for building up an empirical scale of average bond energies, but it is necessary to prove that the average bond energy is determined uniquely by the length of the bond, and is independent of the character of the molecular environment of this bond. The validity of this assumption seems to be particularly doubtful when one compares a given bond in a molecule with the same type of bond in a radical. It is possible that the presence of a free electron in the radical changes the relationship between average bond energy and bond length. However, since the experimental data on bond lengths in radicals are still very scanty the discussion of this subject cannot be taken further for the time being. Nevertheless, we would draw attention to a paper by Wheland[5] who concluded that in quantum-mechanical calculations different sets of values for the integrals α (in the valency bond method) and β (in the molecular orbital method) must be used depending on whether one is dealing with molecules or with radicals. This may imply that different sets of average bond energies must be used in each case.

To illustrate the difficulties encountered in calculating resonance energies let us consider the computation of the resonance energy of the benzene molecule. The calculations by Pauling[1,3] were based on a set of constant (although in some way arbitrarily chosen) values for the average energies of the C−C, C=C, and C−H bonds. These calculations could be modified in several ways, but would still remain uncertain due to the arbitrary nature of the average bond energies used in computation. Further refinements could be introduced:

* The term "average bond energy" used in the present paper corresponds to the term "bond energy" as used by Fajans, and recently by Pauling.

[1] L. Pauling and J. Sherman, J. Chem. Phys. **1**, 606 (1933).
[2] M. Szwarc and M. G. Evans, J. Chem. Phys. **18**, 618 (1950).
[3] L. Pauling, *The Nature of Chemical Bond* (Cornell University Press, Ithaca, 1945).

† The deformability α of a bond is given by

$$\Delta E = \tfrac{1}{2} \cdot \alpha (\Delta x)^2,$$

where ΔE is the increase in the potential energy of a molecule resulting from extending a bond by Δx. α depends, of course, on the stretching force constant and on the relevant cross terms corresponding to the interaction between non-bonded atoms (see reference 2).

[4] A. D. Walsh, J. Chem. Soc. p. 398 (1948).
[5] G. W. Wheland, J. Chem. Phys. **2**, 474 (1934).

1. It is possible to choose a more elaborate scale of average bond energies, by taking into account the variations in the C–H, average bond energies due to variations in their lengths (e.g. Skinner[6]).

2. The average energy of the C–C and C=C bonds in benzene might be modified by making an allowance for the compression of the reference C–C bond to 1.39A, and for the stretching of the reference C=C bond to the same length.[7] Thus, the heat of atomization is calculated in terms of compressed *single* C–C bonds and extended *double* C=C bonds.

3. It is possible to elaborate these computations still further by introducing various values for average bond energies corresponding to various types of hybridization (e.g. Roberts and Skinner[8]).

It is obvious, however, that all these elaborations of the basic method of Pauling introduce so many unknown and undetermined constants that the usefulness of such calculations is questionable.

The new definition of the average bond energy which was proposed by M. G. Evans and the present writer[2] removes the arbitrary nature of this entity, but it offers no possibility of calculating resonance energies from average bond energies, since the sum of the average bond energies defined in the new way *must* always be equal to the heat of atomization of the molecule. It seems, nevertheless, that the new definition of the average bond energy provides a useful basis for comparing the influence of molecular environment on the nature of a bond. The "new" average bond energies are directly related to those properties of bonds which are characteristic of the undissociated molecule, e.g., the bond length. Hence, variations of these average bond energies should reflect the influence of those factors which affect the molecule as a whole but they do not show up the factors affecting the radicals produced by the rupture of the bond. Unfortunately, the estimation of these "new" average bond energies requires a knowledge of the potential energy of the molecule as a function of all internal coordinates, while the experimental data which we possess at present are far from being sufficient for this purpose.

All the difficulties described above are due to the use of the concept of average bond energy in discussing the energy relationships of molecules. It would be desirable, therefore, to look for an alternative approach to this problem, and it seems that the concept of bond dissociation energy‡ might be more useful in this respect than the notion of average bond energy. Moreover, since the bond dissociation energy is a measurable entity, and many experimental methods have been devised for its determination,[9] the conclusions derived from theoretical considérations may be checked by experiments.

Some difficulties arise, however, in discussing the variations of bond dissociation energies. Let us compare, for example, the dissociation energy of a bond linking atoms A and B in a molecule M with the dissociation energy of a similar bond in the molecule N. The difference between these two bond dissociation energies is due to factors which affect the original molecules and to factors which affect the radicals formed in the dissociation process. To illustrate this point let us consider two processes

$$CH_3 \cdot CH_3 \rightarrow 2CH_3 - D(CH_3 - CH_3)$$

and

$$Ph \cdot CH_2 \cdot CH_2 \cdot Ph \rightarrow 2Ph \cdot CH_2 - D(Ph \cdot CH_2 - CH_2 \cdot Ph)$$

$D(Ph \cdot CH_2 - CH_2 \cdot Ph)$ is smaller than $D(CH_3 - CH_3)$ since the benzyl radical is more stable than the methyl radical. However, in addition to this factor which affects the radicals, another factor might influence to a different extent the molecule of ethane and of dibenzyl. In a general case the difference

$$D(CH_3 - CH_3) - D(Ph \cdot CH_2 - CH_2 \cdot Ph)$$

may be expressed as

2 (stabilization of the benzyl radical − stabilization of the methyl radical) plus (stabilization of ethane − stabilization of dibenzyl).

It is impossible to disentangle in an absolute way the factors influencing radicals and molecules. It is necessary, therefore, to introduce some assumptions in order to continue this discussion. Let us take the C–H bond dissociation energy in methane as a standard C–H bond dissociation energy, and let us *assume* that the

TABLE I.*

Compound	$D(R-H)$ kcal./mole	Exp. resonance energy of R kcal./mole
CH_3-H	101	(0)[a]
C_2H_5-H	98(?)	3(?)
$Ph \cdot CH_2-H$	77.5	23.5
$CH_2:CH \cdot CH_2-H$	76	25
$PH_3 \cdot C-H$	75	26
$(CH_3 \cdot CO)-H$	85	16
CCl_3-H	89	12

* The experimental resonance energy of the methyl radical is by definition zero.
[a] For the source of the values of bond dissociation energies quoted in this table see reference 9.

TABLE II.*

Compound	$D(R-Br)$ kcal./mole	$D(CH_3-Br) - D(R-Br)$ kcal./mole	Exp. resonance energy of R kcal./mole
CH_3-Br	67	—	—
$Ph \cdot CH_2-Br$	50.5	16.5	23.5
$CH_2:CH \cdot CH_2-Br$	48	19	25
CF_3-Br	~64	~ 3	?
CCl_3-Br	~48	~19	12

* For the source of the values of bond dissociation energies quoted on this table see reference 9. The value of $D(CCl_3-Br)$ has been obtained recently by M. Szwarc and A. H. Sehon, J. Chem. Phys. **18**, 1685 (1950).

[6] H. A. Skinner, Trans. Faraday Soc. **41**, 645 (1945).
[7] E. H. Lloyd and W. G. Penney, Trans. Faraday Soc. **35**, 835 (1939).
[8] J. S. Roberts and H. A. Skinner, Trans. Faraday Soc. **45**, 339 (1949).
‡ Bond dissociation energy is defined as the endothermicity of the process in which the gaseous molecule $R' \cdot R''$ dissociates into fragments R' and R'' by a rupture of the bond $R'-R''$.
[9] M. Szwarc, Chem. Rev. **47**, 75 (1950).

TABLE III.*

Compound	$D(R'-R'')$ kcal./mole	Weakening due to resonance energy of R' and R'' kcal./mole	Strengthening effect† influencing the molecule $R'-R''$ kcal./mole	Weakening due to steric hindrance kcal./mole
NC−CN	120?	—	37?	—
Ph−Ph	106?	—	23?	—
CH_3-CH_3	83	—	—	—
$Ph\cdot CH_2-CO\cdot CH_3$	63	~40	~20	—
$CH_3\cdot CO-CO\cdot CH_3$	60	~32	~ 9	—
$Ph\cdot CH_2-CH_2\cdot Ph$	47	~47	~11	—
$CH_2{:}CH\cdot CH_2-CH_2\cdot CH{:}CH_2$	42	~50	~ 9	—
$Ph_3\cdot C-C\cdot Ph_3$	11	~52	?	~20

* For the source of the values of bond dissociation energies quoted in this table see reference 9.

† The "strengthening effect" is calculated from the equation "Strengthening effect" = (reson. energy of R_1) + (reson. energy of R_2) + $D(R_1-R_2)$ − $D(CH_3-CH_3)$.

difference between $D(CH_3-H)$ and $D(R-H)$ is due *entirely* to the resonance energy of the radical *R*. This is, of course, an arbitrary assumption, nevertheless it seems to be the most reasonable one.§ Accepting this assumption we are able to derive a series of values which might be called "experimental resonance energies of radicals" and which are presented in Table I.

Some of the information in Table I requires further elucidation. The resonance energy of the benzyl radical is greater than that calculated by quantum mechanics; this point is fully discussed elsewhere.[12] The resonance energy of the allyl radical is of the same order of magnitude as that of the benzyl radical, the small excess in the former being well within the limits of the experimental uncertainties. The resonance energy of the triphenylmethyl radical is not much higher than that of the benzyl or allyl radicals. This result is not surprising in view of the fact that the triphenylmethyl radical has a propeller shape structure and not a planar structure.[12] The comparatively high stabilization energy of the trichloromethyl radical accounts well for the observations of Kharasch and his colleagues.[13] The reason for this stabilization of CCl_3 may be found from steric considerations (see the discussion of $D(CF_3-Br)$ and $D(CCl_3-Br)$ given later in this paper). The calculation of the resonance energy of the acetyl radical might be questioned, and it might be suggested that another "standard" should be chosen for such cases. For compounds which contain three groups (or atoms) linked to a carbon atom which participates in the C−H bond under consideration $D(CH_3-H)$ seems to be undoubtedly the best standard. In cases when such a carbon atom is involved in a double or triple bond this standard might require modification. For the sake of simplicity, however, it is desirable to retain the original standard for the C−H bond dissociation energy, namely $D(CH_3-H)$.

Having obtained the values for the "experimental resonance energies of radicals" we can now discuss the variations in other C−X bond dissociation energies. We start with C−Br bond dissociation energies for which some data have been provided recently by pyrolytic studies. These data are presented in Table II, which reveals the following points:

1. The decrease in the C−Br bond dissociation energies in the series methyl bromide, benzyl-bromide, allyl-bromide is smaller than was to be expected from the "experimental resonance energies" of the respective radicals. These observations might be interpreted in terms of strengthening effects which seem to be greater in the molecules of benzyl bromide and allyl bromide than in the molecule of methyl bromide. It is possible to ascribe this strengthening effect to the ionic contribution,[10] from which it follows that the C−Br bond in benzyl bromide or allyl bromide has a more pronouncedly ionic character than the analogous bond in methyl bromide. Such a conclusion would appeal to the organic chemists, who know that benzyl and allyl bromides hydrolyze more readily than methyl bromide.

2. The difference between $D(CF_3-Br)$ and $D(CCl_3-Br)$ may indicate the greater stability of the CCl_3 radical as compared with the CF_3 radical. It is plausible to interpret this increase in stability of the CCl_3 radical in terms of steric effects. The mutual repulsion between the bulky Cl atoms seems to be greater in the molecule of $CCl_3\cdot Br$ where they are placed at the corners of a tetrahedron than in the CCl_3 radical which is most probably planar. Consequently there is some gain in energy in the dissociation process

$$CCl_3Br \rightarrow CCl_3 + Br.$$

On the other hand, a much smaller gain is expected in the process

$$CF_3Br \rightarrow CF_3 + Br$$

since the radius of the fluorine atom is much smaller than that of the chlorine atom. One has to notice, however, that the difference $D(CH_3-Br)-D(CCl_3-Br)$ is greater than the difference $D(CH_3-H)-D(CCl_3-H)$. This extra weakening of $D(CCl_3-Br)$ seems likely to be due to the repulsion between chlorine atoms and bromine atom in the CCl_3Br molecule.

An interesting set of data is obtained by collecting the values of various C−C bond dissociation energies. Table III shows that the C−C bond dissociation energies are far from being constant. On the contrary, the values presented in this table show a variation by one power of ten, demonstrating clearly that the C−C bond dissociation energy is influenced profoundly by the nature of both the parent molecule and the radicals formed in the dissociation process.

§ This approach was suggested previously by Polanyi and his colleagues, (see reference 10), and the following discussion does not differ essentially from their treatment. However, we shall use here the most recent experimental data, since the dissociation energies used by the above authors are not sufficiently accurate. (See Butler and Polanyi (reference 11) and reference 9.)

[10] Baughan, Evans, and Polanyi, Trans. Faraday Soc. **37**, 377 (1941).

[11] E. T. Butler and M. Polanyi, Trans. Faraday Soc. **39**, 19 (1943).

[12] M. Szwarc, Disc. Faraday Soc. **2**, 39 (1947).

[13] See, e.g., W. A. Waters, *Chemistry of free radicals* (Oxford University Press, London, 1946).

For the discussion of Table III let us assume $D(CH_3-CH_3)$ to be our reference C−C bond dissociation energy. The relative increase in the C−C bond dissociation energy shown by diphenyl and cyanogen indicates an additional bond strengthening which is usually interpreted in terms of conjugation in the molecule. On the other hand, the relative decrease in the C−C bond dissociation energy, as observed in the remaining compounds listed in Table III, might be interpreted in terms of the "experimental resonance energy" of radicals as given in Table I, and of the "strengthening effect" influencing the undissociated molecule. The magnitudes of these effects are shown in the last three columns of Table III, and are computed by comparing $D(CH_3-CH_3)$ with $D(R'-R'')$.

It is interesting to note that although both $D(Ph\cdot CH_2-CH_2\cdot Ph)$ and $D(CH_3CO-CO\cdot CH_3)$ are lower than $D(CH_3-CH_3)$, the relevant C−C bonds seem to be intrinsically stronger by about 11 kcal./mole and 9 kcal./mole respectively than $D(CH_3-CH_2)$. This effect seems to manifest itself in a shortening of the relevant C−C bonds. While the length of the CH_3-CH_3 bond is about 1.54A, the central C−C bond distance in diacetyl is 1.47A,[14] and that in dibenzyl is 1.48A[15] (see in this respect reference 12). The exceptionally low value for $D(Ph_3\cdot C-C\cdot Ph_3)$ seems to be due to steric hindrance.[16]

The reality of the strengthening effect is particularly well demonstrated by values of

$$D(Ph\cdot CH_2-CO\cdot CH_3) = 63 \text{ kcal./mole}$$
$$D(CH_3\cdot CO-CO\cdot CH_3) = 60 \text{ kcal./mole}$$

and

$$D(Ph\cdot CH_2-CH_2\cdot Ph) = 47 \text{ kcal./mole.}$$

Were the gradation in the relevant C−C bond dissociation energies due to the resonance energies of the radicals only, one would expect an inequality of the type:

$$D(Ph\cdot CH_2-CH_2\cdot Ph) < D(Ph\cdot CH_2-CO\cdot CH_3) < D(CH_3\cdot CO\cdot -CO\cdot CH_3).$$

The fact that $D(Ph\cdot CH_2-CO\cdot CH_3)$ is *greater* than both $D(CH_3\cdot CO-CO\cdot CH_3)$ and $D(Ph\cdot CH_2-CH_2\cdot Ph)$ points to the presence of a strengthening effect which stabilizes the molecule of benzyl methyl ketone to a greater extent than the molecules of diacetyl or dibenzyl. It seems that this is not an isolated case but rather an example of a general rule. It is known for example that by mixing hexaphenyl ethane and tetraphenyl hydrazine one obtains a stable compound

$$Ph_3\cdot C\cdot N\cdot Ph_2.$$

This compound does not dissociate into radicals in the temperature range in which both hexaphenyl ethane and tetraphenyl hydrazine dissociate readily. Another well-known example is provided by the series:

$$D(Na-Na) = 17 \text{ kcal./mole}$$
$$D(Cl-Cl) = 57 \text{ kcal./mole}$$
$$D(Na-Cl) = \sim 90 \text{ kcal./mole}$$

and the accepted interpretation of this sequence is based on the idea of an ionic contribution to the NaCl structure.[3] The same kind of explanation might be suggested for the two former cases—one might postulate a contribution by ionic structures such as e.g.

$$Ph\cdot CH_2^+\cdot COCH_3^-$$

or

$$Ph_3\cdot C^+\cdot NPh_2^-.$$

In any case the regularities mentioned above are worth noting, whatever the explanation might be.

Further examples of the strengthening effect in a series of paraffinic hydrocarbons are derived from modern thermochemical data. If $D(CH_3-H)-D(R-H)$ represents the "experimental resonance energy" of radical R, then the strengthening effect in the $R'-R''$ bond (denoted by x) might be found from the equation

$$x = (\text{reson. energy of } R') + (\text{reson. energy of } R'') - D(CH_3-CH_3) + D(R'-R'').$$

Since the resonance energies of R' and R'' cancel out in the final expression for x, the latter quantity is expressed ultimately in terms of heats of formation of $R'H$, $R''H$, and $R'\cdot R''$ in conjunction with the values for $D(CH_3-H)$ and $D(CH_3-CH_3)$. The values of x computed in this way are collected in Table IV, and they indicate that the strengthening effect is smaller for the terminal bonds than for other C−C bonds in the molecule.

The discussion of the variation of bond dissociation energies presented in this paper is, of course, purely tentative. It is based on a number of assumptions, which although plausible are still arbitrary. It is not claimed that these particular assumptions are the best, but it is hoped that they may lead to a better understanding of the subject. The real purpose of this paper is to stress the ambiguities and difficulties encountered in all treatments of molecular energetics which are based on the concept of average bond energy, and to point out another avenue of approach which is more closely linked with experiment since it uses the concept of bond dissociation energy.

TABLE IV. The strengthening effect x (expressed in kcal./mole) refers to the C−C bond, the position of which is indicated by the subscript numbers.

Hydrocarbon	C_1-C_2	C_2-C_3	C_3-C_4	C_4-C_5	C_5-C_6	C_6-C_7	C_7-C_8	C_8-C_9	C_9-C_{10}
$n\cdot C_3H_8$	1.7	1.7							
$n\cdot C_4H_{10}$	2.1	4.3	2.1						
$n\cdot C_5H_{12}$	2.3	4.9	4.9	2.3					
$n\cdot C_6H_{14}$	2.1	5.0	5.4	5.0	2.1				
$n\cdot C_7H_{16}$	2.0	4.7	5.3	5.3	4.7	2.0			
$n\cdot C_8H_{18}$	2.0	4.6	5.0	5.2	5.0	4.6	2.0		
$n\cdot C_9H_{20}$	2.0	4.6	4.9	4.9	4.9	4.9	4.6	2.0	
$n\cdot C_{10}H_{22}$	2.1	4.7	5.0	4.9	4.7	4.9	5.0	4.7	2.1

[14] P. W. Allen and L. E. Sutton, Acta Cryst. **3**, 46 (1950).
[15] G. A. Jeffrey, Proc. Roy. Soc. **A188**, 222 (1947).
[16] H. E. Bent and E. S. Ebers, J. Am. Chem. Soc. **57**, 1242 (1935). Bent, Cuthbertson, Dorfman, and Leary, *ibid.* **58**, 165 (1936). H. E. Bent and G. R. Cuthbertson, *ibid.* **58**, 170 (1936).

The Electric Conductivity of Weak Electrolytes and Ampholytes at High Electric Field Strengths

O. Blüh and F. Terentiuk
Department of Physics, University of British Columbia, Vancouver, Canada
(Received August 23, 1950)

An oscillographic method has been devised for the investigation of the variation of the electrolytic conductivity with the electric field strength up to 100 kv/cm. The method has been used to measure the field effect in various weak electrolytes, particularly in ampholytes.

I

DEVIATIONS from Ohm's law in electrolytic solutions at high electric field strengths were observed, for the first time, by Max Wien. In solutions of strong electrolytes the effect is small and can be accounted for by the theory of ionic atmospheres, while in solutions of weak electrolytes the phenomenon is much larger—in the order of 10 percent for fields of 100 kv/cm—and was explained as a dissociation effect. The literature on the subject has been comprehensively reviewed up to 1938.[1]

Most of the experiments were made with a bridge method devised by Wien, but in two instances a high speed cathode-ray oscilloscope was used.[2] Between 1927 and 1934[1] Wien and his co-workers investigated aqueous and non-aqueous solutions of various salts, acids, and bases. Experiments of a more recent date have mostly been concerned with the effect in non-aqueous solutions.[3] Among the aqueous solutions of weak electrolyes investigated by Schiele[4,5] a relatively great increase in conductivity at rather low fields was found for acetic acid and particularly for glycine (amino acetic acid). Large increases in conductivity were also reported for solutions of agar.

Glycine and agar are ampholytes; glycine solutions are characteristic of the amino acid solutions containing zwitterions or dipolar ions. The question could be raised whether there is a connection between the dipolar properties of the molecules and the large increase in conductivity observed. From this standpoint, it could be expected that similar substances, amino acids, peptides, and proteins, would show comparable dissociation effects.[6]

The aim of the present investigation has been to develop an electronic measuring apparatus and to apply it to the investigation of weak electrolytes of an amopholytic nature and to other biologically important substances. In view of the fact that the effect in these solutions could be expected to be of the order of 10 percent, an attempt was made to develop a method in which simplicity of operation rather than high accuracy is obtained. Previous investigators used a special high speed oscilloscope for recording a current-voltage trace[2] and applied single pulses of extremely short duration in order to reduce heating effects. However, it was thought possible to use an ordinary oscilloscope, to apply voltage pulses of longer duration, and to prevent the heating effects by allowing the electrolyte to flow through the conductivity cell. The method has proved practicable and useful for the investigation of the problem under consideration.

II

The electrolytic cell (cf. Fig. 1) is made of Lucite, with two non-platinized cylindrical platinum electrodes of diameter $\frac{1}{8}$ inch. The distance between the electrode faces can be measured with a travelling microscope. The electrolytic solutions flow through the cell at a rate of 1000 cc/min. Two liters of solution were usually necessary.

The voltage pulses delivered to the conductivity cell are modulated from a minimum voltage up to a maximum voltage approximately five times the minimum voltage. The modulated voltage pulses are generated from sine waves produced by a variable audiofrequency oscillator (Block diagram, Fig. 1. A detailed circuit diagram is given in Fig. 2.) The resulting positive square pulses can be varied in duration by adjustment of a variable resistance (500 K) controlling the time constant of the kipp relay (6N7), but in the present investigation the pulse duration remained constant at 50 microseconds. The modulating saw-tooth wave is generated by a gas triode (884). The pulses from the kipp relay are applied to the cathode circuit of the modulator (807), and the saw-tooth wave is applied to the grid. The output is a series of positive pulses with linear saw-tooth modulation of 100 c.p.s. The saw-tooth wave also provides the horizontal sweep for the cathode-ray oscilloscope.

[1] H. C. Eckstrom and C. Schmelzer, Chem. Rev. **24**, 367 (1939).
[2] W. Fucks, Ann. d. Physik **12**, 306 (1932); W. Hüter, Ann. d. Physik **24**, 253 (1935).
[3] D. J. Mead and Fuoss, J. Am. Chem. Soc. **61**, 2097 (1939); **62**, 1720 (1940). H. A. Strobel and H. C. Eckstrom, J. Chem. Phys. **16**, 827 (1948). W. A. Adcock and R. H. Cole, J. Am. Chem. Soc. **71**, 2835 (1949). R. M. Fuoss, D. Edelson and B. I. Spinrad, J. Am. Chem. Soc. **72**, 327 (1950).
[4] M. Wien (experiments by J. Schiele), Physik. Zeits. **32**, 545 (1931).
[5] J. Schiele, Ann. Physik **13**, 811 (1932); Physik. Zeits. **34**, 60 (1933).
[6] O. Blüh, Protoplasma **23**, 436 (1935). Professor Wien was then prepared to investigate a number of amino acids and polypeptides. Owing to his retirement the experiments were not carried out (O.B.).

The modulated pulses are amplified in three stages. The first is an inverted amplifier (807), which supplies negative pulses to the following driver amplifier stage (807). The output at this stage has an amplitude of about 250 volts, and is applied to the grid of a power triode output stage (304*TH*) whose plate supply can be varied from zero to several thousand volts. The final pulses are brought from the power amplifier stage through a high voltage coupling condenser to the conductivity cell (Fig. 1).

Instead of a continuously increasing voltage being applied to the cell, a sequence of short pulses (50 microseconds), modulated over a certain voltage range, is used. In order for a steady trace to be obtained on the screen of the oscilloscope, the modulated pulses are repeated with a convenient frequency (100 c.p.s.). In series with the conductivity cell is a variable wire resistance which is connected across the vertical deflecting plates of the oscilloscope. The potential drop across the resistor is recorded on the screen instantaneously with the potential applied to the cell (cf. Figs. 3 to 10). The peak voltage at the cell is observed with the help of a rectifying circuit, the pulses being used to charge a condenser, and the peak voltage measured with an electrostatic voltmeter.

The pulse generator and the cell arrangement are assembled in a steel rack, whereas the oscilloscope is placed in a darkroom space made of black-out curtains. The screen of the oscilloscope (Sylvania, Model 132) is seven inches in diameter, but only the central part of $2\frac{1}{2}$-by-$2\frac{1}{2}$-inch square is used. The rest of the screen is masked off with black paper and the open square framed with graph paper. A piece of black cotton is stretched across the screen as a reference line. The photographs of the traces were taken with a 3.5 Univex camera on Kodak Super XX film (size of picture 20 by 25 mm.). Exposures of 10 sec. at full aperture were made at a distance of ten inches.

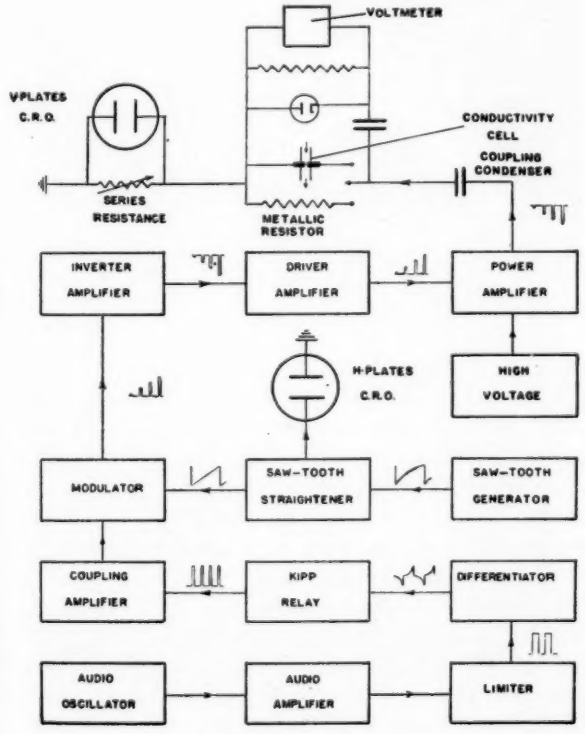

FIG. 1. Block diagram of apparatus.

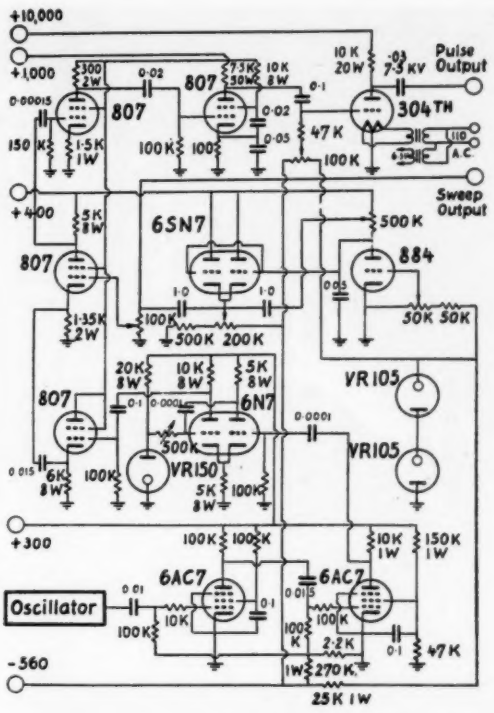

FIG. 2. Pulse-generator circuit diagram.

The linearity of pulse modulation is initially established with the help of metallic resistors at high voltage but low field strength, so that the pulse generator was always operated under the same condition as during the actual measurements. The heads of the pulses are adjusted so as to fall parallel to the string stretched across the screen, and a photograph of the fluorescent trace taken. The metallic resistor is then replaced by the electrolytic cell, and the voltage varied so that the maximum pulse always falls in the upper right-hand corner of the square part of the screen. The lower part of the curve is then approximately parallel to the string. The trace obtained with the electrolyte is recorded on the same film on which the resistor trace was photographed. Finally, the open part of the screen is covered with a square of black paper and the graph paper frame photographed in white light. Several photographic records were obtained for each measurement.

The traces can easily be observed on the screen; they remain very steady during the flow of the liquid, as can be seen from the photographs (Figs. 3 to 10). The steadiness of the trace indicates the constancy of temperature. The flow of the solutions has no effect on the conductivity, as was shown in independent experiments at low

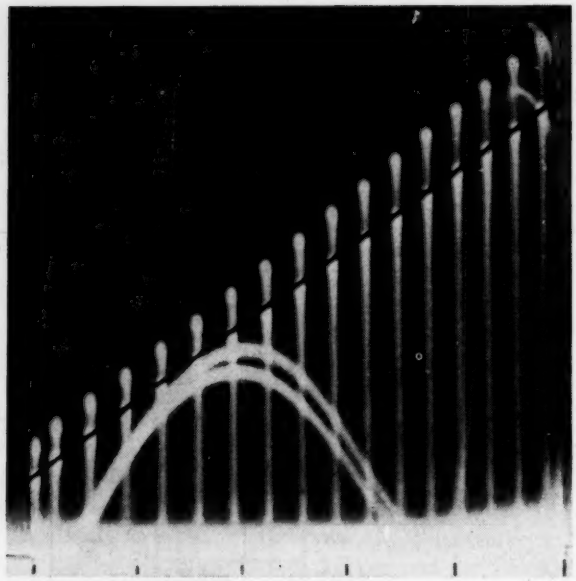

FIG. 3. Hydrochloric acid.

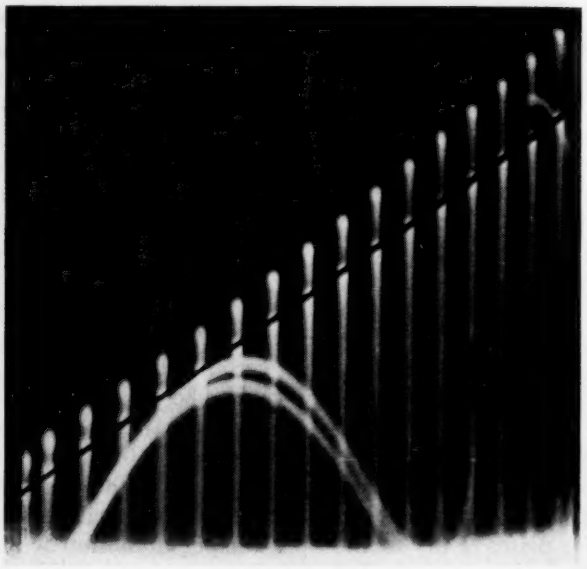

FIG. 5. Acetic acid.

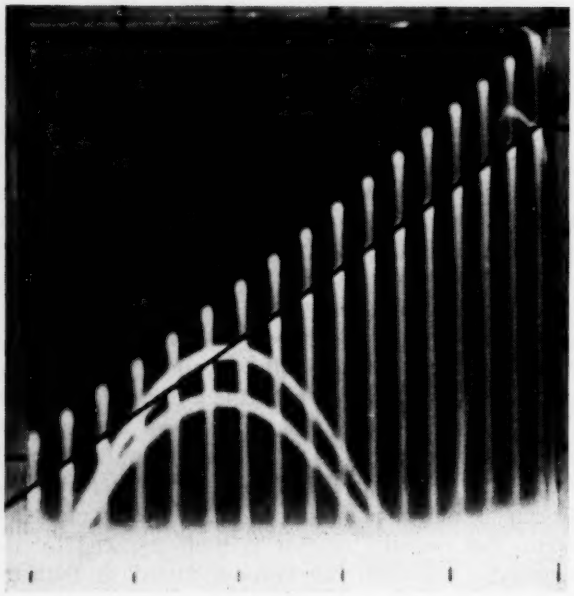

FIG. 4. Lithium chloride.

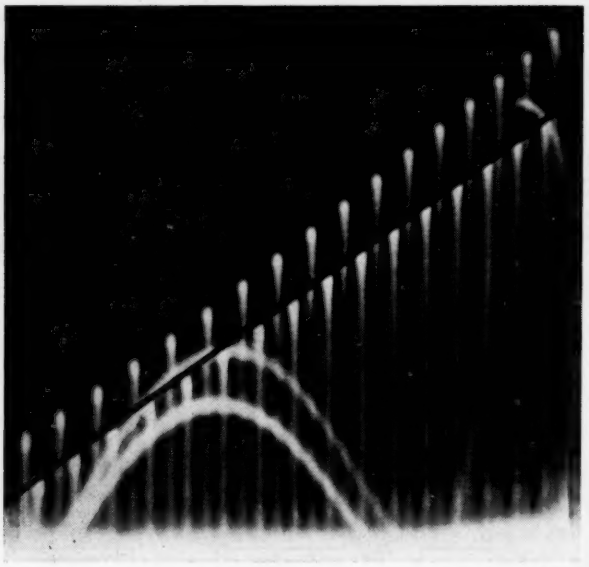

FIG. 6. Glycin.

fields with bridge arrangements at 60 c.p.s. and 1000 c.p.s. The same bridges were used to measure the conductivity of the solutions in a conventional conductivity cell.

III

The general character of the traces for the solutions investigated is a curve deviating continuously upwards from the initial slope at low voltage to greater slopes at the peak voltage. It does not appear that at any point a sharp change occurs. In order to obtain the percentage increase of conductivity for different parts of the trace, the slope of tangents to the curves can be found. For this purpose enlarged photographic copies (3 by 3 inches) of the films were made. A Lucite plate, on which fine straight lines of different slopes were engraved, was placed on top of the photographic copy and moved parallel along a metal bar until one of the straight lines was found to coincide with the imaginary tangent given by three adjacent pulse heads. The slopes of the engraved reference lines varied by half-degrees, and $\frac{1}{4}$ degrees could be interpolated. With a better definition of the trace heads greater accuracy could be achieved. The accuracy of the linear trace was also checked, and found in all cases to be correct to $\frac{1}{2}$ degree. Average values of the slopes were used for calculating

the relative increases. The tangents of the slopes are taken as measures of the conductivity at the corresponding field strength. Only two slopes, at the beginning and the end of the trace, were measured. The maximum field strength was calculated as the ratio of voltage and gap distance.

The constancy of the pulse traces indicates that no heating effect is transferred from pulse to pulse. However, pulses with higher energy produce relatively more heat, and it appears that with the narrow gaps used a sufficient heat dissipation during the pulses is not guaranteed. For this reason a standard trace with solutions of hydrochloric acid was obtained. According to Wien, the very small increase in conductivity with field strength in these solutions is entirely due to a general ionic effect, which would not be noticeable with the present arrangement. In our experiments solutions of hydrochloric acid gave a slightly curved trace, which for a maximum field intensity of 100 kv/cm resulted in a percentage increase in conductivity of 13 percent. This change, very likely due entirely to heating during a single pulse, was deducted from the percentage changes observed for the other solutions. These changes were throughout greater than those for hydrochloric acid, as an inspection of the traces in Figs. 3 to 10 shows. The curvature is best observed by sighting along the pulse heads. The gap distance between the electrodes

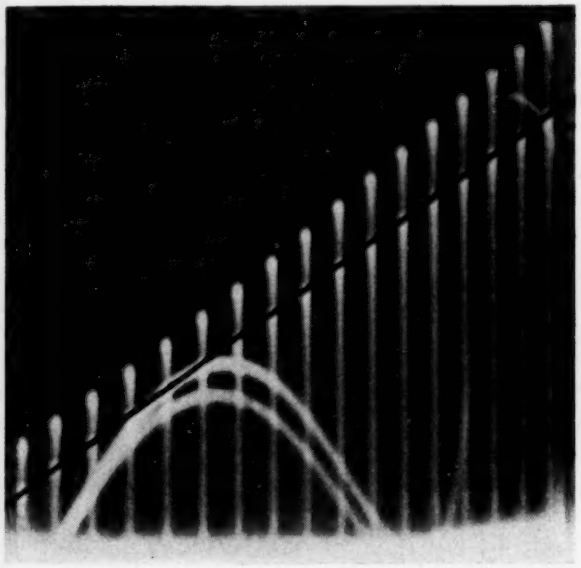

FIG. 7. Glutamic acid.

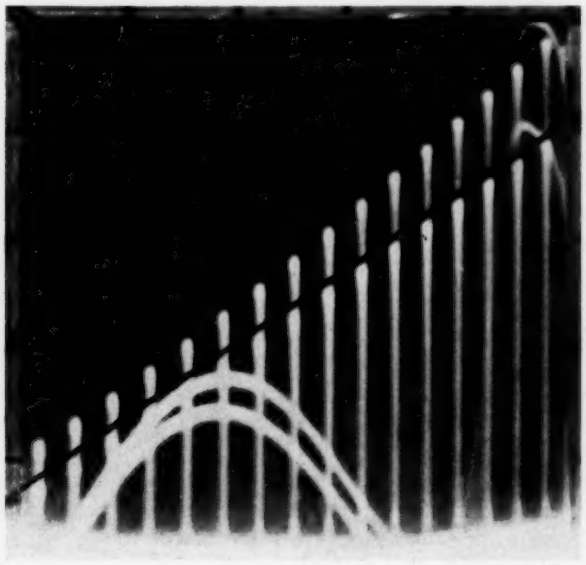

FIG. 9. Heparin.

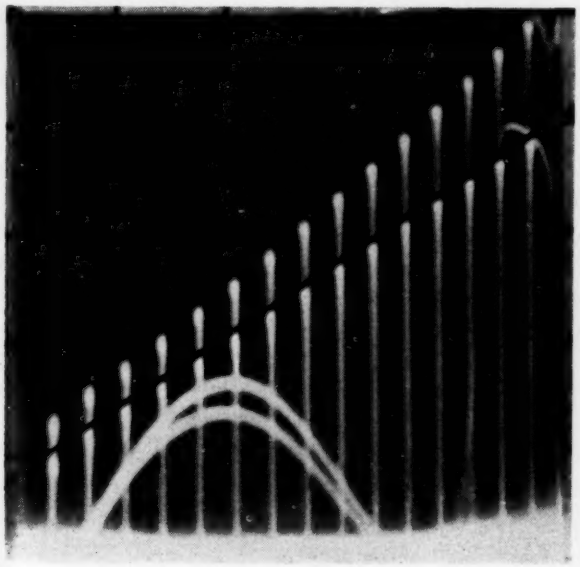

FIG. 8. *m*-benzoic acid.

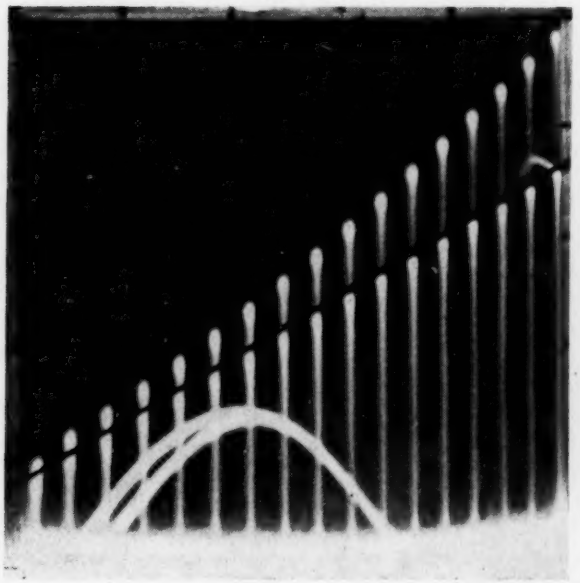

FIG. 10. Agar.

TABLE I. Percentage increase of conductivity (relative to hydrochloric acid).

Number	Substance	Conductivity ohm^{-1} cm^{-1} 1.3×10^{-4} E_{max}= 60 kv/cm Gap= 0.043 cm	1.3×10^{-4} 80 kv/cm 0.027 cm	7.4×10^{-5} 80 kv/cm 0.043 cm	7.4×10^{-5} 100 kv/cm 0.027 cm
1	Sulfuric acid	1.0	1.8	1.3	1.4
2	Potassium chloride	1.8	3.3	2.4	4.2
3	Lithium bromide	2.1	5.8	5.7	7.3
4	Acetic acid	5.9	9.8	9.7	11.6
5	Glycine	4.8	7.6	7.0	10.0
6	Glutamic acid	3.4	8.7	8.6	11.5
7	Benzoic acid				11.6
8	Sulfanilic acid				13.9
9	*o*-Amino benzoic a.				16.3
10	*m*-Amino benzoic a.				16.1
11	*p*-Amino benzoic a.				16.2
12	Proteose	3.1	4.0	6.2	9.5
13	Heparin			12.4	19.6
14	Agar			25.7	
				(Gap=0.027 cm)	

TABLE Ia. Concentration gram/liter.

Number of substance	Conductivity ohm^{-1} cm^{-1} 1.3×10^{-4}	7.4×10^{-5}
1	0.161	0.095
2	0.075	0.040
3	0.126	0.075
4	0.577	0.180
5	64.0	38.1
6	0.888	0.214
7		0.130
8		0.063
9		0.817
10		0.850
11		0.800
12	0.857	0.398
13		4 cc/l
14		9.0

was varied in order to produce a change in heat dissipation, but without a noticeable change in the relative increases of conductivity. (Compare the two columns of figures for 80 kv/cm in Table I.)

The values given in Table I are percentage increases of conductivity relative to hydrochloric acid. The estimated percentage error of the values given is about 10 percent. Besides the substances listed in the table, other substances were investigated, e.g., potassium iodide, barium ferri- and ferrocyanide, leucine, beta-alanine, valine, various peptones, and serum in diluted solution.[7] All these solutions, at low field conductivities of the order of 10^{-4} ohm^{-1} cm^{-1}, show considerable increases of conductivity in the order of 10 percent for maximum fields up to 130 kv/cm.

IV

The values given in Table I are in agreement with those reported by Schiele[4,5] for the same substances. Schiele found for sulfuric acid, relative to hydrochloric acid, at a similar conductivity, and at a field of 100 kv/cm, a 1 percent increase in conductivity; for lithium bromide he obtained 7 percent, and for potassium iodide 2–3 percent; the latter value should be comparable to the potassium chloride values in Table I. For both acetic acid and glycine, Schiele found an increase in conductivity of 5 percent at 100 kv/cm, which is lower than our values. This may be due to differences in the low field conductivities (2×10^{-4} in Schiele's experiments) and in pulse time. Agar gave a similar high percentage increase, as found earlier.

The other substances have been measured for the first time. The aromatic aminoacids show no differences between those which contain dipolar ions (sulfanilic acid, *m*-aminobenzoic acid), and those which do not.[8]

The percentage increases of conductivity of a proteose and heparin (a complex substance similar to mucoitin sulfuric acid) is very striking; higher values have been obtained for other proteoses and for serum.

The dissociation effect has been treated theoretically by Onsager.[9] Considering the molecules of weak electrolytes as ion pairs in Brownian motion, a superimposed electric field influences the latter and effects a change in the dissociation constant. The dissociation of protons from weak acids and amino acids can be understood in the same way, with the difference that in the case of dipolar ions the proton may be expected to dissociate from the amino group. An electrostatic effect from the negative charge of the carboxyl group may hinder the dissociation, while the dissociation of protons from positive glycine ions would be facilitated by the presence of the positive charge on the amino group. On the other hand, the proton dissociation could be directly influenced by the electric field on the proton which has experienced an intramolecular proton shift.

In order to gain insight into the mechanism of proton dissociation, the method will be applied to the systematic study of aminoacids, polypeptides, and proteins, with respect to dipole length, hydrogen ion concentration, viscosity, etc. The experimental arrangement can be improved by the use of fast recording oscilloscopes and single pulse recording with long persistence screens. A study of the effect of pulse time, and of time lags will also be undertaken. The method of modulated high voltage pulses is applicable to the study of the field effect in solid and liquid insulators, to which it has already been applied in preliminary experiments.

This investigation has been assisted by a grant from the Canadian National Research Council. One of us (F. T.) has obtained financial support in the form of scholarship grants. We wish to thank Mr. H. H. A. Davisson, who developed the pulse generator, and Mr. H. Dutton, who assisted in the preliminary stages of the experiments.

[7] F. Terentiuk, *The Conductivity of Amion Acid Solutions in High Electric Fields*, Master's thesis, University of British Columbia (1949).

[8] O. Blüh and J. Kroczek, Zeits. f. physik. Chemie **B27**, 278 (1934); G. Devoto, Gazz. chim. ital. **63**, 247 (1933).

[9] L. Onsager, J. Chem. Phys. **2**, 599 (1934).

THE JOURNAL OF CHEMICAL PHYSICS VOLUME 18, NUMBER 12 DECEMBER, 1950

The Vibrational Spectra and Structure of Inorganic Molecules. III. The Infra-Red Spectra of Nitrosyl Chloride and Nitrosyl Bromide from 2.0 to 25μ*

W. G. BURNS† AND H. J. BERNSTEIN
Division of Chemistry, National Research Council, Ottawa, Canada

(Received August 30, 1950)

The infra-red absorption spectra of nitrosyl chloride and nitrosyl bromide vapors have been examined from 400 to 5303 cm^{-1}, and the spectra explained on the basis of three fundamentals at 1799, 592, and 332 cm^{-1} for NOCl and 1801, 542, and 265 cm^{-1} for NOBr. The force constants and the amplitudes for the fundamental modes were calculated for a central force system. The $P-R$ separation of the predominantly parallel bands and the spacing of rotational bands in one partially resolved mainly perpendicular band in the NOCl spectrum were found to be in good accord with the electron diffraction data for the dimensions of the molecule. Thermodynamic functions for the gases were calculated from 298° to 1500°K. The calculated values of S_{298}^0 for both gases are in good agreement with the experimental values.

I. NITROSYL CHLORIDE

THE infra-red absorption spectrum of NOCl gas has been measured previously by Bailey and Cassie[1] who interpreted their spectrum on the basis of three fundamentals, *viz.*, $\nu_1=1832$ cm^{-1},

$$\nu_2=633 \text{ cm}^{-1}, \text{ and } \nu_3=923 \text{ cm}^{-1}.$$

These fundamentals were shown to be unsatisfactory by Beeson and Yost[2] from comparison of the observed entropy change for the reaction $2NOCl(g)\rightleftarrows 2NO+Cl_2(g)$ with that calculated from the methods of statistical thermodynamics.[3] If the fundamentals suggested by Bailey and Cassie are used to calculate the entropy change for this reaction it is found that $\Delta S°$(calc.)$-\Delta S°$(obs.)$=3.6$ cal./deg./mole. Since this is well outside the range of the experimental error of ±0.3 cal./deg./mole Beeson and Yost concluded that the band at 923 cm^{-1} was a combination of the fundamental at 633 cm^{-1} with a low lying bending frequency at ~290 cm^{-1}. Using this revised assignment to calculate the entropy change for the reaction, gives$\Delta S°$(calc.) $-\Delta S°$(obs.)$=0.4$ cal./deg./mole.

The principal moments of inertia used in the above calculation of the entropy, *viz.*,

$$I_A=9.05\times10^{-40} \text{ g cm}^2, \quad I_B=147.7\times10^{-40} \text{ g cm}^2,$$
$$I_C=156.7\times10^{-40} \text{ g cm}^2$$

were calculated from Ketelaar and Palmer's[4] electron diffraction data, namely $r_{ON}=1.14\pm0.02$A, $r_{NCl}=1.95\pm0.01$A, and $\measuredangle O-N-Cl=116\pm2°$.‡

It is evident that the molecule is very nearly a symmetric top. However, since NOCl has a plane of symmetry, only all bands will be hybrid possessing perpendicular and parallel components. The fine structure spacing of the perpendicular component should be about 6 cm^{-1} which would be readily resolved under our experimental conditions.

This work was undertaken because of the tentative nature of the existing data with regard to choice of fundamentals, and also in the hope of resolving the perpendicular component of a band in order to find a spectroscopic value for the least moment of inertia.

Experimental

The nitrosyl chloride was prepared by the method of Tilden.[5] Nitrosulfuric acid was dropped on dry sodium chloride and the gases evolved according to the equation

$$2NaCl+SO_2OH\cdot ONO\rightarrow Na_2SO_4+HCl+NOCl$$

were collected in a trap immersed in molten chloroform (−63.5°C). The nitrosulfuric acid was prepared by absorbing the nitrosyl chloride obtained from heating aqua regia in concentrated sulfuric acid until the absorbing liquid was a golden brown color. The NOCl was purified in vacuum by keeping it immersed in a bath of solid CO_2/acetone (−78°C) and pumping out the gases through a trap kept in a freezing mixture at −110°C. This caused an efficient separation from the more volatile impurities which did not condense and the less volatile, which remained in the vessel at −78°C. Five such distillations were carried out, rejecting the first and last fractions. Previous work[6] has shown that this was sufficient to reduce the impurities to less than 0.26 percent.

The spectra were obtained with a Perkin-Elmer Model 12*C* infra-red spectrometer used in conjunction with a Brown recorder. The NOCl was introduced into

* Presented at the Symposium on Molecular Structure held at Columbus Ohio (June, 1950).

† National Research Laboratories Postdoctorate Fellow 1949–50.

[1] C. R. Bailey and A. B. D. Cassie, Proc. Roy. Soc. **145A**, 336 (1934).

[2] C. M. Beeson and D. M. Yost, J. Chem. Phys. **7**,,44 (1939).

[3] See G. Herzberg, *Infrared and Raman Spectra of Polyatomic Molecules* (D. Van Nostrand Company, Inc., New York, 1945), p. 501 ff.

[4] J. A. A. Ketelaar and K. J. Palmer, J. Am. Chem. Soc. **59**, 2629 (1937).

‡ The absorption of microwaves by $NOCl^{35}$ and $NOCl^{37}$ gives $I_B=147.33$, $I_C=152.59$, and $I_A=5.27$ for $NOCl^{35}$ [Pietenpol, Rogers, and Williams, Phys. Rev. **77**, 741 (1950)]. These values for I_B and I_C and those obtained by electron diffraction are in good agreement. The I_A obtained by these authors was calculated from $I_C=I_A+I_B$ which is only true for the instantaneous moments of inertia and not to be used here.

[5] W. A. Tilden, J. Chem. Soc. **27**, 630 (1874).

[6] F. S. Dainton and W. G. Burns (unpublished results).

TABLE I. The infra-red spectrum of NOCl gas.

Bailey and Cassie Obs.	Bailey and Cassie Assignment	This work Obs.	This work *PR* separation	This work Assignment
		5303[a] w		$3\nu_1=5397$
		4160 w	15	$2\nu_1+\nu_2=4160$
		3898 w	14	$2\nu_1+\nu_3=3900$
		3568 m	15	$2\nu_1=3598$
		2395 m *PQR*	18	$\nu_1+\nu_2=2391$
2155 m	$2\nu_2+\nu_3$	2131 m *PQR*	20	$\nu_1+\nu_3=2131$
1832 s	ν_1	1799 s *PQR*	19	ν_1
		1248 v.w.		$2\nu_3+\nu_2=1256$
1200 w	$2\nu_2$	1207 v.w.		$\nu_1-\nu_2=1207$
		1184 v.w.		$2\nu_2=1184$
923 s	ν_3	923 s *PR*	15	$\nu_2+\nu_3=924$
		664 v.w.		$2\nu_3=664$
633 s	ν_2	592 s *PR*	18	ν_2
		332[b]		ν_3

[a] The frequency of this band was calculated to be about 5303 cm^{-1} from the observed bands for ν_1 and $2\nu_1$ and then used as a calibration point for this region. Its numerical value may be considerably in error.
[b] Obtained from the combination tones $2\nu_3$, $\nu_2+\nu_3$, $\nu_1+\nu_3$, $2\nu_1+\nu_3$.

TABLE II. Fine structure of band at 664 cm^{-1}

Arbitrary numbering	Cm^{-1}
1	631.0
2	636.9
3	642.5
4	648.6
5	653.0
6	657(?)
7	666.5

the evacuated absorption cell (10 cm in length) from a side arm containing the solid or liquid in a small bulb. The different pressures required were obtained by immersing the bulb in baths of known temperatures and the pressure obtained from the vapor pressure data.[6]

Results and Discussion

Figure 1 shows the bands observed between 400 and 5300 cm^{-1}. Their frequencies are included in Table I (column 3) and the frequencies of the bands obtained by Bailey and Cassie are given in column 1 of Table I for comparison.

The very strong band at 1799 cm^{-1} must be ascribed to a fundamental associated with the NO vibration since it is reasonably close to the fundamental observed in nitric oxide[7] at 1875 cm^{-1}. By reason of its intensity, the band at 592 cm^{-1} may be considered to be another fundamental. The next most intense bands are at 923 and 2131 cm^{-1}. If the band at 923 cm^{-1} is assumed to be a fundamental, it is impossible to explain the relatively strong band at 2131 cm^{-1} by a binary combination. The assignment $2\times592+923=2107$ cm^{-1} which corresponds to the assignment made by Bailey and Cassie, for the band at 2155 cm^{-1} has a large negative anharmonicity and seems to be too intense for a ternary combination tone. The bands at 2131 and 923 cm^{-1} are best explained as combination tones of the fundamentals at 1799 and 592 cm^{-1} with an unobserved fundamental at 332 cm^{-1}. On this basis namely $\nu_1=1799$ cm^{-1}, $\nu_2=592$ cm^{-1}, and $\nu_3=332$ cm^{-1} the assignment in Table I has been made.

From the values of the principal moments of inertia a pure parallel band would be expected to give the usual *PQR* contour with unresolvable fine structure and a *PR* separation[8] of 18.5 cm^{-1}. On the other hand, a pure perpendicular band would have a rotational fine structure with a spacing of about 6 cm^{-1}. Since the molecule has a plane of symmetry only, the observed bands are hybrid with both parallel and perpendicular components. The fundamentals at 1799 and 592 cm^{-1} and all the observed combination tones and overtones appear to have mainly parallel character with no fine structure. The observed separation of the *PR* maxima (19 ± 1 cm^{-1}) agrees quite well with the calculated separation[8] of 18.5 cm^{-1}.

The force constants were calculated assuming a central force field using the equations of Radakovic[9] and the molecular dimensions mentioned above. The values obtained are

$$f_{NO}=13.97\times10^5 \text{ dynes per cm},$$
$$f_{NCl}=1.92\times10^5 \text{ dynes per cm},$$
$$f_{ClO}=1.30\times10^5 \text{ dynes per cm}.$$

The amplitudes of the motions of the atoms in the three fundamental modes of vibration were calculated from the same equation[9] and are shown in Fig. 2. The amplitudes are drawn to a scale which is ten times as large as that for the molecular dimensions. Examination of Fig. 2 suggests that the only vibration in which the rate of change of dipole moment is predominantly perpendicular to the axis of least moment of inertia is the bending vibration $\nu_3=332$ cm^{-1}. The weak overtone at

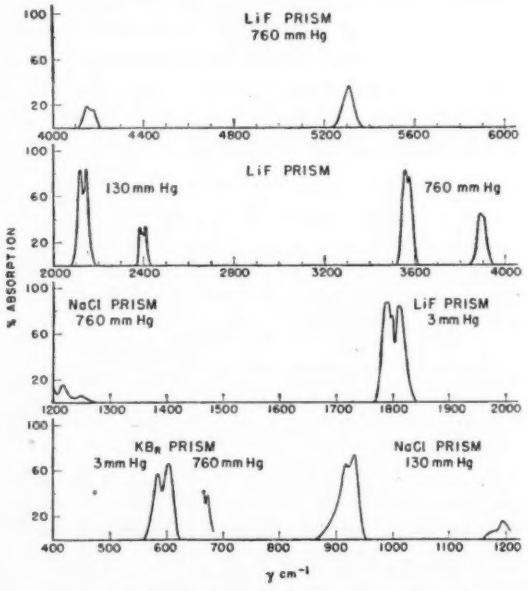

FIG. 1. Infra-red spectrum of gaseous NOCl.

[7] R. H. Gillette and E. H. Eyster, Phys. Rev. **56**, 1113 (1939).
[8] S. L. Gerhard and D. M. Dennison, Phys. Rev. **43**, 197 (1933).
[9] M. Radakovic, Monats. f. Chem. **56**, 447 (1930).

$\sim$664 cm^{-1} was examined at one atmosphere pressure for fine structure and the structure has been partially resolved (Fig. 3). The band is difficult to observe since it is overlapped on one side by the atmospheric CO_2 band at 667 cm^{-1} and on the other side by the tail of the very strong band at 592 cm^{-1}. Since the center of the band was not observed, the individual bands could not be numbered. Their frequencies are given in Table II. The spacing is about equal to the expected value of $\sim$6.0 cm^{-1}. The fact that this overtone was observed and has the expected perpendicular character and the correct fine structure spacing is convincing confirmation of the assignment.

Thermodynamic Functions

Nitrosyl chloride gas is diamagnetic[10] and the molecule appears to have a singlet ground state. On this basis and using the fundamentals given above and the electron diffraction values of the principal moments of inertia, the thermodynamic properties of the gas were calculated using the usual statistical-mechanical formulas. In Table III are listed the calculated values of C_p^0, S^0, and $-(F^0-H_0^0)/T$ for the gas from 300° to 1500°K. The calculated value of the entropy at 298°K, $S_{298}^0(\text{NOCl})g=62.4\pm0.1$ cal./deg./mole, agrees quite well with the observed value $S_{298}^0(\text{obs.})=63.0\pm0.3$ cal./deg./mole.

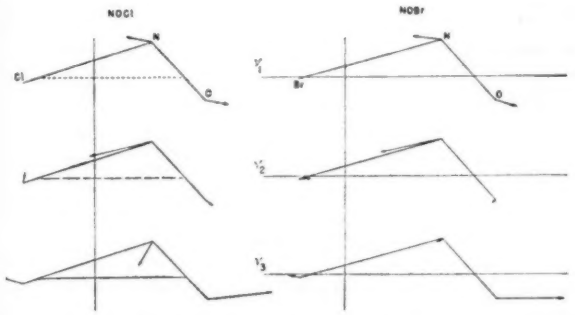

FIG. 2. The amplitudes during the modes of vibration of NOCl and NOBr.

II. NITROSYL BROMIDE

The electron diffraction experiments on nitrosyl bromide give the structure N–Br=2.14±0.02A, N–O=1.15±0.01A, $\measuredangle$O–N–Br=117±3°. The infra-red spectrum has not been previously examined, but the entropy of the gas is available from measurements on the equilibrium[11]

$$2NOBr \rightleftharpoons 2NO+Br_2$$

Experimental

Nitrosyl bromide was prepared by bubbling nitric oxide into bromine. The nitric oxide was prepared by the method given by Johnson and Giauque,[12] but without their stringent precautions for purity. The gases evolved in the reaction

$$2HNO_2+2I^-+2H^+=2NO+I_2+2H_2O$$

were passed in turn through concentrated H_2SO_4, 50 percent KOH, a trap at −78°, and P_2O_5. The nitric oxide was passed next into a trap of bromine (reagent grade) and a mixing bulb, and the gases finally condensed in molten carbon tetrachloride at −23°C. This product was purified in the same manner as the nitrosyl chloride, the first trap being kept at −63.5°C in molten chloroform, and the second at −110°C. The nitrosyl bromide could not be freed from nitric oxide since the mixture of gases due to the above equilibrium contains about seven percent NO at one atmosphere pressure, and room temperature.[11] This was not serious since the spectrum of NO is well known[7] and could be easily identified.

The same type of cell was used as for nitrosyl chloride. Only two pressures were used—a very low pres-

TABLE III. Thermodynamic functions of NOCl.

T°K	$-(F^0-H_0^0)/T$ cal./deg./mole	S^0 cal./deg./mole	C_p^0 cal./deg./mole
298.2	53.291	62.386	10.628
300	53.345	62.450	10.640
350	54.837	64.184	10.954
400	56.031	65.496	11.218
450	57.169	66.931	11.449
500	58.208	68.149	11.658
600	60.048	70.306	12.019
700	61.652	72.183	12.320
800	63.074	73.845	12.566
900	64.355	75.338	12.768
1000	65.523	76.692	12.931
1100	66.595	77.930	13.065
1200	67.588	79.073	13.176
1300	68.513	80.131	13.267
1400	69.379	81.118	13.342
1500	70.192	82.040	13.405

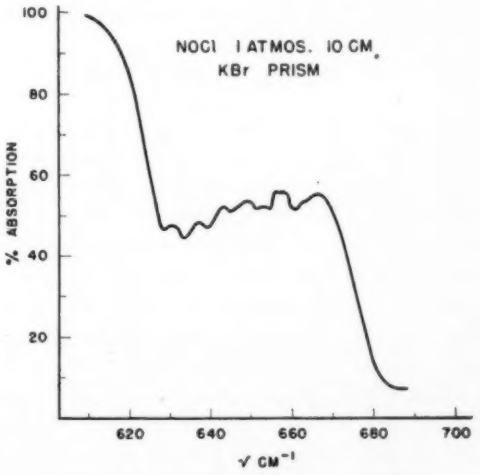

FIG. 3. Fine structure of $2\nu_2$ for NOCl.

[10] C. M. Beeson and C. D. Coryell, J. Chem. Phys. 6, 656 (1938).
[11] Blair, Brass, and Yost, J. Am. Chem. Soc. 56, 1916 (1934).
[12] H. L. Johnson and W. F. Giauque, J. Am. Chem. Soc. 51, 3194 (1929).

TABLE IV. The infra-red spectrum of NOBr gas.

Obs. cm^{-1}	*PR* separation	Assignment
5303[a] w		$3\nu_1=5403$
4103 w		$2\nu_1+\nu_2=4109$
3831 w	14	$2\nu_1+\nu_3=3832$
3567 w	15	$2\nu_1=3602$
2340 w	15	$\nu_1+\nu_2=2343$
2066 w	15	$\nu_1+\nu_3=2066$
1801 v.s.	15	ν_1
807 w	16	$\nu_2+\nu_3=807$
542 v.s.	14	ν_2
265[b]		ν_3

[a] See footnote (a) to Table I.
[b] Obtained from the combination tones $\nu_2+\nu_3$, $\nu_1+\nu_3$, $2\nu_1+\nu_3$.

TABLE V. Thermodynamic functions of NOBr.

T°K	$-(F^0-H_0^0)/T$ cal./deg./mole	S^0 cal./deg./mole	C_p^0 cal./deg./mole
298.2	55.991	65.333	10.865
300	56.047	65.398	10.876
350	57.506	67.096	11.148
400	58.801	68.600	11.378
450	59.966	69.952	11.582
500	61.029	71.183	11.770
600	62.906	73.358	12.101
700	64.538	75.246	12.382
800	65.983	76.195	12.615
900	67.283	78.414	12.806
1000	68.465	79.771	12.963
1100	69.550	81.013	13.091
1200	70.553	82.157	13.198
1300	71.487	83.217	13.285
1400	72.362	84.205	13.359
1500	73.182	85.128	13.420

sure estimated at 5 mm for the fundamentals, and a pressure of one atmosphere which was required for the overtones and combinations, as the spectrum was much less intense than that of the nitrosyl chloride.

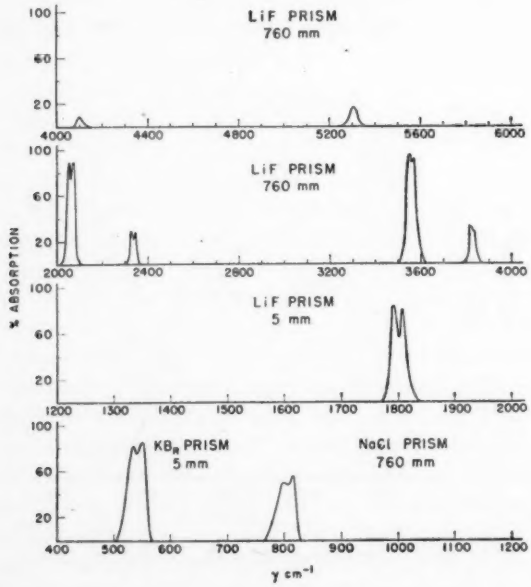

FIG. 4. Infra-red spectrum of gaseous NOBr.

TABLE VI. Comparison of the spectra of NOCl and NOBr.

NOCl cm^{-1}	Assignment	NOBr cm^{-1}
5303 w	$3\nu_1$	5303 w
4160 w	$2\nu_1+\nu_2$	4103 w
3898 w	$2\nu_1+\nu_3$	3831 w
3568 w	$2\nu_1$	3567 w
2395 m	$\nu_1+\nu_2$	2340 w
2131 m	$\nu_1+\nu_3$	2066 w
1799 v.s.	ν_1	1801 v.s.
1248 v.w.	$2\nu_3+\nu_2$	
1207 v.w.	$\nu_1-\nu_2$	
1184 v.w.	$2\nu_2$	
923 s	$\nu_2+\nu_3$	807 w
~664 v.w.	$2\nu_3$	
592 v.s.	ν_2	542 v.s.
332	ν_3	265

TABLE VII. Comparison of some molecular properties of NOCl and NOBr.

Molecular property		NOCl	NOBr
Force constants in units of 10^5 dynes/cm	$f_{N=O}$	14.0	14.0
	f_{N-X}	1.92	2.18
	f_{O-X}	1.30	0.832
Bond distances in angstroms and angle in degrees	R_{NO}	1.14±0.02	1.15±0.04
	R_{N-X}	1.95±0.01	2.14±0.02
	∢ONX	116±2°	117±3°
Moments of inertia in 10^{-40} c.g.s. units	I_A	9.05	9.40
	I_B	147.7	229.7
	I_C	156.7	239.1
Frequencies of fundamentals in cm^{-1}	ν_1	1799	1801
	ν_2	592	542
	ν_3	332	265
Entropy in cal./deg./mole	S^0_{298}(calc.)	62.4±0.1	65.3±0.1
	S^0_{298}(obs.)	63.0±0.3	65.2±0.3

Results and Discussion

Figure 4 shows the bands observed between 400 and 5300 cm^{-1} and Table IV gives the frequencies and the assignment.

Assignment

The assignment follows the same argument as for nitrosyl chloride, since the spectra are very similar. It is even more unlikely with nitrosyl bromide that the band at 807 cm^{-1} is a fundamental since its intensity is so much less than that of the bands at 542 and 1801 cm^{-1}.

Discussion

The principal moments of inertia, calculated from the electron diffraction measurements are

$$I_A=9.40\times10^{-40}\text{ g cm}^2,\quad I_B=229.6\times10^{-40}\text{ g cm}^2,$$
$$I_C=239.0\times10^{-40}\text{ g cm}^2$$

so that a parallel band should have a *PR* separation[8] of

14.6 cm^{-1}, and a perpendicular band should have resolvable fine structure with a separation of ~ 6 cm^{-1}. The force constants were calculated for a central force field[9] as for nitrosyl chloride, and the values obtained were

$$f_{NO} = 14.00 \times 10^5 \text{ dynes per cm},$$
$$f_{NBr} = 2.18 \times 10^5 \text{ dynes per cm},$$
$$f_{BrO} = 0.832 \times 10^5 \text{ dynes per cm}.$$

The amplitudes of the vibrations of the atoms were calculated as for the nitrosyl chloride, and are shown in Fig. 2. No band appears to be predominantly perpendicular. The overtone of 265 cm^{-1} is masked by the strong fundamental at 542 cm^{-1}. All the combination tones were found to be parallel in character, as were the other two fundamentals, and no fine structure was resolved. The observed separation of the *PR* maxima of 15 ± 1 cm^{-1} agrees quite well with the value 14.6 cm^{-1} calculated by the method of Gerhard and Dennison.[8]

Thermodynamic Functions

Using the usual statistical equations, and assuming the usual harmonic oscillator rigid rotator approximation, the values of S^0, $C_p{}^0$, and $-(F^0-H_0{}^0)/T$ were calculated for the gas and are given in Table V. The calculated value of the entropy at room temperature, 65.3 cal./deg./mole, agrees well with the value (65.2 ± 0.3 cal./deg./mole) obtained by Blair, Brass, and Yost[11] from measurements of the equilibrium with nitric oxide and bromine.

A comparison of the spectra of NOCl and NOBr is given in Table VI.

Some of the molecular constants and properties of NOCl and NOBr are compared in Table VII.

The authors are indebted to Miss E. Miller for reduction of the spectra and computational assistance.

Note added in proof: A note on the infra-red spectrum of NOCl has appeared [J. H. Wise and J. T. Elmer, J. Chem. Phys. **18**, 1411, 1950] while our manuscript was in press. The results are in agreement with our conclusions for this molecule.

THE JOURNAL OF CHEMICAL PHYSICS VOLUME 18, NUMBER 12 DECEMBER, 1950

The Multiplicity Forbidden Absorption Bands in the Spectrum of Pyridine

C. Reid
National Research Council, Ottawa, Canada
(Received August 11, 1950)

The two singlet-triplet transitions of pyridine have been studied using very long optical paths. The first of these, a π-electron transition, which was previously observed in the liquid phase only as a region of continuous weak absorption at the long wave end of the main absorption system, has been observed in the gas phase as a well-defined band system between 3000 and 3300A with a maximum molar absorption coefficient, $\epsilon = 0.10$.

The sixty observed bands have been fitted into a vibrational scheme which suggests that the transition responsible for them is allowed by symmetry.

The second transition which involves the non-bonding pair of electrons on the nitrogen atom was observed previously as a low temperature phosphorescence emission. Attempts to observe this transition in absorption using very long paths in the gas phase were unsuccessful, but it has been observed weakly using an optical path of 45 cm of liquid pyridine.

INTRODUCTION

THE ultraviolet absorption spectrum of gaseous pyridine has been investigated by Henri and Angenot,[1] by Sponer and Stucklen,[2] and by Lord.[3] The band of lowest wave number observed by any of these investigators was that at 32488 cm^{-1}, denoted by Henri and Angenot as "extremely weak" when observed with a path length of 53 cm and a pressure of 900 mm of pyridine vapor. The system of bands between 32500 and 38500 cm^{-1} will be henceforth referred to as the Henri-Angenot bands.

Two observations have been made at lower frequencies.[4] Low temperature phosphorescence emission was observed with a high frequency limit at about 25000 cm^{-1} and was identified as due to the lowest triplet→singlet transition involving the non-bonding electron pair on the N atom. In the region 29000 to 33000 cm^{-1} a very weak continuous absorption was observed in 5 cm of liquid pyridine. This was identified as due to a transition from the ground (singlet) state to a second triplet state involving π-electron excitation analogous to the well-known singlet-triplet absorption of benzene.

It appeared of interest to see whether, by using the very long absorption paths now available, these transi-

[1] V. Henri and P. Angenot, J. de Chem. Phys. **33**, 641 (1936).
[2] H. Sponer and H. Stucklen, J. Chem. Phys. **14**, 101 (1946).
[3] R. C. Lord (private communication).

[4] M. Kasha and C. Reid, "π- and n-electron transitions in N heterocyclics" (in preparation).

TABLE I. Observed wave numbers of bands in the 31000-cm^{-1} band system of pyridine.

Observed wave number cm^{-1}	Approximate relative intensity	Distance from O−O band cm^{-1}	Calculated distance from O−O band cm^{-1}	Designation[a]
30279.9	10	−596.0	−604(?)	−604(?)
339.3	5	−536.8	−536.5	$\nu_{10}-1570$
629.8	10	−246.3	−247.8	ν_2-652
694.4	15	−181.7	−182.8	ν_9-1139
734.2	2	−141.9	−146.2	ν_7-1028
748.5	1	−127.6	−126.4	ν_4-710
876.1	100	0	—	—
933.8	20	57.7	53.5	ν_8-884
976.9	5	100.8	104.8	$\nu_{12}-1028$
31083.3	1	207.2	209.6	ν_4-374
102.7	2	226.6	225.1	ν_5-404
164.0	5	287.9	287.2	ν_9-669
208.2	2	332.1	—	ν_1
270.6	10	394.5	391.7	$\nu_{11}-710$
280.3	10	404.2	—	ν_2
345.0	2	468.9	—	ν_3
459.7	80	583.6	—	ν_4
505.2	15	629.1	—	ν_5
698.4	15	822.3	—	ν_6
735.6	2	859.5	858.7	$\nu_{13}-374$
757.9	2	881.8	—	ν_7
790.9	1	914.8	915.7	$\nu_1+\nu_4$
813.6	2	937.5	—	ν_8
832.3	20	956.2	—	ν_9
842.3	2	966.2	961.2	$\nu_1+\nu_5$
866.3	3	990.2	987.8	$\nu_2+\nu_4$
909.6	15	1033.5	—	ν_{10}
934.8	20	1058.7	1052.5	$\nu_3+\nu_4$
977.8	20	1101.7	—	ν_{11}
32008.9	3	1132.8	—	ν_{12}
031.0	5	1154.9	1154.4	$\nu_1+\nu_6$
044.2	30	1168.1	1167.2	$2\nu_4$
108.8	5	1232.7	—	ν_{13}
120.4	30	1244.3	—	ν_{14}
192.9	3	1316.8	—	ν_{15}
216.8	2	1340.7	1341.7	$\nu_2+\nu_8$
247.4	35	1371.3	1360.4(?)	$\nu_2+\nu_9$(?)
264.6	10	1388.5	—	ν_{16}
348.9	5	1472.8	1464.9	$\nu_1+\nu_{12}$
475.0	3	1598.9	1590.3	$\nu_1+2\nu_5$(?)
522.2	30	1646.1	1644.6	$2\nu_6$
538.4	50	1662.3	1662.6	$\nu_5+\nu_{10}$
552.0	10	1675.9	1685.3	$\nu_4+\nu_{11}$
567.8	10	1691.7	1704.0	$\nu_6+\nu_7$
590.0	5	1713.9	1713.2	$\nu_3+\nu_{14}$
605.7	10	1729.6	1730.8	$\nu_5+\nu_{11}$
623.7	10	1747.6	1750.8	$3\nu_4$
628.1	15	1752.0		
660.6	10	1784.5	1785.7	$\nu_3+\nu_{15}$
677.3	10	1801.2	1796.3	$2\nu_4+\nu_5$
708.8	70	1832.7	1827.9	$\nu_4+\nu_{14}$
750.9	20	1874.8	1875.0	$2\nu_8$
784.3	15	1908.2	1912.4	$2\nu_9$
793.9	60	1917.8	1915.3	$\nu_9+\nu_{10}$
817.8	5	1941.7	1945.9	$\nu_5+\nu_{15}$
874.6	65	1998.5	1989.5	$2\nu_4+\nu_6$

[a] Frequencies given numerically in the assignment of "hot" bands are ground-state frequencies according to Kline and Turkevitch (see reference 6).

tions could be observed in the gas phase and the O−O bands thus located more precisely.

EXPERIMENTAL

In the present work the spectrum of pyridine vapor has been examined between 2500 and 5000A in the first order of a 21-ft. grating spectrograph using the long-path multiple reflection technique of White, as described by Bernstein and Herzberg.[5]

The multiple reflection system which employed mirrors of 1 meter radius of curvature was mounted in a brass tube provided with an observation window through which the images on the field mirror could be observed. The light beam entered and left the system through quartz windows sealed into the brass end plate by means of "O ring" seals. The whole tube was provided with a Chromel heating element and was suitably insulated so that its temperature could be raised to 200°C. The heater extended several inches beyond the mirror system at both ends to ensure uniform temperature conditions in the region between the mirrors.

With a path length of 20 meters and pressures of 30 to 50 mm a well-defined band system was observed in the region 3000 to 3300A. A photograph of this system, which is henceforth called the 31000-cm^{-1} band system, with the first-order iron arc used as a comparison spectrum, is shown in Fig. 1. The maximum path length which could be obtained was 80 meters, at a pressure of 760 mm of pyridine. With this pressure and path length no absorption could be detected in the region between 3500 and 5000A. However, absorption bands corresponding to the phosphorescence emission were observed with a small Hilger spectrograph in the spectrum of pure liquid pyridine. The bands appeared in the region 3500 to 4000A with an absorbing path length of 45 cm of liquid.

The pyridine used in these experiments was reagent grade material which had been purified by refluxing for 4 hr. with periodic additions of dry chromic oxide to remove traces of picolines. The resulting liquid was subsequently fractionated and the fraction boiling between 115.2° and 115.3°C used.

DISCUSSION

The bands observed in the 31000-cm^{-1} band system are listed in Table I. These bands are very sharp and in general are degraded slightly to the red. Measurements were made on the violet edges of the bands in all cases.

The most prominent feature of the system is a series of four bands spaced approximately 584.0 cm^{-1} apart, and with the strongest member at 30876.1 cm^{-1}. The most characteristic feature of the Henri-Angenot bands is a series of bands spaced 542 cm^{-1} apart. This series has been interpreted as due to the symmetric carbon ring vibration which in the ground state has the frequency 604 cm^{-1}. We assume that the series which we have observed in the new system is due to the same upper state vibration. If this interpretation is correct the band at 30876.1 cm^{-1} is probably the O−O band of the new electronic transition. Since it is the most prominent band in the system it is probable that the transition in question, although weak, is not forbidden by symmetry selection rules. The strongest

[5] H. J. Bernstein and G. Herzberg, J. Chem. Phys. 16, 30 (1948).

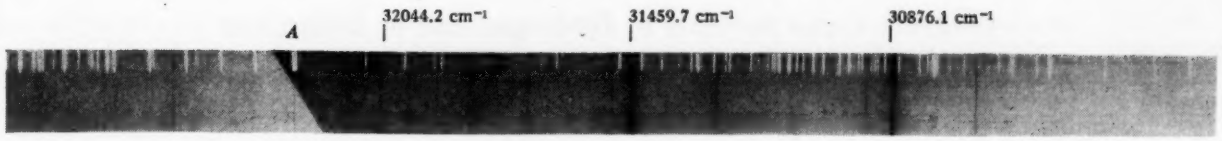

FIG. 1. The 31000-cm^{-1} band system of pyridine. The region to the left of the point marked A is the beginning of the Henri-Angenot bands.

bands of the system have a molar absorption coefficient, $\epsilon = 1/lc \log I_0/I = 0.10$, the weakest, $\epsilon = 0.002$.

Using 16 reasonable upper state frequencies and some of the ground-state frequencies of Kline and Turkevich,[6] it has been found possible to account very well for the 60 bands belonging to this system which have been observed. The number of bands measurable is limited by the overlap of the much stronger band system at shorter wave-lengths. In view of this and the large number of normal vibrations in pyridine, the choice of fundamental frequencies which has been made is probably not an unambiguous one, but it is the one that appears best to fit the available data. Thirteen bands are assigned to be "hot" bands. Of these, only one is assigned to the type 0←1, on the basis of the rather poor agreement between our frequency of 596 cm^{-1} and the strong fundamental variously reported as 601 and 604 cm^{-1}. The remainder appear to be principally 1←1 transitions. This is rather surprising, and it must be admitted is a point against our assignments. No attempt has been made to assign the 16 frequencies used to particular normal vibrations, or even to particular symmetry classes.

Turning to the system of bands between 3600 and 4000A, which were observed in the liquid phase only, we find three diffuse absorption maxima, at approximately 25500, 26490, and 27500 cm^{-1}, with a molar absorption coefficient of about 5×10^{-4}. The separation is approximately the same as that of the three most prominent bands in the phosphorescence spectrum. The bands are still weakly visible with an absorbing path length of 20 cm of pure liquid pyridine, but are absent when 1 meter absorbing path of a 30 percent solution of pyridine in concentrated sulfuric acid is used. Although this result must be interpreted with caution in view of the weakness of the absorption, it is consistent with the identification[1] of the corresponding phosphorescence bands as due to the transition from the ground state to the lowest triplet level in which the two non-bonding electrons on the nitrogen atom have become unpaired (called by Kasha an n-electron singlet-triplet transition). In sulfuric acid these non-bonding electrons are used up in forming a pyridonium ion, $C_5H_5NH^+$, and unpairing is not possible without disruption of this ion (compare NH_4^+).

However, the weakness of the 31000-cm^{-1} band system, although it is allowed by the symmetry selection rules, suggests that it too is due to a transition involving a change in multiplicity, as seemed already probable[1] by analogy with the benzene $T \leftarrow S$ system. Its closeness to the Henri-Angenot bands, which result from a singlet-singlet transition involving an electron of the conjugated π-electron system, suggests that the 31000-cm^{-1} band system is due to the corresponding π-electron singlet-triplet transition.

Thanks are due Dr. M. Kasha and Dr. G. Herzberg for numerous helpful discussions on this topic.

[6] C. H. Kline and J. Turkevich, J. Chem. Phys. **12**, 300 (1944).

Collision Cross Sections of Hydrogen and of Deuterium

I. AMDUR, M. C. KELLS, AND D. E. DAVENPORT
Department of Chemistry, Massachusetts Institute of Technology, Cambridge, Massachusetts
(Received September 8, 1950)

Total collision cross sections have been measured for hydrogen atoms, with energies between 300 and 800 ev, scattered in room temperature hydrogen, and for deuterium atoms, with energies between 500 and 1150 ev, scattered in room temperature deuterium. The $H-H_2$ cross section has a pronounced maximum at 600 volts indicating the presence of inelastic scattering. In the case of $D-D_2$ there is a similar effect, less pronounced, at about 800 volts.

Classical theory has been used to evaluate the repulsive potentials for the two systems on the assumption that smooth curves through the experimental results represent elastic cross sections, and that the atoms and molecules are mass points whose interaction forces are spherically symmetrical. For $H-H_2$, the present potential has been combined with one previously obtained, and the results represented by

$$V(r)=[0.708\exp(-29.9r^2)+0.0607\exp(-0.942r^2)]\times10^{-10}\text{ erg}$$

for r between 0.27 and 0.68A. The relation for $D-D_2$ is

$$V(r)=4.59\times10^{-11}\exp(-5.17r^2)\text{ ergs}$$

for r between 0.29 and 0.56A. The $D-D_2$ potential is considerably larger than that for $H-H_2$ for r between 0.29 and 0.56A, but the difference decreases markedly as r increases. It is suggested that the apparent difference in the potentials may result from the assumption of spherical symmetry which, even on a relative basis, does not exist in the present case because of the difference in the nuclear statistics of H_2 and D_2.

HYDROGEN atoms, with energies in the range 200–800 ev, have been previously scattered in room temperature hydrogen[1] and the total collision cross sections so determined used to evaluate the repulsive potential at small separation distances for the $H-H_2$ system.[2] In order to ascertain if the approximate equality of intermolecular and intramolecular forces which exists for hydrogen and deuterium at large separation distances, persists at small distances, it was decided to measure the collision cross sections of high velocity deuterium atoms scattered in room temperature deuterium. It was considered desirable to repeat the measurements on hydrogen to ensure that the present cross-section determinations for the two systems were under comparable conditions, as well as to check the earlier work.

The apparatus and experimental procedure was the same as that used in the scattering of high energy argon atoms in argon.[3] Since the geometry and, therefore, the angular aperture of the present scattering system differed from that originally used,[1] the present values for the total collision cross sections of hydrogen atoms scattered in hydrogen would not be expected to agree with those previously determined. The repulsive potentials evaluated from the two sets of results, however, might be expected to agree.

Total collision cross sections were determined, as previously, from ratios of beam intensities at two different pressures of scattering gas, and the usual tests were applied for the absence of multiple scattering. A total of 112 cross sections, from 7 to 18 at each voltage, were measured for 300 to 800 ev hydrogen atoms scattered in hydrogen gas. In the case of the deuterium experiments, 65 cross sections, from 4 to 14 at each voltage, were measured for 500 to 1150 ev deuterium atoms scattered in deuterium gas. Hydrogen and deuterium of 99.9 percent purity were used in the experiments. The final results are summarized in Tables I and II which contain values of $\bar{S}$, the arithmetic average of all total collision cross sections measured at a given voltage, S, *elastic* collision cross sections as read from the smooth curves which eliminate the maxima near 600 and 800 volts as shown in Fig. 1, and $\bar{L}$, the average mean free path at 1 mm of Hg and 0°C computed from the relation

$$\bar{L}=1/(n\bar{S}),\qquad(1)$$

where n is the number of scattering molecules per cm³ at 1 mm of Hg and 0°C. The maxima in Fig. 1 are similar to those previously observed in the scattering of hydrogen atoms by hydrogen, and of argon atoms by argon, and are probably due to inelastic scattering processes such as excitation or ionization. The tabulated values of S satisfy the relations

$$\mu v^2/S^{\frac{1}{2}}=[7.48\times10^{-5}\exp(-34.39S)+8.58\times10^{-9}\exp(-4.72S)]\text{ ergs}/A\qquad(2)$$

for the $H-H_2$ system, and

$$\mu v^2/S^{\frac{1}{2}}=[3.04\times10^{-8}\exp(-12.60S)+5.28\times10^{-9}\exp(-1.73S)]\text{ ergs/A}\qquad(3)$$

for the $D-D_2$ system, where μ is the reduced mass, and v, the relative initial velocity of the scattering system. These expressions were derived for use in evaluating the repulsive potential, $V(r)$, as a function of the separation distance, r, by a combination of the methods previously used for the case where the potential cannot be represented by $V(r)=K/r^n$ over the required range of r,[2b]

[1] I. Amdur and H. Pearlman, J. Chem. Phys. **8**, 7 (1940).
[2] (a) I. Amdur, J. Chem. Phys. **11**, 157 (1943); (b) **17**, 844 (1949).
[3] Amdur, Davenport, and Kells, J. Chem. Phys. **18**, 525 (1950).

and where the aperture geometry is determined by several openings in the scattering path.[3] The percentage errors in the last column of each table are the probable errors of the $\bar{S}$ and $\bar{L}$ values.

The repulsive interaction potentials derived from the variation of elastic cross section with energy as given in Eqs. (2) and (3) may be represented as follows:

(a) for the system, $H-H_2$,

$$V(r)=[4.38\times10^{14}\exp(-361r^2)+0.236\exp(-10.8r^2)]\times10^{-10}\text{ ergs}(r\text{ in }A) \quad (4)$$

for r in the range 0.32–0.39A;

(b) for the system, $D-D_2$,

$$V(r)=4.59\times10^{-11}\exp(-5.17r^2)\text{ ergs}(r\text{ in }A) \quad (5)$$

for r in the range 0.29–0.56A.

Recently,[2b] a relation was obtained for the average $H-H_2$ repulsive potential,

$$V(r)=[0.567\exp(-24.9r^2)+0.215r\exp(-2.40r^2)]\times10^{-10}\text{ ergs}(r\text{ in }A) \quad (6)$$

for r in the range 0.27–0.68A. Since the range of separation distance for which Eq. (4) is valid is so much smaller than that of Eq. (5), the present results will be combined with those of Eq. (6) to obtain a relation, based on two separate investigations, which is valid over a range of separation distance comparable to that of the $D-D_2$ system. This relation may be expressed as

$$V(r)=[0.708\exp(-29.9r^2)+0.0607\exp(-0.942r^2)]\times10^{-10}\text{ ergs}(r\text{ in }A) \quad (7)$$

for r between 0.27 and 0.68A. Equation (7) gives $V(r)$ values which, over the appropriate ranges of r, show an average absolute deviation of 12 percent from values computed from Eq. (4) or Eq. (6). This deviation which may be due to possible differences in beam composition in the present experiments (arc pressure, 0.23 mm) and in the earlier experiments (arc pressure, 0.3–0.4 mm), is small in comparison with the difference between the $V(r)$ values for $H-H_2$ and $D-D_2$ at a given separation distance, as shown graphically in Fig. 2.

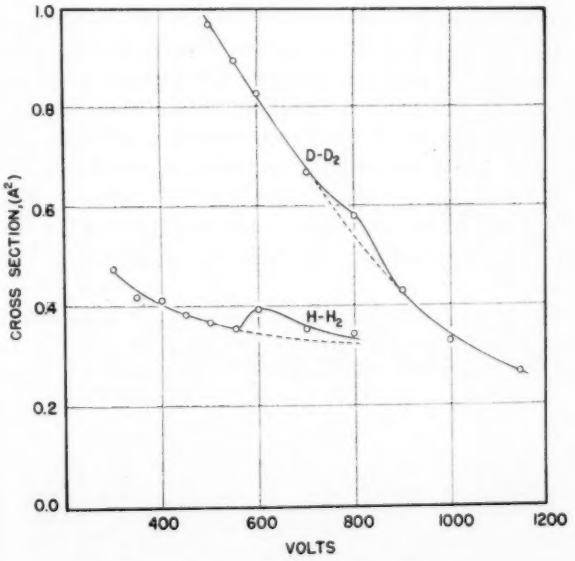

FIG. 1. Total collision cross sections.

TABLE I. Summary of collision cross section results for $H-H_2$.

Voltage	$\bar{S}$ A^2	S A^2	$\bar{L}$ cm	Percent error (±)
300	0.477	0.472	0.593	1.9
350	0.419	0.432	0.675	1.4
400	0.408	0.404	0.693	1.0
450	0.383	0.383	0.738	1.3
500	0.366	0.367	0.773	1.4
550	0.355	0.356	0.797	1.1
600	0.392	0.346	0.721	0.8
700	0.352	0.332	0.803	1.1
800	0.341	0.323	0.829	2.6

TABLE II. Summary of collision cross section results for $D-D_2$.

Voltage	$\bar{S}$ A^2	S A^2	$\bar{L}$ cm	Percent error (±)
500	0.967	0.970	0.292	0.8
550	0.898	0.892	0.315	1.0
600	0.827	0.817	0.342	0.6
700	0.669	0.670	0.423	1.2
800	0.579	0.536	0.488	0.7
900	0.428	0.421	0.661	0.7
1000	0.325	0.338	0.870	4.6
1150	0.265	0.263	1.067	3.5

For separation distances much greater than those involved in the present experiments, the intermolecular and intramolecular forces for hydrogen and deuterium are nearly equal. Wooley, Scott, and Brickwedde[4] have summarized the evidence for this conclusion in reviewing experimental measurements and theoretical treatments of viscosity, thermal conductivity, and compressibility of H_2 and D_2, and Hurlburt and Hirschfelder[5] have shown that band spectra measurements are in accord with the assumption of approximately equal intramolecular forces. In the case of intramolecular forces, evidence is supplied by measurements of the recombination rates of atomic hydrogen and of atomic deuterium.[6]

In the present case, the separation distances between nearest atoms in both systems are smaller than the radius of the first Bohr orbit, 0.53A, as seen in Fig. 2 where r is the distance between the center of the beam atom and the center of gravity of the scattering molecule. Yet, it is somewhat surprising to find the large departure from the approximate equality of interaction potentials observed at larger distances, since widely different potentials have been reported previously only in connection with nuclear interactions, where separa-

[4] Wooley, Scott, and Brickwedde, J. Research Nat. Bur. Stand. **41**, 379 (1948) RP1932.
[5] H. M. Hulburt and J. O. Hirschfelder, J. Chem. Phys. **9**, 61 (1941).
[6] I. Amdur, J. Am. Chem. Soc. **57**, 856 (1935).

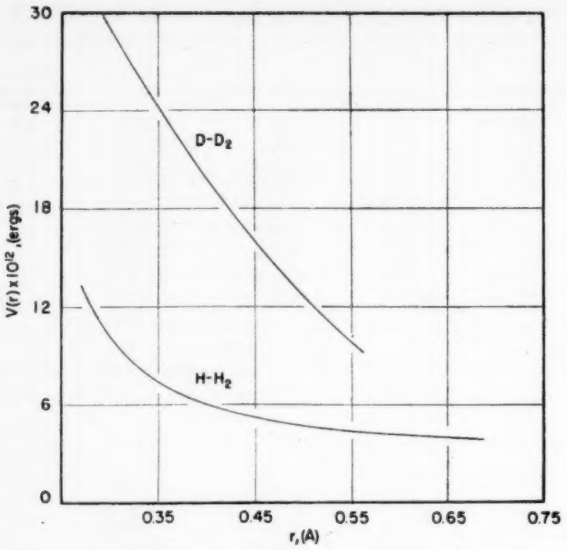

FIG. 2. Average repulsive potentials based on assumption that the atoms and molecules are mass points.

tion distances are extremely small, of the order of 10^{-4}A. There is the possibility that the difference in potentials shown in Fig. 2 may have its origin in apparatus geometry. For example, the condensers which deflect ions from the partially neutralized beam are located near the detector end of the scattering path and may therefore be relatively inefficient in removing ions from the portion of the scattering path near the atom gun. If the cross section for "umladung" or charge transfer for H^+ in H_2 were appreciably greater than that for D^+ in D_2, the observed total cross sections for $H-H_2$ could be smaller than those for $D-D_2$ because of greater enhancement of the intensity of the beam of H atoms, relative to that of the D atoms, during passage through the region scattering path above the condensers. Although possible, this explanation does not seem likely for the following reasons: first, at all voltages, the observed total cross sections were found to be independent of scattering pressure, whereas the presence of a significant amount of enhancement of scattered beam intensity resulting from charge transfer would cause a decrease of cross section with increasing scattering pressure, as in the case of multiple scattering; second, results obtained for He scattered in He (to be published later) in a second apparatus where the scattering gas is restricted to a region into which ions cannot penetrate, are in accord with results previously obtained in the present apparatus for the He—He system; finally, the difference between the two potentials in Fig. 2 diminishes, as anticipated, with increasing separation distance. For example, the $D-D_2$ potential is greater than the $H-H_2$ potential by 18.3×10^{-12} ergs at 0.29A, by 12.3×10^{-12} erg at 0.43A, and by 4.6×10^{-12} erg at 0.56A. If a short extrapolation of the curves is valid, the potentials would appear to coalesce at about 0.69A.

The authors suggest that the apparent difference in the two potentials might result from assuming spherically symmetrical force fields in calculating values of $V(r)$ from values of elastic cross sections as functions of voltage. Although this assumption cannot be true in an absolute sense for the systems under discussion, it might, if the systems behaved completely classically, be expected to give correct relative values of the potential, since, at a given voltage, the ratio of the angular velocity of the room temperature molecules to the linear velocities of the high energy beam atoms is the same for the $D-D_2$ and the $H-H_2$ systems. Under these conditions, both D_2 molecules and H_2 molecules would appear to present all orientations (on a number average basis) to the D atoms and H atoms, respectively, during the time in which the particles were within ranges of separation distance where mutual interactions were significant. However, the nuclear statistics of D_2 and H_2 are different, and at room temperature these molecules do not have exactly equal rotational energies as demanded by classical theory.[7] Thus, the ratios of angular velocity to linear velocity differ slightly and the average configuration in the $D-D_2$ system need not be strictly the same as that in the $H-H_2$ system. Margenau[8] has shown that at small separation distances, different orientations of the H_2 molecule with respect to the H atom produce very large changes in the magnitude of the interaction potential. It therefore seems possible for a relatively small difference in average orientation in the two systems to be responsible for the marked difference in the apparent potentials at small distances. As the separation distance is increased the effect of orientation would be expected to be of less significance and the assumption of spherical symmetry could lead to correct values of the average interaction potential. If a method could be found for analyzing the experimental results without assuming spherical symmetry, it is conceivable that, even at small distances, the interaction potentials for the two systems would turn out to be the same when referred to the *same* average orientation or to the same specific orientation.

[7] A. Farkas, *Orthohydrogen, Parahydrogen, and Heavy Hydrogen* (Cambridge University Press, London, 1935), pp. 17 and 163.
[8] H. Margenau, Phys. Rev. **66**, 303 (1944).

Letters to the Editor

THIS section will accept reports of new work, provided these are terse and contain few figures, and especially few half-tone cuts. The Editorial Board will not hold itself responsible for opinions expressed by the correspondents. Contributions to this section should not exceed 600 words in length and must reach the office of the Managing Editor not later than the 15th of the month preceding that of the issue in which the letter is to appear. No proof will be sent to the authors. The usual publication charge ($8.00 per page) will not be made and no reprints will be furnished free.

Ultraviolet Absorption Spectra of Mercury in Solution

M. K. PHIBBS
Division of Chemistry, National Research Council of Canada, Ottawa, Canada
October 16, 1950

IN a recent paper to this Journal,[1] which dealt with the problem of ultraviolet absorption spectra in solution, Bayliss developed a relation of the form,

$$\Delta\nu = c(n^2-1)/(2n^2+1), \qquad (1)$$

where $\Delta\nu$ (cm^{-1}) represents the shift of the absorption maximum to longer wave-lengths from its position in the gas phase, n is the refractive index of the solvent, and c is a constant whose value depends on the solute only.* Experimental data on merocyanine and bromine were used to confirm the linear relation between $\Delta\nu$ and $(n^2-1)/(2n^2+1)$.

It would seem that the most suitable type of solute for a check of this equation would be an atomic solute such as mercury. In this case, there should be no interference by the solvent "cage" effect, at least as discussed by Bayliss and Rees,[2] because there is no question of modification of vibrational energy levels by the environment. Furthermore, the mercury atom should correspond more closely than any molecule to the Onsager model of a point dipole at the center of a spherical cavity, on which the above development was based.

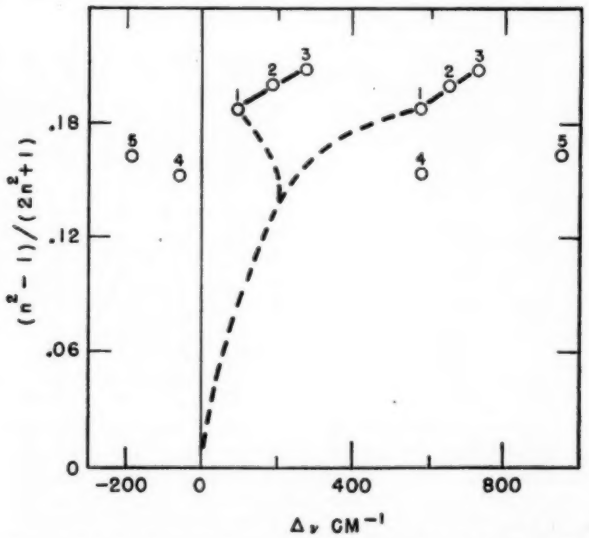

FIG. 1. Relation between the shift of the two peaks of the absorption spectra of Hg in solution and the refractive index of the solvent. The different solvents are represented by numbered points: (1) hexane at 25°C (reference 4), (2) decane at 25°C (reference 4), (3) octadecane at 25°C (reference 4), (4) methanol at 100°C (liquid) (reference 3), and (5) water at 120°C (liquid) (reference 3). The broken lines represent the behavior of the two peaks in hexane as the temperature is raised up to and beyond the critical temperature of hexane (reference 3).

Bonhoeffer and Reichardt[3] have already obtained such data for mercury dissolved in hexane, methanol, and water at several temperatures. In connection with other work[4] similar measurements were made with a Beckmann (Model CU) spectrophotometer using the solvents hexane, decane, and octadecane at 25°C. In all cases the absorption spectra are examples of extreme pressure broadening of the Hg resonance line 2537A, and they exhibit two peaks. The twin peaks have been attributed[3] to the splitting of the triply degenerate ($^3P_1$) upper energy level into a doubly degenerate σ-component and a π-component by the electrical force field of the environment. The data for the shifts of these two peaks† from 2537A in the various solvents are presented in Fig. 1.

It can be seen that there is an approximately linear relation between the $\Delta\nu$ of either peak and $(n^2-1)/(2n^2+1)$ for the three alkanes at 25°C, but the following observations make this agreement with theory of doubtful significance. Neither straight line passes through the origin in contradiction to the equation. This latter contradiction was also found by Bayliss[1] with bromine and merocyanine, for which, as here, the corresponding straight lines cut the $\Delta\nu=0$ ordinate far above the origin. Moreover, the variation of $\Delta\nu$ for the two peaks in hexane with increasing temperature[3] (decreasing $(n^2-1)/(2n^2+1)$) is represented by the dotted lines in Fig. 1; and it is evident that there is no discernible connection between these results and the equation. Finally, the data for methanol and water lie far off the straight lines through the alkane data; and, furthermore, one of the peaks for water and for methanol are shifted to the short wave-length side of 2537A. It seems unlikely that the large deviations from the equation shown by methanol and water could be attributed entirely to the weak inductive forces.

It seems, then, that the equation developed by Bayliss is too simplified to explain the absorption spectra of mercury in solution. It would probably be better, in this case, to try to extend the idea of statistical pressure broadening,[5] applicable to a compressed gas environment, to a liquid medium although the development could not be easy.

Aside from the mercury solutions, a few attempts were made to find absorption spectra for Na, Cd, and Bi in decane at 25°C; but the solubility of the metals was always too low to permit detection of any light absorption. Probably absorption spectra of such solutes would be obtainable at higher temperatures and/or with the right choice of solvent. In any case, further work on atomic solutes might add considerably to the general understanding of absorption spectra in solution.

[1] N. S. Bayliss, J. Chem. Phys. 18, 292 (1950).
* $c=10^{10}f/\nu a^3$, with f=oscillator strength, $2\pi c\nu$=natural frequency, and a=radius of solute particle. Equation (1) implies a linear relation between $\Delta\nu$ and $(n^2-1)/(2n^2+1)$ only if f is independent of environment. This seems to be true for mercury, for which $f\sim0.025$ in the gas phase and in solution in hexane at 63°C. See H. Reichardt, Zeits. f. Physik 70, 516 (1931).
[2] N. S. Bayliss and A. L. G. Rees, J. Chem. Phys. 8, 377 (1940).
[3] H. Reichardt and K. F. Bonhoeffer, Zeits. f. Physik 67, 780 (1930).
[4] M. K. Phibbs and B. deB. Darwent, J. Chem. Phys. 18, 679 (1950).
† The positions of the peaks were taken as the two maxima in each spectrum. Presumably, the actual positions of the peaks of the two component curves making up the over-all absorption spectrum might be slightly displaced from these values, but hardly enough to invalidate the qualitative conclusion presented.
[5] H. Margenau, Phys. Rev. 48, 755 (1935).

Erratum: Proton Magnetic Resonance in Polyethylene

[J. Chem. Phys. 18, 1303 (1950)]

ROGER NEWMAN
Lyman Laboratories, Harvard University, Cambridge, Massachusetts

THE words "intermolecular" and "intramolecular" appearing in the next-to-last paragraph of this note should be interchanged.

Infra-Red and Raman Spectra of para-Difluorobenzene

ARMAND H. DELSEMME
Société Belge de l'Azote Research Laboratories, Liége, and Institut d'Astrophysique, University of Liége, Belgium
September 26, 1950

AMONG the fluorinated derivatives of benzene, the para-difluorobenzene molecule has apparently not been studied spectroscopically in spite of the interest in connection with its relatively great symmetry.

The aim of this work is to assign the observed frequencies to the normal modes of vibrations, with the particular view of understanding the influence of the fluorine atoms on a conjugated link system. Only the experimental part of the work will be reported here.

The infra-red spectrum of para-difluorobenzene has been observed at room temperature for both the liquid and gaseous states, in the range from 3 to 25 microns, covered by the conventional three prisms of LiF, NaCl, and KBr used in the standard 12 C Perkin-Elmer infra-red recording spectrometer.

Two infra-red gas cells having optical thicknesses of 10 and 100 cm were used. The gas pressure ranged from 5 to 45 mm Hg. Three infra-red liquid cells were used, with optical thicknesses of 5, 25, and 100 microns.

The Raman spectrum has been observed for the liquid state only, with a *B* II Huet spectrograph, giving a dispersion of 18A/mm near 4358A. The 4358A line of the mercury arc was the exciting line.

The observed frequencies have been measured within 0.5 cm^{-1} around 500 cm^{-1}, within 1 cm^{-1} around 1000 cm^{-1}, and within 3 cm^{-1} around 3000 cm^{-1} for the infra-red spectrum; they were measured to within 3 cm^{-1} for the whole Raman spectrum. These values are listed in Table I.

TABLE I.

Raman spectrum liquid		Infra-red spectrum gas		liquid		gas		liquid	
3130	*m*	3124	*m*	3125	*s*	1987	*m*	1972	*m*
3090	*vs*	3098	*m*	3089	*vs*	1865	*s*	1870	*s*
3051	*m*	3070	*vs*	3064	*s*	1624	*m*	1632	*s*
2490	*w*	3032	*m*	3022	*m*	1510	*vs*	1504	*vs*
~2450	*vw*	2957	*w*	2957	*s*	1433	*m*	1432	*s*
~2440	*vw*	2929	*vs*	2927	*vs*	···		1305	*w*
~2110	*vw*	2896	*s*	2896	*s*	1223	*vs*	1208	*vs*
1622	*s*	2858	*s*	2858	*s*	1188	*vs*	1182	*vs*
1612	*vw*	2776	*vw*	2796	*vw*	···		1143	*m*
1397	*w*	2792	*w*	2787		1084[a]	*vs*	1085	*vs*
1290	*w*	2760	*w*	2748		1013[b]	*w*	1012	*s*
1247	*vs*	2687	*w*	2686	*m*	···		985	*w*
1177	*m*	2643	*w*	2643	*m*	···		942	*m*
1143	*s*	2560	*w*	2558	*m*	···		927	*m*
1086	*w*	···		2528	*m*	877	*w*	884	*m*
1014	*w*	2472	*s*	2458	*w*	···		858	*w*
859	*vs*	2441	*w*	2441	*s*	846[b]	*vs*	833	*vs*
835	*vs*	2426	*w*	2423	*m*	···		806	*vw*
695	*m*	···		2290	*w*	···		798	*w*
638	*s*	2224	*s*	2226	*s*	740[a]	*vs*	737	*vs*
~ 517	*vw*	2154	*w*	2154	*m*	···		687	*w*
455	*vs*	2068	*s*	2063	*m*	···		636	*w*
160	*w*	···		2051	*s*	505[b]	*s*	510	*s*
145	*w*	···		2042	*m*	412	*w*		

[a] Pseudo-parallel band ($P-R=10$ cm^{-1}).
[b] Pseudo-perpendicular band ($P-R=15$ cm^{-1}).

TABLE II.

	Raman A_{1g}	B_{1g}	B_{2g}	B_{3g}	Infra-red B_{1u}	B_{2u}	B_{3u}
C−H stretching	3090	3051	···	···	···	3070	3096
C−F stretching	1247	···	···	···	···	1188	···
C−C stretching	1622	1397	···	···	···	1433	1510
C−C breathing	859	···	···	···	···	740	1223
C−H bending	1143	1290	835	1086	836	1084	1013
C−F bending	···	638	···	695	505	···	412
C−C−C bending	455	517	···	361	~180	···	···

A preliminary analysis of our results gives the frequency assignments shown in Table II.

Calculations are now being carried out in order to evaluate the vibrational potential function of the molecule. The detailed results of the work will be published elsewhere in the near future.

The author wishes to thank Dr. Jules Duchesne for suggestions and advice, and for lending him a sample of para-difluorobenzene. The sample of this compound was offered Dr. Duchesne by the Imperial Chemical Industries, Ltd., to which we are very much indebted.

The Infra-Red Spectrum of C_2H_2 from 4400 to 8500 cm^{-1}

ROBERT M. TALLEY AND ALVIN H. NIELSEN
The University of Tennessee, Knoxville, Tennessee
September 1, 1950

THIS letter is a preliminary report on the infra-red spectrum of acetylene in the previously unmapped region 4400 to 8500 cm^{-1}. Nineteen bands were observed, of which two had been previously observed with low dispersion and one photographed with high dispersion. The observations were made with the University of Tennessee prism-grating spectrometer utilizing a 15,000 line-per-inch replica grating, and a lead sulfide photoconducting cell with a Wilson-type amplifier as the detecting system. The acetylene was from a commercial cylinder and was purified to eliminate the principal contaminant, acetone. A multiple-path[1] cell 25 in. long capable of 72 light traversals was built for this experiment. For the bands of intensity (m) in Table I, 1 meter-atmosphere of C_2H_2 was used, and for those listed (w) 2 meter-atmospheres, and for those of intensity (vw) 20 meter-atmospheres. The frequencies in Table I given to four significant figures are estimated band centers from *Q* branches of very weak perpendicular bands whose rotational structure could not be observed, or midpoints of very weak parallel bands not well enough

TABLE I. C_2H_2 bands in the region 4400–8500 cm^{-1}.

Band center (obs.) cm^{-1} vac.	Vib. frequency ΔG_V[a] cm^{-1}	Band type and intensity	Upper state $v_1v_2v_3v_4^{l}v_5^{l}$	Lower state $v_1v_2v_3v_4^{l}v_5^{l}$	$B'-B''$ cm^{-1}
4493.92	4493.92	∥ w	0 0 1 2^0 0^0	0 0 0 0^0 0^0	+0.0012
4673.48[b]	4673.48	∥ w	1 0 0 1^1 1^1	0 0 0 0^0 0^0	−0.0036
4722.8?	4722.8?	∥ w	0 0 1 0^0 2^0	0 0 0 0^0 0^0	—
5102.2	5103.4	⊥ vw	0 1 0 4^0 1^1	0 0 0 0^0 0^0	−0.007
5123.9	5125.1	⊥ vw	0 0 1 3^0 0^0	0 0 0 0^0 0^0	—
5773	5771.8	⊥ vw	0 0 2 0^0 0^0	0 0 0 0^0 1^1	—
5785	5783.8	⊥ vw	?	0 0 0 1^0 0^0	—
5818	5919.2	⊥ vw	0 2 0 2^0 1^1	0 0 0 0^0 0^0	—
5837	5835.8	⊥ vw	0 1 1 2^0 0^0	0 0 0 1^0 0^0	—
5851.3	5852.5	⊥ vw	0 1 1 1^0 0^0	0 0 0 0^0 0^0	−0.016
5946	5944.8	⊥ vw	1 0 1 0^0 0^0	0 0 0 1^0 0^0	—
5981	5979.8	⊥ vw	2 0 0 0^0 0^0	0 0 0 0^0 1^1	—
6556.1[b]	6556.1	∥ m	1 0 1 0^0 0^0	0 0 0 0^0 0^0	−0.013
6625.0	6625.0	∥ vw	1 1 0 1^1 1^1	0 0 0 0^0 0^0	—
7396	7399.6	⊥ vw	2 0 0 0^2 2^2	0 0 0 0^0 1^1	—
7418	7419.2	⊥ vw	2 0 0 0^1 1^1	0 0 0 0^0 0^0	—
7468	7469.2	⊥ vw	1 1 0 0^3 1^1	0 0 0 0^0 0^0	—
7732	7732	∥ vw	1 0 1 2^0 0^0	0 0 0 0^0 0^0	—
8513[c]	8513	∥ w	1 1 1 0^0 0^0	0 0 0 0^0 0^0	−0.018

[a] W. H. Shaffer and A. H. Nielsen, J. Chem. Phys. **9**, 847 (1941). ΔG_V is the pure vibration term including the anharmonic constants and may be derived from Eq. (21). Equation (23), the rotational energy, contains a constant term $-B_v(l_4+l_5)^2$ which arises from the angular momentum of vibration l_4 and l_5. When Δl_4 and Δl_5 are zero, or when l_4 and l_5 are oppositely directed, the contribution of this term is zero and ΔG_V is the band center. For this situation, as may be seen in Table I, the numbers in columns one and two are identical. When Δl_4 and Δl_5 are not zero the contribution of this term, ΔF_R, is included in the band center frequency and the band center $=\Delta G_V+\Delta F_R$. Thus the numbers in columns one and two differ in most cases by B_v' or B_v'' which, in the case of C_2H_2, is about 1.2 cm^{-1}.
[b] Previously observed with low dispersion by R. Mecke, Zeits. f. Elektrochemie **36**, 589 (1930); and Zeits. f. Physik **64**, 173 (1930).
[c] Photographed by G. Herzberg and J. W. T. Spinks, Zeits. f. Physik **91**, 386 (1934).

resolved for analysis. There is, therefore, an uncertainty probably not exceeding 1 cm^{-1} in these band centers.

The lower state of the transitions observed was determined by cooling the cell with dry ice, and noting the attenuation of the absorption for transitions arising from excited levels. The results are summarized in Table I using the notation of Herzberg.[2]

These results are to be considered preliminary as there may still be some small uncertainty in the assignment of one or two of the bands, and it may be possible to discover other bands in the water vapor regions at 1.4 and 1.8μ when the relative humidity ceases to be 95 to 100 percent.

[1] J. U. White, J. Opt. Soc. Am. **32**, 285 (1942).
[2] G. Herzberg, *Infrared and Raman Spectra of Polyatomic Molecules* (D. Van Nostrand Company, Inc., New York, 1945), p. 290.

Errata: Quantum-Mechanical Resonance between Identical Molecules

[J. Chem. Phys. **18**, 1150 (1950)]

HERBERT JEHLE
University of Nebraska, Lincoln, Nebraska

FIGURE 3 should be turned around as follows:

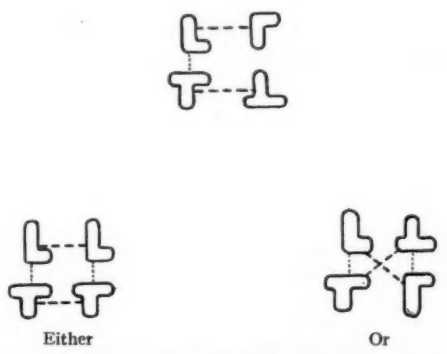

FIG. 3. Orientation before bond formation above. Orientation after bond formation below.

The left side of each of the three pictures may represent two genes of an original chromosome, the right side the genes of the daughter chromosome. Dashed lines indicate the z axes connecting corresponding genes in the pair of chromosomes, dots indicate bonds stringing up neighboring genes.

On a smaller scale, the left sides represent two constituent molecules of an original gene, the right sides the molecules of the daughter gene. Dashes connect corresponding constituent molecules and dots indicate bonds between constituent molecules, cementing them to become genes. The original gene collects from the surrounding medium various small constituent molecules, e.g., peptide rings (cf. Fig. 3, "above"). These molecules, identical with the corresponding ones of the original gene, form various chemical bonds among each other, trying to build up the daughter gene. Only those bond formations, however, which result in molecule complexes identical with the corresponding ones of the original gene will, after orientation in the "or" configuration, be specifically attracted by the original gene and therefore not stroll away under Brownian agitation.

Note to Equation (11.9): When $-(n-1)\lambda/2\kappa^2$ becomes comparable to unity, some levels of the first and also of the higher bunches are lowered towards the ground level, which results in an enormous increase in the partition function and in the attractive force (11.9). In that case, of course, we reach the limits of validity of the present perturbation calculation, but the qualitative result is clearly a very strong attraction.

The Effect of Mass Discrimination on Isotope Abundance Measurements. Relative Abundances of Krypton Isotopes*

OLIVER A. SCHAEFFER
Chemistry Department, Brookhaven National Laboratory, Upton, Long Island, New York

August 28, 1950

UNDER certain operating conditions, mass spectrometers record one of the masses in a particular mass ratio preferentially, and introduce a systematic error into the ratio. This is of prime concern in the careful determination of isotope abundances. An estimate of the magnitude of such errors was presented by Coggeshall,[1] who made a calculation for a simplified ion source free from a magnetic field. This calculation indicates that an error of roughly one percent will be introduced into an isotope ratio of two masses differing by about ten percent if the masses are analyzed by varying the electrostatic field. On the other hand, the same calculation indicates that if magnetic scanning is employed, there will be no such systematic error introduced. A similar calculation, with some refinements, was made by Berry,[2] who also verified the calculation experimentally. Berry's data obtained with a simplified ion source and a fixed ion accelerating potential show that all ions formed initially with thermal distribution of velocity will be focused with the same efficiency independent of their mass.

It is known that certain 60° sector spectrometers, which have more elaborate ion optics in the ion source, show a larger increase in collected ion current with accelerating voltage than the calculation predicts. It should be borne in mind that these spectrometers do not have the simple ion source for which the calculation was made; and as a result, deviations from the calculation which such spectrometers show do not invalidate the calculation. They do, however, show that the calculation is probably only applicable to the simple type source for which it was made.

In lieu of a theoretical analysis for more elaborate ion sources, the ion collection efficiency for ions of different e/m can be determined by the use of separated isotopes or equivalently by a standard sample. Recently, Nier[3] has carefully redetermined the natural isotope abundances of several elements. He corrected for all discrimination errors by using a calibrating mixture prepared from separated argon isotopes. Nier's[3] values allow samples of natural abundance to be used as standards, to the approximation that a given natural abundance sample has the same composition as the sample Nier used. Probably the largest factor in the variation in natural abundance, aside from radioactive decay, arises from chemical exchange processes. As the rare gases are not subject to such processes, it is reasonable to suppose that a given sample of rare gas will be of practically the same isotopic composition as Nier's sample.

In order to compare the accuracy of data obtained with the two usual types of mass scanning, electrostatic and magnetic, the abundances of the krypton isotopes in a sample obtained from Linde Air Products Company were measured by both methods. The masses were scanned by varying the magnetic field at different ion accelerating voltages from 750 to 5000 volts, and also by varying the accelerating voltage at constant magnetic field. The mass spectrometer used has been described previously.[4] The data are presented in Table I. Each set of magnetically scanned values represents the average of two or more individual determinations. There are no evident systematic trends in the magnetically scanned values. The electrostatically scanned value does, however, deviate quite appreciably from any of these values. As the magnetically scanned results are independent of the ion accelerating voltage, one is led to believe that these results are relatively free from voltage discrimination errors. The averages of these are compared with Nier's most recent results and also to previous investigations in Table II. The errors indicated in the table are probable errors calculated from the scatter of the data. It is seen that the present results agree within the

TABLE I. Isotope abundances[a] of krypton with different scanning methods.

Mass	Magnetic scanning 750v	1000v	1500v	2000v	3000v	4000v	5000v	Electrostatic scanning[b]
78	0.350	0.347	0.351	0.353	0.357	0.354	0.358	0.39
80	2.26	2.27	2.27	2.29	2.33	2.32	2.31	2.52
82	11.62	11.63	11.61	11.55	11.55	11.59	11.58	12.03
83	11.51	11.57	11.54	11.47	11.48	11.52	11.51	11.64
84	56.76	56.93	56.96	57.10	56.99	56.90	56.99	56.80
86	17.48	17.25	17.29	17.25	17.30	17.31	17.28	16.62

[a] The abundances have all been corrected for the fact that with the capillary leak used the ratio of the partial pressures of two isotopes in the ion source differs from that in the sample by a factor depending on the square root of the mass ratio. (For a full discussion of this correction see M. G. Inghram, *Advances in Electronics*, Vol. I. (Academic Press, New York, 1948).)
[b] Magnetic field such that mass 78 is focused at 1700 volts ion accelerating potential.

TABLE II. Comparison of various isotopic krypton abundances.

Mass	This research	Nier[a]	Lounsbury, Epstein, and Thode[b]	Nier[c]	Dibeler, Mohler, and Reese[d]
78	0.353±0.001	0.354±0.002	0.34	0.34	0.36
80	2.29 ±0.01	2.27 ±0.01	2.23	2.26	2.25
82	11.58 ±0.01	11.56 ±0.02	11.50	11.50	11.57
83	11.51 ±0.02	11.55 ±0.02	11.48	11.50	11.44
84	56.95 ±0.04	56.90 ±0.10	57.02	56.95	57.14
86	17.31 ±0.03	17.37 ±0.02	17.43	17.41	17.24

[a] See reference 3.
[b] Lounsbury, Epstein, and Thode, Phys. Rev. **72**, 517 (1947).
[c] A. O. Nier, Phys. Rev. **52**, 933 (1937) and private communication to H. G. Thode (see reference 5).
[d] Dibeler, Mohler, and Reese, J. Research Nat. Bur. Stand. **38**, 617 (1947).

precision of the measurements to Nier's most recent data. The agreement shows that it is possible to measure directly isotope abundances free from voltage discrimination errors by the use of magnetic scanning. This conclusion is of importance for measurements of abundances when a calibration mixture is not available.

* This work was conducted under the auspices of the AEC.
[1] N. D. Coggeshall, J. Chem. Phys. **12**, 19 (1944).
[2] C. E. Berry, Phys. Rev. **78**, 597 (1950).
[3] A. O. Nier, Phys. Rev. **77**, 789 (1950); **79**, 450 (1950).
[4] O. A. Schaeffer and J. M. Hastings, J. Chem. Phys. **18**, 1048 (1950).

An Aid in Making Vibrational Assignments

H. J. BERNSTEIN
Division of Chemistry, National Research Council, Ottawa, Canada
September 13, 1950

GENERALLY the only observed frequencies (obtained from Raman and infra-red spectra) which can be assigned unambiguously are those belonging to the totally symmetrical type. The depolarization data makes this possible. As a result, for a molecule of rather high symmetry there remain several more symmetry types to which assignments can be made with difficulty from considerations of the spectra only. Usually, calculations of the frequencies are made from a quadratic potential energy function.[1] The calculated frequencies are used then as a guide in assigning the observed frequencies to their respective types. Since the force constants employed to calculate the frequencies have been obtained from the simple potential function (i.e., no cross terms) for the totally symmetrical type, the calculated frequencies for the other type are at best only a first approximation.

Although the numerical agreement between observed and calculated frequencies under these conditions cannot be expected to be good, there is a definite relation between them which is of use in making the vibrational assignment. When there are n modes in a symmetry type, this relation is of the form

$$\sum_{i=1}^{n} \frac{\Delta\lambda_i}{\lambda_i} \approx 0, \tag{1}$$

where $\lambda = 4\pi^2 c^2 \nu^2$ with ν in cm^{-1}.

From the relation[2]

$$\pi = GF, \tag{2}$$

in which

$\pi = \lambda_1\lambda_2\lambda_3\lambda_4 \cdots \lambda_n$
$G = G$ matrix which is a function of masses only
$F = F$ matrix which is a function of force constants only

we see that

$$\frac{d\pi}{\pi} = \frac{dG}{G} + \frac{dF}{F}$$
$$= \frac{dF}{F} \text{ for no mass changes and no changes in geometry.} \tag{3}$$

For the case outlined above in which the F matrix is a function of the principal force constants only, *viz.* $F = K_1K_2K_3 \cdots K_n$, it is readily seen that

$$\frac{d\pi}{\pi} = \sum_{i=1}^{n} \frac{d\lambda_i}{\lambda_i} = \sum_{i=1}^{n} \frac{dK_i}{K_i}. \tag{4}$$

For the small changes in the force constants introduced when a set of force constants from one symmetry type is used to calculate the frequencies of some other type it can be shown[3] that

$$d\pi = 0 \tag{5}$$

and for larger differences that

$$\Delta\pi \approx 0. \tag{6}$$

Thus (1) follows from (6) and (4).

For a symmetry type containing two modes the relation gives

$$\frac{\Delta\lambda_1}{\lambda_1} \approx -\frac{\Delta\lambda_2}{\lambda_2},$$

i.e., the percent increase between the observed and calculated frequencies of one of the modes is nearly equal to the percent decrease for the other mode.

For the case where the symmetry type contains three modes, if the observed and calculated frequencies of one of the modes are quite close, i.e., $\Delta\lambda \approx 0$, the general expression will reduce to the two-mode case as a first approximation.

This criterion has already been used to advantage in assigning the 35 observed Raman and infra-red bands of the S_8 molecule.[1]

[1] H. J. Bernstein and J. Powling, J. Chem. Phys. **18**, 1018 (1950).
[2] E. B. Wilson, Jr., J. Chem. Phys. **7**, 1047 (1939); **9**, 76 (1941).
[3] This result and others concerned with "the change of frequency accompanying changes in mass, geometry, and force constants of a molecule" are considered in a paper which will appear in the *Canadian Journal of Chemistry* (1951).

Errata: Vibrational Intensities. I. Theory of Diatomic Infra-Red Bands

[J. Chem. Phys. **18**, 983 (1950)]

BRYCE L. CRAWFORD, JR. AND H. L. DINSMORE
School of Chemistry, University of Minnesota, Minneapolis, Minnesota

AN error in our paper has been pointed out by Professor J. C. Decius which necessitates revision of certain of the relations given. In our Eq. (7), we omitted re-emitted radiation on the grounds that it would be isotropic. Actually, this is true only for spontaneous emission; induced emission is in the direction of the inducing radiation.[1] Consequently the term for induced emission should be included, as in our Eq. (7′); this leads to small changes in the subsequent equations.

Fundamentally, we must start from Eq. (7′) instead of Eq. (7). We can regard this as a formal change which replaces $\omega_{v,j}{}^{v',j'}$ by

$\omega_{v,j}{}^{v',j'}[1-\exp(-hc\omega_{v,j}{}^{v',j'}/kT)]$ in Eqs. (10), (25), and (28). The last of these, written out correctly for evaluation, is now

$$A_v{}^{v'}=(8\pi^3N_v/3hcZ)[\Sigma_{j,j'}\,\omega_{v,j}{}^{v',j'}\exp(-E_j/kT)S_{v,j}{}^{v',j'} -\exp(-hc\omega_v{}^{v'}/kT)\Sigma_{j,j'}\,\omega_{v,j}{}^{v',j'} \times\exp(-E_{j'}/kT)S_{v,j}{}^{v',j'}]. \quad (28')$$

The first sum, correctly evaluated in the original paper, led to Eq. (37). The evaluation of the second sum may be avoided by noticing that it is just like the first save for the appearance of $E_{j'}$ in the exponential instead of E_j. If we interchange j and j', the exponential is reduced to the former case; the line strength $S_j{}^{j'}$ is invariant; and we need only examine the effect on $\omega_{v,j}{}^{v',j'}$. This is given in Eq. (31), in terms of the parameter M; it is easy to see that interchange of j and j', which amounts to interchanging the R and P branches, changes the sign of M. Hence the interchange of j and j' reduces the second sum to the first sum, save for a change of sign of the term in $\bar{B}$, and of course multiplication by the vibrational Boltzmann factor.

So we may include these effects by writing Eq. (37) as

$$A_v{}^{v'}=(8\pi^3N_v/3hc)\tilde{\omega}_v{}^{v'}S_v{}^{v'}, \quad (37')$$

where, however, Eq. (46) is revised to read

$$\tilde{\omega}_v{}^{v'}=[\omega_v{}^{v'}+(B_{v'}-B_v)(1+Z)][1-\exp(-hc\omega_v{}^{v'}/kT)] +2\bar{B}[1+\exp(-hc\omega_v{}^{v'}/kT)]. \quad (46')$$

The summation to get the $A^{(n)}$ goes through as before, with the revised definition of $\tilde{\omega}_v{}^{v'}$. The parameter Y_n, defined in Eq. (54), becomes

$$Y_n=[nx_e\omega_e(1-e^{-n\beta})+\alpha_e(1+e^{-n\beta})]/\tilde{\omega}_0{}^n; \quad (54A)$$

with this change Eq. (54) through (57) are correct. Equation (58) is now better written as

$$A_0{}^n=(8\pi^3N/3hcQ)(\mathbf{p}_0{}^n)^2\tilde{\omega}_0{}^n. \quad (58')$$

Here $\tilde{\omega}_0{}^n$ is a special case of $\tilde{\omega}_v{}^{v'}$:

$$\tilde{\omega}_0{}^n=[\omega_0{}^n+(B_n-B_0)(1+Z)](1-e^{-n\beta})+2\bar{B}_0{}^n(1+e^{-n\beta}). \quad (58A)$$

We are grateful to Professor Decius for calling this error to our attention.

[1] W. Heitler, *Quantum Theory of Radiation* (Oxford University Press, London, 1936), pp. 102 ff.

Electrolysis of Aluminum Solutions in a Magnetic Field

CHARLES E. WOOD* AND C. W. TITTLE
North Texas State College, Denton, Texas
October 16, 1950

THE formation of a molten mass-like deposit on the aluminum anode of an electrolytic cell with a platinum cathode and an electrolyte of unspecified concentration consisting of aqueous aluminum sulfate, in the presence of a magnetic field of 2000 gauss has been reported by Antonoff and Rowley.[1] These experiments have been repeated with magnetic inductions up to a maximum of 8160 gauss produced by an electromagnet with pole faces 1.19 cm in diameter and a gap of 7.1 mm. In most of the experiments pure metallic aluminum sheet was used as the anode material and a platinum wire or strip served as the cathode. Direct potential differences of from 5 to 40 volts were supplied by batteries and applied directly to the cell terminals. The total current in the various experiments was in the range of 0.0016 to 2.00 amp. The longest run at maximum magnetic field was 18 minutes in duration. Concentration of the aluminum sulfate solution ranged from 12.5 to 200 grams of $Al_2(SO_4)_3\cdot 18H_2O$ per 100 cc of water. Temperature varied from 26 to 73°C and usually increased steadily during a particular experiment. In some of the experiments, the aluminum strip running from the anode proper to the cell terminal was in contact with the electrolyte; in others, it was insulated with paraffin wax. In one series of runs, Alcoa type 24ST aluminum alloy was used as anode,[2] and in some instances the anode was scored in hopes that the scratches would serve as centers for formation of the deposit.[3] In a few runs, aluminum was used as anode and cathode.

In none of these experiments was a molten mass-like deposit formed on the anode. Corrosion of the anode was evident in all cases and tended to be somewhat more pronounced with the magnetic field. In one instance the pits resembled a crater, but with peaks and indentations reversed. Close inspection showed traces of an unidentified black deposit in the pits, possibly cupric oxide from small amounts of copper impurities.[3] There appeared to be no significant difference in results with and without the magnetic field. With the field, the solution became agitated by the charged gas bubbles, which rotated in spiral orbits. The motion of the liquid tended to remove the polarization gas bubbles and may account for the slight differences observed with and without the field.

If a significant magnetic effect exists under the conditions of the experiments described here, it is certainly difficult to reproduce. If such an effect does exist, one might expect the electromotive force of the cell to depend on the magnetic field. Palumbo and Riccobono[4] found only a slight effect on the emf which could be explained by considerations of thermal effects alone.

* Present address: Paris Junior College, Paris, Texas.
[1] G. Antonoff and A. Rowley, Acta Physica Austriaca **2** (No. 1), 101–3 (1948); J. Phys. Colloid Chem. **52**, 1105–8 (1948).
[2] Following suggestions of G. Antonoff, personal communication.
[3] W. E. Holland, Trans. Am. Electrochem. Soc. **53**, 198 (1928).
[4] D. Palumbo and G. Riccobono, Ric. Scient. **18**, 821–3 (1948).

Erratum: Thermal Diffusion in the Critical Region. II

[J. Chem. Phys. **18**, 1027 (1950)]
E. B. GILLER, R. B. DUFFIELD, AND H. G. DRICKAMER
Department of Chemistry, University of Illinois, Urbana, Illinois

IN Table I, page 1028, the heading of the fourth column should be "$\frac{\rho}{\text{g/cc}}$"; the heading of the fifth column should be "ΔT°C". Also, the values of α' and α corresponding to separation factor of greater than one should be positive; i.e., the values of α' and α for runs 9, 10, 11, 26, 27, 28, 43L, 45, 46, 54L, 55L, 56L, 57L, 73L, 74L, 75L, 76L, 80, 81, 82, 89, 90, 91, 92, 93, 94 should have a positive sign.

Perturbations in the BaO Spectrum

ISTVAN KOVACS
Institute of Spectroscopy, Hungarian University for Technical Sciences, Budapest, Hungary
AND
ALBIN LAGERQVIST
Physics Department, The University, Stockholm, Sweden
September 18, 1950

THE band spectrum of barium oxide—$^1\Sigma-{}^1\Sigma$-system investigated from about λ 5200 to 7000A—contains many perturbations.[1] All the perturbations are found in the upper levels and have been studied for $v'=1, 2, \cdots 5$; no perturbations have been found in $v'=0$. They can be explained as the results of interactions with four perturbing states called X, Y, Z, and Q. Most of the perturbations contain extra lines. The knowledge of the extra lines makes it possible to study the nature of the perturbing states.

A $^1\Sigma^+$-state—for BaO the states are with great probability $^1\Sigma^+$-states—can be perturbed not only by $^1\Sigma^+$ and $^1\Pi$-states but also by $^3\Pi$, $^3\Sigma^+$, and $^3\Sigma^-$-states. The ground states of the atoms, Ba(^1S) and O(^3P), give rise to a $^3\Sigma^-$ and a $^3\Pi$-state. We therefore consider that the states must be found among $^1\Sigma^+$, $^1\Pi$, $^3\Pi$, or

$^3\Sigma$-states. Theoretical treatments of singlet-singlet interactions[2,3] and singlet-triplet interactions[4–6] have been given.

At a perturbation with known extra lines the B-value of the perturbing state can be determined. If perturbations are known, emanating from at least two consecutive vibrational levels of a perturbing state, the ω_e and $x_e\omega_e$-values can be calculated. If several extra lines are found at a perturbation, it may be possible to decide whether the perturbing matrix element is J-dependent or not. The matrix element is independent of J at $^1\Sigma^1\Sigma$-interactions and at $^1\Sigma^3\Pi_0$.

This investigation[1,7] has shown that it sometimes may be possible to determine B-values for perturbing states with almost the same accuracy (4 figures) as for states for which full rotational information is available. It may also be possible to decide whether the perturbing matrix element is J-dependent or not.

The rotational and vibrational constants are of about the same magnitude for all the perturbing states in BaO, $B_e \sim 0.226$, $\omega_e \sim 450$. For the analyzed states Σ and Σ^* the corresponding constants are, B_e: 0.3125 and 0.2584; ω_e: 669.8 and 500. The matrix element for $Y\Sigma^*$ interactions is independent of J. From this we can conclude that Y must be a $^1\Sigma$ or a $^3\Pi_0$ state. The matrix elements for $X\Sigma^*$ and $Z\Sigma^*$ interactions are with great probability J-dependent. About $Q\Sigma^*$ perturbations nothing can be said. The following four interpretations of the perturbing states have been specially discussed:

State:	1	2	3	4
X	$^1\Pi$	$^1\Pi$	$^3\Pi$	$^1\Pi$
Y	$^1\Sigma^+$	$^1\Sigma^+$	$^3\Pi_0$	$^3\Pi_0$
Z	$^1\Pi$	$^3\Sigma^-_{J+1}$	$^3\Sigma^-_{J+1}$	$^3\Pi_1$
Q	Singlet	$^3\Sigma^-_{J-1}$	$^3\Sigma^-_{J-1}$	Singlet

After a thorough investigation of these four possibilities we consider the third interpretation as the most likely.

A detailed discussion is published in *Arkiv för Fysik*.[7]

[1] Barrow, Lagerqvist, and Lind, Proc. Phys. Soc. (to be published) (1950).
[2] I. Kovács, Zeits. f. Physik **93**, 669 (1937).
[3] I. Kovács, Hung. Phys. Acta. (to be published).
[4] A. Budó and I. Kovács, Zeits. f. Physik **109**, 393 (1938).
[5] A. Budó and I. Kovács, Zeits. f. Physik **111**, 633 (1939).
[6] A. Budó and I. Kovács, Hung. Phys. Acta. (to be published).
[7] I. Kovács and A. Lagerqvist, Arkiv. f. Fysik. (to be published).

The Absorption and Reflection Spectra of the Ammonium Halides

L. F. H. Bovey*
Department of Colloid Science, Cambridge, England
October 16, 1950

In a previous letter,[1] the definite result was given that there was no direct spectroscopic evidence which could justify the postulation of free rotation in the ammonium halides. This investigation of the infra-red spectra at various temperatures has now been completed on all the four ammonium salts and this conclusion fully supported. During the course of the investigation, it was noticed that consistent spectra were not obtained and this experimental result could neither be entirely attributed to the difficulties of working in regions of strong water vapor absorption nor to variation in the orientation of the crystallites forming the sample. Further work with crystals and sublimed layers of measured thickness showed that these differences could be largely attributed to the effect of selective reflection from the solid layer and this phenomenon has now been investigated. Table I summarizes the frequencies of strong absorption lines (corrected for any reflection effect) and reflection peaks at −150°C and −120°C respectively. These data are presented since the lines are more narrow at low temperatures, and the experimental errors are less.

Reflection spectra from sublimed layers are similar to those from crystals and in the examination of solids, consideration should be given to the possible influence of reflection on absorption measurements, particularly when the intensities of components of a doublet are compared. In the absence of suitable techniques for cutting thin layers of ionic solids, the reflection spectra from single crystals may again become important in the elucidation of crystal structure, since the orientation of the axes of the crystal may be definitely known.

TABLE I.

NH_4F		NH_4Cl		NH_4Br		NH_4I	
Absorption* cm^{-1}	Reflection cm^{-1}	Absorption* cm^{-1}	Reflection cm^{-1}	Absorption* cm^{-1}	Reflection cm^{-1}	Absorption* cm^{-1}	Reflection cm^{-1}
1484 (30) 1503	1494	1397 (30)	1410	1407 (35) 1430 (25)	1413 1434	1397 (30) 1424 (6)	1403
		1796 (20)		1729 (15)		1685 (5)	
		2022 2068 (10) 2175		1958 (10)		1916 (5)	
2005 (110)	2015						
2080 2135 (10)							
2260 (60)							
2508 2575 (10) 2594							
2830 (85)	2860	2824 (40)		2805 2850 (20)		2795 (12)	
3024 (15) 3100 (100) 3212 (70)		3041 (140) 3132 (110) 3210 (10)	3052 3155	3025 (80) 3122 (85) 3192 (20)	3060 3150	3017 (100) 3070 (100) 3170 (15) 3210 (15)	3030

* Figures in brackets give relative intensities for lines in one compound.

The data at low and room temperatures can be more satisfactorily interpreted if the ammonium ion has a higher symmetry (Wagner and Hornig)[2] than C_{3v} or C_3 (Couture and Mathieu),[3] except in the case of ammonium fluoride where the lower symmetry is also supported from crystallographic data.[4] It should be added that this investigation has also provided spectroscopic evidence for hydrogen bonding in NH_4F.

The spectra taken at temperatures between 20°C and −150°C showed that in the chloride and bromide, changes in the bands occurred in the vicinity of the λ-point temperatures and continued over a range of some 50°C below, with a decrease in the rate of change below −100°C. The ammonium fluoride when cooled, gave essentially only a sharpening of the characteristic room temperature spectrum. No variation corresponding to that in the chloride and bromide was noticed in ammonium iodide and the spectrum showed no definite alteration from that at room temperature until approximately −120°C, when large changes occurred. The variation of the spectra with temperature support an order-disorder theory for the chloride and bromide but the absence of any corresponding effect in the iodide is surprising since dilatometric measurements[5] gave a transition over the range −40°C to −58°C; this difference may be in part influenced by the crystallographic change from the NaCl to CsCl type of structure which occurs at −17°C. Work at Brown University has independently confirmed the results on ammonium iodide.[6]

This investigation has been carried out during the tenure of a Ministry of Education Further Education and Training Scheme Grant.

* Now at Division of Physics, National Research Council, Ottawa, Canada.
[1] L. F. H. Bovey and G. B. B. M. Sutherland, J. Chem. Phys. **17**, 843 (1949).
[2] E. L. Wagner and D. F. Hornig, J. Chem. Phys. **18**, 296 and 305 (1950).
[3] L. Couture and J. P. Mathieu, Proc. Ind. Acad. Sci. **28**, 401 (1948).
[4] W. Zachariasen, Zeits. f. physik. Chemie **127**, 218 (1927).
[5] A. Smits and D. Tollenaar, Zeits. f. physik. Chemie **B52**, 222 (1942).
[6] The author is indebted to Dr. D. F. Hornig for showing him these results prior to publication.

Carrier-Free Radioisotopes from Cyclotron Targets XII. Preparation and Isolation of Be^7 from Lithium

HERMAN R. HAYMOND, WARREN M. GARRISON, AND JOSEPH G. HAMILTON
Crocker Laboratory, Radiation Laboratory, and Divisions of Medical Physics, Experimental Medicine and Radiology; University of California, Berkeley and San Francisco*
October 11, 1950

THE radionuclide, Be^7, produced from lithium by the nuclear reaction[1] $Li^7(p,n)Be^7$ using the 10-Mev proton beam of the 60-in. cyclotron at Crocker Laboratory, has been isolated without added isotopic carrier by a separation procedure based on the radio-colloidal[2] properties of Be^7. Other radioisotopes produced concurrently by proton bombardment of lithium are short-lived and had decayed prior to the separation reported here. The principal radioactive by-product observed was 112-min. F^{18} produced[1] by proton bombardment of the small amount of oxygen which was present as lithium oxide on the target surface.

Five grams of c.p. lithium metal[3] was pressed onto a grooved water-cooled copper plate and bombarded in vacuum for 120 μa hr. at an average beam intensity of 8 μa. The bombarded lithium was dissolved in 100 ml of water with the gradual addition of dilute HCl. The acid solution was filtered and adjusted to pH 9 with dilute NH_4OH.[4] This "solution" containing lithium hydroxide, ammonium hydroxide, and Be^7 presumably as a radiocolloid, was slowly drawn through a Pyrex sintered-glass filter, the pore size of which was of the order of 5 microns. Over 90 percent of the carrier-free Be^7 remained adsorbed on the glass filter disk.[5] After washing the filter with 2 ml of water, which removed less than 5 percent of the activity, the Be^7 was quantitatively removed with 2 ml of 0.1 N HCl. The resultant solution after neutralization was used as a tracer for biological studies. Approximately 30 minutes were required for the separation which had an over-all yield of approximately 90 percent. The Be^7 was identified by the 52-day half-life and 0.48-Mev gamma-ray previously reported.[6,7]

We wish to thank Professor G. T. Seaborg for helpful suggestions and Mr. T. Putnam, Mr. G. B. Rossi, and the crew of the Crocker Laboratory Cyclotron for bombardments.

* This document is based on work performed under Contract No. W-7405-eng-48-A for the AEC.
[1] G. T. Seaborg and I. Perlman, Rev. Mod. Phys. **20**, 585 (1948).
[2] O. Hahn, *Applied Radiochemistry* (Cornell University Press, Ithaca, New York, 1936).
[3] Beryllium could not be detected by spectrographic analyses.
[4] Previous experiments had shown that between pH 2 and pH 9, the amount of Be^7 which could be removed by filtration increased with pH.
[5] Filtration through Whatman No. 40 removed only 30–50 percent of the Be^7.
[6] E. Segrè and C. E. Wiegand, Phys. Rev. **75**, 39 (1949).
[7] S. Rubin, Phys. Rev. **69**, 134 (1946).

Carrier-Free Radioisotopes from Cyclotron Targets XIII. Preparation and Isolation of Sc 44, 46, 47, 48 from Titanium

JEANNE D. GILE, WARREN M. GARRISON, AND JOSEPH G. HAMILTON
Crocker Laboratory, Radiation Laboratory, and Divisions of Medical Physics, Experimental Medicine and Radiology; University of California, Berkeley and San Francisco*
October 13, 1950

THE radioactive[1] scandium was prepared by bombardment of natural titanium with 20-Mev deuterons in the 60-in. cyclotron at Crocker Laboratory. At this energy, radioscandium is produced by the nuclear reactions $Ti^{46}(d,\alpha)Sc^{44}$, $Ti^{46}(d,2p)Sc^{46}$, $Ti^{47}(d,\alpha n)Sc^{44}$, $Ti^{47}(d,2p)Sc^{47}$, $Ti^{48}(d,\alpha)Sc^{46}$, $Ti^{48}(d,2p)Sc^{48}$, $Ti^{49}\times(d,\alpha n)Sc^{48}$, $Ti^{49}(d,\alpha)Sc^{47}$, $Ti^{50}(d,\alpha n)Sc^{47}$, $Ti^{50}(d,\alpha)Sc^{48}$; long-lived radiocalcium and radiovanadium are produced concurrently by the reactions: $Ti^{48}(d,\alpha p)Ca^{45}$, $Ti^{48}(d,2n)V^{48}$, $Ti^{48}(d,n)V^{49}$, $Ti^{47}(d,n)V^{48}$, $Ti^{49}(d,2n)V^{49}$. In the procedure described here, the carrier-free radioscandium is separated as a radiocolloid[2] from an ammonium hydroxide—hydrogen peroxide solution containing the target element and the concurrently produced radioisotopes of calcium and vanadium.

The titanium target (c.p. metal[3] powder supported on a copper target plate with 0.25-mil platinum foil) was bombarded for 100 μa hr. at an average beam intensity of 20 μa. After aging for 24 hours, the bombarded titanium metal powder (approximately 1 g) was dissolved in 40 ml of 18 normal sulfuric acid containing five percent 16 normal nitric acid. A small amount of undissolved inactive material was removed by centrifugation. The supernatant was slowly added to 200 ml of 8 normal ammonium hydroxide containing 15 ml of 30 percent hydrogen peroxide to give a clear yellow "solution" of the following composition: (1) titanium as the soluble pertitanate, (2) radiocalcium, (3) radiovanadium as pervanadate, (4) radioscandium as radiocolloidal aggregates.[2,4] This "solution" was then passed through two consecutive Whatman No. 42 filter papers which retained over 95 percent of the scandium activity as adsorbed radiocolloid. After washing with 10 ml of water, the scandium activity was quantitatively removed in 10 ml of 1 normal hydrochloric acid which after neutralization with the ammonium hydroxide—hydrogen peroxide solution was again passed through filter paper. Three such cycles gave a hydrochloric acid solution of carrier-free radioscandium containing less than 2 gamma of titanium. In a chemical separation performed on this final fraction using added scandium, calcium, titanium, and vanadium carriers, over 98 percent of the activity was recovered in the scandium fraction.

The decay was followed for 45 days and showed initially a composite 2.5-day half-life corresponding to the shorter-lived[1] scandium isotopes (2.2-day Se^{44}, 3.4-day Sc^{47}, 44-hour Sc^{48}). Twenty-four hours after bombardment, absorption measurements in aluminum showed the 1.4-Mev beta-particle of 3.9-hour Sc^{44} which is produced[5] by isomeric transition from 2.2-day Sc^{44}. The gamma-radiation had a half-thickness of 11.0 g/cm^2 in lead. Thirty-six days after bombardment, the activity had an approximately 80-day half-period; aluminum absorption measurements showed the 0.36- and 1.5-Mev beta-particles previously reported[6] for 85-day Sc^{46}.

We are grateful to Professor G. T. Seaborg for helpful suggestions and Mr. T. Putnam, Mr. G. B. Rossi, and the crew of the 60-in. cyclotron for the bombardments.

* This document is based on work performed under Contract No. W-7405-eng-48-A for the AEC.
[1] G. T. Seaborg and I. Perlman, Rev. Mod. Phys. **20**, 585 (1948).
[2] O. Hahn, *Applied Radiochemistry* (Cornell University Press, Ithaca, New York, 1936).
[3] Scandium could not be detected by spectrographic analyses.
[4] M. H. Kurbatov and J. D. Kurbatov, J. Chem. Phys. **13**, 208 (1945).
[5] H. Walke, Phys. Rev. **57**, 163 (1940).
[6] Walke, Williams, and Evans, Proc. Roy. Soc. (London) **A171**, 360 (1939).

The C—Br Bond Dissociation Energy in Trichlorobromomethane

M. SZWARC AND A. H. SEHON
Chemistry Department, The University of Manchester, Manchester, England
October 23, 1950

IT was shown in our previous studies[1,2] that it is possible to estimate the C—Br bond dissociation energy in various organic bromides by pyrolyzing these compounds in a stream of toluene. Under the experimental conditions used in these investigations the bromide molecule RBr dissociates according to Eq. (1)

$$RBr \rightarrow R + Br. \qquad (1)$$

The bromine atom formed in this process reacts rapidly with the toluene which is used as a carrier gas yielding HBr and a benzyl radical

$$Br + C_6H_5 \cdot CH_3 \rightarrow HBr + C_6H_5 \cdot CH_2.$$

Hence, the rate of formation of HBr measures the rate of the initial dissociation of the molecule RBr. Assuming that the recombination process

$$R+Br\rightarrow RBr$$

does not require any activation energy, we consider that the C−Br bond dissociation energy is equal to the activation energy of process (1).

We have recently applied this technique for the determination of the C−Br bond dissociation energies in polyhalogenated bromomethanes, and report here the results obtained for trichlorobromomethane. The evidence of present experiments leaves no doubt that the dissociation takes place according to the equation

$$Cl_3CBr\rightarrow Cl_3C\cdot+Br.$$

Hydrogen bromide* was formed in the pyrolysis. Moreover, the formation of dibenzyl is further proof that the dissociation process involves a radical split of the Cl_3CBr molecule. In accordance with the mechanism outlined above the rate of decomposition was measured by the rate of formation of HBr, and we found that the reaction obeys first-order kinetics. The unimolecular rate constant was not affected by the variation of the partial pressure of Cl_3CBr by a factor of 4.5 (from 0.18 to 0.83 mm Hg) and of the time of contact by a factor of 4 (from 0.3 to 1.3 sec.). The rate constant remained also independent of the pressure of toluene when the latter was varied by a factor of 2 (from 10 to 21 mm Hg). The plot of the unimolecular rate constant against $1/T$ is shown in Fig. 1. The straight line corresponds to an activation energy of 48±1 kcal./mole and to a frequency factor of 1.10^{13} sec.$^{-1}$. The latter value is considered to be an additional proof for the unimolecularity of the dissociation process (1).

Making the usual assumption that the recombination process

$$Cl_3C\cdot+Br\rightarrow Cl_3CBr$$

does not require any activation energy, we conclude that the C−Br bond dissociation energy in trichlorobromomethane is 48±1 kcal./mole.† Three values for $D(Cl_3C-Br)$ can be deduced from investigations of other workers. The study of the photo-oxidation of trichlorobromomethane by Franke and Schumacher[3] leads to a value of about 45 kcal./mole. The studies of bromine exchange reactions makes it possible to estimate the activation energy of the reaction $Cl_3CBr+Br\rightarrow Cl_3C\cdot+Br_2$; and the results obtained by Miller and Willard[4] lead to $D(Cl_3C-Br)<52$ kcal./mole, while those reported by Davidson and Sullivan[5] to $D(Cl_3C-Br)<57$ kcal./mole.

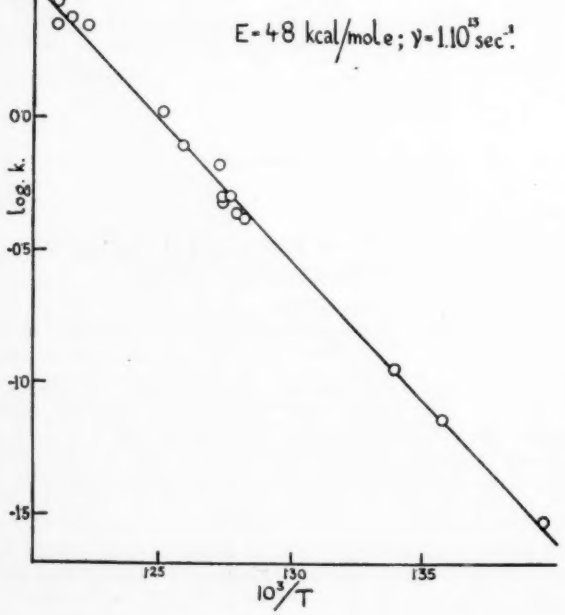

FIG. 1.

The striking point emerging from these studies is the great difference between $D(CH_3-Br)$ and $D(CCl_3-Br)$. For the former bond dissociation energy a value of 68–69 kcal./mole can be deduced on basis of existing thermochemical data and of the known value for $D(CH_3-H)$. Our investigation of the pyrolysis of methyl bromide indicates that $D(CH_3-Br)\approx 67$ kcal./mole. The C−Br bond dissociation energy in trichlorobromomethane is, therefore, lower by about 20 kcal./mole than in methyl bromide. It seems that this decrease is to be attributed mainly to the steric repulsion between the bulky chlorine and bromine atoms in the Cl_3CBr molecule, since our preliminary studies of the pyrolysis of trifluorobromomethane suggests that the difference $D(CH_3-Br)-D(CF_3-Br)$ is about 4 kcal./mole only.

In our opinion two factors contribute to the steric effect responsible for the weakening of the C−Br bond in Cl_3CBr. The strain due to the interaction of the bulky chlorine atoms in any molecule Cl_3CX is released when the molecule dissociates and a planar $Cl_3C\cdot$ radical is formed (see e.g. Brown[6] and Szwarc[7]). This factor is responsible for the known stability of the Cl_3C radical.[8] In the particular case of Cl_3CBr the additional decrease in the C−Br bond strength is due to the bulkiness of the bromine atom. The latter effect becomes evident on comparing the difference $D(CH_3-Br)-D(CCl_3-Br)\approx 20$ kcal./mole, with the difference $D(CH_3-H)-D(CCl_3-H)$‡ which is equal to about 12 kcal./mole only.

A full account of the determination of C−Br bond dissociation energies in polyhalogenated bromomethanes is in course of preparation.

* It was shown that no HCl was produced within the temperature range used for the thermal decomposition of Cl_3CBr, i.e., 718–827°K.

† If, however, some activation energy were required for the recombination process, the $D(CCl_3-Br)$ would be even smaller than 48 kcal./mole.

‡ $D(CCl_3-H)$ is estimated at about 89 kcal./mole from the data of Schumacher *et al.* See H. J. Schumacher and K. Wolf, Zeits. f. physik Chemie **B25**, 161 (1934); J. V. Braunwarth and H. J. Schumacher, Kolloid Zeits. **89**, 184 (1939).

[1] M. Szwarc and B. N. Ghosh, J. Chem. Phys. **17**, 744 (1949).
[2] Szwarc, Ghosh, and Sehon, J. Chem. Phys. (to be published).
[3] W. Francke and H. J. Schumacker, Zeits. f. physik. Chemie **B.42**, 297 (1939).
[4] A. A. Miller and J. E. Willard, J. Chem. Phys. **17**, 168 (1949).
[5] N. Davidson and J. H. Sullivan, J. Chem. Phys. **17**, 176 (1949).
[6] H. C. Brown, *et al.*, J. Am. Chem. Soc. **67**, 378 (1945) and following papers.
[7] M. Szwarc, Disc. Faraday Soc. **2**, 39 (1947).
[8] M. S. Kharash *et al.*, J. Am. Chem. Soc. **69**, 1100, 1105 (1947).

Lattice Frequencies of Benzene Crystal

ISAO ICHISHIMA AND SAN-ICHIRO MIZUSHIMA
Chemical Laboratory, Faculty of Science, Tokyo University, Bunkyoku, Tokyo, Japan

October 23, 1950

FROM the polarization characteristics of the Raman lines of crystalline benzene Fruhling[1] has recently reported in this journal that the 63 (ν_2) and 105 cm^{-1} (ν_4) lines arise from the rotational oscillations about the two axes of inertia situated in the plane of the molecule (hereafter designated as I) and that the 35 (ν_1) and 69 cm^{-1} (ν_8) lines arise from those about the hexagonal axis (hereafter designated as II).

Although the assignment of these lines is not discussed in detail in his paper, the conclusion does not seem to be reconcilable with the Raman measurements recently made by one of us (I.I.) from −10° down to −190°C. In this temperature range all these lines change their frequencies linearly with the absolute temperature T: $\nu_1=69-0.100T$, $\nu_2=89-0.083T$, $\nu_3=112-0.127T$, $\nu_4=141-0.128T$ cm^{-1}.

The ν_4-line has almost the same intensity as the ν_2-line at lower temperatures but the former becomes more diffuse and weaker

than the latter at higher temperatures, so that these two lines cannot be considered to arise from the same kind of molecular motion. An examination of the lattice structure[2] suggests that the energy required for the rotation or tunneling of benzene molecules about their hexagonal axes would be much less than that for the rotation about the axes in the molecular plane. Such motions would considerably affect the potential field described in our previous paper[3] and in consequence the corresponding Raman lines would become diffuse. Since the tunneling or the non-uniform rotation about the hexagonal axes occurs very probably at higher temperatures,[4] it seems more reasonable to assign ν_4 to II rather than to I.

If such an argument be admitted, we cannot assign ν_1 to II, since the intensity of this line increases with rising temperature. The fact that the intensity of ν_1 is very weak at low temperatures might suggest that this frequency corresponds to a forbidden line to be assigned to a translational vibration which tends to appear in the Raman effect at higher temperatures. (The potential field in the benzene crystal has a center of symmetry and, therefore, all the translational oscillations are forbidden in the Raman effect.[3] The large anharmonicity in the molecular oscillation in the lattice which would give rise to the considerable temperature dependence of the lattice frequencies would also be responsible for the appearance of the forbidden Raman lines at higher temperatures.)[5]

This conclusion would be supported by our experimental result on the Raman effect of pyridine crystal whose potential field has no center of symmetry and which would, therefore, show the Raman lines of the translational oscillation. At −190°C we found four lattice frequencies in the Raman effect which are practically equal to those of the crystalline benzene at the same temperature and the lowest frequency (ν_1) was found to be considerably stronger in intensity than that of benzene.

[1] A. Fruhling, J. Chem. Phys. **18**, 1119 (1950).
[2] E. G. Cox, Proc. Roy. Soc. **A135**, 491 (1932).
[3] I. Ichishima and S. Mizushima, J. Chem. Phys. **18**, 1420 (1950).
[4] E. R. Andrew, J. Chem. Phys. **18**, 607 (1950).
[5] In this connection we want to point out the strong distortions of the ellipsoid of polarizabilities due to the large mobility of the π-electrons which was already reported by Fruhling (see reference 1).

Errata: The Photo-Chemical Reduction of Water by Europium (*II*) Ion, and the Magnetic Susceptibilities of Europium (*II*) and Europium (*III*) Ions

[J. Chem. Phys. 17, 1345 (1949)]

DAVID L. DOUGLAS AND DON M. YOST
Gates and Crellin Laboratories of Chemistry, California Institute of Technology, Pasadena, California

AN error has been found in the calculation of the quantum yields tabulated in Table I. The numbers of quanta absorbed should be, reading from top to bottom: 34.0×10^{19}, 31.2×10^{19}, 27.7×10^{19}, and 29.7×10^{19}. The corresponding corrected values of the quantum yield are: 0.15 ± 0.02, 0.16 ± 0.02, 0.18 ± 0.02, and 0.20 ± 0.02.

UNIVERSITY OF MICHIGAN
JAN 11 1951
PHYSICS LIBRARY

THE JOURNAL OF CHEMICAL PHYSICS

VOLUME 18 NUMBER 12

DECEMBER, 1950

Published by the

AMERICAN INSTITUTE OF PHYSICS

Incorporated

LANCASTER, PA., AND NEW YORK, N. Y.

CHEMICAL

BOARD OF EDITORS

JOSEPH E. MAYER, *Editor*

Associate Editors

Term ending December 31, 1951

PAUL E. [illegible]
PAUL EMMETT
C. A. [illegible]CHISON
J. G. KIRKWOOD
R. S. [illegible]LIKEN

Term ending December 31, 1952

FORREST CLEVELAND
BRUCE CRAWFORD, JR.
RALPH HALFORD
GEORGE KIMBALL
K. J. LAIDLER
WILLARD F. LIBBY
J. RUD NIELSEN

Tables may be typewritten on sheets separate from the running text. Each table must have a caption which will make the data in the table intelligible without reference to the text. Avoid complicated column headings.

Wherever possible figures should be planned for the width of a column (3 in.). A convenient reduction ratio is about 2:1 or 3:1. Lettering should be large enough on the original that when reduced it shall not be less than about $\frac{1}{16}$ in. (~1.5 mm). Line drawings must be in *india ink* on white paper or tracing cloth. Coordinate paper is not desirable but if used must be blue lined and the coordinate lines which are to show must be inked over. Photographs should have maximum black and white contrast. Identify each original drawing or photograph on the back with the author's name and the figure number. Figures should be numbered consecutively. Captions should be typed on a separate sheet of paper.

A limited number of alterations in proof are unavoidable, but the cost of making extensive alterations after the article has been set in type will be charged to the author.

Proof and all correspondence concerning papers in the process of publication should be addressed to the Publication Manager, American Institute of Physics, 57 East 55 Street, New York 22, New York.

Subscription Price

	U. S. and Canada	Elsewhere
To members and associate members of the American Institute of Physics	$12.00	$13.00
To all others	15.00	16.00

Back Number Prices

Yearly rate when complete year is available: $13.00.
Single copies: $1.25 each.

Subscriptions, renewals, and orders for single copies should be addressed to the American Institute of Physics, 57 East 55 Street, New York 22, New York.

Changes of address should be sent to the American Institute of Physics.

This Journal of Chemical Physics is published monthly at Prince and Lemon Streets, Lancaster, Pennsylvania.

Entered as second class matter December 20, 1932, at the Post Office at Lancaster, Pa., under the Act of August 24, 1912.

Acceptance for mailing at special rate of postage, provided for in paragraph (d-2), section 34.40, P. L. & R. of 1948, authorized February 5, 1932.